ORNL-4581
UC-4 – Chemistry

CHEMISTRY DIVISION ANNUAL PROGRESS REPORT

FOR PERIOD ENDING MAY 20, 1970

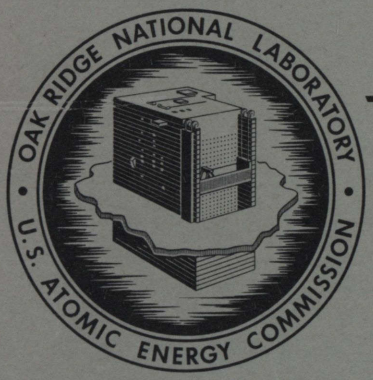

OAK RIDGE NATIONAL LABORATORY
operated by
UNION CARBIDE CORPORATION
for the
U.S. ATOMIC ENERGY COMMISSION

Printed in the United States of America. Available from Clearinghouse for Federal
Scientific and Technical Information, National Bureau of Standards,
U.S. Department of Commerce, Springfield, Virginia 22151
Price: Printed Copy $3.00; Microfiche $0.65

ORNL-4581

Contract No. W-7405-eng-26

CHEMISTRY DIVISION ANNUAL PROGRESS REPORT

for Period Ending May 20, 1970

E. H. Taylor, Director
Sheldon Datz, Associate Director
Ralph Livingston, Associate Director
B. H. Ketelle, Assistant Director

G. E. Moore, Editor of Annual Report

SEPTEMBER 1970

OAK RIDGE NATIONAL LABORATORY
Oak Ridge, Tennessee
operated by
UNION CARBIDE CORPORATION
for the
U. S. ATOMIC ENERGY COMMISSION

Reports previously issued in this series are as follows:

ORNL-2386	Period Ending June 20, 1957
ORNL-2584	Period Ending June 20, 1958
ORNL-2782	Period Ending June 20, 1959
ORNL-2983	Period Ending June 20, 1960
ORNL-3176	Period Ending June 20, 1961
ORNL-3320	Period Ending June 20, 1962
ORNL-3488	Period Ending June 20, 1963
ORNL-3679	Period Ending June 20, 1964
ORNL-3832	Period Ending May 20, 1965
ORNL-3994	Period Ending May 20, 1966
ORNL-4164	Period Ending May 20, 1967
ORNL-4306	Period Ending May 20, 1968
ORNL-4437	Period Ending May 20, 1969

Contents

1. Nuclear Chemistry

2. Chemistry and Physics of Transuranium Elements

3. Isotope Chemistry

4. Radiation Chemistry

RADIATION AND HOT-ATOM CHEMISTRY OF INORGANIC CRYSTALLINE SOLIDS

5. Organic Chemistry

6. Physical Chemistry

AQUEOUS SYSTEMS

MOLTEN SALTS AND RELATED NONAQUEOUS SYSTEMS

CALORIMETRY

ELECTROCHEMISTRY

7. Chemical Physics

NEUTRON AND X-RAY DIFFRACTION

INFRARED AND RAMAN SPECTROSCOPY

MICROWAVE AND RADIO-FREQUENCY SPECTROSCOPY

ELECTRON SPECTROSCOPY

MASS SPECTROMETRY AND RELATED TECHNIQUES

MOLECULAR BEAM STUDIES

Introduction

Again this year, we intend the Table of Contents to serve also as the summary of this report. We have also again modified the arrangement of topics by introducing a new heading, "Physical Chemistry." This provides a place for a number of subgroups of topics which had previously seemed a little inconsistent as separate chapters.

This has been a year in which the Laboratory has explored with considerable intensity possible new directions for part of its effort. Two division members, S. Datz and J. S. Johnson, have been directly concerned with this planning, and many more have examined how these new directions might affect their areas of research. It should perhaps be noted that the Chemistry Division has from the beginning been a major contributor to the first and largest of these new directions; accounts of the Water Research Program have been appearing in our annual report since 1963. Any heavier involvement of the Division in environmental and similar programs seems most likely to fall in this area, particularly since some aspects of it, hyperfiltration and certain applications of electrochemistry, give promise of early practical usefulness and are therefore in need of expanded effort.

Although the needs of applied projects are therefore taking somewhat more of our time and effort than formerly, we have no intention of abandoning those areas of research in which we have productive programs nor of ceasing to look for new areas in which we can make important contributions to pure science. The Table of Contents and the body of this report provide evidence for this continuing and evolving effort. We note two items about new directions, one of which will certainly influence our future plans and results and one of which may or may not: At about the end of the report period a beam of about 15 mA of O^{5+} was obtained at ORIC in a combined effort by the Electronuclear and the Chemistry Divisions to develop a high-intensity, high-charge-state source of carbon, nitrogen, oxygen, and neon. This flexible, intense source together with our unequaled choice of targets from the operations of the HFIR-TRU-calutron complex gives us a unique capability for producing and for identifying as to Z isotopes of elements around 104, a capability which we shall certainly exploit.

As to the other new direction, we have begun during this year actual search for superheavy elements in nature. We have been using fission counting and mass spectroscopy for detection following various kinds of separation. Early in fiscal year 1971 (corresponding roughly to our report year) we expect to have in operation a neutron coincidence counter that will accept 50-kg samples without the necessity of prior chemical separation. Whether the search will be successful depends, of course, on whether such elements do exist. We think that we are bringing to the search enough enthusiasm to find them if they are there, and we are counting on a variety of experts, in and out of house, to ensure that we examine the most promising samples.

1. Nuclear Chemistry

A REEXAMINATION OF THE DECAY OF ^{49}Ca

E. Eichler

Mann and Bloom[1] have recently measured beta-gamma correlations in ^{49}Ca decay to determine the mixing between analog and antianalog states. Analysis of their results depends profoundly on the absence of spreading of the $p_{3/2}$ strength away from the antianalog 3084-keV level in ^{49}Sc. Erskine *et al.*[2] observed in their ^{48}Ca(^{3}He, d) studies a state at 4507 keV with an $l = 1$ character suggesting a $\frac{1}{2}$ or $\frac{3}{2}$ spin assignment. In our earlier study[3] we tentatively identified a 1409-keV transition which might deexcite the suspect 4507-keV level. With our new high-resolution large-volume Ge(Li) detector, I restudied the ^{49}Ca gamma-ray spectrum. The 1409-keV gamma ray was readily shown to decay with the 8.8-min ^{49}Ca half-life. I observed additional new gamma rays; the energies and intensities of all the newly observed transitions are given in Table 1.1. Most of these transitions seem to deexcite previously known levels.

To establish the spin assignment of the 4507-keV level, I measured the 1409-3084 keV gamma-ray directional correlation using two NaI detectors. Since the intermediate spin (that of the 3084-keV level) is $\frac{3}{2}$, the A_4 parameter is zero. Thus an explicit $A2$ value could be extracted from a two-angle experiment. Twenty separate bombardments yielded an $A2$ parameter of about -0.1. Such a value is consistent with a $\frac{1}{2}^-$ assignment, with the reasonable assumption of little or no $E2$ admixture. An assignment of $\frac{3}{2}^-$ would only be possible with 50% or more $E2$ component, unlikely in such a shell-model nucleus.

Table 1.1. Newly Observed ^{49}Ca Gamma Rays

E (keV)	I^a
144.5 ± 0.7[b]	0.038
380.8 ± 0.7[b]	0.018
856.4 ± 0.5	0.14
987.5 ± 0.5	0.083
1144.5 ± 0.5	0.12
1288.6 ± 0.5	0.080
1408.9 ± 0.2	0.68

[a] Relative to the 3084.4-keV gamma ray as 100 units.

[b] These transitions could not be verified by half-life because of their low intensities.

[1] L. G. Mann and S. G. Bloom, *Nucl. Phys.* **A140,** 598 (1970).

[2] J. R. Erskine, A. Marinov, and J. P. Schiffer, *Phys. Rev.* **142,** 633 (1966).

[3] G. Chilosi, G. D. O'Kelley, and E. Eichler, *Nucl. Phys.* **A136,** 649 (1969).

ENERGY LEVELS IN ^{86}Sr FROM THE DECAY OF 14.6-hr ^{86}Y

A. V. Ramayya[1] D. Krmpotić[1,3]
B. van Nooijen[1,2] J. H. Hamilton[1]
J. W. Ford[1] J. J. Pinajian[4]
Noah R. Johnson

An experimental investigation of the ^{86}Sr levels populated in the decay of 14.6-hr ^{86}Y has been in progress for the past several years. This work, which has now been completed, has revealed a wealth of new information on the excited states of ^{86}Sr. Many types of experimental techniques have been utilized in this research. These included performing internal and external conversion measurements with an iron-free double-focusing beta-ray spectrometer, gamma-ray measurements with Ge(Li) spectrometers, and gamma-gamma coincidence experiments with NaI-NaI, NaI-Ge(Li), and Ge(Li)-Ge(Li) coincidence arrangements coupled to two-parameter analyzers.

For the energy measurements, several runs were taken with standards mixed into the source to eliminate any shifts due to source-strength variations. In this manner the energies of the stronger ^{86}Y lines were determined, and in turn these served as internal calibration points. The energy calibration was accomplished by a computer least-squares fit of the standard lines to a third-degree polynomial.

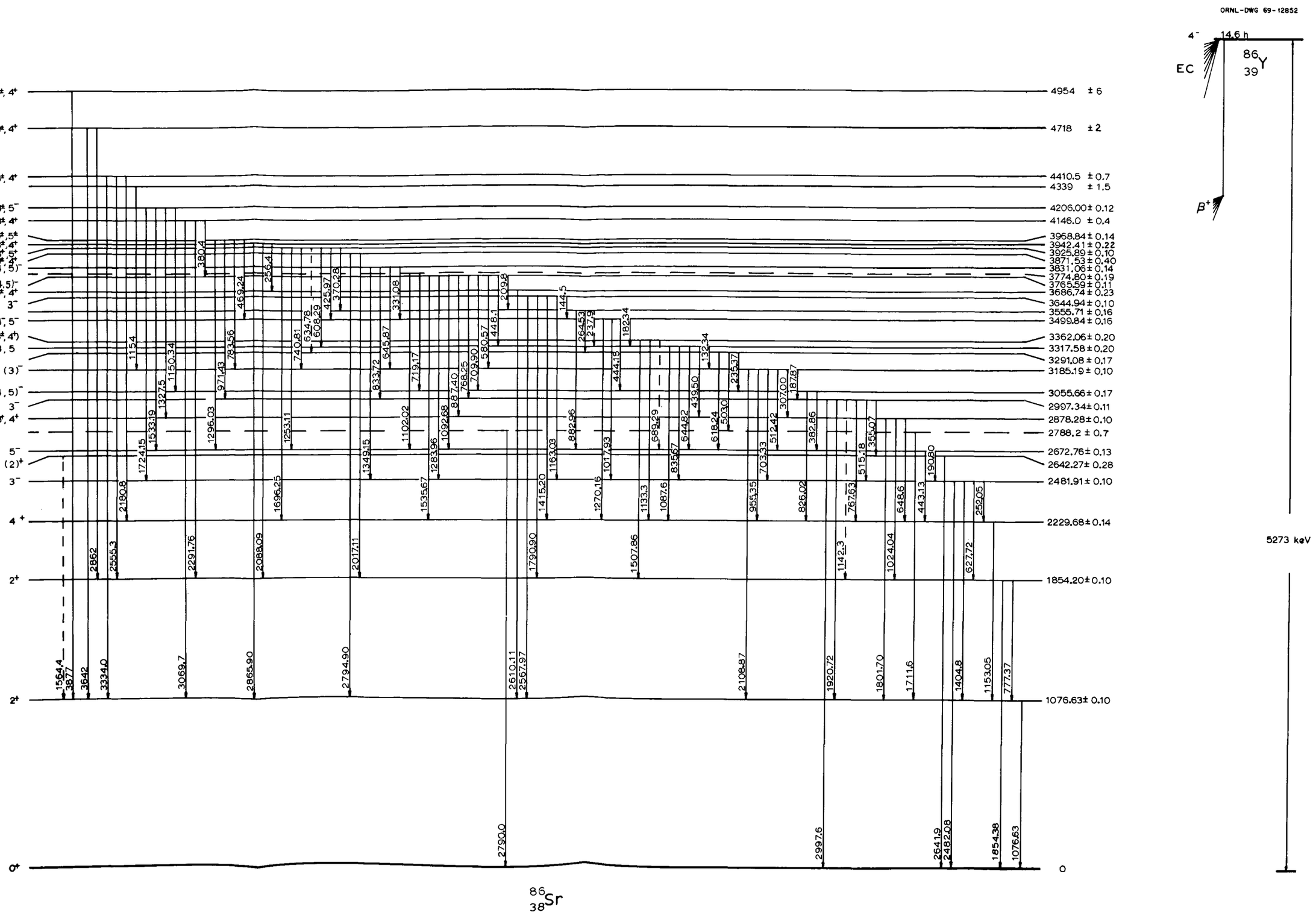

Fig. 1.1. Proposed ^{86}Y Decay Scheme. The dashed levels and dashed transitions indicate cases for which there is only weak evidence.

The coincidence spectra resulting from gating on 38 different transitions were analyzed. As a result of these extensive coincidence measurements along with the numerous other types of experiments performed, a highly consistent and detailed picture of the decay properties of the ^{86}Y nucleus has evolved. This decay scheme is shown in Fig. 1.1.

With the detailed knowledge of the ^{86}Sr levels achieved here, it seems somewhat unfortunate that there are not extensive theoretical calculations with which to compare experiments. Talmi and Unna[5] have made shell-model calculations for a few of the excited states. Their calculations were based on the assumption that the closed $1f_{5/2}$ subshell is stable as far as the low-lying levels are concerned. Note that the ^{86}Sr nucleus consists of 38 protons which fill the $1f_{5/2}$ and lower-lying subshells and of 48 neutrons which leave two holes in the $1g_{9/2}$ subshell. These calculations, which considered only the neutron holes in the $2p_{1/2}$ and $1g_{9/2}$ subshells, predict excited states at 1.08 (2^+), 1.98 (4^+), 2.33 (0^+), 2.35 (6^+), 2.49 (8^+), 2.58 (5^-), and 2.62 (4^-) MeV. As seen, the agreement with experiment is not very good.

It is probable that collective effects also are very important in the ^{86}Sr level structure. The 1076.63-keV 2^+ level may be described as a one-phonon vibrational level, whereas the 1854.2-keV 2^+ level may be described as a member of the two-phonon triplet, and the 2229.68-keV level could be the 4^+ member. Computing the ratio of reduced $E2$ transition probabilities of the 777.37-keV stopover to the 1854.20-keV crossover transitions, one obtains $B(E2; 2_2^+ \rightarrow 2_1^+)/B(E2; 2_2^+ \rightarrow 0_1^+) \cong 102$, where it is assumed that the 777.37-keV line is pure $E2$. The 2481.91-keV 3^- level probably can be interpreted as the one-phonon octupole level because of a relatively strong transition to the ground state. It is not possible to make any predictions about the higher excited states until unique spin assignments become possible.

---

[1] Vanderbilt University, Nashville, Tenn.

[2] Permanent address: Technological University of Delft, Department of Physics, Delft, Holland.

[3] Permanent address: Boris Kidric Institute of Nuclear Science, Belgrade, Yugoslavia.

[4] Isotopes Division.

[5] I. Talmi and I. Unna, *Nucl. Phys.* **19**, 225 (1960).

SEARCH FOR THE 0^+ MEMBER OF THE TWO-PHONON TRIPLET IN ^{110}Cd

M. C. Kelley[1] R. G. Lanier[2]
J. R. Van Hise[1] Noah R. Johnson

Our search for the 0^+ member of the two-phonon state in ^{110}Cd and study of the decay properties of 25-sec ^{110g}Ag (1^+) have been completed. The experi-

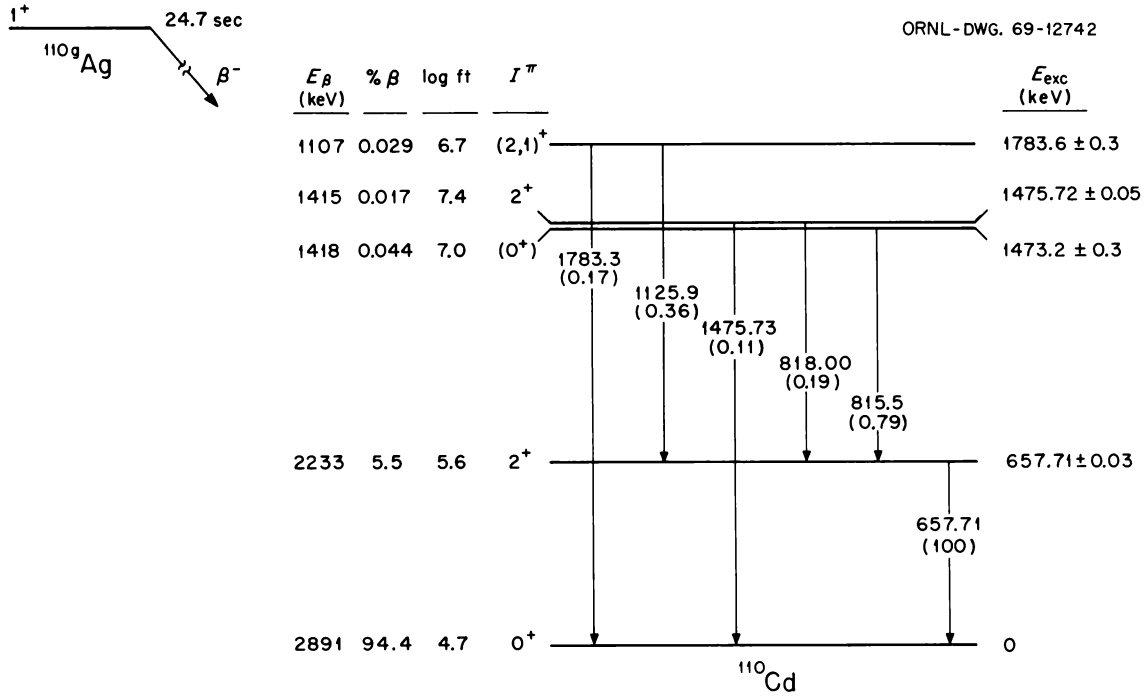

Fig. 1.2. Decay Scheme of ^{110g}Ag. The numbers in parentheses below the transition energies are relative gamma-ray intensities.

mental measurements were carried out with the use of NaI(Tl) and Ge(Li) detectors in both singles and coincidence arrangements. A summary of the observations is best presented in the ^{110g}Ag decay scheme shown in Fig. 1.2.

As we have already pointed out,[3] the low-lying states of many medium-weight even-even nuclei have properties which are reasonably well characterized as quadrupole surface vibrations. Currently there is considerable concern with understanding the behavior of the three members of the two-phonon quadrupole vibrations in these nuclei. From the present measurements it has been concluded with reasonable certainty that the 0^+ member of this triplet in ^{110}Cd exists at 1473.2 keV. The 2^+ member lies only 2.5 keV higher. Both the 2^+ and 4^+ members were seen in the ^{110g}In investigation which is discussed in the following contribution.

The observation of all three members of the two-phonon state in ^{110}Cd thus gives support to a vibrational interpretation for this nucleus. However, there are other data which raise serious questions on this interpretation; these are discussed in the following contribution, "Properties of ^{110}Cd Levels Populated in the Decay of 69-min ^{110g}In.

---

[1]Chemistry Department, Andrews University, Berrien Springs, Mich.

[2]U.S. Atomic Energy Commission Postdoctoral Fellow under appointment with Oak Ridge Associated Universities.

[3]M. C. Kelley, J. R. Van Hise, R. G. Lanier, and Noah R. Johnson, *Chem. Div. Ann. Progr. Rept. May 20, 1969*, ORNL-4437, p. 3.

PROPERTIES OF ^{110}Cd LEVELS POPULATED IN THE DECAY OF 69-min ^{110g}In

D. G. Sarantites[1] Noah R. Johnson
H. W. Boyd[2]

An extensive investigation of the level properties of ^{110}Cd as populated by the decay of 69-min ^{110g}In has been completed. Singles and coincidence gamma-ray measurements were made with both NaI(Tl) and Ge(Li) detectors. The spectra in coincidence with every prominent gamma-ray transition have been measured.

From these experiments a total of 72 transitions were assigned to the decay of ^{110g}In, and most of these have been placed in the level scheme shown in Fig. 1.3. With the log *ft* values and the gamma-ray intensity information determined in this work, it has been possible to place limits on the spin and parity values for many of the levels.

The low-lying states at 657.5 (2^+), 1475.2 (2^+), and 1540.0 (4^+) keV have been studied by means of Coulomb excitation by McGowan *et al.*[3] and by Milner *et al.*[4] These authors have determined $B(E2)$ values for the $4_1^+ \rightarrow 2_2^+$, $2_2^+ \rightarrow 2_1^+$, and $2_1^+ \rightarrow 0^+$ transitions and have compared their results with the predictions of the asymmetric rotor model and the vibrational model. Milner *et al.*[4] have determined the ratio $B(E2, 2_1^+ \rightarrow 2_1^+)/B(E2, 2_1^+ \rightarrow 0^+)$ to be 1.08 ± 0.29 using a branching ratio of 1.83 ± 0.13 for $I(818)/I(1475.5)$. This ratio of $B(E2)$ values is only about half that predicted by the vibrational model and raises some serious question about the validity of this model. These authors[4] also found a large $B(M1)$ value for the $2_2^+ \rightarrow 2_1^+$ in ^{110}Cd as well as for other even-A cadmium nuclei. This raises further question about the vibrational description of these medium-weight even-A nuclei, since in this picture $M1$ transitions should be strictly forbidden. Our data on the beta population of the 2_1^+ and 2_2^+ states in ^{110}Cd also indicate probable differences in the structures of these two states. We find a log *ft* value of 7.0 to the 2_2^+ state at 1475.1 keV. In contrast, we find that the log *ft* to the 2_1^+ state at 657.5 keV is 5.6. This same pattern of log *ft* values for allowed beta transitions to the corresponding two 2^+ states has been observed in other similar nuclei.

---

[1]Washington University, St. Louis, Mo.

[2]Oak Ridge Associated Universities Research Participant from West Georgia College, Carrollton.

[3]F. K. McGowan, R. L. Robinson, P. H. Stelson, and J. L. C. Ford, Jr., *Nucl. Phys.* **66**, 97 (1965).

[4]W. T. Milner, F. K. McGowan, P. H. Stelson, R. L. Robinson, and R. O. Sayer, *Nucl. Phys.* **A129**, 687 (1969).

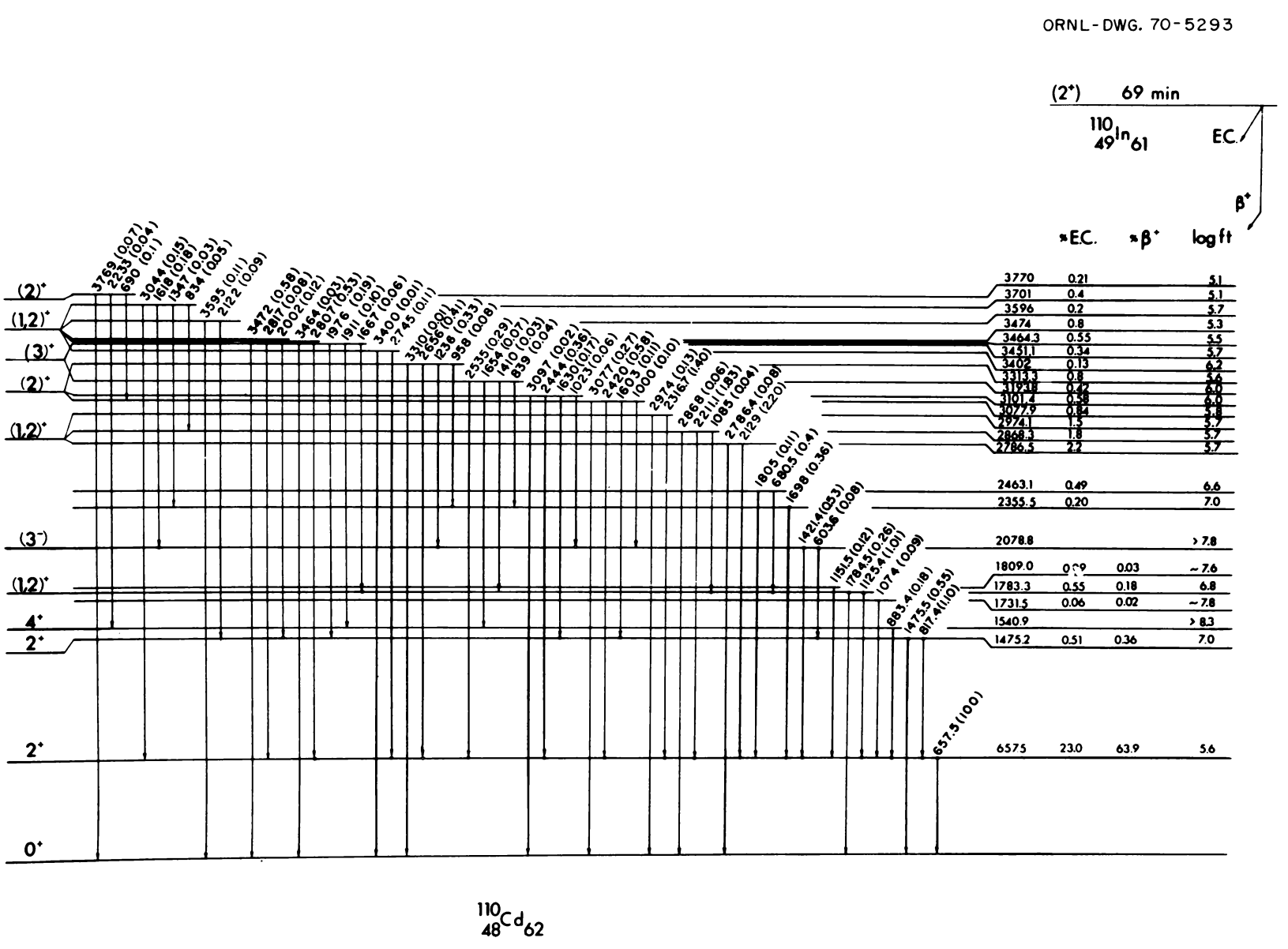

Fig. 1.3. Proposed Decay Scheme for the 69-min ^{110g}In. All energies are given in keV, and the intensities of the observed gamma rays are given in parentheses relative to the 675.5-keV gamma ray taken as 100.

DECAY OF ^{137}Nd, ^{136}Nd, AND ^{136}Pr

B. H. Ketelle A. R. Brosi

More information on the decay schemes of 13.5-min ^{136}Pr, 37-min ^{137}Nd, and 50-min ^{136}Nd is of interest because these isotopes are usually present in cyclotron targets which have been bombarded to produce new isotopes of praseodymium and neodymium on the neutron-deficient side of stability. In recent work emphasis has been on the accumulation of sufficient gamma-gamma coincidence data to deduce energy level diagrams. In the past this has been impossible, because the short-lived sources decayed before data could be acquired. When rates were increased to compensate for the short time available for data acquisition, the loss in energy resolution was intolerable. Recent developments in solid state circuitry have made it possible to resolve these difficulties.

The coincidence counting system used consists of two 40-cc germanium detectors, pulse rejection circuitry, amplitude and rise-time compensated coincidence timing, and a multiparameter pulse analyzer which stores both related coincidence addresses and singles spectra on magnetic tape. In order to accumulate coincidence data on short-lived isotopes as rapidly as possible, the germanium detectors were mounted as close to the source as the positron absorbers would permit. The pulse rejection circuitry eliminated pileup in the last stages of the amplifier and permitted the use of high-intensity sources. This circuitry was also used to discard coincidences between annihilation gamma rays and most of the coincidences due to Compton scattering between detectors.

With ^{136}Pr and ^{137}Nd sources, spectra of satisfactory energy resolution were taken with singles rates as high as 5×10^4/sec on each side and coincidence rates as high as 2×10^3/sec. These rates are about an order of magnitude higher than could be achieved with earlier equipment. A total of 10^7 coincidence events could be accumulated using sources made from a single cyclotron target. Well over a hundred pairs of coincident transitions were observed in the decay of both ^{137}Nd and ^{136}Pr. From these data an energy level diagram with more than 50 levels was constructed for ^{137}Pr, and another with more than 20 levels was constructed for ^{136}Ce.

In the case of sources of ^{136}Nd, coincidence rates were much lower relative to the singles rates than for sources of ^{137}Nd or ^{136}Pr. Several experiments have been done to learn whether the low coincidence rates were the result of delayed gamma emission or whether the gammas were emitted by totally different nuclides, even though they appeared to decay with the same half-life. This work has shown that the most intense gammas are in coincidence with praseodymium x rays and that they depopulate levels with lifetimes of less than a nanosecond. The high-intensity gammas were shown to be emitted in the same relative intensities in targets with different ^{136}Ce isotopic enrichments and regardless of whether the activity was produced by a ^{3}He or a ^{4}He reaction. These experiments confirm our earlier conclusion that ^{136}Nd decays by electron capture to several different levels in ^{136}Pr. The fact that gamma-gamma coincidence counting rates are low indicates that most electron captures occur to energy levels which are depopulated by decay to the ground state.

SEARCH FOR THE OCCURRENCE OF ^{146}Sm IN NATURE

C. E. Bemis H. R. Gwinn[1]
J. Halperin R. L. Bailey[1]
R. W. Stoughton L. T. Newman[1]
K. Spainhour[1]

The nuclide ^{146}Sm with an alpha half-life of $(1.026 \pm 0.048) \times 10^8$ years[2] has previously been produced in ^{4}He ion bombardments of Nd[2,3] and in the ^{147}Sm$(n,2n)$ reaction.[4] This nuclide has the longest half-life of all artificially produced radionuclides, although ^{146}Sm has never been observed in naturally occurring samarium.

We have estimated that if ^{146}Sm was produced approximately 4.5×10^9 years ago in the same yield and manner as ^{144}Sm, presumably a charged-particle reaction, the natural abundance of ^{146}Sm today is approximately 2.5×10^{-15} g per gram of natural samarium.

Approximately 16 kg of naturally occurring samarium was processed during the period 1967–1968 in the calutron facilities at Oak Ridge National Laboratory as part of the regular program to replenish the samarium stable-isotope inventory. Special collection pockets were fabricated and installed to collect the ion beam occurring at the mass 146 position for the entire run. Approximately 17 g of Sm_2O_3 was recovered, chemically processed to remove Nd, and mass analyzed. The average isotopic enhancement factor for this first calutron pass was ~200.

All of the first-pass material was processed in a second calutron run, and about 13 mg of Sm_2O_3 was recovered from the mass 146 pocket. The results of the mass assays of the samarium recovered from the two successive calutron runs are listed in Table 1.2 together

Table 1.2. Abundances of Naturally Occurring Samarium Isotopes and Abundances After Electromagnetic Isotope Separation in the Mass 146 Position

Isotope	Natural Abundance (at. %)	First-Pass Abundance (at. %)	Second-Pass Abundance (at. %)
144	3.09	3.65	1.40
146		<0.005	$\leqslant 0.6 \pm 0.2$ ppm
147	14.97	50.02	76.07
148	11.24	14.23	10.80
149	13.83	10.88	5.78
150	7.44	4.28	1.77
152	26.72	10.16	2.79
154	22.71	6.78	1.37

with the abundances of the isotopes of natural samarium.

We are currently measuring the alpha-particle spectrum of a small portion of the second-pass material prior to a third isotope separation which will use the laboratory-size 150-cm sector separator at the Transuranium Research Laboratory.[5]

At this present stage we can conclude that the natural isotopic abundance of ^{146}Sm is less than $\sim 2.9 \times 10^{-12}$ g per gram of natural samarium based on the mass assays of the second-pass material. The alpha-particle measurements, where the ratio of ^{146}Sm (E_α = 2.55 MeV) to ^{147}Sm (E_α = 2.23 MeV) alphas is determined, are perhaps more sensitive than the mass spectroscopic measurements because of large difference in half-lives. After the third stage of isotopic separation in which we expect an enhancement factor of ~1000 in the ^{146}Sm/^{147}Sm atom ratio, we should be able to measure an abundance for ^{146}Sm in the range of $\gtrsim 10^{-16}$ g per gram of natural samarium.

Although we expect ^{146}Sm to be produced via the ^{147}Sm(n,2n) reaction with cosmic-ray neutrons to the extent of $\sim 10^{-14}$ g per gram of natural samarium, an abundance of ^{146}Sm greater than this value might serve as a sensitive geochronological indicator.

[1] Isotopes Division.

[2] A. M. Friedman *et al., Radiochim. Acta* 5, 192 (1966).

[3] D. C. Dunlavey and G. T. Seaborg, *Phys. Rev.* 92, 206 (1953).

[4] M. Nurmia, D. Geissing, W. Sievers, and L. Varga, *Ann. Acad. Sci. Fennicae, Ser. A*, VI(167), 1 (1965).

[5] L. D. Hunt and C. E. Bemis, Jr., *Chem. Div. Ann. Progr. Rept. May 20, 1969*, ORNL-4437, p. 37.

PRODUCTION OF RARE-EARTH ALPHA EMITTERS WITH ENERGETIC ^{3}He PARTICLES

K. S. Toth[1] M. A. Ijaz[2]
R. L. Hahn W. M. Sample[2]

The work reported here and in the following section is part of a program that deals with the production and characterization of new rare-earth alpha emitters with N = 86 and 87. Earlier publications[3,4] discussed the properties of ^{153,154}Ho and ^{155}Er, nuclides produced by bombarding enriched targets of ^{156}Dy with protons and ^{4}He ions. The maximum proton and ^{4}He energies available at the ORIC are ~65 and ~80 MeV respectively. These energies are not high enough to produce the thulium and ytterbium isotopes with N = 86 and 87 by bombarding the most neutron-deficient stable isotope of erbium, ^{162}Er. Reaction energetics indicated, however, that 100-MeV ^{3}He ions incident on ^{162}Er could induce the (^{3}He,8n) and (^{3}He,9n) reactions necessary to produce the ytterbium nuclides of interest.

A beam of several microamperes of doubly charged 100-MeV ^{3}He ions was developed at the ORIC, and a search for ^{156}Yb and ^{157}Yb was initiated. It soon became clear that a separate investigation with ^{156}Dy as the target nucleus was necessary to establish excitation functions for (^{3}He,xn),(^{3}He,pxn), and (^{3}He, αxn) reactions that would lead to known erbium, holmium, and dysprosium nuclides.[5] These excitation function data could then be used in the mass assignments of the new ytterbium nuclides.

The experiments were performed with a gas-jet system.[6] The radioactive nuclei that recoil out of thin targets are stopped in helium gas in a "high-pressure" chamber (~0.2 to 2 atm) and then carried by the gas through a very small orifice into a "low-pressure" chamber (~0.2 to 0.5 torr), where they are deposited on a catcher foil for assay. Targets consisted of thin layers (~0.6 mg/cm^2) of rare-earth oxide electrodeposited onto platinum or nickel supporting foils. The isotopic compositions of the enriched oxides were such that the target nuclei of interest, ^{156}Dy and ^{162}Er, made up 12.6 and 20.4% of the target materials respectively. During irradiation, targets were positioned so that first the backing foil and then the oxide deposit intercepted the beam. Alpha-particle spectra were measured with Si(Au) detectors coupled through a low-noise charge-sensitive preamplifier, linear amplifier, and post-amplifier to a multichannel analyzer, which was used to store spectra as a function of decay time. The full width at half maximum for the various alpha-particle peaks observed during the experiments was typically 30 to 35 keV.

A series of 20-sec bombardments followed by 6 min of counting was made on a ^{156}Dy target to obtain relative yields for the various alpha emitters produced as a function of ^{3}He bombarding energy. While the initial ^{3}He energy was 102.1 MeV, the maximum available energy without any absorbers was 97.3 MeV, since the ^{3}He ions had to pass through an aluminum window foil and a 2.5-mil platinum target-backing foil.

Figure 1.4 shows spectra taken over a period of time following the bombardment of ^{156}Dy with 97.3-MeV ^{3}He ions. Part *a* represents the sum of the first two 10-sec counts, part *b* the sum of four spectra measured over the next 110 sec of counting, and part *c* the sum of a 1-min and a 2-min count. Eight main alpha groups were observed, and on the basis of alpha energies and half-lives these were assigned to: ^{152}Er, ^{153}Er, ^{151}Ho, ^{151m}Ho, ^{152}Ho, ^{152m}Ho, ^{150}Dy, and ^{151}Dy.

Yields as a function of incident energy are shown in Fig. 1.5. The experimental counting rates were corrected for differences in beam intensity, bombardment time, and available[5] alpha/total branching ratios. The ordinate scale is expressed in relative units because the efficiency for ejection of the recoil products from the ^{156}Dy target and their subsequent collection on the platinum catcher foil is not known. Furthermore, the recoil range is expected to increase with bombarding energy; this increase should not be large in going from 70 to 100 MeV, and the data shown in Fig. 1.5 are not corrected for this effect.

Curves shown in Fig. 1.5 are excitation functions calculated by using the statistical theory[7] of compound nuclear reactions and are normalized to the data points. It is seen that the energy dependence exhibited by the (^{3}He,*xn*) and (^{3}He,*pxn*) data is reproduced reasonably well by the calculated excitation functions. The particular values of the level density and radius parameters used in the calculations were $a = A/20$ and $r_0 = 1.5$ F; these same values were used in our previous studies on holmium[3] and erbium[4] isotopes produced in bombardments of ^{156}Dy with protons and ^{4}He ions. The (^{3}He,*pxn*) yields appear to be 3 or 4 times greater than those from the (^{3}He,*xn*) reactions, while the calculations indicate that the (^{3}He,*xn*) and (^{3}He,*pxn*) products in the region of 70 to 100 MeV should have comparable cross sections. Part or all of this discrepancy may be due to uncertainties in available alpha-decay branching ratios.[5] (The alpha/total branching ratios for ^{152}Er and ^{153}Er have been reported to be 0.90 and 0.95, while those for the holmium alpha emitters are reported to be between 0.20 and 0.30.) Another possible explanation is that recoils originating from (^{3}He,*pxn*) reactions have greater forward momen-

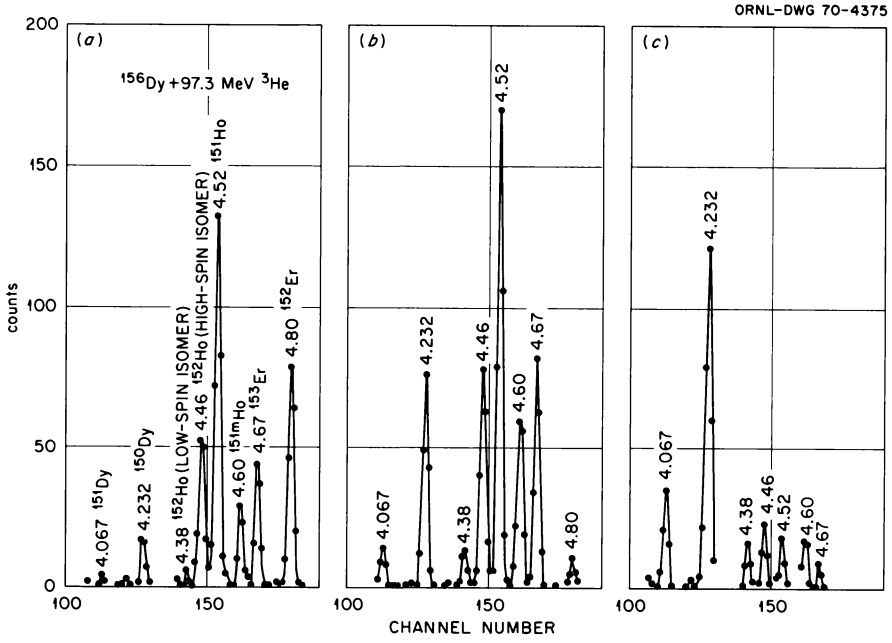

Fig. 1.4. Spectra Obtained from Reactions of 97.3-MeV ^{3}He Ions with ^{156}Dy. Part *a* is the sum of the first two 10-sec counts after end of bombardment, part *b* is the sum of four spectra taken over the next 110 sec, and part *c* is the sum of a 1- and a 2-min count.

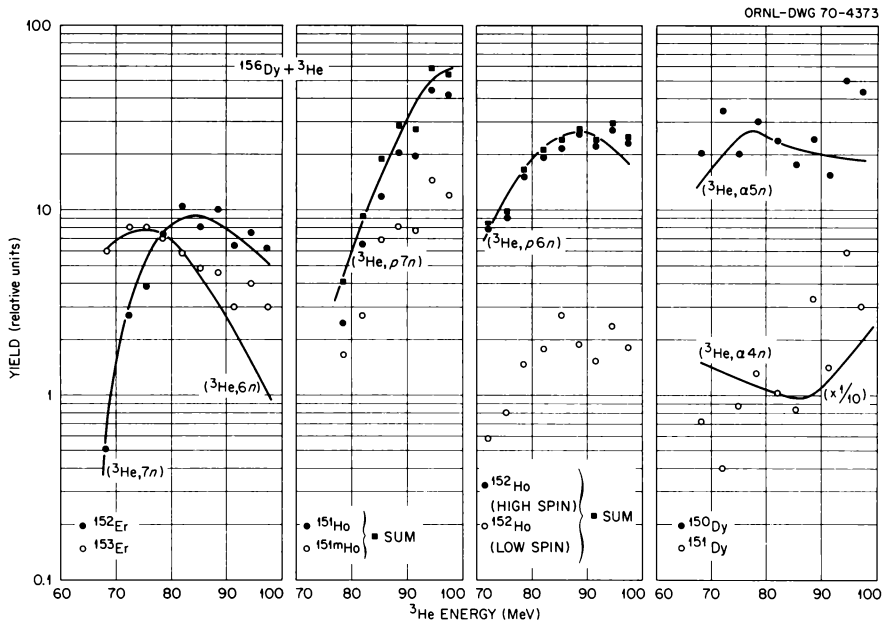

Fig. 1.5. Excitation Functions for Reactions of ^{3}He Particles with ^{156}Dy. The curves are results of statistical-model calculations, normalized to the data.

tum than those resulting from (^{3}He, xn) reactions. This additional momentum could be due to the effect of proton evaporation on the velocity of the recoils or to the fact that a mechanism other than compound-nucleus decay is involved in (^{3}He, pxn) reactions. Since the ^{156}Dy target used was thicker than the ranges of the recoil nuclei, the additional momentum would mean that a greater portion of the target material would be available for (^{3}He, pxn) products.

The counting statistics for the 6-min (^{150}Dy) and 18-min (^{151}Dy) activities were rather poor, as evidenced by the large scatter in the ^{150}Dy and ^{151}Dy data points. Nevertheless it is clear that their yields are comparable with those of the (^{3}He, pxn) products. The calculations, on the other hand, predict that the (^{3}He, αxn) yields should be smaller than the (^{3}He, xn) yields by about a factor of 5. Here again part of the discrepancy may be due to uncertainties in alpha/total ratios[5] (0.18 and 0.06 for ^{150}Dy and ^{151}Dy respectively) or to a greater forward momentum imparted to the (^{3}He, αxn) recoils. But, in contrast to the (^{3}He, pxn) and (^{3}He,xn) results, the shapes of the calculated curves do not reproduce the (^{3}He, αxn) data points. A further complicating factor here is that part of the observed yields for ^{150}Dy and ^{151}Dy could be due to either electron-capture decay from ^{150}Ho and ^{151}Ho or alpha decay from ^{154}Er and ^{155}Er. However, detailed analysis of the data clearly indicates that

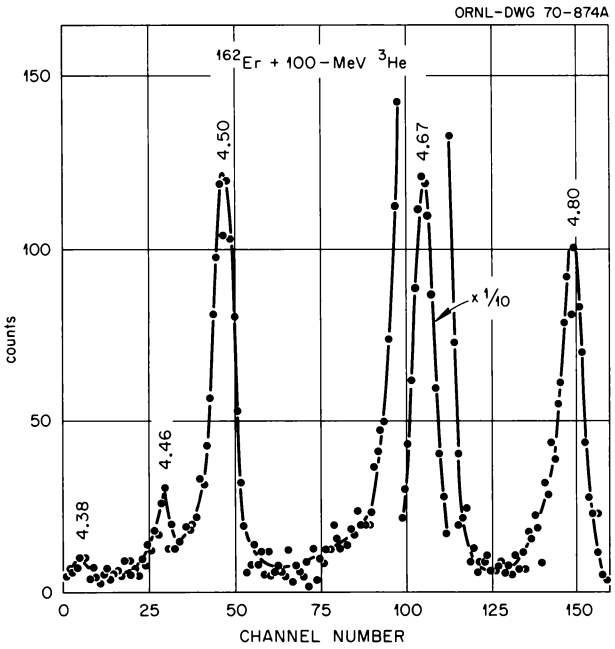

Fig. 1.6. Spectrum Obtained from Reactions of 100-MeV ^{3}He Ions with ^{162}Er.

most of the observed ^{150}Dy and ^{151}Dy yields are produced not by radioactive decay but by (^{3}He, αxn) reactions.

Similar irradiations of the ^{162}Er target with 100-MeV ^{3}He particles yielded the spectra shown in Fig. 1.6.

Thirty 15-sec irradiations were done, each followed by 3 min of counting. Three alpha groups stand out at 4.80, 4.67, and 4.50 MeV. Two smaller peaks appear at 4.46 and 4.38 MeV. Decay curve analyses for the main three peaks indicated that (1) the 4.80-MeV group had a 24-sec half-life and thus could not be ^{152}Er, (2) the intense 4.67-MeV peak had the 36-sec half-life of ^{153}Er, and (3) the 4.50-MeV alpha particle had a 34-sec half-life. The assignment of these peaks will be discussed in the following contribution. The count rates for the peaks at 4.46 and 4.38 MeV were low; the decay curves, however, were consistent with the half-lives of the ^{152}Ho isomers.

Excitation functions for the 4.67-, 4.50-, and 4.80-MeV peaks are shown in Fig. 1.7. Statistical model calculations for the (^{3}He,8n) and (^{3}He,9n) reactions are in agreement with the data for the 4.50- and 4.80-MeV peaks. But the yield of ^{153}Er, produced by the (^{3}He, α8n) reaction, cannot be fitted by the calculated curve. Also, the ^{153}Er yield is significantly larger than that for the (^{3}He,8n) reaction.

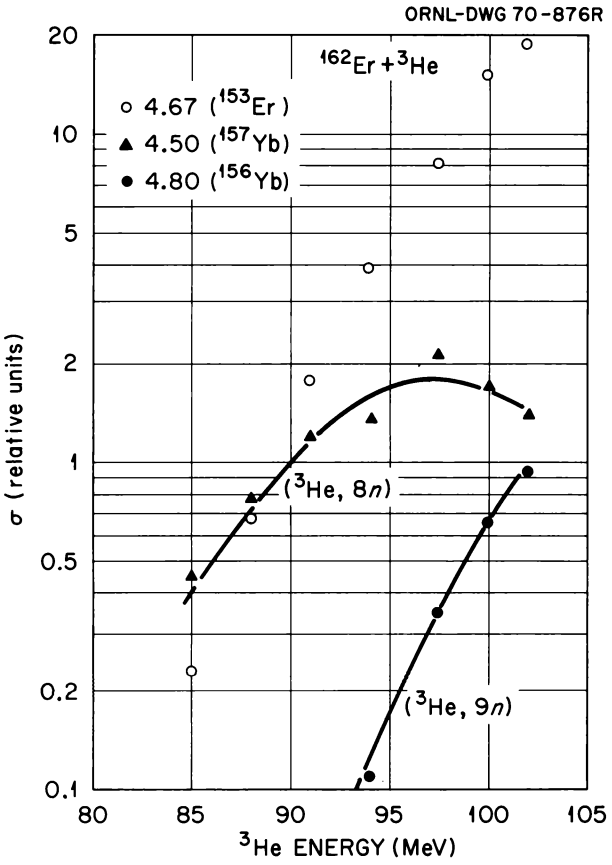

Fig. 1.7. Excitation Functions for the 4.67-, 4.50-, and 4.80-MeV Peaks Observed in the Irradiations of ^{162}Er with ^{3}He Particles. The curves are statistical-model calculations, normalized to the data.

These results are of special interest because they indicate that charged particles, both protons and alphas, are emitted in large yield relative to neutron emission in reactions of ^{3}He particles with rare-earth nuclei. Furthermore, the emission of alpha particles in fairly complex reactions in which several neutrons are also emitted apparently cannot be explained by the usual notions of compound-nuclear reactions.

---

[1] Electronuclear Division.

[2] Physics Department, Virginia Polytechnic Institute, Blacksburg.

[3] R. L. Hahn, K. S. Toth, and T. H. Handley, *Phys. Rev.* **163**, 1291 (1967).

[4] K. S. Toth, R. L. Hahn, M. F. Roche, and D. S. Brenner, *Phys. Rev.* **183**, 1004 (1969).

[5] P. Eskola, *Arkiv Fysik* **36**, 477 (1967).

[6] R. L. Hahn *et al.*, *Chem. Div. Ann. Progr. Rept. May 20, 1969*, ORNL-4437, p. 37.

[7] I. Dostrovsky, Z. Fraenkel, and G. Friedlander, *Phys. Rev.* **116**, 683 (1960).

NEW ISOTOPES: ^{151}Er, ^{156}Yb, AND ^{157}Yb

K. S. Toth[1] M. A. Ijaz[2]
R. L. Hahn W. M. Sample[2]

The data discussed in the preceding contribution were used to characterize three new rare-earth nuclides.

^{151}Er, because it contains 83 neutrons, should decay primarily by electron capture to ^{151}Ho. Indeed, the two alpha-decaying isomers of ^{151}Ho at 4.52 and 4.60 MeV were clearly seen in the reactions ^{156}Dy + ^{3}He. Accordingly, a search for an initial growth period in the ^{151}Ho peaks due to the decay of ^{151}Er was undertaken. None was observed for the more intense 4.52-MeV alpha peak (see Fig. 1.4). The 4.60-MeV group, contrastingly, at ^{3}He incident energies above 90 MeV did show an initial increase in intensity, with the growth period being most pronounced at the highest bombarding energy.

A separate experiment was undertaken to emphasize the period immediately after bombardment so that an accurate determination could be made of the initial growth and decay relationships. Twenty 10-sec bombardments were made, followed, within ~0.2 sec, by forty 10-sec counts. The decay data for the 4.60-MeV peak, shown in Fig. 1.8, are characteristic of radioactive growth and decay. Least-squares analyses of these data indicated that the 47-sec ^{151m}Ho arises in part from

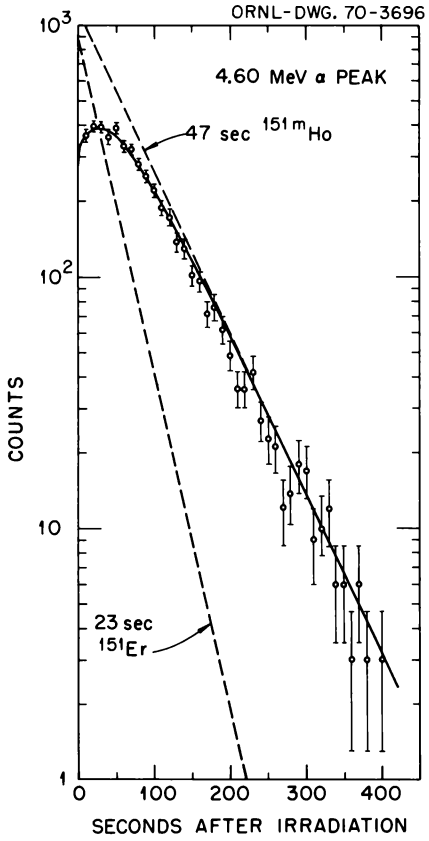

Fig. 1.8. Decay Data for the 4.60-MeV Alpha Peak of ^{151m}Ho, Illustrating Its Growth from ^{151}Er.

the decay of a nuclide with a half-life of 23 ± 2 sec. This new activity, based on the unequivocal parent-daughter relationship, was assigned to ^{151}Er.

The 4.80-MeV alpha peak observed in the reactions ^{162}Er + ^{3}He (Figs. 1.6 and 1.7) also represented a new alpha-decaying isotope. Its excitation function indicated that it was produced in the ^{162}Er(^{3}He,9*n*) reaction leading to ^{156}Yb. Corroboration of this assignment was sought in the decay data for the 4.80-MeV peak.

One hundred irradiations of 10 sec duration followed by 160 sec of counting for each were performed. The summed decay data are shown in Fig 1.9. Least-squares analysis indicated a generic relationship between two radioactive components, one with a half-life of 24 ± 1 sec and the other with a 9.8-sec half-life. Because this latter value is that of ^{152}Er, the parent-daughter relationship clearly establishes the existence of its alpha-decay parent, the new ytterbium nuclide ^{156}Yb. (The alpha-decay energy, 4.80 ± 0.01 MeV, within the resolution capabilities of the detection system used, is the same as that of its alpha-decay daughter, ^{152}Er.)

The assignment of the 4.50-MeV peak to ^{157}Yb from the reaction ^{162}Er + ^{3}He requires considerably more discussion than in the previous cases, ^{151}Er and ^{156}Yb. Although the experimental excitation function (Fig. 1.7) is certainly consistent with that for the ^{162}Er(^{3}He,8*n*) reaction required to make ^{157}Yb, analysis of the decay data for the 4.50 ± 0.01 and 4.67 ± 0.01 MeV alpha peaks is not as straightforward as it was for ^{151}Er and ^{156}Yb.

First of all, as shown in the lower part of Fig. 1.10, the 4.50-MeV peak decays with a half-life of 34 ± 3 sec. This combination of energy and half-life agrees reasonably well with that known for ^{151}Ho. So one must adequately demonstrate that the 4.50-MeV alpha peak cannot be due to ^{151}Ho before considering its assignment to ^{157}Yb.

The experimental excitation function for the 4.50-MeV group (Fig. 1.7) clearly peaks at ~98 MeV, a result that is unreasonable for the (^{3}He,$\alpha p9n$) reaction needed to produce ^{151}Ho in light of the data shown in Fig. 1.5 for the (^{3}He,αxn) and (^{3}He,pxn) reactions. Furthermore, if the 4.50-MeV peak were due to ^{151}Ho, then the 4.60-MeV alpha group of ^{151m}Ho should also be evident in Fig. 1.6. It was not seen.

The possible production of ^{151}Ho from the alpha decay of the unknown nuclide ^{155}Tm, as well as the suggestion that the 4.50-MeV alpha group is due to the

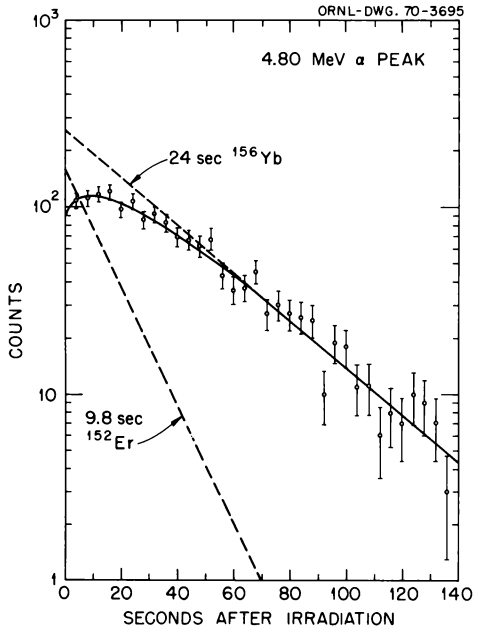

Fig. 1.9. Decay Data for the 4.80-MeV Alpha Peak, Illustrating the Decay of ^{156}Yb and the Growth of Its Daughter, ^{152}Er.

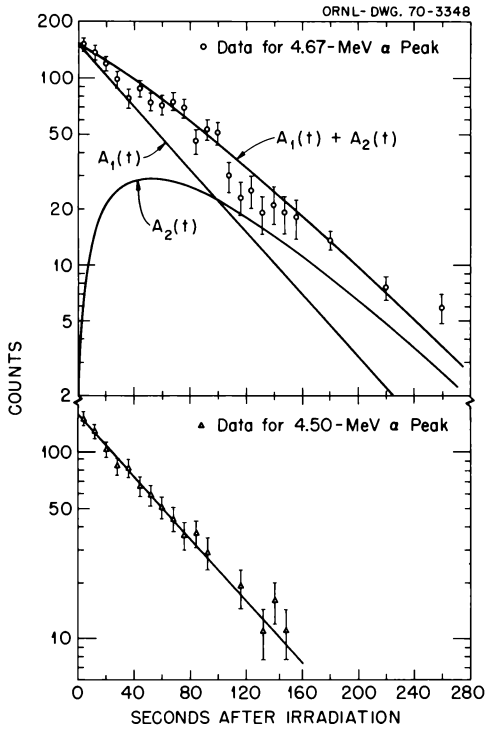

Fig. 1.10. (Lower) Decay Data for the 4.50-MeV Peak, Assigned to the Decay of ^{157}Yb; (Upper) Decay Data for the 4.67-MeV Peak, Ascribed to ^{153}Er. Curve $A_1(t)$ is that calculated for the ^{153}Er present at the end of the irradiation. The calculated growth and decay curve of ^{153}Er due to parent ^{157}Yb is curve $A_2(t)$. The sum of these curves, $A_1(t) + A_2(t)$, agrees quite well with the data.

alpha decay of ^{155}Tm itself, can also be ruled out because the thulium nuclide would have to be made in a (^{3}He,$p9n$) reaction. Again the shape of the observed yield curve is inconsistent with the data shown in Fig. 1.5. Also, the half-life of ^{155}Tm should be >5 sec (that reported[3] for ^{154}Tm), but no initial growth period was observed for the 4.50-MeV peak.

In the series of 100 irradiations at 100 MeV, no alpha activity was observed due to the known[3] 1.65-sec ^{155}Yb nuclide, even though measurements were begun within ~0.2 sec after the end of the bombardment. Thus the 4.50-MeV alpha group cannot be due to either of the two decay sequences:

$$^{155}\mathrm{Yb} \xrightarrow{\alpha} {}^{151}\mathrm{Er} \xrightarrow{\mathrm{E.C.}} {}^{151}\mathrm{Ho}$$

or

$$^{155}\mathrm{Yb} \xrightarrow{\mathrm{E.C.}} {}^{155}\mathrm{Tm} \xrightarrow{\alpha} {}^{151}\mathrm{Ho}\ .$$

Another problem associated with the mass assignment is due to the fact that if the 4.50-MeV peak arises from the decay of ^{157}Yb, then its daughter ^{153}Er should also be observed. The 4.67-MeV alpha peak, decaying with 36-sec half-life, can indeed be attributed to ^{153}Er. But because ^{153}Er is essentially a pure alpha emitter, for every ^{157}Yb alpha decay one should see one alpha event due to ^{153}Er; radioactive growth and decay should be apparent.

The counts observed at 100 MeV (see Fig. 1.6) were such that the ^{153}Er produced independently in the (^{3}He,$\alpha 8n$) reaction obscured any counts that would have grown in from the 4.50-MeV alpha group which we have assigned to ^{157}Yb. At energies below 90 MeV, count rates for both the 4.50- and 4.67-MeV groups were extremely low. An attempt was made to observe growth in the 4.67-MeV alpha peak at a ^{3}He energy of 90.3 MeV. Sixty 20-sec irradiations were made, each followed by 320 sec of counting.

The decay data from these experiments are shown in the upper part of Fig. 1.10. Note that the 4.67-MeV alpha peak no longer exhibits the characteristic half-life of ^{153}Er; instead, the apparent half-life is appreciably longer than 36 sec.

One can perhaps argue that the 4.67-MeV peak observed at 90.3 MeV is due not only to 36-sec ^{153}Er, but also to some other nuclide with a half-life of ~70 sec. The combination of these two components could lead to the experimental decay curve *if* the intensity of the longer component were comparable with that of ^{153}Er. One would expect to see this result reflected in the behavior of the excitation function for the 4.67-MeV peak (see Fig. 1.7). Nothing striking, however, occurs in the excitation function at 90 MeV to indicate that another nuclide besides ^{153}Er is making a marked contribution to the yield of the 4.67-MeV peak.

We can explain the results in Fig. 1.10 by assuming that the 4.67-MeV peak is due to ^{153}Er, growing from the decay of ^{157}Yb. Furthermore, this explanation is consistent with our assignment of the 4.50-MeV peak to the decay of ^{157}Yb. In Fig. 1.10 it is seen that the initial intensities of the 4.50- and 4.67-MeV peaks are comparable, so that the ^{153}Er growing from the alpha decay of ^{157}Yb can have a striking effect upon the observed decay curve for the 4.67-MeV alpha peak. Because parent and daughter have approximately the same half-life, the equation for the growth and decay for ^{153}Er has a special form:

$$A_d(t) = A_p(0)\,\lambda t e^{-\lambda t}\ .$$

Here $A_d(t)$ is the daughter activity at some time t after the end of the irradiation, $A_p(0)$ is the parent activity at the end of bombardment, and λ is the decay

Table 1.3. New Rare-Earth Nuclides

Isotope	Half-Life (sec)	Alpha-Particle Energy (MeV)
^{151}Er	23 ± 2	*a*
^{156}Yb	24 ± 1	4.80 ± 0.01
^{157}Yb	34 ± 3	4.50 ± 0.01

[a]Decay is primarily by electron capture to ^{151m}Ho.

constant, which is taken to be equal for parent and daughter. It is significant that this expression contains the multiplicative factor λt; it does not exhibit the simple exponential dependence upon t that is usually associated with radioactive decay.

The calculated growth and decay curve for ^{153}Er, consistent with the observed intensity of the 4.50-MeV peak that we assign to ^{157}Yb, is labeled $A_2(t)$ in Fig. 1.10. The curve labeled $A_1(t)$, with characteristic 36-sec half-life, is that ascribed to the ^{153}Er present at the end of bombardment. [The ^{153}Er is produced in two ways during the irradiation: by the (^{3}He,$\alpha 8n$) reaction and by decay of ^{157}Yb.] The sum of the two curves, labeled $A_1(t) + A_2(t)$, is seen to agree quite well with the data; at decay times >120 sec, the growth of ^{153}Er from ^{157}Yb [curve $A_2(t)$] has an important effect upon the shape of the observed decay curve.

In conclusion, we assign the 4.50-MeV alpha particle to the new nuclide ^{157}Yb because (1) the excitation function is typically that for the (^{3}He,$8n$) reaction, (2) the data do not support the assignment of the activity to other nuclides, such as ^{151}Ho, and (3) the decay data for the 4.67-MeV peak are consistent with what is expected for ^{153}Er growing in from the alpha decay of ^{157}Yb.

The data for the three new nuclides are summarized in Table 1.3.

[1]Electronuclear Division.

[2]Physics Department, Virginia Polytechnic Institute, Blacksburg.

[3]P. Eskola, *Arkiv Fysik* **36**, 477 (1967).

ALPHA-DECAY ENERGY SYSTEMATICS

K. S. Toth[1] R. L. Hahn

The discovery of unknown isotopes is of significance because it contributes to the understanding of the systematics of radioactive decay and provides measurements of decay energies which can then be used to determine precise values of nuclear masses and binding energies. Alpha-decay energies available[2] for rare-earth nuclei are plotted in Fig. 1.11 as a function of neutron number. Decay energies for new isotopes reported in the preceding contributions[3] and in refs. 4 and 5 are indicated by larger points. With the exception of the data shown for N = 83 nuclides, only experimentally determined decay energies are plotted in Fig. 1.11. Energies given for ^{147}Gd, ^{145}Sm, and ^{143}Nd were calculated by means of closed energy cycles. The method consists in constructing an energy-balance cycle from two alpha- and two beta-decay energies. If three of the four pieces of information that constitute a cycle are known, then the fourth can be calculated. In all three instances the alpha-decay energy of a given N = 83 isotope is ~1.5 MeV less than that of the corresponding N = 84 nuclide. (In Fig. 1.11 the ^{151}Er alpha-decay energy is thus estimated to be ~1.5 MeV less than that of ^{152}Er.) This sudden drop in energy shows the influence of the closed 82-neutron shell. As a result of the major closed shell, the maximum alpha-decay

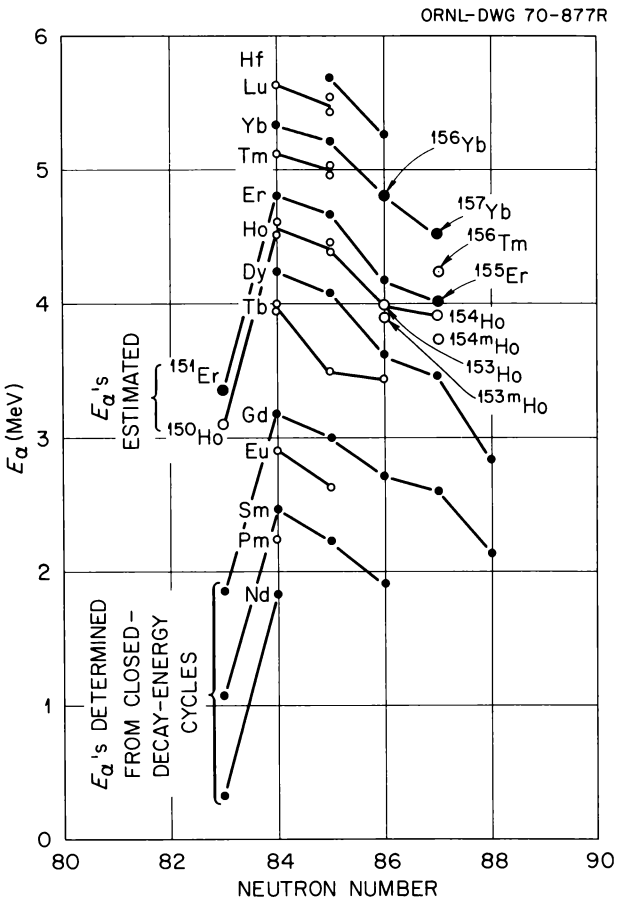

Fig. 1.11. Alpha-Particle Energies for Rare-Earth Nuclides as a Function of Neutron Numbers.

energy for a given element is reached at 84 neutrons, owing to the abnormally low neutron binding energies just beyond the closed shell.

The data for the new Ho, Er, and Yb isotopes, with neutron number $N = 86$ and 87, as well as for Gd and Dy nuclides, are indicative of a pairing energy effect. (A similar pairing effect has been noted[6] for alpha emitters in the $N = 126$ region.) While nuclides with $N = 84$ and $N = 85$ have similar decay energies, the additional pair of neutrons in $N = 86$ nuclides seems to result in added stability and a consequent extra decrease in alpha-decay energy. The effect is even more pronounced in going from $N = 87$ to $N = 88$ nuclides; this would account for the fact that a rather extensive search[4] for alpha activity due to the 88-neutron nuclide ^{155}Ho proved fruitless. A straight line drawn through the energies for ^{151,152,153,154}Ho would yield a decay energy for ^{155}Ho of ~3.7 MeV. Based on the sharp drop in energy between the 87- and 88-neutron isotopes of dysprosium, however, one would estimate the ^{155}Ho alpha-decay energy to be only ~3.3 MeV. A decrease of 0.4 MeV in alpha-decay energy would lead to a greatly increased alpha-decay half-life, which in turn would make the alpha/total branching ratio for ^{155}Ho much less than expected.

The one clear exception in Fig. 1.11 to this pairing effect involves ^{150}Tb. This odd-odd nucleus has an unknown ground-state spin. From decay-scheme studies[2] the level structure in its alpha-decay daughter, ^{146}Eu, has been proposed to be: 0 keV (4^+), 115 keV (3^+), 230 keV (2^+), and 375 keV (1^+). If the ground-state spin of ^{150}Tb were low, then alpha decay would proceed to one of the low-spin excited states in ^{146}Eu rather than to the 4^+ ground state. The observed ^{150}Tb alpha decay would therefore not correspond to the actual energy difference between the two nuclei.

One other point should be made concerning Fig. 1.11: On examination of the $N = 84$ nuclei, one notes a "break" between the gadolinium ($Z = 64$) and terbium ($Z = 65$) nuclides. This "break" had been observed earlier,[7] when it was suggested that the 65th proton is less tightly bound than the other protons in the region. The effect correlates nicely with the fact that there is a proton subshell occurring at $Z = 64$ where the $d_{5/2}$ orbital is closed and the next available orbital is the $h_{11/2}$. As a result of the splitting between the two subshells there would be an extra stabilization for the 64-proton configuration.

[1] Electronuclear Division.

[2] *Nuclear Data Sheets, B,* Academic, New York.

[3] K. S. Toth, R. L. Hahn, M. A. Ijaz, and W. M. Sample, "Production of Rare-Earth Alpha Emitters with Energetic ^{3}He Particles" and "New Isotopes: ^{151}Er, ^{156}Yb, and ^{157}Yb," the two preceding contributions, this report.

[4] R. L. Hahn, K. S. Toth, and T. H. Handley, *Phys. Rev.* **163,** 1291 (1967).

[5] K. S. Toth, R. L. Hahn, M. F. Roche, and D. S. Brenner, *Phys. Rev.* **183,** 1004 (1969).

[6] K. Valli, University of California Radiation Laboratory Report No. 17723, 1967 (unpublished).

[7] J. O. Rasmussen, S. G. Thompson, and A. Ghiorso, *Phys. Rev.* **89,** 33 (1953).

COULOMB EXCITATION OF ^{154}Gd, ^{156}Gd, AND ^{166}Er[1]

L. L. Riedinger[2] J. Fuglsang[3]
E. Eichler G. B. Hagemann[3]
B. Herskind[3]

Coulomb excitation involving 15-MeV alpha and 30- to 55-MeV oxygen ions from the Niels Bohr Institute tandem accelerator has been used to study rotational and vibrational states in ^{154}Gd, ^{156}Gd, and ^{166}Er. The alpha particles were detected in a heavy-particle spectrograph. Gamma rays from decay of the states Coulomb excited by the ^{16}O ions were detected in coincidence with backscattered projectiles. By means of the de Boer–Winther multiple Coulomb excitation program, matrix elements connecting the different states are evaluated from the data. Special emphasis is placed on the interpretation of the properties of the β- and γ-vibrational bands. From the ^{154}Gd(α,α') data, we found a $B(E2)$ value to the 2+ β-vibrational state of 0.024 ± 0.004, very similar to the recently measured value for ^{152}Sm, and a $B(E2; 0 \rightarrow 2\gamma)$ of 0.171 ± 0.012, approximately twice that in ^{152}Sm. In oxygen ion experiments we observed the ground-state rotational levels with spins up to 8+ and the 2+ and 4+ states of the γ bands in ^{154}Gd, ^{156}Gd, and ^{166}Er, while in the former two nuclei, gamma rays from the 0+, 2+, and possibly the 4+ members of the β band were detected.

Our results suggest that the Z_β anomalies observed at ORNL by Riedinger, Johnson, and Hamilton,[4] as well as at other laboratories, may be due specifically to the transition between the 2+ member of the β band and the 4+ of the ground band. This has been suggested also by Fraser *et al.*[5]

[1] Work performed at the Niels Bohr Institute, University of Copenhagen, Denmark.

[2] Present address: Physics Department, Notre Dame University, South Bend, Ind.

[3]Niels Bohr Institute, University of Copenhagen, Denmark.

[4]L. L. Riedinger, Noah R. Johnson, and J. H. Hamilton, *Phys. Rev.* 179, 1214 (1969).

[5]I. A. Fraser *et al.*, *Phys. Rev. Letters* 23, 1047 (1969).

COULOMB EXCITATION EXPERIMENTS AT ORIC

E. Eichler Noah R. Johnson
C. E. Bemis M. Schmorak[1]

The recent development of heavy-ion beams at the Oak Ridge Isochronous Cyclotron (ORIC) has opened up a new area of nuclear research using the technique of Coulomb excitation. The currently available beam of 80-MeV ^{16}O is near the barrier height of the heaviest elements and thus quite suitable for Coulomb excitation in this unexplored region at the outer limits of the periodic system.

We have constructed a reaction chamber and acquired annular silicon surface-barrier detectors and coincidence circuitry needed for gamma-ray–backscattered-oxygen-ion coincidence measurements. In our first three runs we attempted to optimize the beam optical parameters so as to maximize the intensity on the target and minimize that striking the collimator. Even in the singles mode we observed excitation of the ground-state rotational band up to the 10+ state as well as members of the β- and γ-vibrational bands. In our most recent run we recorded gamma-ray spectra from Coulomb excitation of ^{238}U in coincidence with backscattered ^{16}O ions with excellent signal-to-background ratios.

---

[1]Nuclear Data Project.

SOME PROPERTIES OF VIBRATIONAL BANDS IN ^{156}Gd AND ^{158}Gd

A. F. Kluk[1] N. R. Johnson
J. H. Hamilton[2]

The decay properties of 15-day ^{156}Eu and 45-min ^{158}Eu are being investigated with large-volume, high-resolution Ge(Li) detectors. Both gamma-ray singles experiments and multiparameter Ge(Li)-Ge(Li) coincidence experiments have been done on each isotope. Several computer programs have been developed for accurate analysis of the gamma-ray singles spectra and for sorting related address pairs from coincidence experiments. In addition, an Si(Li) spectrometer system has been developed for multichannel pulse-height analysis of electron spectra.

Although the detailed decay properties of these two isotopes are being determined, our experiments have been concerned primarily with the study of the branching ratios of the gamma-ray transitions between the β- and γ-vibrational levels and the 0+, 2+, and 4+ members of the ground-state rotational band. In particular, we are concerned with the ratios of reduced electric quadrupole transition probabilities from the β band.

Earlier it was found[3–5] that these ratios in ^{152}Sm and ^{154}Gd, which are just at the onset of permanent nuclear deformation, were not accounted for by theory. The theory which had seemed to give an adequate description of the $B(E2)$ ratios from the γ band consists of a first-order perturbational treatment of the simple adiabatic model of an axially symmetric deformed nucleus. This treatment is necessary to account for the mixing of the wave functions of the vibrational and rotational bands. These mixings of bands result in corrections to the gamma-ray branching intensity ratios which are proportional to the ratios of the spin-independent part of the matrix elements. The proportionality factor can be determined as a function of a term called a mixing parameter, Z, which according to the theory should have a consistent value for all branching ratios from a given band.

It was felt that since ^{156}Gd is a somewhat better deformed nucleus than ^{152}Sm and ^{154}Gd, the same disagreement may not be present here. However, our high-resolution work with ^{156}Eu indicates that similar anomalies do exist in the branching intensity ratios from the β band of ^{156}Gd. The band mixing parameter is given in Table 1.4 for the various transitions from the 2+ member of the β band. (The 0+ band head is at 1049.45 keV, and the 2+ member is at 1129.47 keV.) As seen in Table 1.4, there is a large variation in the three Z_0 values. In the last column we show the corresponding Z_0 value from the (n,γ) work of Greenwood and Reich.[6] We also observed another $K\pi = 0+$ band with the 0+ level at 1168.12 keV and 2+ level at 1258.02 keV. This band likewise was recently reported by Greenwood and Reich.[6] The data on this band are also given in Table 1.4 and are found to be inconsistent with theoretical predictions.

These discrepancies may be partially explained by recent Coulomb excitation work[7,8] which showed relative magnitudes of the $E2$ matrix elements associated with the decay of the β-vibrational band in several deformed nuclei. It was found[7,8] that the probability for deexcitation of the 2+ level by $E2$ radiation to the 4+ level of the ground-state rotational band is considerably less enhanced than that predicted

by the rotational model modified to include mixing of the intrinsic and rotational wave functions to first order.[3,4] The reason for this lower $B(E2)$ value is not known.

Our values for the Z_2 mixing parameter for the γ-vibrational band of ^{158}Gd are given in Table 1.5 (Z_2 is the mixing parameter between the γ-vibrational and ground states) and compared with those of Paperiello *et al.*,[9] which were obtained from ^{158}Tb decay. In ^{156}Gd the 2+ level of the γ band was considered to be at 1154.01 keV. The wide variation in the three Z_2 values obtained from this level is most surprising, since previous experience with other deformed nuclei has shown much better agreement in the respective values.

Table 1.4. Reduced Transition Probability Ratios for Transitions from the $K\pi = 0+$ Band of ^{156}Gd

Energy Level (keV)	Reduced Transition Probability Ratio	Experimental Value	Theoretical Value[a]	Z_0	
				This Work[b]	Greenwood *et al.*[6]
				$\times 10^{-3}$	$\times 10^{-3}$
		β-Vibrational Band			
1129.47	$\frac{B(E2, 2^{+\prime} \rightarrow 0^+)}{B(E2, 2^{+\prime} \rightarrow 2^+)}$	0.18(1)	0.70	−82(7)	74(4)
	$\frac{B(E2, 2^{+\prime} \rightarrow 0^+)}{B(E2, 2^{+\prime} \rightarrow 4^+)}$	0.14(1)	0.39	−28(3)	18(2)
	$\frac{B(E2, 2^{+\prime} \rightarrow 4^+)}{B(E2, 2^{+\prime} \rightarrow 2^+)}$	1.28(9)	1.79	12(2)	−15(2)
		Other $K\pi = 0^+$ Band			
1258.02	$\frac{B(E2, 2^{+\prime\prime} \rightarrow 0^+)}{B(E2, 2^{+\prime\prime} \rightarrow 2^+)}$	0.25(2)	0.70	−68(7)	73(5)
	$\frac{B(E2, 2^{+\prime\prime} \rightarrow 0^+)}{B(E2, 2^{+\prime\prime} \rightarrow 4^+)}$	0.07(1)	0.39	−55(6)	47(4)
	$\frac{B(E2, 2^{+\prime\prime} \rightarrow 4^+)}{B(E2, 2^{+\prime\prime} \rightarrow 2^+)}$	3.28(24)	1.79	−25(5)	18(4)

[a]Based on adiabatic asymmetric rotor model.

[b]The difference in the signs on our values from those of Greenwood *et al.*[6] arises merely from the sign convention used in writing the wave functions of the states.

Table 1.5. Reduced Transition Probability Ratios for Transitions from the $K\pi = 2^+$ Band of ^{158}Gd

Energy Level (keV)	Reduced Transition Probability Ratio	Experimental Value	Theoretical Value[a]	Z_2	
				This Work	Paperiello *et al.*[b]
				$\times 10^{-3}$	$\times 10^{-3}$
1186.8	$\frac{B(E2, 2^{+\prime\prime} \rightarrow 0^+)}{B(E2, 2^{+\prime\prime} \rightarrow 2^+)}$	0.448	0.699	77(8)	~40
	$\frac{B(E2, 2^{+\prime\prime} \rightarrow 4^+)}{B(E2, 2^{+\prime\prime} \rightarrow 2^+)}$	0.046[c]	0.050	−10(1)	~0.0
	$\frac{B(E2, 2^{+\prime\prime} \rightarrow 0^+)}{B(E2, 2^{+\prime\prime} \rightarrow 4^+)}$	9.79[c]	13.89	33(4)	

[a]Based on the adiabatic symmetric rotor model.

[b]C. J. Paperiello, B. G. Funk, and J. W. Mihelich, Univ. of Notre Dame, to be published.

[c]The $2^{+\prime\prime} \rightarrow 4^+$ transition intensity was obtained from G. Ewan, R. L. Graham, and J. S. Geiger, *Nucl. Phys.* **29**, 153 (1962).

Our feelings at this time are that additional experiments must be done to clarify the situation. This is very important in that the presently listed values seem to imply for the first time a highly impure γ-vibrational band. Detailed data analyses on the γ-vibrational band of ^{156}Gd have not been completed.

[1] Oak Ridge Graduate Fellow from Vanderbilt University, Nashville, Tenn. under appointment with Oak Ridge Associated Universities.

[2] Vanderbilt University, Nashville, Tenn.

[3] L. L. Riedinger, N. R. Johnson, and J. H. Hamilton, *Phys. Rev. Letters* **19**, 1243 (1967).

[4] L. L. Riedinger, N. R. Johnson, and J. H. Hamilton, *Phys. Rev.* **179**, 1214 (1969).

[5] I. Liu, D. B. Nielsen, P. Salling, and O. Skilbreid, *Izv. Akad, Nauk SSSR, Ser. Fiz.* **31**, 63 (1967).

[6] R. C. Greenwood and C. W. Reich, *Nucl. Technol. Branch Ann. Progr. Rept. January 1970,* IN-1317, p. 78; A. Backlin *et al.*, presented at the symposium on Neutron Capture Gamma-Ray Spectroscopy, Aug. 11–15, 1969, Studsvik, Sweden.

[7] J. S. Greenberg, presented at International Conference on Radioactivity in Nuclear Spectroscopy, Vanderbilt University, Aug. 11–15, 1969.

[8] L. L. Riedinger, E. Eichler, J. Fuglsang, G. B. Hagemann, and B. Herskind, presented at the International Conference on Nuclear Reactions Induced by Heavy Ions, Heidelberg, Germany, July 15–18, 1969.

[9] C. J. Paperiello, B. G. Funk, and J. W. Mihelich, University of Notre Dame, to be published.

$M1$ ADMIXTURE IN THE $2^+_\beta \rightarrow 2^+_g$ TRANSITION IN ^{178}Hf

J. H. Hamilton[1] A. V. Ramayya[1]
P. E. Little[1] Noah R. Johnson

In some of our previous work[2,3] on levels in ^{152}Sm and ^{154}Gd aimed at a better understanding of the β-vibrational bands in deformed nuclei, there existed considerable question about the nature of the electromagnetic radiation from the 2^+ members of the bands. Specifically, it appeared that the reduced electric quadrupole transition probability for the $2^+_\beta \rightarrow 2^+_g$ transition was about twice the value expected for the apparent degree of mixing between the wave functions of the ground and β bands. It was surmised that there may be a large $M1$ component present to account for this apparent discrepancy.

However, Hamilton *et al.*[4] did angular correlation measurements for the $2^+_\beta \rightarrow 2^+_g \rightarrow 0^+_g$ cascade in ^{154}Gd and found that the 692-keV $2^+_\beta \rightarrow 2^+_g$ transition had less than a 2% $M1$ admixture. Using two NaI detectors, Nielsen, Nielsen, and Rud[5] have reported more recently that for an even better deformed nucleus, ^{178}Hf, there is (83 ± 10)% $M1$ admixture in the corresponding transition from the 2^+ state at 1276.6 keV. From our results and other results reported[6,7] recently for ^{152}Sm, it seemed somewhat surprising that such a large $M1$ component should be present in ^{178}Hf. Therefore we decided to repeat the ^{178}Hf experiments using an NaI detector in conjunction with a high-resolution Ge(Li) detector.

Our preliminary results are similar to those of Nielsen *et al.*[5] in that we find $87.4\ ^{+4.4}_{-5.4}$% $M1$ radiation in this $2^+_\beta \rightarrow 2^+_g$ transition. Whereas the value of Nielsen *et al.*[5] gave a consistent picture for the $B(E2)$ ratios based on a general perturbational treatment for the mixing of the two bands, our result is just outside that needed for agreement with the theory. The present value has error limits a factor of 2 smaller than those of Nielsen *et al.*,[5] but we are repeating the measurements in order to reduce these still further.

The absence of sizable $M1$ components in the $2^+_\beta \rightarrow 2^+_g$ transitions in ^{152}Sm and ^{154}Gd, which are just at the beginning of a deformed region, and their presence in similar transitions in more strongly deformed nuclei like ^{178}Hf presents an even greater dilemma than that emphasized earlier by Mottelson.[8] The accumulating experimental evidence on lowest excited $K = 0$ states and the rotational bands built on them in the above three nuclei suggests that their usual description as collective quadrupole vibrations of the β type may be in error. It appears that the wave functions describing these states are strongly admixed with other components and that probably this admixture is quite different in ^{178}Hf from that in ^{152}Sm and ^{154}Gd. The need for a detailed theoretical understanding of these nuclei is obvious, although it may have to await the accumulation of additional data on excited 0^+ states in other deformed nuclei.

[1] Vanderbilt University, Nashville, Tenn.

[2] L. L. Riedinger, N. R. Johnson, and J. H. Hamilton, *Phys. Rev. Letters* **19**, 1243 (1967).

[3] L. L. Riedinger, N. R. Johnson, and J. H. Hamilton, *Phys. Rev.* **179**, 1214 (1969).

[4] J. H. Hamilton, A. V. Ramayya, L. C. Whitlock, and A. Meulenberg, *Proc. Intern. Conf. on Nuclear Structure, Tokyo, Sept. 7–13, 1967,* ed by J. Sanada, p. 667.

[5] H. L. Nielsen, K. B. Nielsen, and N. Rud, *Phys. Letters* **27B**, 150 (1968).

[6] J. S. Greenberg, *International Conference on Radioactivity in Nuclear Spectroscopy: Modern Techniques and Applications,* Gordon and Breach, 1969; I. A. Fraser, J. S. Greenberg, S. H.

Sie, R. G. Stokstad, and D. A. Bromley, *Contribution – International Conference on Properties of Nuclear States, Montreal, 1969.*

[7]F. K. McGowan, *International Conference on Radioactivity in Nuclear Spectroscopy: Modern Techniques and Applications,* Gordon and Breach, 1969; F. K. McGowan, R. O. Sayer, P. H. Stelson, R. L. Robinson, and W. T. Milner, *Bull. Am. Phys. Soc.* **13,** 845 (1968).

[8]B. R. Mottelson, *Proc. Intern. Conf. on Nuclear Structure, Tokyo, Sept. 7–13, 1967,* ed by J. Sanada, p. 87.

FRAGMENT ENERGY CORRELATION MEASUREMENTS FOR THE FISSION OF ^{232}Th BY 8- TO 13-MeV PROTONS[1]

Robert L. Ferguson Franz Plasil[2]
H. W. Schmitt[2]

In order to complete our study of the systematics of heavy-element proton-induced fission, we have carried out two-parameter fragment energy correlation measurements on the fission of ^{232}Th bombarded by protons at several energies in the range 8 to 13 MeV. Previously we reported studies on the fission of ^{233}U, ^{235}U, ^{238}U, and ^{239}Pu by protons of 7 to 13 MeV.[3,4] Experimental details and methods of analysis in the present work were essentially identical to those described earlier.[5]

Thorium-232 has the lowest values of Z and A among the target nuclei included in our survey, and it exhibits features not shown by the uranium and plutonium isotopes. In the mass distributions shown in Fig. 1.12 for E_p = 8 and 13 MeV, a third peak centered about symmetric mass division appears at low values of the total fragment kinetic energy. This symmetric peak becomes more prominent as the bombarding energy is increased, as has been observed previously in the fission of radium[6] (where it actually predominates at higher bombarding energies) and of thorium.[7]

Because this feature is apparent at relatively low excitation energy in ^{232}Th, a relatively heavy nucleus, it may become attractive to attempt an analysis of our results in terms of a two-component hypothesis including molecular-model considerations, as proposed by Konecny, Nörenberg, and Schmitt.[8] In this context the thorium-plus-proton system would allow exploration of a transition region between the distinctly triple-peaked radium fission and normal heavy-element asymmetric fission.

General features of the functions and distributions obtained in this work are qualitatively consistent with our earlier results on uranium and plutonium[3,4] (see Fig. 1.13). Note that the symmetric peak is not apparent in these mass distributions, even at 13 MeV bombarding energy.

When ratios of peak to valley yields in the mass distributions are plotted against bombarding energy, as in Fig. 1.14, we observe a break between 8 and 9 MeV which may be indicative of the onset of second-chance fission. At 9 MeV bombarding energy the compound-nucleus excitation energy may be sufficiently high to allow the emission of a neutron before fission, thus lowering the average excitation energy relative to that at 8 MeV bombarding energy and increasing the contribution from asymmetric fission. In spite of the occurrence of a symmetric peak in both the thorium and radium results, we note that values of the peak-to-valley ratio for thorium follow more closely those found for uranium and plutonium isotopes than those for radium.

---

[1]This work was performed in collaboration with the Physics Division and has also been reported in *Phys. Div. Ann. Progr. Rept. Dec. 31, 1969,* ORNL-4513, p. 79. Similar collaborative efforts were also reported on pp. 76–84 of that report.

[2]Physics Division.

[3]R. L. Ferguson, S. C. Burnett, Frances Pleasonton, F. Plasil, and H. W. Schmitt, *Chem. Div. Ann. Progr. Rept. May 20, 1968,* ORNL-4306, p. 12.

[4]R. L. Ferguson, F. Plasil, Frances Pleasonton, and H. W. Schmitt, *Chem. Div. Ann. Progr. Rept. May 20, 1969,* ORNL-4437, p. 26.

[5]R. L. Ferguson, S. C. Burnett, Frances Pleasonton, F. Plasil, and H. W. Schmitt, *Phys. Div. Ann. Progr. Rept. Dec. 31, 1967,* ORNL-4230, p. 79.

[6]See E. Konecny and H. W. Schmitt, *Phys. Rev.* **172,** 1213 (1968); *Phys. Rev.* **172,** 1226 (1968); and references therein.

[7]See, for example, I. F. Croall and J. G. Cuninghame, *Nucl. Phys.* **A125,** 402 (1969).

[8]E. Konecny, W. Nörenberg, and H. W. Schmitt, *Nucl. Phys.* **A139,** 513 (1969).

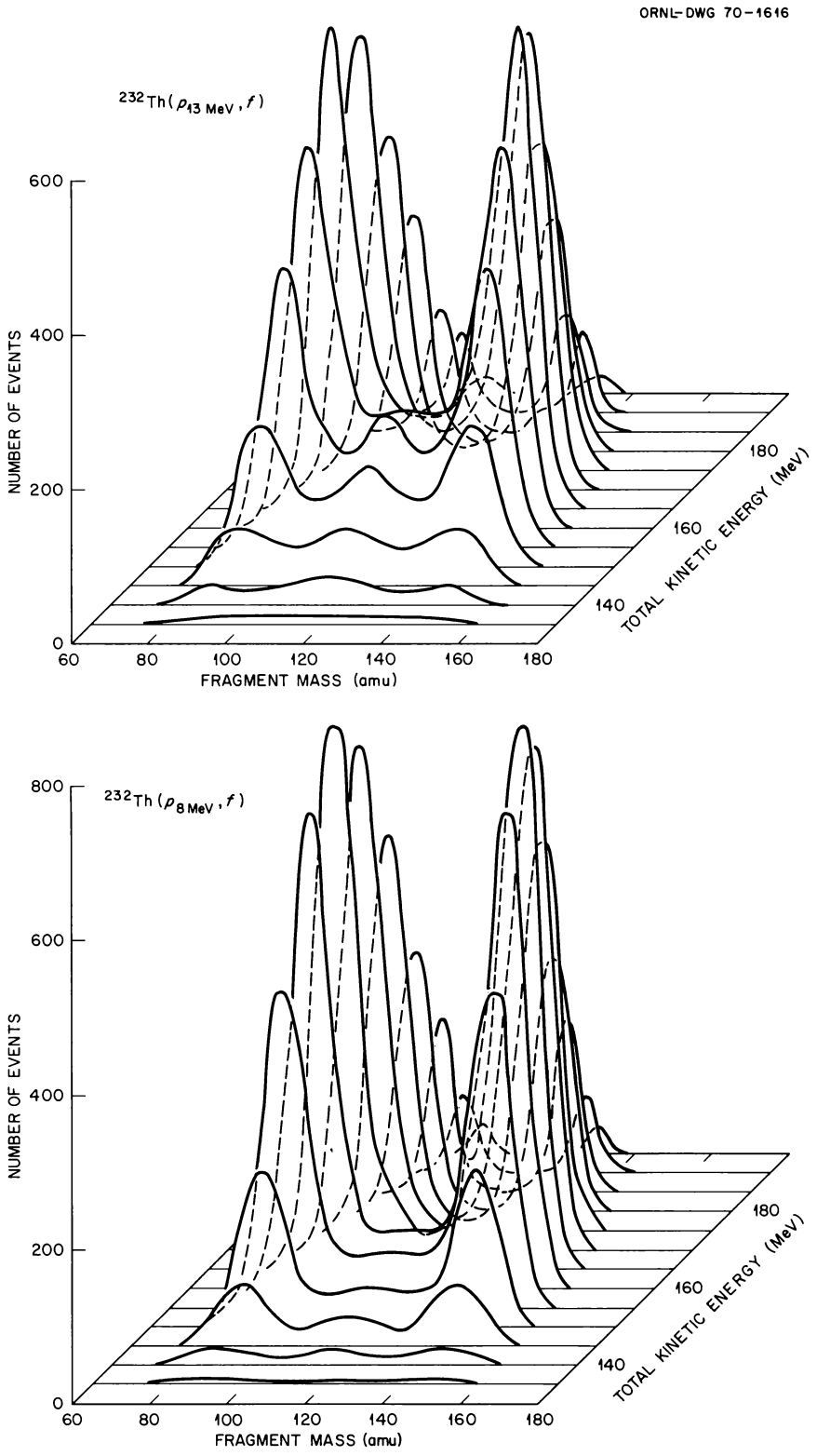

Fig. 1.12. Isometric Projections of ^{232}Th(p,f) Mass-Energy Correlations. E_p = 8 MeV, lower portion; E_p = 13 MeV, upper portion. Mass distributions, given as a function of the total fragment kinetic energy, were smoothed by averaging over boxes 5 amu by 5 MeV and symmetrized by reflection about fragment mass 116.5.

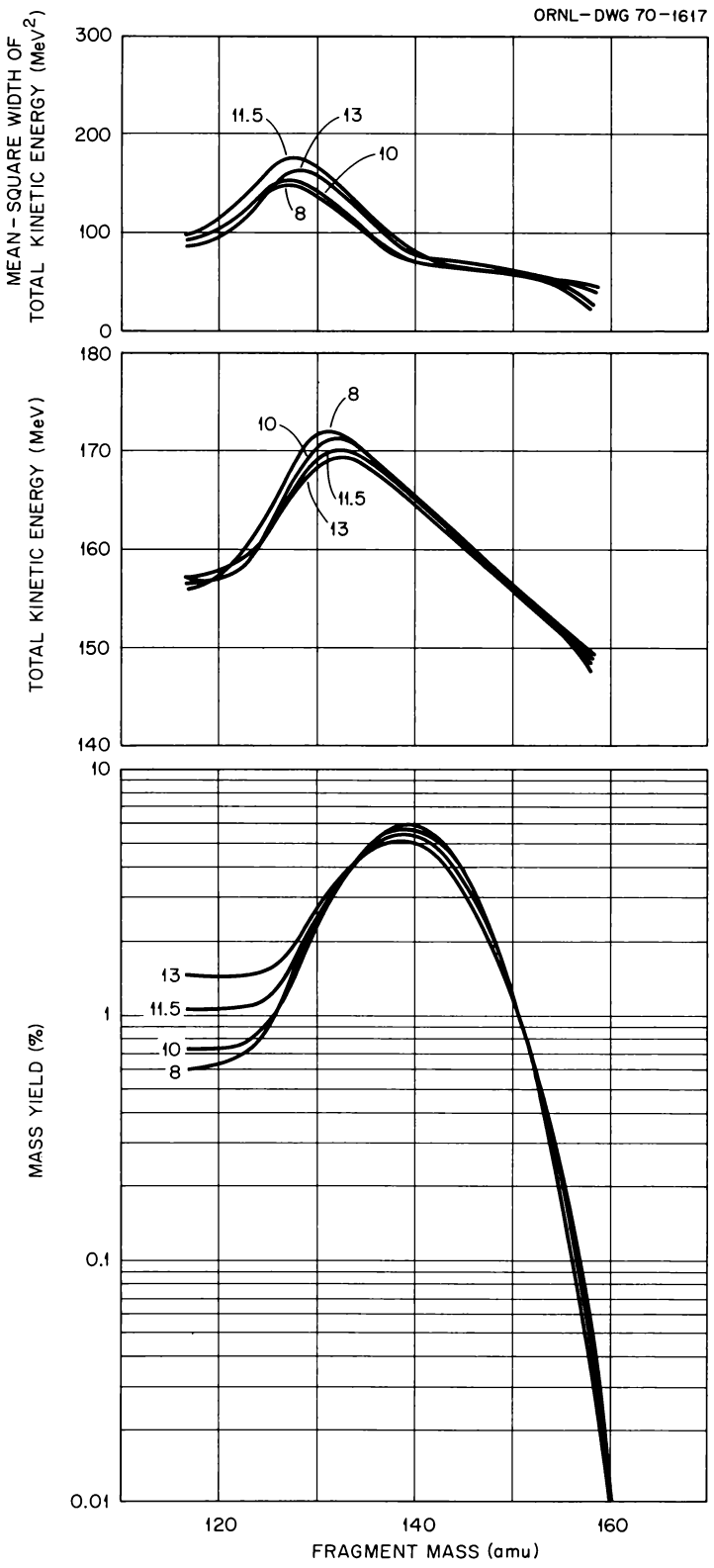

Fig. 1.13. Mass Distributions, Average Total Kinetic Energies, and Mean-Square Widths of the Total Kinetic Energy Distributions as Functions of Fragment Mass for Fission of ^{232}Th by Protons of 8, 10, 11.5, and 13 MeV. The curves, labeled with the proton bombarding energy, were symmetrized by averaging complementary points.

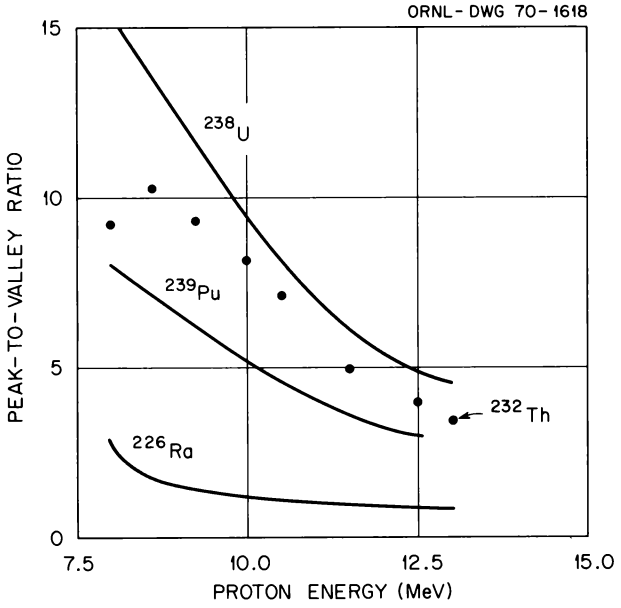

Fig. 1.14. Fragment Mass Distribution Peak-to-Valley Ratios for Proton-Induced Fission of ^{232}Th as a Function of Bombarding Energy. Shown for comparison are results for the proton-induced fission of ^{226}Ra, ^{238}U, and ^{239}Pu.

FRAGMENT ENERGY CORRELATION MEASUREMENTS IN THE FISSION OF SPONTANEOUSLY FISSIONING ISOMERS[1]

Robert L. Ferguson G. D. Alam[3]
Franz Plasil[2] H. W. Schmitt[2]

In recent years a large number of spontaneously fissioning isomers have been discovered.[4] Theoretical calculations of Strutinsky[5] and others predict the existence of a second minimum in the nuclear potential-energy surface, giving rise to a double fission barrier. A popular explanation of the observed isomers is that they are due to nuclear states in this second potential-energy minimum. Data on spontaneously fissioning isomers consist largely of half-life measurements (typically in the nanosecond to microsecond region) and of excitation functions, although some measurements of single-fragment kinetic energies have been made,[6,7] and there has been one brief report of a mass distribution.[8] In our work we have measured the kinetic energies of fragment pairs and have obtained fragment mass distributions and total kinetic energies in an effort to determine to what extent the fission of the isomers differs from prompt fission.

Known isomers[4] were made with 13-MeV protons and deuterons in the reactions: ^{240}Pu$(p,2n)^{239m}$Am, ^{239}Pu$(d,2n)^{239m}$Am, ^{235}U$(d,p)^{236m}$U, ^{238}U$(d,np)^{238m}$U, and ^{237}Np$(d,2n)^{237m}$Pu. Targets of typical thickness ~50 μg/cm^2 were bombarded with 1- to 3-μA beams. The isomer nuclei recoiled out of the target, and energies of coincident fission fragments from the fission of the recoiling nuclei were measured by a pair of silicon surface-barrier detectors located downstream from the target. The detectors were so arranged that their active surfaces were shielded from the target. The number of events ranged from about 1000 in the case of ^{239m}Am to about 200 in the case of ^{238m}U. The pulse-height data were transformed to mass and total kinetic energy data in the usual manner.[9] The masses obtained here are related to pre-neutron-emission masses. They are the "provisional masses" of ref. 9, but since neutron emission data are not available in these cases, it is not possible to make the small corrections which give "final" masses.

The mass distributions are shown in Fig. 1.15. All distributions are shown to be peaked at asymmetric mass divisions and have the general appearance of mass distributions from low-excitation-energy prompt fission. The number of events is insufficient to determine peak-to-valley ratios. Table 1.6 gives the average light-fragment and heavy-fragment masses, $\langle\mu_L\rangle$ and $\langle\mu_H\rangle$; the average fragment total kinetic energy after neutron emission, $\langle E_K\rangle$; root-mean-square width of the light- or heavy-fragment masses, σ_μ; and the rms width of the kinetic energy distribution, σ_{E_K}. In the case of ^{236m}U, for comparison purposes, values are also given for the thermal-neutron-induced fission of ^{235}U. In this case the fission of the isomer is, within the accuracy of our measurements, identical to the low-excitation prompt-fission case. Two different methods were used to obtain ^{239m}Am; these results are also identical within experimental errors. Uncertainties are not given in the table because error estimates are not completed. The error in the average kinetic energies, however, is expected to be of the order of ±2.0 MeV, while the error in the average masses is expected to be about ±1.5 amu. The position of the heavy-fragment peak of the mass distributions, characterized by $\langle\mu_H\rangle$ in Table 1.6, remains constant (with the possible exception of ^{237m}Pu) for both prompt and isomer fission. This effect has been observed over a wide range of low-excitation direct-fission cases.

From this work it appears that the mass and total kinetic energy distributions are determined at the same stage of the fission process (i.e., in the same region of the multidimensional potential-energy surface describing the system) in isomer fission as in direct fission. However, while there appears to be little difference

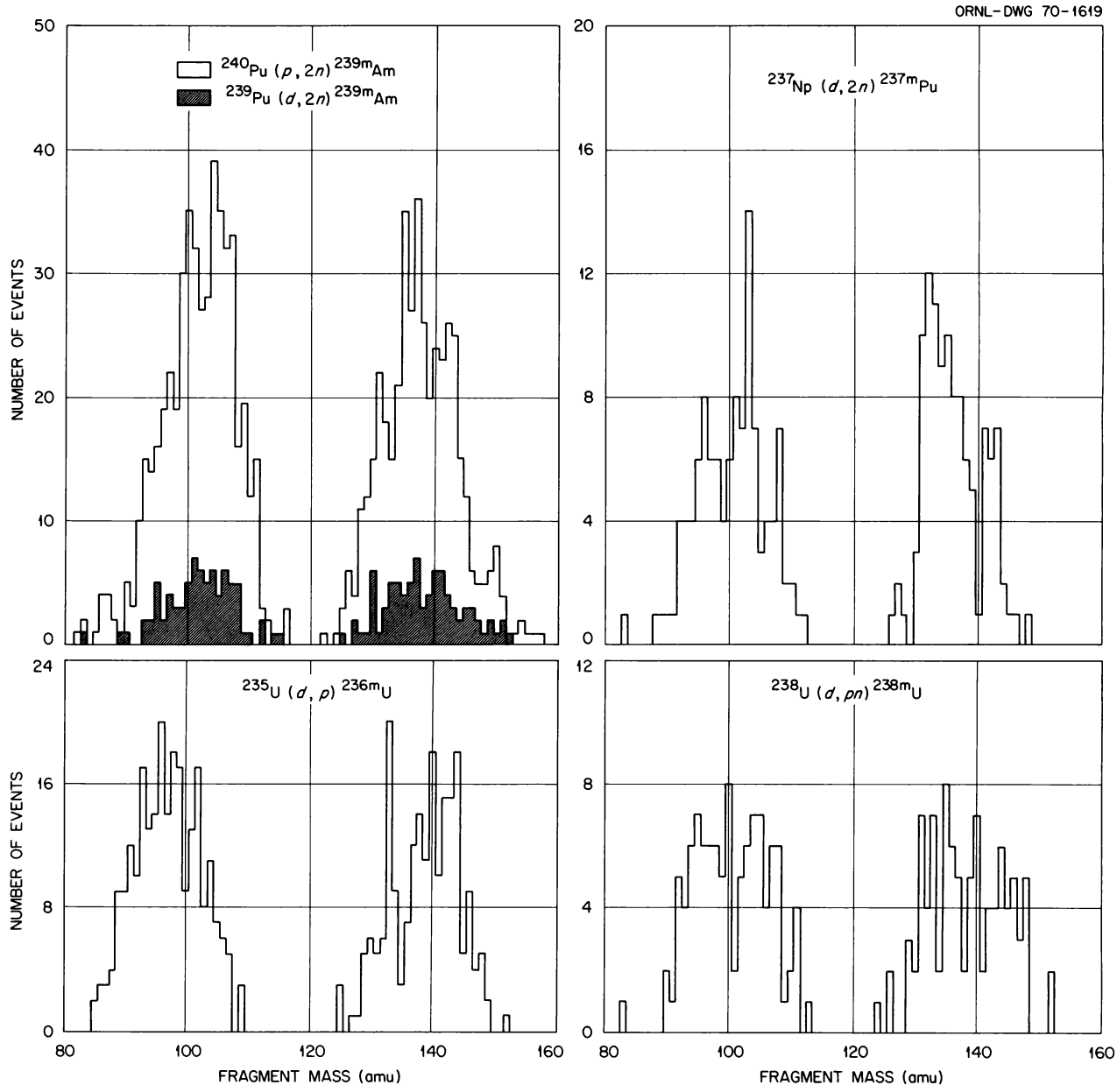

Fig. 1.15. Mass Distributions from Isomeric Fission. Reactions by which isomers were obtained are shown.

Table 1.6. Mean Values and Widths of Fission Fragment Distributions

	^{239m}Am[a]	^{239m}Am[b]	^{236m}U	^{236}U[c]	^{238m}U[d]	^{237m}Pu
$\langle\mu_L\rangle$	101.6	101.8	96.9	96.6	100.5	100.4
$\langle\mu_H\rangle$	137.8	138.3	138.8	139.4	138.5	136.2
σ_μ	6.1	5.9	5.4	5.4	6.1	5.3
$\langle E_K\rangle$	183.2	181.0	172.1	171.9	172.5	182.3
σ_{E_K}	13.0	12.3	10.0	10.9	11.7	11.9

[a]Obtained from the reaction ^{240}Pu$(p,2n)^{239m}$Am.
[b]Obtained from the reaction ^{239}Pu$(d,2n)^{239m}$Am.
[c]Prompt fission of ^{235}U induced with thermal neutrons.
[d]Originally assigned to ^{239m}Np.

between the two cases at the distribution-determining stage of fission, we are not able to determine from our data to what extent the paths to scission are similar, and we are equally unable to deduce information on the nature of the saddle. Further discussion can be found in a letter[10] reporting preliminary results on two of the cases presented here.

[1]This work was performed in collaboration with the Physics Division and has also been reported in *Phys. Div. Ann. Progr. Rept. Dec. 31, 1969,* ORNL-4513, p. 84. Similar collaborative efforts were also reported on pp. 76–84 of that report.

[2]Physics Division.

[3]Visiting scientist from PINSTECH, P.O. Nilore, Rawalpindi, Pakistan.

[4]See, for example, N. L. Lark, G. Sletten, J. Pedersen, and S. Bjornholm, *Nucl. Phys.* **A139**, 481 (1969); or for a recent review see S. M. Polikanov and G. Sletten, unpublished preprint.

[5]V. M. Strutinsky, *Nucl. Phys.* **A95**, 420 (1967); **A122**, 1 (1968).

[6]B. H. Erkkila and R. B. Leachman, *Nucl. Phys.* **A108**, 689 (1968).

[7]D. S. Brenner, L. Westgaard, and S. Bjornholm, *Nucl. Phys.* 89, 267 (1966).

[8]*Fundamental Nuclear Energy Research 1969,* p. 105, U.S. Government Printing Office, Washington, D.C., 1970.

[9]H. W. Schmitt, J. H. Neiler, and F. J. Walter, *Phys. Rev.* **141**, 1146 (1966).

[10]R. L. Ferguson, Franz Plasil, G. D. Alam, and H. W. Schmitt, accepted for publication in *Phys. Letters.*

PRIMORDIAL RADIONUCLIDE ABUNDANCES, SOLAR-PROTON AND COSMIC-RAY EFFECTS, AND AGES OF APOLLO 11 LUNAR SAMPLES[1]

G. D. O'Kelley
J. S. Eldridge[2]
E. Schonfeld[3]
P. R. Bell[4]
V. A. McKay[5]
R. T. Roseberry[5]
R. E. Wintenberg[5]
K. J. Northcutt[2]

The high-sensitivity gamma-ray spectrometer with low background described in previous reports[6] was employed at the Lunar Receiving Laboratory (LRL) at Houston, Texas, for nondestructive analysis of samples returned from the moon by the Apollo 11 mission. The experimental methods are described in detail elsewhere,[6,7] and preliminary results of these studies have been published.[7–9]

Gamma-ray spectrometry can be used to determine the concentrations of the primordial elements K, Th, and U. Because the moon has neither an atmosphere nor a significant magnetic field to protect it from bombardment by galactic cosmic rays and heavy charged particles from the sun, a variety of radioactive nuclei are constantly being formed by nuclear reactions in the lunar surface. A study of these induced activities is expected to yield important information concerning the bombardment history of the material and the history of the particle fluxes responsible for production of the observed species.

Because of the complex operations involved in handling lunar material, analysis of the first sample did not begin until late on July 25, 1969, four days after samples arrived at the LRL and nearly nine days after the samples were collected. Thus radioactive nuclides with half-lives of less than a few days were undetectable.

Results on whole rocks and fines are summarized in Table 1.7. Concentrations were obtained by calibrating the detector system with replicas filled with radionuclide standards. The data on crystalline rocks and fines were obtained by calibration with replicas which accurately reproduced the shape, bulk density, and electronic density of the samples. Radionuclide concentrations of breccias were obtained by calibration with extended sources of iron powder containing the radionuclide standards.

Bulk densities for seven samples were obtained from the sample weights and the volumes of accurate replica shells. It will be noted that the crystalline rocks,

Table 1.7. Gamma-Ray Analyses of Whole Rocks and Fines from Apollo 11

Values for short-lived nuclides have been corrected for decay to 0000 hours, CDT, July 21, 1969

Sample No. (type)[a]	10057,1(*A*)	10072,1(*A*)	10003,0(*B*)	10017,0(*B*)	10018,1(*C*)	10019,1(*C*)	10021,1(*C*)	10002,6(*D*)
Weight (g)	897	399	213	971	211.5	234	157	301.5
Bulk density (g/cc)	2.73 ± 0.14	2.37 ± 0.24	2.88 ± 0.35	3.00 ± 0.15	2.0 ± 0.2	2.02 ± 0.15		1.55 ± 0.05
K (ppm)[b]	2550 ± 130	2300 ± 120	480 ± 25	2430 ± 120	1420 ± 70	1200 ± 60	1600 ± 80	1100 ± 60
Th (ppm)[b]	3.30 ± 0.20	2.80 ± 0.17	1.01 ± 0.06	3.25 ± 0.18	2.30 ± 0.20	1.90 ± 0.19	2.50 ± 0.25	1.92 ± 0.10
U (ppm)[b]	0.79 ± 0.06	0.76 ± 0.06	0.26 ± 0.03	0.83 ± 0.07	0.60 ± 0.09	0.43 ± 0.06	0.54 ± 0.08	0.49 ± 0.04
^{7}Be (dpm/kg)[c]	<70		<100	<60				<80
^{22}Na (dpm/kg)	41 ± 4	46 ± 5	41 ± 4	39 ± 4	55 ± 8	47 ± 7	55 ± 8	51 ± 5
^{26}Al (dpm/kg)	75 ± 8	73 ± 8	74 ± 8	73 ± 8	108 ± 16	101 ± 15	110 ± 15	120 ± 12
^{44}Ti (dpm/kg)[c]	<2.5	<2.5		2.1 ± 1.3				<2.5
^{46}Sc (dpm/kg)	10 ± 2	8 ± 2	13 ± 3	13 ± 3	13 ± 4	10 ± 3	13 ± 4	8 ± 2
^{48}V (dpm/kg)			12 ± 9	11 ± 7				
^{52}Mn (dpm/kg)			35 ± 20				33 ± 21	
^{54}Mn (dpm/kg)	32 ± 6	20 ± 4	35 ± 7	33 ± 7	38 ± 10	28 ± 9	21 ± 6	28 ± 7
^{56}Co (dpm/kg)	31 ± 8	40 ± 10	43 ± 10	26 ± 7	33 ± 10	35 ± 10	50 ± 15	40 ± 7
^{60}Co (dpm/kg)				1.1 ± 0.8				

[a]Petrologic classification: *A*, fine-grained crystalline rock; *B*, medium-grained crystalline rock; *C*, breccia; *D*, fine material.

[b]Standardization for assay of K, Th, and U with reference to terrestrial isotopic abundances. Equilibrium of thorium and uranium decay series also assumed.

[c]Upper limits are 2σ evaluated from least-squares analyses.

breccias, and fines show a distinct correlation between bulk density and sample type.

The breccias and fines are very similar in their chemical compositions, as evidenced by their similar concentrations of K, Th, and U. This substantiates the hypothesis that the breccias were compacted mostly from the fine material.

With the exception of sample 10003, the crystalline rocks from the Apollo 11 landing site form a distinct group with K, Th, and U contents significantly higher than those of the breccias and fines. Sample 10003 is a coarsely crystalline rock which resembles in texture the terrestrial gabbro and differs from the other crystalline rocks in its lower concentrations of K, Th, and U. This suggests that it may have come from another region of the moon, that it may be the product of an igneous process different from that which formed the other crystalline rocks examined, or that it may have originated in a stratigraphically different location in the same general region.

The concentrations of potassium are low compared with the average value for the earth's crust, but the thorium and uranium contents are near those of terrestrial basalts. Thus the contribution by potassium to radiogenic heating of the moon must be small relative to that of thorium and uranium. The degree of differentiation required to produce the apparent depletion of potassium and enrichment of thorium and uranium seen here must have come about through melting of the lunar surface to depths >100 km; however, the source of the heat is at present open to question.

Radionuclide concentration gradients at the surfaces of rocks were shown to have arisen from intense bombardment by the low-energy protons of solar flares, especially the flare of April 12, 1969. Solar proton activation is the principal source of ^{48}V and ^{56}Co; in addition, ^{26}Al, ^{22}Na, and ^{54}Mn are produced both by solar and cosmic-ray protons. The steep concentration gradient of ^{56}Co was used to identify the surface of rock 10017 that had faced the sun. This orientation information was needed so that oriented samples of 10017 could be distributed to other investigators for analysis. The long half-life of ^{26}Al (0.74×10^{6} years) and its surface concentration gradient due to solar-flare effects suggest that the erosion rate of the rocks due to micrometeoroid bombardment must be less than about 3 mm/10^{6} years.

Some of the information obtained in this study may be combined with gas analysis data to provide estimates of crystallization and cosmic-ray exposure ages. In Table 1.8 we show gas retention ages for four rocks, derived from elemental analyses for K, Th, and U reported in Table 1.7, combined with concentrations of radiogenic ^{4}He and ^{40}Ar from the literature.

Except for rock 10003, for which the U, Th-^{4}He age is only about half the K-^{40}Ar age, both gas retention ages are concordant. These results suggest that radio-

Table 1.8. Estimation of Gas Retention Ages and ^{22}Na-^{21}Ne Exposure Ages for Crystalline Rocks of Apollo 11

Sample No.	10003[a]	10017[b]	10057[b]	10072[b]
	Gas Retention Ages (10^6 years)[c]			
U, Th-^{4}He	2300	2450 ± 150	2700 ± 150	2750 ± 150
K-^{40}Ar	3970	2220 ± 150	2400 ± 150	3200 ± 230
	Exposure Ages (10^6 years)[c]			
^{22}Na-^{21}Ne	90	340 ± 40	38 ± 5	160 ± 20
^{3}He	110	310	44	190

[a]Gas contents from ref. 13.

[b]Gas contents from ref. 12.

[c]Errors quoted for K-^{40}Ar and ^{22}Na-^{21}Ne ages are combined analytical errors of gas concentrations and our radioactivity determinations of K, Th, U, or ^{22}Na. Errors for gas concentrations of samples 10017, 10057, and 10072 were taken as 5% (J. G. Funkhouser, O. A. Schaeffer, D. D. Bogard, and J. Zähringer, private communication, January 1970).

genic ^{4}He is located in retentive sites but that rock 10003 may have undergone some significant heating not experienced by the other rocks.

Gas retention methods are generally found to give somewhat shorter ages than other methods, due to loss of gas from interstitial phases. The ^{87}Rb-^{87}Sr internal isochrons for rocks 10017 and 10057 yield an age of 3.65×10^9 years.[10] If the event which formed the mare materials did occur 3.65×10^9 years ago, the K-^{40}Ar age of 4.0×10^9 years determined here for rock 10003 is quite remarkable. This result suggests that the origin of rock 10003 may be different from that of the other rocks examined.

Estimates of cosmic-ray exposure ages were made by the ^{22}Na-^{21}Ne method. From similar work on meteorites[11] it was assumed that the effective cross sections for production of ^{22}Na and ^{22}Ne were equal, that is, a ratio of production rates $P_{Na}/(P_{Na} + P_{Ne}) = 0.50$. The ratio of these production rates would not be expected to vary greatly with chemical composition, since both spallation products have the same mass and differ only by one atomic number. Specific activities of ^{22}Na from the present work were used in combination with neon concentrations obtained by Funkhouser *et al.*[12] or Hintenberger *et al.*[13] The ^{3}He exposure ages were calculated on the basis of 10^{-8} cm^3 of ^{3}He per gram per million years exposure. The variations in cosmic-ray exposure ages of a factor of 10 seen here are consistent with the concept of a continual series of disturbances of the lunar surface due to impact.

[1]Sponsored by the National Aeronautics and Space Administration through interagency agreements with the U.S. Atomic Energy Commission.

[2]Analytical Chemistry Division.

[3]NASA Manned Spacecraft Center.

[4]Director's Division.

[5]Instrumentation and Controls Division.

[6]*Chem. Div. Ann. Progr. Rept. May 20, 1969,* ORNL-4437, pp. 16–19, and references therein.

[7]G. D. O'Kelley, J. S. Eldridge, E. Schonfeld, and P. R. Bell, *Geochim. Cosmochim. Acta,* Suppl. I, vol. 2, pp. 1407–23 (1970).

[8]The Lunar Sample Analysis Planning Team (including P. R. Bell, J. S. Eldridge, and G. D. O'Kelley), *Science* **165**, 1211–27 (1969).

[9]G. D. O'Kelley, J. S. Eldridge, E. Schonfeld, and P. R. Bell, *Science* **167**, 580–82 (1970).

[10]A. L. Albee *et al.*, *Science* **167**, 463–66 (1970).

[11]G. Spannagel and C. Sonntag, in *Radioactive Dating and Methods of Low-Level Counting,* ed. by IAEA, pp. 231–38, International Atomic Energy Agency, 1967.

[12]J. G. Funkhouser *et al.*, *Science* **167**, 561–63 (1970).

[13]H. Hintenberger *et al.*, *Science* **167**, 543–45 (1970).

RADIONUCLIDE CONCENTRATIONS IN APOLLO 12 LUNAR SAMPLES BY NONDESTRUCTIVE GAMMA-RAY SPECTROMETRY[1]

G. D. O'Kelley P. R. Bell[4]
J. S. Eldridge[2] V. A. McKay[5]
E. Schonfeld[3] R. T. Roseberry[5]
K. J. Northcutt[2]

Eleven samples were analyzed by nondestructive gamma-ray spectrometry during the preliminary examination of the Apollo 12 lunar samples[6] at the Lunar Receiving Laboratory, Houston, Texas. The gamma-ray spectrometer, on-line computer data acquisition system, and general technique were the same as described previously for Apollo 11 studies.[7] All samples were mounted in thin-walled stainless steel cans with indium gasket seals.

For preliminary study, calibrations were obtained with a series of radioactive standards prepared by dispersing known amounts of radioactivity in quantities of iron powder. Time did not permit recording a library of standard spectra with the standard sources placed inside the steel containers actually used. Empirical corrections for the effects of the containers were applied; these corrections were least important for the ^{40}K data and most serious for the ^{26}Al and ^{22}Na results. The results are summarized in Table 1.9. Because of the preliminary nature of the investigation,

Table 1.9. Gamma-Ray Analyses of Lunar Samples from Apollo 12

Sample No.	Weight (g)	K (wt %)	Th (ppm)	U (ppm)	^{26}Al (dpm/kg)	^{22}Na (dpm/kg)	Other Radionuclides Detected
				Crystalline Rocks			
12002	1530	0.043 ± 0.004	0.95 ± 0.10	0.23 ± 0.03	72 ± 14	53 ± 10	^{54}Mn, ^{52}Mn, ^{56}Co, ^{46}Sc, ^{48}V
12004	502	0.048 ± 0.004	0.88 ± 0.09	0.25 ± 0.03	112 ± 22	65 ± 13	^{54}Mn, ^{56}Co, ^{46}Sc, ^{48}V
12039	255	0.060 ± 0.005	1.20 ± 0.12	0.31 ± 0.04	80 ± 16	45 ± 9	^{56}Co, ^{54}Mn
12053	879	0.051 ± 0.004	0.89 ± 0.09	0.25 ± 0.03	85 ± 17	42 ± 9	^{56}Co, ^{48}V, ^{46}Sc, ^{54}Mn
12054	687	0.052 ± 0.004	0.77 ± 0.08	0.21 ± 0.03	50 ± 11	42 ± 9	^{48}V, ^{56}Co, ^{54}Mn, ^{46}Sc
12062	730	0.052 ± 0.004	0.81 ± 0.08	0.21 ± 0.03	65 ± 13	34 ± 7	^{48}V, ^{56}Co, ^{54}Mn, ^{46}Sc
12064	1205	0.053 ± 0.004	0.88 ± 0.09	0.24 ± 0.03	58 ± 12	44 ± 9	^{56}Co, ^{46}Sc, ^{48}V, ^{54}Mn
				Miscellaneous Samples			
12034[a]	154	0.44 ± 0.04	13.2 ± 1.3	3.4 ± 0.4	58 ± 12	27 ± 6	^{54}Mn
12073[a]	405	0.278 ± 0.022	8.2 ± 0.8	2.0 ± 0.3	125 ± 25	60 ± 12	^{56}Co, ^{54}Mn, ^{46}Sc
12070[b]	354	0.206 ± 0.016	6.0 ± 0.6	1.5 ± 0.2	140 ± 25	65 ± 13	^{56}Co, ^{48}V, ^{46}Sc, ^{54}Mn
12013[c]	80	2.02 ± 0.16	34.3 ± 3.4	10.7 ± 1.6			

[a]Breccia.
[b]Fine material.
[c]Highly feldspathic breccia of complex origin.

rather large errors have been assigned. These errors include, in addition to the statistical errors of counting, estimates of possible systematic errors due to uncertainties in the detector efficiency calibration.

Although there are many qualitative similarities between the radiation counting data on samples from Apollo 11 and Apollo 12, there are also some notable differences. The potassium concentration of the crystalline rocks of Apollo 12 is remarkably constant at about 0.05 wt %, and the ratio K/U is about 2200. These properties appear significantly lower than the typical crystalline rocks[7] from Apollo 11; however, one of the coarsely crystalline Apollo 11 rocks (sample 10003) did resemble very closely the chemical composition of the crystalline rocks shown in Table 1.9. The ratio Th/U is about 4 for all typical materials in Table 1.9, as found for the materials from Tranquillity Base (Apollo 11). The concentrations of the radioactive elements K, Th, and U in the crystalline rocks of Table 1.9 are all remarkably constant and on the average much lower than comparable Apollo 11 rocks. Because so few samples from the two sites can be compared, it is not possible to discount biased sampling of the lunar surface material as a factor.

The breccia and fines are quite different from the crystalline rocks in several respects. The ratio K/U is only 1400 to 1500, compared with an average value of about 2700 for the Apollo 11 materials. Thus these samples show even greater differences from terrestrial rocks and meteorites than did the surface material from Tranquillity Base. Although the ratio Th/U remains at about 4, the concentrations of all the radioactive elements are much higher in the breccias than in the crystalline rocks. This is the reverse of the situation observed at Tranquillity Base, and poses an interesting problem: If the fines and breccias are derived from crystalline rocks, why do the crystalline rocks from the Ocean of Storms (Apollo 12) show such differences in their chemistry? The answer may lie in sampling bias or in different origins of these materials.

Sample 12013 exhibits dramatic differences in chemistry from all lunar samples examined so far. The sample is a small feldspar-rich specimen which appears to be a breccia made up of material characteristic of the late stage of crystallization from a melt. Accordingly, it contains higher amounts of K, Th, and U than previously encountered.

In general the amounts of cosmogenic ^{26}Al and ^{22}Na appear saturated but show variations which may be related to chemical composition or to cosmic-ray exposure. For example, sample 12034 was recovered from a trench dug during the lunar surface activities. When collected, it was buried to a depth of 15 to 20 cm. The saturation activities of ^{26}Al and ^{22}Na are reduced by the amount expected due to attenuation of the irradiation flux in the lunar soil.

Cosmic-ray exposure ages and gas-retention ages for four rocks were computed from the data of Table 1.9

and rare-gas data published by the Preliminary Examination Team.[6] Exposure ages ranged from 37 to 200 million years, and $^{40}K/^{40}Ar$ gas-retention ages ranged from 2400 to 2700 million years. The cosmic-ray exposure history of the Apollo 12 rocks appears to be similar to that of the Apollo 11 materials; however, the average age of the Apollo 12 rocks is about 500 million years younger than those of Apollo 11.

---

[1]Sponsored by the National Aeronautics and Space Administration through interagency agreements with the U.S. Atomic Energy Commission.

[2]Analytical Chemistry Division.

[3]NASA Manned Spacecraft Center, Houston, Tex.

[4]Director's Division.

[5]Instrumentation and Controls Division.

[6]Lunar Sample Preliminary Examination Team (including P. R. Bell, J. S. Eldridge, V. A. McKay, G. D. O'Kelley, and R. T. Roseberry), *Science* **167**, 1325–39 (1970).

[7]G. D. O'Kelley *et al.*, "Primordial Radionuclide Abundances, Solar-Proton and Cosmic-Ray Effects, and Ages of Apollo 11 Lunar Samples," preceding contribution, this report.

2. Chemistry and Physics of Transuranium Elements

LARGE YIELDS FOR CHARGED-PARTICLE EMISSION IN REACTIONS OF PROTONS WITH ACTINIDE TARGETS

R. L. Hahn K. S. Toth[1] M. F. Roche[1]

Theoretical treatments, usually based upon the compound-nucleus model, have been developed for complex nuclear reactions in heavy elements.[2] Because of the large Coulomb barriers encountered in these reactions, the theories have often neglected the emission of charged particles; the two modes of nuclear breakup usually considered are neutron emission and fission.

In our studies at ORIC of proton-induced reactions to produce alpha-emitting nuclides of neptunium[3] and uranium,[4] we have observed that the yields of products from reactions involving the emission of protons or alpha particles are comparable with or even larger than the yields from reactions involving only neutron emission. For example, we show in Fig. 2.1 some alpha spectra obtained from the reactions ^{231}Pa + p. At a bombarding energy of 44 MeV, the spectrum (*a*) taken during the first 2.5 min after bombardment is dominated by the decay chain of the (p,5n) product, ^{227}U; in *b*, taken from 9 to 20 min after bombardment, the ^{228}U decay chain from the (p,4n) reaction is readily apparent. Note, however, that peaks due to the decay chains of ^{227}Pa, the (p,p4n) product, and ^{225}Th, the (p,α3n) product, also contribute appreciably to spectrum *b*. At a bombarding energy of 63 MeV, neither of the (p,xn) products, ^{228}U or ^{227}U, is seen to any great extent. In spectrum *c*, taken shortly after the bombardment, the (p,p5n) product, ^{226}Pa, and its decay daughters are seen, while ^{227}Pa, ^{225}Th, and possibly ^{226}Th are seen at later counting times in spectrum *d*.

The experimental yields of the alpha-active products observed in the reactions ^{231}Pa + p are shown in Fig. 2.2. These values have been corrected for differences in beam intensity, bombardment time, and alpha/total branching ratios. We see that the yields of the (p,p4n), (p,p5n), and (p,α3n) reactions are clearly not negligible compared with the (p,4n) and (p,5n) yields.

Because of the experimental method used, some qualifying remarks are in order at this point. The experiments were done by collecting on a catcher foil the recoil nuclei knocked out of a ^{231}Pa target during irradiation with protons. The catcher foil was then assayed with an alpha spectrometer to give spectra such as those shown in Fig. 2.1. Because ^{231}Pa is radioactive, one has to be certain that the products of interest, such as ^{225}Th, are not formed in (p,xn) reactions on ^{227}Ac, which is the alpha-decay daughter of ^{231}Pa. So special care was given to preparing ^{231}Pa separated from its daughters; the main step in the separation scheme involved extracting the Pa from an HNO_3 solution into 0.5 *M* TTA in xylene. After the separation the concentration of radioactive daughters from the ^{231}Pa decay chain was $\sim 10^{-7}$ relative to ^{231}Pa; the reaction products observed are clearly due to nuclear reactions induced in ^{231}Pa, not in its daughters.

The yields shown in Fig. 2.2 have not been corrected for effects related to target thickness. That is, the calculated range[5] in ^{231}Pa of a heavy recoil such as ^{228}U from a bombardment with 65-MeV protons is $\sim$35 μg/cm^2. Since the targets used in our experiments were usually thicker than this value, the fraction of the recoils that escaped from the target was less than unity. Determining the value of this fraction is not a simple task when intensely radioactive targets such as ^{231}Pa are used; thus the data in Fig. 2.2 are expressed in relative units.

However, there are other effects related to target thickness that are rather subtle but still can affect the reaction yields of Fig. 2.2. First of all, the recoil range is thought to be a linear function of the energy of the recoil;[4] the fraction of recoils escaping from a thick target thus will increase with increasing bombarding energy. So, for example, the yield curve for ^{228}U in Fig. 2.2 is not identical with its relative excitation function; the experimental curve is skewed to higher values at high energies. Furthermore, since the (p,pxn) yields occur at higher energies than do the (p,xn) yields, they may be larger than expected because of the recoil-energy relation. This effect can be as large as a factor of 2 increase in going from 30 to 60 MeV.

A second point to consider is that the energy of a recoil nucleus, and thus its range, depends upon the mechanistic details of the nuclear reaction in which it

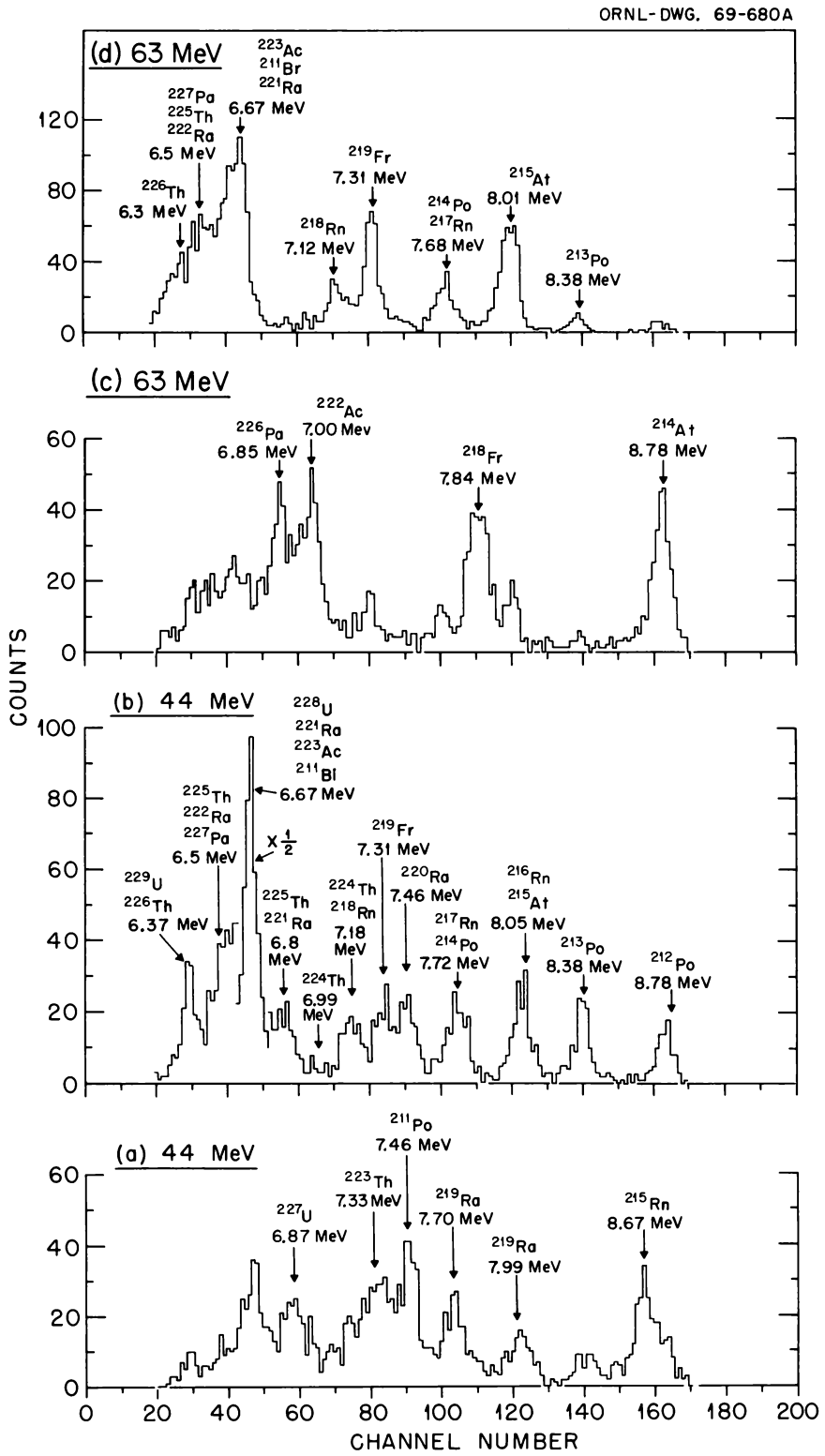

Fig. 2.1. Spectra of Alpha-Active Products from the Reactions of ^{231}Pa + p at 44 and 63 MeV. Spectra *a* and *c* were taken shortly after the end of bombardment; spectra *b* and *d* were taken at later counting times. See text for details.

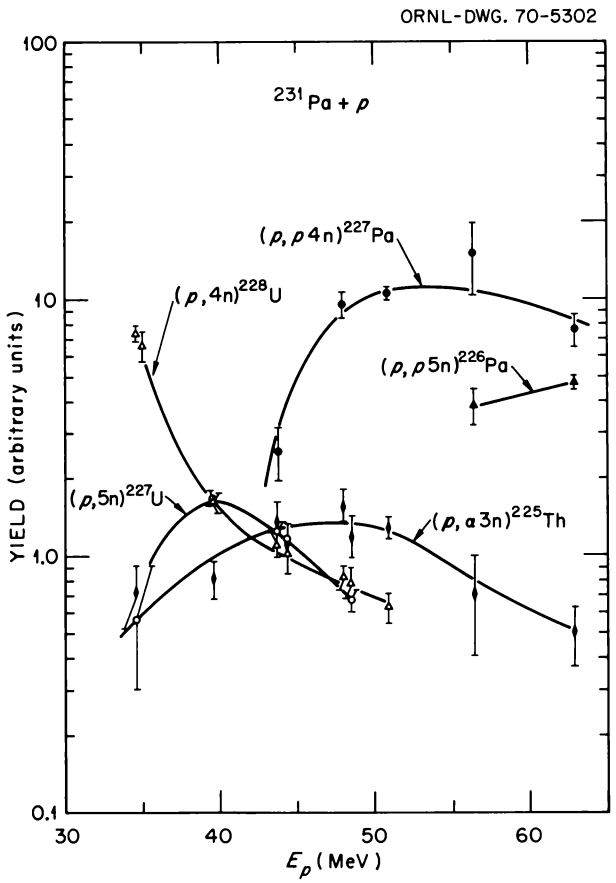

Fig. 2.2. Yields of Recoil Products vs Bombarding Proton Energy E_p for Reactions ^{231}Pa + p.

was produced. In a compound-nucleus reaction, the full momentum of the projectile is imparted to the compound system, whereas in other, noncompound processes less than the full value is transformed into recoil momentum.[6] If ^{227}Pa, the (p,$p4n$) product, were formed in some noncompound process, then its recoil energy, and accordingly its recoil yield, would be less than if it were made by compound-nucleus formation (note that this effect would mean that the ^{227}Pa cross section, relative to that for ^{228}U, which we might assume is a compound-nucleus product, would be even larger than that shown in Fig. 2.2).

And yet, even if all of the products observed were formed in compound-nucleus reactions, their recoil ranges could still differ from one another. Because of the large Coulomb barrier in protactinium, the average energy of an evaporated proton or alpha particle is of necessity much greater than that for a neutron. The kinetic energy of the recoil is related to the kinetic energy of the evaporated particle.[7] Thus the recoil energies, ranges, and yields of the products of reactions involving charged-particle emission can be greater than those of products of (p,xn) reactions; for a reaction involving proton evaporation, this effect can conceivably increase the observed yields of (p,pxn) products by as much as 50% (this value is based upon expressions given in ref. 7).

It should be noted that although these effects upon the observed relative yields can't be evaluated very precisely, the yields of (p,pxn) products relative to (p,xn) products have been enhanced at most by no more than a factor of ~3. Even if we correct the yields by this factor, it is apparent that the (p,pxn) and (p,αxn) yields are still not negligible.

Nuclear reaction calculations are currently being done to see if we can interpret our data. Two models are being tried: (1) compound-nucleus formation and decay, and (2) an intranuclear cascade initiated by the incoming proton, followed by compound-nucleus decay. In both models the processes of charged-particle evaporation and of fission are explicitly considered during the compound-nucleus phase of the reaction; some of the details of the theoretical treatment are discussed in the next section.

---

[1] Electronuclear Division.

[2] See, for example, J. D. Jackson, *Can. J. Phys.* **34**, 767 (1956); T. Sikkeland, A. Ghiorso, and M. J. Nurmia, *Phys. Rev.* **172**, 1232 (1968).

[3] R. L. Hahn, M. F. Roche, and K. S. Toth, *Nucl. Phys.* **A113**, 206 (1968).

[4] R. L. Hahn, M. F. Roche, and K. S. Toth, *Phys. Rev.* **182**, 1329 (1969).

[5] J. Lindhard, M. Scharff, and H. E. Schiott, *Kgl. Danske Videnskab. Selskab, Mat.-Fys. Medd.* **33**, No. 14 (1963).

[6] G. B. Saha and N. T. Porile, *Phys. Rev.* **149**, 880 (1966).

[7] L. Winsberg and J. M. Alexander, *Phys. Rev.* **121**, 518 (1961).

INCLUSION OF CHARGED-PARTICLE EMISSION AND FISSION IN NUCLEAR REACTION CALCULATIONS

R. L. Hahn

The compound-nucleus and intranuclear-cascade models present two very different physical pictures of how protons interact with nuclei. In the former model the proton reacts with the target nucleus as a whole to form a system whose decay can be treated by statistical mechanical methods. In the latter case the proton is assumed to interact with individual nucleons in the

nucleus via a series of two-body interactions; then, if the product of these interactions is left with some excitation energy, its subsequent decay is taken to be that of a compound nucleus.

We wish to use both of these models to calculate excitation functions to be compared with the data discussed in the preceding contribution. To do so, we must consider neutron emission, charged-particle emission, and fission in the calculations. It is not clear, however, how to treat fission as a series of nucleon-nucleon interactions in the intranuclear cascade, so we shall confine ourselves only to the compound-nucleus decay.

Traditionally, one has ignored charged-particle emission from heavy compound nuclei and considered only neutron emission and fission.[1,2] Thus the probability that a particular compound nucleus evaporates a neutron in the absence of fission can be written as

$$P_n = \left[\Gamma_n / \sum_j \Gamma_j\right], \tag{1}$$

where Γ_j is the emission width for particle j and the sum in the denominator is over all possible decay modes, except fission. After the emission of the neutron, a new compound nucleus is formed whose decay is independent of its mode of formation. So the probability that a first and then a second neutron is emitted is given by the product of the probabilities that each neutron is emitted,

$$P_{2n} = P_{n1} P_{n2} = \prod_{i=1}^{2} \left[\Gamma_n / \sum_j \Gamma_j\right]_i . \tag{2}$$

If the fission process can also occur, the width for fission (Γ_f) must be added to the denominator of Eq. (1). Then the probability that a neutron is emitted when fission is possible is

$$P_{n,f} = \left[\Gamma_n / \left(\sum_j \Gamma_j + \Gamma_f\right)\right] = P_n \left[\sum_j \Gamma_j / \left(\sum_j \Gamma_j + \Gamma_f\right)\right] . \tag{3}$$

Now in heavy elements the calculated widths for emission of charged particles, Γ_p, are usually small ($\lesssim$10%) compared with neutron emission,[3,4] so that $\Gamma_n > \Gamma_p$ or $\sum_j \Gamma_j \approx \Gamma_n$, and

$$P_{n,f} \approx P_n [\Gamma_n / (\Gamma_n + \Gamma_f)] . \tag{4}$$

Similarly

$$P_{2n,f} \approx P_{2n} \prod_{i=1}^{2} [\Gamma_n / (\Gamma_n + \Gamma_f)]_i , \tag{5}$$

where the term in brackets shows that fission competes with neutron emission at each step in the evaporation chain.

It should be stressed that although $\Gamma_n > \Gamma_p$, it may not necessarily follow that charged-particle emission may be neglected, for the probability for emission of a given particle, as in Eq. (5), also depends upon the fission-competition factor. To see this more clearly, let us not neglect the possible emission of charged particles in our calculations. We write, as in Eqs. (1) and (3),

$$P_p = \left[\Gamma_p / \sum_j \Gamma_j\right], \tag{6}$$

$$P_{p,f} = P_p \left[\sum_j \Gamma_j / \left(\sum_j \Gamma_j + \Gamma_f\right)\right] . \tag{7}$$

Now, instead of taking $\Gamma_p \approx 0$ as is usually done,[2] we use the less severe approximation $\sum_j \Gamma_j \approx \Gamma_n$. Then

$$P_{p,f} \approx P_p [\Gamma_n / (\Gamma_n + \Gamma_f)] . \tag{8}$$

We see that the fission factor has the same form as in Eq. (4), irrespective of the particle being evaporated.

Then for the case of *pn* emission we have

$$P_{pn,f} \approx P_{p1} P_{n2} \prod_{i=1}^{2} [\Gamma_n / (\Gamma_n + \Gamma_f)]_i , \tag{9}$$

where the subscripts $p1$ and $n2$ denote that the proton is emitted before the neutron. It should be stressed that although the form of Eq. (9) is similar to that of Eq. (5), the P_j values and the fission terms in the brackets are different because different nuclei are produced in the $2n$ and pn reactions. So $P_{pn,f}$ is not necessarily small compared with $P_{2n,f}$.

The various P_j terms in the equations are given by the usual Monte Carlo evaporation calculation.[3,4] With the aid of O. W. Hermann,[5] we have modified the computer calculation to multiply these probabilities by the appropriate fission terms, which are evaluated by a simple prescription given by Sikkeland *et al.*[2] The calculations are currently being done for the reactions ^{231}Pa + *p*.

[1] J. D. Jackson, *Can. J. Phys.* **34**, 767 (1956).

[2] T. Sikkeland, A. Ghiorso, and M. J. Nurmia, *Phys. Rev.* **172**, 1232 (1968).

[3] I. Dostrovsky, Z. Fraenkel, and G. Friedlander, *Phys. Rev.* **116**, 683 (1959).

[4] See, for example, H. W. Bertini, H. E. Francis, and M. I. Guthrie, "Instructions for the Operation of Codes Associated with the Low-Energy Intranuclear Cascade Calculation," ORNL-3844 (1966).

[5] Computing Technology Center.

THE DECAY OF THE ISOMERS OF ^{240}Np AND ^{244}Cm AND THE RESULTANT STATES OF ^{240}Pu

C. E. Bemis, Jr. M. R. Schmorak[1]
M. J. Zender[2]

We have investigated the nuclear energy states in ^{240}Pu by observing gamma rays emitted following the beta decay of the ^{240}Np isomers and following the

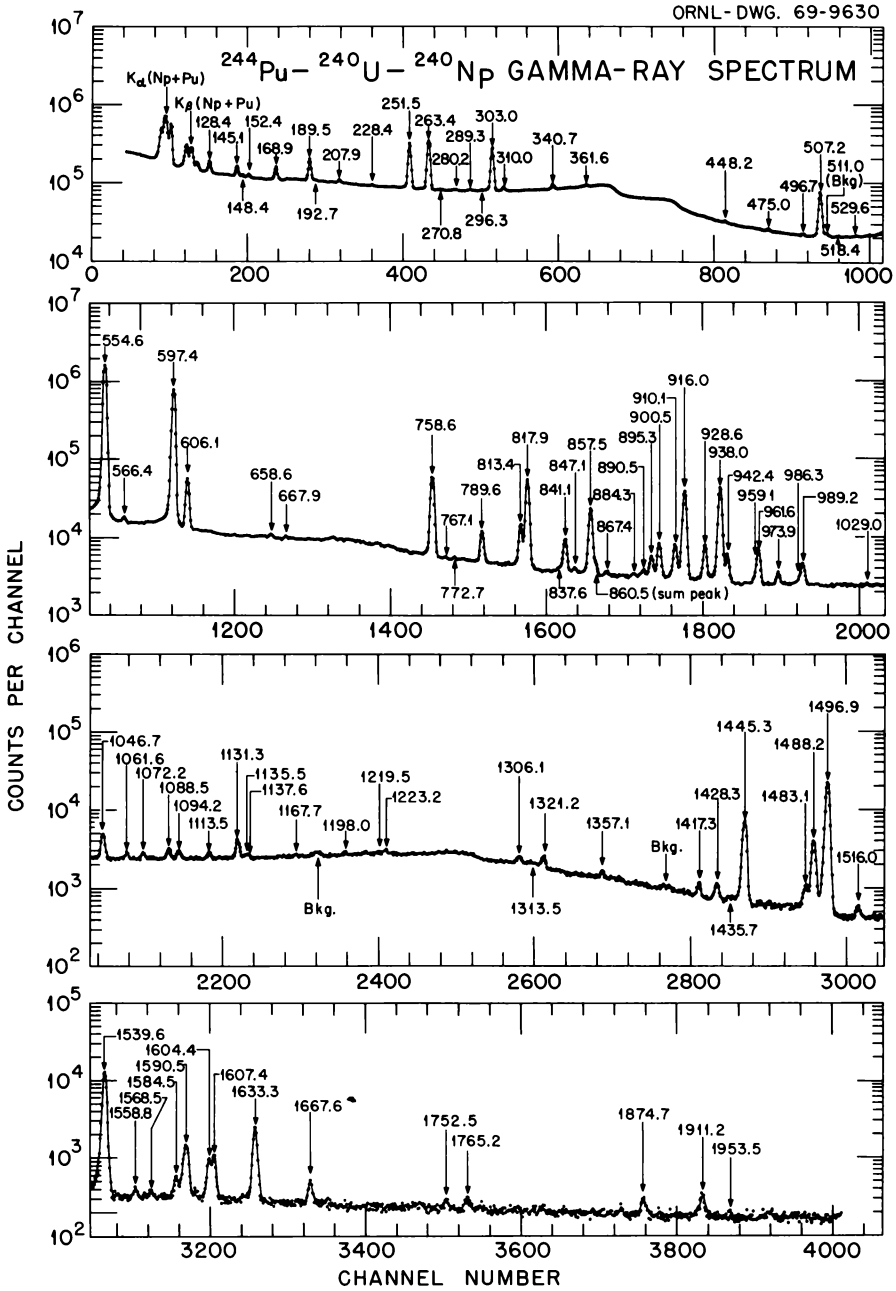

Fig. 2.3. Gamma-Ray Spectrum Observed in the β^- Decay of the 7.3-min Isomer of ^{240}Np with $KI^{\pi} = 01^-$.

ORNL-DWG. 70-5968

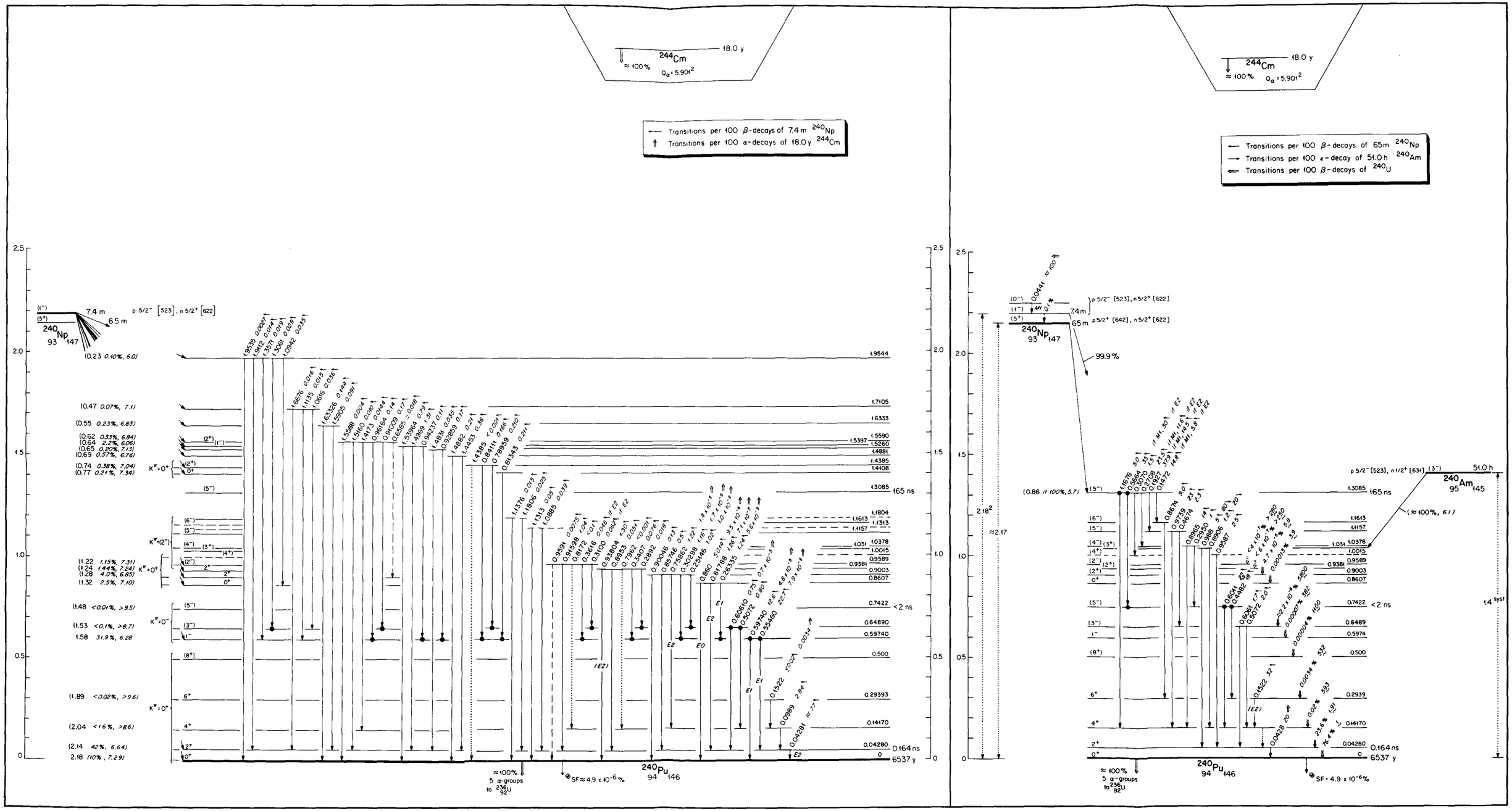

Fig. 2.4. Complete Level Scheme for ^{240}Pu. Derived from the decay of the ^{240}Np isomers and from the ^{244}Cm decay (this work), together with the previously published results for ^{240}Am decay.

alpha decay of ^{244}Cm. A 15-mg isotope-separated source of 99% ^{244}Pu ($t_{1/2}$ = 8.28 × 10^7 years) was used as the equilibrium grandparent activity for 7.3-min ^{240m}Np ($KI^{\pi} = 01^-$). Approximately 10 μg of ^{244}Cm was prepared using the Transuranium Research Laboratory isotope separator[3] for studies of the gamma rays in ^{240}Pu following the alpha decay of ^{244}Cm.

We have found approximately 100 gamma-ray transitions in the ^{240}Np decay using a 35-cm^3 Ge(Li) detector. A representative singles gamma-ray spectrum is shown in Fig. 2.3. We have also used a thin-window planar Ge(Li) detector for the investigation of gamma rays in the low-energy region (20 to 200 keV).

Gamma-gamma coincidence measurements were performed with a 3 × 3 in. NaI(Tl) detector and the 35-cm^3 Ge(Li) detector. All of the transitions with an absolute intensity greater than ~0.01% per decay were placed in the level scheme shown in Fig. 2.4, which summarizes essentially all of our work, including the results for ^{240}Am decay which were previously published.

Our voluminous results for ^{240}Pu and the interpretation are currently being prepared for publication.[4,5] The features of the states in ^{240}Pu uncovered in this work provide a wealth of information on doubly even nuclei in the transuranium element region.

[1] Nuclear Data Group.

[2] Oak Ridge Associated Universities Research Participant from Fresno State College, Fresno, Calif., summer 1969.

[3] L. D. Hunt and C. E. Bemis, Jr., *Chem. Div. Ann. Progr. Rept. May 20, 1969*, ORNL-4437, p. 37.

[4] C. E. Bemis, Jr., M. R. Schmorak, and M. J. Zender (to be published).

[5] M. R. Schmorak, C. E. Bemis, Jr., M. J. Zender, F. E. Coffman, A. V. Ramayya, and J. H. Hamilton, to be published; "A Two-Phonon Octupole Vibrational Band in ^{240}Pu," following contribution, this report.

A TWO-PHONON OCTUPOLE VIBRATIONAL BAND IN ^{240}Pu

M. R. Schmorak[1] F. E. Coffman[3]
C. E. Bemis, Jr. A. V. Ramayya[3]
M. J. Zender[2] J. H. Hamilton[3]

The study[4] of the β^- decay of 7.3-min ^{240}Np and the resultant states in ^{240}Pu led to the identification of two states at excitation energies of 1410.8 and 1438.5 keV in ^{240}Pu which appeared to be members of a $K^{\pi} = 0^+$ rotational band with peculiar gamma-ray deexcitation patterns. A partial decay scheme including these states is given in Fig. 2.5. These states were confirmed in gamma-ray–gamma-ray coincidence experiments; the transitions from these states only populated the $I = 1^-$ and 3^- members of the $K = 0$ octupole band, as would be expected for collective-nuclear vibrational states of the two-phonon octupole type with $\lambda = 3$. Although the one-phonon vibrational states with $\lambda = 2$ and $\lambda = 3$ are well established in nuclei, only the $\lambda = 2$ two-phonon shape vibrational states have been previously identified, with only one such case in permanently deformed nuclei.

To characterize these states in ^{240}Pu even further, we have performed gamma-gamma directional correlation experiments between the gamma rays deexciting these states and the transitions deexciting the one-phonon octupole band. Using a rotatable 2 × 2 in. NaI(Tl) detector set to record only the photopeaks of the 554.6-, 597.6-, 507.1-, and 606.1-keV transitions, the coincidence spectrum was recorded using a 50.4-cm^3 Ge(Li) detector. The coincidence spectra were recorded sequentially at 90, 135, and 180°. The experimental correlation coefficients were determined and corrected for finite-solid-angle effects. These values are given in Table 2.1; when taken together with our limit of $\leqslant 2.8 \times 10^{-2}$ for the K-shell conversion coefficients for the 813.4-, 789.6-, and 841.1-keV transitions, they are conclusive proof of the 0^+ assignment for the 1410.8-keV state and confirm spin 2 for the 1438.5-keV state.

The limit on the K-shell conversion coefficient restricts the gamma-ray multipolarities to $E1$ or $E2$ transitions with $\leqslant$20% $M1$ admixture. The latter is not allowed within the limits of our correlation experiment, which is proof of positive parity for these states. Our values for the gamma-ray intensity ratios and beta branching ratios for these states are given in Table 2.2, together with the theoretical values which clearly indicate $K = 0$.

The limits we were able to set on the crossover transitions to the ground-state band, $\leqslant 1 \times 10^{-3}$% per decay, indicate highly hindered $E2$ transitions with hindrance factors of at least 10. These transitions are expected to be hindered, as the exchange of more than one phonon in electromagnetic transitions is strictly forbidden in the harmonic limit.

It would be of great interest to excite these states in ^{240}Pu via multiple Coulomb excitation (double $E3$), which would lend additional confirmatory proof for the existence of the two-phonon octupole vibration. The population of the two-phonon octupole band should also be possible in radioactive decay for other nuclei in the heavy-mass deformed region.

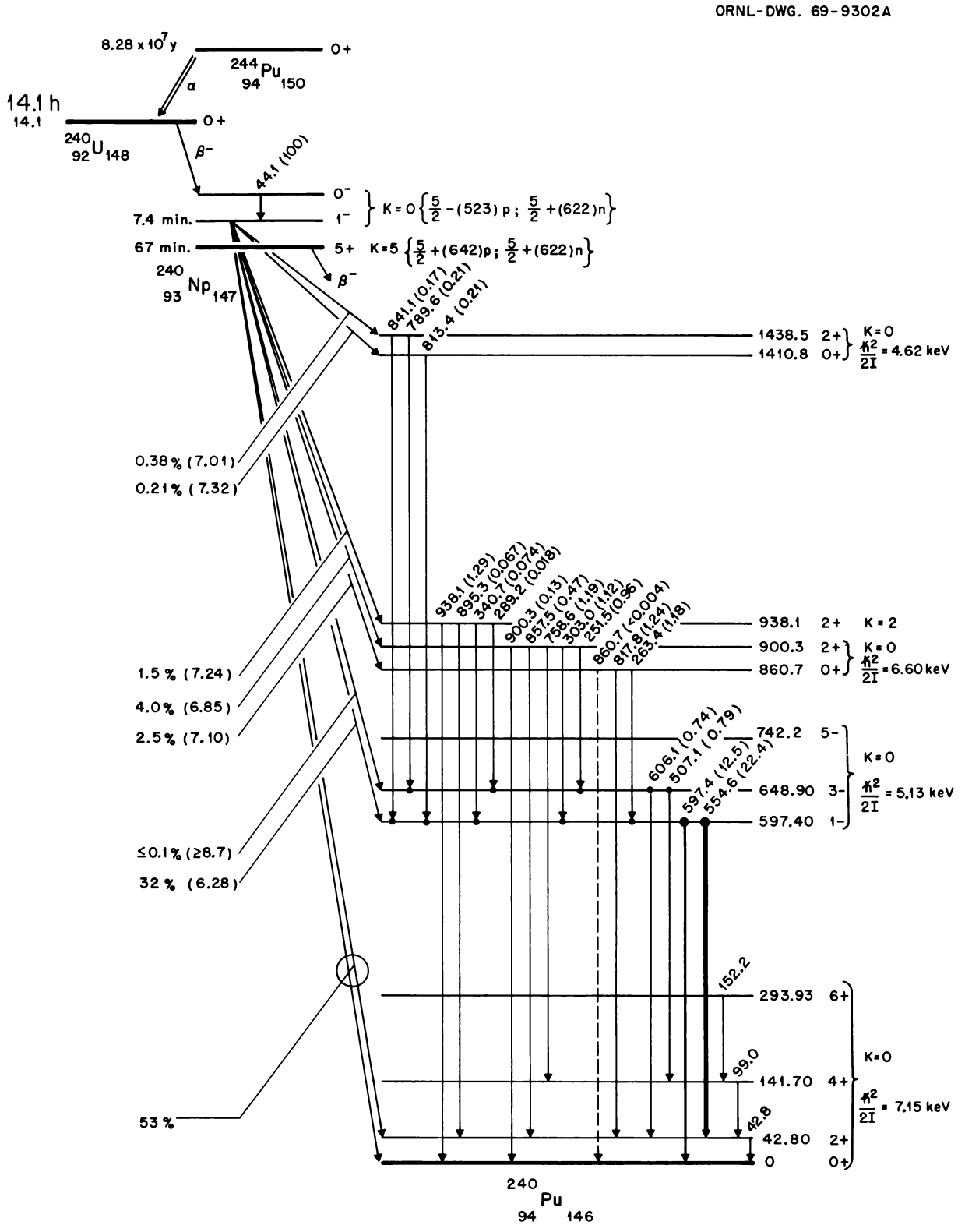

Fig. 2.5. Partial Level Scheme of ^{240}Pu. The two-phonon octupole bands (1410.8- and 1438.5-keV states) and their resultant decay pattern are shown.

Table 2.1. Experimental Directional Correlation Coefficients for Cascades from the 1410.8- and 1438.5-keV Levels in ^{240}Pu

Level Energy (keV)	Gamma-gamma (θ) (keV)	Experimental Correlation Coefficients[a]	Theoretical Correlation Coefficients[b]	Level Spin and Parity
1410.8	813.4-554.6	$A_2 = 0.062 \pm 0.015$	$A_2 = 0.050(0\rightarrow1\rightarrow2)$	0^+
	813.4-597.4	$A_2 = 0.62 \pm 0.15$	$A_2 = 0.500(0\rightarrow1\rightarrow0)$	
1438.5	789.6-507.1	$A_2 = 0.11 \pm 0.05$	$A_2 = 0.050(2\rightarrow3\rightarrow4)$	$2^{(\pm)}$
	789.6-606.1	$A_2 = 0.26 \pm 0.13$	$A_2 = 0.120(2\rightarrow3\rightarrow2)$	
	841.1-554.6	$A_2 = -0.014 \pm 0.024$	$A_2 = 0.005(2\rightarrow1\rightarrow2)$	
	841.1-597.4	$A_2 = -0.14 \pm 0.24$	$A_2 = 0.050(2\rightarrow1\rightarrow0)$	

[a]All of the measured A_4 values are consistent with zero, as expected for spin 1 intermediate states and for the cascades through the 3^- state, which is expected to decay via pure electric dipole transitions to the 2^+ and 4^+ members of the ground band.
[b]Calculated assuming pure dipole transitions and the cascades as given above.

Table 2.2. Absolute Gamma-Ray Intensities, Reduced Transition-Intensity Ratios, and Beta Branching to the Two-Phonon Octupole Band in ^{240}Pu

Level Energy (keV)($K^\pi I$)	Gamma-Ray Transition (keV)	Absolute Gamma-Ray Transition Intensity (%)[a]	Normalized Reduced Intensity[b]	Normalized Theoretical Reduced Intensities	
				$K = 0$	$K = 1$
1410.8(0^+0)	813.43 ± 0.14	0.211 ± 0.025			
1438.5(0^+2)	789.59 ± 0.10	0.210 ± 0.020	1.49 ± 0.115	1.50	0.666
	841.11 ± 0.10	0.166 ± 0.012	1.00	1.00	1.00

Level Energy (keV)	Beta Feeding[c] (%)	log ft	Normalized ft Values	Normalized Theoretical Reduced Intensities	
				$K = 0$	$K = 1$
1410.8(0^+0)	0.211 ± 0.025	7.32	1.00	1.00	1.00
1438.5(0^+2)	0.376 ± 0.023	7.01	0.501 ± 0.031	0.500	2.00

[a]Intensity units are in percent per decay of ^{240m}Np.
[b]Assuming electric dipole character. The E_γ^3 dependence on the transition rate has been removed.
[c]Beta feedings were derived from total gamma-ray intensities using theoretical $E1$ conversion coefficients.

[1]Nuclear Data Group.

[2]Oak Ridge Associated Universities Research Participant from Fresno State College, Fresno, Calif., summer 1969.

[3]Vanderbilt University, Nashville, Tenn.

[4]See C. E. Bemis, Jr., M. R. Schmorak, and M. J. Zender, "The Decay of the Isomers of ^{240}Np and ^{244}Cm and the Resultant States of ^{240}Pu," preceding contribution, this report.

LONG-LIVED SPONTANEOUS-FISSION ISOMERISM IN ^{241}Pu?

C. E. Bemis, Jr. J. E. Bigelow[1]
R. J. Silva A. M. Friedman[2]

The recent report by Nisle and Stephan[3] of the existence of a (0.34 ± 0.11)-year isomeric state in ^{241}Pu has generated much theoretical and experimental interest. Nilsson and coworkers[4] have associated this isomer with spontaneous-fission isomerism and attribute the long half-life to the presence of the $1\,1/2^-[505]$ neutron orbital at the Fermi surface at the large distortion characteristic of fission isomers.

The possible presence of a ~0.3-year spontaneous-fission isomer in ^{241}Pu and the unexcelled opportunities it would afford for detailed studies of shape and fission isomerism in nuclei have prompted us to make an exhaustive search for this isomer using a variety of production modes. We have attempted to produce this isomer in the ^{240}Pu(n,γ) reaction, the ^{242}Pu$(n,2n)$ reaction, and the ^{238}U(α,n) reaction.

We irradiated ^{240}Pu (99.994%) in carefully monitored experiments at the Oak Ridge Research Reactor, examined the plutonium fraction from a 1.5-year irradiation of ^{242}Pu in the High Flux Isotope Reactor, and bombarded ^{238}U with 40-MeV ^{4}He ions at the Argonne 60-in. cyclotron. All samples were carefully processed chemically after the irradiation to recover the plutonium fraction, which was assayed for alpha and fission activities. The irradiated ^{240}Pu sample and the ^{242}Pu sample were isotopically enriched in ^{241}Pu using the 150-cm isotope separator in the Transuranium Research Laboratory.

The small number of fission events observed in these experiments was entirely accounted for by the fission branching decays of ^{240}Pu or ^{242}Pu which were present in the samples in known quantities. Upper limits for the cross sections for the production of a ~0.3-year spontaneous-fission activity were derived from the absence of fission events, from the isotopic composition of our samples, and from the monitored irradiation histories. These values are listed in Table 2.3.

Our data have also been analyzed in terms of a 0.3-year isomer of ^{241}Pu which undergoes independent alpha or beta decay. A limit of $\leq 6 \times 10^{-9}$ for the atom ratio of ^{241m}Pu/^{241g}Pu was determined for an alpha-decay isomer and a limit of $\sim 10^{-3}$ for beta decay. Although these values are not as sensitive as the fissioning-isomer experiments given in Table 2.3, the values are well below the corresponding ratio reported by Nisle and Stephan.[3]

In conclusion, we are unable to explain the results of Nisle and Stephan[3] in terms of a 0.3-year isomer that decays by spontaneous fission or even by alpha or beta decay. In light of our negative results, the elegant theoretical interpretation by Nilsson *et al.*[4] seems somewhat premature.

Table 2.3. Upper Limits for the Production of ~0.3-Year ^{241m}Pu in Various Reactions

Reaction	Energy (MeV)	^{241m}Pu/^{241g}Pu	Isomer Formation Cross Section (cm^2/atom)
^{240}Pu(n,γ)	Thermal	$\leq 7.6 \times 10^{-12}$	$\leq 2.2 \times 10^{-33}$
^{240}Pu(n,γ)	≥ 1	$\leq 6.6 \times 10^{-12}$[a]	$\leq 1.5 \times 10^{-35}$
^{242}Pu($n,2n$)	≥ 6.2	$\leq 6.6 \times 10^{-12}$[a]	$\leq 2.9 \times 10^{-33}$
^{238}U(α,n)	46	$\leq 5.0 \times 10^{-9}$	$\leq 2.5 \times 10^{-35}$

[a]These values do not necessarily represent the actual isomer ratios but are the ratios of ^{241m}Pu produced by the indicated reaction to total ^{241g}Pu produced by all of the reactions possible with reactor-spectrum neutrons on ^{240}Pu and ^{242}Pu.

[1]Chemical Technology Division.

[2]Chemistry Division, Argonne National Laboratory, Argonne, Ill.

[3]R. G. Nisle and I. E. Stephan, *Nucl. Sci. Eng.* **39**, 257 (1970).

[4]S. G. Nilsson, G. Ohlén, C. Gustavson, and P. Möller, *Phys. Letters* **30B**, 437 (1969).

THE FISSION THERMAL-NEUTRON CROSS SECTION AND RESONANCE INTEGRAL OF ^{245}Cm, ^{247}Cm, AND ^{249}Cf

J. Halperin J. H. Oliver R. W. Stoughton

Measurements of the thermal-neutron fission cross sections and resonance integrals of ^{245}Cm, ^{247}Cm, and ^{249}Cf have been carried out employing the method of solid-state track recording. The technique lends itself to picogram (10^{-12} gram) and smaller sample sizes and allows the measurement of fissionability in various neutron-spectrum configurations. We have irradiated nuclides deposited upon thin nickel foils in contact with Lexan film (biphenol-A polycarbonate plastic) in selected neutron spectra. Following the irradiation the Lexan film is etched in an NaOH medium to develop the tracks caused by the fission fragments. The etched tracks, approximately 20 μ in length and each representing individual fission events, are counted under a microscope. The efficiency of the system for our experimental configuration was found to be 92%, determined by calibrating the film with a known fissioning source.

The samples were each measured a number of times in two distinct neutron spectra. An almost pure-Maxwellian room-temperature neutron spectrum is available in the D_2O tank adjacent to the BSR (Bulk

Shielding Reactor). Here samples were irradiated with gold neutron monitors to measure thermal cross sections. The monitors were dilute (~0.1%) alloys of gold in aluminum to minimize self-shielding. The thermal-neutron measurements were normalized to a 2200-m/sec value of 98.8 b for gold.

Epithermal reaction rates were measured in the pneumatic-tube facility of the ORR, where the ratio of thermal to resonance flux per unit lethargy is ~35. Samples were irradiated within 40-mil cylindrical cadmium filters together with gold monitors for short periods of time. The epithermal neutron measurements were normalized to $I(\mathrm{Au}) = 1580$ b.

The accuracy of the method is comparable with the usual activation cross-section measurements of 5 to 10%. However, the accumulation of sufficient statistical precision tends to be more tedious in the counting of events under the microscope. In general all the measurements listed in Table 2.4 were found to be consistent within the statistics of the number of tracks enumerated. The neutron fluences (which ranged up to 10^{15} thermal neutrons/cm^2 and 10^{13} epithermal neutrons per unit lethargy per square centimeter) were evaluated by measuring the 411.8-keV gamma ray in the decay of 2.70-day ^{198}Au. The gold activity was followed over a period of several half-lives to evaluate the amount of ^{198}Au formed during the irradiation. The efficiency of the NaI detector was established by 4π beta-gamma coincidence measurements.

^{245}Cm

A sample containing 76.5% ^{245}Cm and 23.1% ^{244}Cm was available from the calutron isotope-separations group.[1] It contained a negligible amount of ^{247}Cm. A 2200-m/sec fission cross section $\sigma_f = 1920 \pm 180$ b and a fission resonance integral $I_f = 1140 \pm 100$ b are reported here. The thermal cross section within the limits of error agrees with the 2040 b reported by Diamond[2] but is distinctly larger than the cross section of 1550 b used for production calculations for the TRU facility.[3]

By combining the value of the capture cross section and resonance integral previously reported[4] the ratio of $\alpha_{epi}/\alpha_{th} = 0.50$ ($\alpha = \sigma_c/\sigma_f$). This ratio is somewhat smaller than earlier estimates and is in the direction of making a resonance reactor less attractive than a thermal reactor for the production of californium.

^{247}Cm

A sample of curium containing 22% ^{247}Cm, 48% ^{244}Cm, and 0.6% ^{245}Cm was made available from the calutron isotope separations group.[1] Approximately 30% of the thermally induced fissions were due to the ^{245}Cm in the sample. However, only some 3% of the fissions were due to ^{245}Cm in the epithermal-neutron measurement. There is also a small correction due to the 1-b thermal-fission cross section and 12-b fission resonance integral in ^{244}Cm. A 2200-m/sec value of the fission cross section $\sigma_f = 120 \pm 12$ b and a fission resonance integral of $I_f = 1060 \pm 110$ b are reported here for ^{247}Cm. The value within the limits of error agrees with that reported by Diamond,[2] $\sigma_f = 108$ b, but is substantially smaller than the HFIR radiation cross section of $\sigma_f = 280$ b.[3] The fission resonance integral is consistent with the value of 1000 b used as a production cross section for the TRU facility.[3]

^{249}Cf

A particularly pure preparation of the 352-year ^{249}Cf was obtained by milking a source of 311-day ^{249}Bk.[5] The sample was assayed by measuring its alpha-decay spectrum. A 2200-m/sec fission cross section $\sigma_f = 1690 \pm 160$ b and a fission resonance integral of $I_f = 2940 \pm 280$ b are reported here. The thermal cross section may be compared with the 1730-b production cross section reported by Metta.[6] The resonance integral is considerably higher than the 1800 b reported by MacMurdo.[7]

---

[1] We are indebted to L. O. Love and his coworkers for these separated curium isotopes.

[2] H. Diamond *et al., J. Inorg. Nucl. Chem.* **30,** 2553 (1968).

[3] W. D. Burch, J. E. Bigelow, and L. J. King, *Transuranium Processing Plant Semiann. Rept. of Production, Status, and Plans, Dec. 31, 1968,* ORNL-4428 (1969).

[4] J. Halperin, R. E. Druschel, and R. E. Eby, *Chem. Div. Ann. Progr. Rept. May 20, 1969,* ORNL-4437, p. 20.

[5] We are indebted to R. D. Baybarz, Chemical Technology Division, for making this sample available.

[6] D. Metta *et al., J. Inorg. Nucl. Chem.* **27,** 33 (1965).

[7] K. W. MacMurdo, "Measurement of Fission Cross Section and Spontaneous Fission Half Life By Solid State Track Recorder," Presented at the 21st Southeastern Regional Meeting of the American Chemical Society, Richmond, Va., Nov. 5–8, 1969.

Table 2.4. Fission Cross-Section Measurements

Type of Irradiation	^{245}Cm				^{247}Cm				^{249}Cf			
	Number of Measurements	Total Tracks Counted	σ_{2200} (b)	I (b)	Number of Measurements	Total Tracks Counted	σ_{2200} (b)	I (b)	Number of Measurements	Total Tracks Counted	σ_{2200} (b)	I (b)
Thermal neutron	2	7500	1920		6	1500	120		2	2800	1690	
Epithermal neutron	4	9100		1140	3	1900		1060	2	2900		2940

ENERGY SPECTRUM OF DELAYED NEUTRONS FROM THE SPONTANEOUS FISSION OF ^{252}Cf

E. T. Chulick[1] C. E. Bemis, Jr.
P. L. Reeder[2] E. Eichler

Delayed-neutron energy spectra from fission product precursors are of interest in the field of fast-reactor kinetics and as a nuclear spectroscopic tool for studying the properties of nuclear states. As reported previously,[3] we have remeasured the delayed-neutron group half-lives and group abundances from the spontaneous fission of ^{252}Cf and have briefly described our very preliminary results for delayed-neutron energy measurements using the time-of-flight technique.

Our experimental procedure in the energy spectra measurements was to collect fission product recoils from a ~10-μg ^{252}Cf source on Mylar magnetic tape for a predetermined collection time. After the collection period the tape containing the fission product recoils was rapidly transferred a distance of about 3 m from the ^{252}Cf source to the counting position, using the drive system from a magnetic-tape transport. Neutron shielding (consisting of high-density concrete blocks, cadmium sheets, and paraffin blocks loaded with lithium and boron) was interspersed between the ^{252}Cf source and the counting position of our time-of-flight spectrometer to reduce the prompt fission-spectrum neutron background.

The time-of-flight spectrometer consisted of a beta detector located 0.5 cm above the tape and a neutron detector located 20.0 or 25.0 cm horizontally from the tape. The beta detector was a disk of NE-102 plastic scintillator, and the neutron detector was a stilbene crystal; both were mounted on RCA-8575 photomultipliers. A block diagram of the time-of-flight instrumentation including the neutron–gamma-ray discrimination system is shown in Fig. 2.6. The time resolution of this system under the conditions of the actual experiments was 1.4 nsec.

Our recoil-collection and counting-time cycle emphasized mostly the 2-sec and the 0.5-sec delayed-neutron groups. Of the total neutrons that we observed, 48% were due to the 2-sec group and 28% were due to

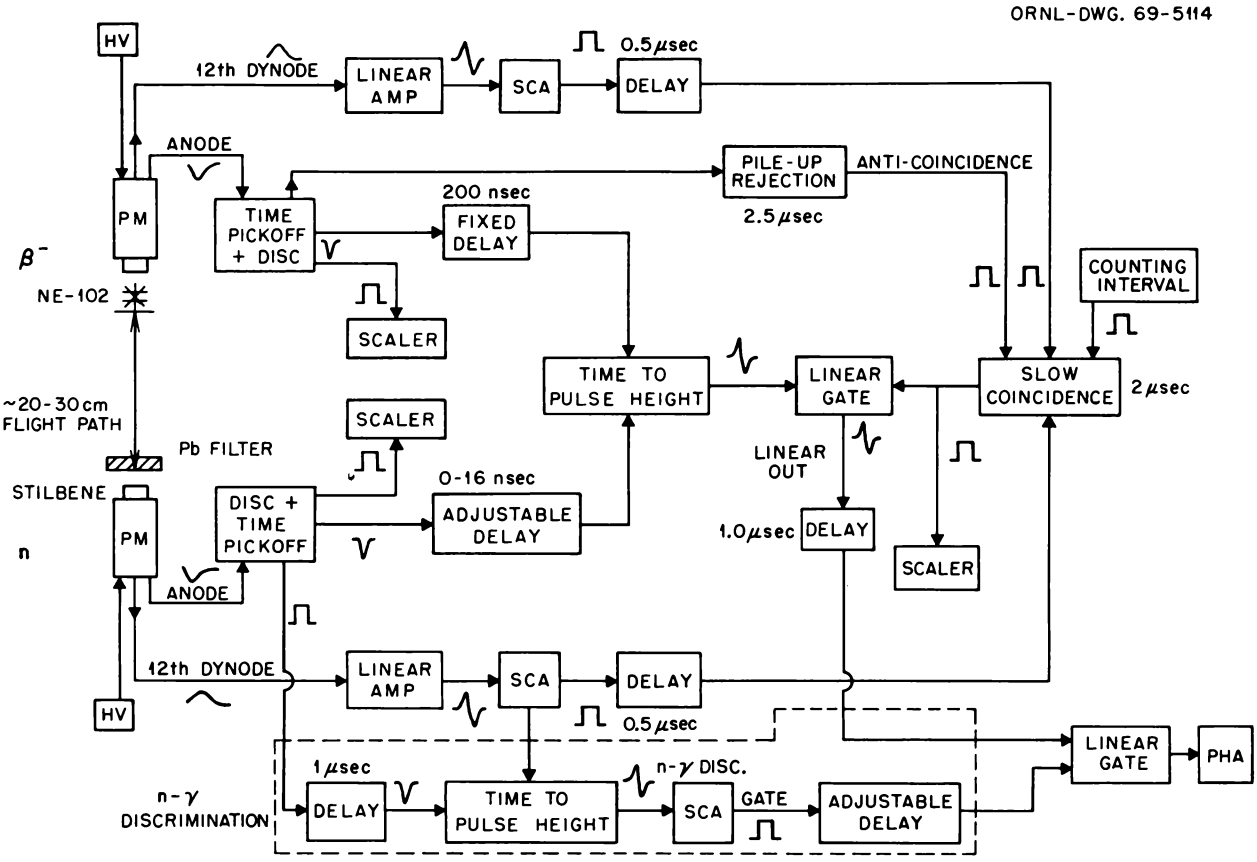

Fig. 2.6. Block Diagram of the Instrumentation Used for Delayed-Neutron Time-of-Flight Experiments.

the 0.5-sec group. Our neutron time-of-flight counting rate was about 1 count/cycle, and the cycles were repeated continuously for a two-week period to obtain statistically significant data. Experiments at 20.0-cm and at 25.0-cm flight distance were performed to identify the neutron groups unequivocally by virtue of their shift in time for the two different flight paths. The energies of the most prominent discrete neutron energy groups for the two different flight paths are given in Table 2.5 together with their average energy. In Fig. 2.7 our 20.0-cm-flight-path time spectrum has been converted to an energy spectrum and compared with the 2-sec group energy spectrum measured by Batchelor and Hyder.[4] Although the Batchelor and Hyder spectrum was measured with a ^{3}He spectrometer with poorer energy resolution and for the fission of ^{235}U, the agreement is interesting.

This work is being prepared for publication.

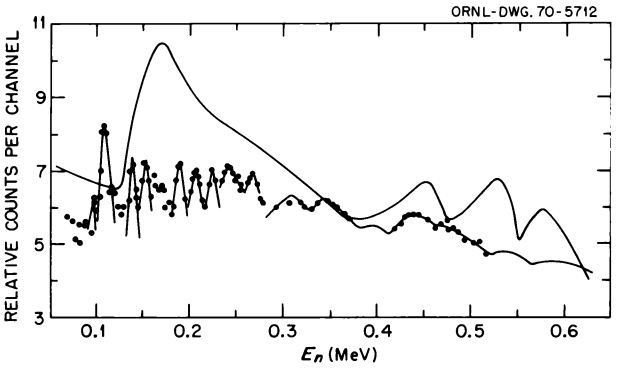

Fig. 2.7. Comparison of Delayed-Neutron Energy Spectra for the 2.0-sec Group. Top curve from the work of Batchelor and Hyder; bottom curve, this work.

Table 2.5. Energies of Delayed-Neutron Peaks for the 2.0-sec Group from the Spontaneous Fission of ^{252}Cf

20.0-cm Flight Path (MeV)	25.0-cm Flight Path (MeV)	Average Energy (MeV)
0.096 ± 0.005	0.093 ± 0.005	0.095 ± 0.007
0.107 ± 0.005	0.101 ± 0.006	0.104 ± 0.008
0.138 ± 0.007	0.132 ± 0.007	0.135 ± 0.010
0.155 ± 0.009	0.160 ± 0.013	0.158 ± 0.016
0.190 ± 0.012	0.185 ± 0.016	0.188 ± 0.020
0.205 ± 0.014	0.205 ± 0.018	0.205 ± 0.023
0.225 ± 0.016	0.225 ± 0.021	0.225 ± 0.026
0.240 ± 0.018		0.240 ± 0.018
0.265 ± 0.020	0.265 ± 0.027	0.265 ± 0.034
0.340 ± 0.030	0.340 ± 0.041	0.340 ± 0.051
0.440 ± 0.040	0.420 ± 0.050	0.430 ± 0.064

[1]Cyclotron Institute, Texas A & M University, College Station.

[2]Department of Chemistry, Washington University, St. Louis, Mo.

[3]E. T. Chulick, P. L. Reeder, E. Eichler, and C. E. Bemis, Jr., *Chem. Div. Ann. Progr. Rept. May 20, 1969,* ORNL-4437, p. 24.

[4]R. Batchelor and H. R. McK. Hyder, *J. Nucl. Energy* **3**, 7 (1956).

ALPHA-DECAY STUDIES OF NEUTRON-DEFICIENT CALIFORNIUM ISOTOPES

R. J. Silva M. L. Mallory
R. L. Hahn P. F. Dittner
C. E. Bemis, Jr. O. L. Keller
K. S. Toth[1]

The recently developed ^{12}C ion beam of the Oak Ridge Isochronous Cyclotron (ORIC) was used to produce neutron-deficient californium isotopes for alpha-decay studies. The carbon-ion energy was 118 MeV but could be adjusted to lower energies by interposing beryllium foils of appropriate thicknesses. The beam intensity varied from ½ to 1 particle microampere of current.

The targets of highly enriched ^{238}U, ^{235}U, ^{234}U, and ^{233}U were prepared by molecular plating of approximately 1 mg of material onto 1-mil-thick beryllium backing foils over a 1-cm-square area. The uranium targets served as beam-entrance windows for a helium-filled gas-jet chamber. The californium product atoms recoiling from the target were stopped in the gas and pumped through a 13.5-mil orifice into an evacuated chamber where the helium gas jet impinged on a platinum disk upon which the atoms were deposited. The platnium disk was attached to the end of a polyethylene "rabbit" that could be transferred pneumatically through a ⅝-in.-diam polyethylene tube to the chemistry laboratory in ~5 sec after the irradiation period. At the chemistry laboratory end of the tube the "rabbit" was received in a device that allowed it to be rotated in front of a 2-cm^2 Si(Au) alpha-particle detector.

After suitable amplification the pulses from the detector were fed into two pulse-height analyzers where alpha-particle pulses in the energy range of 6.00 to 8.50 MeV were recorded. One of the analyzers was a 1600-channel device which was divided into eight 200-channel sections in order to follow decay of various alpha-particle groups through preset time intervals. The other was a 1024-channel analyzer which provided a

continuous sum spectrum at higher channel resolution than the first analyzer so that accurate energy values could be obtained. The measured resolution of the system was ~18 keV FWHM for the 5.4988-MeV alpha group of ^{238}Pu.

Alpha-particle spectra of ^{245}Cf were obtained in bombardments of ^{238}U with 67-MeV ^{12}C ions. The low bombarding energy was used to eliminate the production of the interfering ^{244}Cf activity. In addition to the known alpha group of 7.12 MeV[2] (remeasured in this experiment to be 7.135 ± 0.003 MeV at 93.2% abundance), peaks at 7.103 (3.7%), 7.074 (3.1%), and 6.964 (<0.5%) MeV were recorded.

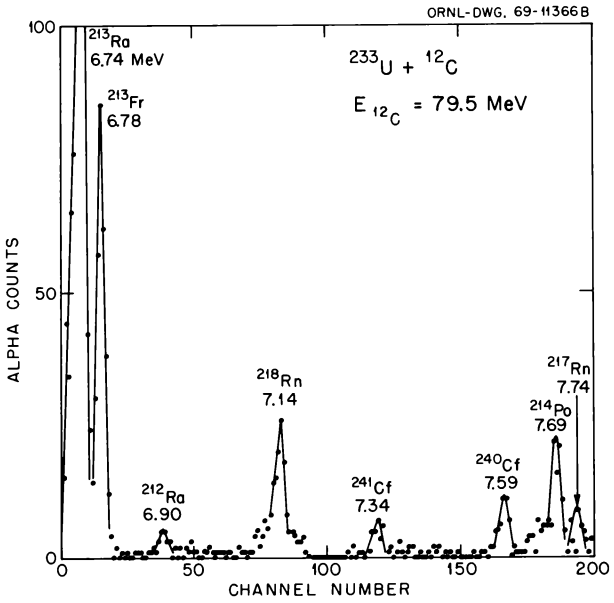

Fig. 2.8. Alpha-Particle Spectrum Obtained in the Bombardment of ^{233}U with 79.5-MeV ^{12}C Ions.

Figure 2.8 shows a typical alpha-particle spectrum obtained in the bombardment of ^{233}U with 79.5-MeV ^{12}C ions where both the new activities of 7.335 ± 0.005 and 7.590 ± 0.010 MeV can be seen. The former activity was also seen in bombardments of ^{235}U and ^{234}U. The half-lives of these activities were determined to be 3.1 ± 1.2 and 0.90 ± 0.15 min respectively. In addition, we were able to obtain a more precise energy value for the ground-state decay of ^{242}Cf[3,4] of 7.385 ± 0.004 MeV with measured half-life of 3.3 ± 0.4 min. Analysis of the data also showed an alpha group of 7.351 ± 0.006 MeV energy. The half-life of this activity was the same as ^{242}Cf, and the intensity was about 20% of the 7.385-MeV group. The energy difference of ~40 keV and the relative intensity are consistent with the alpha-decay systematics to first excited states of even-even transuranium isotopes. It was therefore assigned as the alpha decay of ^{242}Cf to the first excited state of ^{238}Cm.

The excitation functions for production of ^{242}Cf and the alpha activities of 7.335 and 7.590 MeV are given as the points in Fig. 2.9 for the ^{235}U, ^{234}U, and ^{233}U irradiations. The solid curves are theoretical calculations based on compound-nucleus and optical-model theory[5] of the variation of reaction cross section with bombard-

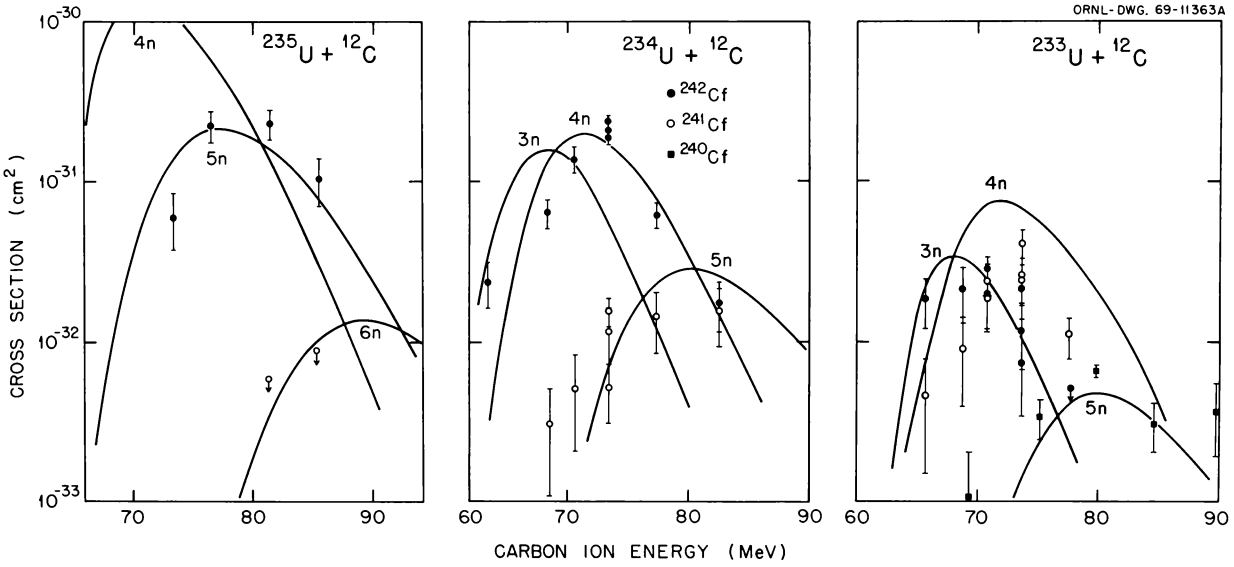

Fig. 2.9. Excitation Functions for Production of ^{242}Cf, ^{241}Cf, and ^{240}Cf. Points are experimental values, and solid lines are theoretical calculations.

ing energy. As some of the experimental collection efficiency parameters were not well known, the experimental data for ^{242}Cf were adjusted in magnitude but not energy to fit the calculated curve for the ^{235}U. The same factor was then used for the ^{234}U and ^{233}U cases. The behavior of the 7.335-MeV and 7.590-MeV activities is that expected for the assignment of the former to the decay of ^{241}Cf and the latter to ^{240}Cf.

[1] Electronuclear Division.

[2] A. Chetham-Strode, G. R. Choppin, and B. G. Harvey, *Phys. Rev.* **102**, 947 (1956).

[3] P. R. Fields, R. F. Barnes, R. K. Sjoblom, and J. Malsted, *Phys. Letters* **24B**, 340 (1967).

[4] T. Sikkeland and A. Ghiorso, *Phys. Letters* **24B**, 331 (1967).

[5] T. Sikkeland, A. Ghiorso, and M. J. Nurmia, *Phys. Rev.* **172**, 1232 (1968).

STATES IN ^{250}Bk POPULATED IN THE ALPHA DECAY OF ^{254}Es

C. E. Bemis, Jr. E. Eichler

We are currently investigating the states in ^{250}Bk that are populated in the alpha decay of 276-day ^{254}Es ($KI^{\pi} = 77^{+}$). As was shown in the earlier work of McHarris *et al.*,[1] the four low-lying rotational bands observed in odd-odd ^{250}Bk could be explained by the various couplings between the $7/2^{+}[633\uparrow]$ and $3/2^{-}[521\uparrow]$ proton states and the $1/2^{+}[620\uparrow]$ and $7/2^{+}[613\uparrow]$ neutron states according to the Gallagher-Moszkowski coupling rules.[2]

We have reinvestigated this decay with the much larger sources of ^{254}Es that have been produced at ORNL. Using silicon surface-barrier detectors for alpha particles and a thin-window Ge(Li) detector for gamma rays, we have performed alpha-gamma coincidence experiments in addition to singles measurements. Although these experiments are still in progress, we have identified two new, higher-lying, rotational bands in ^{250}Bk which most probably involve the $7/2^{+}[633\uparrow]$ proton state and the neutron state $3/2^{+}[622\uparrow]$ for one of these bands and the $5/2^{+}[642\uparrow]$ proton and the $5/2^{+}[642\uparrow]$ neutron states for the other band. Our work is in favorable agreement with most of the assignments of McHarris *et al.*,[1] although we have not analyzed all of our data. Six new alpha groups and ten previously unobserved gamma rays have been measured in the alpha-gamma coincidence experiments.

An isotopically separated ^{254}Es source will be used for studies of the internal-conversion-electron spectrum with the $\pi\sqrt{2}$ spectrometer. We are attempting to observe both members of a given Gallagher-Moszkowski doublet, which should be possible in ^{250}Bk. This identification would provide information on the neutron-proton interaction in nuclei.

[1] W. McHarris, F. S. Stephans, F. Asaro, and I. Perlman, *Phys. Rev.* **144**, 1031 (1966).

[2] C. J. Gallagher and S. A. Moszkowski, *Phys. Rev.* **111**, 1288 (1958).

THE NEUTRON ABSORPTION CROSS SECTION OF ^{257}Fm

C. E. Bemis, Jr. J. Halperin
R. E. Druschel R. D. Baybarz[1]

Measurements have been made of the neutron absorption cross section and resonance integral of ^{257}Fm. This measurement probably involves the heaviest nuclide thus far examined for this property.

A sample of the 97-day alpha-emitting ^{257}Fm containing some 10^{8} atoms became available as a part of the transuranium production program at the HFIR. A measurement of the "burnout" of the fermium in a carefully monitored neutron irradiation was used as the method of measuring the absorption cross section. Curium-244, with a relatively small and well-known cross section, was added to the fermium sample to serve as an internal standard. Aliquots of this sample were deposited in quartz ampuls and irradiated in an assembly containing cadmium filters designed to measure the response to epithermal as well as thermal neutrons. Dilute alloys of cobalt (~0.1%) irradiated with the samples were used to measure the neutron fluence. The samples were irradiated in the ORR to a thermal-neutron fluence of 6.27×10^{19} neutrons/cm^2 at a position where the ratio of thermal to resonance flux per unit lethargy was found to be 9.56.

Following the irradiation the samples were dissolved and passed through a "cleanup column." The actinides were adsorbed onto an anion exchange column and washed with 0.1 *N* HCl, which removed various fission products and other activated impurities from the irradiated sample. Then elution with 2 *N* HCl removed the actinides as a group. The washes and the column were carefully examined to verify that no loss of fermium or curium had taken place. Samples were assayed with a silicon-detector alpha spectrometer to determine the ratio of ^{257}Fm (6.519 MeV, 94%) to ^{244}Cm (5.806 MeV, 76.4%) in the unirradiated and the several irradiated samples.

Approximately 0.58% of the ^{244}Cm which served as a standard of comparison in this burnout experiment was calculated to have been transmuted in the unfiltered irradiation and somewhat less was transmuted in the epithermal-neutron experiment. After correcting for sample decay, the cadmium-filtered sample ratio was found to be unchanged from the unirradiated sample ratio within the limit of sensitivity of the measurement (~2%), implying that the absorption resonance integral $I_{abs} \leqslant 5000$ b. In a similar manner the fermium in the thermal-neutron-irradiated sample was found to be reduced 31.3% from its initial value relative to the curium, yielding an absorption cross section for the reactor-neutron spectrum of $\sigma_{eff}^{abs} = 6100 \pm 600$ b. The upper bound placed on the resonance integral implies that $\sigma_{th}^{abs} \geqslant 5600 \pm 600$ b and less than the value of σ_{eff}^{abs}.

The large thermal absorption cross section, presumably largely associated with neutron-induced fission, can be used to estimate the thermal-neutron capture cross section of ^{257}Fm using correlations of σ_f/σ_c with the neutron binding energy (B_n) and fission activation energy (E_0) for ^{258}Fm. This correlation was first pointed out by Huizenga and Duffield,[2] although we have used the revised correlation parameters of Prince[3] to estimate a value of 7.2 for the ratio σ_f/σ_c; this implies a capture cross section of ~850 b.

The recently measured value[4] of ~300 μsec for the half-life of ^{258}Fm coupled with the above estimate of the ^{257}Fm capture cross section is in agreement with the limits of these values set by a recent ^{258}Fm identification attempt at the HFIR.[5]

---

[1] Chemical Technology Division.

[2] J. R. Huizenga and R. B. Duffield, *Phys. Rev.* 88, 529 (1952).

[3] A. Prince, private communication, September 1969.

[4] E. K. Hulet, private communication, April 1970.

[5] C. E. Bemis, Jr., E. K. Hulet, and R. W. Lougheed, *Chem. Div. Ann. Progr. Rept. May 20, 1969*, ORNL-4437, p. 24.

STUDIES ON THE SEPARATION OF RECOIL ATOMS OF HEAVY ELEMENTS

P. G. Laubereau[1] R. J. Silva

Investigations were started to find improved procedures for rapid separation of the heaviest elements ($Z > 100$). These elements are likely to be produced as energetic recoil nuclei ejected from a target as a result of a nuclear reaction,[2] and we are interested in obtaining information about the chemical and energetic state of such recoil nuclei. We especially wished to investigate the possibility of the solid-phase halogenation of these nuclei after catching them on thin layers of various materials and of subsequently separating these halides by sublimation. In a parallel study we were interested in finding solids useful for gas-solid phase separation columns.

Our first experiments were aimed at developing a method of separation of element 104 from 103. In these experiments ^{169}Lu and ^{170}Hf, produced by irradiating a ^{159}Tb target with 67-MeV ^{14}N ions from the ORIC cyclotron, were used as chemical substitutes for elements 103 and 104. Element 104 (ekahafnium) is expected to form a fairly volatile tetrachloride, while lawrencium (ekalutetium) trichloride is not readily volatile. The target was mounted in a "gas-jet apparatus,"[3,4] and the recoils in the helium jet were allowed to impinge on the surface of various collector materials; pellets of ZrF_4, $NaBF_4$, KBr, and KI and single crystals of $MnCl_2$, LiF, NaCl, KBr, and KCl were used. However, it was not possible under high vacuum and at elevated temperatures to sublime a significant fraction of the collected isotopes from the catcher material, even under conditions where the collector material itself was completely sublimed; most of the activity remained on the nonvolatile backing material.

In a second series of experiments, recoils were collected on quartz, platinum, and several different kinds of graphite, and the collectors then were subjected to chlorination with CCl_4, Cl_2/He, Freon 12, Freon 13, or Freon 22. With "single-crystal" graphite as collector and chlorination with CCl_4 at 650 to 700°C for about 5 min, about 30 to 40% of the ^{170}Hf activity was sublimed, while nearly 100% of the ^{169}Lu activity remained on the graphite. Experiments are planned in which attempts will be made to increase the separation efficiency while decreasing the separation time.

These investigations also revealed that so-called "carrier-free" radioactive isotopes (e.g., ^{95}Zr, ^{95}Nb, ^{153}Gd, and ^{181}Hf), when deposited on the various surfaces by evaporation of acid solutions, do not serve as good models for the behavior of recoil atoms in experiments of this kind. This may be due to the method of deposition or to the presence in the samples of small but nevertheless "weighable" amounts of the stable isotopes of Zr, Nb, Gd, and Hf used in the reactor productions of the radioactive samples. One might expect the chemical behavior of a few thousand atoms on a foreign surface to be significantly different from that of weighable numbers of atoms, depending on the nature of the experiment.

A frontal gas-chromatography apparatus using graphite columns was designed for the rapid separation from neighboring elements of element 106 (eka-tungsten), which is predicted to form a volatile hexacarbonyl.

[1] Guest scientist from Federal Republic of Germany, Bonn.

[2] See, for example, R. J. Silva *et al.*, "Alpha-Decay Studies of Neutron-Deficient Californium Isotopes," a previous contribution to this chapter of this report.

[3] R. L. Hahn, *Chem. Div. Ann. Progr. Rept. May 20, 1968*, ORNL-4306, p. 37.

[4] R. L. Hahn *et al.*, *Chem. Div. Ann. Progr. Rept. May 20, 1969*, ORNL-4437, p. 37.

K X RAYS OF THE HIGHER ACTINIDES

P. F. Dittner C. E. Bemis, Jr.
R. J. Silva

Recent interest in superheavy elements and in the problem of their identification (atomic number) has spurred theoretical predictions of the energies of the *K* x rays of elements having $Z > 95$. These predictions[1] are in part dependent upon experimental values of known *K* x rays. With this in mind we have embarked upon a program to measure the *K* x rays of elements 96 through 102. Beyond americium ($Z = 95$) the quantities of material available are too small to use the method of fluorescence excitation. We have measured the *K*-series emission lines following either alpha, electron-capture, or β^- decay using suitable actinide radioactivities. Production of *K*-shell vacancies from these processes results in the emission of a *K* x ray as the fluorescence yield is close to 100%.[2]

The x rays are detected by a Ge(Li) detector, and the output pulses are amplified and stored in a 4096-channel pulse-height analyzer. The *K* x-ray spectrum of curium has been recorded using a ^{249}Cf source, which alpha decays to ^{245}Cm. The use of a ^{254}Es source, which decays by alpha emission to ^{250}Bk which subsequently beta decays to ^{250}Cf, allowed us to record both the berkelium and californium *K* x-ray spectra. These spectra are currently being analyzed to determine the energies of the *K* x rays and their relative intensities for each element. In order to determine the energies, the unknown spectra were simultaneously recorded with well-known standards (i.e., Pu *K* x rays, ^{182}Ta, ^{243}Am and ^{57}Co gamma rays). For the relative intensities, the efficiency of the Ge(Li) detector has been calibrated using the known gamma-ray intensities of ^{241}Am, ^{57}Co, ^{203}Hg, and ^{160}Tb.

The *K* x-ray energies and intensities for elements 99–102 will be determined in the same way, using parent elements produced with alpha and heavy-ion beams at the ORIC.

[1] T. A. Carlson, C. W. Nestor, Jr., F. B. Malik, and T. C. Tucker, *Nucl. Phys.* **A135**, 57 (1969).

[2] A. H. Wapstra, G. J. Nijgh, and R. van Lieshout, *Nuclear Spectroscopy Table*, North-Holland, Amsterdam, 1959.

STUDIES OF PLEOCHROIC HALOS

R. V. Gentry[1] J. W. Boyle
Russell Baldock

Pleochroic halos (minute regions of discoloration surrounding microscopic inclusions in various minerals) are usually observed in thin mineral sections as one or more concentric circular rings. These halos are now generally considered to result from alpha-particle bombardment over geologic time from the decay of uranium, thorium, or other radioactive elements present in the inclusions. Many halos can be explained in this way—for example, the common uranium and thorium halos in which the radii of the concentric rings correspond to the ranges of the various alpha particles in the decay chains which end in stable lead. However, there are some halos which cannot be explained by any of the known naturally occurring radioactive elements. Some of these unexplained halos are larger than uranium and thorium halos (giant halos) and some are smaller (dwarf halos). Studies are under way to try to explain the genesis of these anomalous halos.

One approach which has been initiated with the rare dwarf halos consists in leaching the samples[2] containing the halos with boiling nitric acid, separating the resulting solution into various fractions by standard ion exchange techniques, and analyzing these fractions for their atomic composition using the Chemistry Division's two-stage mass spectrometer. The analyses so far have shown the presence of both uranium and thorium and have shown that the lead is mainly radiogenic. Specifically, the lead isotope of mass 206 is approximately one and one-half times more abundant than the isotope of mass 208, whereas in natural (nonradiogenic) lead masses 206 and 208 are present in abundances of 23.6 and 52.3% respectively. Subsequent measurements by another laboratory[3] are in agreement with these findings. Work is to continue, with special effort to be expended in the rare-earth and actinide regions of the periodic table and also in the superheavy region.

[1] Visiting scientist from the Institute of Planetary Science, Columbia Union College, Takoma Park, Md.

[2] A Precambrian biotite from the Ytterby quarry near Stockholm, Sweden.

[3] Analyses were made by C. A. Anderson of the Hasler Research Center, Applied Research Laboratory, Galeta, Calif.

SEARCH FOR SUPERHEAVY ELEMENTS IN NATURE: EKAPLATINUM

J. S. Drury

An international search is currently in progress to find certain superheavy elements (atomic numbers 108–120) in nature. Members of several different groups in the Chemistry Division are collaborating in this effort. The work reported here and in the following contribution is concerned primarily with the discovery of ekaplatinum, atomic number 110, and ekaosmium, atomic number 108.

An assumption was made that the chemical properties of element 110 would be as noble as, or more noble than, its light predecessor in Group VIII. Using this criterion, we sought to identify and select samples in which the superheavy element would tend to be concentrated, either naturally, in the earth's rocks, or artificially, by man's intervention. The natural or artificial concentrate would then be concentrated further before being analyzed by some distinctive analytical technique, such as spontaneous- or induced-fission counting, or multiple neutron counting.

Our first choice for samples judged likely to be naturally concentrated in element 110 was ultrabasic rocks known to contain platinum values, such as harzburgite or dunite from the Transvaal region. These rocks were finely ground, and by means of the "fire-assay" technique, all noble-metal values were concentrated in a 1-mg bead of carrier gold. This operation could be expected to concentrate any superheavy noble elements present in the initial sample by a factor of 15,000. The gold beads were dissolved in aqua regia, and all noble elements were electroplated as thin films on nickel disks. These disks were then monitored for fission in 2π counters which were set to reject particles having energies less than 15 MeV. The limit of detection of this method was estimated to be about 1 ppb, assuming a favorable fission half-life for the ekaelement.

Following is a list of typical samples examined: platinum-bearing rock from the Transvaal; dunite from North Carolina and from New Zealand; norite from the Stillwater Complex in Montana; basalt from the East Pacific Rise (Juan de Fuca); basalt from the Mid-Atlantic Ridge (equator); magnetite concentrate from 100 lb of basalt from the Snake River region; gabbro from Ontario; hornblende from Quebec; pyroxenite from Colorado and North Carolina. Samples were also taken from certain mills in which ore concentration processes were thought likely to concentrate the superheavy element.

At the time of writing, fission-fragment activity has been detected in samples from only one source – a flue dust from a Western lead refinery. The source of this activity has not been identified.

SEARCH FOR SUPERHEAVY ELEMENTS IN NATURE: EKAOSMIUM

D. A. Lee

Although the volatility of osmium tetraoxide is well known, very little general information exists concerning the solution chemistry of osmium. This information is desirable, not only to serve as a basis for predicting where in nature ekaosmium might be concentrated but also to suggest how this superheavy element might be further concentrated once a natural or artificial concentrate of the element is available. For these reasons we have studied the distribution of osmium between two immiscible phases under controlled conditions. Extraction coefficients of Os(VIII), $D = [\mathrm{Os}]_{org}/[\mathrm{Os}]_{aq}$, were determined by measuring the extraction of osmium(VIII) from aqueous solutions by CCl_4 as a function of equilibrium pH, the concentration of different alkali-metal hydroxides, NH_4^+ concentration, the concentration of various mineral acids, osmium concentration, CCl_4 concentration in heptane, and the effect of various oxidants added to maintain osmium as Os(VIII). From the slopes of the plots of log D vs the various parameters, the osmium species involved were proposed.

From the loading isotherm (Fig. 2.10) it was concluded that the extracted osmium species was in the same polymeric state as the aqueous species. Osmium tetraoxide in organic solvents is monomeric;[1] therefore OsO_4 in acid solution is monomeric.

Osmium tetraoxide was extracted from solutions of HNO_3, HCl, H_2SO_4, and $HClO_4$ over a concentration range from 0.1 to 5.0 N for each acid. A slope of 0 was determined for the plot of the extraction coefficient against acid activity for each acid, and there was no difference in the magnitude of the extraction coefficient for a particular acid. It was necessary to

maintain osmium as Os(VIII) in the tracer solution with 10^{-3} *M* KIO_4.

The effect of ammonium ion concentration on osmium tetraoxide extraction was measured in a series of experiments in which the ammonium ion concentration was varied from 0.005 *M* to 5.0 *M* in 0.1 *M* and 0.5 *M* HNO_3. There was no change in the extraction coefficient over the entire range of ammonium ion concentration in either acid concentration.

The dependence of Os(VIII) extraction upon equilibrium pH was studied using KOH, NaOH, LiOH, and NH_4OH. Os(VIII) extracts readily from acidic solutions; however, from basic solutions the extraction coefficient is smaller. Also, osmium is more easily reduced in basic solutions. A plot of log *D* vs equilibrium pH for the various bases is given in Fig. 2.11. The slope for KOH and NaOH solutions of OsO_4 was −1, which indicates that the osmium species in those basic aqueous solutions was $OsO_4 \cdot KOH$ and $OsO_4 \cdot NaOH$. $K[OsO_4(OH)H_2O]$ has been described as a possible compound formed by the reaction of OsO_4 with KOH.[1] For NH_4OH solutions of OsO_4, the plot of log *D* vs pH proceeds smoothly from slope 0 to −2, indicating a stepwise addition of two hydroxyls to osmium. The species obtained by using LiOH was not easily determined. At high pH the basicity of the solution increased very minutely with a large increase in LiOH concentration. The best estimate for the slope was −4, which indicates a species $OsO_4 \cdot 4LiOH$ in the aqueous phase.

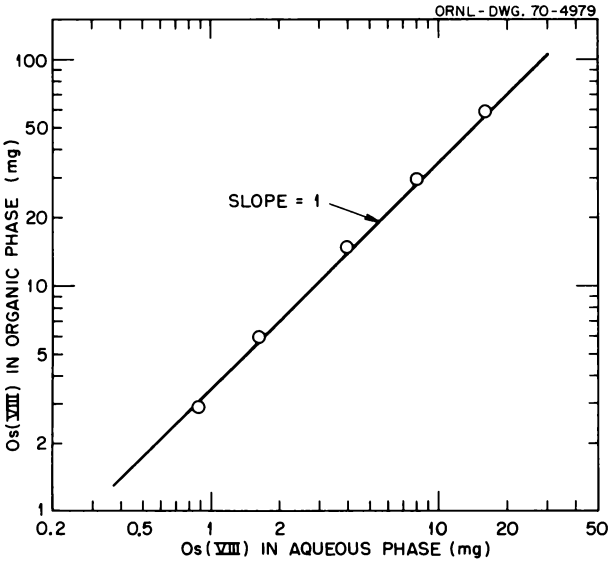

Fig. 2.10. Loading Isotherm for OsO_4 Extraction.

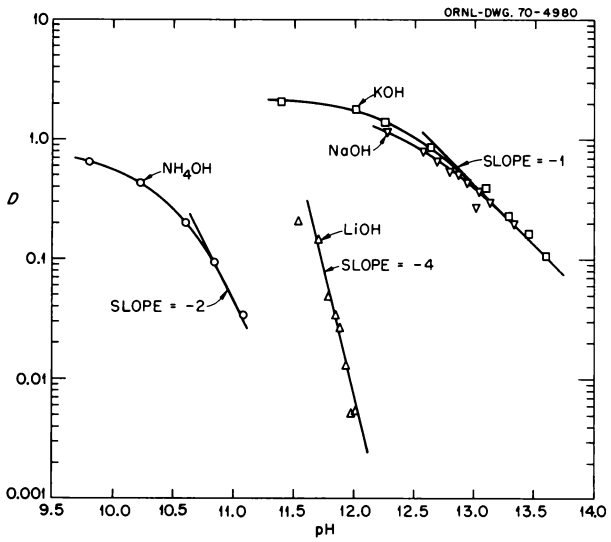

Fig. 2.11. Dependence of Extraction Coefficient on pH.

To determine whether or not CCl_4 formed a complex with OsO_4 and thereby extracted osmium, an experiment was made to determine CCl_4 dependence. The molar concentration of CCl_4 in heptane was varied from 0.00325 *M* to 10.4 *M* (100% CCl_4), and a series of extractions of OsO_4 were made from 5 *M* HNO_3. Over the entire CCl_4 concentration range the extraction coefficients were the same. Therefore CCl_4 is not a complexing reactant but simply extracts OsO_4 as a neutral species.

In all these experiments special precaution had to be taken to keep osmium oxidized to Os(VIII). In early experiments the osmium tracer, assumed to be Os(VIII), was actually Os(VI), and from acid solutions the extraction of Os(VI) was first order with acid activity; each osmium atom extracted was bound to one acid molecule. Usually KIO_4 was added to the tracer solution and was the most effective oxidant used; however, in basic lithium solutions insoluble $LiIO_4$ formed, which caused difficulty in the osmium extractions. For the lithium systems, H_2O_2 proved effective. $(NH_4)_2S_2O_8$ was also tried, but it did not keep osmium oxidized in all cases.

[1] W. P. Griffith, *Quart. Rev.* 19, 254 (1965).

ELECTRON-TRANSFER ABSORPTION IN SOME ACTINIDE(III) AND LANTHANIDE(III) TRICYCLOPENTADIENIDES AND THE STANDARD II-III CATION OXIDATION POTENTIALS[1]

L. J. Nugent G. K. Werner[3]
P. G. Laubereau[2] K. L. Vander Sluis[3]

Electron-transfer absorption bands have been detected in the reflectance spectrum of a single microcrystal of $^{249}CfCp_3$ (Cp^- = cyclopentadienyl ion) at room temperature. The lowest energy band appears near 5510 Å; this is assigned as electron-transfer absorption on the basis of a correlation with the californium standard II-III oxidation potential (+2.0 V) and corresponding data in the lanthanide series for the $EuCp_3$, $YbCp_3$, $SmCp_3$, and $TmCp_3$ compounds. The fact that electron-transfer absorption is not observed in $AmCp_3$ above 3600 Å permits a lower limit of +2.6 V to be set for the americium standard II-III oxidation potential. Prospects for the detection of electron-transfer absorption in the other lanthanide and actinide tricyclopentadienide analogs are discussed[1] in relation to theoretical estimates of the standard II-III oxidation potentials for these series.

---

[1]Abstract of paper appearing in *Proceedings of the 8th Rare-Earth Research Conference*, Reno, Nev., Apr. 19–22, 1970.

[2]Visiting scientist from Federal Republic of Germany, Bonn.

[3]Physics Division.

THEORY OF THE TETRAD EFFECT IN THE LANTHANIDE(III) AND ACTINIDE(III) SERIES

L. J. Nugent

Peppard *et al.*[1-3] have recently found a "tetrad effect" in the variation with atomic number Z of their liquid-liquid extraction data for the partition of the lanthanides(III) and actinides(III) between various solvents. In Fig. 2.12 we show some of their typical results illustrating this effect for the equilibrium distribution of the Ln(III) species and two of the An(III) species between the solution di-2-ethylhexyl chloromethylphosphonate $(ClCH_2)PO(OC_6H_{12}\cdot C_2H_5)_2$ in benzene and an aqueous solution of 11.4 F LiBr + 0.5 F HBr at 22 ± 2°C. The equilibrium constant K is the ratio of the concentration of the metal cation in the organic phase to that in the aqueous phase. These workers point out that in addition to the expected discontinuity at the ½ point, attributable to the half-filled-shell effect in the electronic structure of the Gd(III) or the Cm(III) ion, there is a minor dip at the ¼ point between elements 60 and 61 and at the ¾ point between elements 67 and 68.

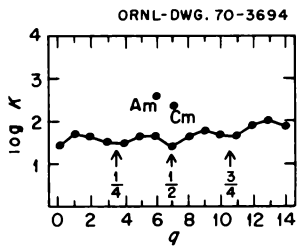

Fig. 2.12. Example of the Tetrad Effect. Variation of log K with q for lanthanide(III) species in 0.6 F DEH [ClMP] (benzene) vs 11.4 F LiBr + 0.5 F HBr (from ref. 1).

Analogous tetrad relationships appear in their Ln(III) and An(III) data for other liquid-liquid systems, in the data of others on reversed-phase partition chromatography, and in several other comparative properties for these series.[3-6] Thus the effect is in general well established for the Ln(III) and An(III) series; this has led Peppard *et al.*[3] to make the following general hypothesis:

"In systems involving all 15 lanthanides(III), the points on a plot of the logarithm of a suitable numerical measure of a given property of these elements vs Z may be grouped, through the use of four smooth curves without inflections, into four tetrads with the gadolinium point being common to the second and third tetrads and the extended smooth curves intersecting, additionally, in the 60-61 and 67-68 Z regions. In a similar plot for actinides(III), an analogous tetrad effect is apparent with the curium point being common to the second and third tetrads."

The purpose of the present paper is to put forward an electronic energy argument which explains the half-filled-shell effect, and to show that the one-fourth- and three-fourths-filled-shell effects can be explained on a similar, though not identical, basis for both the Ln(III) and the An(III) series.

In the well-known lanthanide contraction the Ln(III) crystal radii decrease approximately linearly by about 17% going from Ce(III) to Lu(III).[7] Classical electrostatic theories attempting to account for the solvation energy as a function of these Ln(III) radii, such as the simple theory of Born[8,9] or others,[10] show no tetrad effect because the corresponding effect is not apparent in the ionic radii. Cunningham[8] has calculated the hydration energies for some of the Ln(III) and An(III) ions from the Born equation; he shows this interaction

with H_2O to be quite large (~36 eV), and similar interactions are undoubtedly influential in stabilizing these III oxidation states in most media. There is no evidence from such calculations, however, that classical solvation-energy variations with the commonly accepted cation radii[7] indicate a tetrad effect in either the Ln(III) or the An(III) series.

Next in magnitude after the classical solvation energy is the quantum-mechanical interelectron-repulsion energy H_r of the q electrons in each f^q configuration. This interaction removes the degeneracy of those terms with different L and S, or of the same L and S but different seniority quantum number, leaving the J and M_J degeneracy intact. The value of H_r is different for the free ion and for the ion in the solution, or in the present cases for the two interfaced solutions, and, as will be shown, its variation with q or Z has the same symmetry as the tetrad effect.

Jørgensen[11] has developed a convenient treatment of H_r by noting that it can be expressed to a good approximation for f^q configurations simply by

$$H_r(q, s) = \frac{q(q-1)E^0}{2} + (^9/_8)\langle S(S+1)\rangle E^1 - (^9/_8)S(S+1)E^1 \ , \quad (1)$$

where S is the total electron-spin angular-momentum quantum number in the usual Russell-Saunders basis for the state of interest in the f^q configuration (in the present case the ground state), $\langle\ \rangle$ indicates a degeneracy or $2J + 1$ weighted average over each term in the configuration, and E^0 and E^1 are the first two Racah parameters of interelectronic repulsion. The first two terms in Eq. (1) represent the degeneracy-weighted average value, or baricenter, of the entire configuration, while the last term gives the deviation of the baricenter of those terms with quantum number S from the baricenter of the entire configuration. The first, E^0-dependent term in Eq. (1) is simply a quadratic monotonically increasing function of q which, as such, cannot account for the tetrad effect; therefore it will not be considered any further here. The last two, E^1-dependent terms are what Jørgensen calls the spin-pairing energy. Experimentally determined values for E^1 are listed in Table 2.6 for the Ln(III) and An(III) series. Using these values with the last two terms of Eq. (1), we show next that the variation in the spin-pairing energy with q has the same symmetry as the half-filled-shell effect.

Jørgensen[11] has noted that for any l^q configuration $(^9/_8)\langle S(S+1)\rangle = (^{27}/_{32})q[1 - (q-1)/(4l+1)]$, and this value minus $(^9/_8)S(S+1)$ from Eq. (1) is listed in Table 2.6 as the coefficient of E^1 for the ground state of each Ln(III) and An(III) ion. The product of E^1 times the coefficient of E^1, the spin-pairing energy, is plotted vs q as a solid line in Fig. 2.13 for the Ln(III) series and as a solid line in Fig. 2.14 for the An(III) series. The variation in the spin-pairing energy here with q shows the half-filled-shell effect, and this is undoubtedly why the latter is observed experimentally. This does not, however, explain the one-fourth- and three-fourths-filled-shell effects. In order to explain the latter we must develop Eq. (1) to a better approximation.

In the original development of Eq. (1), the terms linear in the Racah parameters E^2 and E^3 were not explicitly considered,[11] probably because they are mainly smaller and more difficult to generalize than the

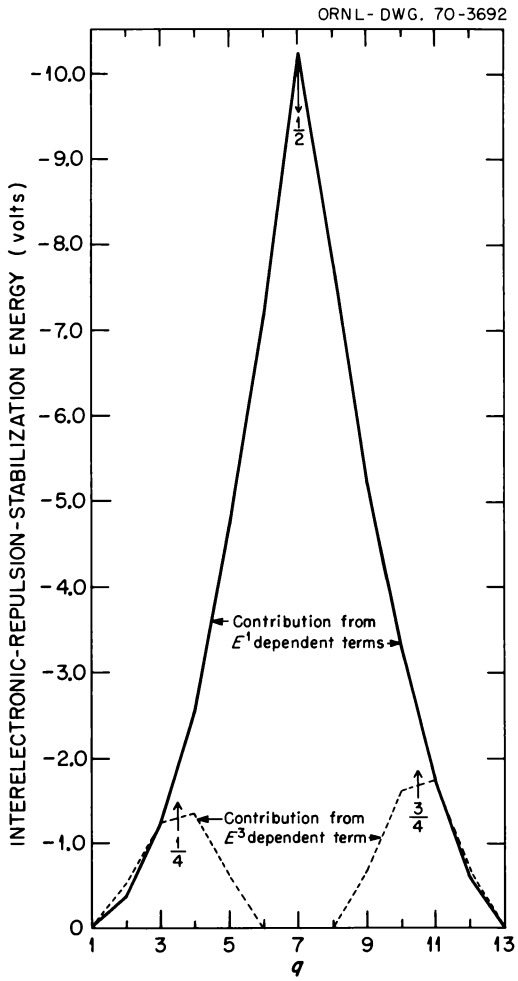

Fig. 2.13. Ground-State Interelectronic-Repulsion-Stabilization Energy for the Ln(III) Aqueous Ions vs q for the $4f^q$ Configurations.

first three terms. For the ground electronic states of the f^q configurations, the coefficients of the E^2-dependent terms are all zero, so they make no contribution here to the tetrad effect. The coefficients of many of the E^3-dependent terms, on the other hand, are not zero, and they display the exact q dependence required to match the one-fourth- and three-fourths-filled-shell effects. These coefficients for the ground electronic states are listed in Table 2.6; they are easily obtained with the aid of Jørgensen's paper on the refined spin-pairing-energy theory for electron transfer bands, where their consecutive differences are presented.[12] Experimentally determined values for E^3 are also listed adjacent to the corresponding values for E^1 in Table 2.6. The product of E^3 times the coefficient of E^3 is plotted vs q as the dotted line in Fig. 2.13 for the Ln(III) series and as the dotted line in Fig. 2.14 for the An(III) series. It can be seen there that the theoretical one-fourth- and three-fourths-filled-shell effects have the same sign as the half-filled-shell effect and that they are about a factor of 6 smaller in magnitude.

The variations in $\log K$ at the one-fourth-, one-half-, and three-fourths-filled points, constituting the tetrad effect, can now be shown to follow from simple thermodynamic equilibrium considerations. Thus, taking the standard free-energy change

$$\Delta G^\circ = \Delta H^\circ - T\,\Delta S^\circ = -2.30RT \log K \qquad (2)$$

Table 2.6. Parameters of Significance for the Theoretical Development of the Tetrad Effect in the Lanthanide(III) and the Actinide(III) Series

Element (III)	Ground State	q	E^1 (V)[a,b]	E^3 (V)[a,b]	Coefficient of E^1	Coefficient of E^3
Ce	$^2F_{5/2}$	1			0	0
Pr	$^3H_4$	2	0.56389	0.0579	−9/13	−9
Nd	$^4I_{9/2}$	3	0.58758	0.0602	−27/13	−21
Pm	$^5I_4$	4	0.61019	0.0652	−54/13	−21
Sm	$^6H_{5/2}$	5	0.68152	0.0689	−90/13	−9
Eu	$^7F_0$	6	0.69095	0.0691	−135/13	0
Gd	$^8S_{7/2}$	7	0.7142	0.0722	−189/13	0
Tb	$^7F_6$	8	0.74655	0.0755	−135/13	0
Dy	$^6H_{15/2}$	9	0.75872	0.0756	−90/13	−9
Ho	$^5I_6$	10	0.79851	0.0774	−54/13	−21
Er	$^4I_{15/2}$	11	0.83934	0.0802	−27/13	−21
Tm	$^3H_6$	12	0.88552	0.0836	−9/13	−9
Yb	$^2F_{7/2}$	13			0	0
Th	$^2F_{5/2}$	1			0	0
Pa	$^3H_4$	2	(0.320)	(0.032)	−9/13	−9
U	$^4I_{9/2}$	3	0.3859	0.0355	−27/13	−21
Np	$^5I_4$	4	0.4208	0.0394	−54/13	−21
Pu	$^6H_{5/2}$	5	0.4621	0.0434	−90/13	−9
Am	$^7F_0$	6	(0.517)	(0.047)	−135/13	0
Cm	$^8S_{7/2}$	7	0.5730	0.0495	−189/13	0
Bk	$^7F_6$	8	(0.616)	(0.0540)	−135/13	0
Cf	$^6H_{15/2}$	9	(0.667)	(0.0577)	−90/13	−9
Es	$^5I_6$	10	(0.716)	(0.0614)	−54/13	−21
Fm	$^4I_{15/2}$	11	(0.765)	(0.0650)	−27/13	−21
Md	$^3H_6$	12	(0.815)	(0.0687)	−9/13	−9
No	$^2F_{7/2}$	13			0	0

[a]Ref. 13 for the Ln(III) aqueous ions.

[b]J. B. Gruber, W. R. Cochran, J. Conway, and A. T. Nicol, *J. Chem. Phys.* **45**, 1423 (1966), for the An(III) ions in various crystalline hosts. The values in parentheses were obtained by a linear extrapolation against atomic number.

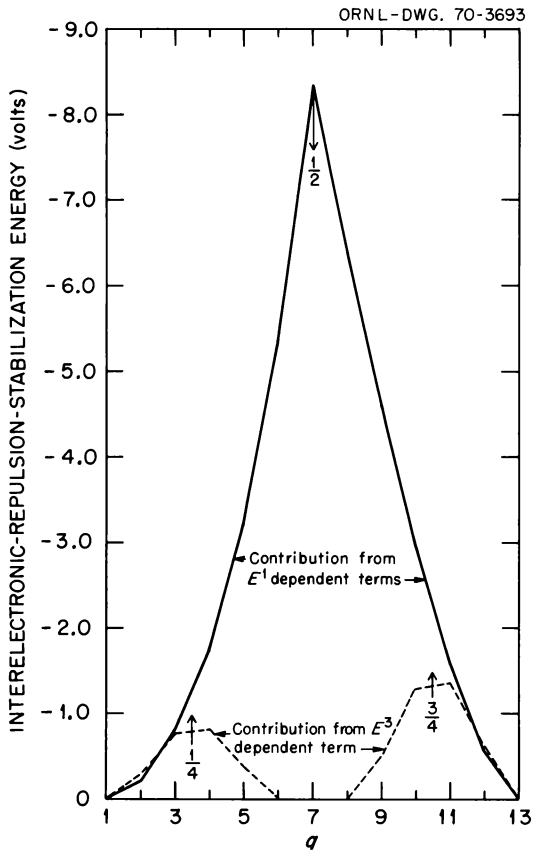

Fig. 2.14. Ground-State Interelectronic-Repulsion-Stabilization Energy for the An(III) Ions vs q for the $5f^q$ Configurations.

for the Ln(III) or An(III) ion between the aqueous phase and the organic phase and taking

$$\Delta G^{\circ\prime} = \Delta H^{\circ\prime} - T\,\Delta S^{\circ\prime} = -2.30RT\,(\log K)' , \qquad (3)$$

where by the prime we mean only those components in each term of Eq. (2) which are accounted for by the E^1-dependent and the E^3-dependent interelectron-repulsion terms, and making the reasonable assumption that $\Delta S^{\circ\prime}$ can be neglected in Eq. (3), we obtain

$$\Delta H^{\circ\prime} = -2.30RT\,(\log K)' . \qquad (4)$$

An examination of Fig. 2.12 shows that at the one-fourth- or three-fourths-filled points, the tetrad effect diminishes log K by about 0.2, and this must be accounted for by the E^3-dependent contribution in Fig. 2.13. Accordingly, setting $(\log K)' = -0.2$ in Eq. (4), we obtain $\Delta H^{\circ\prime} = 0.01$ eV for the difference between the energy of the E^3-dependent term in the organic phase and the energy of the E^3-dependent term in the aqueous phase. From Fig. 2.13 the E^3-dependent term contributes to about -1 to -2 eV in the aqueous phase at the one-fourth and three-fourths points, so this requires the value of E^3 in the organic phase to be smaller than the value of E^3 in the aqueous phase by about 1 to ½%. Since variations in E^3 values by this amount are typical for the Ln(III) ions in various media,[13] these considerations account very well for the one-fourth- and three-fourths-filled-shell effects.

The half-filled-shell effect in Fig. 2.12 can now be independently estimated from the above results for the one-fourth- and three-fourths-filled-shell effects, since variations of 1 or ½% in E^3 between various media are commonly accompanied by corresponding 1 or ½% variations in E^1.[13] From the latter and from Eq. (4), $(\log K)' = -1$ at the half point; this is in reasonable accord with the data of Fig. 2.12, considering that the dip here is growing in all the way from the $q = 1$ or $q = 13$ points following the E^1-dependent contribution shown in Fig. 2.13.

It is worth noting that observed differences in E^1 between two media and the corresponding differences in E^3 are not always of the same sign.[13] This means that although the one-fourth- and three-fourths-filled-shell effects will always occur in the same direction, the half-filled-shell effect can go either in the same direction or it can go in the opposite direction relative to the others, depending upon the particular media involved. Thus it may be possible to find an experimental arrangement which shows an "alternating" tetrad effect.

In conclusion, it is emphasized that the theoretical treatment of H_r above is based on well-defined values for the L and S quantum numbers, that is, upon Russell-Saunders states. It is well known that the Russell-Saunders basis is only an approximation when the relativistic spin-orbit ($\zeta\mathbf{L}\cdot\mathbf{S}$) interaction terms are included in the theoretical treatment of f^q electronic energies.[13-15] It is a simple matter to include first-order spin-orbit interactions in the above considerations, and the coefficients of these terms also display a q dependence matching the one-fourth- and three-fourths-filled-shell effects.[11] Estimates for both series indicate, however, that these first-order contributions are neither as sharply q dependent nor as large as those originating from the E^3-dependent term; so it is not a bad approximation to neglect them here. A treatment of higher-order spin-orbit interactions, on the other hand, is not simple, but it isn't necessary either, since the present approximate treatment provides an adequate theoretical substantiation of the observed tetrad effects for both the Ln(III) and the An(III) series.

[1]D. F. Peppard, G. W. Mason, and S. Lewey, *J. Inorg. Nucl. Chem.* 31, 2271 (1969).

[2]D. F. Peppard, G. W. Mason, and S. Lewey, *J. Inorg. Nucl. Chem.* 27, 2065 (1965).

[3]D. F. Peppard, C. A. A. Bloomquist, E. P. Horwitz, S. Lewey, and G. W. Mason, *J. Inorg. Nucl. Chem.* 32, 339 (1970).

[4]E. Hesford, E. E. Jackson, and H. A. C. McKay, *J. Inorg. Nucl. Chem.* 9, 279 (1959).

[5]I. Fidelis and S. Siekierski, *J. Inorg. Nucl. Chem.* 28, 185 (1966).

[6]I. Fidelis and S. Siekierski, *J. Chromatog.* 17, 542 (1965).

[7]J. R. Peterson and B. B. Cunningham, *Inorg. Nucl. Chem. Letters* 3, 327 (1967).

[8]B. B. Cunningham, "Comparative Chemistry of the Lanthanide and Actinide Elements," paper presented at the XVII International Congress of Pure and Applied Chemistry, Munich, 1959, pp. 64–81.

[9]W. M. Latimer, *The Oxidation States of the Elements and Their Potentials in Aqueous Solution,* Prentice-Hall, New York, 1952.

[10]E. A. Moelwyn-Hughes, *Physical Chemistry,* chap. 18, Pergamon, New York, 1961.

[11]C. K. Jørgensen, *Orbitals in Atoms and Molecules,* Academic, New York, 1962.

[12]C. K. Jørgensen, *Mol. Phys.* 5, 271 (1962), Table II.

[13]W. T. Carnall, P. R. Fields, and K. Rajnak, *J. Chem. Phys.* 49, 4442, 4443, 4447, 4450 (1968).

[14]J. G. Conway, *J. Chem. Phys.* 40, 2504 (1964).

[15]J. B. Gruber and J. G. Conway, *J. Chem. Phys.* 34, 632 (1961).

INVESTIGATIONS ON THE ORGANOMETALLIC CHEMISTRY OF ACTINIDES AND LANTHANIDES

P. G. Laubereau[1] J. H. Burns L. Ganguly[2]

Our studies on the use of cyclopentadiene, C_5H_6, as a ligand for actinide and lanthanide elements have been extended to the synthesis and growth of crystals of the following compounds: $Cm(C_5H_5)_3$, $Nd(C_5H_5)_3$, $Eu(C_5H_5)_3$, $Gd(C_5H_5)_3$, $Tm(C_5H_5)_3$, $Yb(C_5H_5)_2Cl$, and $Pr(C_5H_5)_3 \cdot CHIN$, where CHIN = cyclohexylisonitrile.

The $Cm(C_5H_5)_3$ was synthesized by the microtechnique used to prepare $Bk(C_5H_5)_3$ and $Cf(C_5H_5)_3$;[3] $Yb(C_5H_5)_2Cl$ resulted from the same method when $YbCl_3$ and $Be(C_5H_5)_2$ were employed. Gram quantities of $Gd(C_5H_5)_3$ and $Tm(C_5H_5)_3$ were made by reaction of the respective trichlorides with a melt of $Mg(C_5H_5)_2$. Reaction of $EuCl_3$ and molten $Be(C_5H_5)_2$ at 70°C yielded $Eu(C_5H_5)_3$; gram amounts were subsequently isolated in analytically pure form by extraction with pentane. The use of NdF_3 in preparing $Nd(C_5H_5)_3$ is described elsewhere.[4] A procedure described by Fischer and Fischer[5] for the heavier lanthanides was followed in synthesizing $Pr(C_5H_5)_3 \cdot CHIN$.

For identification, the methods of x-ray diffraction and/or mass spectrometric analysis were used, and in the case of $Eu(C_5H_5)_3$ a full elemental analysis was performed. Crystallographic data for all these compounds, including those previously reported, are summarized in Table 2.7.

[1]Supported by Bundesministerium für wissenschaftliche Forschung, Bonn, Federal Republic of Germany.

[2]Visiting scientist from the Chemistry Department, Louisiana State University, Baton Rouge.

[3]P. G. Laubereau and J. H. Burns, *Chem. Div. Ann. Progr. Rept. May 20, 1969,* ORNL-4437, p. 34; *Inorg. Chem.* 9, 1091 (1970).

[4]P. G. Laubereau, J. A. Fahey, and J. H. Burns, "An Improved Synthesis of Tricyclopentadienyl Complexes in Microquantities," following contribution, this report.

[5]E. O. Fischer and H. Fischer, *J. Organometal. Chem.* 6, 141 (1966).

Table 2.7. Crystallographic Data for Organometallic Compounds of Actinides and Lanthanides

Compound	Unit-Cell Dimensions (Å)			Space Group
	a	*b*	*c*	
$Pr(C_5H_5)_3$	14.20	17.62	9.79	*Pbcm*
$Nd(C_5H_5)_3$	14.24	17.66	9.77	*Pbcm*
$Pm(C_5H_5)_3$	14.12	17.60	9.76	*Pbcm*
$Sm(C_5H_5)_3$	14.15	17.52	9.77	*Pbcm*
$Eu(C_5H_5)_3$	14.06	17.54	9.75	*Pbcm*
$Gd(C_5H_5)_3$	14.09	17.52	9.65	*Pbcm*
$Tb(C_5H_5)_3$	14.20	17.28	9.65	*Pbcm*
$Tm(C_5H_5)_3$	19.98	13.82	8.59	*Pnam* or *Pna*2_1
$Cm(C_5H_5)_3$	14.16	17.66	9.69	*Pbcm*
$Bk(C_5H_5)_3$	14.11	17.55	9.63	*Pbcm*
$Cf(C_5H_5)_3$	14.10	17.50	9.69	*Pbcm*
$Yb(C_5H_5)_2Cl$	13.57	16.21	13.60	$P2_1/c$
		$\beta = 92°30'$		
$Pr(C_5H_5)_3 \cdot CHIN$[a]	8.03	21.65	11.55	$P2_1/c$
		$\beta = 105°9'$		

[a]CHIN = cyclohexylisonitrile.

AN IMPROVED SYNTHESIS OF TRICYCLOPENTADIENYL COMPLEXES IN MICROQUANTITIES

P. G. Laubereau[1] J. A. Fahey[2] J. H. Burns

Previously we prepared $Cm(C_5H_5)_3$,[3] $Bk(C_5H_5)_3$,[4] $Cf(C_5H_5)_3$,[4] and $[Bk(C_5H_5)_2Cl]_2$[5] by reacting the

actinide trichlorides with $Be(C_5H_5)_2$. The procedure involved in situ chlorination with HCl gas of the actinide oxides to the anhydrous chlorides. Usually this gave good results, but in some cases the HCl reacted with the stopcock grease in the system and produced interfering oils. Hence a different path of synthesis was sought which would avoid use of HCl in the system.

A synthesis according to the general scheme

$$2MF_3 + 3Be(C_5H_5)_2 \text{ [at 70°C in molten } Be(C_5H_5)_2\text{]} \rightarrow 2M(C_5H_5)_3 + 3BeF_2 ,$$

where M = lanthanide or actinide element, was studied. The fluorination of the lanthanide or actinide oxides was carried out in a separate furnace. The fluorides were stable in air and could be transferred easily into the reaction system described previously;[4] there they reacted with high yield to form tricyclopentadienyls. By this method $Nd(C_5H_5)_3$ and $^{243}Am(C_5H_5)_3$ were synthesized; they were identified by their x-ray diffraction patterns. The *d* values (Å) for the strongest powder lines of $Am(C_5H_5)_3$ are: 7.42, 7.11, 5.92, 4.85, 3.98, 2.95, 2.47, in full agrement with the ones obtained from orthorhombic tricyclopentadienyls of the actinides and the lanthanides.

[1]Supported by the Bundesministerium für wissenschaftliche Forschung, Bonn, Federal Republic of Germany.

[2]Graduate student, University of Tennessee, Knoxville.

[3]P. G. Laubereau and J. H. Burns, *Inorg. Nucl. Chem. Letters* **6**, 59 (1970).

[4]P. G. Laubereau and J. H. Burns, *Inorg. Chem.* **9**, 1091 (1970); *Chem. Div. Ann. Progr. Rept. May 20, 1969,* ORNL-4437, p. 34.

[5]P. G. Laubereau, *Inorg. Nucl. Chem. Letters,* submitted; also, P. G. Laubereau and J. H. Burns, "The Formation of Dicyclopentadienylberkelium Chloride," following contribution, this report.

THE FORMATION OF DICYCLOPENTADIENYLBERKELIUM CHLORIDE

P. G. Laubereau[1] J. H. Burns

It was found that in the course of a reaction of $BkCl_3$ with $Be(C_5H_5)_2$, not only $Bk(C_5H_5)_3$ was formed as described earlier,[2] but also $[Bk(C_5H_5)_2Cl]_2$.[3] The synthesis presumably followed the reaction equation

$$2BkCl_3 + 2Be(C_5H_5)_2 \rightarrow [Bk(C_5H_5)_2Cl]_2 + 2BeCl_2 .$$

The new berkelium compound was isolated together with $Bk(C_5H_5)_3$ in a quartz capillary by high-vacuum sublimation above 220°C. Identification was achieved by comparison of the x-ray powder pattern with that of dicyclopentadienylsamarium chloride. This latter complex was found by mass spectrometry[4] to exist as a dimer. Because of the very similar properties of the berkelium and samarium complexes, for example, powder patterns, needle-like crystal morphology, and sublimation temperature, the new berkelium compound is assigned the formula: $[Bk(C_5H_5)_2Cl]_2$.

Dicyclopentadienylberkelium chloride is amber, somewhat lighter in color than $Bk(C_5H_5)_3$. Optical spectra in the 400 to 990 nm range were recorded[5] and are shown in Fig. 2.15 with the spectra of $Bk(C_5H_5)_3$[5] and Bk^{3+} for comparison.

[1]Supported by Bundesministerium für wissenschaftliche Forschung, Bonn, Federal Republic of Germany.

[2]P. G. Laubereau and J. H. Burns, *Inorg. Chem.* **9**, 1091 (1970); *Chem. Div. Ann. Progr. Rept. May 20, 1969,* ORNL-4437, p. 34.

[3]P. G. Laubereau, *Inorg. Nucl. Chem. Letters,* submitted.

[4]Mass spectrum recorded by W. T. Rainey, Jr., and W. H. Christy, Analytical Chemistry Division.

[5]L. J. Nugent, P. G. Laubereau, G. K. Werner, and K. L. Vander Sluis, work in progress.

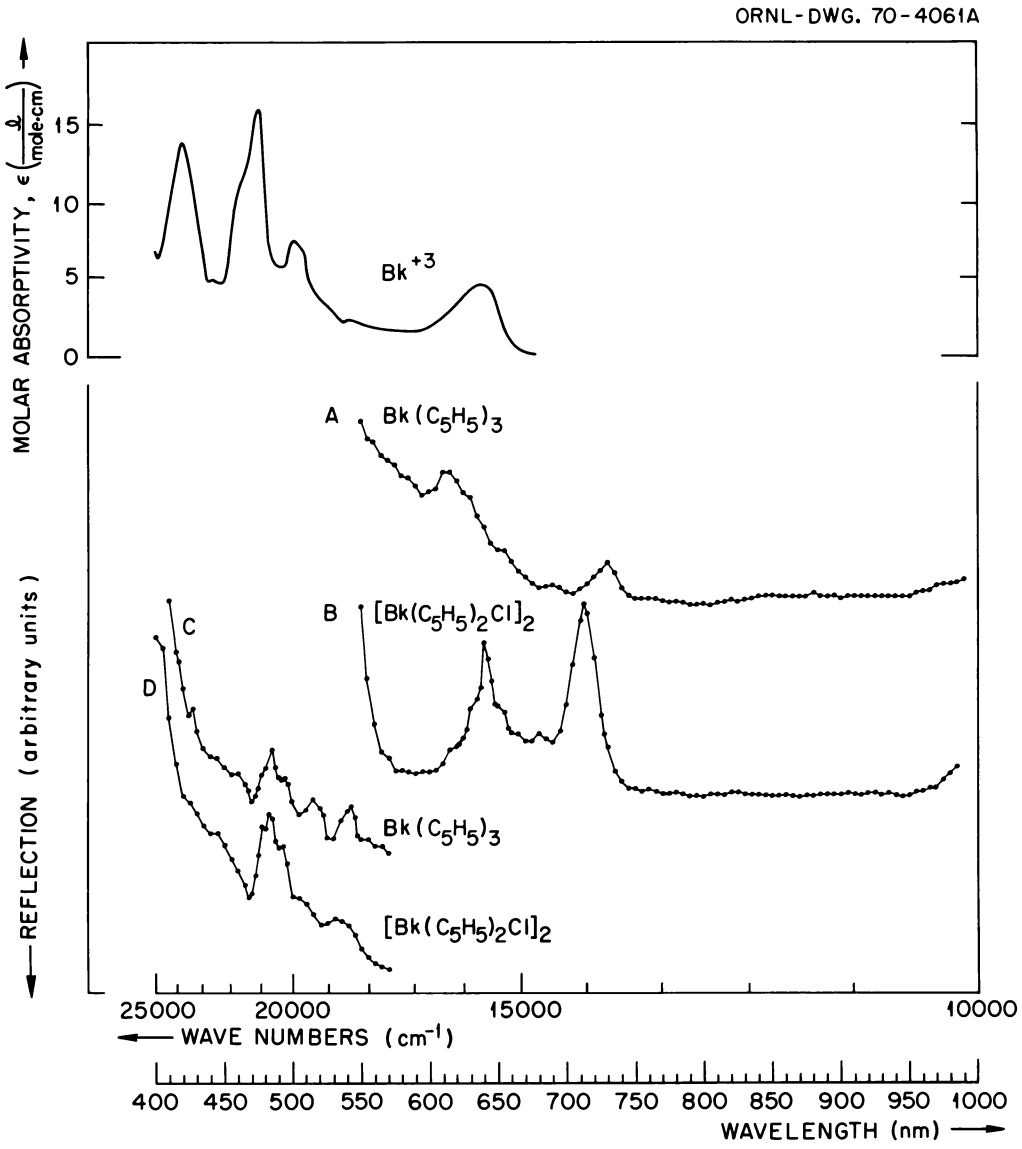

Fig. 2.15. Reflection Spectra of $^{249}Bk(C_5H_5)_3$ and $[^{249}Bk(C_5H_5)_2Cl]_2$ Microcrystals and the Absorption Spectrum of 5.6×10^{-3} *M* $^{249}Bk^{3+}$ in 1.0 *M* $DClO_4$. Spectra *A* and *B* recorded with dry-ice-cooled S-1 phototube detector, spectra *C* and *D* recorded with S-5(1P28) phototube detector. Spectra *A* and *C* recorded 44 hr after the isolation of the complex. Spectra *B* and *D* recorded 2 hr after the isolation of the complex (no significant changes observed after 44 hr). Data for absorption spectrum of Bk^{3+} from R. D. Baybarz, J. R. Peterson, and J. R. Stokely, personal communication.

RARE-EARTH AND AMERICIUM CHELATES

M. D. Danford J. H. Burns
C. E. Higgins J. R. Stokely, Jr.[1]
W. H. Baldwin

Preparation of $CsLn(hfa)_4$ Using Cation Exchange Resin. – Study of these chelates, where Ln is lanthanum or europium and hfa is the anion from 1,1,1,5,5,5-hexafluoro-2,4-pentanedione, has continued.[2] An aqueous solution of Cs(hfa) was passed into a column of Dowex 50 loaded with lanthanide ion, and the cesium lanthanide tetrachelate was obtained from the eluate in 70 to 85% yield. In a modification of this synthesis, the lanthanide was exchanged onto the resin, and then cesium ions were exchanged onto the excess resin sites. $CsLn(hfa)_4$ resulted in 83% yield when the resin was eluted with Cs(hfa). The identity of the product was established through its melting point and through mixed melting point measurements with authentic specimens prepared earlier.[2]

The advantages of using the cation exchange resin for the preparation of lanthanide and actinide compounds include relatively easy separation from other cations and from excess acid.

Preparation of $Cs_2La(hfa)_5$. – The monohydrate, $CsLa(hfa)_4 \cdot H_2O$, was dissolved in *n*-butanol, and part of the solvent was removed until crystals separated. The product, $Cs_2La(hfa)_5$, mp 226–27°C, was identified by analysis for C, H, Cs, La, H_2O, and equivalent weight. Derivatives of this type have considerable interest since the lanthanide atom may be ten coordinated, a rare situation.

$Cs^{243}Am(hfa)_4$.[2,3] – This chelate is a yellow crystalline material that sublimes at 130 to 140°C at 10^{-6} torr and melts at 193–94°C. The product decomposes by self-radiolysis; after eight days in air the melting point had fallen to 168–174°C. In another instance, in which the compound stood in air for about one month, the residue contained significant quantities of AmF_3 (identified by x-ray powder diagram).

^{243}Americium-tris(2,2,6,6-tetramethyl-3,5-heptanedione).[2,3] – This compound sublimes at 124 to 135°C at 10^{-5} torr and melts at 216 to 218°C after softening at 205°C.

[1] Analytical Chemistry Division.

[2] M. D. Danford, C. E. Higgins, and W. H. Baldwin, *Chem. Div. Ann. Progr. Rept. May 20, 1969*, ORNL-4437, p. 36.

[3] M. D. Danford and J. H. Burns, *Chem. Div. Ann. Progr. Rept. May 20, 1968*, ORNL-4306, p. 44.

REACTION OF AQUEOUS LANTHANIDE CHLORIDE SOLUTIONS WITH 2,2-DIMETHOXYPROPANE

W. H. Baldwin T. H. Handley[1]

Existing methods for the preparation of anhydrous lanthanide and actinide trihalides, which are used for the synthesis of many derivatives including some organometallic compounds, require elevated temperatures and sometimes high pressure. In our search for milder reaction conditions we found that the well-known reaction of ketals with water,

$$CH_3C(OCH_3)_2CH_3 + H_2O \rightleftharpoons CH_3COCH_3 + 2CH_3OH,$$

has already been applied, however a priori, to the dehydration of several crystalline hydrates. We have studied this reaction and have attempted to extend its use to aqueous solutions of lanthanide chlorides that result from the action of oxide with excess hydrochloric acid. An endothermic reaction takes place when 2,2-dimethoxypropane is added to the aqueous solution of lanthanide chloride. The reaction mixture is dried in vacuo, and in addition to the anhydrous lanthanide chloride, a small amount of nonvolatile black residue also remains. Quantitative estimates of the amount of this residue are being made. The ratio of Cl/lanthanide in the product was the expected 3.00 ± 0.05.

[1] Analytical Chemistry Division.

PHOTOCHEMICAL REACTIONS INITIATED BY UO_2^{2+}. REACTION OF BUTYRALDEHYDE WITH DIETHYL MALEATE

W. H. Baldwin

The condensation (formation of C–C bonds) of aldehydes with diethyl maleate,

$$RCHO + EtOOCCH{=}CHCOOEt \rightarrow RCOCH(COOEt){-}CH_2COOEt,$$

has previously been accomplished in the presence of dibenzoyl peroxide.[1] This reaction using butyraldehyde has now been carried out photochemically with uranyl ion activation. No attempt has been made to find optimum conditions, but a 35% yield of diethyl butyrylsuccinate was obtained along with an equal weight of higher-boiling material, evidence of extensive

reaction. This reaction is useful for the synthesis of high-molecular-weight branched polar aliphatic compounds whose specific interactions with metallic ions produce metallic salts soluble in organic solvents.

[1] T. M. Patrick, *J. Org. Chem.* 17, 1009 (1952).

THE CRYSTAL AND MOLECULAR STRUCTURE OF TRIS(2,2,6,6-TETRAMETHYL-3,5-HEPTANEDIONATO)NEODYMIUM(III) AND -AMERICIUM(III)

M. D. Danford J. H. Burns

Our studies on the crystal structures of volatile chelates of lanthanide and actinide elements[1] were continued with the elucidation of the structure of $Nd(thd)_3$, where thd = 2,2,6,6-tetramethyl-3,5-heptanedione. The analogous actinide compound $Am(thd)_3$ was shown by x-ray powder diffraction to be isostructural with it.

While our work on $Nd(thd)_3$ was in progress, a completed structure determination of the isostructural compound $Pr(thd)_3$ based on film-recorded data was reported.[2] Using these workers' parameters as a starting point, we refined the structure of $Nd(thd)_3$ with our data collected by a diffractometer. There are no important differences between the two results within the error limits of the two determinations.

The most interesting structural feature is the existence of dimeric molecules, $Nd_2(thd)_6$, in which two of the chelating oxygen atoms form bridges between neodymium atoms. Through dimerization, each neodymium atom achieves seven coordination by oxygen, more than possible in the monomer but still less than normal for an ion of this size (0.995 Å). Higher polymerization is prevented by the steric hindrance from the bulky *t*-butyl groups of the ligands. The molecular character of this crystal accounts for its volatility and ability to sublime without decomposition.

The bond lengths in one $Nd_2(thd)_6$ molecule obtained from this determination are shown diagram-

ORNL-DWG. 70-1456

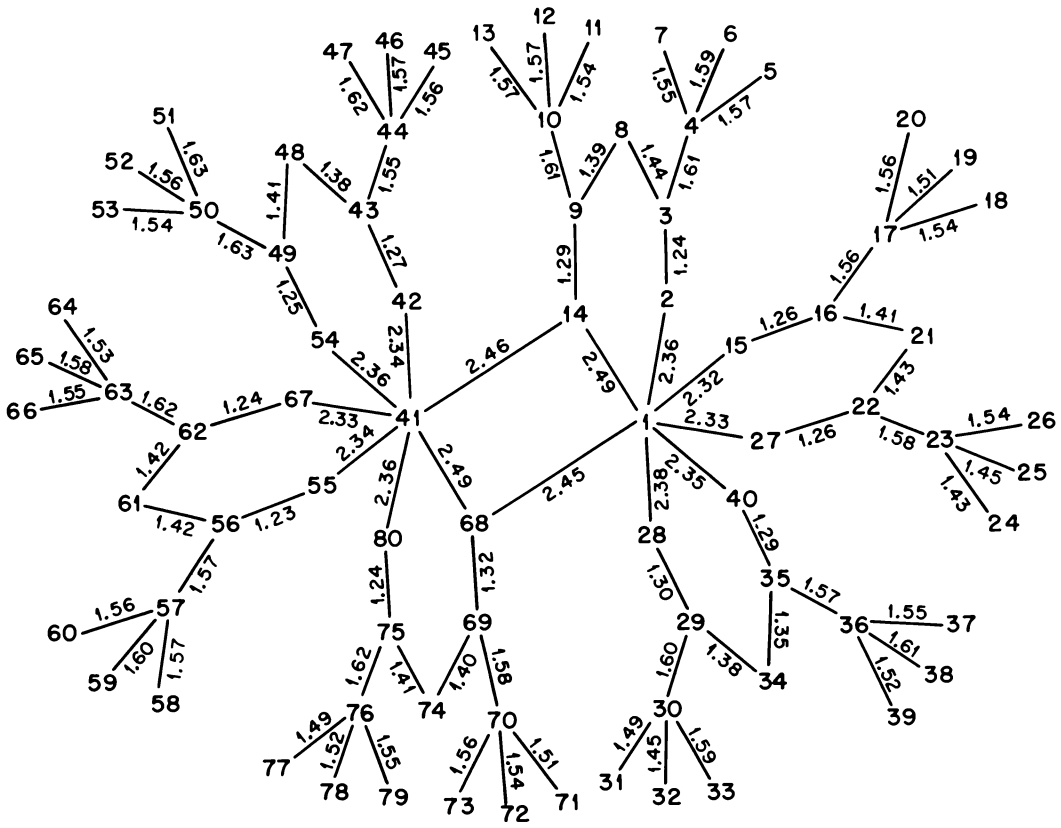

Fig. 2.16. Schematic Drawing Showing the Bond Lengths in One $Nd(thd)_3$ Dimer. Atoms 1 and 41 are neodymium; the remainder are oxygen and carbon atoms.

matically in Fig. 2.16. Average values for the standard errors (Å) are: Nd–O (0.01); O–C (0.02); and C–C (0.02), except for terminal methyl groups, where the value is C–C (0.03). The thermal parameters for the terminal methyl atoms are quite large and have anisotropies indicative of large librational motions. Monoclinic unit-cell dimensions are: $Nd(thd)_3$, a = 12.38(1) Å, b = 28.08(2) Å, c = 22.27(1) Å, β = 107.40(3)°; and for $Am(thd)_3$, a = 12.2(2) Å, b = 28.3(3) Å, c = 22.4(3) Å, β = 106.4(9)°.

[1] M. D. Danford and J. H. Burns, *Chem. Div. Ann. Progr. Rept. May 20, 1968*, ORNL-4306, p. 44.

[2] C. S. Erasmus and J. C. A. Boeyens, *Acta Cryst.* **A25**, S162 (1969).

TRISINDENYLSAMARIUM: SYNTHESIS AND CRYSTAL STRUCTURE

J. L. Atwood[1] J. H. Burns P. G. Laubereau[2]

In a search for preparative methods and for suitable starting materials from which organic ligands can be added to transuranic elements, we have used lanthanide elements as a substitute for the actinides. During these experiments we synthesized trisindenylsamarium, $Sm(C_9H_7)_3$, by reaction of indenylmagnesium bromide with anhydrous $SmCl_3$ in ether solution, and we purified the compound by extraction with toluene. Trisindenylsamarium forms deep red-brown platelike crystals which are very sensitive to moisture and air.

Single-crystal studies with a precession camera and a computer-controlled x-ray diffractometer yielded the orthorhombic unit-cell dimensions and space group: a = 15.568(3) Å, b = 31.348(8) Å, c = 8.265(2) Å, *Pbca*. Subsequent strucutre analysis by Patterson methods found the samarium atoms to be located in the general eightfold positions of *Pbca*. Electron-density maps then showed the positions of the 27 independent carbon atoms, also in general positions. Refinement is still in progress, but a qualitative description of the structure can be given as follows: Each samarium atom is bonded to the π-electron system of the cyclopentadienyl ring of each of three indenyl moieties. The centers of the five-membered rings form an approximately equilateral triangle with the samarium atom at its center. Distances between these trisindenylsamarium molecules are normal.

[1] Department of Chemistry, University of Alabama, University.

[2] Supported by the Federal Republic of Germany, Bonn.

CRYSTALLOGRAPHIC STUDIES OF ANHYDROUS TRANSPLUTONIUM TRICHLORIDES

J. H. Burns J. R. Peterson[1]

A study of the crystal structures of the series of isomorphous transplutonium trichlorides is in progress, with the aim of obtaining a useful set of ionic radii for the trivalent actinide elements. The hexagonal unit-cell dimensions, which are already known,[2] are not sufficient to obtain accurate interatomic distances from which to extract radii; the variable atomic positions for chlorine must also be determined.

We reported previously[3] the refinement of the structure of $AmCl_3$. The study has been extended to include $^{248}CmCl_3$, $^{249}BkCl_3$, and $^{249}CfCl_3$ by use of the indicated isotopes, recently available. A complete structure refinement of $CmCl_3$ was carried out on a crystal grown from the melt. A similarly prepared specimen of $BkCl_3$ was not adequate for structure analysis but provided unit-cell dimensions. Further work is under way on this compound.

Previous studies[4] of $CfCl_3$ have shown it to have the same hexagonal structure as the other trichlorides, but a crystal grown by slow cooling of the melt has a different structure; it is isomorphous with orthorhombic $TbCl_3$.[5] This implies dimorphism in $CfCl_3$, and the orthorhombic structure is probably the high-temperature form. The change in structure type occurs in the actinide series at about the same ionic size as in the lanthanide series. It is reasonable that this change results from the actinide (lanthanide) contraction, since in the hexagonal form the metal is nine coordinated, while in the orthorhombic form it is eight coordinated.

Table 2.8 summarizes the results, including the unit-cell dimensions, refined positional parameters, and tentative ionic radii derived from these.

[1] Chemistry Department, University of Tennessee, Knoxville.

[2] J. R. Peterson and B. B. Cunningham, *J. Inorg. Nucl. Chem.* **30**, 823 (1968).

[3] J. H. Burns and J. R. Peterson, *Chem. Div. Ann. Progr. Rept. May 20, 1969*, ORNL-4437, p. 33.

[4] J. L. Green and B. B. Cunningham, *Inorg. Nucl. Chem. Letters* **3**, 343 (1967).

[5] J. D. Forrester, A. Zalkin, D. H. Templeton, and J. C. Wallmann, *Inorg. Chem.* **3**, 185 (1964).

Table 2.8. Crystallographic Data for Transplutonium Trichlorides

Compound	a (Å)	b (Å)	c (Å)	Space Group	x_{Cl}	y_{Cl}	Ionic Radius (Å)
$AmCl_3$	7.382		4.214	$P6_3/m$	0.38772	0.30187	0.984
$CmCl_3$	7.374		4.185	$P6_3/m$	0.38790	0.30127	0.973
$BkCl_3$	7.388		4.129	$P6_3/m$			
$CfCl_3$	7.393		4.090	$P6_3/m$			
$CfCl_3$	3.869	11.75	8.561	$Cmcm$			

THE TRANSURANIUM RESEARCH LABORATORY ISOTOPE SEPARATOR

L. D. Hunt C. E. Bemis, Jr.

A description of the 150-cm-radius laboratory isotope separator installed in the Transuranium Research Laboratory has been included in an earlier report.[1] This instrument is now fully operational and has been integrated into the nuclear research activities of the Transuranium Element Research Group.

The majority of our research separations have been with the actinide elements to provide isotopically enriched sources for nuclear spectroscopic investigation and small quantities of enriched isotopes for integral neutron cross-section measurements that are of importance in the transuranium element production program at ORNL.

For the transuranic separations the charge material, usually $\leqslant 100$ μg, is evaporated from nitrate solutions onto quartz wool in a quartz sample tube and heated in air to convert the material to the oxide. The tube is inserted into an outlet hole in the ion source, where the sample at ~500 to 700°C is chlorinated in situ at a controlled rate with CCl_4 vapor. Our overall efficiencies using this procedure average 5 to 6% for the actinides. Our average single-pass enhancement factors for isotopes separated by one mass unit exceed ~800 and are about 8000 for isotopes differing by two mass units in the mass 230 to 260 region. We are currently investigating the use of various chlorinating agents other than CCl_4 vapor, such as Freon-11 (CCl_3F), Freon-12 (CCl_2F_2), Freon-13 ($CClF_3$), and Freon-22 ($CHClF_2$) in an attempt to reduce the amount of CCl_4 breakdown products deposited in the vicinity of the ion source.

The separator has been used in an attempt to identify the recently reported ^{241}Pu fission isomer,[2] to produce isotopically enriched 17.8-day ^{253}Cf for nuclear spectroscopic and neutron cross-section measurements,[3] and to produce isotopically pure ^{244}Cm for the investigation[4] of states in ^{240}Pu, and it will be used to enhance the ^{146}Sm content of a second-pass calutron product in an attempt to find ^{146}Sm in nature.[5]

---

[1] L. D. Hunt and C. E. Bemis, Jr., *Chem. Div. Ann. Progr. Rept. May 20, 1969*, ORNL-4437, p. 37.

[2] C. E. Bemis, Jr., R. J. Silva, J. E. Bigelow, and A. M. Friedman, "Long-Lived Spontaneous-Fission Isomerism in ^{241}Pu?," another contribution in this chapter, this report.

[3] C. E. Bemis, Jr., R. E. Druschel, and J. Halperin, *Nucl. Sci. Eng.* (in press).

[4] C. E. Bemis, Jr., M. R. Schmorak, and M. J. Zender, "The Decay of the Isomers of ^{240}Np and ^{244}Cm and the Resultant States of ^{240}Pu," another contribution in this chapter, this report.

[5] C. E. Bemis, Jr., *et al.*, "Search for the Occurrence of ^{146}Sm in Nature," a contribution in chap. 1, this report.

A MASS INDICATOR FOR SECTOR ISOTOPE SEPARATORS

J. R. Tarrant L. D. Hunt C. E. Bemis, Jr.

In a sectorial homogeneous magnetic field of strength B_0 (G) a singly charged ion of mass M (amu) with a kinetic energy E (V) will traverse a path of radius R_0 (cm) according to the following relationship:

$$M = \frac{(R_0 B_0)^2}{2.062 \times 10^4 \times E} . \quad (1)$$

The parameters which determine the position of a focused ion beam in the focal plane in the Transuranium Research Laboratory Isotope Separator[1] are the potential through which the ions are accelerated and the magnetic field strength of the 150-cm, 90° homogeneous-field sector magnet.

Since both of these parameters are independently adjustable for a particular isotope separation, we have designed and constructed an instrument which provides a digital indication of the mass in amu throughout the entire range of both the magnetic field and the acceleration potential. This device allows for the rapid optimization of all other separation parameters for a given experiment.

We use a rotating-coil gaussmeter (Rawson-Lush model 9221) which provides a 31.25-Hz ac voltage proportional to the magnetic field strength over the range 500 to 6000 G. This alternating voltage is converted to a dc voltage level using commercially available modules. A dc voltage proportional to the acceleration potential is derived from the reference divider string for the acceleration power supply (0 to 90 kV). Using a quadratic transconductor with appropriate normalization, the dc analog level proportional to the magnetic field strength is squared, and the ratio of this analog signal to the signal proportional to the acceleration potential is taken using a four-digit ratio voltmeter according to Eq. (1).

The calibration constants required to make the digital voltmeter read directly in amu are determined experimentally using known singly charged ion beams in the range 10 to 270 amu. The accuracy of our mass meter over this range is approximately 0.25 amu, which is sufficient to determine either the position in the focal plane of a known ion beam or the mass of an unknown ion beam.

[1] L. D. Hunt and C. E. Bemis, Jr., *Chem. Div. Ann. Progr. Rept. May 20, 1969,* ORNL-4437, p. 37.

A FAST-CLOSING VALVE TO PROTECT ORIC FROM RADIOACTIVE CONTAMINATION

R. L. Hahn J. R. Tarrant
R. L. Stone[1] L. D. Hunt

In our research with transuranium nuclides at the Oak Ridge Isochronous Cyclotron (ORIC), we have often irradiated targets of alpha-particle-emitting isotopes[2] such as ^{233}U, ^{231}Pa, ^{241}Am, ^{253}Es, and ^{248}Cm. The target material is usually deposited upon a thin foil, which serves as the window between the cyclotron vacuum ($\sim 10^{-4}$ torr) and a chamber containing helium gas at pressures from ~0.2 to 2 atm. Thus the danger exists, should the foil rupture during irradiation, that a shock wave traveling at approximately sonic velocity in helium would carry the gas and some of the alpha-active material into ORIC.

Protection of the cyclotron in the event of such a rupture could be achieved by a fast-acting valve placed between the radioactive target and the cyclotron; in case of target rupture, the valve would close before the shock wave could travel past it. The beam line and associated vacuum pumps from target to valve would have to be decontaminated, but the cyclotron itself could continue in operation.

Valves that close a 2.5-cm opening in $\lesssim 6$ msec have been constructed previously,[3] but their rapid operation results from the ignition of an explosive charge such as gunpowder. These valves have to be dismantled and cleaned frequently to remove the residues of the explosive mixture, and some of the valve parts become deformed after a few firings because of the great impact delivered by the moving valve plate when it slams shut in the valve seat. Accordingly, we have built a reliable, leak-tight valve that does not derive its fast action from explosives.

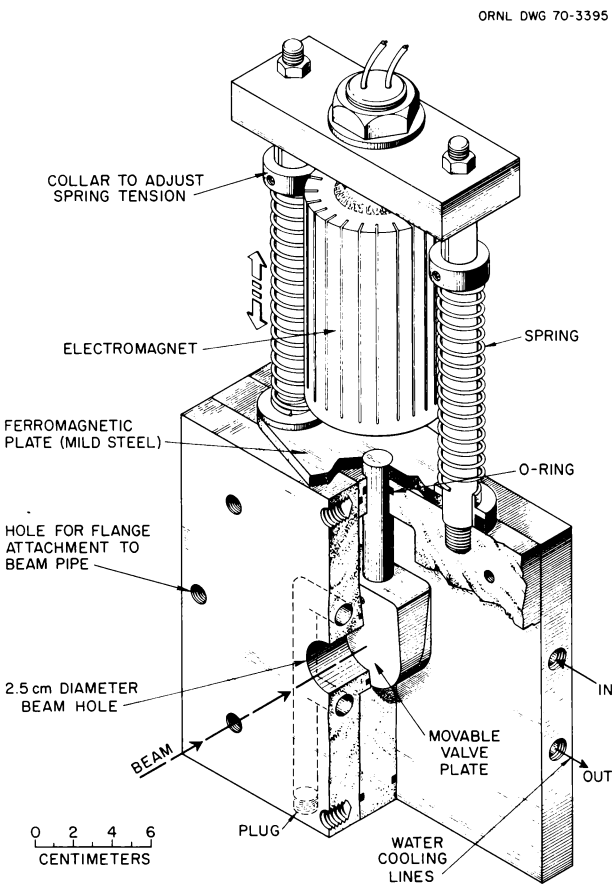

Fig. 2.17. Details of the Construction of the Fast Valve.

This valve, shown in Fig. 2.17, consists of a movable plate that is held by an electromagnet, against the tension of two compressed springs, above the cyclotron beam line. If the current to the electromagnet is interrupted, as by shorting, the magnetic field rapidly collapses, and the springs then drive the plate downward to close off a 2.5-cm opening in the beam line. The valve housing is water cooled to reduce thermal effects caused by the cyclotron beam hitting the valve plate after it has closed.

In actual operation the valve must close only if the target has been broken; otherwise the irradiation should not be interrupted. Since target rupture is accompanied by a rapid rise in pressure along the evacuated beam pipe, a pressure sensor near the target chamber can indicate the condition of the target foil. We have used an automobile spark plug, with an electrode gap of 0.01 cm and an impressed potential of 2000 V, which will discharge in helium at pressures from ~200 μ to >1 atm but not at lower pressures. The discharge of the spark plug can be made to trigger an electronic circuit that shorts the current to the electromagnet and thus actuates the closing of the safety valve.

A schematic diagram of a mockup that has been constructed and the course of events following target rupture are shown in Fig. 2.18. A plunger with a sharp cutting edge is used to break the foil and simulate foil rupture. A helium leak detector is connected to the system beyond the safety valve to obtain a sensitive measure of the effectiveness of the method. Timing tests indicate that the valve closes $\lesssim$30 msec after the target foil is broken.

A closing time of 30 msec is unsatisfactorily slow for shock waves in helium (sonic velocity = 970 m/sec at N.T.P.). However, annular baffles are extremely effective in reducing the velocity and pressure of a shock wave,[4] and provided that they do not interfere with the cyclotron beam reaching the target, they may sufficiently impede the progress of a shock wave from target to cyclotron to make this valve system still useful. Baffles were designed taking into account the cyclotron beam characteristics along the beam pipe,[5] constructed with concentric holes (2.5 to 5.0 cm) that were twice as large as the calculated maximum beam dimensions to assure complete beam transmission, and installed near the valve and near the target chamber in the mockup at intervals of 25.4 cm (Fig. 2.18).

With this arrangement and for helium pressures in the target chamber as high as 2 atm, no indication of helium having passed the valve was given by the leak detector in mockup tests. The combination of fast valve and baffles should prevent not only the helium but also any radioactive material carried along by the helium from getting past the valve. The valve has been tested hundreds of times without apparent reduction in its speed or reliability.

The use of the baffles is most significant. A valve system that inherently is not fast enough to stop a

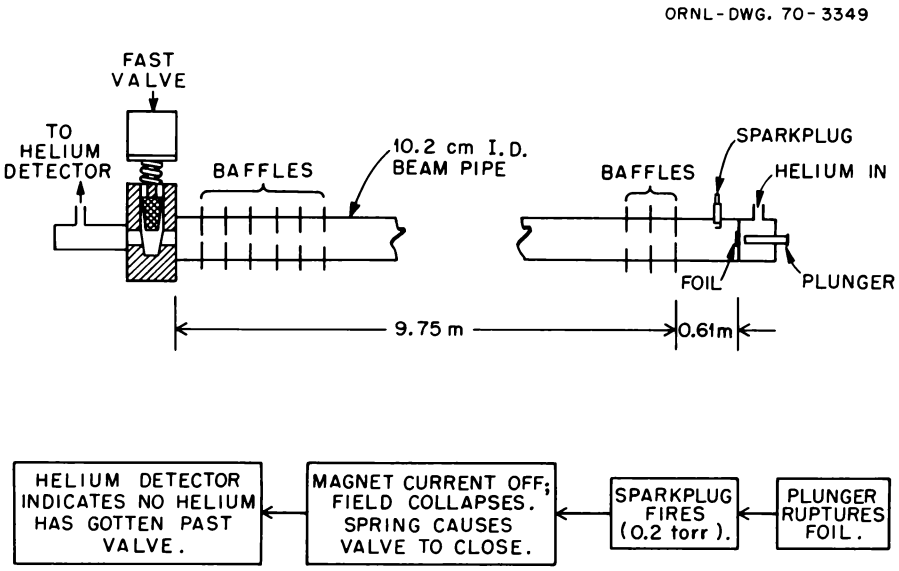

Fig. 2.18. Schematic Drawing of the Complete Valve System. The sequence of events from simulated foil rupture to valve closing is indicated.

helium shock wave works quite well because of the addition of baffles. One is thus not required to build extremely fast valves. This result can be put to general use at accelerators, not only in greatly reducing chances of radioactive contamination but also in avoiding shutdowns caused by accidental loss of accelerator vacuum.

[1] Plant and Equipment Division.

[2] See, for example, R. J. Silva *et al.*, "Alpha-Decay Studies of Neutron-Deficient Californium Isotopes," another contribution in this chapter, this report.

[3] A. Hartwig, Lawrence Radiation Laboratory, Berkeley; private communication.

[4] L. Dresner and C. V. Chester, "Attenuation of Shock Waves in Long Pipes by Orifice Plates, Rough Walls, and Cylindrical Obstacles," ORNL-4288, unpublished (1968).

[5] Performed with computer code OPTIK, T. J. Devlin, UCRL-9727, unpublished (1961).

3. Isotope Chemistry

DEUTERIUM ENRICHMENT

D. A. Lee

Heavy water (D_2O) is a widely used neutron moderator for natural uranium reactors. Most of the presently available supply of this material was separated chemically from natural water by means of the exchange reaction

$$HHO(l) + HDS(g) = HDO(l) + HHS(g) .$$

In every instance the resulting process streams were refluxed by the "dual-temperature" technique. This combination of chemical exchange and reflux method has been very successful: it has produced D_2O at a lower unit cost than any other method. Nevertheless, even this arrangement leaves something to be desired. The dual-temperature refluxing technique requires larger and longer exchange columns and more elaborate heat exchange equipment than conventionally refluxed systems. This appreciably increases the required capital investment. The effective separation factor for the exchange reaction is much smaller for dual-temperature plants than for plants refluxed normally. The fraction of deuterium which can be removed from the feed stream is also reduced in plants employing the dual-temperature refluxing technique. Furthermore, although the corrosive effects of H_2S can be tolerated, there is no doubt that a less corrosive material would be more economical.

In view of these conditions, we have begun a search for a chemical exchange reaction which will permit a new approach to this problem. Specifically, we wish to find a reaction by which water can be reversibly exchanged with a molecular addition compound of water, as indicated in the following equation:

$$\text{Donor·HOH} + HOD = \text{Donor·DOH} + HOH . \qquad (1)$$

If a complex can be found which has an enthalpy of formation of the order of 10 to 20 kcal/mole, it seems likely that reaction (1) would have a single-stage isotopic separation factor large enough to be interesting (>1.1) and a short enough half-time of exchange to be useful in large-scale equipment. It is certain that the separation factor for such a reaction would be smaller than that for the NH_3-H_2 or the H_2O-H_2S system, but this disadvantage could well be offset by the prospect of a greatly simplified refluxing process:

$$\text{Donor·DOH} \xrightarrow{\Delta} \text{Donor} + \text{DOH} ,$$

$$\text{DOH} + \text{Donor} \xrightarrow{\text{cool}} \text{Donor·DOH} .$$

Experiments to evaluate the suitability of possible systems were carried out using tritium rather than deuterium in order to take advantage of simplified analysis by radioactive counting. Of course the separation factors in the D-H systems would not be expected to be as large as in the T-H systems. The results of preliminary studies are encouraging. Following are the measured separation factors (between T and H) for the first few systems examined:

Donor	Aqueous Phase	Separation Factor at 25°C (T-H System)
Trioctylphosphine oxide in *p*-xylene	H_2O	1.15
	0.5 *N* $AlCl_3$	1.05
	0.5 *N* K_2CO_3	1.06
	0.5 *N* HCl	1.08
Tetraheptylammonium bromide in *p*-xylene	H_2O	1.12
Trioctylpropylammonium bromide	H_2O	1.13

The observed separation factors are relatively small (for hydrogen isotope systems). Nevertheless, they are sufficiently large to be encouraging at this stage of the investigation. Further studies of this new approach to the problem of separating hydrogen isotopes will be conducted.

FRACTIONATION OF CARBON ISOTOPES: THE CYANEX SYSTEM

L. L. Brown

The development of the CYANEX system for the fractionation of carbon isotopes continued at the

bench-scale level. This chemical exchange system is based on the exchange reaction

$$R_2C(OH)^{12}CN(org) + {}^{13}CN^-(aq) = R_2C(OH)^{13}CN(org) + {}^{12}CN^-(aq),$$

which has a single-stage fractionation factor of 1.04 at 25°C. Reflux of the product stream is achieved by heating the organic phase to 61°C in the presence of a small stoichiometric excess of HCO_3^-. The cyanohydrin in the organic phase is reconstituted in the waste-end refluxer by countercurrent contact with the aqueous CN^- solution at about 8°C.

Integrated operation of the entire CYANEX system (waste-end refluxer, exchange column, and product-end refluxer) was demonstrated during this report period. The longest of these runs continued for 72 hr, during which time good mechanical operation was achieved. Each refluxer also performed well chemically. Although the chemical stability of the system was not adequately tested by such short runs, it appeared that solution decomposition was not excessive.

Other observations were less favorable. The rate of exchange of carbon between the immiscible phases decreased rapidly as the stoichiometric excess of HCO_3^- was increased from 0 to 25%. Further, mass transfer of carbon-containing species from the aqueous to the organic phase was observed as each run progressed. This latter objectionable characteristic of the CYANEX system stems from the use of free ketone as the solvent of the organic phase. An obvious adjustment would be to dissolve the alkyl cyanohydrin in an inert solvent rather than in free ketone. We have ascertained that xylene is physically suitable for this purpose, and we are now performing additional integrated column runs to establish the usefulness of a modified CYANEX system.

THE CYANEX BENCH-SCALE PILOT PLANT

A. A. Palko

A bench-scale pilot plant was constructed to aid in testing the CYANEX system under process operating conditions. The pilot plant consisted of three main parts: a waste-end reflux system, an exchange column, and a product-end reflux system.

Pulse columns were used in each subsystem to contact the aqueous cyanide solution with the cyanohydrin contained in the organic phase. These pulse columns were made from 1-ft-long sections of 1-in.-i.d. jacketed glass pipe. The pipe sections were hand fitted with perforated stainless steel plates which were strung on a $\frac{1}{8}$-in.-diam stainless steel rod alternately with $\frac{1}{8}$-in.-i.d. Teflon spacers. Several of these assemblies were joined with standard glass-pipe flanges to produce columns of the required length.

The waste-end reflux assembly consisted of two 8-ft jacketed and insulated pulse columns in series. Plates for these columns were stamped from 0.020-in.-thick sheet perforated with 0.030-in.-diam holes (22% open area). Plates were spaced 1 in. apart. Heat exchangers were installed on all feed and exit lines. A water-chilling unit furnished cold water to the column jackets and heat exchangers.

The exchange column was made from 5 ft of unjacketed pulse column. The plates and spacing were the same as for the waste-end reflux section.

The product-end reflux assembly consisted of one 6-ft jacketed and insulated pulse column, a high-temperature water bath, and heat exchangers for all feed and exit lines. Plates for this column were stamped from perforated stainless sheet 0.015 in. thick with 0.015-in.-diam holes and 22% open area. Plate spacing was $\frac{3}{4}$ in.

The pulse generators for all four columns were made from seamless stainless steel bellows which were $1\frac{1}{8}$ in. i.d., $1\frac{5}{8}$ in. o.d., and 3 in. long. The bellows were actuated by a cam-driven arm attached to a Zero-Max speed changer. Pulse frequency could be varied from 0 to 500 cycles/min at fixed pulse amplitudes of $\frac{1}{4}$, $\frac{3}{8}$, or $\frac{1}{2}$ in.

Type 316 stainless steel was used throughout the system for pumps, bellows, sieve plates, valves, and flanges. Microbellows pumps were used for process streams, while centrifugal pumps were used for water circulation. Teflon tubing was used for transfer lines. Liquid levels and interfaces in the columns were controlled by gravity legs. Once steady state was reached, the apparatus would operate automatically and continuously for weeks with only occasional minor adjustments to operating variables. Twenty thermocouples monitored temperatures throughout the system, while 18 sample ports were available to monitor the system chemically.

^{17}O FACILITY

D. Zucker

Last year's efforts to correct the performance of the water distillation cascade appear successful, and the isotopic gradient in this cascade is recovering. Dif-

ficulties with regulating the flow of feedwater to distillation column 4 were eliminated by replacing the feed line and rotameter and by adding more air deentrainment. A low-pressure alarm was also added to the condenser water system. Removal of product water from the distillation cascade began at a reduced rate about the middle of the report period.

The installation of gas circulating pumps in the thermal diffusion cascade, begun last year, was completed. These pumps consist of annealed Plexiglas U-tubes containing mercury and two check valves. The mercury is pulsed by externally applied air pressure, displacing the process gas in the circulation loop. The only wearing parts contacting the process stream are the check valves; these move so slightly they are expected to last for years.

A number of changes were made in the physical plant to ensure greater working and operating safety. The low-oil-pressure and high-temperature cutoff controls for the emergency power supply were disconnected from the diesel control and connected to an alarm instead. This protects the emergency power against failure of the sensing element. Should there be diesel trouble instead of element failure, several additional minutes would now be available in which to take corrective action.

As noted previously, last year's repairs interrupted the normal operation of the ^{17}O facility and decreased its productivity. In spite of this, 14.3 g of water enriched in ^{18}O to 97.3% and 5.4 liters of oxygen gas enriched in ^{18}O to 99.7% were transferred to Isotope Sales inventory. In addition, 4 liters of gas containing ^{18}O at a purity of 95% were also prepared. The total value of these materials exceeded $18,000.

PHOTOCHEMICAL SEPARATION OF ISOTOPES

W. H. Fletcher[1]

Study of the problems associated with the photochemical separation of isotopes continued.[2] The work reported here deals with our efforts to excite the Cl_2 molecule to the discrete $^3\Pi_0^+$ state and to cause it to react with selected substrates without generation of the Cl· radical, which, if formed, would destroy the desired isotopic specificity of the photochemically induced reaction.

Molecular chlorine was chosen for study, not so much because of interest in the isotopes of this element per se, but because this was the only molecule of interest for which sufficient spectroscopic data were available by which frequencies of the various activated states could be computed. The potential well for the $^3\Pi_0^+$ excited state of Cl_2 has a depth of approximately 7400 cal, and the 5145-Å argon laser line will excite the molecule to a vibrational level 4200 cal below the dissociation limit.

The following reactions were chosen for investigation:

$$CO + Cl_2 \rightarrow COCl_2 ,$$

$$C_4F_8 \text{ (perfluorobutene-2)} + Cl_2 \rightarrow C_4F_8Cl_2 ,$$

$$CH_2 = CF_2 + Cl_2 \rightarrow ClH_2C\text{-}CF_2Cl ,$$

$$C_2H_4 + Cl_2 \rightarrow C_2H_4Cl_2 .$$

These molecules do not react with Cl_2 in a clean cell at room temperature if light is excluded and the Cl_2 pressure is low. Irradiations were made on mixtures of Cl_2 with CO, C_4H_8, and $C_2H_2F_2$, using a filtered 5145-Å beam and a light-tight box so that only 5145-Å radiation traversed the sample. Ratios of reactant to Cl_2 pressures were varied from 1:1 to 90:1, and the Cl_2 pressures used were 10, 25, and 30 mm. In all cases the reaction proceeded by a chain mechanism. Quantum yields ranged from 20 to 100 or more.

The conclusion indicated by the results of these experiments is that a free-radical mechanism is involved in all of these reactions. There are at least two mechanisms by which this could occur:

1. The excited Cl_2 may form a complex with the reactant molecule, then lose a Cl atom before the complex can lose its excess energy and become a stable molecule.
2. Repeated collisions of an activated Cl_2 molecule with other molecules may cause it to gain the additional 4 kcal it requires to dissociate. This seems improbable, but this path cannot be disregarded until more data are in hand.

At higher pressures of Cl_2 (0.5 to 1 atm), $CH_2=CF_2$ reacts even in the dark at room temperature. CO does not appear to react with 1 atm of Cl_2 *if* it is in a clean cell and light is carefully excluded.

---

[1]Consultant, Department of Chemistry, University of Tennessee, Knoxville.

[2]W. H. Fletcher, *Chem. Div. Ann. Progr. Rept. May 20, 1968*, ORNL-4306, p. 53.

MOLECULAR SPECTROSCOPY[1]

G. M. Begun

The use of the laser as a light source has greatly expanded the domain of Raman spectroscopy; in particular, it has become much easier to obtain Raman spectra of fused salts. We have used this new capability to study the species present in alkali chloroaluminate melts varying in composition from 50-50 mole % $AlCl_3$-NaCl to pure Al_2Cl_6.

Figures 3.1 and 3.2 show the spectra of pure molten Al_2Cl_6 and $AlCl_4^-$ ($AlCl_3$-NaCl, 50-50 mole %) respectively. Although these spectra have been reported before there is considerable disagreement in the literature. We believe our laser-excited spectra to be superior to any so far reported. Table 3.1 summarizes the data for Al_2Cl_6 and the $AlCl_4^-$ ion. We believe our assignment of the low-frequency peak for $AlCl_4^-$ as ν_2 to be better than previously reported choices. We confirm the value reported by Carlson[2] of 490 cm^{-1} for ν_3 rather than the higher frequencies previously accepted. In addition we have observed two bands at ~270 and ~310 cm^{-1}. Both bands may be combination bands (see Table 3.1); alternately, the band at ~310 cm^{-1} may be due to $Al_2Cl_7^-$ (see below). Our spectrum of liquid Al_2Cl_6 is in reasonable agreement with the literature except at very low frequencies, where we observed two peaks at 119 and 104 cm^{-1}.

The variation of the spectra of the melt with composition is shown in Figs. 3.3 and 3.4, and the frequencies are tabulated in Table 3.2.

Lines due to $Al_2Cl_7^-$ can be located if we assume that the only Raman-active species present in the concentration range 50-50 to 58-42 mole % are $AlCl_4^-$ and $Al_2Cl_7^-$. One peak is easily identified (313 cm^{-1}); it is highly polarized and has an intensity similar to the

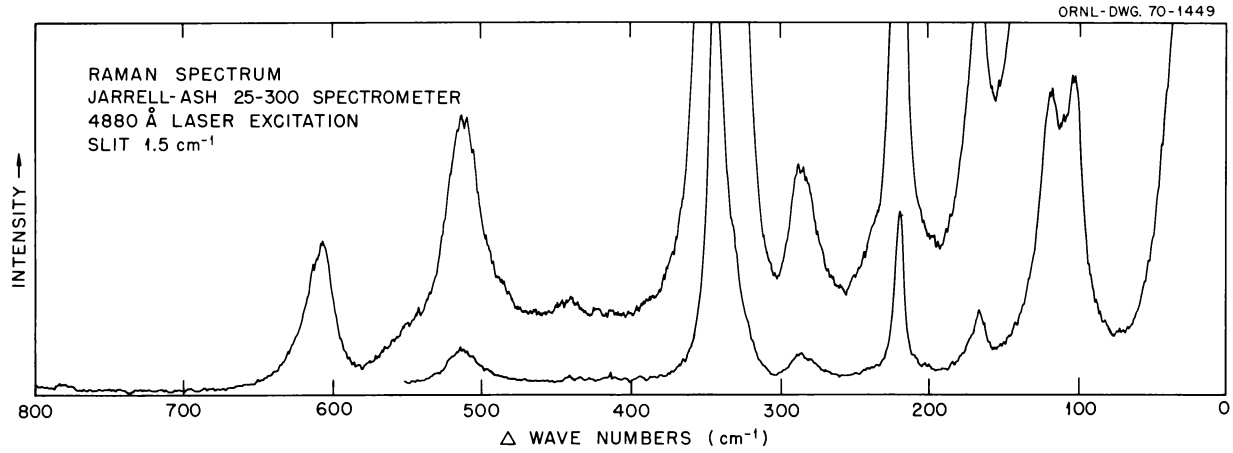

Fig. 3.1. Raman Spectrum of Al_2Cl_6 Liquid at ~225°C.

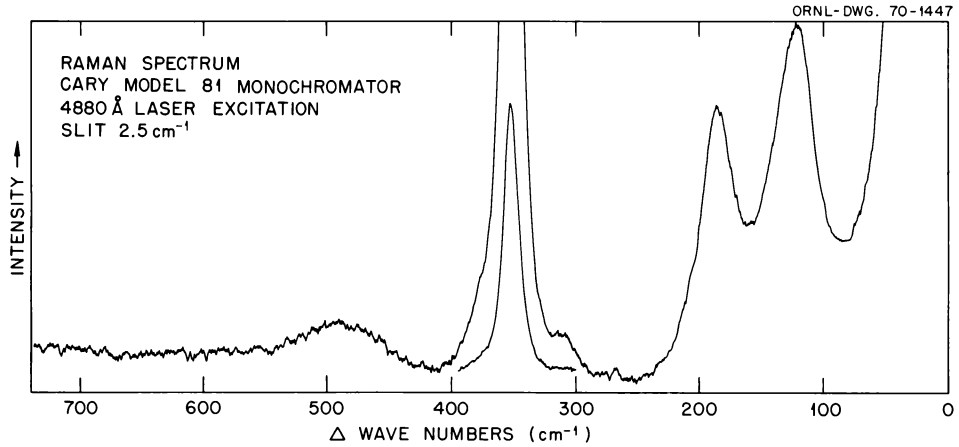

Fig. 3.2. Raman Spectrum of Molten $AlCl_3$-NaCl (50-50 Mole %) at ~225°C.

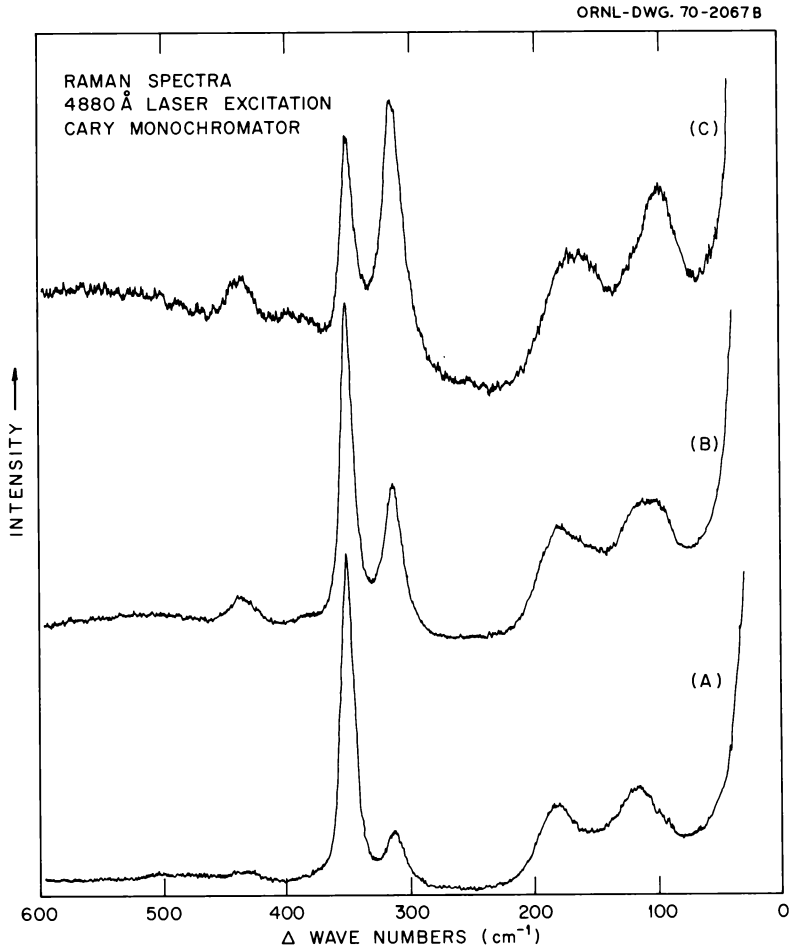

Fig. 3.3. Raman Spectra of Molten $AlCl_3$-NaCl at ~225°C. Composition: *A*, 52-48 mole %; *B*, 54-46 mole %; *C*, 64-36 mole %.

Table 3.1. Raman Frequencies of Molten Al_2Cl_6 and $AlCl_4^-$ at 225°C

Frequency (cm^{-1})	Polarization	Assignment
	Al_2Cl_6	
104 s[a]	P	
119 s	D	
166 w	D?	
218.5 vs	P	
290 m	P	
341 vs	P	
440 w		
512 m	P	
608 m	P?	
	$AlCl_4^-$	
121 s	D	$\nu_2\ E$
186 s	D	$\nu_4\ F_2$
268 vw	?	$\nu_1 - \nu_4$ (?)
306 w	?	$\nu_2 + \nu_4$ (?)
351 vs	P	$\nu_1\ A_1$
490 m	D	$\nu_3\ F_2$

[a]s, strong; m, medium; w, weak; v, very; D, highly depolarized; P, polarized.

350-cm^{-1} peak of $AlCl_4^-$. We also assign the peaks at 435, ~165, and ~100 cm^{-1} to $Al_2Cl_7^-$. The variation of the spectra with composition cannot be explained solely on the basis of $AlCl_4^-$, $Al_2Cl_7^-$, and Al_2Cl_6. The existence of at least one more Raman-active species may be deduced from the following observations:

1. The appearance of a new peak near 390 cm^{-1} for compositions with high $AlCl_3$ content (for example, 73-27 mole % composition).
2. The presence of the strong 350-cm^{-1} peak due to $AlCl_4^-$ in compositions in which Al_2Cl_6 (as evidenced by the 218-cm^{-1} peak) is either not present (67-33 mole %) or present in very low concentrations (73-27 mole %).

Assuming only $Al_2Cl_7^-$ and Al_2Cl_6 at the composition 73-27 mole % (certainly an incorrect assumption), the ratio $Al_2Cl_6/Al_2Cl_7^-$ should be 0.35. If the equilibrium

$$2Al_2Cl_7^- \rightleftharpoons Al_2Cl_6 + 2AlCl_4^- \quad (1)$$

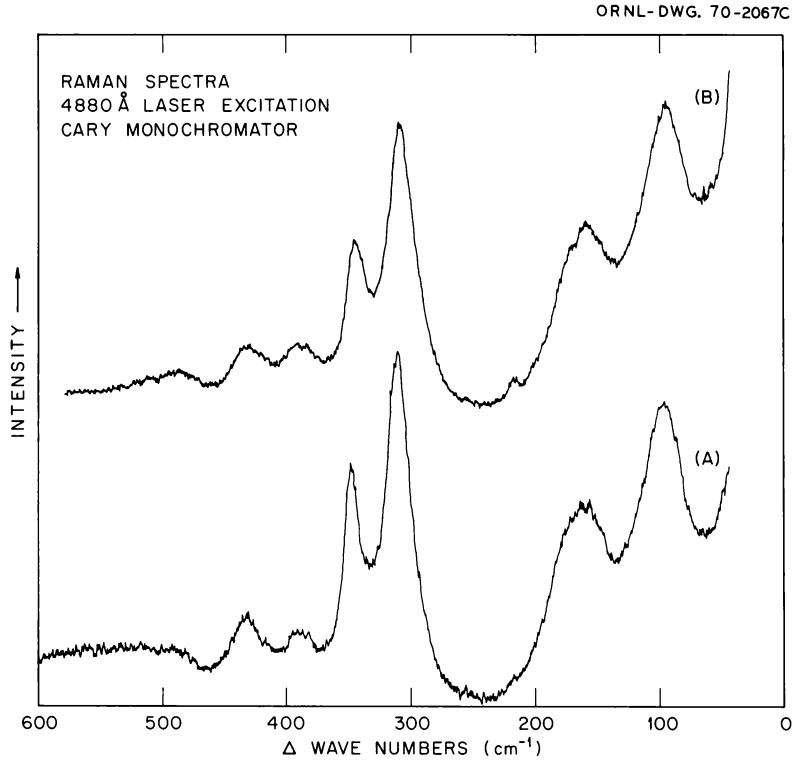

Fig. 3.4. Raman Spectra of Molten $AlCl_3$-NaCl at ~225°C. Composition: *A*, 67-33 mole %; *B*, 73-27 mole %.

Table 3.2. Raman Frequencies of the System $AlCl_3$-NaCl at 225°C

Composition (mole %)	Frequency (cm^{-1}) and Polarization							
	D[a]	D	P	P	P	P	P	D?
51-49	119 s	184 s		313 w	351 vs			490 b,w
52-48	118 s	182 s		313 m	350 vs		436 w	490 b,w
54-46	116 s	183 s		313 m	350 vs		434 w	490 b,w
58-42	108 s	154 sh, 178 s		313 s	350 vs		436 w	
62-38	98 s	165 s		313 vs	350 vs		436 w	
64-36	98 s	165 s		312 vs	350 s		434 w	
67-33	97 s	162 s		312 vs	348 s	388 w	432 m	
73-27	96 s	159 s	218 vw	310 vs	346 m	388 w	432 m	495 b,w

[a]vs, very strong; s, strong; m, medium; w, weak; b, broad; sh, shoulder; D, highly depolarized; P, polarized.

is the predominant one, an even larger ratio should result. Since the concentration of Al_2Cl_6 appears to be much lower than estimated above (in comparison to $Al_2Cl_7^-$), other equilibria such as

$$2Al_2Cl_7^- \rightleftharpoons Al_3Cl_{10}^- + AlCl_4^- \quad (2)$$

or

$$Al_2Cl_7^- \rightleftharpoons AlCl_4^- + AlCl_3 \quad (3)$$

are indicated. No definite conclusions may be drawn at this time regarding the nature of the new species appearing in compositions of high $AlCl_3$ content. The presence of monomeric $AlCl_3$ is unlikely, however, since it is not present in appreciable concentrations in pure liquid aluminum chloride. Evidence of $Al_3X_{10}^-$ species may be inferred from phase diagram studies.[3]

We have observed the Raman spectra of solid and melted samples of triphenylene (C_8H_{12}) in order to make comparisons between observed and calculated

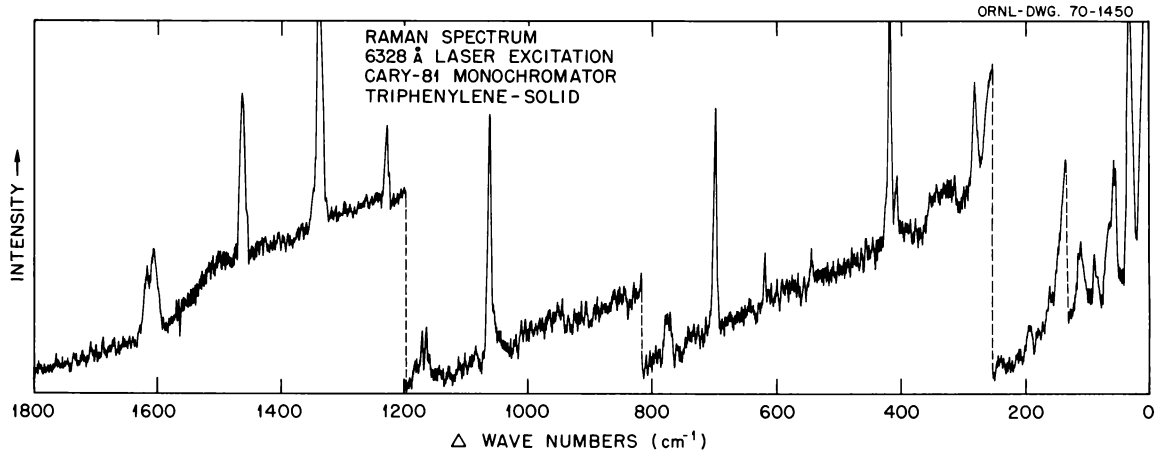

Fig. 3.5. Raman Spectrum of Solid Triphenylene.

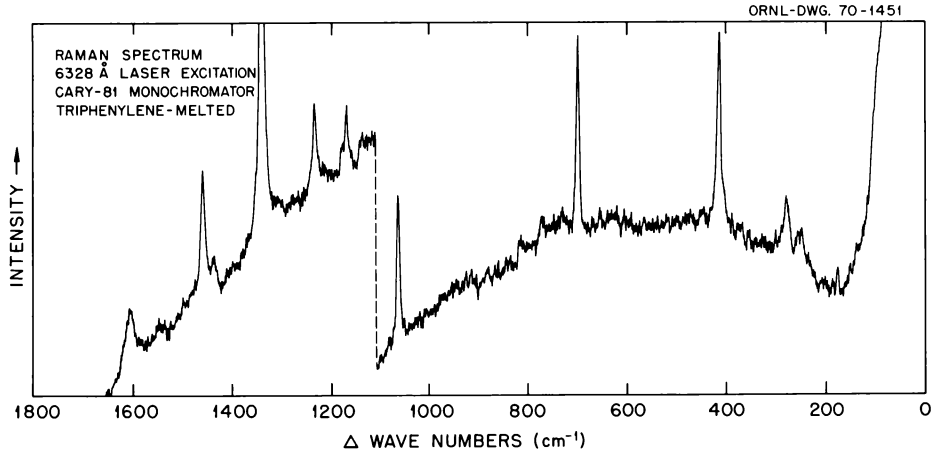

Fig. 3.6. Raman Spectrum of Melted Triphenylene.

vibrational frequencies. Previous observations of the Raman spectrum of triphenylene were poor due to fluorescence of the sample. Our observations were made using the 6328-Å helium-neon laser line for excitation. Figure 3.5 shows our Raman spectrum of solid triphenylene, and Fig. 3.6 is a reproduction of the spectrum of the melted compound. Polarization measurements were also made on the melted sample. The Raman spectral results are shown in Table 3.3.

C. H. King[4] performed an a priori calculation of the planar normal vibrations of triphenylene and found good agreement between the calculated and observed frequencies. The results of these calculations and the comparisons between calculated and observed vibrational frequencies have been prepared for publication.

---

[1]G. Torsi, G. Mamantov, C. H. King, and W. E. Deeds of the University of Tennessee, Knoxville, have participated in this research.

[2]G. L. Carlson, *Spectrochim. Acta* **19**, 1291 (1963).

[3]J. Kendall, E. D. Crittenden, and H. K. Miller, *J. Am. Chem. Soc.* **45**, 963 (1923).

[4]Ph.D. candidate at the University of Tennessee, Physics Department, working under the direction of Dr. W. E. Deeds.

Table 3.3. Raman Spectrum of Triphenylene

Frequency (cm^{-1})[a]		Species Assignment
Solid	Melt	
32 s		Lattice
58 m		Lattice
91 m		Lattice
108 m		Lattice
282 m	279 m	
408 w		E_1'
420 s	416 s,P	A_1'
544 w		
620 w		
698 s	699 s,P	A_1'
770 vw		
776 w		
1061 s	1061 s,P	A_1'
1163 w		E'
1172 w	1171 w,P	A_1'
1229 m	1231 m,P	A_1'
1340 vs	1336 vs,P	A_1'
1457 s	1458 s,P	A_1'
1603 m	1605 m,D	A_1'
1616 m		
2995 w		E'
3034 w		A_1'
3092 w		A_1'

[a]w, weak; m, medium; s, strong; v, very; P, polarized; D, highly depolarized.

ISOTOPIC MASS SPECTROMETRY

L. Landau

During this report period samples of CO_2 and O_2 were analyzed routinely for enrichment of ^{17}O and ^{18}O in order to monitor the performance of the water distillation and the thermal diffusion cascades in the ^{17}O facility. The oxygen samples were also inspected for N_2, Ar, and CO_2 to aid in the detection and location of leaks.

Samples of CO and CO_2 were examined by the ratio method to determine ^{13}C enrichment factors in single-stage experiments and to evaluate the performance of the COCO and the CYANEX systems in column runs under different operating conditions.

A continuing analysis of a set of standard CO_2 samples, used to evaluate the mass spectrometer's performance, now shows a comparison of the 45/44 ratios of the two standards to be $1.03030 \pm 0.00008_5$ (95% C.L.). This is the average of 15 sets of measurements over a period of 11 years. The previous average[1-3] was 1.03029.

Samples of HCN, Xe, and CO_2 enriched in ^{18}O were analyzed for other groups. A total of 450 samples were analyzed.

[1] *Chem. Div. Ann. Progr. Rept. June 20, 1963,* ORNL-3488, p. 33.

[2] *Chem. Div. Ann. Progr. Rept. June 20, 1964,* ORNL-3679, p. 29.

[3] *Chem. Div. Ann. Progr. Rept. May 20, 1967,* ORNL-4164, p. 34.

PREPARATION OF ^{13}CO

L. Landau

CO containing 60% ^{13}C was prepared by reducing isotopically enriched CO_2 over zinc at 400°C. The CO_2 was recycled for several hours through a loop containing a U-tube filled with heated zinc granules. The mass spectrometric analysis of the product showed that more than 99% of the initial CO_2 was reduced to CO.

4. Radiation Chemistry

FLASH PHOTOLYSIS OF AQUEOUS NITRIC OXIDE SOLUTIONS

C. J. Hochanadel J. A. Ghormley
J. W. Boyle

The primary processes in the photolysis of aqueous solutions of NO and O_2[1] have been investigated by flash techniques. Both of these solutions have continuous absorption spectra which extend to much longer wavelengths than the absorptions of the individual components themselves. These spectra have been attributed to charge transfer processes, which, for NO solution, can be written as

$$NO(aq) \xrightarrow{h\nu} NO^*(aq) \rightarrow NO^- + H_2O^+ \left(\xrightarrow{H_2O} H_3O^+ + OH\right).$$

On flashing NO-saturated water (1.9×10^{-3} *M*) we observe the transient spectrum shown in Fig. 4.1 with peaks at 3840 and 2520 Å. Part of the absorption is produced during the flash, but most of it grows in after the flash, reaching a maximum in ~250 μsec. At natural pH the transient decays in ~6 msec, leaving a residual, long-lived absorber with the spectrum of NO_2^-. The decay rate increases with increased acidity. The transient appears to be identical to that observed recently by Seddon[2] in the pulse radiolysis of NO solution. He suggested that the transient is $N_2O_2^-$ produced by reaction of NO with NO^-, which was shown to originate from the fast reaction $e^-(aq) + NO \rightarrow NO^-$. The $N_2O_2^-$ decays by protonation to give N_2O and OH, and the OH reacts rapidly with NO to give HNO_2. The comparison with pulse radiolysis indicates that the primary process in photolysis is essentially as written above. The analogous reaction in O_2-saturated water would produce O_2^- and OH. We observed O_3 as one of the final products in this system,[1] whereas the reactions of O_2^- and OH generally considered in radiation chemistry and photochemistry would give only O_2 and H_2O_2 as stable products. Possible mechanisms for O_3 formation include: combination of O_2^-, reaction of HO_3 (produced by $OH + O_2 \rightarrow HO_3$) with itself or with O_2^-, or by reactions of HO_3^- (produced by $OH + O_2^- \rightarrow HO_3^-$). In attempting to learn more about the reactions of OH in this system we studied the flash photolysis of solutions of $H_2O_2 + O_2$ (OH is produced by photolysis of H_2O_2), $H_2 + O_2$, and $CO + O_2$, where the H_2 and CO are OH scavengers. However, the results thus far have not been conclusive.

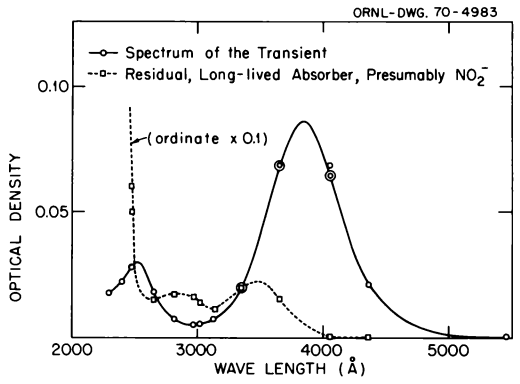

Fig. 4.1. Absorption Spectra Produced in the Flash Photolysis of Solutions of Nitric Oxide in Water. Solid curve – spectrum of the transient; dotted curve – residual long-lived absorber, presumably NO_2^-.

[1] *Chem. Div. Ann. Progr. Rept. May 20, 1969,* ORNL-4437, p. 49.

[2] W. A. Seddon, AECL-3477, p. 59 (Sept. 30, 1969).

PULSE RADIOLYSIS OF SODIUM NITRATE CRYSTALS

J. A. Ghormley C. J. Hochanadel

The pulse technique was used to study the radiolysis of sodium nitrate crystals at room temperature. In the steady radiolysis of alkali nitrates the final products are NO_2^- and O_2, with 100-ev NO_2^- yields ranging from 0.02 for $LiNO_3$ to 0.25 for $NaNO_3$ and 1.6 for KNO_3.[1] A number of studies[2–4] employing optical or esr detection after irradiation, usually at low temperature, have indicated several intermediates, the most prominent being NO_3, NO_3^{2-}, and NO_2.

On irradiating $NaNO_3$ crystals with a 30-nsec pulse of electrons, we observe the formation of transient absorption bands with maxima at 6800, 4100, and 3400 Å (Fig. 4.2). The absorbers are tentatively identified as NO_3, NO_2, and NO_3^{2-}, based on comparisons with reported spectra in the gas phase and/or solution[5] and evidence cited above from esr and optical measurements following steady radiolysis. All three absorbers are produced mostly during the pulse, and the formation-decay characteristics of any one species do not seem to be related to either of the others. The band at 6800 Å (NO_3) decays by first-order kinetics with a lifetime of ~0.5 μsec. Apparently it does not decay to NO_2 (4100 Å). The amount produced and the decay kinetics are independent of the previous history of the sample, for example, previous irradiation and bleaching. There is a shoulder on this band at ~5600 Å which decays at a rate similar to the NO_3 but appears to belong to a different species, possibly related to a crystal defect or an impurity. The yield of absorber was different for three different crystals [two samples grown from the melt (Harshaw) and one grown from solution], and the shoulder is either greatly reduced or not produced at all on a crystal that had previously been irradiated and bleached. The band at 4100 Å (NO_2), produced mostly during the pulse, decays thermally in ~5 sec by something between first- and second-order kinetics. Approximately the same amount is produced on the first pulse as on a crystal that had received many pulses, suggesting that NO_2^- is not its precursor. The band at 3400 Å (NO_3^{2-}) also reaches its maximum during the pulse and is stable for many hours. It can be photobleached, leaving a weak residual absorption in the same region (3450 Å) due to NO_2^-. There is some delayed light emission in the wavelength region from ~3000 to 5000 Å for a period of 1½ μsec following a pulse.

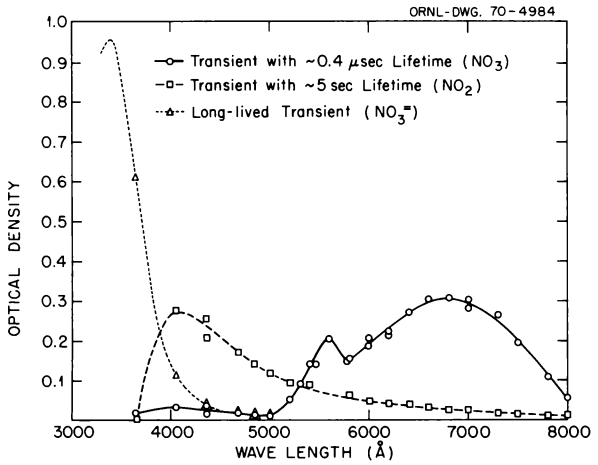

Fig. 4.2. Absorption Spectra of Transients Produced in the Pulse Radiolysis of $NaNO_3$ Crystals. Solid curve – transient with ~0.4-μsec lifetime (NO_3); dashed curve – transient with ~5-sec lifetime (NO_2); dotted curve – long-lived transient (NO_3^{2-}).

Thus far measurements of short-lived species have been limited to wavelengths above 3650 Å. Therefore it has not been possible to observe the behavior of other possible transients such as O, O^-, O_2^-, O_3, NO, N_2O_3, NO_2^{2-}, $ONOO^-$, etc., nor is it possible to observe the formation of final products directly. A complete mechanism for formation of products has not yet been established.

---

[1] C. J. Hochanadel and T. W. Davis, *J. Chem. Phys.* **27**, 333 (1957).

[2] P. Pringsheim, *J. Chem. Phys.* **23**, 369 (1955).

[3] J. Cunningham, *J. Chem. Phys.* **41**, 3522 (1964).

[4] H. Zeldes and R. Livingston, *J. Chem. Phys.* **37**, 3017 (1962); R Livingston and H. Zeldes, *J. Chem. Phys.* **41**, 4011 (1964); H. Zeldes, *Paramagnetic Resonance,* vol II, p. 764, Academic Press, New York, 1963.

[5] L. Dogliotti and E. Hayon, *J. Phys. Chem.* **71**, 3809 (1967).

PULSE RADIOLYSIS OF GASES

C. J. Hochanadel J. A. Ghormley
P. J. Ogren[1]

Energy Transfer in NO-Ar and NO-N_2 Mixtures

In studies of energy transfer and energy degradation, we measured yields of $NO_2 + N_2O_3$ (from the rapid equilibration $NO_2 + NO \rightleftharpoons N_2O_3$) and of NO ($v = 1$) in the above mixtures over the entire composition range at a total pressure of 1 atm, using a 30-nsec electron pulse at a dose rate of $\sim 10^{12}$ rads/sec. In pure NO the yields of $NO_2 + N_2O_3$ had been evaluated as 10.6 per 100 eV.[2] In mixtures with argon the yield remains nearly constant down to about 5% NO, below which it falls rapidly. In N_2 the yield falls slowly with decreasing partial pressure of NO, but at 0.5% NO it is still ~60% of the full yield.

The principal "energy transfer" reactions are likely to be charge exchange from N_2 or Ar to NO and reaction of NO with excited Ar or N_2 or with N atoms produced by dissociation of excited N_2. Charge neutralization is likely to be by $NO^+ + NO^- \rightarrow N + O + NO$ following electron capture by NO. Reactions leading to NO_2 formation are $N + NO \rightarrow N_2 + O$ followed by $O + NO \rightarrow NO_2$. From the W values for NO, N_2, and Ar of 27.5,

36.3, and 26.4, respectively, and assuming an equal yield of excited states leading to NO_2 formation, the estimated maximum yields of NO_2 from energy initially absorbed in NO, N_2, or Ar are 14.6, 11.0, and 15.2, respectively, thereby accounting for the high yields of $NO_2 + N_2O_3$ even at low partial pressures of NO. Further refinement in interpretation will require studies of effects of pressure and dose rate.

The yield of vibrationally excited NO ($v = 1$) in the electronic ground state as a function of composition showed behavior similar to the $NO_2 + N_2O_3$ yields, both in Ar and in N_2.

Luminescence and NO Formation in N_2-O_2 Mixtures

In the pulse radiolysis of oxygen at high dose rate ($\sim 10^{12}$ rads/sec) O_3 is produced in high yield.[3] In mixtures with N_2 the O_3 yield is nearly constant down to ~10% O_2 and then falls rapidly.[4] No oxides of nitrogen were observed in the N_2-O_2 mixtures, possibly because of the low sensitivity for their detection by optical absorption. Light emission is observed in these systems and interferes with absorption measurements. Light emission may, however, offer a means to study NO formation since emission is observed both in the second positive system of N_2 ($C^3\Pi_u \rightarrow B^3\Pi_g$) for (1,0), (0,0), and (0,1), and in the gamma system of NO ($A^2\Sigma^+ \rightarrow X^2\Pi_r$) for (0,1), (0,2), (0,3), (0,4), and (0,8). The strongest emission from N_2 is in the (0,0) transition and from NO in the (0,2) transition. The maximum emission, either from N_2 or NO, occurs at very low O_2 concentrations [11 ppm O_2 or pure N_2 (3 ppm O_2)]. Emission is much less at 495 ppm O_2, and in air there is no detectable NO emission and only faint N_2 emission. The maximum emission from N_2 occurs during the pulse, followed by decay with a lifetime ~1 μsec. The NO emission reaches a maximum in 2 to 3 μsec and undergoes first-order decay with a lifetime of 3 to 5 μsec; the decay is not very sensitive to O_2 concentration in the range 11 to 1100 ppm. Measurements of NO ($v = 1$) quenching in NO-Ar and NO-N_2 mixtures gave $P = 2.1 \times 10^{-4}$ for NO and $<10^{-6}$ for Ar and N_2. Efficiencies of NO, Ar, and N_2 as the third body in the reaction O + NO + M were also estimated.

---

[1] Department of Chemistry, Maryville College, Maryville, Tenn.

[2] C. J. Hochanadel, J. A. Ghormley, and P. J. Ogren, *J. Chem. Phys.* 50, 3075 (1969).

[3] J. A. Ghormley, C. J. Hochanadel, and J. W. Boyle, *J. Chem. Phys.* 50, 419 (1969).

[4] J. A. Ghormley, C. J. Hochanadel, and J. W. Boyle, *Chem. Div. Ann. Progr. Rept. May 20, 1967*, ORNL-4164, p. 41.

DENSITY AND REFLECTIVITY OF AMORPHOUS ICE

J. A. Ghormley C. J. Hochanadel

Ice formed when water vapor is condensed on a surface cooled to 140°K or below gives only broad bands by x-ray diffraction and is generally considered to be amorphous.[1] In studies of the radiation chemistry, surface properties, and thermodynamics of amorphous ice, we have visually examined many samples during crystallization and have seen no change in volume or other indication of the existence of ice with a density of 2.3 g/cm^3 reported recently.[2] This very high density was determined by computing the volume of a known weight of so-called "glassy" ice from photographs of a copper cone with and without the ice deposit.

We have now measured directly, by the buoyancy in liquid oxygen, the density of six samples of amorphous ice prepared by condensation of water vapor on a copper surface at temperatures from 82 to 110°K and deposition rates from 16 to 69 $\times 10^{-6}$ g cm^{-2} sec^{-1}, conditions comparable with those reported for preparation of "superdense" ice. The average density was 0.940 ± 0.012 g/cm^3, with no evidence for a "superdense" ice. Other samples, prepared under a wide variety of conditions by deposition on copper or aluminum or on glass in an all-glass system, all floated in liquid oxygen and sank in liquid nitrogen, indicating a density between 1.14 and 0.808 g/cm^3.

When samples of amorphous ice were observed visually during warming, the change in appearance from translucent to opaque white was so gradual it was not possible to determine the time or temperature at which the change occurred. However, by using a photomultiplier we were able to follow the reflectivity continuously during buildup and warming of the ice; results from a typical sample are shown in Fig. 4.3. Diffuse reflectivity of the ice increased slowly during deposition and continued a slow increase when deposition was stopped and warming begun. At about 150°K a small decrease in reflectivity was usually observable, followed at about 153°K, where crystallization occurs, by a small but sudden rise in reflectivity followed by a continuous increase to a maximum at 210°K. At this point the reflectivity was about 90% of that of freshly deposited MgO. Any large change in density of the ice during crystallization would be expected to break up

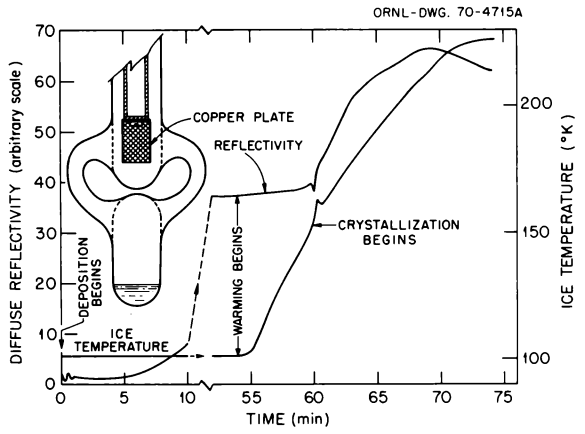

Fig. 4.3. Diffuse Reflectivity of a Typical Sample of Ice During Initial Period of Deposition on a Black Surface at 101°K and During Subsequent Warming.

the deposit and cause a significant increase in reflectivity accompanying the sudden rise in temperature which indicated crystallization. A thin layer of amorphous ice greatly reduced the specular reflectivity of polished copper.

[1] J. A. Ghormley, *J. Chem. Phys.* 48, 503 (1968).

[2] A. H. Delsemme and A. Wenger, *Science* 167, 44 (1970).

REDUCTION OF CERIUM(IV) IN AQUEOUS 4.0 *M* H_2SO_4 SOLUTIONS INDUCED BY HYDROLYSIS OF PEROXYDISULFURIC ACID

H. A. Mahlman T. J. Sworski

We previously reported[1] evidence for a primary yield of SO_4^- radicals in the radiolysis of aqueous sulfuric acid solutions. This evidence was obtained from a kinetic study of the effect of variations in both cerium(III) concentration and either formic acid or 2-propanol concentration on cerium(IV) reduction in aqueous 4.0 *M* H_2SO_4 solutions. We assumed for our kinetic study, as previously reported,[2] that any peroxymonosulfuric acid and peroxydisulfuric acid formed during irradiation were stable products.

Mariano[3] recently reported that both peroxymonosulfuric acid and peroxydisulfuric acid do react with cerium(IV) in sulfuric acid solutions. To remove any doubt in our mind about the validity of our kinetic evidence for a primary yield of SO_4^- radicals, we investigated the reduction of cerium(IV) induced by hydrolysis of peroxydisulfuric acid in aqueous 4.0 *M* H_2SO_4 solutions. Peroxydisulfuric acid reportedly[4] hydrolyzes in sulfuric acid solutions to yield peroxymonosulfuric acid, which further hydrolyzes to yield hydrogen peroxide. Some typical results are shown in Fig. 4.4.

When the initial cerium(III) concentration is 0.026 *M*, the reduction of cerium(IV) is attributable solely to reduction by hydrogen peroxide according to the following expressions:

$$d[H_2S_2O_8]/dt = -k_1[H_2S_2O_8] , \quad (I)$$

$$d[H_2SO_5]/dt = k_1[H_2S_2O_8] - k_2[H_2SO_5] , \quad (II)$$

$$d[H_2O_2]/dt = k_2[H_2SO_5] - k_3[Ce^{IV}]^2[H_2O_2]/[Ce^{III}] , \quad (III)$$

$$d[Ce^{IV}]/dt = -k_3[Ce^{IV}]^2[H_2O_2]/[Ce^{III}] , \quad (IV)$$

$$d[Ce^{III}]/dt = -d[Ce^{IV}]/dt . \quad (V)$$

We have previously determined[5] the value of k_3 in aqueous 4.0 *M* H_2SO_4 solutions. Values for k_1 and k_2

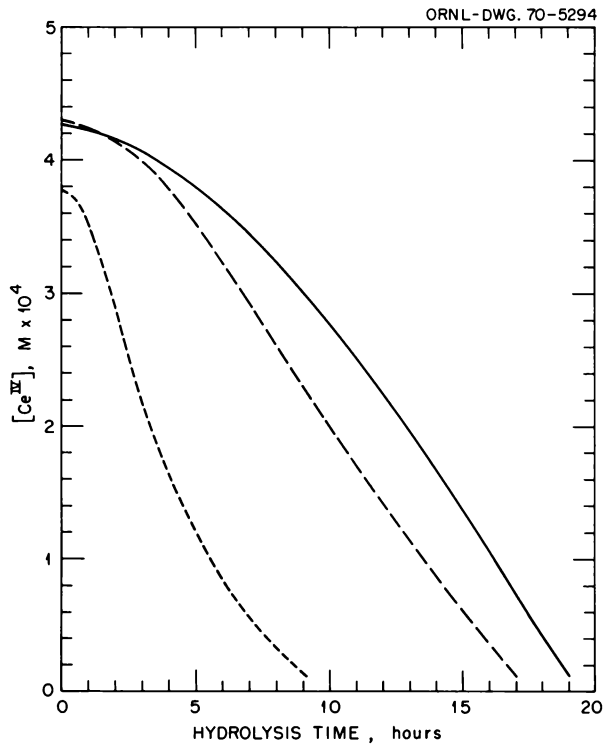

Fig. 4.4. Reduction of Cerium(IV) Induced by Hydrolysis of 0.01 *M* Peroxydisulfuric Acid in Aqueous 4.0 *M* H_2SO_4 Solutions at 25°C. Initial concentrations of cerium(III): —— 0.026 *M*; --- 0.0026 *M*; —— 0.00026 *M*.

are being determined by numerical integration of Eqs. (I)–(V) and are about 4×10^{-5} and 4×10^{-7} sec^{-1} respectively.

The marked inflection in the curves of Fig. 4.4 for cerium(III) concentrations of 0.0026 and 0.00026 *M* is attributed to reduction of cerium(IV) by peroxymonosulfuric acid, inhibited by high concentrations of cerium(III), in agreement with Mariano.[3] No kinetic study of cerium(IV) reduction by peroxymonosulfuric acid has been previously reported. We have been able to interpret our results quite well by assuming the following reaction mechanism:

$$Ce^{IV} + H_2SO_5 \rightleftharpoons Ce^{III} + H^+ + HSO_5 , \quad (4)$$

$$2HSO_5 + H_2O \rightarrow H_2SO_5 + H_2SO_4 + O_2 . \quad (5)$$

If we further assume that k_5 is negligibly small compared with k_{-4}, then the rate of cerium(IV) reduction by peroxymonosulfuric acid is given by:

$$d[Ce^{IV}]/dt = -2k_5k_4^2 [Ce^{IV}]^2 [H_2SO_5]^2/(k_{-4}[Ce^{III}])^2 . \quad (VI)$$

The value of $k_5k_4^2/k_{-4}^2$ is being determined by numerical integration of Eqs. (I)–(V), with Eqs. (II) and (IV) modified to take into account Eq. (VI), and is about 0.01.

We do not confirm the reaction between cerium(IV) and peroxydisulfuric acid reported by Mariano.[3] We conclude that reduction of cerium(IV) by both peroxydisulfuric acid and peroxymonosulfuric acid was negligible under the experimental conditions employed by Boyle[2] and in our determination of $G_{SO_4^-}$ in aqueous 4.0 *M* H_2SO_4 solutions.

---

[1] R. W. Matthews, H. A. Mahlman, and T. J. Sworski, *Chem. Div. Ann. Progr. Rept. May 20, 1969,* ORNL-4437, p. 52.

[2] J. W. Boyle, *Radiation Res.* **17**, 427 (1962).

[3] M. H. Mariano, *Anal. Chem.* **40**, 1662 (1968).

[4] H. Palme, *Z. Anorg. Chem.* **112**, 97 (1920).

[5] H. A. Mahlman, R. W. Matthews, and T. J. Sworski, *Chem. Div. Ann. Progr. Rept. May 20, 1968,* ORNL-4306, p. 61.

KINETIC EVIDENCE FOR A PRIMARY YIELD OF NO_3 RADICALS IN THE RADIOLYSIS OF AQUEOUS NITRIC ACID SOLUTIONS[1]

R. W. Matthews[2] H. A. Mahlman
T. J. Sworski

Evidence for a primary yield of SO_4^- radicals in the radiolysis of aqueous 4.0 *M* H_2SO_4 solutions was previously obtained[3] from a kinetic study of the effects of both cerium(III) and either formic acid or 2-propanol concentrations on cerium(IV) reduction. Similarly, a kinetic study of the effects of both cerium(III) and formic acid concentrations on cerium(IV) reduction has now yielded evidence for a primary yield of NO_3 radicals in the radiolysis of 4.0 *M* HNO_3 solutions.

At constant cerium(III) concentration, the dependence of $G(Ce^{III})$ in 4.0 *M* HNO_3 on formic acid concentration adheres well to:

$$G(Ce^{III}) = G(Ce^{III})^* + 2G^*_{OH}/\left(1 + (k_1[Ce^{III}] + k_2[HNO_3])/(k_4[HCOOH])\right) . \quad (I)$$

This suggests simple competition for the OH radical according to the following reaction mechanism:

$$OH + Ce^{III} \rightarrow OH^- + Ce^{IV} , \quad (1)$$

$$OH + HNO_3 \rightarrow H_2O + NO_3 , \quad (2)$$

$$NO_3 + Ce^{III} \rightarrow NO_3^- + Ce^{IV} , \quad (3)$$

$$OH + HCOOH \rightarrow H_2O + COOH , \quad (4)$$

$$COOH + Ce^{IV} \rightarrow CO_2 + H^+ + Ce^{III} . \quad (5)$$

Values of $G(Ce^{III})^*$, G^*_{OH}, and the kinetic parameter $(k_1[Ce^{III}] + k_2[HNO_3])/k_4$ were obtained for each cerium(III) concentration by fitting the experimental data to Eq. (I) by the method of least squares.[4]

The dependence on cerium(III) concentration of both G^*_{OH}, shown in Fig. 4.5, and the kinetic parameter, shown in Fig. 4.6, is clearly inconsistent with Eq. (I).

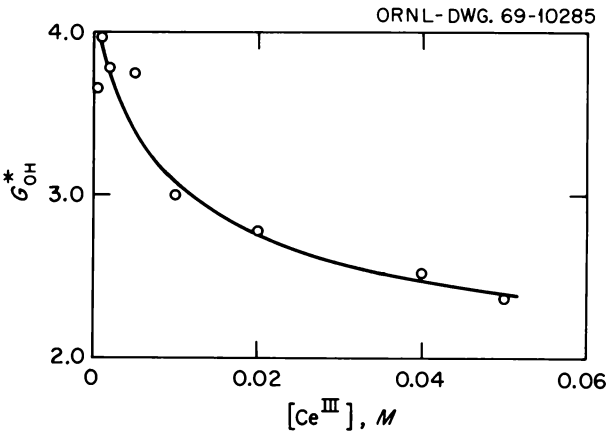

Fig. 4.5. Dependence of G^*_{OH} on Cerium(III) Concentration as Determined by Least-Squares Fit of the Experimental Data to Eq. (I).

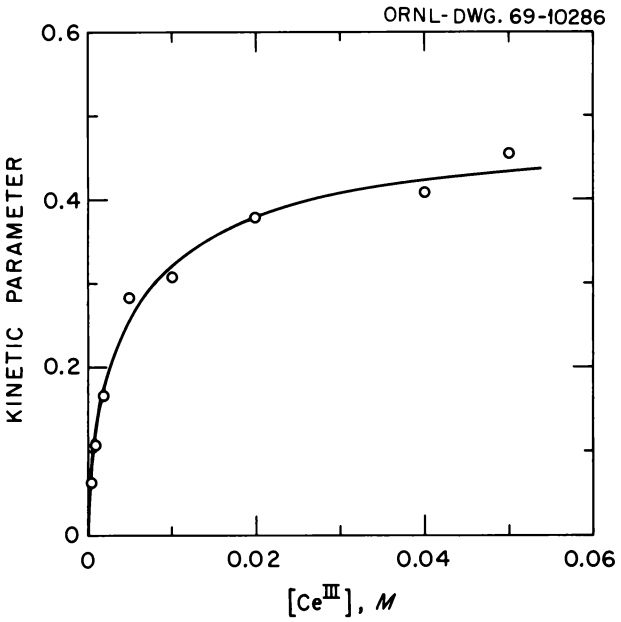

Fig. 4.6. Dependence of the Kinetic Parameter $(k_1[Ce^{III}] + k_2[HNO_3])/k_4$ on Cerium(III) Concentration as Determined by Least-Squares Fit of the Experimental Data to Eq. (I).

The kinetic parameter should be a linear function of the cerium(III) concentration, while G^*_{OH} should be essentially constant. This inconsistency is only another example of why one should vary the concentration of more than one solute in a kinetic study.

A similar dependence of both G^*_{OH} and kinetic parameter on cerium(III) concentration was previously observed[3] in 4.0 *M* H_2SO_4 solutions, perhaps for the same reason. Therefore, we assume for the radiolysis of nitric acid solutions that (1) there is a primary yield of NO_3 radicals and (2) the NO_3 radical can react also with formic acid:

$$NO_3 + HCOOH \rightarrow NO_3^- + H^+ + COOH \,. \qquad (6)$$

Then the dependence of $G(Ce^{III})$ on cerium(III) and formic acid concentrations should be given by

$$G(Ce^{III}) = G(Ce^{III})^* + \frac{2G_{OH}\left(1 + k_2[HNO_3]/\left(k_4[HCOOH]\left(1 + k_3[Ce^{III}]/(k_6[HCOOH])\right)\right)\right)}{1 + (k_1[Ce^{III}] + k_2[HNO_3])/(k_4[HCOOH])}$$

$$+ 2G_{NO_3}/\left(1 + k_3[Ce^{III}]/(k_6[HCOOH])\right) \,. \qquad (II)$$

The experimental data adhere well to Eq. (II), and a least-squares fit[4] yields values of $G_{OH} = 2.04 \pm 0.09$, $G_{NO_3} = 1.56 \pm 0.12$, $k_1/k_4 = 4.0 \pm 0.9$, $k_2[HNO_3]/k_4 = 0.21 \pm 0.03$, $k_3/k_6 = 143 \pm 11$, and eight values of $G(Ce^{III})$ for eight cerium(III) concentrations.

Whereas our relative reactivities[3] of SO_4^- with Ce(III), formic acid, and 2-propanol agree well with published[5] values of absolute rate constants, our relative reactivities of NO_3 with Ce(III) and formic acid are in serious disagreement with published[5] values which yield $k_3/k_6 = 1.8$.

---

[1] Presented at the XXII International Congress of Pure and Applied Chemistry, Sydney, Australia, Aug. 20–27, 1969.

[2] Visiting scientist from the Australian Atomic Energy Commission Research Establishment, Lucas Heights, New South Wales.

[3] R. W. Matthews, H. A. Mahlman, and T. J. Sworski, *Chem. Div. Ann. Progr. Rept. May 20, 1969*, ORNL-4437, p. 52.

[4] M. H. Lietzke, *A Generalized Least-Squares Program for the IBM 7090 Computer*, ORNL-3259 (Mar. 21, 1962).

[5] L. Dogliotti and E. Hayon, *J. Phys. Chem.* 71, 3802 (1967).

PRIMARY PROCESSES IN THE RADIOLYSIS OF WATER

T. J. Sworski

Kinetic evidence was previously reported[1] for a new unobserved primary product in the radiolysis of water: "excited water," which decays by a first-order process. Excited water, instead of e^-(aq), was claimed to be the principal precursor of molecular hydrogen in the spur; it was proposed to be electronically excited water in equilibrium, by a shift of an H atom in a hydrogen bond, with the H_3O-OH radical pair. An increase in yield of excited water with increase in LET was attributed[2] to formation of excited water via electron capture by H_2O^+.

Faraggi and Desalos[3] confirmed that the dependence of G_{H_2} on solute concentration was consistent with a precursor of hydrogen which decays by a first-order process. They proposed that H^- was the primary product which reacts with water by a pseudo first-order

process to yield hydrogen as proposed originally by Platzman,[4]

$$H^- + H_2O \rightarrow H_2 + OH^- . \quad (1)$$

This proposal suffers from the lack of any mechanism for an increase in yield of H^- with increase in LET.

Draganic and Draganic[5] reported that the dependence of $G_{H_2O_2}$ on solute concentration was also consistent with a precursor of hydrogen peroxide which decays by a first-order process, but they attached no significance to it. Sawai and Hamill[6] also reported that the dependence of $G_{H_2O_2}$ on chloride ion concentration was consistent with a precursor of hydrogen peroxide which decays by a first-order process and proposed that excited water was the dry H_2O^+-e^- ion pair. They presented evidence that the nitrate ion reacts with dry H_2O^+ (precursor of OH radical) to yield the NO_3 radical,

$$H_2O^+ + NO_3^- \rightarrow H_2O + NO_3 , \quad (2)$$

and also with dry e^- to reduce G_{H_2} ,

$$e^- + NO_3^- \rightarrow NO_3^{2-} . \quad (3)$$

Our determinations of $G_{OH} = 2.04 \pm 0.09$ and $G_{NO_3} = 1.56 \pm 0.12$ for 4.0 *M* HNO_3 solutions[7] and $G_{OH} = 1.78 \pm 0.03$ and $G_{SO_4^-} = 0.94 \pm 0.03$ for 4.0 *M* H_2SO_4 solutions (the previously reported[8] values for 4.0 *M* H_2SO_4 solutions have been changed as a result of taking into consideration the hydrolysis of the SO_4^- radical) may invalidate the proposal of Sawai and Hamill. With the approximation that energy partition between water and acid is proportional to the electron fraction of each component, G_{OH} for acid water can be calculated from the sulfuric and nitric acid yields: $1.78/0.70 = 2.54 \pm 0.05$ and $2.04/0.79 = 2.58 \pm 0.12$, equal within standard errors and equal to the reported[9] value for pure water of $G_{OH} = 2.59$. The proposal of Sawai and Hamill would be valid only under the unlikely conditions that an increase in H_2O^+ yield by occurrence of reaction (3) would be compensated by an equal loss in yield of H_2O^+ by occurrence of reaction (2). A conclusion which may be more valid is that neither 4.0 *M* nitrate ion nor 4.0 *M* sulfuric acid anions have any effect on formation of OH radical from H_2O^+.

[1] T. J. Sworski, *Advan. Chem. Ser.* **50**, 263 (1965).

[2] T. J. Sworski, p. 315 in *The Chemistry of Ionization and Excitation*, Taylor and Francis Ltd., London, 1967.

[3] M. Faraggi and J. Desalos, *Intern. J. Radiation Phys. Chem.* **1**, 335 (1969).

[4] R. L. Platzman, "Physical and Chemical Aspects of Basic Mechanisms in Radiobiology," *Natl. Acad. Sci.–Natl. Res. Council, Publ.* **305**, 22 (1953).

[5] Z. D. Draganic and I. G. Draganic, *J. Phys. Chem.* **73**, 2571 (1969).

[6] T. Sawai and W. H. Hamill, *J. Chem. Phys.* **52**, 3813 (1970).

[7] R. W. Matthews, H. A. Mahlman, and T. J. Sworski, "Kinetic Evidence for a Primary Yield of NO_3 Radicals in the Radiolysis of Aqueous Nitric Acid Solutions," preceding contribution, this report.

[8] R. W. Matthews, H. A. Mahlman, and T. J. Sworski, *Chem. Div. Ann. Progr. Rept. May 20, 1969*, ORNL-4437, p. 52.

[9] C. J. Hochanadel and R. Casey, *Radiation Res.* **25**, 198 (1965).

ENERGY TRANSFER AND THE RADIOLYSIS OF LIQUID ALIPHATIC CARBOXYLIC ACIDS

A. R. Jones

The energy of fast charged particles decelerating in organic matter is thought to be absorbed by the electrons of the matter to yield electronically excited and ionized molecules in a variety of states. The stabilization and interaction of these excited and ionized molecules is commonly held to produce a conglomeration of chemically active species – atoms, free radicals, radical ions, electrons, and stable and excited product molecules – which then interact in complex fashion.

It has been found, however, that the products of the radiolytic decomposition of some organic compounds apparently result from a single specific decomposition of the parent molecule. This effect has been most extensively investigated for the alpha radiolysis of the homologous series of normal aliphatic carboxylic acids. It was concluded that 90%[1] or 95%[2] of the carbon-to-carbon bond breakage caused by the radiolysis occurred at the R–COOH bond and that there was no evidence of a variety of free radical decompositions.[3]

Such selective bond breakage must be due to selective localization of electronic energy; that is, the energy must be localized on a molecule before its bonds are broken or it is ionized. In order to provide further information pertinent to this process, the gamma radiolysis of the homologous series of linear aliphatic acids is being studied. The results of this work have confirmed the reference reports that selective bond breakage is produced by radiolysis. For the first 24 members of the series the production of carbon dioxide is linear with dose to about 3% decomposition of the

starting material. No acids of lower molecular weight than the starting material were detected in samples radiolyzed to 30% decomposition, showing that decarboxylation is the only radiolytically induced alteration of the carbon skeleton. The carbon dioxide yields were unaffected by the presence of iodine, water, and oxygen. They were temperature independent when the acids were irradiated in the liquid state. Above C_2 the carbon dioxide yields decreased smoothly as the chain length increased. Dimerization in the alpha position, demonstrating the formation of the corresponding free radical, occurred only in the presence of water.

A simple explanation of the behavior of the carboxylic acid homologs is that a random absorption of energy occurs in the material arising purely from the Coulombic interactions of the secondary electrons with the electrons of whatever part of a long-chain carboxylic acid molecule is within effective distance of the track, that there is no exchange of energy intra- or intermolecularly, and that a direct decomposition of those molecules containing electronic energy at the site of chemical change takes place. The alternative, that a preferential attack by electrons or hydrogen atoms occurs at the position of chemical change, appears unlikely since the presence of scavengers of these

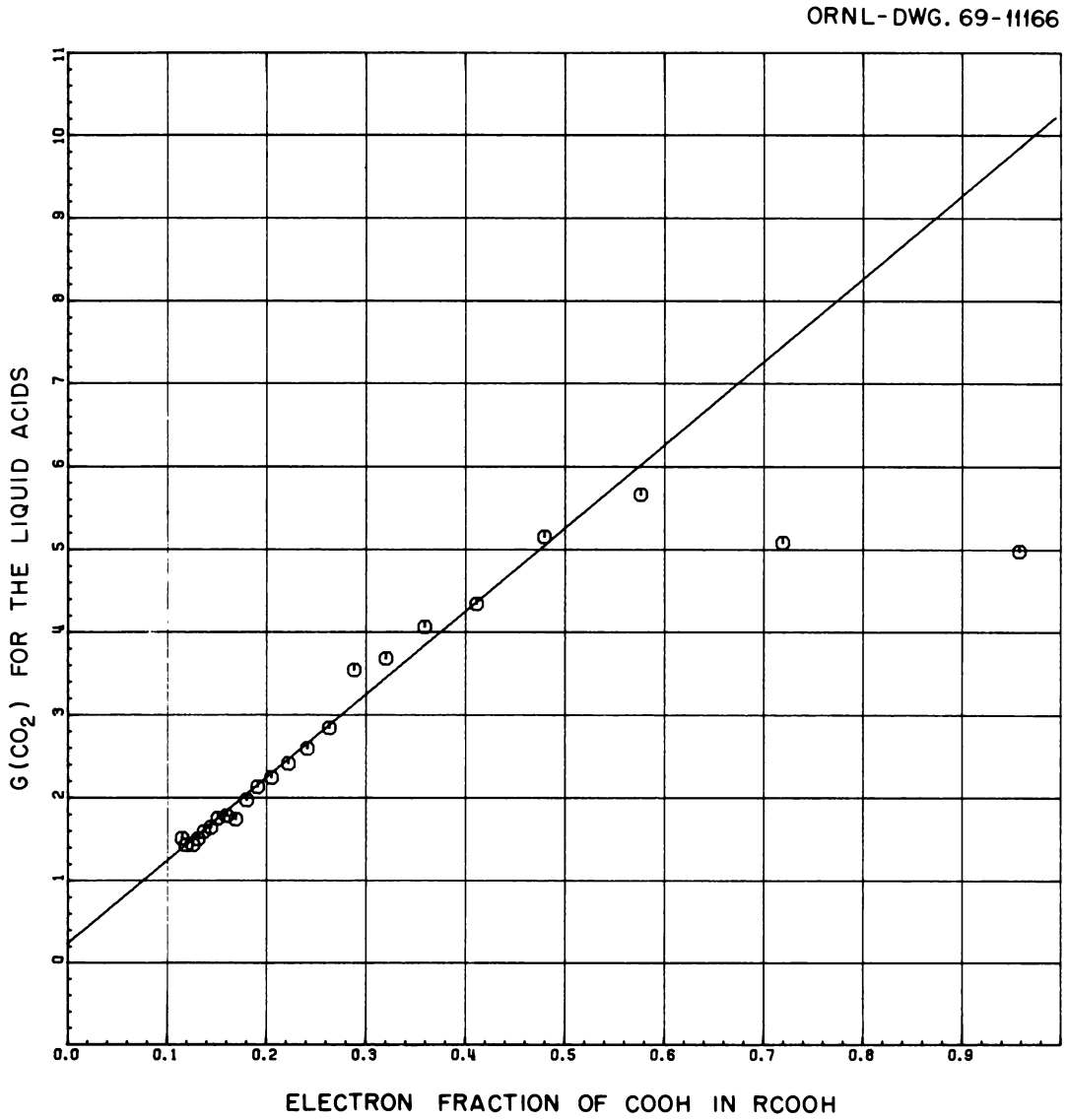

Fig. 4.7. Correlation of the Yield of Carbon Dioxide from the Gamma Radiolysis of Liquid Normal Aliphatic Carboxylic Acids with the Carboxylic Electron Fraction in the Acid.

reactive fragments (oxygen, iodine, or water) does not affect the yield of CO_2.

This proposal is easily tested, since with these assumptions a plot of the carbon dioxide yields from each acid vs the electron fractions of COOH in each acid should give a straight line. Such a relationship is indeed found and is shown in Fig. 4.7. Excluding the points which represent formic and acetic acids, a straight line may be drawn satisfactorily through the remaining yield values; it passes as closely as one might hope through a zero yield of carbon dioxide for an electron fraction of COOH equal to zero.

[1] R. E. Honig, *Science* **104**, 27 (1946).

[2] C. W. Sheppard and V. L. Burton, *J. Am. Chem. Soc.* **68**, 1636 (1946).

[3] W. L. Whitehead, C. Goodman, and I. A. Breger, *J. Chim. Phys.* **48**, 184 (1951).

RADIATION AND HOT-ATOM CHEMISTRY OF INORGANIC CRYSTALLINE SOLIDS

CHEMISTRY OF ^{128}I AND ^{130}I RECOILS IN NEUTRON-IRRADIATED CRYSTALLINE POTASSIUM IODATE AND POTASSIUM PERIODATE[1]

G. E. Boyd Q. V. Larson

Radioactive ^{128}I and ^{130}I recoils formed by neutron capture in crystalline KIO_3 and KIO_4 appeared as iodide, iodate, and periodate ions on analysis of alkaline aqueous solutions of the irradiated solids. With KIO_3 more than two-thirds of the radioiodine was retained as radioiodate, and small amounts of radioperiodate were found. With KIO_4 nearly 90% of the recoils appeared as radioiodate, while the periodate retention was slightly less than 10%. The relative concentrations of the radioiodine oxidation states varied with the time and temperature of the neutron bombardment. Radioiodide was readily converted to iodate and periodate on heating or on exposing the neutron-irradiated solids to ^{60}Co gamma rays. Iodine-131 added in tracer concentrations to crystalline KIO_3 or KIO_4 as iodide ion was rapidly oxidized to iodate and to periodate on heating the solids above room temperature. There was only a small isotopic effect in the yields of the iodine valence states in which ^{128}I and ^{130}I were combined.

[1] Abstract of published paper: *J. Am. Chem. Soc.* **91**, 4639 (1969).

INVESTIGATIONS ON THE THERMAL AND RADIOLYTIC DECOMPOSITION OF ANHYDROUS CRYSTALLINE POTASSIUM CHLORITE[1]

G. E. Boyd L. C. Brown[2]

Measurements of the radiolysis at *ca.* 38° of anhydrous crystalline $KClO_2$ by ^{60}Co gamma rays showed that the chlorite ion decomposed in the solid (Fig. 4.8) via the overall reaction

$$3ClO_2^- \rightsquigarrow Cl^- + 2ClO_3^- .$$

Radiolytic yields for a dose of 1.0×10^{23} eV per mole of $KClO_2$ were: $G(-ClO_2^-) = 33.5 \pm 1.7$; $G(Cl^-) = 10.7 \pm 0.2$; $G(ClO^-) = 0.0$; $G(ClO_3^-) = 22.5 \pm 0.8$; and $G(ClO_4^-) = 0.0$ molecule per 100 eV absorbed. The energy absorbed (3.3 eV/molecule) in the decomposition of ClO_2^- was nearly the same as that required to break a Cl–O bond. The thermal decomposition of $KClO_2$ was strongly exothermic between 135 and 165°, and the stoichiometry of the reaction was identical with that observed in the radiolysis (Fig. 4.9). A reaction mechanism based on the production of oxygen atoms and their addition to ClO_2^- ions in the crystal lattice was suggested.

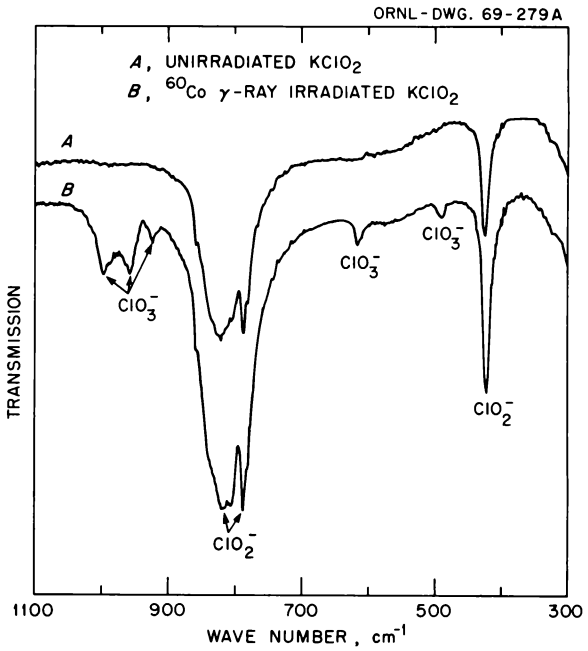

Fig. 4.8. Infrared Absorption Spectrum of $KClO_2$(c) at Room Temperature. KBr pellet technique: concentration of $KClO_2$ *ca.* 0.2% by weight; dose to irradiated $KClO_2$: 1.0×10^{23} eV/mole.

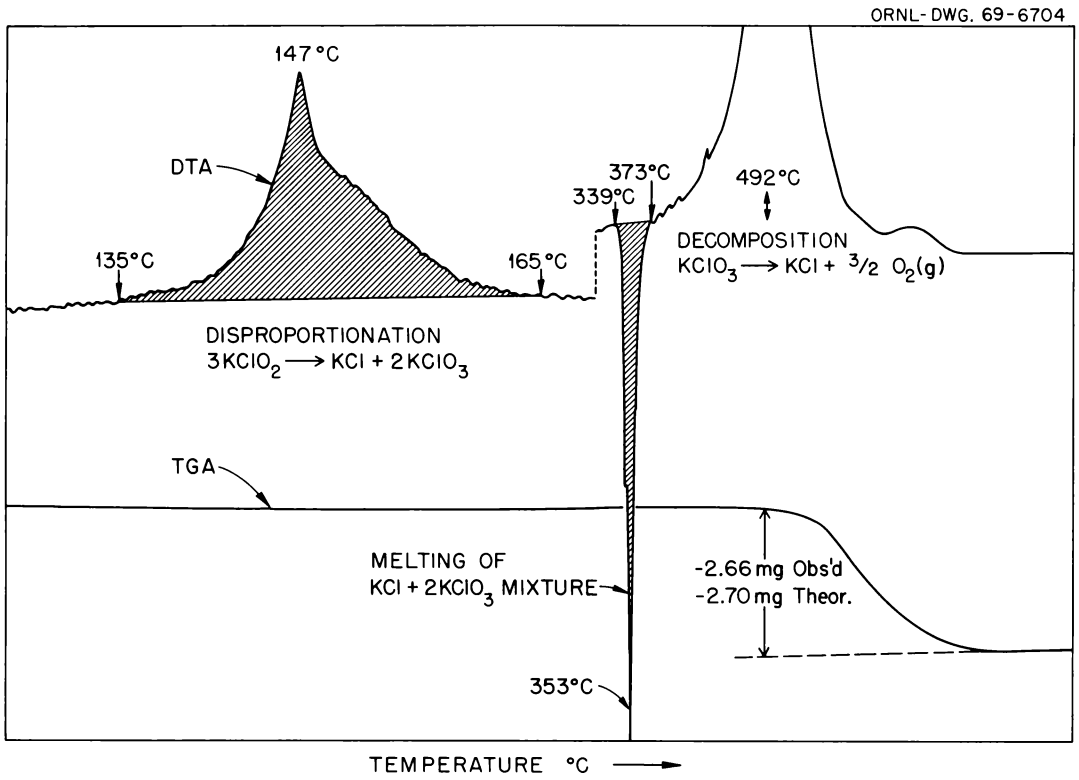

Fig. 4.9. Thermal Analysis Data for the Decomposition of $KClO_2$ (c). 9.0-mg sample heated in argon gas at 6°/min to 120°, then at 0.5°/min to 175° and at 6°/min to 600°C.

[1]Abstract of published paper: *J. Phys. Chem.* 74, 1691 (1970).

[2]Now with the Isotopes Division.

FURTHER OBSERVATIONS ON PRODUCTS FORMED IN THE RADIOLYSIS OF ALKALI-METAL HALATES AND PERHALATES BY ^{60}Co GAMMA RAYS[1]

G. E. Boyd L. C. Brown[2]

Spectroscopic and chemical techniques were employed to identify and measure the concentrations of the stable radiolytic products formed at room temperature in crystalline $KClO_3$, $CsBrO_3$, $CsIO_3$, $KClO_4$, $KBrO_4$, and KIO_4 by ^{60}Co gamma rays. The ultraviolet absorptions of $KClO_3$ (Fig. 4.10) and $CsBrO_3$ (Fig. 4.11) measured with diffuse reflectance techniques indicated the presence of ClO^-, ClO_2^-, and O_3^-, and of BrO^- and O_3^- ions, respectively, in these solids. The spectrum of heavily irradiated $CsIO_3$, however, showed no new features except for a broad band at 460 nm attributable to I_2 in the crystal. The infrared absorptions of $KClO_4$ (Fig. 4.12), $KBrO_4$ (Fig. 4.13), and KIO_4 (Fig. 4.14) showed that ClO_3^- and ClO_2^-, BrO_3^-, and IO_3^- ions, respectively, were formed by radiolysis.

Chemical determinations (Fig. 4.15) of the amounts of BrO^-, BrO_2^-, and BrO_4^- ions[3] produced in $CsBrO_3$ by increasing gamma-ray exposure revealed that constant concentrations were approached for large doses, suggesting that decomposition reactions of a thermal and/or radiolytic nature must occur. The rate of increase in the BrO^- ion concentration at very low dose suggested that this species is not a primary radiolysis product. The excess oxidizing power of $CsBrO_3$ above that from hypobromite and bromite ions was attributed to O_3^- ion rather than to BrO_2 as assumed earlier.

A synopsis of the current state of knowledge about the radiolysis of halate ions in crystals is given.

---

[1]Expanded abstract of paper submitted to the *Journal of Physical Chemistry* (1970).

[2]Now with the Isotopes Division.

[3]Perbromate ion, BrO_4^-, was determined by the microanalytical method described in the following contribution, this report, "Microanalytical Method for Determination of Perbromate Ion in the Presence of Macro Amounts of Other Bromine Anions" by L. C. Brown and G. E. Boyd.

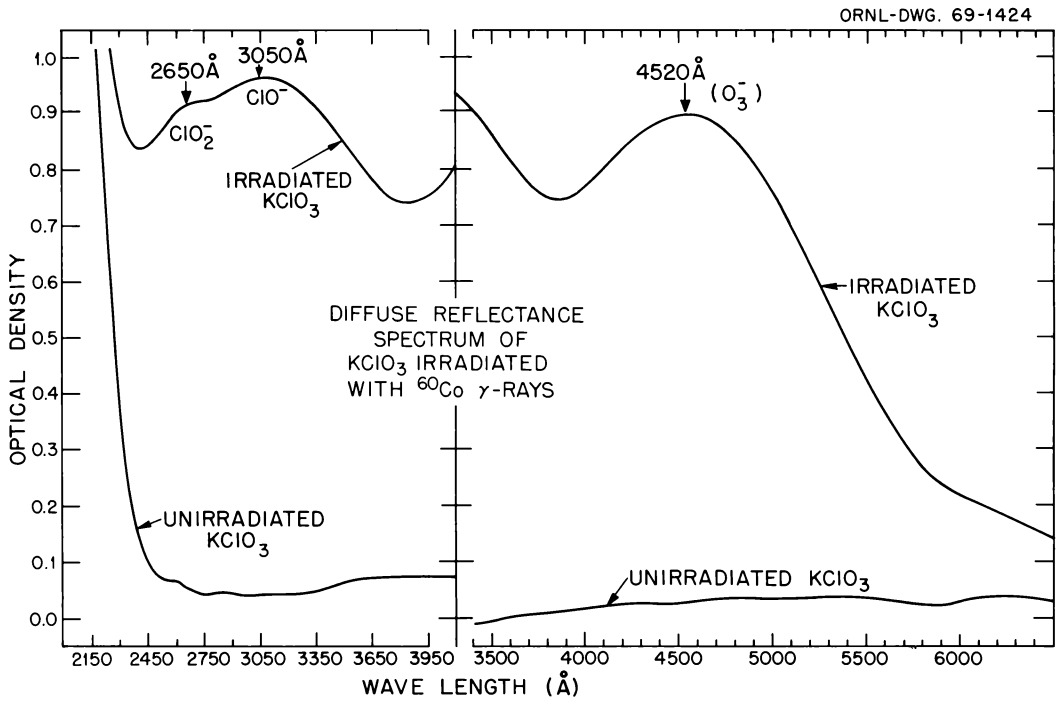

Fig. 4.10. Diffuse Reflectance Spectrum of Crystalline $KClO_3$ Irradiated at 35°C with ^{60}Co Gamma Rays. Absorbed dose = 4.1×10^{23} eV/mole.

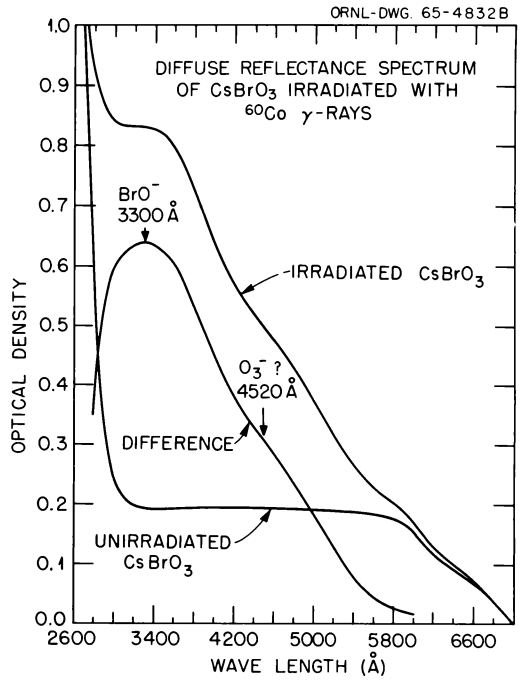

Fig. 4.11. Diffuse Reflectance Spectrum of Crystalline $CsBrO_3$ Irradiated at *ca.* 35° with ^{60}Co Gamma Rays. Absorbed dose = 2.2×10^{24} eV/mole.

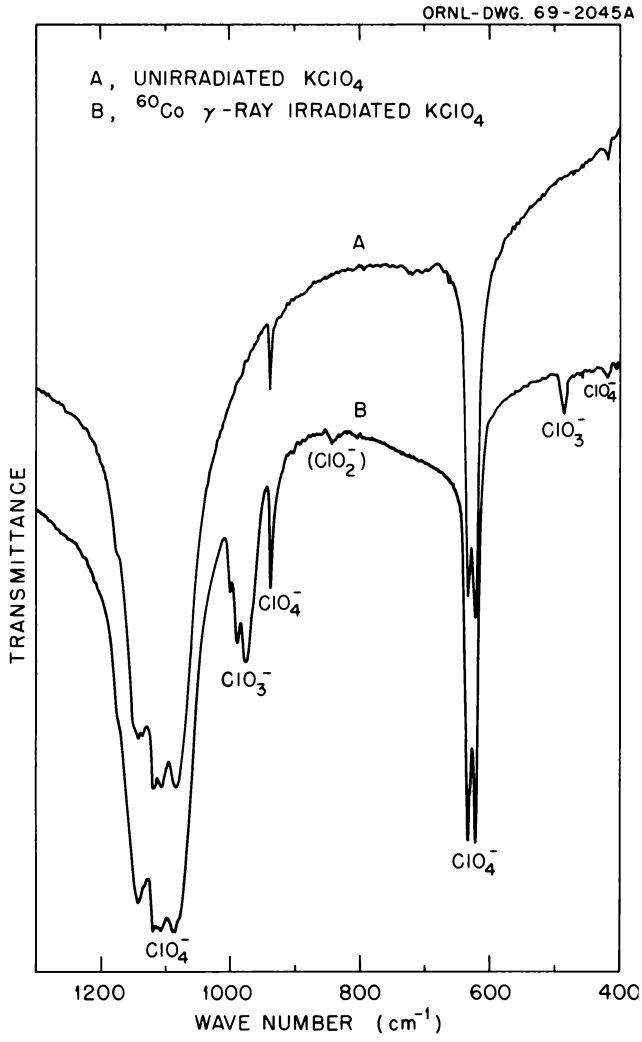

Fig. 4.12. Infrared Spectrum of Crystalline $KClO_4$ Irradiated at *ca.* 35° with ^{60}Co Gamma Rays. Absorbed dose = 1.7 × 10^{24} eV/mole; KBr pellet technique.

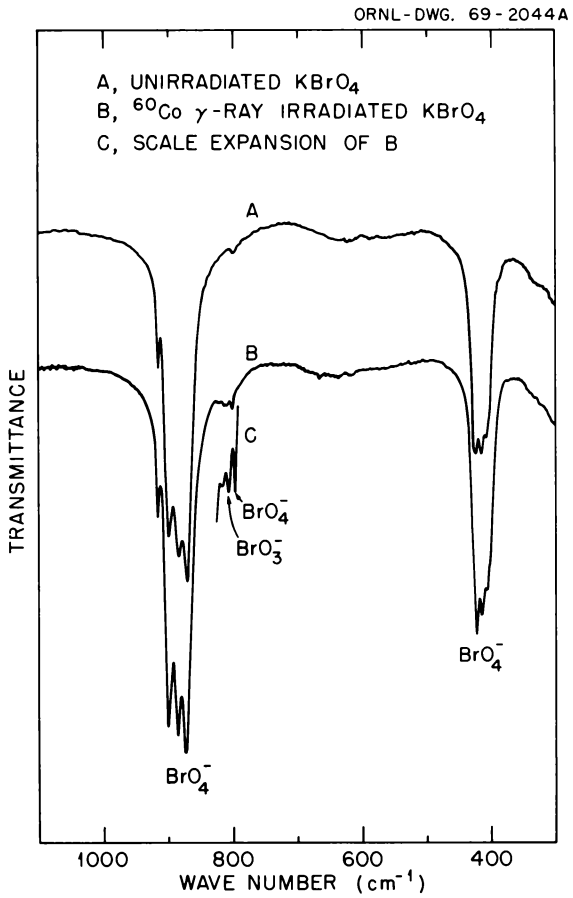

Fig. 4.13. Infrared Spectrum of Crystalline $KBrO_4$ Irradiated at *ca.* 35° with ^{60}Co Gamma Rays. Absorbed dose = 1.5 × 10^{23} eV/mole; KBr pellet technique; 0.2 wt % $KBrO_4$ in KBr.

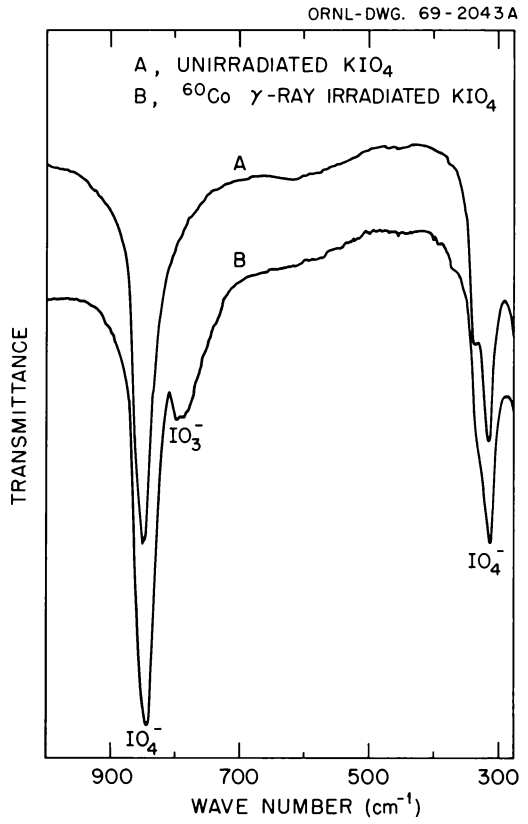

Fig. 4.14. Infrared Spectrum of Crystalline KIO_4 Irradiated at *ca.* 35° with ^{60}Co Gamma Rays. Absorbed dose = 1.9 × 10^{24} eV per mole of KIO_4; KBr pellet technique.

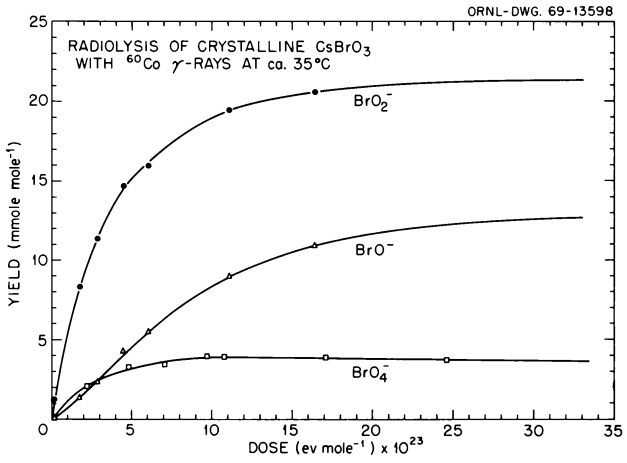

Fig. 4.15. Dose Dependence of the Concentrations of Radiolytic Products Formed at *ca.* 35° in Crystalline $CsBrO_3$ by ^{60}Co Gamma Rays.

MICROANALYTICAL METHOD FOR DETERMINATION OF PERBROMATE ION IN THE PRESENCE OF MACRO AMOUNTS OF OTHER BROMINE ANIONS[1]

L. C. Brown[2] G. E. Boyd

The need for a sensitive, rapid, and convenient analytical method for the determination of perbromate ion in its compounds and in the presence of much larger concentrations of bromate and/or bromide ion arose as a consequence of the discovery of BrO_4^- ion in radiolyzed crystalline $KBrO_3$ and $CsBrO_3$.[3]

Previous analyses[4,5] for perbromate have employed either reduction to Br_3^- by 12 *M* HBr followed by Br_3^- oxidation of I^- to I_3^- which was titrated with thiosulfate, or reduction to Br^- by Mo(VI)-catalyzed $SnCl_2$ in 6 *M* HCl followed by chlorine oxidation of Br^- to BrCN in neutral cyanide solution, reduction of BrCN by acid iodide, and titration of I_3^- with thiosulfate. Both methods are accurate, but they are also long and tedious and work best for relatively pure BrO_4^- samples. If appreciable amounts of other bromine oxyanions are present, for example, BrO_3^-, a preliminary step must be performed in *ca.* 1.5 *M* HBr to reduce those species to Br_2, which is then sparged from solution with an inert gas.

The microanalytical procedure developed in this investigation was an adaptation of the Crystal Violet solvent-extraction–spectrophotometric method for the determination of ClO_4^- ion.[6] Concentrations of 1 to 10 × 10^{-6} *M* BrO_4^- ion were determined in the presence of 1000 times larger amounts of bromate or bromide ion with good accuracy.

---

[1] Résumé of published paper: *Anal. Chem.* **42**, 291 (1970).

[2] Now with the Isotopes Division.

[3] L. C. Brown, G. M. Begun, and G. E. Boyd, *J. Am. Chem. Soc.* **91**, 2250 (1969).

[4] E. H. Appelman, *J. Am. Chem. Soc.* **90**, 1900 (1968).

[5] E. H. Appelman, *Inorg. Chem.* **8**, 223 (1969).

[6] S. Uchikawa, *Bull. Chem. Soc. Japan* **40**, 798 (1967).

RADIOLYSIS OF ^{18}O-ENRICHED POLYCRYSTALLINE KNO_3

M. H. Brooker[1] G. E. Boyd

The effects of an oxygen atmosphere of normal isotopic abundance on the ^{60}Co gamma radiolysis of ^{18}O-enriched KNO_3 are being studied by infrared and Raman spectroscopy. Preliminary experiments show that atmospheric $^{16}O_2$ can be incorporated into the

reactant KNO_3 and into the radiolysis product KNO_2. Infrared and Raman vibrational-band assignments have been facilitated by earlier investigations[2-4] of the frequency shifts characteristic of nitrate and nitrite ions substituted to different degrees with ^{18}O.

Oxygen-18-enriched KNO_3 (51.7% ^{18}O) purchased from Isomet Corporation was used after treatment with Norit A decolorizing carbon in distilled water and subsequent recrystallization. The ^{18}O enrichment was determined by the Raman line intensity method.[4] Raman band intensities in the symmetric stretching region (ν_1) of the different isotopically substituted nitrate ions were in excellent agreement with calculated band intensities on the basis of a random distribution of the ^{18}O atoms (Table 4.1). Two samples of 51.7% ^{18}O-enriched KNO_3 were irradiated simultaneously in the center position of a ^{60}Co source to a dose *ca.* 2×10^{21} eV/g. One of the samples had been degassed at 120°C and sealed under vacuum (*ca.* 10^{-4} mm), while the other sample was left open to the atmosphere.

Vibrational bands characteristic of nitrate ion species were detected at 1271 and 1252 cm^{-1} in the infrared and at 806 and 787 cm^{-1} in the Raman spectra of both samples. These bands are assigned to the $N^{16}O_2^-$ and $N^{16}O^{18}O^-$ species respectively. The ^{18}O enrichment of the KNO_3 sample irradiated in air decreased from 51.7 to 41.6%, but no detectable change occurred in the sample irradiated in vacuo. Although the effect in air unequivocally indicates the existence of the back reaction

$$O + NO_2^- \rightarrow NO_3^- ,$$

the marked difference between samples irradiated in air and in vacuo emphasizes the importance of the reaction

$$O_2 \rightsquigarrow 2O .$$

Replacement of ^{16}O for ^{18}O in the NO_3^- ion during irradiation in air is not a random process but exhibits a selective isotopic effect. The percent of the total nitrate present as $N^{18}O_3^-$ and $N^{16}O^{18}O_2^-$ is greater than calculated on the basis of random distribution, whereas the $N^{16}O_2{}^{18}O^-$ and $N^{16}O_3^-$ species are less concentrated than calculated (Table 4.1). Previously, this effect had been noted in the form of a 13% lower nitrite yield for the irradiation of ^{18}O-enriched KNO_3.[5,6] It is unlikely that isotopic substitution could change the N–O force constant; therefore, it seems most probable that because of its greater mass, ^{18}O has a lower recoil velocity than ^{16}O after the reaction

$$NO_3^- \rightsquigarrow NO_2^- + O$$

and consequently is more easily retained on the original nitrate ion by the back reaction

$$NO_2^- + O \rightarrow NO_3^- .$$

[1] Visiting scientist; National Research Council of Canada Postdoctoral Fellow, 1969–70.

[2] M. H. Brooker and G. E. Boyd, "Infrared and Raman Spectral Studies on ^{18}O-Enriched Polycrystalline KNO_3," Chap. 7, this report.

[3] R. Kato and J. Rolfe, *J. Chem. Phys.* **47**, 1901 (1967).

[4] A. J. Melveger, E. R. Johnson, and E. N. Ladov, *J. Inorg. Nucl. Chem.* **32**, 337 (1970).

[5] H. B. Pogge and F. T. Jones, *J. Phys. Chem.* **74**, 1700 (1970).

[6] E. N. Ladov and E. R. Johnson, *J. Am. Chem. Soc.* **91**, 7601 (1969).

Table 4.1. Comparison Between Observed ^{18}O-Enriched NO_3^- Species Concentrations and Predicted Concentrations on the Basis of Random Distribution

	Percent of Total Nitrate			
	$N^{16}O_3^-$	$N^{16}O_2{}^{18}O^-$	$N^{16}O^{18}O_2^-$	$N^{18}O_3^-$
Original KNO_3 sample, not irradiated, 51.7% ^{18}O				
Observed	11.0	36.6	38.5	13.8
Calculated	11.0	36.7	38.6	13.8
Irradiated KNO_3 sample, *ca.* 2×10^{21} eV/g, 41.6% ^{18}O				
Observed	16.2	37.1	34.7	12.0
Calculated	19.9	42.5	30.5	7.2

5. Organic Chemistry

PREPARATION AND DEAMINATION OF 5-*exo*-PHENYL-5-HYDROXY-2-*exo*-NORBORNYLAMINE AND 5-*endo*-PHENYL-5-HYDROXY-2-*exo*-NORBORNYLAMINE

Ben M. Benjamin Clair J. Collins

Certain refinements in our measurements[1] of the yields of the products obtained on deamination of the title compounds (**1** and **2**) have now been made. The scheme for deamination of the two reactants is outlined in Chart I. The deaminations were carried out either with glacial acetic acid as a solvent or with glacial acetic acid–sodium acetate mixtures. Yields of the minor products were obtained by isotope dilution analysis, starting with labeled reactants **1** and **2**. The results are summarized in Table 5.1. From these data we can draw the following conclusions:

1. The carbonium ion intermediates are best interpreted as the classical Wagner-Meerwein pair A ⇌ B which do not reach equilibrium before they suffer attack to yield the products, for from **1** the ratio **5:6** is 2.3:1, whereas from **2** this ratio is 1:1.7.
2. The *rearranged* ion B (from **1**) and the rearranged ion A (from **2**) produce much smaller yields of *endo* products than the *unrearranged* ions (A from **1** and B from **2**), and we interpret these results to mean that pathways **1** → **4** and **2** → **7** take place through S_N2-like processes.
3. The product ratios **6:7** (from **1**) of 166 and **5:4** (from **2**) of 650 provide the first measurement of a lower limit for the stereospecificity of *exo:endo* attack by anion or solvent on a classical substituted norbornyl carbonium ion.

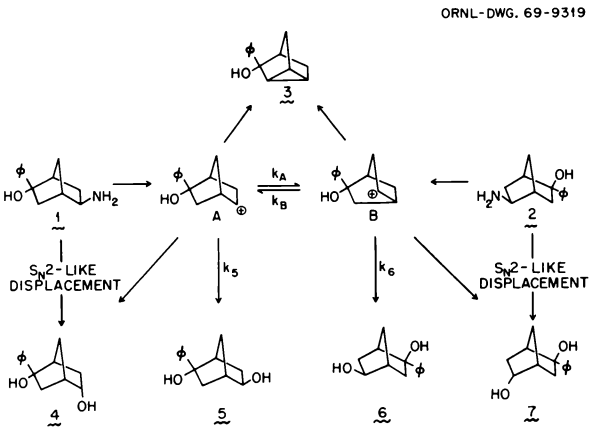

Chart I

Table 5.1. Yields of Products and Product Ratios on Deamination[a] of Amines 1 and 2 (See Chart I)

Products[b]	From 1		From 2
	Glacial HOAc	HOAc-NaOAc	HOAc-NaOAc
	Yields		
3	43.5	35.0	29.6
4	3.4[c]	2.4[c]	0.039[c]
5	36.7	43.5	25.6
6	16.5	19.0	42.6
7	0.075[c]	0.114	2.2[c]
	Ratios		
5:6	2.2:1	2.3:1	1:1.7
5:4	10.5:1	18:1	650:1
6:7	220:1	166:1	19:1
4:7	45:1	21:1	1:56

[a]Deaminations were performed at ambient temperature.

[b]The monoacetates of **4**–**7** were obtained on deamination, and these were converted to the diols with lithium aluminum hydride. Smaller yields of three other compounds[a] (resulting from hydride shift in the ions A and B) were also obtained.

[c]These products were crystallized repeatedly with the addition of hold-back carrier until the radioactivity contents were constant.

[1] B. M. Benjamin and C. J. Collins, *Chem. Div. Ann. Progr. Rept. May 20, 1969,* ORNL-4437, p. 57.

SYNTHESIS AND DEAMINATION OF 5-*exo*-HYDROXY-5-PHENYL-2-*endo*-NORBORNYLAMINE

Ben M. Benjamin Clair J. Collins

The title compound (**8** in Chart II)[1] was synthesized[2] and subjected to deamination in acetic acid–sodium

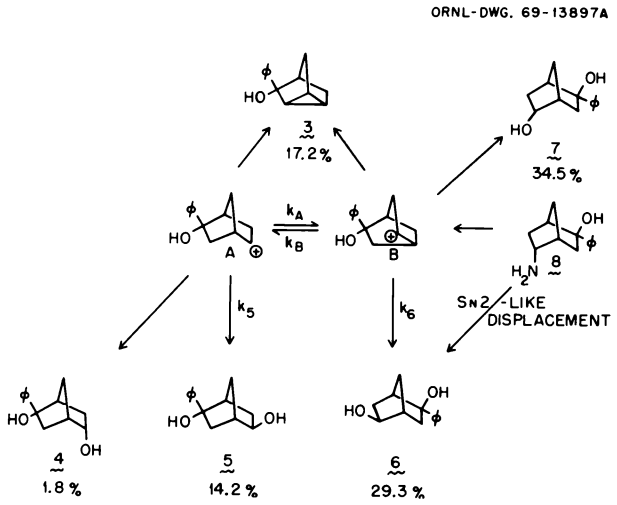

Chart II

acetate solution at room temperature. The mixture of products (as the acetates) was treated with lithium aluminum hydride, and the yields of **3** and the diols **4**–**7** were determined spectrally; these yields are shown under the appropriate structures in the chart. In addition, the products were isolated by column chromatography. In a second deamination of **8** the yield of **4** was determined with a ^{14}C isotope dilution experiment to be 1.8%, in agreement with our estimation of the yield by isolation.

From the data in the chart, the following conclusions can be drawn:

1. The isolation of diol **4** clearly means that the classical ion A must be its precursor. Thus classical ion B (B is attacked from the *exo* direction to yield **6**, and from the *endo* direction to yield **7**) undergoes Wagner-Meerwein rearrangement to classical ion A, which can be attacked from both the *exo* and *endo* directions to give **5** and **4** respectively. There is no evidence here for a bridged ion.
2. The ratio of the yields of diols **5** and **6** was 1:2.1 when they were obtained from **8** and was 1:1.7 (Table 5.1) when they were obtained from the *exo* amine **2** (Chart I); here we have further evidence for the presence of S_N2-like processes which for **2** would produce *endo* diol **7** (2.2%), but for **8** should result in an increase in the yield of **6** as compared with **5**. In addition, S_N2 attack from the *exo* direction on **8** should be favored over *endo* S_N2 attack on **2**; from the data it can be calculated that 2.2% of the *exo* amine **2** and at least 5% of the *endo* amine **8** undergo S_N2-like processes.
3. The relatively high total yield of **7** and **4** together, obtained from **8**, is significant; the *endo* diol **7** is produced in *greater* yield than the *exo* diol **6**, whereas deamination of **2** (Chart I) produces **6** and **7** in a ratio of 19:1 (Table 5.1). These results, we believe, offer clear evidence for the configuration-holding ability of the counter acetate ion.

---

[1]To preserve continuity and readability, the numbering system used in the preceding section is preserved.

[2]The synthesis was through the following route: norbornenone + PhMgBr → 2-*exo*-phenyl-2-norbornenol (borohydration) → 2-*exo*-phenyl-2-*endo*-hydroxy-5-*exo*-norbornenol (mixture) → 2-*exo*-phenyl-2-*endo*-hydroxy-5-*exo*-norbornyl tosylate (hydrolysis) → mixture of diols **5** and **6** (plus smaller yields of several other products). Diol **6** was oxidized with chromic acid to the ketone, which was converted to the oxime. The oxime was then treated with lithium aluminum hydride to yield the amine **8**. Elemental analyses and spectral data were consistent with the assigned structure.

DEGRADATION OF 2-*exo*-NORBORNEOL-^{14}C

Charles E. Harding[1] Clair J. Collins

In the past two years[2,3] we have reported our preliminary results on the "π-route"[4] and "σ-route"[5] syntheses of 2-*exo*-norbornyl acetate and the degradations which were worked out to determine ^{14}C distributions in the 1 and 2 positions of the title compound. Our experiments are now complete; they have been carried out with much higher levels of radioactivity (18.0 mCi ^{14}C per mole) than were used in our earlier[2] experiments.

Because a direct and unequivocal synthesis of 2-*exo*-norbornyl-4-^{14}C tosylate (compound **B**) appeared too difficult, we employed the so-called "π-route" synthesis.[4] Accordingly we prepared 2-(Δ^3-cyclopentenyl-1-^{14}C)-ethyl tosylate (compound **A**) by the method shown in abbreviated form in Chart III, starting with

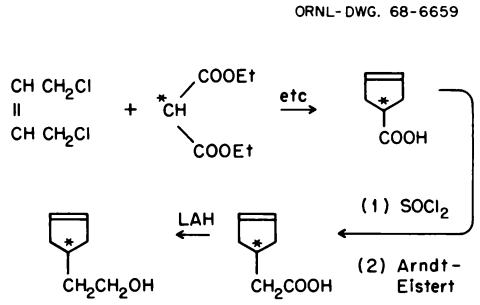

Chart III

cis-1,4-dichlorobutene-2 and malonic-2-^{14}C ester. The tosylate **A** was then acetolyzed[4,6] in buffered (with urea) acetic acid at 50.0 ± 0.2°. The labeled norbornyl-^{14}C acetate was isolated, and the distribution of ^{14}C at positions 1 and 2 was determined. The results are given in Table 5.2. The norbornyl-^{14}C acetate containing most of its ^{14}C at C_4 and a known fraction of its ^{14}C at C_1 and C_2 was converted to the tosylate **B** and acetolyzed in buffered acetic acid at 50.0 ± 0.2°. The product 2-*exo*-norbornyl-^{14}C acetate was reconverted to 2-*exo*-norbornyl-^{14}C tosylate and reacetolyzed. This procedure was repeated until a total of four acetolysis cycles were completed. The fractions of ^{14}C in C_2 were determined after the second and fourth cycles. The fraction of ^{14}C in C_1 was also determined after the fourth cycle. These results are also given in Table 5.2. The ^{14}C content of the 2 position of product was determined by reducing the 2-*exo*-norbornyl-^{14}C acetate with lithium aluminum hydride to 2-*exo*-norborneol-^{14}C, which was oxidized to 2-norbornanone-^{14}C. The ketone was treated with phenylmagnesium bromide, and the resulting product, after hydrolysis, was oxidized to benzoic-^{14}C acid, whose ^{14}C content was determined. The radioactivity in C_1 was determined by use of the degradative scheme outlined in last year's report.[3] The fraction of ^{14}C calculated for C_1 is subject to some uncertainty, for during the treatment of 2-*exo*-methylnorborneol-2 with formic acid,[7] the occurrence of 6,2 hydride shift would distribute the ^{14}C originally in C_1 between C_2 and C_6 of 1-methyl-2-*exo*-norborneol. Thus the radioactivity assay of the benzoic-^{14}C acid of Chart V in last year's report[3] is a minimum measure of the ^{14}C which has wandered to the 1 position during acetolysis of **A** or **B**.

Since in the acetolysis of **B** the reactant was prepared from the product of acetolysis of **A**, we must subtract the radioactivity already present (experiment 1, Table 5.2) in C_1 and C_2. By averaging the increase in ^{14}C content in C_1 and C_2 for four acetolysis cycles of **B**, we find that for each cycle the ^{14}C contents of C_1 and C_2 increase 0.25 and 0.15% respectively. From these data we calculate that the ratios of 6,2 hydride shift to 3,2 hydride shift in the acetolyses of **A** and **B**, are ⩽116 and ⩽250 respectively.

Table 5.2. Distribution of ^{14}C in Norbornyl-^{14}C Acetates

Experiment No.	Reactant	No. of Cycles	Percent ^{14}C in –	
			C_1	C_2
1	A	1	0.52	0.33
2	B	2		0.46
3	B	4	1.52	0.92

[1] Oak Ridge Graduate Fellow from University of Tennessee, Knoxville, under appointment with Oak Ridge Associated Universities. Present address: Chemisches Institut der Universität, Tübingen, Germany.

[2] V. F. Raaen, C. E. Harding, and C. J. Collins, *Chem. Div. Ann. Progr. Rept. May 20, 1968,* ORNL-4306, p. 66.

[3] C. E. Harding, V. F. Raaen, and C. J. Collins, *Chem. Div. Ann. Progr. Rept. May 20, 1969,* ORNL-4437, p. 58.

[4] R. G. Lawton, *J. Am. Chem. Soc.* **83**, 2399 (1961); P. D. Bartlett and S. Bank, *J. Am. Chem. Soc.* **83**, 2591 (1961).

[5] S. Winstein and D. Trifan, *J. Am. Chem. Soc.* **71**, 2953 (1949).

[6] K. Humski, S. Borčić, and D. E. Sunko, *Croat. Chem. Acta* **37**, 3–10 (1965).

[7] P. von R. Schleyer, *J. Am. Chem. Soc.* **89**, 3901 (1967).

DEAMINATION OF 3-*endo*-PHENYL-3-HYDROXYL-2-*exo*-*d*-2-*endo*-NORBORNYLAMINE

Vernon F. Raaen Ben M. Benjamin
Clair J. Collins

We reported previously[1] our determination – with ^{14}C isotope dilution analysis – of the yields of compounds **3** and **4** (Chart IV) upon deamination, in acetic acid–sodium acetate solutions, of the amines **1** and **2**. (From **1**, 4.25% **3**, 2.7% **4**; from **2**, 6.3% **3**, 3.7% **4**.) The title compound (**2**) has now been synthesized with deuterium in the 2-*exo* position. To make the nmr

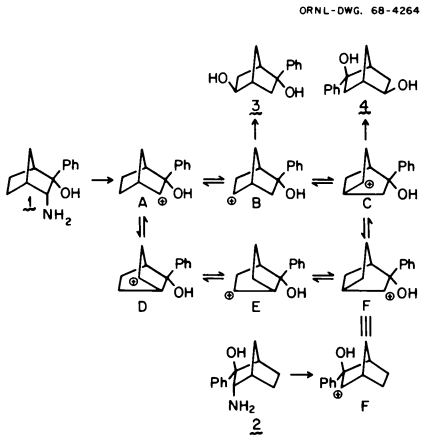

Chart IV

analysis easier, deuteriums were also present at the *exo*-6 and *anti*-7 positions.[2] Nmr analyses of the deuterated products **3** and **4** obtained on deamination of appropriately deuterated **2** indicate that approximately 90% of **3** and 75% of **4** are formed from **2** through the clockwise course. This means that approximately 25% of **4** and 10% of **3** are produced through the counterclockwise course. The results indicate that ions B and C are equilibrating classical ions and not a single nonclassical bridged ion. We hope to refine the measurements by nmr analysis of appropriate derivatives of the deuterated samples of **3** and **4**.

[1] V. F. Raaen and C. J. Collins, *Chem. Div. Ann. Progr. Rept. May 20, 1969*, ORNL-4437, p. 58.

[2] The starting point for the synthesis was 3-*endo*-phenyl-2-norbornanone-5-*exo*-7-*anti*-d_2; B. M. Benjamin and C. J. Collins, *J. Am. Chem. Soc.* 88, 1556 (1966).

ANION CONTROL OF STEREOSELECTIVITY DURING DEAMINATIONS[1]

Clair J. Collins Michael D. Eckart[2]
Vernon F. Raaen

During the deamination, in acetic acid–sodium acetate solution, of 3-*endo*-hydroxy-3-*exo*-phenyl-2-*endo*-norbornylamine (**1** in Chart V), the products **3** and **4** were produced in nearly equal amounts (see Chart V). Upon deamination of the amine **2**, however, nearly 30% of **4** was produced, and only a trace of **3**. Supplementary isotopic labeling experiments (with deuterium) were performed, and from these experiments it was shown that both **3** and **4** are formed from the carbonium ion D. This difference in behavior of D when produced from the two different reactants (**1** and **2**) is a "memory effect" which we ascribe to partial control of product formation by the counter anion (acetate).

ORNL-DWG. 69-10710

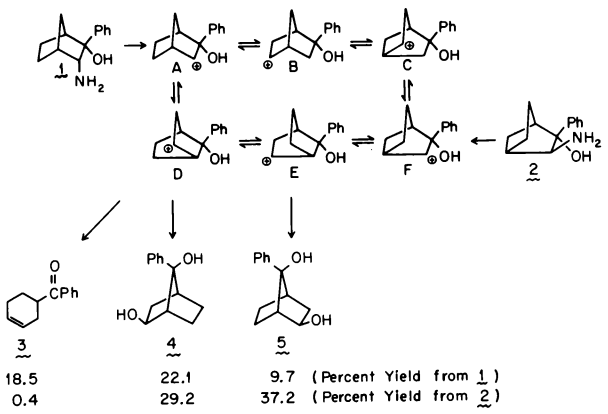

Chart V

[1] Abstract of published paper: C. J. Collins, M. D. Eckart, and V. F. Raaen, *J. Am. Chem. Soc.* 92, 1787 (1970).

[2] Oak Ridge Graduate Fellow from the University of Tennessee, Knoxville, under appointment with Oak Ridge Associated Universities, June 1966–June 1968; present address: Tennessee Eastman Corp., Kingsport, Tenn.

DETERMINATION OF THE STEREOCHEMISTRY OF 1,2 GLYCOLS BY NUCLEAR MAGNETIC RESONANCE

Ben M. Benjamin Michael S. Green[1]

In an earlier report[2] data were presented which related the stereochemistry of a series of α glycols to the nmr chemical shifts of the hydroxyl proton resonances. For any diastereomeric pair of α glycols the hydroxyl proton of the *threo* (or *racemic*) isomer gave a signal at lower field strength than that of the *erythro* (or *meso*) isomer at the same concentration in deuterochloroform. All of the compounds studied contained aromatic groups.

It is of interest to determine whether the same trend is observed (1) in solvents other than $CdCl_3$ and (2) in compounds containing only aliphatic groups. Table 5.3 contains data for several glycols whose nmr spectra were observed in carbon tetrachloride and deutero-1,2-dibromoethane, and Table 5.4 contains data for two pairs of aliphatic glycols. 2,3-Butanediol[3] was prepared by the reduction of diacetyl with lithium aluminum hydride. The mixture of *racemic* and *meso* isomers was separated by preparative gas chromatography. 3,4-Hexanediol[4] was prepared by the ultraviolet irradiation of *n*-propyl alcohol containing 1% hydrogen peroxide or by irradiation of *n*-propyl alcohol containing 10% propionaldehyde. The *meso* form was purified by fractional crystallization, and the *racemic* form was recovered from the crystallization residues by preparative gas chromatography.

As can be seen from Tables 5.3 and 5.4, in every case the hydroxyl proton signals of the *threo* (or *racemic*) isomers appear at lower field strength. This technique can be useful in determining the structure of new pairs of diastereomeric α glycols when both isomers are available.

Table 5.3. Chemical Shifts of Hydroxyl Protons of Diastereomeric Aromatic Glycols as a Function of Concentration in Carbon Tetrachloride and Deutero-1,2-dibromoethane

Compound	Isomer	Concentration, Mole Fraction in CCl_4	Chemical Shift (ppm)	Concentration, Mole Fraction in $C_2D_4Br_2$	Chemical Shift (ppm)
2,3-Diphenyl-2,3-butanediol	*meso*	0.0207	1.933	0.0026	2.150
		0.0108	1.835	0.0015	2.132
		0.0061	1.803		
	racemate	0.0076	2.223	0.0033	2.562
		0.0040	2.233	0.0016	2.495
		0.0020	2.213		
1,2-Diphenyl-1,2-propanediol	*erythro*	0.0121	2.317	0.0039	2.372
		0.0076	2.008	0.0022	2.348
		0.0044	2.044		
	threo	0.0091	2.477	0.0045	2.565
		0.0058	2.290	0.0025	2.552
		0.0038	2.292		
1-Phenyl-2-*p*-tolyl-ethanediol	*erythro*	0.0047	1.98	0.0030	2.183
		0.0035	1.95	0.0015	2.159
	threo	0.0033	2.581	0.0037	2.799
		0.0018	2.482	0.0019	2.753
		0.0012	2.421		
1,2-Diphenylethanediol	*meso*	Not soluble		0.0019	2.263
				0.0011	2.253
	racemate			0.0034	2.832
				0.0021	2.809

Table 5.4. Chemical Shifts of Hydroxyl Protons of Diastereomeric Aliphatic Glycols as a Function of Concentration in Deuterochloroform

Compound	Isomer	Concentration (mole fraction)	Chemical Shift (ppm)
2,3-Butanediol	*meso*	0.0539	3.079
		0.0253	2.473
		0.0159	2.168
	racemate	0.0502	3.234
		0.0290	2.834
		0.0144	2.078
3,4-Hexanediol	*meso*	0.0191	2.097
		0.0118	1.938
		0.0082	1.892
	racemate	0.0245	2.287
		0.0105	2.050
		0.0080	2.032

[1]Participant in the Academic Year Institute in Physical Science, Special Training Division, Oak Ridge Associated Universities.

[2]B. M. Benjamin, *Chem. Div. Ann. Progr. Rept. June 20, 1964*, ORNL-3679, p. 49.

[3]L. P. Kuhn, *J. Am. Chem. Soc.* **80**, 5950 (1958).

[4]G. Leuchner and K. Pfordte, *Ann. Chem.* **619**, 1 (1958).

ISOTHERMAL ANALYSIS OF GRAPHITE-IMPREGNATED TEFLON

C. E. Higgins D. R. Nelson[1]
W. H. Baldwin

It has become necessary for work proposed in the Health Physics Division to ascertain the composition and uniformity of electrodes made from Teflon impregnated with graphite. A method of analysis has been developed based on the facts that Teflon decomposes at elevated temperatures leaving no residue[2] and that graphite survives high temperatures in an oxygen-free atmosphere.[3]

To test the proposed analytical method, mixtures of known amounts of graphite and Teflon in 1 X 1 X 7.5 cm platinum boats were placed inside a 2-cm-diam Vycor tube that contained a nitrogen atmosphere. We found that the nitrogen flow must exceed a minimum rate (>28 ml/min) to avoid carrying graphite out of the boat; flow rates of 40 to 100 ml/min were satisfactory. At temperatures of 640 to 750°C, sample mixtures containing at least 10% graphite gave results reproducible to ±1% of the weight of the residue. As expected, smaller amounts of graphite gave greater weighing errors.

Other polymers that can be volatilized without leaving a residue, for example, polystyrene and polyethylene, can also be analyzed in admixtures with graphite. Polymethyl methacrylate decrepitates during heating with loss of graphite. Nylon, polyethylene glycol, polyvinyl acetate, polyvinyl alcohol, and polyvinyl chloride leave residues (2–8%) when heated alone at 530°C for 10 min.

Commercially prepared electrodes were analyzed by heating 0.5- to 1-g samples at 750° in a nitrogen stream of 65 ml/min for 30 min. Their composition was uniform and close to that stated by the manufacturer (15.1% graphite, the mean of 12 determinations on nominally 15% material).

[1]Health Physics Division.

[2]E. B. Yelton, *Chem. Abstr.* **40**, 4909 (1946).

[3]E. Abrahamzhik, *Chem. Abstr.* **33**, 2437 (1939).

WET OXIDATION OF CELLULOSE

W. E. Clark[1] W. H. Baldwin

A process[2] is being studied for the treatment of cellulosic materials, such as paper, as a means of waste disposal. This is an interesting heterogeneous reaction in which cellulose in the ratio of 10 g to 100 ml of water is placed in an autoclave with twice the theoretical quantity of oxygen gas and heated to the temperature range of 200 to 250°C.

We initiated several runs with filter paper (a source of cellulose with minimum ash) in order to learn something of the course of this reaction.

Most of the carbon is converted to carbon dioxide, but a measurable quantity remains as compounds of carbon dissolved in the residual aqueous solution. Continuous extraction of the aqueous solution with diethyl ether was used to concentrate an acidic fraction in which acetic and formic acids were identified by gas chromatography. The ratio of formic to acetic acid is less at higher temperatures, presumably because faster oxidation of formic acid occurs at the higher temperature.

The nonvolatile aqueous-soluble residue that remained after freeze drying of the aqueous solution was examined by infrared spectrometry. Evidence was found for bonded hydroxyl groups, carbonyl groups, and perhaps vinyl groups. Quantitative volumetric analysis for functional groups revealed, per gram of nonvolatile residue, 1.5 meq acid, 7.8 meq hydroxyl, and <0.8 meq carbonyl. Undoubtedly this residue is a mixture of organic compounds.

Studies of the mechanisms involved in this reaction, as well as its scope and limitations in practical waste disposal, are being continued.[3]

[1]Civil Defense Project.

[2]F. J. Zimmermann, *Chem. Eng.* **65**, 117 (1958).

[3]W. E. Clark, *Civil Defense Project Ann. Rept. March 1969–March 1970*, ORNL-4566, in press.

6. Physical Chemistry

AQUEOUS SYSTEMS

FREE ENERGIES OF ELECTROLYTE MIXTURES

J. S. Johnson, Jr. G. Scatchard[1]
R. M. Rush

Ion-Component Treatment of Free Energy Data[2]

In a previous annual report[3] we discussed the ion-component treatment of free energy data recently proposed by Scatchard[4] and preliminary results of the application to the mixtures involving NaCl, Na_2SO_4, $MgSO_4$, and $MgCl_2$ in aqueous solution. We have now completed the derivation of the equations for the osmotic and activity coefficients and a more detailed analysis of the data mentioned above as well as other data. These results have been submitted for publication.[5]

One of the major advantages of the ion-component treatment is the ability to estimate free energies (and osmotic and activity coefficients) for three-ion mixtures (common-ion mixtures) for data on two-ion (single salt) systems and for four-ion mixtures from data on two- and three-ion mixtures. This is illustrated for the four-ion mixtures of the systems mentioned above by the deviation plots of osmotic coefficients shown in Fig. 6.1. The plots on the left are for the earlier (neutral electrolyte) treatment, and those on the right are for the ion-component treatment. It is clear that the ion-component treatment gives a much better estimate than the neutral-electrolyte treatment when only two-ion (single salt) data are used. The plots labeled "3-ion" are estimates using both two- and three-ion data and involve no direct measurements on the four-ion mixtures. These estimates are about as good as the direct fit to the experimental data obtained by the neutral-electrolyte treatment.

Calculations of the activity coefficient of NaCl in several of the mixtures are shown in Figs. 6.2 and 6.3. The results for the NaCl-$MgCl_2$ mixtures (Fig. 6.2) indicate rather clearly the superiority of the ion-component treatment in estimating the activity coefficient for NaCl in this mixture. The ion-component treatment provides a distinctly better fit using only two-ion data. With the addition of terms obtained by fitting osmotic coefficients of three-ion solutions, the ion-component treatment agrees better with direct measurements of log $\gamma_{\pm NaCl}$ by emf methods[6] than the neutral-electrolyte treatment does, particularly with respect to the curvature at high $MgCl_2$ fractions.

The ability of the ion-component treatment to provide an estimate of the activity coefficients in a four-ion mixture is illustrated by the results for Na_2SO_4-$MgCl_2$ mixtures (Fig. 6.3). It should be emphasized that the solid line was *not* derived from the

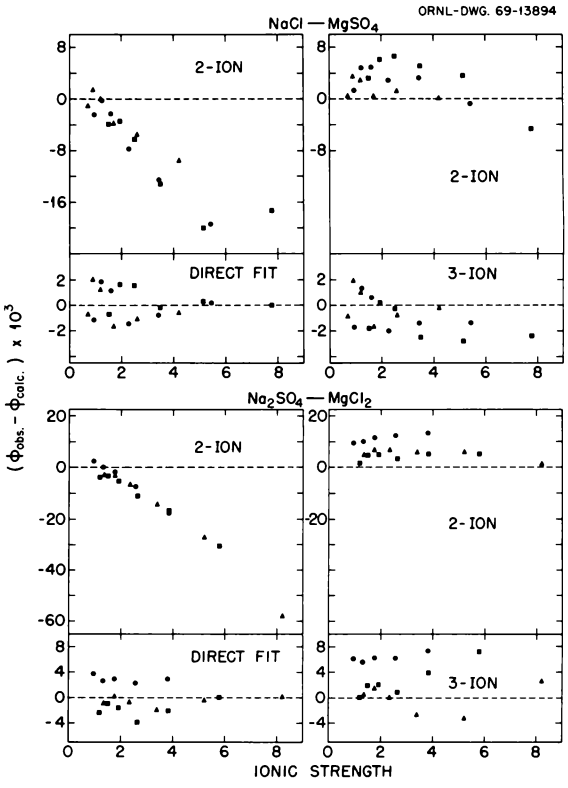

Fig. 6.1. Deviation Plots for Four-Ion Data. Neutral-electrolyte treatment (left) and ion-component treatment (right). Ionic strength fractions for second component: ▲ 0.25, ● 0.5, and ■ 0.75.

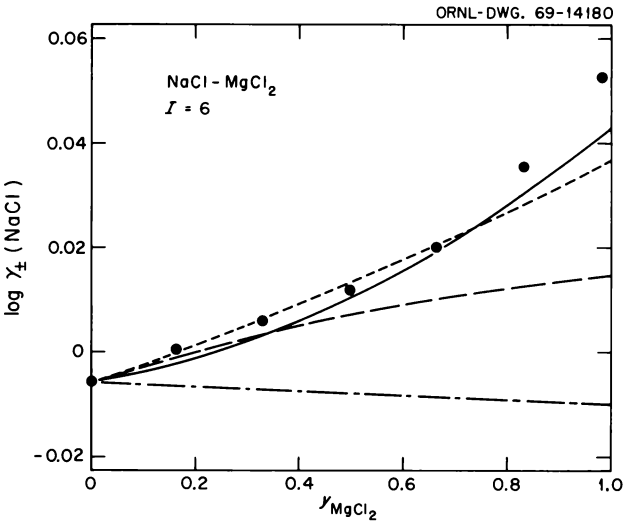

Fig. 6.2. Activity Coefficients of NaCl in NaCl-$MgCl_2$ Mixtures. —– Neutral-electrolyte treatment, two-ion parameters; –– ion-component treatment, two-ion parameters; ···· neutral-electrolyte treatment, direct fit; —— ion-component treatment, three-ion parameters; • emf measurements (ref. 6).

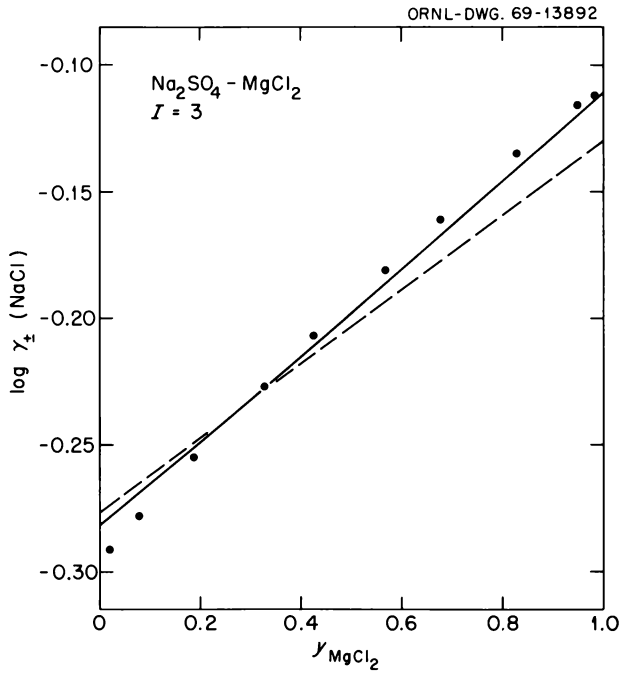

Fig. 6.3. Activity Coefficients of NaCl in Na_2SO_4-$MgCl_2$ Mixtures. ––Ion-component treatment, two-ion parameters; —— ion-component treatment, three-ion parameters; • emf measurements from Y. C. Wu, R. M. Rush, and G. Scatchard, *J. Phys. Chem.* 73, 2047, 4434 (1969).

measurements on the Na_2SO_4-$MgCl_2$ mixtures; it was calculated using only data on the single salts and the appropriate common-ion mixtures. It is not possible to make estimates such as these with the neutral-electrolyte treatment (except at the ends and the midpoint).

For this system, at least, the ion-component treatment provides a better estimate of the osmotic and activity coefficients when only data on the two-ion (single salt) systems are available and provides as good a fit to the three-ion (common ion) data. In addition, for any four-ion system, it provides a means of estimating values using only parameters derived from the two- and three-ion data.

Osmotic Coefficients of Mixed Perchlorate Solutions

Our other studies of solutions of common inorganic electrolytes have continued to concentrate on the perchlorates, which are widely used in studies of complexing and reaction kinetics. Analysis of the data for the mixtures involving $UO_2(ClO_4)_2$ is essentially complete. Experimental work on mixtures of $Ba(ClO_4)_2$ with $HClO_4$ and $NaClO_4$ is nearing completion.

The osmotic coefficient data for the systems $HClO_4$-$UO_2(ClO_4)_2$-H_2O and $NaClO_4$-$UO_2(ClO_4)_2$-H_2O have been analyzed by both the neutral-electrolyte treatment and the more recent ion-component treatment. The relative abilities of the two methods to fit the experimental data are shown in Table 6.1. When terms characteristic of the mixtures (cross terms; three-ion terms in the case of the ion-component treatment) are included, both methods provide a quite satisfactory fit to the data. When only terms derived from data on the single salts (without cross terms; two-ion terms in the case of the ion-component treatment) are included, the results indicate a better estimate for the neutral-electrolyte treatment in the case of $NaClO_4$-$UO_2(ClO_4)_2$ and for the ion-component treatment in the case of $HClO_4$-$UO_2(ClO_4)_2$. This is rather discouraging in view of the consistently better fit obtained with the ion-component treatment for the solutions containing Na^+, Mg^{2+}, Cl^-, and SO_4^{2-} (see above). In the case of $NaClO_4$-$UO_2(ClO_4)_2$ the measurements covered an extended concentration range (ionic strength I from 0.8 to 12.7), and osmotic coefficients of the two solutes are very different, as shown in Fig. 6.4. For $HClO_4$-$UO_2(ClO_4)_2$ the ionic strength range was from 0.6 to 9.4, and the individual solutes have osmotic coefficients relatively close together. It may be

Table 6.1. Standard Deviations

$$s = \sqrt{\frac{\Sigma(\phi_{obs.} - \phi_{calc.})^2}{\text{no. of observations}}}$$

Solutes	Without Cross Terms		With Cross Terms	
	N.E.[a]	I.C.	N.E.	I.C.
$NaClO_4$-$UO_2(ClO_4)_2$	0.0474	0.1480	0.0023	0.0022
$HClO_4$-$UO_2(ClO_4)_2$	0.0185	0.0090	0.0031	0.0030

[a]N.E. = neutral-electrolyte treatment; I.C. = ion-component treatment.

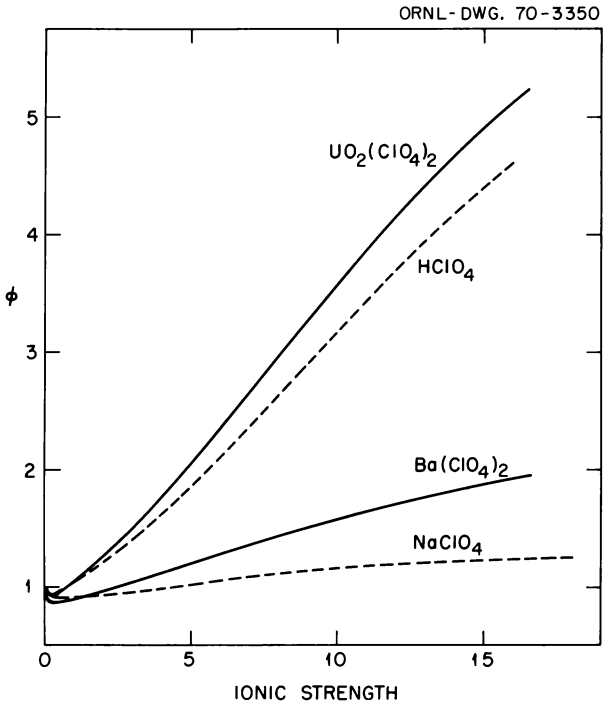

Fig. 6.4. Osmotic Coefficients of Perchlorate Salts. $NaClO_4$, ORNL data; others, literature data.

that the neutral-electrolyte treatment is better able to cope with the extended concentration range and the wide divergence of the individual osmotic coefficients. We have not yet checked the computations thoroughly, so there still may be an error in the analysis of these results.

The difference in the two treatments is also indicated by the activity coefficients shown in Figs. 6.5 and 6.6. The various estimates and procedures are fairly close together for $HClO_4$ (Fig. 6.5) but differ quite a lot for $NaClO_4$ (Fig. 6.6).

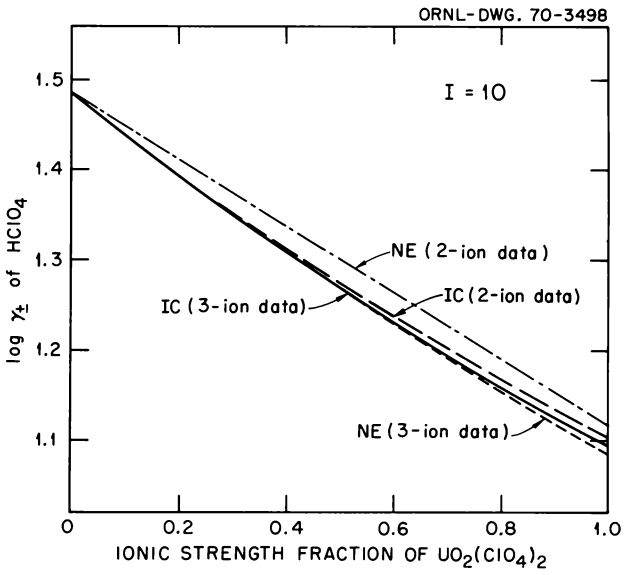

Fig. 6.5. Activity Coefficients of $HClO_4$ in $HClO_4$-$UO_2(ClO_4)_2$-H_2O.

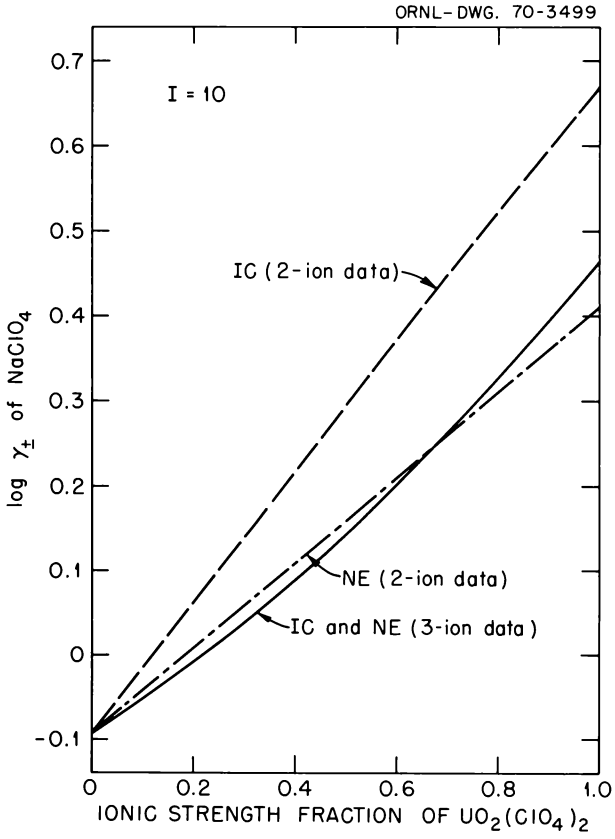

Fig. 6.6. Activity Coefficients of $NaClO_4$ in $NaClO_4$-$UO_2(ClO_4)_2$-H_2O.

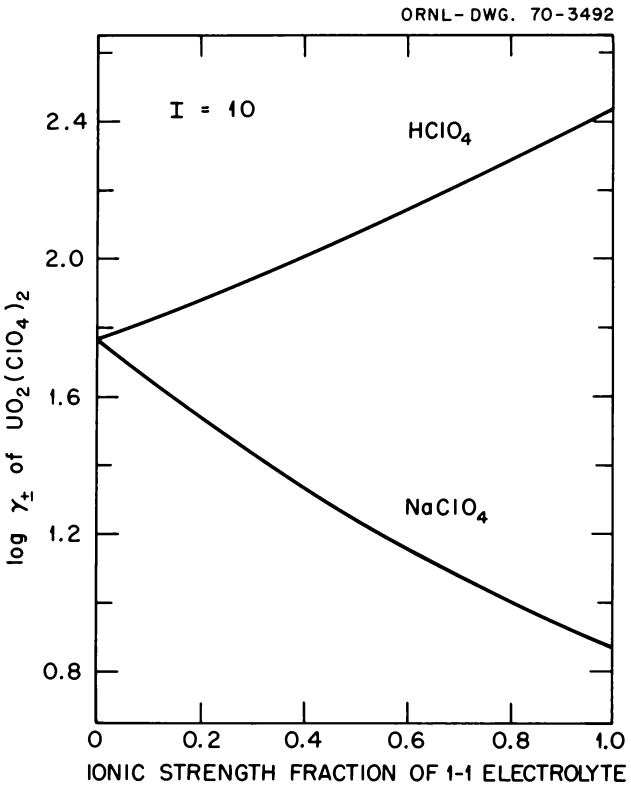

Fig. 6.7. Activity Coefficients of Uranyl Perchlorate in Mixed Electrolyte Solutions.

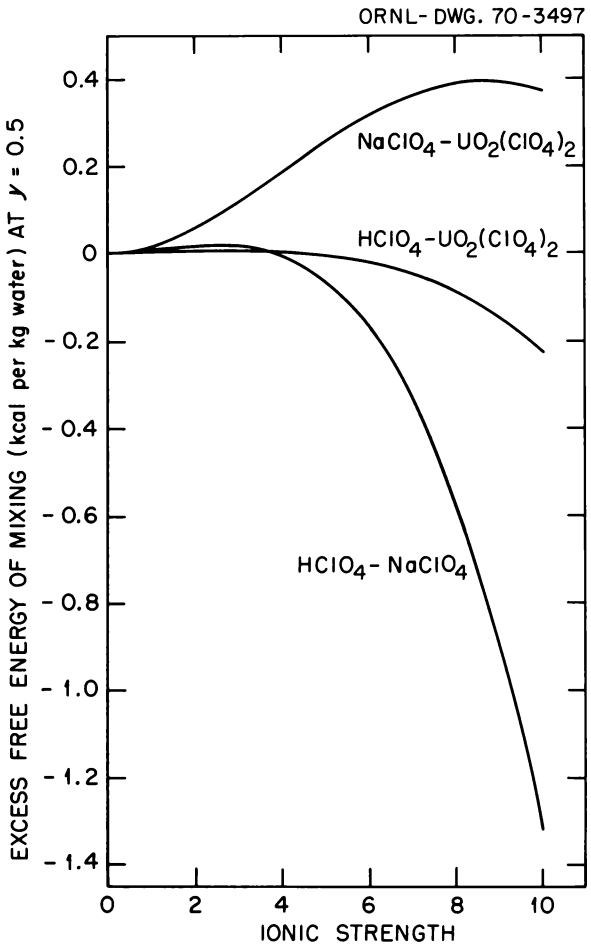

Fig. 6.8. Free Energies of Mixing, Perchlorate Solutions.

The vastly differing effects of $HClO_4$ and $NaClO_4$ on the activity coefficients of $UO_2(ClO_4)_2$ are shown in Fig. 6.7. The magnitude of the effect is even more clearly illustrated by the activity coefficients themselves. At an ionic strength of 10, for pure $UO_2(ClO_4)_2$ $\gamma_\pm$ = 58.4; in "pure" $HClO_4$ ["trace" $UO_2(ClO_4)_2$] $\gamma_\pm$ = 273, a change by a factor of almost 5; in "pure" $NaClO_4$ $\gamma_\pm$ = 7.29, a change in the opposition direction by a factor of 8.

These great changes at high concentrations are also apparent from the excess free energies of mixing. Figure 6.8 shows the excess free energy of mixing for equal ionic strength fractions (y) at constant ionic strength.

[1]Consultant; Professor of Physical Chemistry, Emeritus, Massachusetts Institute of Technology, Cambridge.

[2]Research jointly sponsored by the Office of Saline Water, U.S. Department of the Interior, and U.S. Atomic Energy Commission under contract with Union Carbide Corp. and under contract No. AT(30-1)-905 with Massachusetts Institute of Technology.

[3]R. M. Rush *et al., Chem. Div. Ann. Progr. Rept. May 20, 1969,* ORNL-4437, p. 69.

[4]G. Scatchard, *J. Am. Chem. Soc.* **90,** 3124 (1968); **91,** 2410 (1969).

[5]G. Scatchard, R. M. Rush, and J. S. Johnson, submitted for publication to the *Journal of Physical Chemistry.*

[6]R. D. Lanier, *J. Phys. Chem.* **69,** 3992 (1965).

THE THERMODYNAMIC PROPERTIES OF HCl-NaCl-$MgCl_2$ MIXTURES

M. H. Lietzke R. J. Herdklotz[1]

No extensive study has been made of the thermodynamic properties of aqueous solutions containing four different ionic components. One of the few systems studied[2] has been HCl-CsCl-$BaCl_2$, where the results of emf and isopiestic measurements were combined to calculate the activity coefficient of each component in the mixtures as a function of temperature, total ionic strength, and ionic strength fraction of

each component. Since it will be necessary to have data on a variety of different systems in order to develop and test mathematical representations, a study is being undertaken of four mixtures each containing HCl, an alkali metal chloride, and the adjacent alkaline earth metal chloride. The system reported here, HCl-NaCl-$MgCl_2$, is the second in the series.

Emf measurements of the cell

$$Pt\text{-}H_2(p = 1) \mid HCl(m_2)\, NaCl(m_3)\, MgCl_2(m_4) \mid AgCl, Ag$$

were performed over the temperature range 25 to 75° using solutions of total ionic strengths from 0.5 to 5.0 in which both the total fractions of acid and salt were varied as well as the ionic-strength ratios of the two salts at fixed fractions of total salt. Isopiestic data on the NaCl-$MgCl_2$ mixtures were taken from the literature.[3]

The emf and isopiestic data were fitted by least squares, and the activity coefficients of each component in the mixtures were calculated using a treatment[2] which focuses attention on the "neutral" species in solution, for example, HCl or NaCl, rather than on the ions themselves. This will be referred to as the "neutral-electrolyte" treatment.[4] An attempt was made to compute the activity coefficient of each electrolyte in the mixtures at 25° from data on pure HCl, NaCl, and $MgCl_2$ solutions as well as on HCl-NaCl, HCl-$MgCl_2$, and NaCl-$MgCl_2$ mixtures. The purpose of this calculation was to test the ability of an ion-component treatment[5] to predict the properties of a more complicated mixture from measurements on simpler systems. Details of the method of calculation will be reported elsewhere;[6] only the results of the calculations will be given here.

In Fig. 6.9 the solid lines are plots of the logarithm of the activity coefficient of HCl (×10) in HCl-NaCl-$MgCl_2$ mixtures at $I = 0.5$ and 1.0 at 25° as computed using the neutral-electrolyte treatment. The abscissa $x_4/(x_3 + x_4)$ represents the ratio of the fraction of $MgCl_2$ in the mixtures x_4 to the total fraction of salt in the mixtures $(x_3 + x_4)$, where x_3 is the fraction of NaCl. Note that the curves are concave downward and that the amount of curvature increases as the fraction of acid in the mixtures (x_2) decreases. The solid circles in Figs. 6.9–6.12 refer to the activity coefficient of the pure HCl at the same total ionic strength. For comparison the corresponding plots in HCl-CsCl-$BaCl_2$ mixtures are shown in Fig. 6.10. Here the curves are concave upward, but again the amount of curvature is greatest in the mixtures containing the lowest fraction of acid. In both cases the amount of curvature increases as the total ionic strength increases.

The open circles in Fig. 6.9 represent activity coefficient values computed using the ion-component treatment. The agreement with the observed values is very good at both total ionic strengths.

Plots of the logarithm of the activity coefficient of HCl (×10) in the HCl-NaCl-$MgCl_2$ mixtures at three different temperatures and a total ionic strength of 3.0 are shown in Fig. 6.11. Note that the amount of curvature decreases as the temperature increases. At this ionic strength, values of the activity coefficient computed using the ion-component treatment (open circles) agree very well with the observed values only for solutions in which the fraction of acid is 0.75 and 0.50. At the lower fractions of acid, the plots of the observed values show much more curvature than do the values computed by the ion-component method, and the

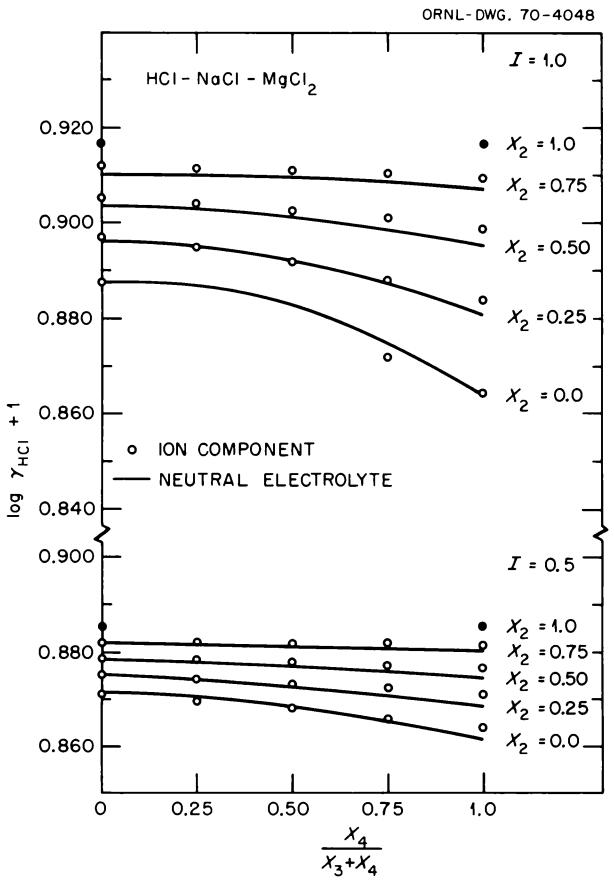

Fig. 6.9. Plots of the Logarithm of the Activity Coefficient of HCl (×10) in HCl-NaCl-$MgCl_2$ Mixtures vs $x_4/(x_3 + x_4)$. $I = 0.5$ and 1.0; temperature = 25°; x_2, x_3, and x_4 refer to the fractions of HCl, NaCl, and $MgCl_2$ respectively; solid circles refer to pure HCl at the same total ionic strength.

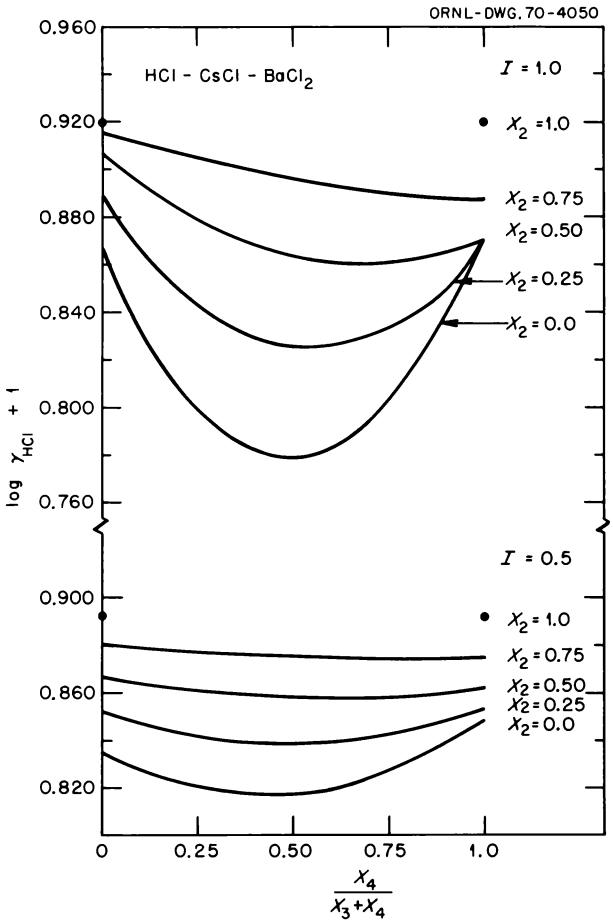

Fig. 6.10. Plots of the Logarithm of the Activity Coefficient of HCl (×10) in HCl-CsCl-$BaCl_2$ Mixtures vs $x_4/(x_3 + x_4)$. I = 0.5 and 1.0; temperature = 25°; x_2, x_3, and x_4 refer to the fractions of HCl, CsCl, and $BaCl_2$ respectively; solid circles refer to pure HCl at the same total ionic strength.

agreement is good only at the extremes. Hence the intermediate values of these computed values are not shown at x_2 = 0.25 and 0.0.

The plots of the logarithm of the activity coefficient of HCl (×10) in the mixtures at I = 5.0 at 25°, shown in Fig. 6.12, continue the trend of greater curvature at higher ionic strength. At this ionic strength, values of the activity coefficient of the HCl computed using the ion-component treatment show good agreement with the observed values only at the highest fraction of acid.

The variation of the logarithms of the activity coefficients (×10) of NaCl and of $MgCl_2$ in the HCl-NaCl-$MgCl_2$ mixtures with x_2, the fraction of HCl in the mixtures, at I = 1.0 and 25° is shown in Fig. 6.13. As the fraction of $MgCl_2$ in any of the mixtures increases at the same total fraction of acid, the activity coefficient of the NaCl increases. The same is true with the $MgCl_2$ activity coefficient: as the fraction of NaCl increases at constant fraction of acid, the activity coefficient of the $MgCl_2$ increases. This is exactly the reverse of the behavior shown in the HCl-CsCl-$BaCl_2$ mixtures by the activity coefficient of the CsCl when the fraction of acid is greater than 0.06 and by the activity coefficient of the $BaCl_2$ at all fractions of acid. As can be seen in Fig. 6.14, addition of $BaCl_2$ at constant fraction of acid above 0.06 *decreases* the activity coefficient of the CsCl, while at any fraction of

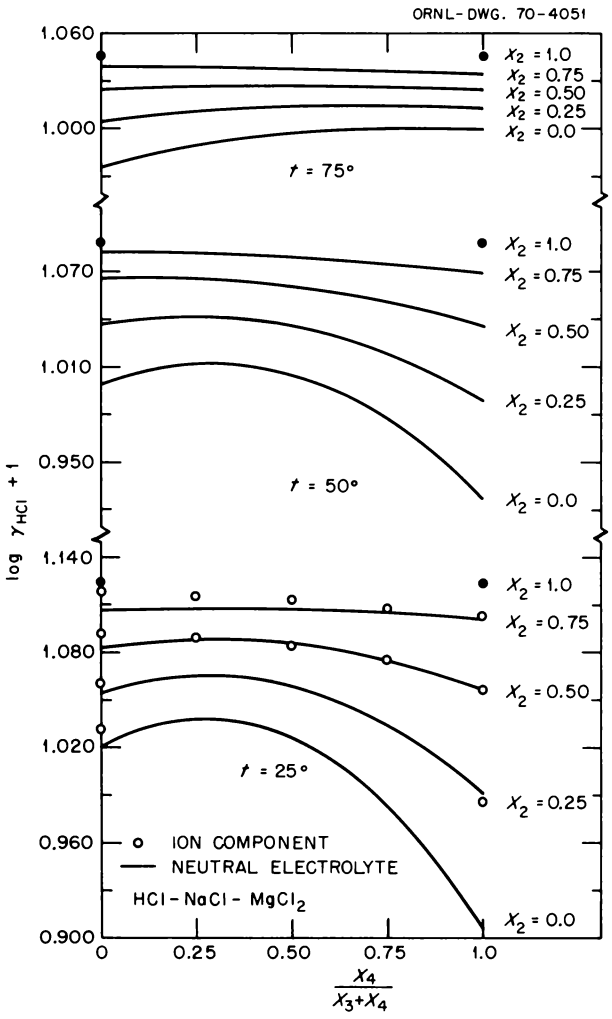

Fig. 6.11. Plots of the Logarithm of the Activity Coefficient of HCl (×10) in HCl-NaCl-$MgCl_2$ Mixtures vs $x_4/(x_3 + x_4)$. I = 3.0; temperature = 25, 50, and 75°; x_2, x_3, and x_4 refer to the fractions of HCl, NaCl, and $MgCl_2$ respectively; solid circles refer to pure HCl at the same total ionic strength.

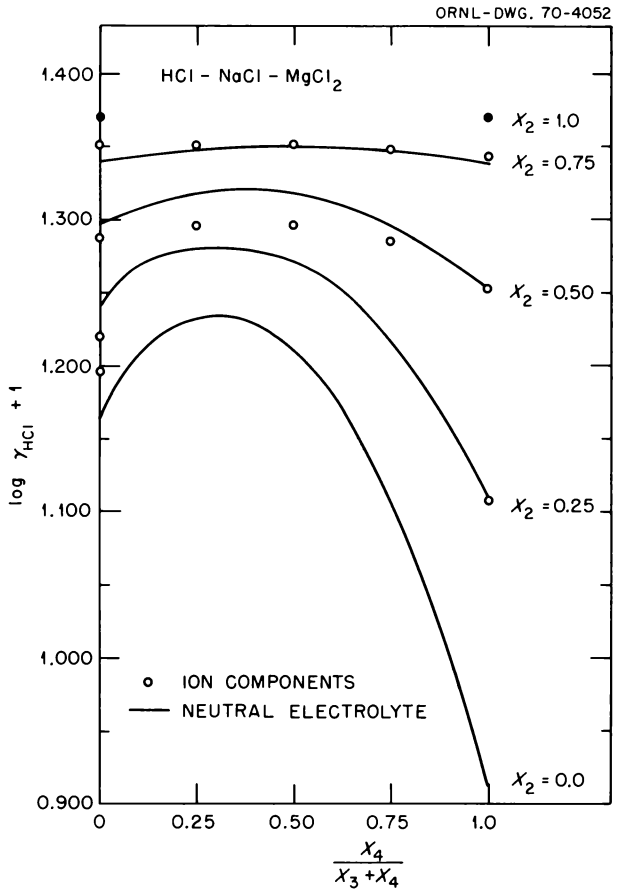

Fig. 6.12. Plots of the Logarithm of the Activity Coefficient of HCl (×10) in HCl-NaCl-$MgCl_2$ Mixtures vs $x_4/(x_3 + x_4)$. I = 5.0; temperature = 25°; x_2, x_3, and x_4 refer to the fractions of HCl, NaCl, and $MgCl_2$ respectively; solid circles refer to pure HCl at the same total ionic strength.

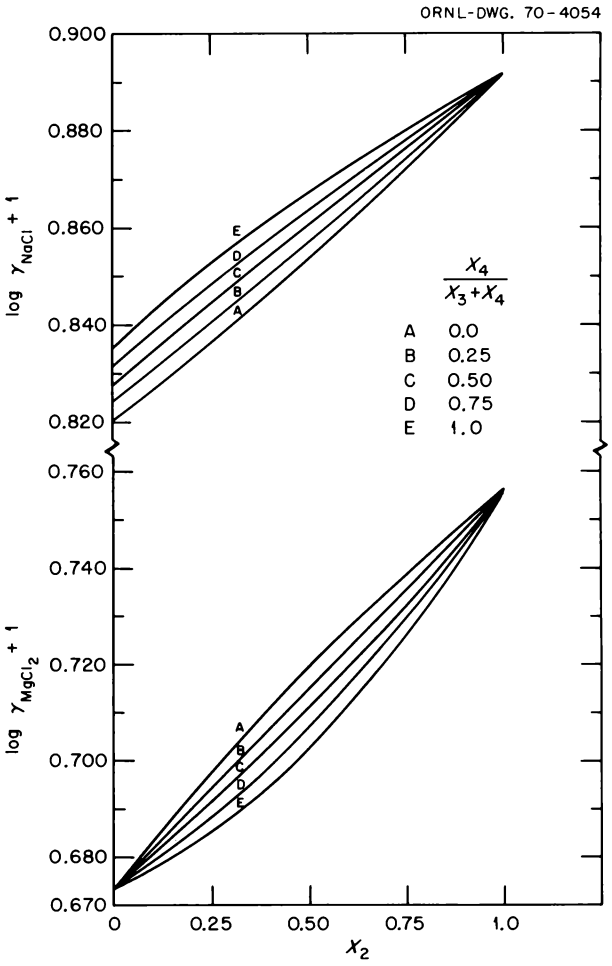

Fig. 6.13. Plots of the Logarithms of the Activity Coefficients (×10) of NaCl and $MgCl_2$ vs x_2. I = 1.0; temperature = 25°; x_2, x_3, and x_4 refer to the fractions of HCl, NaCl, and $MgCl_2$ respectively.

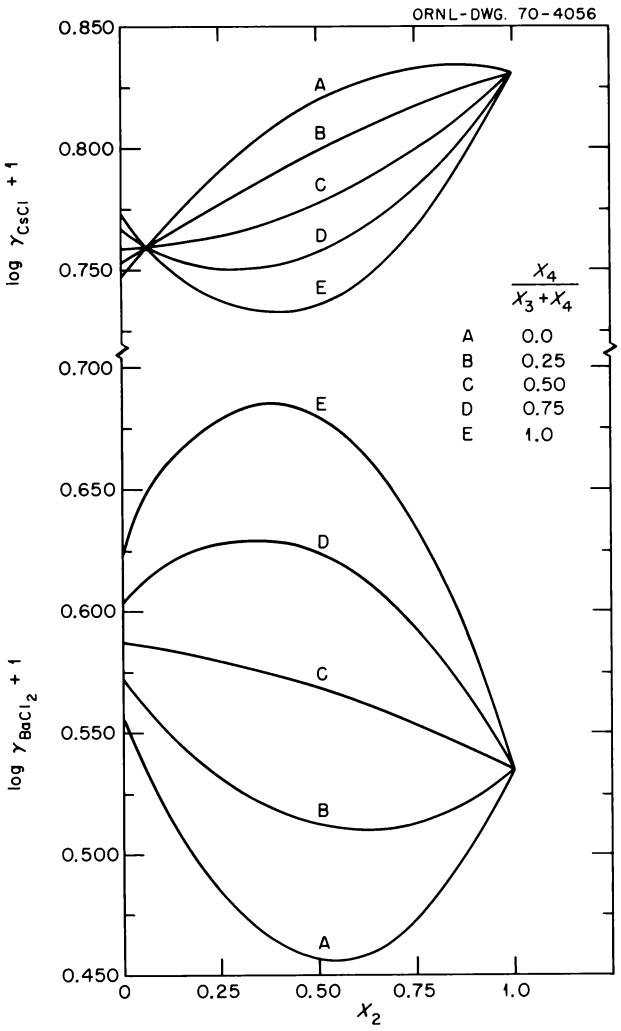

Figure 6.14. Plots of the Logarithms of the Activity Coefficients (X10) of CsCl and $BaCl_2$ vs x_2. I = 1.0; temperature = 25°; x_2, x_3, and x_4 refer to the fractions of HCl, CsCl, and $BaCl_2$ respectively.

acid the addition of CsCl also decreases the activity coefficient of the $BaCl_2$. When the fraction of acid is less than 0.06 in the HCl-CsCl-$BaCl_2$ mixtures, the activity coefficient behavior of the CsCl is the same as that of NaCl in HCl-NaCl-$MgCl_2$ mixtures at all fractions of acid.

Further studies in this program will include the investigation of both HCl-KCl-$CaCl_2$ and HCl-RbCl-$SrCl_2$ mixtures.

[1]Oak Ridge Graduate Fellow from the University of Tennessee, Knoxville, under appointment with Oak Ridge Associated Universities.

[2]M. H. Lietzke, H. B. Hupf, and R. W. Stoughton, *J. Inorg. Nucl. Chem.* **31**, 3481 (1969).

[3]R. F. Platford, *J. Phys. Chem.* **72**, 4053 (1968).

[4]G. Scatchard, *J. Am. Chem. Soc.* **83**, 2636 (1961).

[5]G. Scatchard, R. M. Rush, and J. S. Johnson, submitted for publication to the *Journal of Physical Chemistry;* see also J. S. Johnson, Jr., G. Scatchard, and R. M. Rush, "Free Energies of Electrolyte Mixtures," preceding contribution, this report.

[6]R. J. Herdklotz, Ph.D. dissertation, University of Tennessee, Knoxville, August 1970.

SALT-INDUCED CRITICAL-TYPE TRANSITIONS IN AQUEOUS SOLUTION. HEATS OF DILUTION OF THE LITHIUM AND SODIUM HALIDES

Fred Vaslow

Measurements of the heats of dilution of the halide (except fluoride) salts of both lithium and sodium have been completed. Salt solutions initially between 1.0 and 1.5 *M* were diluted with water in increments, each of about 4% of the total volume; each diluted solution was the starting point for the next dilution.

Ten to twenty dilutions were made on each initial solution, and two runs were made for each salt except NaCl, where six were made, although the first three were of a preliminary nature. The precision of the results is about ±0.0025 cal in a total heat change ranging from 0.5 to 6 cal, depending on the salt and the concentration. Each measurement gives the change $\Delta\phi_H$ of the apparent molal heat content of the salt, or the average slope $\Delta\phi_H/\Delta\sqrt{m}$ over the interval $\Delta\sqrt{m}$ (m is molality).

With the possible exception of one of the preliminary NaCl curves ($\Delta\phi_H/\Delta\sqrt{m}$ vs $\sqrt{m}$) each of these 16 curves shows a small apparent discontinuity close to or within a chord where, with the exception of LiCl, a discontinuity in $\Delta\phi_v/\Delta\sqrt{c}$ vs $\sqrt{c}$ curves (c is molarity) was observed previously.[1] Selected curves for each lithium salt are shown in Fig. 6.15 and for the Na salts in Fig. 6.16. A vertical arrow shows the position of the apparent discontinuity, and a horizontal arrow indicates the position of the discontinuity in the $\Delta\phi_v/\Delta\sqrt{c}$ curves. The heat of dilution curves that are not shown are very similar.

For LiCl solutions a discontinuity in the $\Delta\phi_v/\Delta\sqrt{c}$ curves could not be resolved (i.e., the transition was diffuse). The only other significant difference in the position of the discontinuity between the heat and volume curves occurs for LiBr and amounts to about 0.1 unit in $\sqrt{c}$ or $\sqrt{m}$. Since hysteresis and lag effects are a normal occurrence in the measurement of first- or

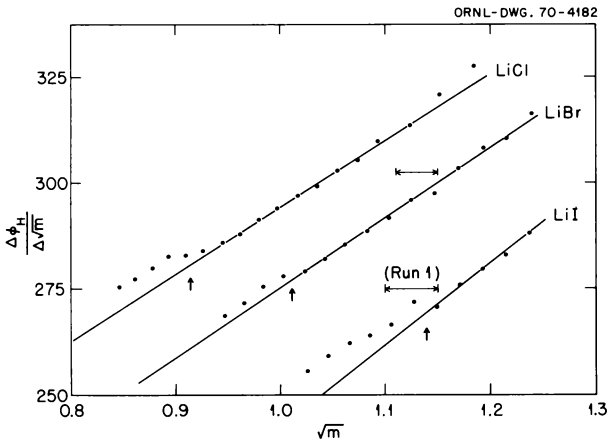

Fig. 6.15. Differential Heats of Dilution Data for LiCl, LiBr, and LiI. Units of $\Delta\phi_H/\Delta\sqrt{m}$ are cal $(kg\ H_2O)^{1/2}$ mole $^{-3/2}$.

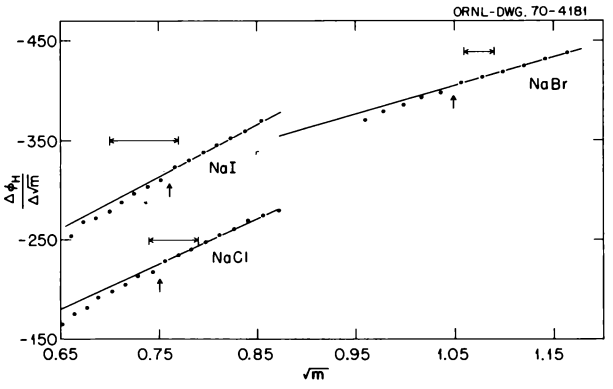

Fig. 6.16. Differential Heats of Dilution for NaCl, NaBr, and NaI. Units of $\Delta\phi_H/\Delta\sqrt{m}$ are cal $(kg\ H_2O)^{1/2}$ mole$^{-3/2}$.

higher-order thermodynamic transitions, this small difference is not unexpected, and the results are not considered to be in disagreement.

While the nature of the transition remains highly speculative, some of the data suggest a closer agreement with the Samoilov theory[2] (transition of solvent structure from that of pure water) rather than with the Kirkwood theory[3] (change in form of the ion radial distribution function). According to the Kirkwood theory the transition should occur at $\kappa a = 1.03$ (κ is the Debye-Hückel parameter proportional to $\sqrt{c}$, and a is the distance-of-approach parameter), or between 0.4 and 0.6 M for the salts studied. While the general concentration predicted is reasonable, the sequence predicted on the basis of ion sizes is wrong, since the salts with the larger values of a give the transition at the higher concentration, contrary to the Kirkwood theory.

Li^+ ion is regarded as a water-structure stabilizer and might be expected to preserve the water structure to a higher concentration in agreement with the Samoilov theory. Similarly the relatively high concentration of the transition for NaBr compared with NaCl and NaI might be interpreted as indicating an optimum stability for Br^- ion in the cavities of water, with Cl^- and I^- being too small and too large, respectively, for maximum stability.

---

[1] F. Vaslow, *J. Phys. Chem.* 73, 3745 (1969).

[2] O. Ya. Samoilov, *The Structure of Aqueous Solutions and the Hydration of Ions,* English Transl., p. 141, Consultants Bureau, New York, 1965.

[3] J. G. Kirkwood, *Chem. Rev.* 19, 275 (1936).

VARIATION OF OSMOTIC COEFFICIENTS OF AQUEOUS SOLUTIONS OF TETRAALKYLAMMONIUM HALIDES WITH TEMPERATURE. THERMAL AND SOLUTE EFFECTS ON SOLVENT HYDROGEN BONDING[1]

S. Lindenbaum G. E. Boyd
L. Leifer[2] J. W. Chase[3]

Osmotic coefficients have been measured at 65° for aqueous solutions of tetra-*n*-butylammonium fluoride; tetramethyl-, tetra-*n*-propyl-, and tetra-*n*-butylammonium chloride; and tetramethyl- and tetra-*n*-propylammonium iodide. These data were combined with the available thermodynamic data at 25° to estimate relative partial molal entropies of the solvent. The thermodynamic properties of symmetric tetra-*n*-alkylammonium halide solutions have been interpreted in terms of the effect of increasing anion size and increasing temperature on the local structure of water. This interpretation is justified in terms of the recently published x-ray diffraction results on water and on aqueous ammonium halide and tetra-*n*-butylammonium fluoride solutions. The concept of "water-structure-enforced ion pairing" has been used to explain the reversal in the sequence of the magnitude of the osmotic coefficients on substituting iodide for chloride ions. It is suggested that this concept is not valid in cases involving either cations or anions which *reduce* the amount of local order in the solvent. However, osmotic coefficient reversals may be accounted for on the basis of the competition between *increased* hydrogen bonding of water as the size of the R_4N^+ cation increases and *decreased* hydrogen bonding as the size of the halide ion increases.

[1] Abstract of published paper: *J. Phys. Chem.* **74**, 761 (1970).

[2] Michigan Technological University, Houghton.

[3] Xerox Corporation Research Laboratories, Rochester, N.Y.

THERMODYNAMIC STUDIES ON AQUEOUS SOLUTIONS OF SALTS OF CARBOXYLIC ACIDS

Siegfried Lindenbaum

Physical properties of aqueous solutions containing large organic cations such as tetraalkylammonium ions[1-4] have suggested that these ions promote structure or increase hydrogen bonding of water. The special interaction between these "hydrophobic" ions and water has also been referred to as "hydration of the second kind."[5] It has been pointed out,[6,7] for example, that the B coefficient of the Jones-Dole viscosity equation has large positive values for these large organic cations, and the larger the cation the more positive the B coefficient. This is in contrast to the behavior of alkali-metal ions, which show decreasing B values with increasing crystallographic cation size. A similar comparison may be made with heat of dilution data. These are given in Fig. 6.17*a* as apparent molal heat contents ϕ_L for alkali-metal chlorides and tetra-*n*-alkylammonium chlorides in 1 m aqueous solutions. For the alkali-metal ions, ϕ_L decreases with increasing crystallographic ion size, whereas for the large organic ions ϕ_L increases markedly with increasing cation size. Many physical measurements have been reported, all of which demonstrate this remarkable difference between the properties of large organic cations and those of inorganic cations. The purpose of this work is to determine whether this difference also exists between inorganic anions and large organic anions.

We have measured heats of dilution of aqueous solutions of sodium salts of butyric (C_4) and valeric (C_5) acids. These are given in Fig. 6.17*b*, together with ϕ_L values of sodium fluoride, chloride, bromide, iodide, and acetate in 1 m solutions. The ϕ_L values of sodium butyrate (NaBut) and sodium valerate (NaVal) are also given in Fig. 6.18 as a function of concentration. The inorganic salts show the expected dependence on ion size, namely, the larger the anion the smaller the value for ϕ_L. The sodium salts of the carboxylic acids gave large positive values of ϕ_L, increasing with anion size, suggesting that these anions cause increased hydrogen bonding in the solvent.

Low values of osmotic and activity coefficients[2,8] of tetraalkylammonium iodides in aqueous solution have led to the suggestion[9] that large cations and large anions are extensively ion paired by a special non-Coulombic mechanism ("water-structure-enforced ion pairing"). In view of this suggestion, a study of the thermodynamic properties of aqueous solutions of salts consisting of both large organic cations and large organic anions seemed to be of interest. Osmotic coefficients of aqueous solutions of tetra-*n*-butylammonium butyrate and tetra-*n*-butylammonium valerate were measured by the gravimetric isopiestic vapor pressure comparison method (Fig. 6.19). In both cases

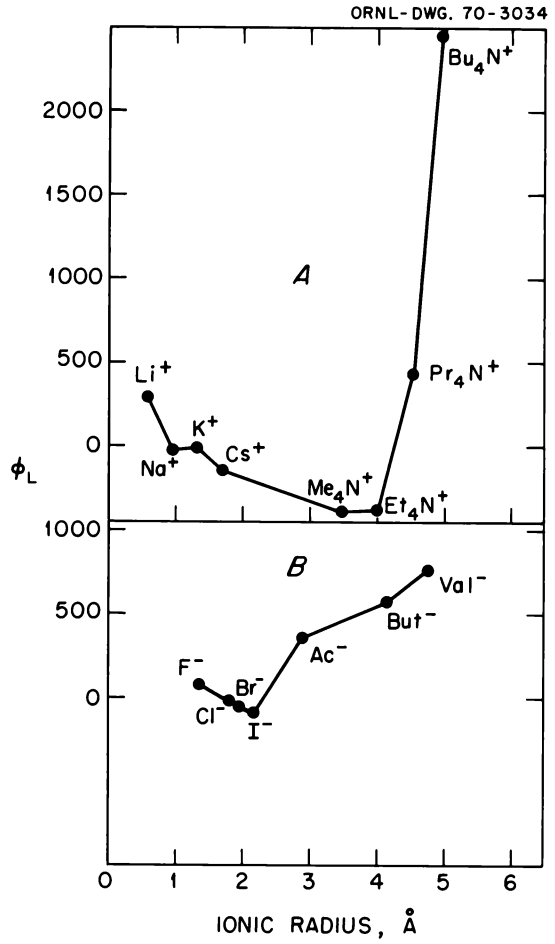

Fig. 6.17. Apparent Molal Heat Contents of 1 m Aqueous Solutions at 25°. (*A*) Chloride salts, (*B*) sodium salts. Ionic radii for acetate, butyrate, and valerate were estimated from molecular models. Other ionic radii are taken from tables in R. A. Robinson and R. H. Stokes, *Electrolyte Solutions*, 2d ed., Academic, New York, 1959. ϕ_L values of sodium fluoride, chloride, bromide, iodide, and acetate and lithium, sodium, potassium, and cesium chloride are taken from V. B. Parker, *Thermal Properties of Aqueous Uniunivalent Electrolytes*, NSRDS-NBS 2, National Bureau of Standards, Washington, D.C., 1965.

the osmotic coefficients were greater than 1.0 for all concentrations greater than 0.3 *m*. This may be taken as a strong indication that ion pairing does not occur in these solutions and casts serious doubt on the validity of the water-structure-enforced ion pairing concept.

Heats of dilution also were measured on aqueous solutions of tetra-*n*-butylammonium salts of butyric (Bu_4NBut), valeric (Bu_4NVal), and heptanoic (Bu_4NHept) acids. These are given in Fig. 6.18, together with the ϕ_L values of Bu_4NF[10] for comparison. The results for Bu_4NBut are also compared in Table 6.2 with ϕ_L values of tetrabutylammonium chloride (Bu_4NCl),[3] NaBut, and NaCl for 1 *m* aqueous solutions. Heats of mixing of 1 *m* solutions of Bu_4NBut with NaCl, and NaBut with Bu_4NCl, were also obtained from measurements of heats of dilutions of equimolar

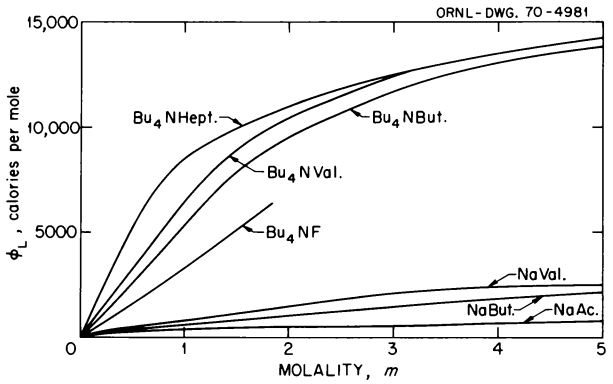

Fig. 6.18. Apparent Molal Heat Contents of Aqueous Solutions of Carboxylates at 25°C.

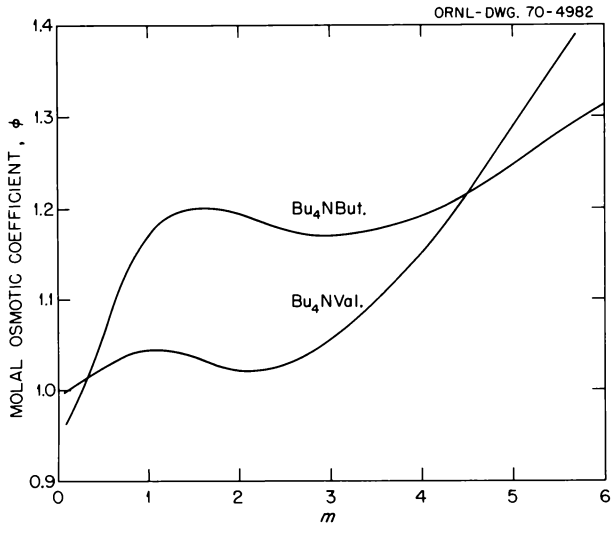

Fig. 6.19. Molal Osmotic Coefficients of Tetra-*n*-butylammonium Butyrate and Valerate at 25°C.

Table 6.2. Apparent Molal Heat Contents of 1 *m* Aqueous Solutions at 25°

Salt	ϕ_L (cal/mole)
Bu_4NBut	5266
NaBut	565
Bu_4NCl	2455
NaCl	−23
Bu_4NCl + NaBut	$\Delta Hm_1 = 170$
Bu_4NBut + NaCl	$\Delta Hm_2 = -941.5$

$$\phi_L(Bu_4NBut) = \phi_L(Bu_4NCl) + \phi_L(NaBut) - \phi_L(NaCl) + 2\Delta Hm_1 - 2\Delta Hm_2$$

mixtures of Bu_4NBut and NaCl. These are given in Table 6.2 also. The ϕ_L of Bu_4NBut is seen to be considerably larger than the sum of ϕ_L for NaBut and Bu_4NCl. This difference is due mainly to the heat of mixing ΔHm_2 of Bu_4NBut + NaCl and to a lesser extent the heat of mixing ΔHm_1 of Bu_4NCl and NaBut. These results suggest that in Bu_4NBut solutions, both anion and cation cause increased solvent hydrogen bonding, whereas in solutions of NaBut or Bu_4NCl the hydration of the sodium ions and chloride ions competes with the water-structure promotion caused by the hydrophobic butyrate or tetrabutylammonium ions.

[1] H. S. Frank and W-Y Wen, *Discussions Faraday Soc.* **24**, 133 (1957).

[2] S. Lindenbaum and G. E. Boyd, *J. Phys. Chem.* **68**, 911 (1964).

[3] S. Lindenbaum, *J. Phys. Chem.* **70**, 814 (1966).

[4] A. H. Narten and S. Lindenbaum, *J. Chem. Phys.* **51**, 1108 (1969).

[5] H. G. Hertz and M. D. Zeidler, *Ber. Bunsenges. Physik. Chem.* **68**, 821 (1964).

[6] R. L. Kay, T. Vituccio, C. Zawoyski, and D. F. Evans, *J. Phys. Chem.* **70**, 2336 (1966).

[7] R. A. Horne and R. P. Young, *J. Phys. Chem.* **72**, 1763 (1968).

[8] J. Lange, *Z. Physik. Chem. (Leipzig)* **139A**, 584 (1968).

[9] R. M. Diamond, *J. Phys. Chem.* **67**, 2513 (1963).

[10] S. Lindenbaum, *J. Phys. Chem.* **73**, 4334 (1969).

TRACER DIFFUSION COEFFICIENTS IN AQUEOUS SOLUTIONS OF ORGANIC ION EXCHANGER MODEL COMPOUNDS: COMPARISON OF AQUEOUS SODIUM *p*-ETHYLBENZENE-SULFONATE WITH CROSS-LINKED POLYSTYRENESULFONATES

M. J. Pikal[1]

The purpose of this study was to determine tracer diffusion coefficients for inorganic ions in concentrated

aqueous electrolyte solutions of "model compounds" for organic ion exchangers. It was expected that this research would yield information on the nature of ion-ion and ion-water interactions in aqueous systems containing large organic ions and that information would be obtained on how these interactions affect the mobilities of inorganic ions in ion exchangers.

Tracer diffusion measurements at 25°C with HTO, $^{36}Cl^-$, $^{65}Zn^{2+}$, and $^{24}Na^+$ were carried out in aqueous sodium *p*-ethylbenzenesulfonate (NapEBS) solutions of 0.1, 0.3, 1.0, and 3.0 *m* concentration using the Stokes diaphragm-cell technique. In addition, measurements in 0.1 and 1.0 *m* NapEBS solutions were completed with the species $^{45}Ca^{2+}$, $^{88}Y^{3+}$, and $^{42}K^+$; measurements with 3.3 *m* NapEBS are in progress.

From the data accumulated thus far, above 0.1 *m* the diffusion coefficients of all species decreased rapidly with an increase in NapEBS concentration. In fact, at 3.0 *m* sodium *p*-ethylbenzenesulfonate, the diffusion coefficients were only about 30% of their respective values at infinite dilution. This change is more than twice the decrease observed with a typical 1-1 supporting electrolyte such as sodium chloride. One interesting feature of the diffusion data is the slow initial decrease in $D_{Zn^{2+}}$ as the concentration of NapEBS

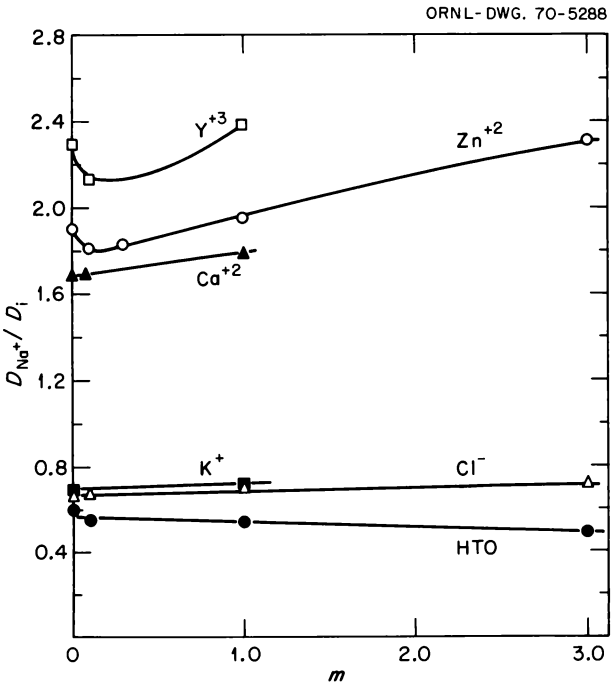

Fig. 6.20. Diffusion Coefficient Ratios for Various Species as a Function of Molality of Aqueous Sodium *p*-Ethylbenzenesulfonate.

increases from zero. This effect is more pronounced for Y^{3+}, where the data indicate an increase in the diffusion coefficient between zero and 0.1 *m*. This unexpected behavior is illustrated in Fig. 6.20, where the ratios D_{Na^+}/D_i are plotted: i = Y^{3+}, Zn^{2+}, Ca^{2+}, K^+, Cl^-, HTO. These data show that at low concentrations the mobilities of Y^{3+} and Zn^{2+} decrease less rapidly with increasing concentration than does the Na^+ mobility. However, at higher concentrations this trend reverses, and the mobilities of Zn^{2+} and Y^{3+} ions decrease more rapidly than does the mobility of Na^+ ion. The latter behavior is qualitatively consistent with the effects of long-range electrostatic forces (i.e., the relaxation effect). A similar trend is found with ion exchange resins of the Dowex 50 type. We note that the Ca^{2+} data appear to be quite normal. While the low-concentration behavior found for Y^{3+} and Zn^{2+} is believed to be real, the physical origin for the effect is not understood. It should also be observed, from Fig. 6.20, that both the K^+ and Cl^- ion mobilities decrease slightly faster than does the mobility of Na^+ ion. This observation, which is qualitatively consistent with the relaxation effect, indicates the absence of specific non-Coulombic forces between Na^+ (or K^+) and $pEBS^-$. It seems reasonable to generalize this result and to assert that no specific non-Coulombic force exists between alkali-metal cations and the sulfonate anion group in organic ion exchangers of the Dowex 50 type.

The decrease of D_{HTO} with increasing NapEBS concentration was much greater than the corresponding decrease of D_{H_2O} in NaCl solutions. From this observation one might be tempted to conclude that the $pEBS^-$ ion is a strong "structure maker." However, all that is observed is that the translational freedom of the water molecules is greatly restricted. Such an effect would also be observed in a solution of large noninteracting spheres in a continuum. The large spheres would effectively block part of the total area available to diffusion and would therefore decrease the mobility of a small species such as H_2O. This effect is the so-called "obstruction effect" whose magnitude may be calculated from hydrodynamic theory. Preliminary calculations for HTO diffusion in the NapEBS solutions studied in this research indicate that most, perhaps all, of the rapid decrease in D_{HTO} may be accounted for by the obstruction effect.

The tracer diffusion coefficients of Na^+ and Zn^{2+} are compared in Figs. 6.21 and 6.22, respectively, in a "typical" 1-1 inorganic electrolyte, in the model compound (NapEBS), and in cross-linked polystyrene-sulfonate-type ion exchangers. It should be noted that although NapEBS is believed to be a far better model

for the exchanger than a 1-1 inorganic electrolyte, diffusion of a cation in the model-compound solution is much faster than in the exchanger. Further, the model-compound and the polystyrenesulfonate curves do not seem to be approaching one another.

The diffusion of HTO in the model-compound (NapEBS) solution is compared with the diffusion of $H_2{}^{18}O$ in a Dowex-50-type ion exchanger in Fig. 6.23. Although the hydrogen form of the resin is used for the comparison, a comparison with the sodium form of the resin should give nearly identical results, because H^+ and Na^+ ions are known from experiment to have nearly identical effects on the mobility of H_2O. The

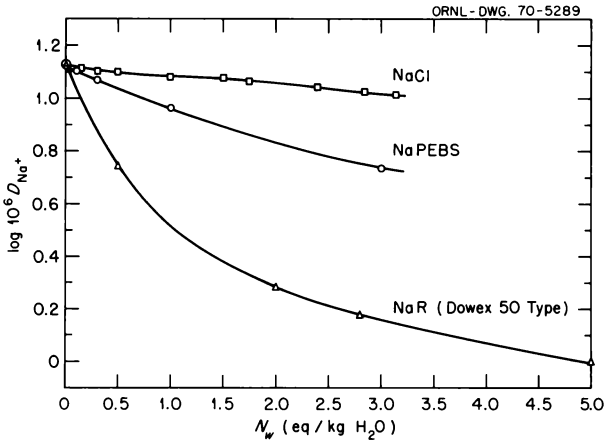

Fig. 6.21. Tracer Diffusion Coefficients of Na^+ for Various Electrolyte Systems.

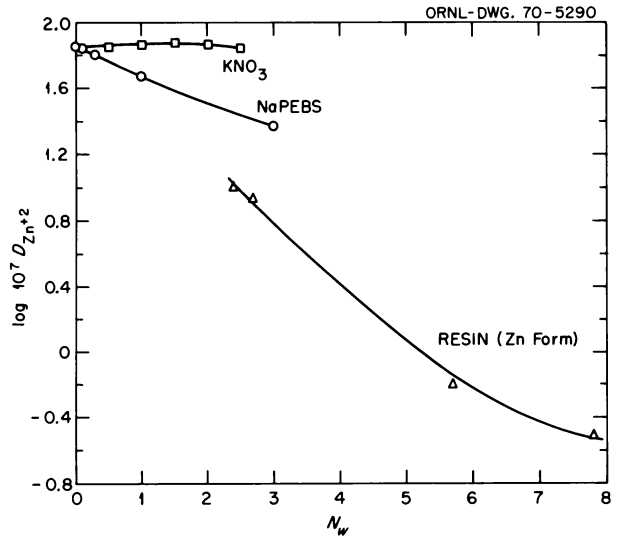

Fig. 6.22. Tracer Diffusion Coefficients of Zn^{2+} for Various Electrolyte Systems.

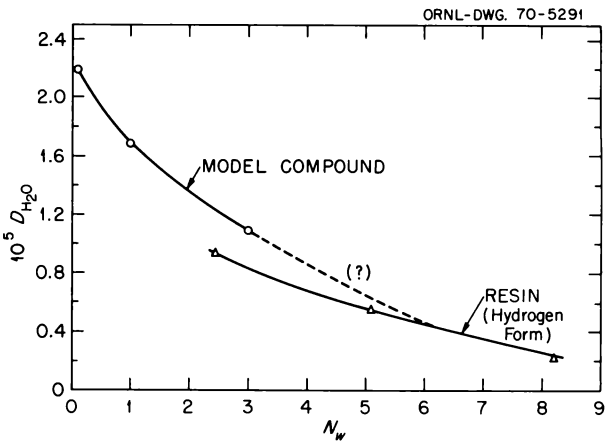

Fig. 6.23. Comparison of the Diffusion Coefficients of HTO in Sodium *p*-Ethylbenzenesulfonate with the Diffusion Coefficients of $H_2{}^{18}O$ in a Dowex-50-Type Ion Exchange Resin.

data in Fig. 6.23 show a semiquantitative agreement between the mobility of H_2O in the model compound and in the cross-linked ion exchanger at concentrations common to the two sets of data. Further, the model-compound curve seems to extrapolate into the resin curve. Thus it seems that the model compound, NapEBS, is a better model for the ion exchanger when diffusion of neutral species is compared rather than diffusion of ions. This observation suggests that the principal difference between an ion exchange resin and its "model compound" is in the nature of the distribution of counter ions around a moving ion.

In addition to diffusion measurements in 3.3 *m* NapEBS, diffusion measurements in ion exchangers of the Dowex 50 type will be made in the near future. The latter measurements will serve two purposes: (1) it is desirable to check the literature values of D_{H_2O} in cross-linked polystyrenesulfonate to establish whether the differences between the ion exchanger and the model-compound data are real or due to experimental error in the former data, and (2) the available data with ion exchangers are not suitable for quantitative comparisons of D_{Na^+}/D_i (i = other species) between exchanger and model-compound solutions. The ion exchange resin measurements planned will provide data suitable for this purpose.

[1] Visiting scientist from the Department of Chemistry, University of Tennessee, Knoxville.

MASS TRANSFER IN ION EXCHANGE TUBES

F. Nelson

In a previous annual report[1] a generalized expression for the limiting current obtainable from oxidation-reduction reactions in porous and tubular electrodes as a function of the parameters of the system (reactant concentration, volume flow rate, diffusion coefficient of the reactant species, and capillary length) and valid for both low and high flow rates was derived [Eq. (2) of ref. 1]. Good agreement between theory and experimental limiting currents of redox reactions in tubular platinum and graphite electrodes was demonstrated over the entire range of flow rates, including the transition region between rate control by surface reaction and by convective diffusion.

This equation has now been modified to express the efficiency of adsorption of ions in tubular adsorbents such as ion exchanger tubes:

$$i_m = u_v c_0' \left\{1 - \exp[-5.43(\mathbb{D}l/u_v)^{2/3}]\right\}, \qquad (1)$$

where i_m is the mass transport diffusion current (moles/sec), u_v is the solution flow rate (cm^3/sec), c_0' is the concentration of diffusing species (moles/cm^3), $\mathbb{D}$ is the diffusion coefficient (cm^2/sec), and l is the length of the tube (cm). The equation applies to conditions where the "back reaction" is negligible.

Two tests of Eq. (1) were undertaken in experiments measuring mass transport in ion exchange tubes by radiochemical techniques. First, at sufficiently high flow rate Eq. (1) reduces to

$$i_m = 5.43 c_0' u_v^{1/3} \mathbb{D}^{2/3} l^{2/3} . \qquad (2)$$

Confirmation of the dependence of the mass transport rate on the two-thirds power of the tube length at high flow rate was demonstrated by passing measured volumes of 10^{-3} M HCl containing tracer $^{22}Na^+$ through tubes lined with a cation exchange membrane (American Machine and Foundry C-60 membrane, H^+ form, 0.54 cm in diameter and 10 cm long) at a linear flow rate of 0.87 cm/sec (0.20 cm^3/sec) for 25 min. Under these conditions desorption of adsorbed tracer was negligible. At the end of each experiment the cation exchanger was cut into sections 1 or 2 cm long and analyzed for ^{22}Na activity, which is proportional to i_m. A log-log plot (Fig. 6.24) of the ^{22}Na activity summed over consecutive membrane sections vs the total length of the assayed sections shows a linear relationship with slope *ca.* $\frac{2}{3}$, as expected from Eq. (2).

Equation (1) was tested further under conditions of large adsorbability and of negligible desorption of ions, in which case F, the fraction of tracer adsorbed, is equal to $i_m/(u_v c_0')$. Then

$$F = 1 - \exp[-5.43(\mathbb{D}l/u_v)^{2/3}] . \qquad (3)$$

The solid curve in Fig. 6.25 describes this equation, and the points in the figure are the results of experiments carried out similarly to those described above at three different flow velocities and for several segments (l) of the tubular exchanger. The agreement of the data with the theoretical curve is excellent.

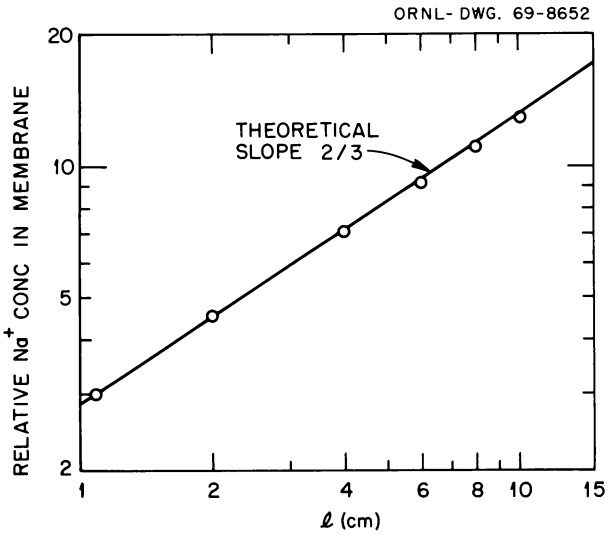

Fig. 6.24. Adsorption of Trace Na^+ in a Tubular Cation Exchanger. AMF C-60, i.d. = 0.54 cm, flow rate = 0.87 cm/sec.

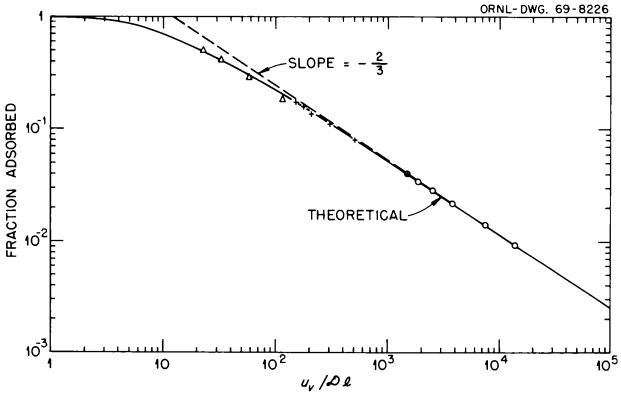

Fig. 6.25. Adsorption of Na^+ in a Cation Exchange Tube. Trace Na^+ in 10^{-3} M HCl; membrane AMF C-60, H^+ form, thickness 0.3 mm; tube length 1 to 10 cm, diameter 0.54 cm. Symbols correspond to experiments at different flow velocities.

In the case of very small loading of the exchanger, that is, small F, Eq. (3) reduces to

$$F = 5.43(u_v/\mathbb{D}l)^{-2/3} , \quad (4)$$

which is still applicable at both high and low flow rates. The log-log plot of F vs the dimensionless parameter $(u_v/\mathbb{D}l)$ of Fig. 6.25 shows that in the limit of small F, the data do indeed fall upon a straight line of proper slope as predicted by Eq. (4).

[1] K. A. Kraus *et al., Chem. Div. Ann. Progr. Rept. May 20, 1967,* ORNL-4164, p. 86.

MASS TRANSFER IN SHALLOW ION EXCHANGE BEDS

Fred Nelson

The previously considered electrochemical aspects of oxidation-reduction reactions in porous, screen, and tubular electrodes[1,2] have been applied successfully to mass transfer in ion exchange tubes.[3] A logical extension of these studies is mass transfer in ion exchange beds.

Consider an ion exchange column consisting of layers of ion exchange beads, each layer in close-packed array but the layers randomly stacked. In each layer the solution may be pictured as passing through the discrete openings or "channels" between the individual beads. Flow through each channel is considered to be laminar (except at very high flow rates), but considerable mixing between layers would be expected because, ideally, the exiting stream for each channel in one layer would not flow smoothly into a channel in the next layer below, but rather would impinge on ion exchange beads. This is assumed to result in complete mixing of the solution between layers. It should be noted that the ion exchange process considered here is not an equilibrium one but concerns adsorption from a flowing solution, with the exchanger acting as an infinite sink for ions; therefore, the back reaction (desorption) is negligible.

This model is similar to the "capillary model" applied earlier[2] to porous electrodes, which were considered to be a labyrinth of capillary tubes. The difference here is that each layer of beads consists of an "array of capillary tubes" through which the flow is laminar, but complete mixing of solution occurs between arrays. The shape of the channel between the beads is, to a first approximation, not important, for in the electrochemical analogy, the capillary diameter at constant volume flow rate has no effect on the limiting current in the laminar flow regime.

One consequence of this model is that the adsorption over a relatively large number of layers may be expressed by:

$$c_n/c_0 = (c_1/c_0)^n , \quad (1)$$

where c_0, c_1, and c_n are the concentrations of trace ion in the inflowing solution, in the effluent from one layer of beads, and from n layers of beads respectively.

To test the model, the rate of adsorption of ions at tracer concentration in shallow beds of cation exchange resins has been measured as a function of solution flow rate over a wide range of linear velocities. Solutions containing a radioactive tracer, $^{109}Cd^{2+}$, of high specific activity were used so that loading of the small beds would be minimal. To assure that desorption of the adsorbed tracer was negligible, the supporting electrolyte concentration was kept low (10^{-3} M HCl). The beds had a cross-sectional area of 0.5 cm^2 and were prepared from spherical cation exchange resins (Amberlite IR-120 or Dowex 50) of uniform size (20 or 35 mesh). Bed heights varied from a single monolayer of beads to as many as 20 layers. A few measurements were also made with beds containing nonuniform-sized beads, 20 to 35 mesh and 35 to 75 mesh.

Figure 6.26 shows the change in mass transfer current i_m (i.e., the amount of $^{109}Cd^{2+}$ adsorbed per second) with volume flow rate u_v for various numbers of layers

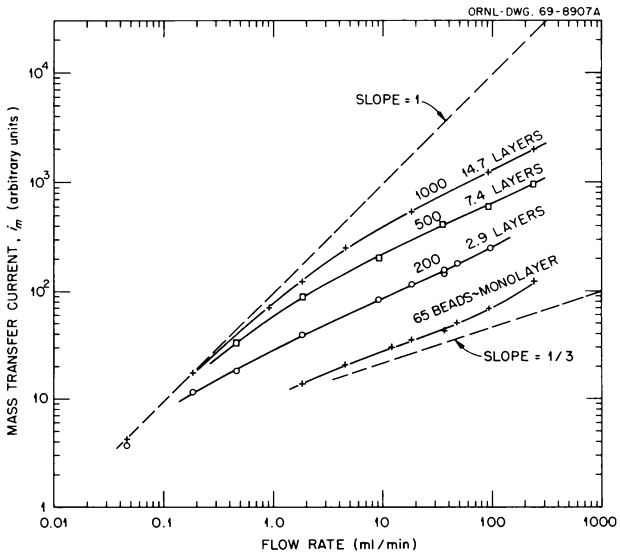

Fig. 6.26. Adsorption of Trace Cd^{2+} in 10^{-3} M HCl in Shallow Beds of Cation Exchange Resin as a Function of Flow Rate. Amberlite IR-120, 20 mesh, 0.5 cm^2 bed area.

of Amberlite IR-120 ion exchange beads. The dashed line in the figure represents i_m for 100% adsorption, a situation which is reached experimentally only at very slow flow rate. At faster flow rates the efficiency of adsorption decreases, and at sufficiently high flow rate the value of i_m should change with the cube root of u_v, as indicated in Eq. (2) of the preceding contribution,[3] that is, a log-log plot of i_m vs u_v should in the limit become a straight line of slope $^1/_3$, as already has been shown for tubular, porous, and screen electrodes[1,2] and tubular cation exchangers.[3] This is seen to be approximately the case in Fig. 6.26 for shallow beds of an ion exchanger over a range of intermediate flow rates.

A test of the validity of Eq. (1) is shown in Fig. 6.27, in which log (c_n/c_0) for $^{109}Cd^{2+}$ in 10^{-3} M HCl is plotted against the number of layers of beads (20-mesh Amberlite IR-120 cation exchange resin) for a range of fast flow rates. The linearity of the plot is in accord with Eq. (1).

The correspondence of these experimental results with the theoretical relationship previously derived [Eq. (3) of the preceding contribution[3] and the solid curve in Fig. 6.25] can also be tested. This is possible since each slope in Fig. 6.27 is equal to log (c_1/c_0) at the given flow rate. Since $F = 1 - (c_1/c_0)$ is the fraction of tracer ions in solution that has been removed by adsorption on the ion exchanger, one can calculate F experimentally and, through Fig. 6.25, find the corresponding theoretical value of $u_v/(\mathbb{D}l)$. The volume flow rate per channel, u_v, is equal to UA/N, where U is the linear flow rate (cm/sec), that is, the fluid velocity in the empty column; A is the cross-sectional area of the column (cm^2); and N is the number of channels per layer of beads. Hence,

$$u_v/(\mathbb{D}l) = UA/(N\mathbb{D}l) ,$$

and the product Nl is the only unknown. The magnitude and constancy of Nl over the range of experimental flow rates is a test of the reasonableness of the model. The results are summarized in Table 6.3.

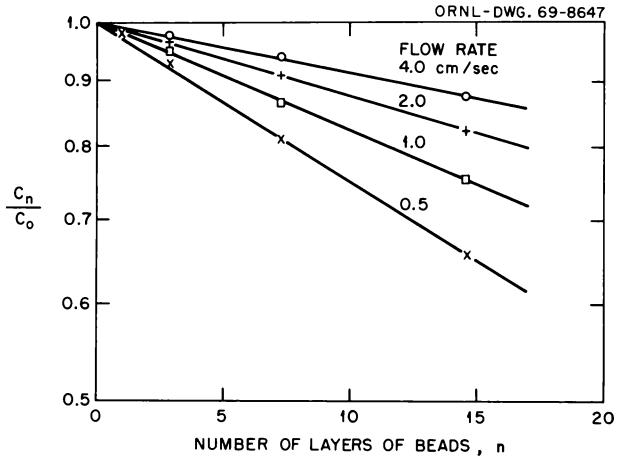

Fig. 6.27. Adsorption of Trace Cd^{2+} in 10^{-3} M HCl in Shallow Beds of Cation Exchange Resin as a Function of the Number of Layers of Beads. Amberlite IR-120, 20 mesh, 0.5 cm^2 bed area.

Although the values of Nl are not constant but show a gradual increase with increasing flow rate, agreement of the data with the capillary model is considered satisfactory, since drifts in the value of Nl could result from variations in channeling, wall effects, and bed packing from experiment to experiment. It appears significant that the magnitude of the drift is less for the 35-mesh than the 20-mesh resin beds, presumably because wall effects become relatively less important with finer resins in columns of fixed cross-sectional area.

A further test of the reasonableness of the model can be made by comparing values of N computed from Nl (assuming l equal to the diameter of the beads) with values of N estimated from geometrical considerations. Thus from Nl values of Table 6.3, N is found to range from 144 to 204 and from 358 to 482 (per square centimeter) for 20- and 35-mesh resin beds, respectively, in the flow-rate region 0.25 to 2.0 cm^3/sec. The number of openings (channels) per sphere is 2 for an ideal hexagonal close-packed array of spheres in an infinite plane. From the measured number of beads (per cubic centimeter) in the beds and assuming isotropic distribution of the particles, the mean number of beads per layer may be computed. These values correspond to N = 136 and 376 channels/cm^2 for 20- and 35-mesh resin beds respectively. Considering that wall effects are ignored, the estimated values of N agree well with those computed from Nl.

Finally, Eq. (4) of the preceding contribution[3] predicts that at sufficiently high flow rates, the ratio of the fractions of elements adsorbed from solution should vary with the $^2/_3$ power of the diffusion coefficients of the tracers. Table 6.4 summarizes rapid-flow experiments carried out with tracer Na^+ and Cd^{2+} in 10^{-3} M HCl; after each experiment the beds were analyzed radiometrically for both Na^+ and Cd^{2+}, and the fraction of each element adsorbed from the solution, $F = 1 - (c_n/c_0)$, was computed. The last column of Table 6.4 shows that the ratio F_{Na}/F_{Cd} is approximately equal to $(\mathbb{D}_{Na}/\mathbb{D}_{Cd})^{2/3}$, as expected.

Table 6.3. Test of "Capillary-Layer" Model of Mass Transfer in Shallow Ion Exchange Beds

Adsorption of tracer Cd^{2+} in 10^{-3} *M* HCl in shallow beds of Amberlite IR-120 resin
$\mathbb{D}_{Cd^{2+}} = 0.72 \times 10^{-5}$ cm²/sec
bed area (*A*) = 0.5 cm²

U (cm/sec)	u_v (cm³/sec)	$-\log (c_1/c_0)$	*F*	$u_v/(\mathbb{D}l)^a$	*Nl* (cm)
				$\times 10^3$	
		20-Mesh Resin			
4.0	2.0	0.00393	0.0090	14.7	18.9
2.0	1.0	0.00574	0.0131	8.40	16.5
1.0	0.5	0.00840	0.0191	4.75	14.6
0.5	0.25	0.01247	0.274	2.82	12.7
		35-Mesh Resin			
4.0	2.0	0.00485	0.0111	10.7	26.0
2.0	1.0	0.00730	0.0167	5.80	24.0
1.0	0.5	0.0106	0.0229	3.10	21.3
0.5	0.25	0.0157	0.0355	1.85	19.3

[a]Dimensionless parameter from Fig. 6.25 corresponding to the listed values of *F*.

Table 6.4. Adsorption of Trace Na^+ and Cd^{2+} in 10^{-3} *M* HCl in Shallow Beds of Cation Exchange Resins

bed size: 0.5 cm² by 0.5 cm
flow rate = 3.2 cm/sec

Resin	Mesh Size	Fraction Adsorbed		F_{Na}/F_{Cd}
		F_{Na}	F_{Cd}	
IR-120	20	0.082	0.0550	1.49
IR-120	35	0.168	0.108	1.55
IR-120	20–35	0.129	0.0864	1.49
Dowex 50W	35	0.179	0.116	1.54
Dowex 50W	35–75	0.456	0.317	1.46

$(\mathbb{D}_{Na}/\mathbb{D}_{Cd})^{2/3} = (1.33/0.72)^{2/3} = (1.85)^{2/3} = 1.51$

[1]K. A. Kraus *et al., Chem. Div. Ann. Progr. Rept. May 20, 1967*, ORNL-4164, p. 86.

[2]F. Nelson, P. M. Lantz, and K. A. Kraus, *Chem. Div. Ann. Progr. Rept. May 20, 1968*, ORNL-4306, p. 103.

[3]F. Nelson, "Mass Transfer in Ion Exchange Tubes," preceding contribution, this report.

SWELLING OF LOW-CROSS-LINKED ION EXCHANGE RESINS

F. Nelson K. A. Kraus D. C. Michelson

Studies of swelling characteristics of relatively low cross-linked cation and anion exchange resins in electrolyte solutions were continued. These materials are of interest because they show large volume changes with change of electrolyte concentration; in addition, some of them show significant salt-rejecting properties when finely ground and used as film-forming additives in hyperfiltration experiments.[1,2]

Strong acid and strong base resins having two different types of networks were investigated: polystyrene-divinylbenzene resins (Dowex 50 and Dowex 1) and cross-linked dextran resins (SE-Sephadex and QAE-Sephadex).[3] The capacities of the resins on a dry basis were similar, ranging from 2.3 to 5.2 equivalents per kilogram of dry Na^+-form or Cl^--form resin. Typical swelling measurements for NaCl solutions are shown in Figs. 6.28 and 6.29 as plots of bed volume (in liters per kilogram of dry resin) vs molality of NaCl. The degree of cross-linking in the Sephadex resins was not specified by the manufacturer; however, resins designated C-50 and A-50 are stated to be less cross-linked than corresponding C-25 or A-25 resins, a relative order consistent with their observed swelling properties. For each resin the bed volume asymptotically approaches a constant (maximum) value at very low NaCl concentrations.

An equation which correlates water uptake with the capacity of water-swollen resin and with the osmotic and activity coefficients of the electrolyte in the resin and solution phases has been derived. Since the osmotic coefficients and activity coefficients of NaCl in these resins are unknown, a complete test of the validity of the derived expression is not yet possible; the necessary measurements are now being carried out. However, with certain simplifying assumptions (e.g., that the ratios

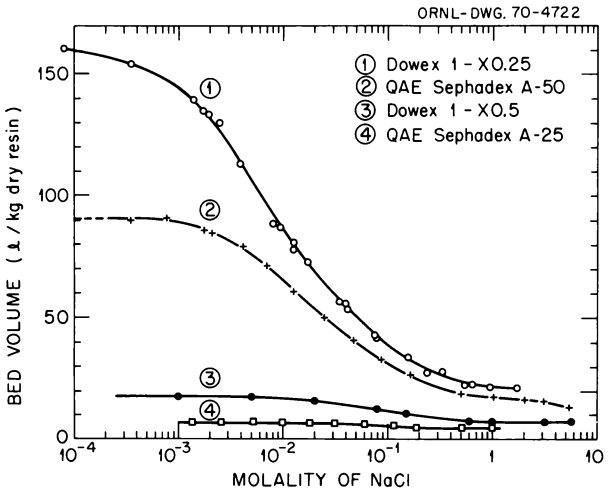

Fig. 6.28. Bed Volume of Some Low-Cross-Linked Anion Exchange Resins in NaCl Solutions (25°C).

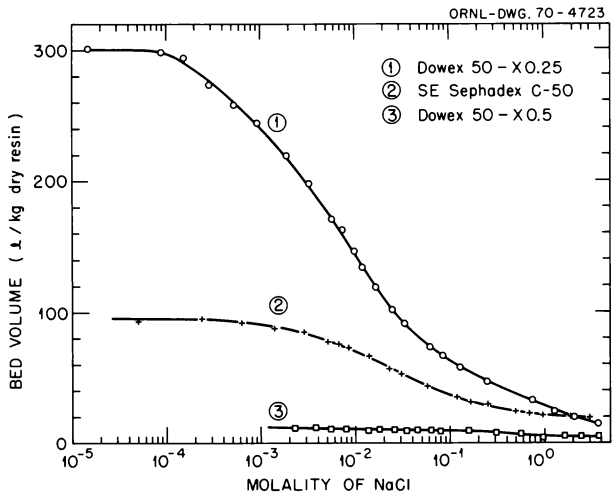

Fig. 6.29. Bed Volume of Some Low-Cross-Linked Cation Exchange Resins in NaCl Solutions (25°C).

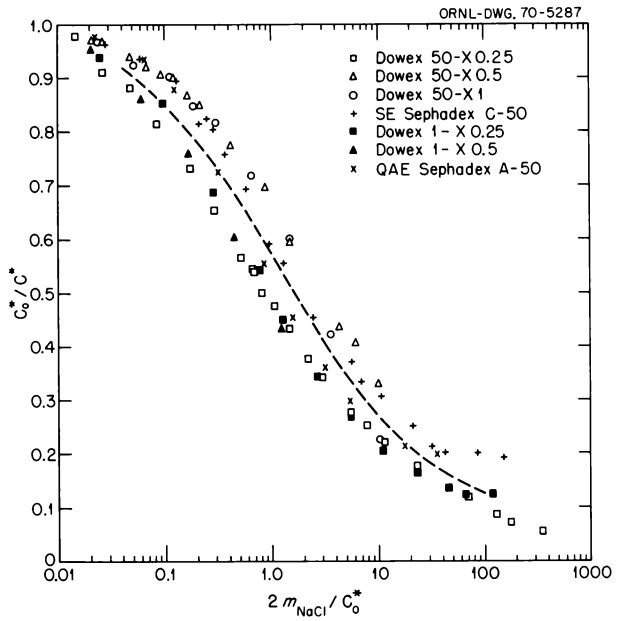

Fig. 6.30. Correlation of Swelling Data for Low-Cross-Linked Ion Exchange Resins in NaCl Solutions (25°C).

between the resin and the solution phases of the osmotic coefficients and of the activity coefficients of the electrolyte are unity), the equation can be reduced to an expression relating C_0^*/C^* and the quantity $2m_{NaCl}/C_0^*$, where C_0^* is the capacity of the swollen resin in water (in moles of sites per kilogram of H_2O in the resin) and C^* is its capacity in NaCl solution of concentration m_{NaCl}. This relationship is shown in Fig. 6.30, which satisfactorily correlates the swelling data for seven different cation and anion exchange resins. Furthermore, the simplified treatment predicts that C_0^*/C^* should be ~0.5 at $2m_{NaCl}/C_0^* = 1.5$, which is seen to be approximately the case from Fig. 6.30.

For resins of high water content, the ratio C_0^*/C^* is approximately equal to the ratio of the bed volume of resin in NaCl solution to that in water. Hence Fig. 6.30 should also be useful for estimating relative bed volume changes of highly swollen resins in NaCl solutions when the water-swollen volume is known.

---

[1] K. A. Kraus, A. J. Shor, and J. S. Johnson, Jr., *Desalination* 2, 243 (1967).

[2] S. B. Sachs, W. H. Baldwin, and J. S. Johnson, *Desalination* 6, 215 (1969).

[3] Pharmacia Fine Chemicals, Uppsala, Sweden. The prefixes *SE-* and *QAE-* designate the *s*ulfonate and *q*uaternary *a*mine resins respectively. Correspondingly, the suffixes *C-* and *A-* refer to these *c*ation and *a*nion resins.

HYPERFILTRATION WITH DYNAMICALLY FORMED MEMBRANES

W. H. Baldwin
M. S. Bautista[1]
J. Csurny
J. A. Dahlheimer[2]
L. Dresner[3]
J. M. Ganzer[1]
Neva Harrison
J. R. Hart[4]
C. E. Higgins
J. S. Johnson
K. A. Kraus[5]
J. R. Love[2]
R. H. Mayer[1]
A. K. Mehta[1]
W. R. Mixon[2]
J. W. Myers[4]
D. C. Michelson
H. O. Phillips
A. J. Shor[4]
Warren Sisson[6]
D. G. Thomas[2]
C. G. West
C. G. Westmoreland

Hyperfiltration studies under the Water Research Program continued to emphasize development of dynamically formed membranes for desalination, supported by the Office of Saline Water, and for processing of effluents from conventional primary and secondary treatment of municipal sewage, supported by the Federal Water Quality Administration, both sponsors being agencies of the U.S. Department of the Interior. Numerous additives, porous supports, and procedures have been tested during the year. Theoretical studies were resumed, particularly in the areas of transport through membranes of multicomponent salt solutions and of concentration polarization with multicomponent solutions. Because this work is to be reported in detail to the appropriate agencies, we shall confine this account to a brief description of dual-layer hydrous oxide–polyacrylic acid (PAA) membranes, in some ways the most interesting development during the year.

In recent years we have tended to stress membranes of organic polyelectrolytes, since the pH of their optimum performance frequently matches acidities of natural brackish waters. Polyacrylic acid membranes have been of interest to us for some time.[7] Salt removal by these is generally higher than by other organic polyelectrolytes. However, there have been certain disadvantages. Fluxes are usually lower than those of other members of the dynamic class, and presence of polyvalent counterions in feeds, while not as deleterious as with many ion exchange membranes, still has serious effects. We have also had trouble in forming polyacrylate membranes on many porous supports, a difficulty which perhaps is associated with irreproducibility of properties and which does not bode well for practical applications.

Hydrous oxide membranes, when operated at optimum pH values and in contact with feeds containing no polyvalent counterions, are usually easy to form on a wide variety of supports and have interesting rejections and high fluxes,[8] particularly if formed at high circulation velocity. An example is given in Fig. 6.31; since rejections are presented as $\mathbf{R}_{obs}$, obtained by comparison of feed and product concentrations, they underrate the salt-filtering capability of the membranes. At such high fluxes, salt buildup at the feed-membrane interface affects results substantially. From concentration polarization theory[9] we estimate the rejection **R**, based on the difference in concentration between the effluent and that computed for the feed-membrane interface, to be 81%, compared with $\mathbf{R}_{obs}$ = 57% for the point in Fig. 6.31 for the 0.45-μ support at 140 min (~1400 gpd/ft^2). With hydrous oxide membranes, however, best salt rejections are usually found at high anion exchange capacities, which usually occur at acidities higher than those of most natural waters. Hydrous oxide anion exchangers also tend to be particularly prone to poisoning by sulfate and other polyvalent counterions.

We have found that some of the advantages of hydrous oxide and polyacrylate membranes can be combined by forming a hydrous oxide sublayer, exposing it at acidic pH to a feed containing polyacrylic acid, and then adding base to bring feed pH into the neutral range. Table 6.5 illustrates a typical membrane formation. A hydrous Zr(IV) oxide membrane, formed from a colloidal dispersion, filtered out 62% of salt from a 0.05 *M* NaCl solution. At pH 6, rejection of the Zr(IV) membrane dropped, since ion exchange capacity is lower under this condition. Rejection remained low on

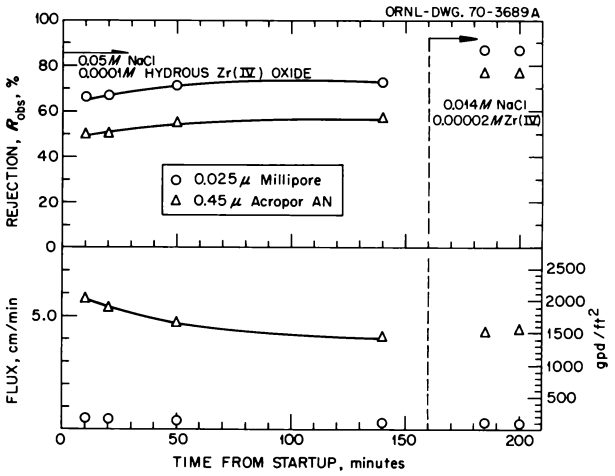

Fig. 6.31. Hyperfiltration with Hydrous Zr(IV) Oxide Membrane Formed at High Circulation Velocity. 50 ft/sec, pH 4 to 4.5.

Table 6.5. Formation of Hydrous Zr(IV) Oxide–Polyacrylate Membrane

0.05 *M* NaCl, 1000 psig, 37 fps, 0.45-μ Acropor AN support on tube

Additive	pH	R_{obs} (%)	Flux (gpd/ft^2)
0.001 *M* hydrous Zr(IV) oxide	3.1	62	630
None	6.0	32	690
20 ppm PAA	5.6	23	700
20 ppm PAA	2.7	53	370
20 ppm PAA	5.6	82	210

addition of neutralized polyacrylic acid. However, on adding HCl to pH 2.7 and then NaOH to bring the pH back to 5.6, rejection rose to 82%.

It is not necessary to introduce the polyacrylate in the salt form, but only to expose the hydrous oxide sublayer to polyacrylic acid under acid conditions, preferably pH below 4. Apparently some of the small fraction of carboxyls ionized at acidic pH become attached to the anion exchange sites of the hydrous oxide, and the attachment is not broken on adding base unless high pH values [~pH 11 for hydrous Zr(IV) oxide] are reached. On raising pH the attached polyacrylic acid is converted to the salt form, and rejection increases with increasing cation exchange capacity. At high alkalinity, membrane rejection may be decreased by loosening of the polyelectrolyte from the hydrous oxide, but it is usually restored by a cycle through acidic pH.

The effect of pH on rejection of NaCl is shown in Fig. 6.32. The results are qualitatively similar to those given in Fig. 3 of ref. 7 for a simple polyacrylate membrane. Rejections are a few percent higher for the dual-layer membrane, and the difference is greater than indicated by direct comparison, since Fig. 6.32 gives rejections as R_{obs} and Fig. 3 of ref. 7, as **R**. The increase in rejection with increasing pH to pH ~8 is consistent with acid-base titration of PAA; full neutralization is approached at about this pH. Fluxes are higher for the dual-layer than for the simple membrane.

Table 6.6 lists a sequence of rejections, including values for a salt with a polyvalent coion (Na_2SO_4) and a polyvalent counterion ($MgCl_2$). The rejections are in the order expected of a cation exchange membrane – highest for Na_2SO_4, intermediate for NaCl, and lowest for $MgCl_2$. The rejection of $MgCl_2$ (64%) is considerably higher than with a simple polyacrylate membrane, <40% in Fig. 3 of ref. 7. Exposure to Mg^{2+} caused a drastic decrease in flux, and much of the decrease persisted after return to an NaCl feed in this case. The effect of Mg^{2+} has appeared to be more rapidly reversible in some experiments.

Of more practical importance is the performance of the membrane with feed solutions of compositions typical of natural waters, containing usually sulfate, magnesium, and calcium in addition to sodium and chloride ions. Figure 6.33 summarizes tests of membranes on supports of two different pore sizes carried out about two weeks later in the same run in which the results in Fig. 6.32 and Table 6.6 were obtained. Some of the tests were at twice and three times the usual compositions,[10] to simulate the effect of concentrating feeds as product is removed. Rejections, based on total anion (by-passage of samples through a column of chloride-form anion exchanger and determination of chloride in the effluent), scatter between 85 and 95% for brackish waters and were surprisingly high even at seawater concentrations. Figure 6.33 also includes values for a simple polyacrylate membrane (half-shaded points) taken from Table IV of ref. 7. It can be seen

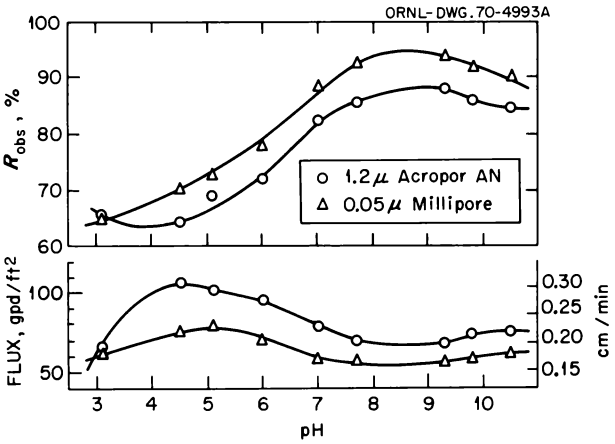

Fig. 6.32. Effect of pH on Hyperfiltration Properties of Polyacrylate Membrane Dynamically Formed on a Hydrous Zr(IV) Oxide Sublayer. 0.05*M* NaCl; 1000 psig; 35ft/sec.

Table 6.6. Hyperfiltration of Na_2SO_4 and $MgCl_2$ by Hydrous Zr(IV) Oxide–PAA Membranes

pH = 7, P = 1000 psig, velocity = 35 fps, 0.05-μ Millipore

Feed	R_{obs} (%)	Flux (gpd/ft^2)
0.05 *M* NaCl	82	73.5
0.025 *M* Na_2SO_4	98	72
0.025 *M* $MgCl_2$	64	8.8
0.05 *M* NaCl	90	28

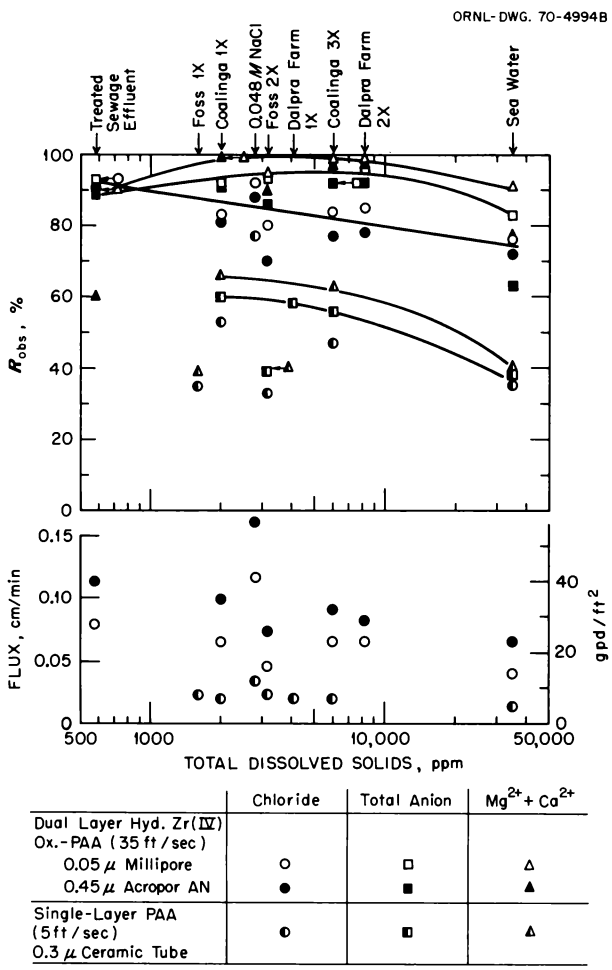

Fig. 6.33. Hyperfiltration of Natural Water Compositions with Dynamically Formed Polyacrylate Membranes. 1000 psig.

that for these practical desalination feeds, both rejections and fluxes of the dual-layer membranes are much higher than for the single-layer polyacrylate membranes. The differences are considerably more than can plausibly be expected from differences in experimental conditions.

Dual-layer membranes also are interesting for sewage treatment applications. Figure 6.34 summarizes a ten-day test carried out in our mobile loop at the Oak Ridge East Sewage Plant with membranes preformed in our laboratory corrosion-resistant loop. The double-layer membrane was the same discussed in connection with Table 6.5, and its properties are compared in Fig. 6.34 with another dual layer prepared simultaneously on 0.025-μ Millipore and with membranes prepared, in a separate run, of homogenized low-cross-linked Dowex 50 (polystyrenesulfonate) ion exchangers; some results with the latter type of membrane were reported last year.[11] The feed was effluent from primary treatment, to which 500 ppm NaCl was continuously added to allow testing at higher dissolved solids than the relatively low-salinity Oak Ridge sewage permitted.

An initial test at the sewage plant with water and 500 ppm NaCl indicated deterioration of rejections of all membranes from values measured at the end of the preforming runs. Whether these lower rejections were caused by moving the membranes or by effect of residual impurities in the mobile loop is not clear, but rejections recovered somewhat on exposure to sewage, presumably because of plugging of defects. Fluxes through both types of membranes on 0.025-μ Millipore were so much lower than through membranes on supports of larger pore size that we shall not discuss them further.

With the 0.45-μ supports both rejections and fluxes in this experiment were higher for the dual-layer hydrous oxide–PAA membrane than for the homogenized ion exchanger. Over the period of the test, fluxes through the dual-layer membrane declined from 100 to 50 gpd/ft²; decline through the Dowex 50 was from 60 to 20 gpd/ft². Chloride rejections by the Zr(IV)-PAA were mostly between 60 and 70%, and rejections of organic carbon were 90 to 95% between 50 and 200 hr.

The product rates for the dual-layer membrane on the 0.45-μ support in Fig. 6.34 are much higher, by something like a factor of 10, than those through cellulose acetate in tests known to us for similar

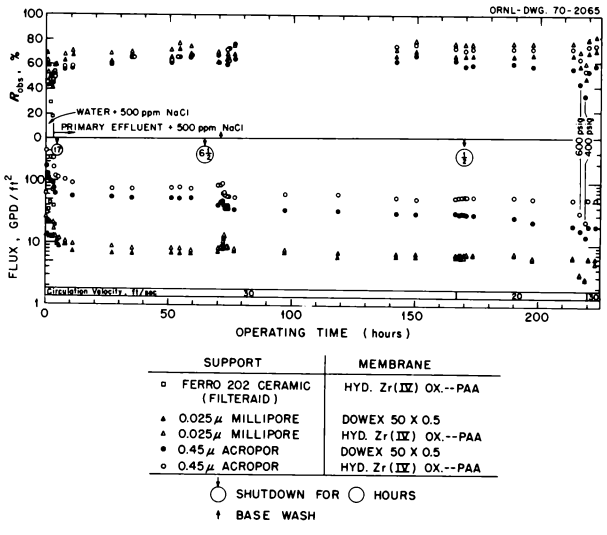

Fig. 6.34. Hyperfiltration of Effluent from Primary Treatment of Sewage with Dynamically Formed Membranes. 1000 psig, unless noted.

applications. Rejections are probably adequate for most purposes. Perhaps the main difficulty (besides the necessity for development of a suitable support module) which must be resolved before practical application to sewage treatments is the high circulation velocities. Fast feed flows seem necessary to maintain high production rates with both these types of membranes, as well as for homogenized Sephadex CM-C25, a dextran-based carboxylate ion exchanger marketed for gel filtration, another promising candidate for sewage treatment.

In summary, dual-layer hydrous oxide–polyacrylate membranes usually have higher fluxes and somewhat higher rejections than simple polyacrylate membranes. With compositions typical of natural waters, salt filtration is much more efficient with the dual-layer type. It may well be that hydrous oxides from corrosion products have contributed to the performance of PAA membranes we have studied earlier. In our corrosion-resistant loop, we have had difficulty forming simple polyacrylate membranes on 0.45-μ supports. In seven tests the best values of $\mathbf{R}_{obs}$ obtained for 0.05 *M* NaCl scattered between 25 and 60%. Only when Fe(III) was introduced and an acid cycle was carried out were high rejections consistently attained.

Hydrous Sn(IV) oxide, as well as oxides of Fe(III) and Zr(IV), has served successfully as a sublayer. In some recent tests, hydrous Zr(IV) oxide premixed with excess polyacrylic acid appears to form membranes having properties similar to the dual-layer type. Two-step formation may therefore not be necessary.

---

[1] Massachusetts Institute of Technology School of Chemical Engineering Practice. R. H. Mayer, Director, and M. S. Bautista, Assistant Director, of the Oak Ridge Station.

[2] Reactor Division.

[3] Neutron Physics Division.

[4] Reactor Chemistry Division.

[5] Director's Division.

[6] Chemical Technology Division.

[7] S. B. Sachs, W. H. Baldwin, and J. S. Johnson, *Desalination* **6**, 215 (1969).

[8] A. J. Shor, K. A. Kraus, W. T. Smith, Jr., and J. S. Johnson, Jr., *J. Phys. Chem.* **72**, 2200 (1968).

[9] T. K. Sherwood, P. L. T. Brian, R. E. Fisher, and L. Dresner, *Ind. Eng. Chem. Fundamentals* **4**, 113 (1965).

[10] Compositions approximated from values given in Office of Saline Water Research and Development Report 134 and personal communication from H. E. Podall. Natural seawater used in test without hydrous oxide sublayer. Coalinga: 0.0028 *M* $NaHCO_3$, 0.0096 *M* Na_2SO_4, 0.0018 *M* $CaCl_2$, 0.0020 *M* $MgCl_2$. Foss reservoir: 0.005 *M* $MgSO_4$, 0.005 *M* $CaSO_4$, 0.0014 *M* NaCl, 0.0026 *M* $NaHCO_3$. Dalpra farm: 0.008 *M* $NaHCO_3$, 0.019 *M* Na_2SO_4, 0.003 *M* $MgSO_4$, 0.003 *M* $CaCl_2$, 0.00004 *M* $FeCl_3$, 0.00002 *M* $MnCl_2$. Seawater: 0.47 *M* NaCl, 0.03 *M* $MgSO_4$, 0.04 *M* $MgCl_2$, 0.002 *M* $NaHCO_3$.

[11] *Chem. Div. Ann. Progr. Rept. May 20, 1969*, ORNL-4437, p. 78.

POLYMER STUDIES

Neva Harrison C. E. Higgins
J. Csurny W. H. Baldwin

Polymer Degradation by Shear

Alexander and Fox[1] have demonstrated the decrease in the viscosity of polymethacrylic acid by ultrasonics and by high-speed stirring in a Waring blender (rated 20,000 rpm). They interpret this decrease in viscosity to be a reflection of the decrease in molecular weight.

We have confirmed this decrease in viscosity by stirring polyethylene oxide (WSR-205, 5 g/liter) at high speed in a Waring blender for 5 min; the intrinsic viscosity of the solution was decreased by a factor of 2.

If reductions of molecular weight are truly produced by mechanical action, significant effects may be observed in the hyperfiltration process using dynamic membranes where one circulates a solution of a polymer to form the membrane.[2] Further, such diminution of molecular weight may result during polymer preparation, since one often stirs polymers with solvents in a blender during purification.

Preparation of Polystyrenesulfonate with Low Degrees of Cross-Linking

Polyelectrolytes with low degrees of cross-linking were desired for testing as dynamic membranes in hyperfiltration.[2] Two methods were used wherein cross-linking was obtained by sulfone formation during the sulfonation step, and a third method where a small quantity of divinylbenzene was copolymerized with styrene to form the cross-linked polyhydrocarbon which probably was further cross-linked during the sulfonation step.

Reaction of polystyrene (mol. wt 2×10^5) with concentrated sulfuric acid (5 ml per gram of polystyrene) at 150°C for 5 hr yielded a gel containing 0.14 g of solid per gram of gel and analyzing 4.4 milliequivalents of acid per gram of dry polymer. Reaction with chlorosulfonic acid in CCl_4 produced a gel of 0.027 g of solid per gram of gel and 5.7 milliequivalents of acid per gram of dry polymer. The product from

sulfonation of poly(styrene-co-divinylbenzene) with chlorosulfonic acid contained 0.04 g of solid per gram of gel and 4.2 milliequivalents of H^+ per gram of dry polymer.

Equilibria in the System: Poly(Hydroxypropyl Acrylate-co-Tetraethylene Glycol Dimethacrylate), Water, and Electrolyte

The title polymer, when already equilibrated with water, shows a considerable increase in volume when equilibrated with 0.5 *M* NaCl–0.02 *M* NaOH solution.[3] This unexpected swelling is definitely the result of hydrolysis of the polymer (see Table 6.7). The amount of swelling varies with the degree of hydrolysis for the monovalent electrolytes. Cupric ion does not follow the pattern of monovalent electrolytes and may be the result of additional cross-linking that prevents swelling.

[1] P. Alexander and M. Fox, *J. Polymer Sci.* 12, 533 (1954).

[2] J. N. Baird *et al.*, *Chem. Div. Ann. Progr. Rept. May 20, 1969*, ORNL-4437, pp. 78–84.

[3] C. E. Higgins and W. H. Baldwin, *Chem. Div. Ann. Progr. Rept. May 20, 1968*, ORNL-4306, p. 71.

Table 6.7. Equilibration[a] of Poly(Hydroxypropyl Acetate-co-Tetraethylene Glycol Dimethacrylate) with Aqueous Electrolytes

Electrolyte	Exchange Capacity (milliequivalent per gram of dry polymer)	Swelling[b]
LiOH	10	20
NaOH, CsOH	9	20
$(CH_3)_4NOH$	7	19
Na_2CO_3	3	12
Na_2HPO_4	0.9	5.8
$NaHCO_3$	0.9	5.5
Sodium acetate	0.8	5.4
Cupric acetate	1.1	1.1

[a] 0.1 *M* electrolyte solution, nine days at room temperature.

[b] Volume of gel in 0.1 *M* electrolyte / volume in distilled water

APPLICATION OF CROSS-FLOW FILTRATION TO POLLUTION CONTROL PROBLEMS[1]

H. A. Mahlman K. A. Kraus
W. G. Sisson[2] J. Csurny
H. O. Phillips

Cross-flow filtration is a separations process in which solid suspensions or colloidal solutions under pressure flow tangentially past a filtering surface under hydrodynamic conditions that prevent buildup of filter cake. An experimental system has been designed and constructed to evaluate cross-flow filtration for converting primary sewage effluent into potable water. Concurrently we have begun construction of a mobile test loop inside a semitrailer which will be placed at the Oak Ridge East Sewage Plant for on-site operation.

A primary objective of our research is optimizing the efficiency of separation at high flow rates from both primary and clarified sewage effluents of finely divided carbon, added as an adsorbent.

[1] Work sponsored by the Federal Water Quality Administration, U.S. Department of the Interior.

[2] Chemical Technology Division.

"POLYWATER," RAMAN AND INFRARED SPECTRA

M. A. Bredig[1]

Following the papers by Deryagin *et al.* on "anomalous water," the report last June by Lippincott *et al.*[2] on infrared and Raman spectra was the first to create really intense and widespread interest among both the general public and the scientific community. I was then prompted to attempt bolstering, by a careful scrutiny of the spectroscopic evidence, the very strong skepticism which I shared with others at this Laboratory in regard to the existence of a new form of liquid water. Suggestions that because of its alleged high-temperature stability "polywater" might find practical applications, including some in nuclear reactor technology, appeared to be attended by the spending of considerable research effort throughout the country. This seemed to call for an earnest attempt at quick refutation.

My efforts were directed toward a demonstration that the spectra, reportedly unique, could in fact be interpreted in terms of impurities or of simple well-known chemical entities, the presence of which was suggested by the experimental conditions.

The Raman Spectrum

A search through the Raman spectra of many compounds, especially those suspect as contaminants, yielded no satisfactory fit. What may be taken as the one exception was the spectrum of the SiF_6^{2-} ion.[3] Its strongest band, $\nu_1 \approx 654 \pm 5$ cm^{-1}, greatly resembles in relative intensity and width the strong band of "poly-

water" centered at 644 or 630 cm^{-1}, depending on which of two spectra reported[2] is taken for comparison. The discrepancy of 10 or 24 cm^{-1} is uncomfortable but, in fact, hardly greater than that between the two spectra reported or greater than the half width of the band. If the "conventional methods" of cleaning glass reportedly used[2] included hydrofluoric acid (cf. also Deryagin *et al.*), the presence of SiF_6^{2-}, perhaps in the form of solid Na_2SiF_6, could be understood. Of the only other two, much weaker, Raman bands of SiF_6^{2-}, one ($\nu_2 \approx 471 \pm 5$ cm^{-1}) might be compared with the similarly weak band at 463 cm^{-1} appearing in "polywater." Identification of the second band ($\nu_5 \approx 401 \pm 5$ cm^{-1}) is impaired by the termination of the "polywater" spectrum at 400 cm^{-1} and the steeply rising background. [Like the band at 1050 cm^{-1}, ascribed by Lippincott *et al.* to the quartz capillary but most likely due to the argon laser lines 19,448 and 19,435 cm^{-1} ($\Delta\nu$ = 1044 and 1057), that background is definitely not attributable to fused quartz, because a strong band at 800 cm^{-1}, very characteristic of fused quartz, was not observed.]

A strong point in support of "polywater" has been made of the absence of Raman frequencies in the region between 3000 and 4000 cm^{-1} for the O–H stretch characteristic of normal liquid water.[2] From experience in our laboratory with laser-excited Raman spectra of minute quantities of water in narrow capillaries, it would not be surprising if in Lippincott's measurements part of the sample had distilled quickly out of the range of the intense exciting beam, leaving a residue containing the SiF_6^{2-} ion behind.

A very weak, very narrow band at 3420 cm^{-1} was ascribed by Lippincott *et al.* "to traces of residual water." This conclusion must astonish anyone familiar with the very broad Raman band of water, having a width many times that of the band at 3420 cm^{-1}.

It seems that at least a provisional identification of the particular single Raman spectrum published thus far for "polywater" as that of the SiF_6^{2-} ion has been achieved.

The Infrared Absorption Spectrum

The only two infrared spectra in the characteristic range between 4000 and 500 cm^{-1} reported thus far by the proponents[2,4] of "polywater" differ considerably from each other by the following features (Fig. 6.35).

In spectrum II, more recently reported by Page, Jakobsen, and Lippincott,[4] which we consider first, two strong, broad absorption regions from 3600 to 2900 cm^{-1} (the O–H stretch region) and 950 to 650 cm^{-1} appear, both of which were essentially absent in spectrum I of Lippincott *et al.*[2] (Fig. 6.35). These absorptions represent considerable amounts of normal liquid water; consequently, the strong absorption band near 1600 cm^{-1} must be assigned principally to the H–O–H bending mode of normal liquid water rather than to a new species, "polywater."

Both the distinct peak at 1455 cm^{-1}, ignored by the authors,[4] and the weaker one at 1665 cm^{-1}, on the shoulder of the strongest band at 1600 cm^{-1}, were absent in the original "polywater" spectrum I. The addition of the peak at 1455 cm^{-1} reduced the resolution of the "polywater" bands. The peak at 1665 cm^{-1} was interpreted[4] as the H–O–H bending mode of normal liquid water and referred to as "1645." In the background spectrum this H–O–H vibration is seen at 1615 cm^{-1}. Therefore, the 1665-cm^{-1} peak in the spectrum of the sample cannot be the same species. Apparently a discrepancy of 50 cm^{-1} was simply ignored. I much prefer the assignment of both the 1665- and 1455-cm^{-1} absorptions to the rather distinctly separate two branches of the H–O–H bending vibration (ν_0 = 1595 cm^{-1}) in water *vapor* which was evidently in imbalance within the double-beam spectrometer used.[4] [The small quantity of water vapor thus indicated to have been present in the sample beam may perhaps have arisen throughout the scanning period from the sample as it warmed up in the strong infrared radiation. A similar though much lesser imbalance in water vapor appears in the background spectrum, in addition to the *liquid* water bands around 3300 and 1600 cm^{-1}, the presence of *liquid* water in the background spectrum being unexplained. It evaporated during the scan from 4000 to 400 cm^{-1} (no liquid water absorption band between 950 and 650 cm^{-1}). The presence of water vapor is indicated by the undulation, small but distinctly visible, in the H–O–H bending region, on both sides of the corresponding band for liquid water, appearing at 1615 cm^{-1}.] Superimposition of the water vapor spectrum upon the absorption band of (normal) liquid water may explain why the 1600-cm^{-1} band in the "polywater" spectrum is somewhat stronger than expected in comparison with the O–H stretch band around 3300 cm^{-1}.

Most significant is the observation that the second strongest absorption band, centered around 1380 cm^{-1}, previously ascribed[4] to unresolved "polywater" vibrations at 1410 and 1360 cm^{-1}, perfectly fits the strongest peak, at 1390 cm^{-1}, which one obtains for aqueous carbonate solutions (Fig. 6.35).

Other peaks in spectrum II, weak ones at 1168 and 1040 cm^{-1} and a strong one at 1110 cm^{-1}, appeared

similarly in spectrum I. They correspond to the strongest absorptions for silicate and sulfate respectively. I prepared highly viscous solutions of sodium oxide and sulfate in water glass (sodium polysilicate). Spectra obtained between Irtran 2 (zinc sulfide) plates from minute samples exposed briefly to the carbon dioxide of the air were characteristic of carbonate, silicate, sulfate, and water and closely resembled spectrum II of "polywater" (Fig. 6.35).

The significance of these results was enhanced by refractive index measurements on such mixtures. I obtained values up to 1.46–1.48, similar to those reported for "polywater."[5]

The interpretation of spectrum I (ref. 2), obtained with diamond platelets, presents greater difficulty, mainly for the following reason: the band near 1600 cm^{-1} cannot readily be assigned to the H–O–H bending mode of normal liquid water because its other important absorption, near 3300 cm^{-1}, for the O–H stretch, was reported to be absent. However, two alternate interpretations come to mind, which I find as difficult flatly to dismiss as to accept. One is similar to that given to spectrum II but involves the reluctant assumption of an awkward experimental procedure leading to the presence of one, and the absence of the other, band of normal liquid water. The other, quite different, interpretation, but also entailing only common chemical species, seems not less tenuous. I failed in trying with sufficient assurance to verify postulates about unusual experimental conditions that could have affected the measurements. One is frustrated by the uncommon paucity of experimental detail available in the paper[2] or from other sources.

We may be left with a mystery as far as spectrum I is concerned. At the same time we seem to be able to ascribe the later spectrum II of Page, Jakobsen, and

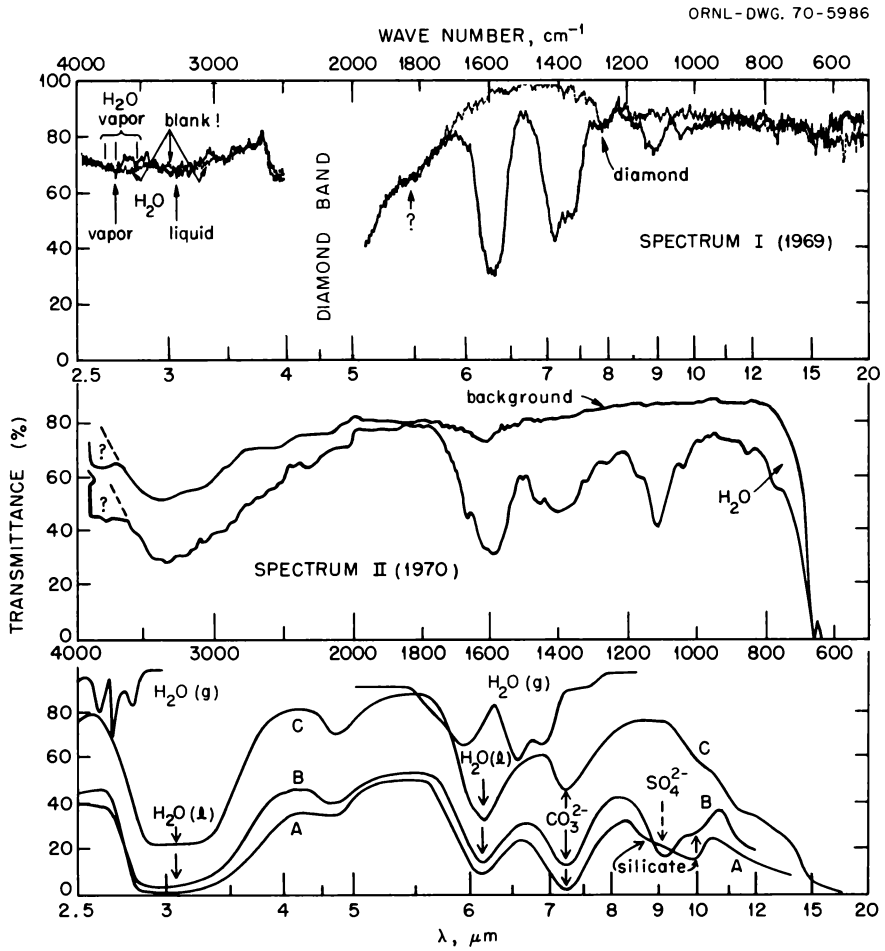

Fig. 6.35. Comparison of Polywater Infrared Spectra I (ref. 2) and II (ref. 4) with Spectra of Mixtures of Carbonate, Sulfate, Silicate, and Water. (*A*) Water glass + Na_2CO_3, aq; (*B*) water glass + Na_2CO_3, aq + Na_2SO_4, aq; (*C*) water glass + $Na_2O + H_2O + CO_2$ (air).

Lippincott[4] to a mixture of the simple species carbonate, sulfate, silicate, normal liquid water, and water vapor rather than as unlikely a chemical entity as "a new liquid form of water."[6]

(Note added in proof: Results of a most recent paper by W. D. Bascom *et al.*[7] may suggest that much of the 1600-cm^{-1} band of both spectra I and II might be assigned to *solid potassium bi*carbonate rather than normal water. $KHCO_3$ would also improve the fit in the region 3000 to 2000 cm^{-1} of spectrum II. One contradiction is the predominance of sodium over potassium in polywater analyses,[6] solid *sodium* bicarbonate absorbing most strongly near 1300 cm^{-1} rather than 1400 cm^{-1}. Another is the existence, in $KHCO_3$, of other bands of medium intensity near 1000 and 830 cm^{-1}, which are weak or nonexistent in the polywater spectra. The spectrum shown in Fig. 7 of ref. 7 does not fully satisfy comparison with polywater on account of the reversal in relative intensities of the 1600 and 1400 cm^{-1} bands and an overemphasis on the silicate band.)

---

[1]Thanks for valuable assistance and helpful discussions are due to many ORNL staff members, too numerous to list here.

[2]E. R. Lippincott, R. R. Stromberg, W. H. Grant, and G. L. Cessac, *Science* **164**, 1482 (1969).

[3]G. M. Begun and A. C. Rutenberg. *Inorg. Chem.* **6**, 2212 (1967).

[4]T. F. Page, Jr., R. J. Jakobsen, and E. R. Lippincott, *Science* **168**, 51 (1970).

[5]G. A. Castellion, D. G. Grabar, J. Hesson, and H. Burkhard, *Science* **167**, 867 (1970).

[6]After completion of the work described here, the papers by D. R. Rousseau and S. P. S. Porto, *Science* **167**, 1715 (1970) and by S. L. Kurtin, C. A. Mead, W. A. Mueller, B. C. Kurtin, and E. D. Wolf, *Science* **167**, 1722 (1970) appeared with strong evidence against the existence of a new liquid form of water.

[7]W. D. Bascom, E. J. Brooks, and B. N. Worthington III, NRL Report 7115 (Apr. 21, 1970).

ON THE EXISTENCE OF SO-CALLED "ANOMALOUS WATER"

E. H. Taylor

For about two years there has been widespread interest in claims for the existence of a new form of liquid water, called "anomalous water" or "polywater" by various groups of proponents.[1,2] I found the experimental and theoretical bases for these claims so unconvincing, and the degree of acceptance of them so surprising, that I repeated some of Deryagin's experiments and spent some time trying to explain the various phenomena on more prosaic grounds. Most of the effort was devoted to experiments on the formation of the material and on measurement of a few of its properties; independently, M. A. Bredig[3] undertook a study of the infrared spectroscopic experiments.[2]

I was able to duplicate the principal results of Deryagin and his school on the formation of anomalous water, in particular the random nature of its occurrence, the growth and disappearance as a function of the partial pressure of water, and the formation on flat surfaces as well as in capillaries. All of these observations could readily be explained as the condensation of water on minute amounts of soluble impurities, specks of dust, inclusions in the glass, or local residues of some cleaning agent.

There remained the problem of accounting for the supposedly anomalous properties reported for the material. A careful reading of the original papers showed that some of the properties could be explained as being simply those of electrolyte solutions of believable concentrations. These included freezing and melting behavior,[4] thermal expansion,[4] and vapor pressure lowering.[5] The viscosity measurements[6] (*ca.* 15 times the viscosity of water) were obviously distorted by the large surface forces resulting from nonuniform wetting of the capillary. The high density[7] (1.4 g/cm^3) could conceivably be that of a salt solution, particularly since the method of measurement (density gradient column) allowed extraction of water during the measurement. The high refractive index[8] was harder to reconcile with the impurity hypothesis, since there was not an obvious mechanism for concentrating the solution as there was in the density measurement. Bredig[3] observed that rather high solute concentrations were required to match the refractive index if the impurities were sodium carbonate and silicate.

Deryagin reported a high thermal stability,[5] basing this on an experiment in which anomalous water was distilled from one end of a capillary to another through an intermediate zone maintained at high temperatures. To explain this on the basis of an impurity requires either that a new portion of impurity be present in the far end of the capillary, or that the required impurity be transported in the vapor or by spray. Both these seem unlikely, but there was so little detail given for the original experiment that it seems preferable to discount this experiment rather than to accept the idea of another form of liquid water.

Although most of the experimental results (including the spectra, described by M. A. Bredig[3]) can be explained reasonably well by a simple hypothesis of impurities, there are some quantitative difficulties, and it would be desirable to be able to refute the existence

of anomalous water on more general grounds. One basis for such rejection is the widely supported observation that anomalous water grows for only a limited time. It appears as a droplet in a capillary, becomes a slug which grows in length for a time, and then ceases to grow. Since the formation is attributed to catalysis, the stoppage is attributed to poisoning, but it has not been realized that this leads to a contradiction with other observations. Briefly, the contradiction is demonstrated by noting that the poisoning must be complete when the surface is covered by a monolayer and by calculating from that the maximum fraction of anomalous water that could be formed. (The bulk of the slug must be ordinary water condensed on the layer of anomalous water.) A simple calculation shows this fraction to be *ca.* $3 \times 10^{-3}\ n/D$, where n is the number of sheets of closely bound H_2O units in the supposed polymer (anomalous water) and D is the capillary diameter in microns. Since n is unlikely to be as large as 10 and D is typically 30, the fraction expected is around 10^{-3}. This is much less than the claims of various observers which include the following values of this fraction of anomalous component derived from the stated property: vapor pressure lowering,[5] 0.07; volume change on freezing,[9] 0.02 to 0.6; refractive index,[10] 0.2 to 1.0; molecular spectra, almost no ordinary H_2O.[2]

Because of this contradiction, one must reject either the quoted measurement, the simple argument based on standard ideas from kinetics, or the existence of a new liquid form of water. Rejecting the measurements would be tantamount to rejecting anomalous water, since its existence is inferred from such data. Since the simple impurity hypothesis (with allowance for experimental uncertainties) is sufficient to explain the observations, it seems unwise to abandon well-tried concepts in favor of so wild a hypothesis as the existence of anomalous water.

---

[1] B. V. Deryagin, *Discussions Faraday Soc.* **42**, 109 (1966).

[2] E. R. Lippincott, R. R. Stromberg, W. H. Grant, and G. L. Cessac, *Science* **164**, 1482 (1969).

[3] M. A. Bredig, "'Polywater,' Raman and Infrared Spectra," preceding contribution, this report.

[4] B. V. Deryagin, I. G. Ershova, B. V. Zheleznyi, and N. V. Churaev, *Dokl. Akad. Nauk SSSR* **170**, 876–79 (1966).

[5] B. V. Deryagin, N. V. Churaev, N. N. Fedyakin, M. V. Talaev, and I. G. Ershova, *Izv. Akad. Nauk SSSR, Ser. Khim.*, No. 10, 2178 (1967).

[6] B. V. Deryagin, N. N. Fedyakin, and M. V. Talaev, *Dokl. Akad. Nauk SSSR* **167**, 376 (1966).

[7] B. V. Deryagin, D. S. Lychnikov, K. M. Merzhanov, Ya. I. Rabinovich, and N. V. Churaev, *Dokl. Akad. Nauk SSSR* **181**, 823 (1968).

[8] B. V. Deryagin, Z. M. Zorin, and N. V. Churaev, *Dokl. Akad. Nauk SSSR* **182**, 811 (1968).

[9] B. V. Deryagin, B. V. Zheleznyi, N. N. Zakhavaeva, O. A. Kiseleva, A. I. Konovalov, D. S. Lychnikov, Ya. I. Rabinovich, M. V. Talaev, and N. V. Churaev, *Dokl. Akad. Nauk SSSR* **189**, 1282 (1969).

[10] G. A. Castellion, D. G. Grabar, J. Hession, and H. Burkhard, *Science* **167**, 865 (1970).

MOLTEN SALTS AND RELATED NONAQUEOUS SYSTEMS

HEAT CONTENT OF ALKALI METAL FLUOROBORATES[1]

A. S. Dworkin M. A. Bredig

We have completed our high-temperature heat content measurements of $NaBF_4$, KBF_4, $RbBF_4$, and $CsBF_4$. The equations which represent our results for $H_T - H_{298}$ (cal/mole) are given in Table 6.8. Table 6.9 summarizes the heats and entropies of melting and transition.

KBF_4, $RbBF_4$, and $CsBF_4$ all undergo a solid-state transition from the $BaSO_4$-type orthorhombic structure to the high-temperature cubic structure.[2-4] $NaBF_4$, on the other hand, exists as the orthorhombic (pseudo-tetragonal) $CaSO_4$ type of structure[5] at room temperature and in a noncubic form above the transition temperature.[4,6] This latter structure has recently been reported[6] to be monoclinic with four molecules per unit cell. However, a lowering of the symmetry at higher temperature without a lowering of the number of molecules per unit cell is quite unlikely. The structure was derived from a powder pattern, and the authors state that their assignment is not necessarily correct or unique. We believe that this inconsistency may be avoided by showing that the x-ray spacings (Table 2, ref. 6) are compatible with the assumption of a mechanical mixture of the orthorhombic low-temperature phase with a high-temperature phase of hexagonal, rather than monoclinic, structure. These data (Fig. 6.36) give c/a = 1.55, which may be compared with the high-temperature form of $CaSO_4$, also shown[7] to be hexagonal rather than cubic, with c/a = 1.54, that is, slightly distorted from the ideal "close-packed" symmetry, c/a = 1.63, as in wurtzite, ZnS.

Although the entropies of fusion of $NaBF_4$ and KBF_4 are similar (Table 6.9), the entropy of transition of KBF_4 is much larger than that of $NaBF_4$ (5.93 to 3.13 eu). This may be explained qualitatively on the basis

Table 6.8. Equation Coefficients for Enthalpy Data for Equation:
$H_T - H_{298}$ (cal/mole) $= a + bT + cT^2 + dT^{-1}$

Compound	a	b	c	d	Average Percent Error	Temperature Range (°K)
	$\times 10^3$		$\times 10^{-2}$	$\times 10^4$		
$NaBF_4$	−3.820	3.148	3.703	−12.17	0.3	298–516
	−9.785	36.48			0.1	516–679
	−8.605	39.52			0.1	679–750
KBF_4	−6.325	15.62	1.943	−1.737	0.2	298–556
	−7.800	34.95			0.2	556–843
	−7.710	39.94			0.1	843–900
$RbBF_4$	−7.430	18.77	1.697	+9.677	0.2	298–518
	−7.897	34.34			0.1	518–855
	−7.985	39.92			0.1	855–1000
$CsBF_4$	−7.614	17.63	2.009	+17.01	0.2	298–443
	−8.673	34.18			0.1	443–828
	−8.390	39.36			0.1	828–1000

Table 6.9. Heats and Entropies of Melting and Transition of Alakli Metal Fluoroborates

	T_m (°K)	ΔH_m (kcal/mole)	ΔS_m (eu/mole)	T_{tr} (°K)	ΔH_{tr} (kcal/mole)	ΔS_{tr} (eu/mole)	$\Delta S_m + \Delta S_{tr}$ (eu/mole)
$NaBF_4$	679	3.25	4.78	516	1.61	3.1	7.9
KBF_4	843	4.30	5.10	556	3.30	5.9	11.0
$RbBF_4$	855	4.68	5.5	518	2.86	5.5	11.0
$CsBF_4$	828	4.58	5.5	443	1.94	4.4	9.9

of the differing structures of both the low- and high-temperature solids, which in turn are due to the large difference in the size of the cations. The $NaBF_4$ structure is more disordered below the transition, which is reflected by the fact that at 500°K $S_T - S_{298}$ is more than 1 eu larger for $NaBF_4$ than for KBF_4. In addition, the high-temperature cubic structure of KBF_4 most probably is more compatible with anionic rotational or librational disorder than is the structure of $NaBF_4$ of lower symmetry.

KBF_4, $RbBF_4$, and $CsBF_4$ are isodimorphous and therefore can be considered as a series separate from $NaBF_4$. Table 6.9 shows that although the enthalpies and temperatures of melting are similar there is a decrease in temperature, entropy, and enthalpy of transition of 21, 25, and 41%, respectively, with increasing cation size in this series. The particularly large relative change in the enthalpy may be attributed to the decrease in lattice energy with increasing size of the cation, which also facilitates the rotation or libration of the fluoroborate ion. The large decrease in enthalpy as compared with the entropy of transition also explains the relatively low temperature of transition found for $CsBF_4$.

[1]This work also has been reported in the *MSR Program Semiann. Progr. Rept. Feb. 28, 1970.*

[2]M. J. R. Clark and H. Lynton, *Can. J. Chem.* **47**, 2579 (1969).

[3]D. J. Huettner *et al.*, *J. Chem. Phys.* **48**, 1739 (1968).

[4]C. Finbak and O. Hassel, *Z. Physik. Chem.* **32B**, 433 (1936).

[5]G. Brunton, *Acta Cryst.* **B24**, 1703 (1968).

[6]C. W. F. T. Pistorius, J. C. A. Boeyens, and J. B. Clark, *High Temperatures–High Pressures* **1**, 41 (1969).

[7]M. A. Bredig, *Chem. Div. Ann. Progr. Rept. May 20, 1968,* ORNL-4306, p. 129.

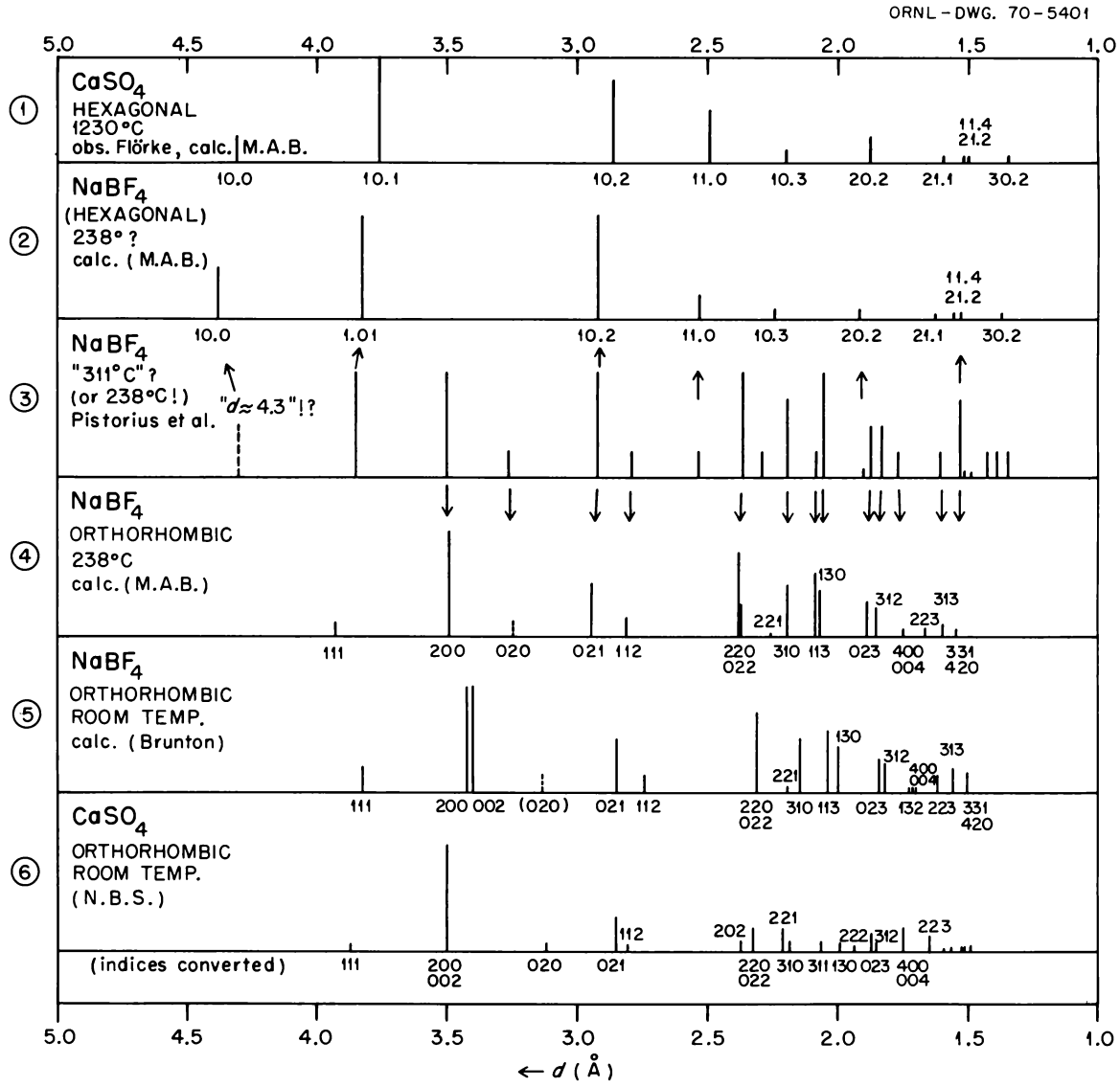

Fig. 6.36. Interpretation of High-Temperature X-Ray Powder Pattern of $NaBF_4$ (ref. 6) as That of a Phase Mixture. Note correspondence of most reflections of pattern 3 (observed) with those of 2 and 4 (calculated). Isodimorphous $CaSO_4$ (Nos. 1 and 6) for comparison (ref. 7).

THE SOLUBILITY OF THORIUM METAL IN THORIUM TETRAFLUORIDE[1]

A. S. Dworkin M. A. Bredig

Thermal-analysis measurements were made to determine the eutectic temperature in the Th-ThF_4 system and, through combination with the entropy of fusion of ThF_4, the solubility of thorium in ThF_4. The eutectic temperature was found to be only 1 to 2° lower than the melting point (1110°C) of ThF_4, indicating a solubility of about 0.1 to 0.2 mole % thorium in ThF_4. This is of the same low order of magnitude as the solubility in $3LiF \cdot ThF_4$ and as the solubilities of La, Ce, and Nd in their respective trifluorides, which we had measured earlier.

The low solubility of thorium in ThF_4 indicates that the formation of a stable trivalent thorium fluoride in any appreciable concentration is unlikely.

[1]This work has also been reported in the *MSR Program Semiann. Progr. Rept. Aug. 31, 1969,* ORNL-4449, p. 135.

THE SYSTEM YTTRIUM METAL–YTTRIUM TRICHLORIDE AT HIGH TEMPERATURES

A. S. Dworkin M. A. Bredig R. J. Katt[1]

As a result of our previous work, we have been able to correlate solubilities of alkali and alkaline-earth metals in their own halides both at temperatures near the melting points of the salts and at much higher consolute temperatures above which the systems are completely miscible. For the lanthanide systems the solubility of the metals in their halides is known in most cases only at temperatures within a few hundred degrees of the melting point of the salt. We have extended these measurements to much higher temperatures (~1550°C) in an attempt to find a consolute temperature for at least one trivalent salt-metal system.

The Y-YCl_3 system was chosen for study because vapor pressure studies reported in the Russian literature gave a solubility at about 1350°C of 35 mole % yttrium, which is high enough to indicate the possibility of complete miscibility at all temperatures below the melting point of yttrium (~1550°C).

Our measurements show the literature data to be incorrect. At 1350°C we find the solubility of yttrium in YCl_3 to be only about 15 mole %. At the monotectic temperature of 1480°C, we find that a large miscibility gap exists from about 22 to 96 mole % yttrium. We also estimate the consolute temperature to be much higher than 1600°C.

From the above results and a careful study of the literature, we conclude that there are in all probability no lanthanide metal-halide systems with a consolute temperature less than 1600°C, with the exception of those involving the largely divalent europium and ytterbium metals.

---

[1]Oak Ridge Associated Universities Summer Student Trainee from Williams College, Williamstown, Mass., Summer 1969.

A REFERENCE ELECTRODE SYSTEM FOR USE IN FLUORIDE MELTS

Harry R. Bronstein

Nuclear fuel technology has focused interest on the chemical and thermodynamic properties of fluoride melts. One of the best means of gaining such information directly is to determine the emf of electrochemical cells incorporating the materials of interest. However, the half-cell of interest must be coupled through some junction to a reference electrode system; therefore, for the determination of thermodynamic properties, the junction potential must be eliminated or its magnitude and stability established.

An electrochemical cell

$$(-)\ Be^0 \,\Big|\, \underset{(liq)}{LiF\text{–}BeF_2} \,\Big|\, \begin{matrix}Ta\\ frit\end{matrix} \,\Big|\, \begin{matrix}CaF_2\\ single\ crystal\end{matrix} \,\Big|\, \left.\begin{matrix}NiF_2\\ Ni\\ pellet\end{matrix}\right\} Ni(+)$$

reported previously[1] yielded an initial voltage at 600°C of 1.870 V, in fairly good agreement with the calculated value of 1.900 V.[2,3] This potential remained constant for a very short period, and then a slow downward drift commenced, terminating at the end of 12 hr in a fairly steady potential of 1.35 V. This result may be explained by (1) the eventual saturation by CaF_2 (≈12 mole %) of the LiF-BeF_2 melt within the tantalum frit which may (but not likely) give a liquid-junction potential of 0.5 V; (2) a mixed potential at the beryllium electrode due to impurities in the melt;[2] (3) the establishment of a redox potential by a lower-valent species of beryllium produced by reaction of the metal and normal beryllium ions of the melt; or (4) a combination of any of the above phenomena. An examination of the CaF_2 crystal showed some solvation action of the melt. However, the beryllium electrode had undergone extensive attack – much more than would be expected from trace impurities.

In the course of events, D. L. Manning of the Analytical Chemistry Division and I became aware of our independent but similar approaches to a reference electrode for use in fluoride melts. The combining of our individual experiences evolved the Bronstein-Manning reference electrode system (Fig. 6.37). The single-crystal LaF_3 has sufficient conductance, supplied virtually 100% by the mobile F^- ion, which permits the elimination of a liquid-solid junction potential if the melts at both ends of the crystal are essentially the same. The saturated NiF_2 solution (10^{-3} mole fraction) would hardly alter the slight solubility of LaF_3 (≈1 mole % by analogy to CeF_3[4]) in the upper melt held within the cup portion of the LaF_3 crystal. The single-crystal LaF_3, on account of its low solubility, could make contact directly with the melt, but slight temperature gradients within the melt could cause mass transfer from the small crystal and thus limit its lifetime. The fine-porosity nickel frit limits the area of contact of the main bulk of the melt with the crystal.

The Ni-Ni(II) couple in fluoride melts shows Nernstian reversibility and fairly large exchange currents.[5] With the expected elimination of junction potentials and with the free energy of formation of

crystalline NiF_2 well established,[3] the use of this couple in the LiF-BeF_2 (67-33 mole %) melt saturated with NiF_2 as the electrode of constant potential should provide a very reliable reference electrode for use in fluoride melts.

The magnitude of the liquid-solid junction potential to be eliminated was found to be 50 mV by measuring the potential of the cell

(+) Ni | LiF, NiF_2 (c) | BeF_2 (sat'd) | LaF_3 single crystal | Ni frit | LiF BeF_2 melt | Ni frit | LaF_3 crystal | Ni NiF_2 } pellet 50–50% by volume (–)

It was also experimentally confirmed that the difference in the potentials generated at the surfaces of the LaF_3 crystal under identical conditions was quite small, 15 mV, and probably due to an asymmetry potential. Asymmetry potentials for the glass electrode commonly fall in the range 0 to ±10 mV.[6]

In tests of this electrode vs the Be^0 |BeF_2-LiF system, the expected voltage,[2,3] 1.900 V, was obtained. However, after a short period of stability this potential would gradually decay to a value approximately 0.5 V below the initial voltage. This voltage would then remain constant for the duration of the experiment. The beryllium electrodes when removed from the melts showed catastrophic attack. In separate experiments where highest-purity materials were used the same phenomenon occurred. According to Hitch and Baes[2] high-purity materials obviated the poisoning of their beryllium electrodes. However, in the present circumstances the beryllium electrodes if poisoned should not have shown such severe attack. Analysis of the melt and electrode materials before and after the experiments showed the presence of insignificant quantities of impurities, quantities very much below the levels necessary to cause such attack. In some experiments the melts were pretreated with beryllium chips in order to remove any impurities which could poison or attack the electrode. In all cases the beryllium electrodes still underwent attack, and the potentials were 0.5 V below the calculated value. In order to gain some insight into the phenomenon occurring at the beryllium electrode, the beryllium electrode was made cathodic by pulsing a current between it and the nickel container. As a result of this current pulse, the potential of the beryllium electrode vs the reference electrode was 1.900 V, in agreement with the calculated value. However, this potential would shortly decay to the value previously measured. Apparently by plating a fresh surface of beryllium upon the electrode, the Be/Be^{2+} potential could be maintained. An anodic current had no effect on restoring the electrode to the Be/Be^{2+} potential.

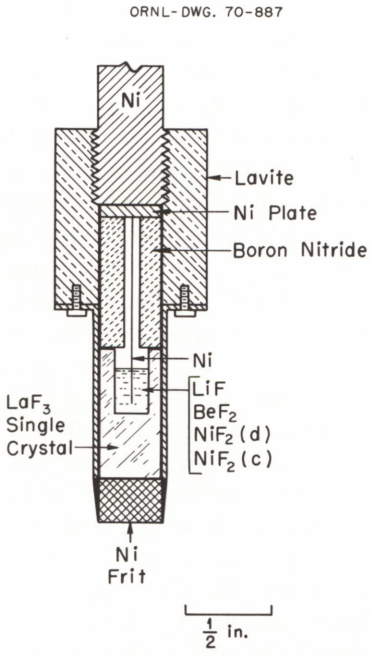

Fig. 6.37. Bronstein-Manning Reference-Electrode System for Use in Fluoride Melts.

Formation of a subvalent species through an attack on the electrode according to the reaction Be + BeF_2 → 2BeF would explain the lower potential in terms of a redox couple Be^+/Be^{2+} and the effect of cathodic and anodic current upon the electrode. However, the work of Hitch and Baes[2] seemingly eliminates this mechanism.

Another system investigated which showed similar behavior was the Zr/ZrF_4 couple in the melt LiF-BeF_2, ZrF_4 (5.0 mole %). Here again the initial potential of the cell, 1.620 V, was in good agreement with the calculated value[7] (1.590 V), but after a short period of time (10 min) the potential decayed to the value 1.000 V and remained thereafter at this potential for the duration of the experiment – several days. Examination of the zirconium electrode revealed severe attack. Again one is tempted to invoke the formation of a subvalent species of zirconium as an explanation. What occurs at the metal electrodes bears further investigation.

In spite of the special difficulties described here occurring at the beryllium and zirconium electrodes, it may be said that the somewhat new concept for a reference electrode for use in fluoride melts has been successfully tested and should prove quite versatile.

[1] H. R. Bronstein, *Chem. Div. Ann. Progr. Rept. May 20, 1969*, ORNL-4437, p. 102.

[2]B. F. Hitch and C. F. Baes, Jr., *EMF Study of LiF-BeF_2 Solutions,* ORNL-4257 (July 1968); *Inorg. Chem.* 8, 201 (1969).

[3]R. J. Heus and J. J. Egan, *Z. Physik. Chem. (Frankfurt)* 49(1–2), 38–43 (1966).

[4]J. A. Fredricksen, L. O. Gilpatrick, and C. J. Barton, *Solubility of Cerium Trifluoride in Molten Mixtures of LiF, BeF_2, and ThF_4,* ORNL-TM-2335 (January 1969).

[5]H. W. Jenkins, G. Mamantov, and D. L. Manning, *J. Electroanal. Chem.* 19, 385 (1968).

[6]D. J. G. Ives and G. J. Janz, *Reference Electrodes,* p. 255, Academic, 1961.

[7]C. F. Baes, Jr., *Nuclear Metallurgy,* vol. 15, AIME Symposium on Reprocessing Nuclear Fuels, pp. 615–44 (1969).

CALORIMETRY

LOW-TEMPERATURE HEAT CAPACITY OF POTASSIUM HEXACHLOROTECHNETATE(IV)

R. H. Busey R. B. Bevan, Jr. R. A. Gilbert

The interest in the chemical thermodynamic properties of potassium hexachlorotechnetate(IV), K_2TcCl_6, as well as the $TcCl_6^{2-}$ ion in aqueous solution, stems from the fact that the $TcCl_6^{2-}$ ion is the stable species of technetium in strong hydrochloric acid,[1] and knowledge of its properties is basic to the thermodynamics of technetium. Similar in behavior to the corresponding rhenium compound, K_2TcCl_6 is expected to become antiferromagnetic at low temperatures[2] and exhibit a heat capacity anomaly at the Néel temperature.[3] Finally, we are very interested in determining if K_2TcCl_6, with its large octahedral anion, will undergo the phase changes shown by K_2ReCl_6[3] and K_2ReBr_6[4] and exhibit the peculiar thermal-history behavior discovered in K_2ReBr_6[4] and K_2ReI_6.[5,6]

The preparation of the calorimetric sample was described last year.[7] We report at this time only qualitative results of the heat capacity observations, because we discovered at the conclusion of the measurements that the sample had undergone some kind of decomposition during the course of the measurements. This decomposition was evidenced by a pronounced color change of the sample from yellow to green. An unused portion of the sample stored in a glass bottle within a desiccator also exhibited the same color change, a fact which shows that the decomposition was not the result of cooling the sample to low temperatures. The radioactivity of the ^{99}Tc is not responsible for the decomposition by radiolysis, because we have a small sample of K_2TcCl_6 prepared several years ago which shows (colorwise) no evidence whatever of decomposition.

The heat capacity of K_2TcCl_6 exhibits a lambda-type heat capacity anomaly with a maximum at 7.0 ± 0.1°K indicative of a cooperative-type transition. By comparison with data[2,3] on K_2ReCl_6, there is no doubt that this anomaly represents the transition from an ordered antiferromagnetic state below 7.0°K to a disordered paramagnetic state above this temperature. This is the first unequivocal evidence that complex halide salts of technetium, K_2TcX_6, become antiferromagnetic at low temperatures.

The Néel temperature of K_2TcCl_6, 7.0°K, is considerably lower than that of K_2ReCl_6, 11.9°K.[2,3] This order is to be expected since it has been recognized for a long time that exchange interaction forces increase rapidly in going from first- to third-transition-series-element compounds, giving rise to low magnetic moments for paramagnetic compounds of the third-transition-series elements.[8] It should be appreciated that both these compounds are magnetically dilute; that is, the magnetic ions [Re(IV) or Tc(IV)] are separated by a distance of many Angstrom units by diamagnetic chloride ions. Thus the superexchange forces giving rise to antiferromagnetism at these temperatures are remarkably large.

The heat capacity observations also revealed that K_2TcCl_6 may exhibit thermal-history behavior similar to that observed in K_2ReBr_6[4] and K_2ReI_6.[5,6] There was a small spontaneous evolution of heat around 145°K which was found to be associated with a heat capacity anomaly around 200°K. If the heat evolution was avoided by cooling the sample to only 160°K, then the anomaly at 200°K was not observed. These observations need confirmation, however, on a sample of high purity.

Potassium hexachlorotechnetate(IV) has a face-centered cubic structure, a_0 = 9.82 Å, at room temperature.[9] The heat capacity results indicate no crystal structure change at low temperatures. This behavior resembles that of K_2PtCl_6[10] and contrasts with that of K_2ReCl_6, which is cubic at room temperature, a_0 = 9.82 Å,[9] but undergoes several structure modifications below room temperature.[3] According to Brown,[11] for face-centered cubic structures A_2MX_6 (where A is an alkali metal cation and MX_6 is an octahedral anion), if the ratio of the radius of the cation A to the radius of the cavity of X atoms in which it resides is equal to or greater than 0.98, the compound will remain cubic at low temperatures. Using this empirical rule, the cell parameter, and our observation that K_2TcCl_6 remains cubic, it may be estimated that the Tc-Cl bond distance in the $TcCl_6^{2-}$ ion in the crystal is 2.39 ± 0.04 Å. This result may be compared

with 2.36 ± 0.02 Å for the average Tc-Cl distance in $TcCl_4$[12] (distorted octahedral coordination), and 2.35 Å in the $Tc_2Cl_8^{3-}$ ion.[13] The Re-Cl bond length in K_2ReCl_6 is 2.37 Å.[14]

[1] R. H. Busey, *Chem. Div. Ann. Progr. Rept. June 20, 1959,* ORNL-2782, p. 13.

[2] R. H. Busey and E. Sonder, *J. Chem. Phys.* **36**, 93 (1962).

[3] R. H. Busey, H. H. Dearman, and R. B. Bevan, Jr., *J. Phys. Chem.* **66**, 82 (1962).

[4] R. H. Busey, R. B. Bevan, Jr., and R. A. Gilbert, *J. Phys. Chem.* **69**, 3471 (1965).

[5] R. B. Bevan, Jr., R. A. Gilbert, and R. H. Busey, *Chem. Div. Ann. Progr. Rept. May 20, 1966,* ORNL-3994, p. 107.

[6] R. B. Bevan, Jr., R. A. Gilbert, and R. H. Busey, *Chem. Div. Ann. Progr. Rept. May 20, 1967,* ORNL-4164, p. 102.

[7] R. B. Bevan, Jr., and R. H. Busey, *Chem. Div. Ann. Progr. Rept. May 20, 1969,* ORNL-4437, p. 115.

[8] J. H. Van Vleck, "Theory of Electric and Magnetic Susceptibilities," Oxford University Press, Oxford, 1932.

[9] J. Dalyiel, N. S. Gill, R. S. Nyholm, and R. D. Peacock, *J. Chem. Soc. (London)* **1958**, 4012.

[10] L. V. Coulter, K. S. Pitzer, and W. M. Latimer, *J. Am. Chem. Soc.* **62**, 2845 (1940).

[11] I. D. Brown, *Can. J. Chem.* **42**, 3758 (1964).

[12] M. Elder and B. R. Penfold, *Inorg. Chem.* **5**, 1197 (1966).

[13] F. A. Cotton and C. E. Coffee, *J. Am. Chem. Soc.* **81**, 7 (1959).

[14] B. Aminoff, *Z. Krist.* **94**, 246 (1936).

ENTHALPIES OF FUSION AND TRANSITION OF LEAD FLUORIDE

C. W. Linsey[1] R. A. Gilbert R. H. Busey

The orthorhombic-to-cubic transition in PbF_2 is highly irreversible, and the enthalpy of transition cannot be determined directly by drop calorimetry. The enthalpy of transition at 25°C (240 ± 9 cal/mole), determined by solution calorimetry as the difference in the enthalpy of solution of the two modifications in 1 *M* $Fe(NO_3)_3$, was reported previously.[2] The additional data required to determine the enthalpy of transition at the transition temperature, ΔH_{trans}, have now been determined.

The transition temperature was determined from enthalpy measurements by drop calorimetry on a sample of orthorhombic PbF_2. The furnace temperature was increased only 1 to 2° between enthalpy determinations. Only the cubic-to-orthorhombic transition is extremely sluggish; the reverse transition is apparently rapid. Below the transition temperature the enthalpy measurements gave $(H_T^O - H_{273}^O)$, where H_T^O and H_{273}^O represent the enthalpies of orthorhombic PbF_2 at temperature T and at the ice point, 273.15°K, respectively. When the furnace temperature finally exceeded the transition temperature, the enthalpy measurements gave $(H_T^C - H_{273}^C)$ where H_T^C is the enthalpy of cubic PbF_2 at temperature T, and the enthalpy values fell on a higher curve. In this manner the transition temperature was established to be between 582° and 584°K, and was taken to be 583 ± 1°K. The enthalpy difference, $[(H_T^C - H_{273}^C) - (H_T^O - H_{273}^O)]$, where T is now the transition temperature, was observed to be 145 cal/mole.

The only additional data required to obtain the enthalpy of transition at the transition temperature from that at 25°C is $[(H_{298}^C - H_{273}^C) - (H_{298}^O - H_{273}^O)] = 12$ cal/mole, obtained from enthalpy measurements on the two modifications. The enthalpy of transition at 583°K is then 373 ± 9 cal/mole, and the entropy of transition is 0.64 ± 0.02 cal deg^{-1} $mole^{-1}$.

The enthalpy data on the orthorhombic PbF_2 obtained during the course of the transition-temperature measurement discussed above were found to be in disagreement by approximately 2.5% from earlier measurements.[2] A thorough examination and check of various possible sources of error have revealed that the enthalpy of the Nichrome V capsules varied from capsule to capsule, although the capsules had been prepared from the *same* rod. Earlier results[3] in this Laboratory using Nichrome V capsules revealed no such errors, but measurements at the National Bureau of Standards showed that Nichrome V capsules made from adjacent sections of the same rod could have enthalpies differing by approximately 1.5%.[4] Additional measurements on the lead halides are being made using platinum–10% rhodium capsules to obtain corrections to be applied to the original data.

Additional measurements on the enthalpy of fusion of PbF_2 lead to a final result of 3.52 kcal/mole and 1103°K for the melting point. The low entropy of fusion, 3.19 cal deg^{-1} $mole^{-1}$, reflects the result of the large configurational entropy (3.6 cal deg^{-1} $mole^{-1}$) which develops from the order-disorder transition[2] below the melting point. The sum of these two entropies, ~6.8 cal deg^{-1} $mole^{-1}$, which might be considered as the "normal" entropy of fusion (i.e., in the absence of the order-disorder transition), compares favorably with the entropies of fusion of $PbCl_2$ and $PbBr_2$, 6.81 and 6.10 cal deg^{-1} $mole^{-1}$ respectively.[2]

[1] Oak Ridge Graduate Fellow from North Texas State University, Denton, under appointment with Oak Ridge Associated Universities.

[2]C. W. Linsey, R. A. Gilbert, and R. H. Busey, *Chem. Div. Ann. Progr. Rept., May 20, 1969,* ORNL-4437, p. 111.

[3]R. A. Gilbert, *J. Phys. Chem.* 67, 1143 (1963).

[4]T. B. Douglas and J. L. Dever, *J. Res. Natl. Bur. Std.* 54, 15 (1966).

FREE ENERGY AND ENTHALPY OF FORMATION OF K_2ReBr_6

R. H. Busey E. D. Sprague[1] R. B. Bevan, Jr.

The availability of high-purity K_2ReBr_6 used in low-temperature heat capacity studies[2] prompted the measurements reported here for the determination by solution calorimetry of the enthalpy of formation of the compound. These measurements complete the determination of the thermodynamic properties of K_2ReBr_6.

The enthalpy of hydrolysis of K_2ReBr_6 in alkaline solution at 25°C is given in Table 6.10. The calorimetric procedure, including the precautions to exclude oxygen from the solution, have been described.[3] The reaction is assumed to be

$$K_2ReBr_6(c) + 4OH^- = ReO_2 \cdot 2H_2O(c) + 2K^+ + 6Br^- , \quad (1)$$

similar to that in the hydrolysis of K_2ReCl_6.[4] The standard enthalpy of the reaction at infinite dilution is −64.0 ± 0.2 kcal/mole.

There has recently been a new determination of the enthalpy of formation of $Re_2O_7(c)$ at 25°C by solution calorimetry,[5] $\Delta H_f^\circ[Re_2O_7(c)] = -301.9 \pm 1.8$ kcal/mole, which is superior to previous measurements. This new result, together with a recent enthalpy of solution determination,[6] gives a revised result for the enthalpy of formation of the perrhenate ion, $\Delta H_f^\circ[ReO_4^-(aq)] = -190.9$ kcal/mole.

The enthalpy of formation of K_2ReBr_6 determined from the enthalpy of hydrolysis is $\Delta H_f^\circ[K_2ReBr_6(c)] = -248.8$ kcal/mole at 25°C. This result is based upon a revised[4] $\Delta H_f^\circ[ReO_2 \cdot 2H_2O(c)$, freshly ppt.] = −238.3 kcal/mole which incorporates the above new enthalpy of formation of $ReO_4^-(aq)$. Other enthalpies of formation required for reaction (1) and for the revisions were taken from the revised *National Bureau of Standards Bulletin* 500.[7] At 25°C the entropy of formation[2,7] is −39.6 cal deg^{-1} $mole^{-1}$, and the free energy of formation is $\Delta F_f^\circ = \Delta H_f^\circ - T\,\Delta S_f^\circ = -236.9$ kcal/mole.

Table 6.10. Enthalpy of Hydrolysis of K_2ReBr_6 at 298.15°K

Run No.	Sample Weight (g)	$[OH^-]$ (*M*)	$-\Delta H$ (kcal/mole)
28	0.2550	0.100	64.33
29	1.0073	0.400	65.10
30	0.5055	0.103	64.25
31	0.5022	0.300	64.66
32	0.5011	0.0521	63.97
33	0.4998	0.397	64.54
34	0.5011	0.203	64.42
35	0.5009	0.395	64.86
36	0.5002	0.347	64.87
37	0.4105	0.0509	63.86
38	0.5019	0.148	64.34
39	0.3683	0.0595	64.15
			$\Delta H^\circ = -64.0 \pm 0.2$ kcal/mole

[1]Temporary employee, Summer 1967.

[2]R. H. Busey, R. B. Bevan, Jr., and R. A. Gilbert, *J. Phys. Chem.* 69, 3471 (1965).

[3]R. H. Busey, E. D. Sprague, and R. B. Bevan, Jr., *J. Phys. Chem.* 73, 1039 (1969).

[4]R. H. Busey, K. H. Gayer, R. A. Gilbert, and R. B. Bevan, Jr., *J. Phys. Chem.* 70, 2609 (1966).

[5]E. G. King, D. W. Richardson, and R. V. Mrazek, U.S. Bureau of Mines, *Rept. of Investigation No. 7323* (November 1969).

[6]J. C. Ahluwalia and J. W. Cobble, *J. Am. Chem. Soc.* 86, 5377 (1964).

[7]D. D. Wagman *et al.*, "Selected Values of Chemical Thermodynamic Properties," *Natl. Bur. Std. Tech. Notes* No. 270-3 and 270-4 (January 1968). $\Delta H_f^\circ(K^+)$ taken from W. M. Latimer, *Oxidation Potentials,* 2d ed., Prentice-Hall, New York, 1952.

ELECTROCHEMISTRY

KINETICS OF THE CHARGE AND DISCHARGE OF THE FILM ON SUPERPASSIVE IRON

G. H. Cartledge

The last annual report[1] presented measurements of the rate of charge and discharge of the film on iron between two fixed potentials above the passivation potential in an inhibiting solution of potassium pertechnetate. It was shown that the rates are described by an equation derived on the prior assumption[2] that the superpassive state arises when a number of electron holes are formed in the fully oxidized [Fe(III)] film. In the steady state, an equivalent number of protons will have been transferred to the electrolyte. When the potential is then suddenly lowered, the difference in the

mobility of electrons and protons causes a transient potential difference to be set up which lowers the activation energy for the rate-determining return of protons to the film.

During the past year the study was extended to other inhibiting electrolytes, the molybdate ion being studied extensively. The earlier results were fully confirmed, and the rate constants were quite similar, in spite of considerable differences in the thickness of the films.

The results mean that "passive iron" does not owe its passivity merely to the presence of a film containing Fe(III) compounds, but rather to the unique properties acquired by the passivating interface when the film is supercharged either electrolytically or by vigorous chemical electron acceptors. The detailed interpretation has been given in a recent publication.[3]

[1]G. H. Cartledge, *Chem. Div. Ann. Progr. Rept. May 20, 1969*, ORNL-4437, p. 87.

[2]G. H. Cartledge, *Corrosion* **24**, 223 (1968).

[3]G. H. Cartledge, *Chimia* **23**, 450 (1969).

THE ELECTROCHEMISTRY OF TECHNETIUM

G. H. Cartledge

Initiation of a study of the electrochemical properties of iron alloyed with 0.1 wt % technetium disclosed the need for an investigation of the anodic behavior of elementary technetium itself. Anodic polarization of the alloy was shown to be attended by a large increase in the concentration of technetium in the surface, and this had a very considerable effect on the overvoltage of the alloy in both anodic and cathodic polarization.

The study on elementary technetium embraced anodic polarization in various acid media, chiefly 1 *N* H_2SO_4, in an atmosphere of helium. Other measurements were made on technetium, platinum, or gold substrates which had been coated with a film of hydrous oxide by cathodic reduction of a pertechnetate. Such electrodes were found to give a number of reproducible potentials in acidic media and over a sufficient range of pH values as to leave no doubt that they correspond to definite couples between the element and one of its hydroxides or between two such compounds containing the element in different valence states.

The study is incomplete, but certain conclusions are possible. When technetium is coated under suitable conditions, the electrode gives a potential for the couple

$$Tc + 4H_2O \rightleftharpoons Tc(OH)_4 + 4H^+ + 4e^-,$$

from which the free energy of formation of $Tc(OH)_4$ may be calculated directly. Figure 6.38 shows a series of measurements of this couple over a wide range of acidities. The calculated free energy, −199.7 kcal/mole, is in good agreement with the value, −202 kcal/mole, derived from a determination of the heat of combustion of technetium to pertechnic acid[1] and the reversible potential of the Tc(IV-VII) couple.[1,2]

Several other couple potentials were observed, and it was possible to identify them as including the new compounds TcOH, $Tc(OH)_2$, $Tc(OH)_3$, and Tc_3O_4 as components of surface films. The identification was based on an empirical relation found to exist when the free energy of formation, *per equivalent*, of oxides of a given metal in different valence states is plotted against the valence. The agreement between observed halts or inflections in potential-time curves with potentials calculated from the approximated free energies was unambiguous and provided data for calculating free energies of formation for all the oxides. Certain features of the experiments indicate the probable need to consider the influence of the beta radiation of technetium and of the radiolytic products in the electrolyte.

The corrosion potential of technetium in 1 *N* H_2SO_4 is approximately 20 mV noble to the reversible potential of a hydrogen electrode in the same solution. After a film of TcOH has been formed, the electrode remains essentially passive, the anodic current density remaining in the order of 10^{-6} A/cm^2 until the potential is raised by about 500 mV, when oxidation of the film to TcO_4^- sets in. The study is continuing.

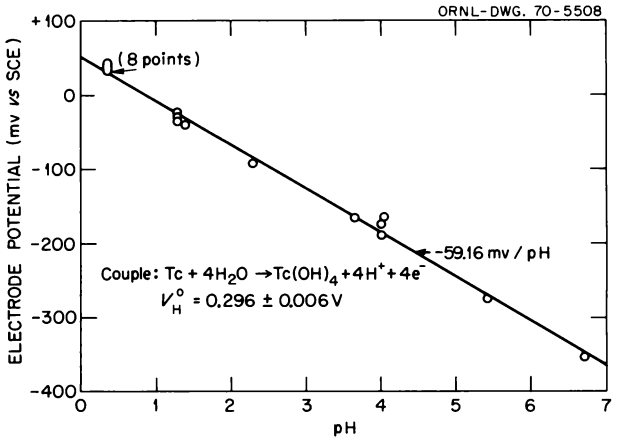

Fig. 6.38. Electrode Potential of the Tc-Tc(OH)$_4$ Couple as a Function of pH. Potentials are referred to sce.

[1] J. W. Cobble, W. T. Smith, Jr., and G. E. Boyd, *J. Am. Chem. Soc.* **75**, 5777 (1953).

[2] G. H. Cartledge and W. T. Smith, Jr., *J. Phys. Chem.* **59**, 1111 (1955).

ELECTROCHEMICAL BEHAVIOR OF TITANIUM

E. J. Kelly

This report describes the effects of chloride, iodide, and hydrogen ions and of the hydrogen evolution reaction on polarization curves for the dissolution of zone-refined titanium in H_2-saturated acidic sulfate media. The experiments represent part of a continuing program which has as its goal the determination of the mechanisms of dissolution of titanium in the active and active-passive transition states and of the related phenomena of corrosion inhibition and pitting corrosion.

In Fig. 6.39 curves *A* and *D* illustrate the effect of pH on the anodic polarization curves. At the corrosion potential E_c (cf. curve *A*), titanium undergoes spontaneous active-state dissolution. As the potential is made increasingly positive, the anodic current corresponding to the dissolution reaction rises to a maximum (i_m) at the "critical potential" (E_m) and then decreases as the metal is transformed from the active to the passive state. As is shown by curve *D*, an increase in pH is accompanied by a decrease in i_m and a displacement of E_m toward more negative values. In an earlier report[1] it was shown that $d \log i_m/dE_m$ and dE_m/d pH are essentially constant, from which it follows that d log i_m/d pH must also be constant. Although various authors have verified one or more of these functional relationships,[2] the values assigned to the constants have been characterized by a lack of agreement and even internal inconsistencies, that is, violations of the requirement that

$$d \log i_m/d \text{ pH} = (d \log i_m/dE_m)\cdot(dE_m/d \text{ pH}) .$$

The existence of such simple functional relationships greatly restricts mechanisms proposed for titanium dissolution. However, in order to further limit the mechanistic possibilities, precise values of the derivatives are required, and this has necessitated taking into account the effect of the hydrogen evolution reaction on the measured values of i_m and E_m. In Fig. 6.39 the cathodic polarization curve (curve *E*) exhibits a Tafel region with a slope of −120 mV/decade. The cathodic Tafel line (curve *G*), which corresponds to the hydrogen evolution reaction, must be extrapolated into the anodic potential region and added to curve *D* in order to obtain curve *F*, which corresponds to just the titanium dissolution reaction. As a consequence of this correction, it is seen that the correct value for i_m (curve *F*) is somewhat greater than the apparent value given by curve *D*, and, similarly, the true value of E_m is more negative than the apparent value.

As the pH decreases, the correction for the effect of the hydrogen evolution reaction diminishes, and for curve *A* it is negligible. In Fig. 6.40 curve I shows that log i_m is a linear function of E_m, and curve II shows that log i_m is a linear function of pH. From curves I and II one obtains

$$d \log i_m/dE_m = (\tfrac{1}{2})\cdot(F/2.303RT)$$

and

$$d \log i_m/d \text{ pH} = -\tfrac{2}{3} .$$

It follows that

$$dE_m/d \text{ pH} = -(\tfrac{4}{3})\cdot(2.303RT/F) .$$

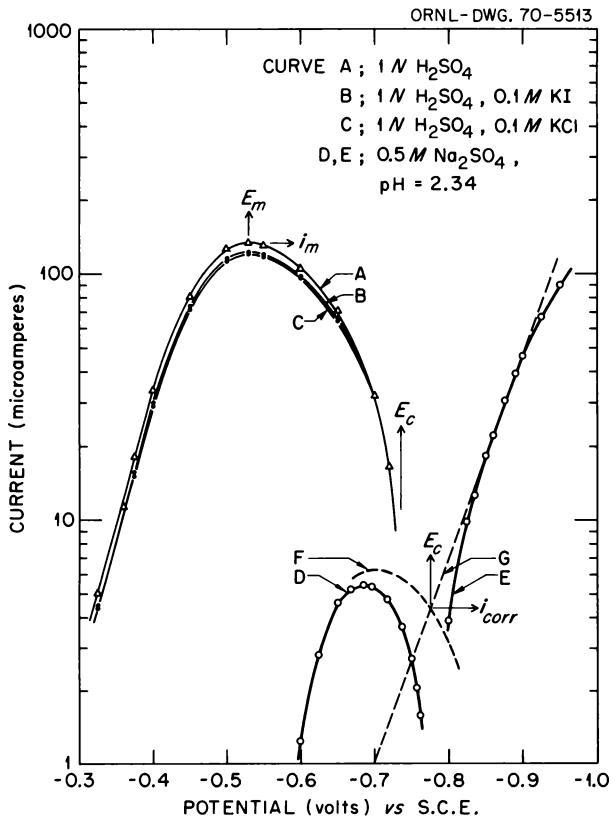

Fig. 6.39. Effects of pH, Chloride Ions, and Iodide Ions on the Polarization Characteristics of Titanium at 30°C.

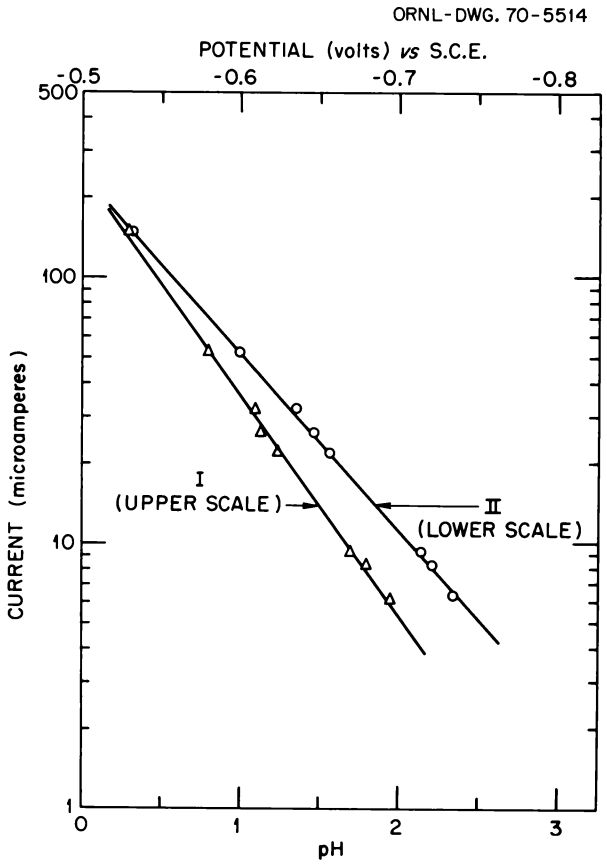

Fig. 6.40. Variation of i_m with E_m (Curve I) and with pH (Curve II) in 0.5 M Na_2SO_4 Solutions at 30°C.

The nature of these constants is of prime diagnostic significance in the elucidation of the mechanism of titanium dissolution.

The presence of chloride or iodide ions at concentrations of 10^{-3} and 10^{-2} M had no discernible effect on the anodic polarization curves of titanium in 1 N H_2SO_4. However, at a concentration of 10^{-1} M, both I^- and Cl^- lower the curve, as is shown by curves B and C, respectively, in Fig. 6.39. As measured at i_m, the reduction amounts to approximately 8% for I^- and 10% for Cl^-. No effect on E_m is observed. The significance of these results derives from the fact that for other metals which undergo active-state dissolution in 1 N H_2SO_4 (e.g., Fe and Co), the iodide ion is a powerful inhibitor of the dissolution reaction. In the case of iron, for example, the adsorption of iodide from 1 N H_2SO_4 solutions containing even lower concentrations of iodide than those employed in this work is sufficient to lower the anodic polarization curve by several orders of magnitude.[3] The effect of Br^- is less, and that of Cl^- is relatively insignificant. In the case of active iron, the surface is occupied almost completely by adsorbed water molecules only,[4] which are displaced by the adsorbed inhibitor. In the case of titanium, the results obtained in this investigation suggest the existence of a surface occupied not by water molecules but rather by adsorbed surface intermediates such as TiO and TiO·OH. The inability of iodide ions or chloride ions to displace these adsorbed species could account for the results described above.

---

[1] E. J. Kelly, *Chem. Div. Ann. Progr. Rept. May 20, 1969*, ORNL-4437, p. 89.

[2] N. T. Thomas and K. Nobe, *J. Electrochem. Soc.* **116**, 1748 (1969).

[3] K. E. Heusler and G. H. Cartledge, *J. Electrochem. Soc.* **108**, 732 (1961).

[4] E. J. Kelly, *J. Electrochem. Soc.* **115**, 1111 (1968).

CHRONOPOTENTIOMETRY AND VOLTAMMETRY OF THE Ag-AgCl ELECTRODE IN FLOWING STREAMS – EXPERIMENTAL[1]

R. E. Meyer P. M. Lantz
M. C. Banta[2] F. A. Posey

In previous reports[3,4] we described a chronopotentiometric technique for the analysis of solutions containing chloride ion. This work has been extended to include chronopotentiometric and voltammetric analyses of the chloride ion in flowing streams by use of a channel electrode. A schematic diagram of a channel electrode is shown in Fig. 6.41. Flow of solution is assumed to take place along the x direction. The electrode length in the x direction is denoted by l (cm), and the width of the working surface of the electrode is w (cm). The dimensions of the channel which determine the flow pattern are the width d, the height h,

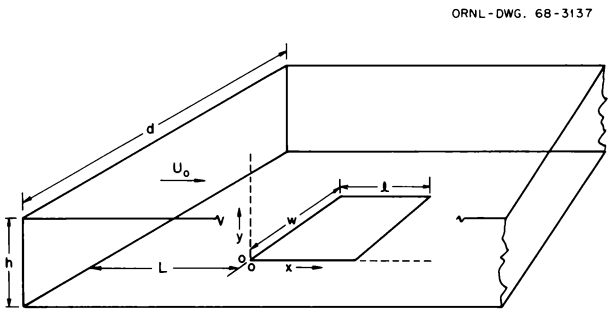

Fig. 6.41. Typical Experimental Configuration for Electroanalysis in Flowing Solution.

and the distance from the entrance of the channel to the leading edge of the electrode L.

Two modes of operation were investigated in this work. In the voltammetric mode we were primarily interested (1) in the relation between the limiting current which results from oxidation of a silver electrode in the presence of chloride ions and the parameters which determine flow rate, and (2) in applying these results to the analysis of solutions containing low concentrations of chloride ion ($<10^{-3}$ M). For analysis of solutions containing higher concentrations of chloride ion, we investigated the chronopotentiometric mode of operation.

In terms of volume flow rate and the parameters of Fig. 6.41, the limiting current is given by[5,6]

$$I_L = 1.467zwFC_0\left(\frac{Dl}{h}\right)^{2/3}\left(\frac{U_v}{d}\right)^{1/3}, \qquad (1)$$

where I_L is the limiting current due to convective diffusion (A), z is ion charge, F is the Faraday constant (coulombs/equivalent), C_0 is bulk reactant concentration (moles/cm^3), D is the diffusion coefficient (cm^2/sec), and U_v is the volume flow rate (cm^3/sec). Several cells were constructed which had the geometry of Fig. 6.41, and a number of experiments were carried out to see if the limiting current conformed to the predictions of Eq. (1). Experimentally observed relations between limiting current and flow rate, electrode length, and bulk concentration of chloride ions are shown in Figs. 6.42–6.44. These results show that Eq. (1) holds to a high degree of accuracy. In Fig. 6.43 a blank current is first subtracted from the polarization curves to get the horizontal lines which correspond to the limiting currents. These results demonstrate that successful analyses may be carried out by use of this technique, since limiting currents are directly proportional to the bulk concentration of chloride ions.

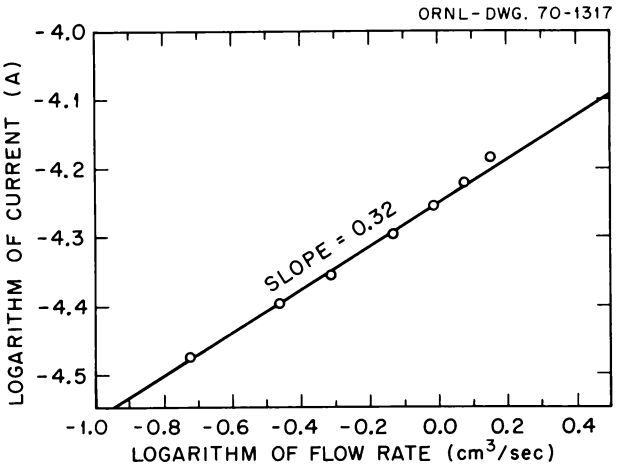

Fig. 6.42. Limiting Current as a Function of Volume Flow Rate. 0.5 × 1.5 cm electrode, 5 × 10^{-4} M NaCl, 0.25 M KNO_3, +0.300 V vs sce.

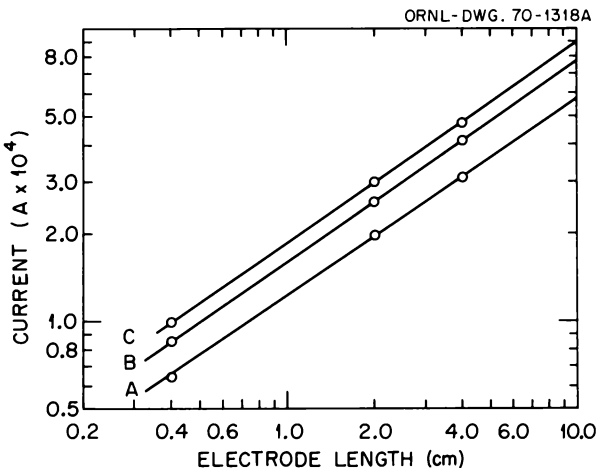

Fig. 6.43. Limiting Current as a Function of Electrode Length at Various Flow Rates. 2.5 × 10^{-3} M NaCl, 0.25 M KNO_3, +0.300 V vs sce. Flow rates: curve A, 0.189 cm^3/sec; curve B, 0.485 cm^3/sec; and curve C, 0.737 cm^3/sec. Slope of straight lines = 0.66.

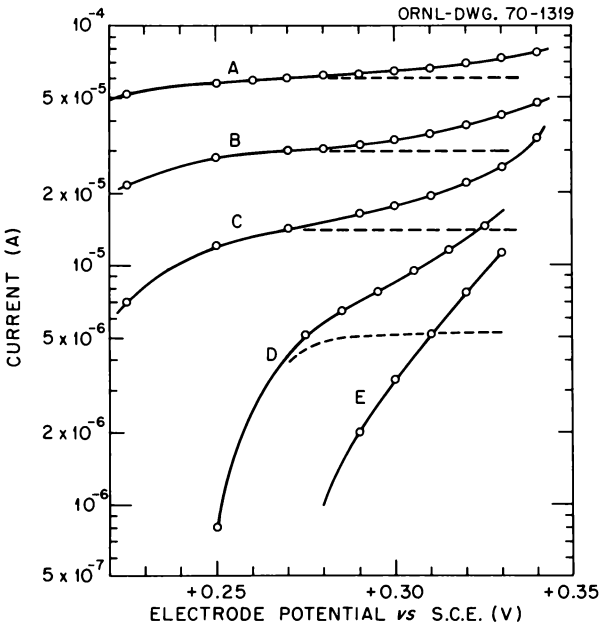

Fig. 6.44. Limiting Current as a Function of NaCl Concentration. 0.25 M KNO_3, 0.5 × 1.5 cm electrode, volume flow rate = 0.189 cm^3/sec; (A) 10^{-3} M NaCl, (B) 5 × 10^{-4} M NaCl, (C) 2 × 10^{-4} M NaCl, (D) 10^{-4} M NaCl, (E) blank.

Voltammetric measurements were found to be useful for chloride analysis in the concentration range 1 X 10^{-4} to 5 X 10^{-3} *M* Cl^- (approximately 4 to 200 ppm).

In the chronopotentiometric mode of operation, the effect of increasing the solution flow rate is to increase the transition time and to broaden or retard the transition of the potential from the Ag-AgCl electrode reaction to the next available reaction. This broadening effect is shown in Fig. 6.45, where chronopotentiograms for various flow rates are shown for a solution of 5.63 X 10^{-3} *M* NaCl. Little change in the initial sections of the curves is noted, but in the final section the slope of the rising portion decreases considerably. It is quite difficult to determine the transition time by conventional graphical techniques, but with a derivative technique transition times may be determined with considerable precision. The potential derivative vs time curves for these chronopotentiograms are shown in Fig. 6.46. As expected, the derivative peaks broaden, but the transition time, that is, the maximum point, may be determined with reasonable precision. It was found that the transition time obtained with a channel electrode is a reproducible function of the flow rate and is also a reproducible function of the usual parameters, current density and reactant concentration. By use of appropriate calibration procedures, precise chronopotentiometric analyses (±0.5%) may be carried out with a channel electrode over the concentration range 3 X 10^{-4} to 10^{-1} *M* Cl^- (approximately 10 to 3500 ppm).

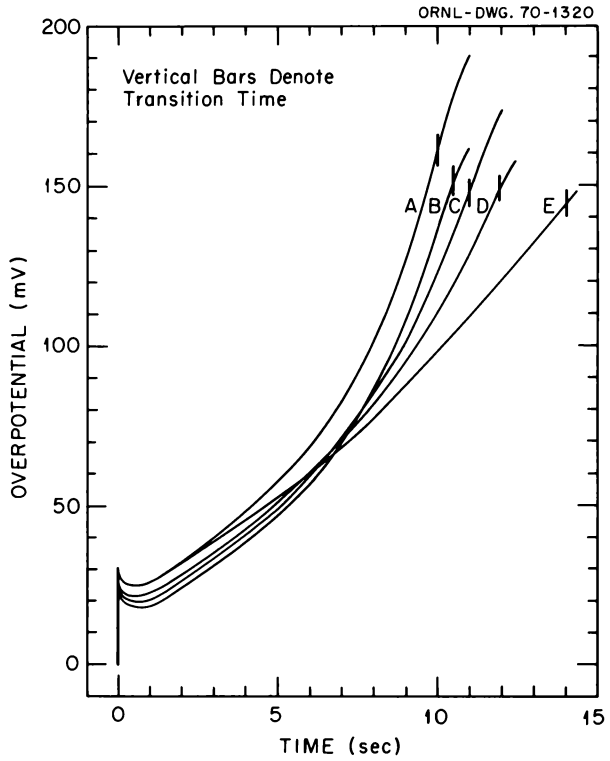

Fig. 6.45. Effect of Flow Rate on Chronopotentiograms. 5.63 X 10^{-3} *M* NaCl, 0.25 *M* KNO_3, 0.5 X 1.5 cm electrode, *I* = 0.518 mA; (*A*) 0.0 cm^3/sec, (*B*) 0.162 cm^3/sec, (*C*) 0.273 cm^3/sec, (*D*) 0.392 cm^3/sec, (*E*) 0.565 cm^3/sec.

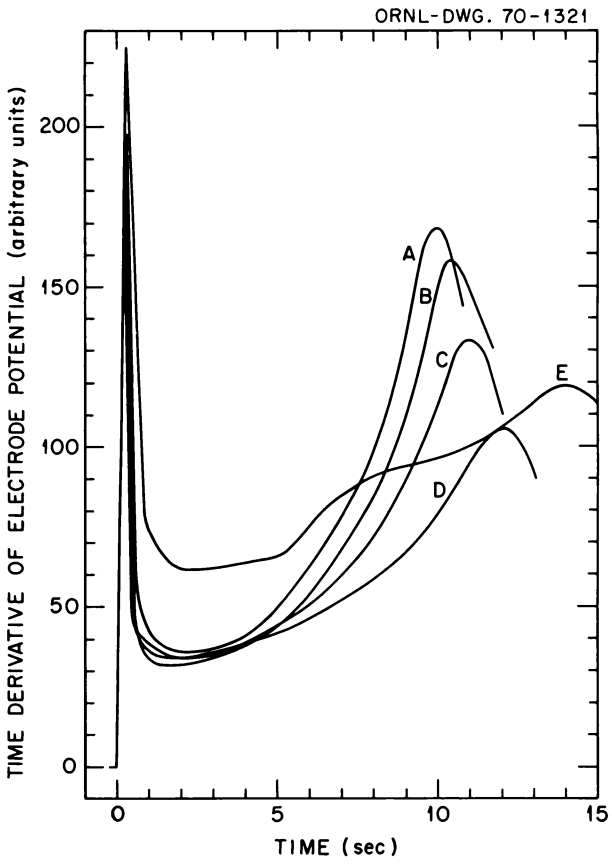

Fig. 6.46. Effect of Flow Rate on Derivatives of Chronopotentiograms. 5.63 X 10^{-3} *M* NaCl, 0.25 *M* KNO_3, 0.5 X 1.5 cm electrode, *I* = 0.518 mA; (*A*) 0.0 cm^3/sec, (*B*) 0.162 cm^3/sec, (*C*) 0.273 cm^3/sec, (*D*) 0.392 cm^3/sec, (*E*) 0.565 cm^3/sec.

---

[1] Research jointly sponsored by the Office of Saline Water, U.S. Department of the Interior, and by the U.S. Atomic Energy Commission under contract with Union Carbide Corporation.

[2] Department of Chemistry, Sam Houston State University, Huntsville, Tex.

[3] R. E. Meyer *et al., Chem. Div. Ann. Progr. Rept. May 20, 1967*, ORNL-4164, p. 87.

[4]R. E. Meyer *et al., Chem. Div. Ann. Progr. Rept. May 20, 1968,* ORNL-4306, p. 113.

[5]V. G. Levich, *Physicochemical Hydrodynamics,* p. 112, Prentice-Hall, Englewood Cliffs, N.J., 1962.

[6]F. A. Posey and R. E. Meyer, "Chronopotentiometry and Voltammetry of the Ag-AgCl Electrode in Flowing Streams. II. Theoretical," submitted to the *Journal of Electroanalytical Chemistry.*

CHRONOPOTENTIOMETRY AND VOLTAMMETRY OF THE Ag-AgCl ELECTRODE IN FLOWING STREAMS – THEORETICAL[1]

F. A. Posey R. E. Meyer

Solutions to the equation of convective diffusion were obtained for chronopotentiometry and voltammetry of an electrode located in a channel where the electrode process involves formation of a solid phase. The relations derived for voltammetry permit computation of reactant concentration from experimental polarization curves, polarization resistances, or limiting currents with a knowledge of solution flow rate, applied current, electrode and channel dimensions, and other parameters. An approximate method of solution of the equation of convective diffusion, based upon a Nernstian diffusion layer approximation, was used to obtain a useful expression for the effect of flow rate and other pertinent variables on transition times for chronopotentiometry in flowing streams.

The theoretical relations proved to be useful in the interpretation of voltammetric and chronopotentiometric measurements on the Ag-AgCl channel electrode, which has application to rapid chloride analysis in flowing streams. Two manuscripts on experimental and theoretical aspects of the Ag-AgCl channel electrode have been submitted for publication to the *Journal of Electroanalytical Chemistry.*

[1]Research jointly sponsored by the Office of Saline Water, U.S. Department of the Interior, and by the U.S. Atomic Energy Commission under contract with Union Carbide Corporation.

INSTRUMENT AND CELL DEVELOPMENT FOR RAPID CHRONOPOTENTIOMETRIC ANALYSIS OF CHLORIDE ION[1]

R. E. Meyer

A rapid method of chronopotentiometric analysis of chloride ion has been described previously.[2-4] Because practical application of an analytical method depends on the availability of convenient and reliable apparatus, a new cell was designed, constructed, and tested. In addition a new instrument was designed and built for use with the cell.[5]

Chronopotentiometric analysis of the chloride ion is based upon accurate determination of the time required to deplete the boundary layer (transition time) when an anodic current is applied to a silver electrode in the presence of chloride ion. Accurate analysis requires precise control of the applied current density and the geometry of the cell. In addition, electrodes should be easily replaceable, and the entire cell should be easy to disassemble and clean. These requirements are met by the cell shown in Fig. 6.47. The main body of the cell is machined from a cylinder of Lucite. The area of the electrode is precisely defined by pressing the silver disk against the machined flat surface of the Lucite. The vertical sides of the cell at the electrode edges shield the

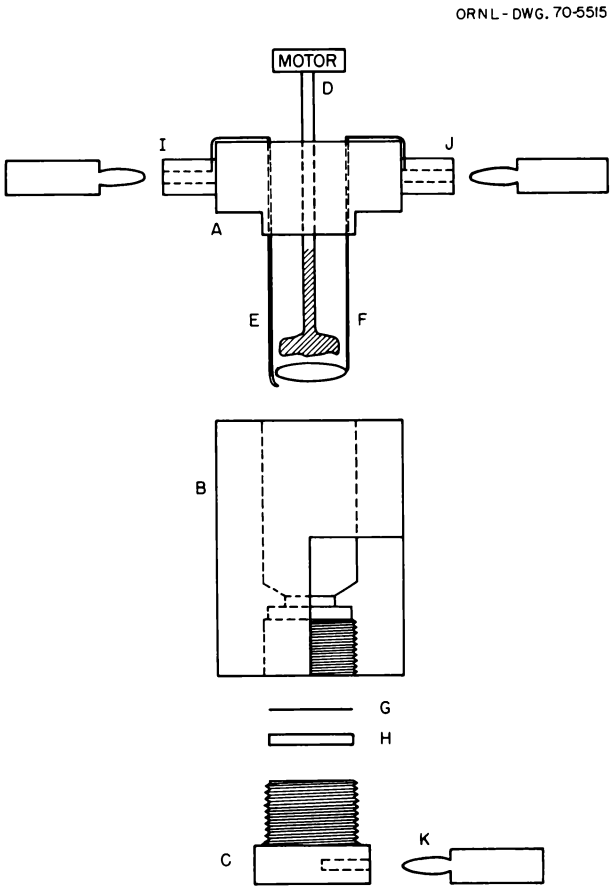

Fig. 6.47. Chloride Test Cell Assembly. (*A*) Teflon support; (*B*) Lucite reservoir; (*C*) stainless steel electrode support; (*D*) epoxy-coated stirrer; (*E*) epoxy-coated Ag-AgCl reference electrode; (*F*) silver polarizing electrode; (*G*) silver disk; (*H*) stainless steel washer; (*I*) reference electrode connector; (*J*) polarizing electrode connector; (*K*) test electrode connector.

electrode in order to prevent interference by horizontal components of mass transport of the reactant at the edges. Total volume of the cell is about 15 cm^3, but as little as 5 or 6 cm^3 is sufficient for analysis.

The electronic instrument designed for use with this cell incorporates three basic functions in one instrument. Three integrated-circuit miniature operational amplifiers (Fairchild UA741C) are used. One of the amplifiers is used to control the current to a preset value and will maintain a constant current regardless of changes in cell impedance. The magnitude of the current is determined by settings on a digital potentiometer and a range switch. The other amplifiers are used for measurement of the electrode potential and the time derivative of the electrode potential. The time derivative is used for precise determination of the transition time.[4] A switch converts the control circuit to a potentiostat for operation of the test electrode at constant potential. This instrument may be used as a generalized electrochemical instrument designed for easy portability and low cost (less than $500).

An instruction manual has been written for both the instrument and the cells. This apparatus has been used and tested for several months, resulting in a considerable increase in precision of measurement and convenience of operation.

---

[1]Research jointly sponsored by the Office of Saline Water, U.S. Department of the Interior, and by the U.S. Atomic Energy Commission under contract with Union Carbide Corporation.

[2]R. E. Meyer *et al., Chem. Div. Ann. Progr. Rept. May 20, 1967,* ORNL-4164, p. 87.

[3]R. E. Meyer *et al., Chem. Div. Ann. Progr. Rept. May 20, 1968,* ORNL-4306, p. 113.

[4]R. E. Meyer, F. A. Posey, and P. M. Lantz, *J. Electroanal. Chem.* 19, 99 (1968).

[5]The invaluable advice and assistance of J. L. Lovvorn, Instrumentation and Controls Division, is gratefully acknowledged.

7. Chemical Physics

NEUTRON AND X-RAY DIFFRACTION

INTERPRETATION OF THE STRUCTURES OF SOME ALKALINE EARTH CHLORIDES IN TERMS OF INTERIONIC FORCES

W. R. Busing

An earlier report[1] presented some of the reasons for establishing a model to interpret crystal structures in terms of interionic and intermolecular forces and described a computer program which can adjust the parameters of such a model on the basis of experimentally observed crystal structures. These calculations have now been improved to include as observations thermochemical information on lattice energies, to allow for the weighting of observations according to their estimated errors, and to permit information about several substances to be used in adjusting common parameters of the model. The form of the interatomic repulsion potential has been revised so that the expression for the lattice energy is

$$W=\frac{1}{2}\sum_i\sum_j\left[\frac{Q_iQ_j}{r_{ij}}-\frac{D_iD_j}{r_{ij}^6}+(B_i+B_j)\exp\frac{A_i+A_j-r_{ij}}{B_i+B_j}\right].$$

Here r_{ij} is the distance between two ions, Q_i is the ionic charge, and D_i is a coefficient in the van der Waals term. The repulsion term is in the form suggested by Gilbert,[2] in which A_i is a radius and B_i is a hardness parameter.

The present study, which is described in more detail elsewhere,[3] considers four related substances with different structure types: $MgCl_2$, a $CdCl_2$-type layer structure; $CaCl_2$, a distorted rutile arrangement; $SrCl_2$, the fluorite structure; and $BaCl_2$, the orthorhombic $PbCl_2$ structure. Values of the Q_i's, D_i's, and B_i's were established on a theoretical basis. Parameters A_i for the five kinds of ions and one factor multiplying the van der Waals contributions were adjusted for a least-squares fit to the 17 observed structural parameters and the four lattice energies. The resulting model was then tested by adjusting the structural parameters of each substance to minimize the calculated energy W. Table 7.1 shows a comparison of observed and calculated

Table 7.1. Comparison of Observed and Calculated Lattice Parameters, Atomic Coordinates, Interatomic Distances, and Lattice Energies for $MgCl_2$, $CaCl_2$, $SrCl_2$, and $BaCl_2$

	Observed	Calculated	Difference
Lattice Parameters (Å) and Atomic Coordinates			
$MgCl_2$			
a	3.596	3.587	−0.009
c	17.590	17.502	−0.088
Cl *z*	*a*	0.273	*a*
$CaCl_2$			
a	6.24	6.310	0.070
b	6.43	6.310	−0.120
c	4.20	4.261	0.061
Cl *x*	0.275	0.304	0.029
y	0.325	0.304	−0.021
$SrCl_2$			
a	6.977	7.004	0.027
$BaCl_2$			
a	9.415	9.353	−0.062
b	7.878	7.969	0.091
c	4.731	4.831	0.100
Ba *x*	0.118	0.108	−0.010
y	0.250	0.248	−0.002
Cl(1) *x*	0.431	0.422	−0.009
y	0.356	0.357	0.001
Cl(2) *x*	0.829	0.839	0.010
y	0.473	0.486	0.013
Interatomic Distances (Å)			
Mg-Cl	*a*	2.32	*a*
Ca-Cl	2.70	2.72	0.02
	2.76	2.76	0.00
Sr-Cl	3.02	3.03	0.01
Ba-Cl(1)	3.06	3.06	0.00
	3.07	3.09	0.02
	3.14	3.13	−0.01
Ba-Cl(2)	3.24	3.14	−0.10
	3.26	3.25	−0.01
	3.56	3.74	0.18
Lattice Energies (kcal/mole)			
$MgCl_2$	−602.8	−601.6	1.2
$CaCl_2$	−538.2	−537.3	0.9
$SrCl_2$	−514.0	−517.6	−3.6
$BaCl_2$	−489.3	−489.0	0.3

[a]Not yet observed.

lattice parameters, coordinates, interatomic distances, and lattice energies. In general the agreement is good, showing that the model is a reasonable first approximation. For $CaCl_2$, however, this model predicts the tetragonal rutile structure rather than the orthorhombic distortion which is observed.

It is now fairly clear that the model must be elaborated to allow for the polarization of the ions due to the presence of their neighbors. Earlier attempts[1] to include deformable ions failed to produce stable structures because the form of the restoring force allowed the dipole moments to increase indefinitely. New attempts using an exponential restoring force seem to be more successful, and there are indications that this model will account for the orthorhombic structure of $CaCl_2$.

In an attempt to explain the four different structural arrangements found for these compounds, further calculations were made assuming each of the three alternative structure types for each substance. The values found previously were used for the parameters of the energy expression, and each hypothetical structure was adjusted to minimum energy. For $CaCl_2$ and $SrCl_2$ the results of these calculations were satisfactory in that all of the alternative arrangements were less stable than those observed. On the other hand, the calculations imply that both the rutile and fluorite structures for $BaCl_2$ and the rutile structure for $MgCl_2$ would be more stable than the observed structures. This is a further indication that the model is not yet complete.

The work is continuing, and efforts are being made to include polarization effects as mentioned above. The result of adding van der Waals terms in r^{-8} and r^{-10} will also be examined.

[1] W. R. Busing, *Chem. Div. Ann. Progr. Rept. May 20, 1968*, ORNL-4306, p. 139.

[2] T. L. Gilbert, *J. Chem. Phys.* **49**, 2640 (1968).

[3] W. R. Busing, *Trans. Am. Cryst. Assoc.* **6** (1970), to be published.

SITE SYMMETRY RESTRICTIONS ON THERMAL-MOTION TENSOR COEFFICIENTS

C. K. Johnson

When an atom (or molecule) in a crystal is situated on a site of special symmetry of the unit cell of the crystal, the components of any tensor representing a property of the atom (or molecule) are restricted according to the point symmetry of the site.[1] The existing tabulations for these restrictions are inadequate for modern thermal-motion studies because they are either limited to second-rank symmetric polar tensors[2] or are limited to one orientation of the site point group.[1]

A comprehensive tabulation for second-, third-, and fourth-rank symmetric polar tensors used in the cumulant-expansion structure-factor equation[3] and for second-rank general axial tensors used in rigid-body analysis[4] has now been derived for all possible settings of the special positions in the crystallographic space groups. This tabulation, which covers all subgroups of point groups *m*3*m* and 6/*mmm* including conjugate subgroups, will appear as part of a chapter[5] on thermal-motion analysis in a forthcoming volume of *The International Tables for X-Ray Crystallography.*

A computer program using the FORMAC (*FOR*mula *MA*nipulation *C*ompiler) programming system[6] was written to evaluate algebraically the appropriate tensor transformation equations[1] and to sum the tensors resulting from all the different transformations of a given subgroup.[2] The groups of transformations were formed from generator elements[1,7] by the group-multiplication-table method. The restrictions among the tensor coefficients for a given site symmetry were found by inspection of the algebraic form of the tensor sums and were recorded in a notation which could be verified algebraically by another FORMAC program. There are 98 subgroups of point group *m*3*m* and 54 subgroups of 6/*mmm* (including conjugate sets). For the contravariant components of the tensors mentioned, a total of 230 different tensor-component restrictions were found. In addition, the restrictions for all covariant components and certain mixed covariant-contravariant combinations were derived for the hexagonal axis system, in which covariant and contravariant components have different symmetry restrictions.

[1] R. R. Birss, *Symmetry and Magnetism,* North-Holland, Amsterdam, 1964.

[2] W. J. A. M. Peterse and J. H. Palm, *Acta Cryst.* **20**, 147 (1966).

[3] C. K. Johnson, *Acta Cryst.* **A25**, 187 (1969).

[4] V. Schomaker and K. N. Trueblood, *Acta Cryst.* **B24**, 63 (1968).

[5] C. K. Johnson and H. A. Levy, "Thermal Motion Analysis Using Bragg Diffraction Data" in *International Tables for X-Ray Crystallography,* Suppl. to Vols. II, III (eds. W. A. Hamilton and J. A. Ibers), Kynoch Press, Birmingham (in press).

[6] R. Tobey, J. Baker, R. Crews, P. Marks, and K. Victor, *PL/I-FORMAC Interpreter User's Reference Manual,* IBM Contributed Program Library No. 360D-03.3.004, Hawthorne, N.Y., 1967.

[7] S. C. Miller and W. F. Love, *Tables of Irreducible Representations of Space Groups and Co-Representations of Magnetic Space Groups,* Pruett Press, Boulder, 1967.

A NEW STRUCTURE-FACTOR EQUATION FOR ANALYZING SKEWNESS AND KURTOSIS IN THERMAL-MOTION DENSITY FUNCTIONS

C. K. Johnson

The Gaussian probability density function is used widely to approximate the thermal motion of atoms in crystals. Skewness and kurtosis, the deviations of odd and even symmetry from the Gaussian density function, can provide valuable characterizations for anharmonic vibration effects. The cumulant-expansion structure-factor equation[1,2] has been used successfully for the determination of skewness in thermal-motion density functions. The skewness coefficient tensor in the cumulant expansion adds ten parameters per atom to the nine parameters per atom normally determined in a crystal-structure refinement. The kurtosis coefficient tensor in the cumulant expansion has not been used because it introduces an additional 15 parameters per atom. A new model with fewer parameters clearly is needed. The structure-factor equation described here utilizes the properties of contracted multidimensional Hermite polynomials to obtain a reduced set of skewness and kurtosis parameters which are orthogonal to the usual atomic position and temperature-factor parameters.

The structure-factor equation incorporating the contracted Hermite polynomials is

$$F(\mathbf{t}) = \sum_{\text{atoms}} f(\mathbf{t}) \exp\left(i \sum_{j=1}^{3} x^j t_j\right) \left\{ \exp\left(-\frac{\alpha}{2} \sum_{j,k=1}^{3} \sigma^{jk} t_j t_k\right) \times \left[1 - \frac{i}{10} \sum_{m=1}^{3} c_m \, {}^3G^m(\mathbf{t}) + \frac{1}{28} \sum_{m,n=1}^{3} d_{mn} \, {}^4G^{mn}(\mathbf{t})\right]\right\}, \quad (1)$$

where $f(\mathbf{t})$ is the atomic scattering factor and $\mathbf{t} = 2\pi\mathbf{h}$, with $\mathbf{h}$ the vector of Miller indices. The nine normal coefficients x^j and $\alpha\sigma^{jk}$ ($j, k = 1, 2, 3; j \leqslant k$) are the parameters for the mean position vector $\mathbf{x}$ and the dispersion matrix $\alpha\boldsymbol{\sigma}$, of the Gaussian density function for an atom. The ten new parameters are the "orthogonalization scalar" α, the "contracted skewness vector" $\|c_j\| \equiv \mathbf{c}$, and the symmetric "contracted kurtosis matrix" $\|d_{jk}\| \equiv \boldsymbol{d}$. The polynomial tensors with components ${}^3G^m(\mathbf{t})$ and ${}^4G^{mn}(\mathbf{t})$ are derived by contracting[3] the third- and fourth-order G Hermite polynomial tensors[4-6] with components ${}^3G^{jkm}(\mathbf{t})$ and ${}^4G^{jkmn}(\mathbf{t})$, with respect to the tensor with components p_{jk}, where the matrix $\|p_{jk}\| \equiv \boldsymbol{p}$ is the inverse of the matrix $\boldsymbol{\sigma}$. The singly contracted polynomials are

$${}^3G^m(\mathbf{t}) = (Q - 5)s^m \quad (2)$$

and

$${}^4G^{mn}(\mathbf{t}) = (Q - 7)s^m s^n - (Q - 5)\sigma^{mn}, \quad (3)$$

where the components s^j of the vector $\mathbf{s}$ are given by

$$s^j = \sum_{k=1}^{3} \sigma^{jk} t_k$$

and the scalar Q is

$$Q = \sum_{j=1}^{3} s^j t_j .$$

The density functions obtained by Fourier transformation of Eq. (1) are basically power-series expansions about the Gaussian thermal-motion density functions; however, they are rather cumbersome expressions (because of the parameter α) and are not shown here.

The orthogonalization scalar α is an empirical parameter serving as an approximation for the first- and second-order correction terms[7] which are omitted from Eq. (1) because of their functional redundancy with the normal first- and second-order terms containing the parameters $\mathbf{x}$ and $\boldsymbol{\sigma}$. The scalar α is adjusted to minimize interactions between x^j and c_j and between σ^{jk} and d_{jk} ($j, k = 1, 2, 3$) which arise in a least-squares refinement. When $\alpha = 0.5$, the factor enclosed by the braces in Eq. (1) becomes a three-term tensor series of biorthogonal[4,7] Hermite functions (i.e., parabolic cylinder functions[8]); however, the experimentally derived values for α which minimize the above interactions have been found to be in the range 0.2 to 0.4. The parameter α allows the character of the Fourier-transformed series[9] in direct space to change from a power-series expansion about the Gaussian when $\alpha = 1$ to a Gram-Charlier differential expansion[6,10] when $\alpha \to 0$. If the atom displays significant skewness or kurtosis, α can be adjusted as an ordinary least-squares parameter; alternatively, α may be adjusted empirically to minimize the correlation coefficients for the above interactions. In general, a single overall value for α will work reasonably well; however, the least-squares program written for these studies provides an α parameter for each atom.

In practice, the three skewness coefficients c_j ($j = 1, 2, 3$) account for about half the total improvement in

the agreement factor R that can be realized when the full ten-parameter skewness tensor is used. The skewness vector $\mathbf{w} \equiv \sigma\mathbf{c}$ (in crystal coordinates) is along the direction of maximum asymmetry of the density function and may be compared with the downward-pointing shaft of a beach umbrella.

The singly contracted kurtosis tensor with components d_{jk} has six unique elements. The three scalars λ_k and the three vectors $\mathbf{v}_k$ in the matrix equation

$$d\mathbf{v}_k = \lambda_k p\mathbf{v}_k \tag{4}$$

give the principal axes of leptokurtosis (positive λ's) and platykurtosis (negative λ's) in the density function. The matrix p is the inverse of σ, and the vectors $\mathbf{v}_k$, which are not necessarily orthogonal, are resolved along the crystal axes.

An example of a "kurtose"[11] thermal-motion density function is that for the xenon atom in the square planar molecule XeF_4.[12] The xenon atom in the crystal cannot display skewness because it is on a center of symmetry; however, kurtosis is allowed, and four of the six coefficients d_{jk} have magnitudes from 1.3 to 1.6 times their standard errors as determined by the method of least squares. The principal axes of kurtosis calculated with Eq. (4) indicate that the density normal to the plane of the XeF_4 molecule is leptokurtic and that the in-plane density is platykurtic. This pattern of kurtosis suggests that certain modes of internal molecular vibration are anharmonic. The fluorine atoms are relatively free of kurtosis, but they do have appreciable skewness which is reasonably consistent with that calculated for rigid-body libration.[13]

---

[1] C. K. Johnson, *Acta Cryst.* **A25**, 187 (1969).

[2] C. K. Johnson, chap. 9 in *Thermal Neutron Diffraction*, ed. by B. T. M. Willis, Oxford University Press, London, 1970.

[3] H. Grad, *Phys. Fluids* **6**, 147 (1963); see Appendix, p. 178.

[4] Erdélyi (ed.), Bateman Manuscript Project, *Higher Transcendental Functions*, vol. II, pp. 264 ff., McGraw-Hill, New York, 1953.

[5] P. A. Tortrat, "Les Fonctions Orthogonales D'Hermite à Plusieurs Variables et Relations D'Incertitude De Heisenberg," Thèses, Université de Paris, 1953.

[6] P. I. Kuznetsov, R. L. Stratonovich, and V. I. Tikhonov, *Theory of Probability Appl. (USSR) English Transl.* **5**, 80 (1960).

[7] The redundant first- and second-order correction terms omitted from the series enclosed by brackets in Eq. (1) are

$$i \sum_{j=1}^{3} a^{j\,1} H_j(\mathrm{t})$$

and

$$\frac{i^2}{2} \sum_{j,k=1}^{3} b^{jk\,2} H_{jk}(\mathrm{t}) .$$

These omitted terms incorporate H Hermite polynomials rather than G Hermite polynomials in order to ensure orthogonality between different-order terms. The G and H Hermite polynomials are biorthogonal relative to the weighting function

$$\Phi(\mathrm{t}) = \exp\left(-\frac{1}{2} \sum_{j,k=1}^{3} \sigma^{jk} t_j t_k\right) ;$$

that is, the integral

$$\int_{-\infty}^{\infty} \Phi(\mathrm{t})\, {}^{m}G^{\alpha_1 \ldots \alpha_m}(\mathrm{t})\, {}^{n}H_{\beta_1 \ldots \beta_n}(\mathrm{t})\, d\mathrm{t}$$

is nonzero only if $m = n$ *and* the sequence of tensor indices $\alpha_1 \ldots \alpha_m$ is the same as or a permutation of the sequence $\beta_1 \ldots \beta_n$.

[8] N. N. Lebedev, *Special Functions and Their Applications*, chap. 10, Prentice-Hall, Englewood Cliffs, N.J., 1965.

[9] N. Ja. Vilenkin, *Special Functions and the Theory of Group Representations*, 565 pp., Am. Math. Soc., Providence, R.I., 1968.

[10] M. G. Kendall and A. Stuart, *The Advanced Theory of Statistics*, vol. 1, Griffin, London, 1963.

[11] The adjective "kurtose," from the noun kurtosis, is coined to complement the adjective skew in describing aberrations of the Gaussian density function.

[12] J. H. Burns, P. A. Agron, and H. A. Levy, p. 211 in *Noble-Gas Compounds*, ed. by H. H. Hyman, University of Chicago Press, Chicago, 1963.

[13] C. K. Johnson, *Chem. Div. Ann. Progr. Rept. May 20, 1969*, ORNL-4437, p. 122.

A PRELIMINARY STUDY OF THE USE OF POSITION-SENSING DETECTORS IN X-RAY AND NEUTRON DIFFRACTION STUDIES

H. A. Levy R. D. Ellison

A study of the use of position-sensing neutron and x-ray detectors in single-crystal diffraction experiments was begun. Our preliminary results apply to both of the detection systems being developed by members of the Instrumentation and Controls Division: the system using image-intensification and television techniques designed by J. B. Davidson[1] and the position-sensing proportional-counter technique of M. K. Kopp and C. J. Borkowski.[2] Because of its potential for use in neutron diffraction investigations where only a relatively low neutron flux is available, experimental evaluation of the former will be undertaken first.

Best use of these detectors may be had in recording the diffraction patterns of crystals with large unit-cell dimensions where many diffraction peaks occur simultaneously. We have written a computer program to calculate the position and size at the detector of each

diffracted beam for the case of a crystal rotating about a single axis. A search is made for spatial overlap of reflections that occur simultaneously.

The method used was to generate the indices of reflections of interest and to calculate the rotation required to orient the crystal for a reflection and the coordinates of that reflection on the face of the detector. The spread of the reflection on the detector was calculated as the sum of the effects due to the divergence of the incident beam, its wavelength variation, the size of the crystal, and, for the neutron case, the correlation of wavelength variation with incident beam direction. The range of crystal rotation required to integrate over the reflection was calculated from an assumed mosaicity of the crystal, the beam divergence, the wavelength spread, and the correlation. The list of reflections was put in the order of appearance as the crystal rotates; the disappearance of each reflection was also entered into the list. As each reflection was entered into the ordered list, the detector coordinates of its boundaries were compared with those of reflections that had begun but not yet ended. Simultaneous reflections that were separated by less than the semi-dimension of the one that required the largest detector area were considered to overlap.

For the x-ray case, the calculation was performed subject to the following experimental conditions: beam divergence of 0.27° vertical and 0.07° horizontal (approximately those currently used with our single-crystal diffractometer); a hypothetical monoclinic crystal 0.5 mm along each edge and with unit-cell parameters of a = 30 Å, b = 35 Å, c = 40 Å, cos β = −0.087 and a mosaic angular spread of 0.5°; a detector placed 212 mm from the crystal; and Cu $K\alpha$ radiation. The area of the detector was kept relatively small (25 × 250 mm), as was the total crystal rotation (5°), to reduce computing time. Results of this calculation were encouraging: as many as 67 simultaneous reflections may be expected to appear with no overlaps in the range of Bragg angles covered. A total of 99 reflections is expected during 5° of crystal rotation; the rotation required to cover one equatorial reflection is as much as 0.78°. If each reflection were measured separately using the same angular velocity of crystal rotation, the time required for measuring all 99 reflections would be 99 × 0.78/5 = 14.7 times that required using the position-sensing detector. Larger advantage factors would be expected for crystals with larger unit cells.

[1] J. B. Davidson, abstract VIII-7, Collected Abstracts of the Eighth International Congress of Crystallography, *Acta Cryst.* **A25**, part S3, p. S66 (1969).

[2] C. J. Borkowski and M. K. Kopp, *Rev. Sci. Instr.* **39**, 1515 (1968).

A LEAST-SQUARES METHOD FOR THE ABSOLUTE SCALING AND NORMALIZING OF OBSERVED STRUCTURE FACTORS[1]

H. A. Levy W. E. Thiessen[2] G. M. Brown

The usual single-crystal diffraction experiment provides, for the various reflections **h** recorded, values of the observed structure-factor square $|F_o(\mathbf{h})|^2$ which are correctly scaled relative to each other (apart from minor experimental errors) but not absolutely scaled. Generally methods of solution for the crystal structure require at least an approximation to absolute scaling at the beginning, and structure determination is facilitated if an estimate of an over-all temperature factor for all the atoms in the crystal can be made as well. Knowledge of both the absolute scale and the temperature factor is essential for the calculation of the normalized structure factors required in the powerful direct methods of solution which have been applied so successfully in recent years.[3] It is important that the best possible estimates be made for the scale and temperature factors so that the normalized structure factors calculated from the observations will represent as faithfully as possible the normalized structure factors, $E(\mathbf{h})$, defined in the theory of direct methods:[4]

$$|E(\mathbf{h})|^2 = \frac{|F_o(\mathbf{h})|^2}{kps_2},$$

in which k is the reciprocal of the factor required to put the observations on an absolute scale and p is the known mean value of E^2 for a particular subset of reflections; p is always unity for general reflections in primitive space groups but may take on higher integral values in centered cells or for zones or rows specially affected by a symmetry element.[5] The sum of squares of the atomic scattering factors (including thermal attenuation), s_2, is assumed to be factorable:

$$s_2 = \sum_{j=1}^{N} f_j^2(|\mathbf{h}|)\, T_j(\mathbf{h}) = \sum_{j=1}^{N} f_j^2(|\mathbf{h}|)\, T(\mathbf{h}) = \sigma_2(|\mathbf{h}|)\, T(\mathbf{h}).$$

Here σ_2 is the sum of squares of the scattering factors of all N atoms in the unit cell at rest, and T represents an over-all temperature-factor function which may take various forms. In the Wilson plot method,[6] which is widely used to calculate normalized structure factors, T

is assumed to have the Gaussian form $\exp(-B|\mathbf{h}|^2/2)$. Averages of $F_o^2/p\sigma_2$ over small ranges of $|\mathbf{h}|$ are calculated, and their natural logarithms are plotted against $|\mathbf{h}|^2$; the straight line best fitting the points is assumed to have a slope of $-B/2$ and an intercept at $\ln k$. The K-curve method[7] is similar but does not assume a Gaussian temperature factor; the averages are plotted directly vs $|\mathbf{h}|$, and the value of T at any $|\mathbf{h}|$ is estimated from a smooth curve drawn through the points.

Although these methods do not readily lend themselves to anisotropic forms of $T(\mathbf{h})$, Maslen[8] has described an addition to the normal Wilson plot process involving a second series of plots against six products of the Miller indices. This method has a fault in common with the Wilson plot itself: the results are affected, sometimes strongly, by the choice of intervals for the averaging process.

We have developed an alternative way employing the method of least squares for fitting the $|F_o(\mathbf{h})|^2$ to the mean values of the Wilson distribution. The function

$$S = \sum_{\mathbf{h}} w_{\mathbf{h}} [|F_o(\mathbf{h})|^2 - kp\,\sigma_2(|\mathbf{h}|)\,T(\mathbf{h})]^2$$

is minimized by adjusting k and the parameters implicit in $T(\mathbf{h})$. The weights are given by

$$w_{\mathbf{h}} = [\text{var}\,(F_o^2) + (kp\sigma_2 T)^2\ \text{var}\,(E^2)]^{-1}\ ,$$

where var (F_o^2) is the experimental variance and var (E^2) is the variance of the theoretical distribution:

$$\text{var}\,(E^2) = 1 - \sigma_4/\sigma_2^2$$

for the acentric distribution, and

$$\text{var}\,(E^2) = 2 - 3\sigma_4/\sigma_2^2$$

for the centric distribution,[6] where

$$\sigma_4 = \sum_{j=1}^{N} f_j^4(\mathbf{h}).$$

The second term predominates. Although the $w_{\mathbf{h}}$ formally depend on the adjustable parameters, they are properly held constant for the minimization of S.

We have had occasion to compare the Wilson plot and least-squares methods during the course of solving the structure of a steroid-isocyanide addition compound,[9] $C_{40}H_{50}O_3N_2$ (space group $P2_12_12_1$; $Z = 4$; 4267 independent reflections measured using Cu $K\alpha$ radiation). Anisotropy in the thermal attenuation of intensities was noted during data collection.

Normalized structure factors calculated using the isotropic function $T(h) = \exp(-B|\mathbf{h}|^2/2)$ in the least-squares method were quite different from those calculated from a Wilson plot using seven intervals of $|\mathbf{h}|$ but were practically identical to those calculated with 25 intervals. Changing the form of the temperature factor to

$$T(\mathbf{h}) = \exp(-2\tilde{\boldsymbol{h}}\boldsymbol{\beta}\boldsymbol{h})$$

led to a dramatic change in the magnitudes of E. In this equation $\boldsymbol{h}$ is the column matrix of reflection indices and $\tilde{\boldsymbol{h}}$ is its transpose. The matrix $\boldsymbol{\beta}$ is the usual 3×3 matrix of anisotropic thermal parameters. It is apparent from Table 7.2 that agreement between the experimental values of E and those calculated from the solved structure for reflections with large E values is considerably improved; the value of

$$R_E \equiv \Sigma\big||E_o| - |E_c|\big| \,/\, \Sigma|E_c|$$

is 0.120 for the isotropic model and 0.078 for the anisotropic. The values for the 106 reflections having $E_c > 2.00$ are $R_{\text{iso}} = 0.108$ and $R_{\text{aniso}} = 0.086$. The quality of the correction for anisotropy can be judged by comparison of the average value of E^2 vs Miller indices in Figs. 7.1 and 7.2. The drift observed with the

Table 7.2. Comparison of the 13 Largest Normalized Structure Factors for the Steroid-Isocyanide Addition Compound[9] $C_{40}H_{50}O_3N_2$, Derived from the Observations Using an Isotropic Form of the Temperature Factor, an Anisotropic Form of the Temperature Factor, and Calculated from the Solved Structure

h	k	l	E_{iso}	E_{aniso}	E_{calc}
0	26	0	3.42	3.38	3.71
10	9	0	3.95	3.53	3.50
10	17	0	3.84	3.44	3.41
0	1	4	3.06	3.21	3.29
0	2	1	2.24	2.22	3.27[a]
12	9	0	3.21	2.75	3.09
9	16	0	3.42	3.12	2.99
5	0	5	2.81	2.97	2.90
3	19	5	2.68	2.89	2.86
11	9	3	3.21	2.91	2.80
0	34	2	2.13	2.15	2.79
3	32	0	2.53	2.49	2.78
9	10	0	3.03	2.76	2.77

[a]This reflection severely affected by extinction.

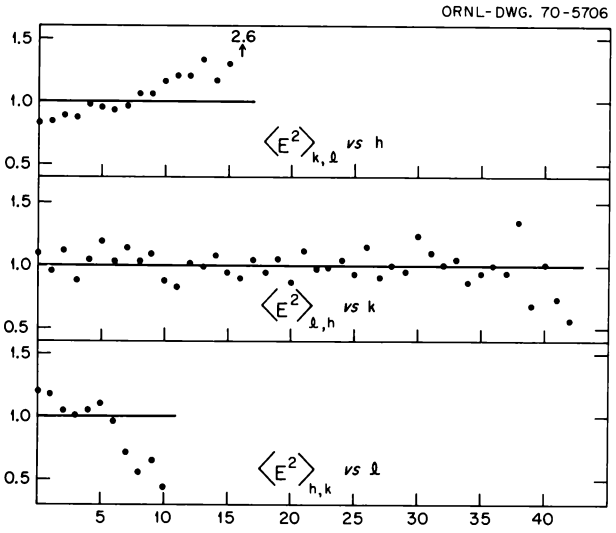

Fig. 7.1. Plots of Average Values of E^2 Derived from a Wilson Plot Using an Isotropic Temperature-Factor Correction vs Miller Indices.

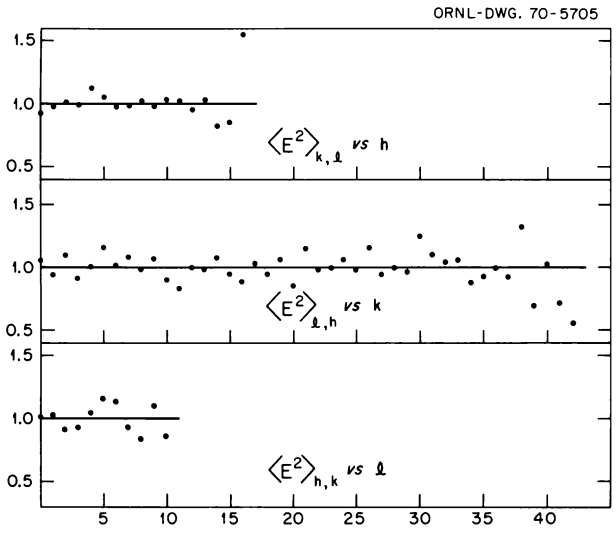

Fig. 7.2. Plots of Average Values of E^2 Derived from the Least-Squares Fit Using an Anisotropic Temperature-Factor Correction vs Miller Indices.

isotropic temperature correction (Fig. 7.1) has been eliminated by the anisotropic treatment (Fig. 7.2).

[1] A preliminary account of this work was given at the American Crystallographic Association Winter Meeting, March 1–5, 1970, held at Tulane University, New Orleans, La.

[2] National Institutes of Health Special Postdoctoral Fellow.

[3] J. Karle and I. L. Karle, *Acta Cryst.* **21**, 849 (1966).

[4] J. Karle, "The Phase Problem in Structure Analysis," pp. 131–222 in *Advances in Chemical Physics*, I. Prigogine and S. A. Rice, eds., Interscience, New York, 1969.

[5] D. Rogers, "Statistical Properties of Reciprocal Space," chap. 15 in *Computing Methods in Crystallography*, J. S. Rollett, ed., Pergamon, Oxford, 1965.

[6] A. J. C. Wilson, *Elements of X-Ray Crystallography*, chap. 8, Addison-Wesley, Reading, Mass., 1970.

[7] J. Karle and I. L. Karle, "Phase Determination for Centrosymmetric Crystals by Probability Methods," chap. 17 in *Computing Methods in Crystallography*, J. S. Rollett, ed., Pergamon, Oxford, 1965.

[8] E. N. Maslen, *Acta Cryst.* **22**, 945 (1967).

[9] W. E. Thiessen, "The Addition Product of an Isocyanide with a Steroidal α,β-Unsaturated Ketone: Structure Determination," following contribution, this report.

THE ADDITION PRODUCT OF AN ISOCYANIDE WITH A STEROIDAL α,β-UNSATURATED KETONE: STRUCTURE DETERMINATION[1]

W. E. Thiessen[2]

In 1969 Zeeh[3] reported that the boron trifluoride-catalyzed addition of two moles of an organic isocyanide to certain steroidal α,β-unsaturated ketones led to products having the 2,3-diiminooxetane structure. For instance, the product from *t*-butyl isocyanide and Δ^4-cholestenone was assigned structure **I**, and that from 2,6-dimethylphenyl isocyanide and 17β-acetoxy-1-methyl-1-androsten-3-one (methenolone acetate) was assigned structure **II** (Fig. 7.3). These structure proposals were based on chemical transformations of the cholestenone product to known compounds, on the spectral properties of the products (which are very similar), and on analogy to the reactions of saturated ketones with isocyanides, which are known to yield 2,3-diiminooxetanes.[4]

Because the structural assignments were not certain, crystals of **I** and **II** were sent to ORNL for structure analysis. Crystals of **I** were invariably twinned and had two molecules per asymmetric unit (space group $P2_1$, $Z = 4$, $a = 10.47$ Å, $b = 18.14$ Å, $c = 19.10$ Å, $\beta = 98.5°$). The methenolone acetate adduct **II** appeared to be crystallographically tractable and, furthermore, was of some pharmaceutical interest.

Methenolone and its acetate are used in treatment of a wide variety of debilitating diseases, since they have the property of promoting growth, particularly of muscle tissue, through increased efficiency of protein utilization. This anabolic activity was first observed in testosterone, **III**, the natural male hormone, which cannot itself be used as an anabolic agent because of its undesirable side effects (development of masculine

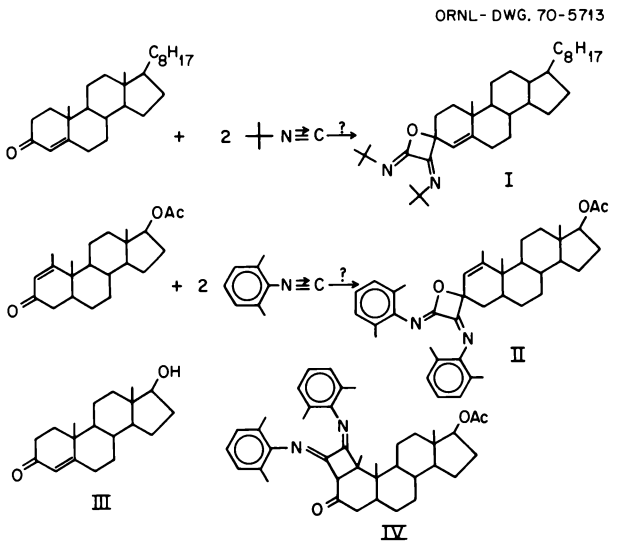

Fig. 7.3. (I and II) Structures Proposed[3] for the 2:1 Addition Products of Isocyanides with α,β- Unsaturated Ketones; (III) the Structure of Testosterone; (IV) the Correct Structure of the 2:1 Adduct.

secondary sex characteristics, etc.). The changes in structure from testosterone to methenolone (the change in position of the double bond and introduction of a methyl group) have the effect of reducing the side effects while maintaining the desired anabolic activity.[5] Whatever the structure of the isocyanide addition product, it seemed likely that one or more new carbon-carbon bonds had been formed in that part of the molecule in which structural changes produce changes in biological activity.

Crystals of the methenolone adduct are orthorhombic [space group $P2_12_12_1$, a = 12.9791(4) Å, b = 33.526(13) Å, c = 7.885(9) Å, Z = 4]. A sample of irregular shape with no dimension less than 0.2 mm or greater than 0.5 mm was mounted on the Oak Ridge computer-controlled x-ray diffractometer. Intensity measurements were carried out with Cu $K\alpha$ radiation from 2θ = 60° to 2θ = 161.5° by the 2θ scan technique and at smaller scattering angles by an ω scan technique. In addition the accessible Cu $K\beta$ reflections outside the limit given above were surveyed, and integrated intensity measurements were performed on 185 of the strongest of these. The usual processing of the data included an absorption correction.

The observed intensities were reduced to normalized structure factors, E, by a new least-squares technique.[6] The phases assigned arbitrarily to define the origin and enantiomorph[7] and those phases which were indicated above the 0.75 probability level from the Σ_1 relationship[7] are given in Table 7.3.

The key to the solution of the structure lay in relating $\phi_{0,\overline{26},0}$, $\phi_{\overline{8},\overline{12},0}$, and $\phi_{8,38,0}$. These phases, plus the four arbitrarily assigned, were sufficient to relate the entire set of 312 reflections having $E > 1.8$. A basic contradiction is immediately obvious: all three of these phases are predicted to have the value π by Σ_1, but the more powerful Σ_2 relationship, on which the tangent formula[8] is based, predicts that the sum of these phases should be zero since their indices add to zero.

The tangent formula approach outlined in an accompanying report[9] was applied by assuming in turn that each one of the Σ_1 indications was incorrect. The three resulting phase sets had values of the inconsistency index[9] Q of 0.32, 0.37, and 0.41 respectively. An E map based on the most consistent set revealed the positions of 39 of the nonhydrogen atoms among the 45 highest peaks, and the steroid skeleton was immediately recognizable from a stereo plot of these 45 peak positions produced in the program ORTEP.[10]

A Fourier synthesis based on all reflections immediately revealed the remaining "heavy" atoms. All of the hydrogen atoms were subsequently discovered in difference Fourier maps, and full-matrix least-squares refinement with anisotropic "heavy" atoms and isotropic hydrogen atoms brought the final $R(F)$ value to 0.045.

It is worth noting that the crucial Σ_2 relationship would not have been available without the Cu $K\beta$ data, since the reflection 8,38,0 is outside the limits of the

Table 7.3. Initial Phase Assignments (ϕ_i) and Final Phase Values (ϕ_f) in the Solution of the Structure of the 2:1 Adduct via the Tangent Formula

h	k	l	E	ϕ_i	ϕ_f
		To Specify Origin and Enantiomorph			
10	9	0	3.50	0	0
7	0	10	3.15	π	π
β9	16	0	3.10	$\pi/2$	$\pi/2$
5	0	5	2.88	$\pi/2$	$\pi/2$
		From Σ_1			
0	26	0	3.33	π	0
8	12	0	2.79	π	π
β8	38	0	2.64	π	π
4	4	0	2.51	0	π
0	34	2	2.17	π	π
12	0	4	2.09	0	0
0	36	4	2.02	π	0
β18	0	2	1.97	π	π

ORNL-DWG. 70-2068

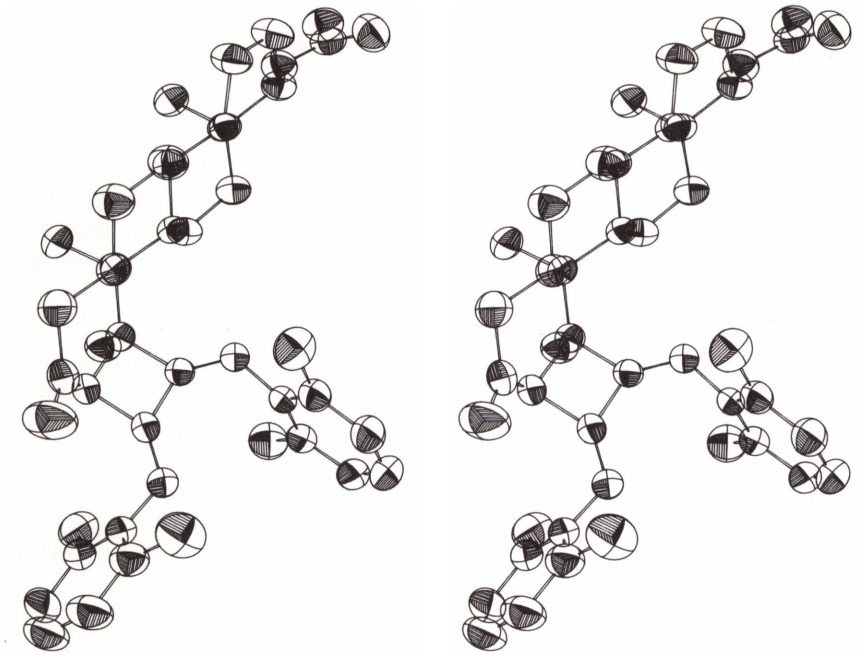

Fig. 7.4. Stereoscopic View of the 2:1 Adduct Between 2,6-Dimethylphenylisocyanide and Methenolone Acetate. The ellipsoids describe the volume within which the probability of finding the atomic center is 0.5.

diffractometer with Cu $K\alpha$ radiation. This experience recalls the similar ease of solution of the structure of sedoheptulosan hydrate described in an earlier report[11] which also employed Cu $K\beta$ data.

The structure actually determined for the methenolone adduct (**IV**) differs from the proposed structure in that addition of the isocyanide moieties has taken place at the carbon-carbon double bond rather than at the carbonyl group, as previously postulated. Whether modification of the addition product will produce biologically active compounds remains to be seen. In any case, knowledge of the correct structure will enable organic chemists to plan further reactions intelligently.

A stereoscopic drawing of the molecule (omitting hydrogen atoms for clarity) is given in Fig. 7.4. Although detailed analysis of the molecular geometry is not yet complete, two structural features of interest are apparent:

1. The 2,6-dimethylphenyl groups attached to the imino nitrogens cannot achieve coplanarity with the imino groups for steric reasons. The angles between their planes and those of the imino groups (87 and 73°) bespeak conjugation with the nitrogen lone pairs.

ORNL-DWG. 70-5714

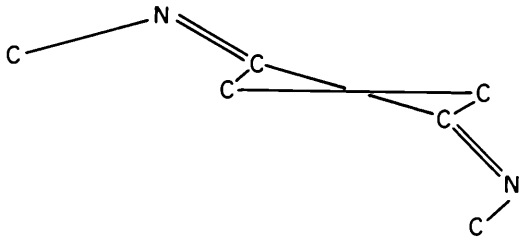

Fig. 7.5. A Schematic Representation of the Cyclobutane Ring in the 2:1 Adduct Viewed Edge On.

2. The cyclobutane ring is, as expected, puckered; the angle between the (approximate) planes of the C–C=N groups is 14°. In addition, the imino groups

are not strictly planar; the nitrogen atoms are forced away from each other, presumably by dipole-dipole interactions. This effect is illustrated schematically in Fig. 7.5.

[1]A preliminary account of this work was given at the American Crystallographic Association Winter Meeting, March 1–5, 1970, held at Tulane University, New Orleans, La.

[2]National Institutes of Health Special Postdoctoral Fellow.

[3]B. Zeeh, *Tetrahedron Letters.* **1969**(2), 113.

[4]H.-J. Kabbe, *Angew. Chem.* **80**, 389 (1968); *Angew. Chem. Intern. Ed.* **7**, 389 (1968); T. Saegusa, N. Takaishi, and H. Fujii, *Tetrahedron* **24**, 3795 (1968).

[5]G. K. Suchowsky and K. Junkmann, "Recent Findings in Anabolic Steroids," pp. 155–59 in *Hormonal Steroids; Biochemistry, Pharmacology, and Therapeutics,* vol. 2 of the Proceedings of the First International Congress on Hormonal Steroids, L. Martin and A. Pecile, eds., Academic, New York, 1965.

[6]H. A. Levy, W. E. Thiessen, and G. M. Brown, "A Least-Squares Method for the Absolute Scaling and Normalizing of Observed Structure Factors," preceding contribution, this report.

[7]J. Karle and H. Hauptmann, *Acta Cryst.* **9**, 635 (1956).

[8]J. Karle and I. L. Karle, *Acta Cryst.* **21**, 849 (1966).

[9]W. E. Thiessen, "Structure and Stereochemistry of α- and β-Cubebene from the Crystal Structure of Nor-β-cubebone," following contribution, this report.

[10]Program ORTEP, written by C. K. Johnson, AEC Document No. ORNL-3794, Revised (June 1965).

[11]G. M. Brown and W. E. Thiessen, *Chem. Div. Ann. Progr. Rept. May 20, 1969,* ORNL-4437, p. 129.

STRUCTURE AND STEREOCHEMISTRY OF α- AND β-CUBEBENE FROM THE CRYSTAL STRUCTURE OF NOR-β-CUBEBONE[1]

W. E. Thiessen[2]

α- and β-Cubebene, isomeric hydrocarbons from the oil of *Piper cubeba* L., have been assigned structures **I** and **II** (Fig. 7.6), respectively, by Ohta, Sakai, and Hirose.[3] The chemical evidence adduced by these workers does not establish the stereochemistry at the centers indicated by wavy lines in Fig. 7.6, nor does it rule out alternate structures of type **III** (Fig. 7.7). In order for a rational synthetic scheme for these natural products to be devised, an experiment distinguishing among these structural possibilities was necessary.

Degradation work on the cubebenes is complicated at the outset by the difficulty of separating the α and β isomers. Ozonolysis of the hydrocarbon mixture followed by treatment with hydrogen peroxide gives, after separation of the acidic products derived from α-cubebene, the norketone **IV** (Fig. 7.6) derived from β-cubebene. This crystalline ketone can be reconverted in good yield to β-cubebene by reaction with triphenylphosphinemethylene, demonstrating that no rearrangement has occurred in the ozonolysis.[4] Crystal structure analysis of this nor-β-cubebone was therefore under-

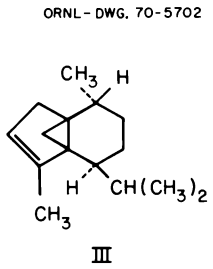

Fig. 7.7. An Alternative Structure for α-Cubebene.

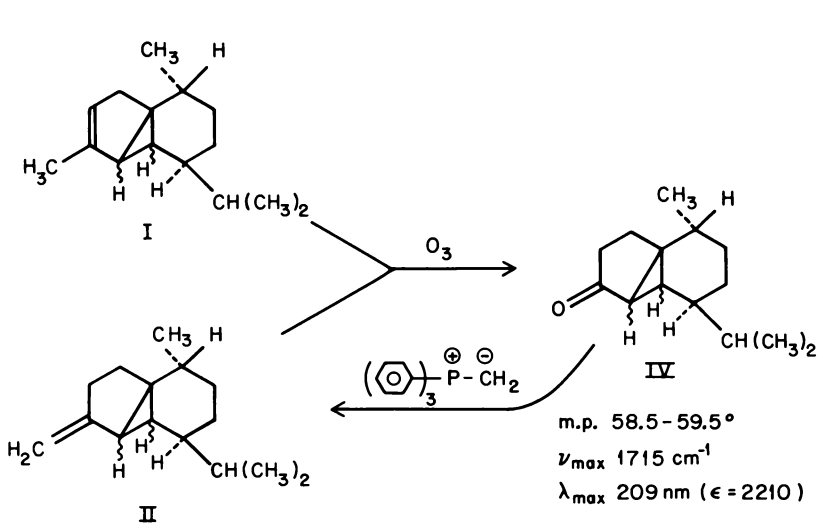

Fig. 7.6. Structural Relationships Between α- and β-Cubebene and Nor-β-cubebone.

taken to ascertain the structures of the natural products and, as a bonus, to determine the accurate molecular geometry of a conjugated cyclopropyl ketone system. The spectral characteristics of nor-β-cubebone given in Fig. 7.6 indicate some degree of electronic interaction between the three-membered ring and the carbonyl group.

Preliminary Weissenberg photographs displayed systematic absences and symmetry uniquely consistent with the orthorhombic space group $P2_12_12_1$. The tendency of the crystalline ketone to sublime at an appreciable rate at room temperature was first noted at this stage. Consequently, after a sphere approximately 0.35 mm in diameter was selected from several which had been ground from single crystals, it was coated with a thin film of white glue prior to mounting on the Picker automatic diffractometer. A least-squares fit of angle data from 14 reflections (T = 24°; Cu $K\alpha$ radiation, λ = 1.54051 Å) yielded the following cell dimensions: a = 8.4800(16) Å, b = 23.5020(54) Å, c = 6.3138(10) Å.

Intensity data for 1598 reflections accessible with Cu $K\alpha$ radiation below $2\theta = 160°$ were measured with the diffractometer in automatic mode by the 2θ-θ scan technique. The intensities of standard reflections decreased steadily with time, showing that the attempt to prevent sublimation was not entirely successful. This loss of intensity was nearly linear, the final standard measurement showing 58% of the initial intensity. A decay correction employing linear interpolation between successive standards was applied along with Lorentz and polarization corrections. No absorption correction was attempted in view of the uncertainty of shape of the crystal as it evaporated.

The observed structure factors were put on an absolute scale and corrected by an average isotropic temperature factor by use of a Wilson plot program to give normalized structure factors $E_{\mathbf{h}}$.[5] Four zonal reflections of proper parity[6] were chosen from among those with the largest values of $E_{\mathbf{h}}$ for arbitrary phase assignments to define origin and enantiomorph (Table 7.4). In addition, one general reflection (364) was allowed to take on initial values from 0 to $7\pi/4$ in steps of $\pi/4$ in order to begin the phase determination for the 125 reflections with $E_{\mathbf{h}} > 1.62$ by the tangent formula,[7]

$$\tan \phi_h \cong A/B ,$$

where

$$A = \sum_{\mathbf{k}} |E_{\mathbf{k}} E_{\mathbf{h}-\mathbf{k}}| \sin (\phi_{\mathbf{k}} + \phi_{\mathbf{h}-\mathbf{k}}) ,$$

$$B = \sum_{\mathbf{k}} |E_{\mathbf{k}} E_{\mathbf{h}-\mathbf{k}}| \cos (\phi_{\mathbf{k}} + \phi_{\mathbf{h}-\mathbf{k}}) .$$

Of the eight sets of phases produced in this way, the four in which ϕ_{364} had been originally set to a cardinal point (0, π, or $\pm \pi/2$) had values of the inconsistency index

$$Q = \sum_{\mathbf{h}} |E_{\mathbf{h}} - t_{\mathbf{h}} E_{\mathbf{h}}| / \sum_{\mathbf{h}} |E_{\mathbf{h}}| ,$$

where

$$t_{\mathbf{h}} = (A^2 + B^2)^{1/2} / \sum_{\mathbf{k}} |E_{\mathbf{k}} E_{\mathbf{h}-\mathbf{k}}| ,$$

of 0.32 to 0.33. The other four had Q greater than 0.37.

Only one of the four of the most self-consistent phase sets is in complete agreement with the Σ_1 predictions listed in Table 7.4. An E map was accordingly calculated from this set. Of the six strongest peaks in this map, five made up a very plausible arrangement consisting of the expected cyclopropane ring with two more atoms connected to one apex at reasonable distances and angles. Fourier methods, using the Sim-Woolfson weighting scheme,[8] and refinement of phases by the method of Karle[9] led to chemically reasonable positions for 12 atoms but also produced obviously spurious peaks. No placement of the remaining atoms from chemical reasoning or from analysis of the Patterson map was found which led to even approximate agreement of observed and calculated structure factors.

Phase determination of the 193 reflections with $E_{\mathbf{h}} \geqslant 1.47$ was therefore attempted, allowing ϕ_{364} to take values from 0 to $19\pi/20$ in increments of $\pi/20$. These sets converged in 18 to 30 cycles; and of the three most nearly self-consistent sets, two were very similar and had the predicted values for those phases known from

Table 7.4. Initial Values of Phases Assigned to Reflections with Large Normalized Structure Amplitudes

To Specify Origin and Enantiomorph:					From Σ_1:				
h	k	l	E	ϕ	h	k	l	E	ϕ
1	29	0	3.41	$\pi/2$	0	18	0	2.60	0
0	9	2	2.90	$\pi/2$	0	28	0	2.30	π
0	19	1	1.96	$\pi/2$	0	6	6	2.30	π
10	11	0	2.13	0	2	28	0	1.74	0

Σ_1, but the arbitrary starting value for $\phi_{1,29,0}$ had been changed from $\pi/2$ to $-\pi/2$. An E map calculated from the slightly more nearly self-consistent of these two sets revealed positions for 14 of the 15 nonhydrogen atoms among the 21 strongest peaks. One of the methyl carbons of the isopropyl group was missing but was revealed by a subsequent Fourier synthesis based on all reflections. Full-matrix least-squares refinement of these atom positions, together with isotropic and then anisotropic temperature factors, reduced $R(F)$ to 0.11. A difference Fourier map showed peaks corresponding to calculated positions for all 22 hydrogen atoms. Further refinement (keeping hydrogen atoms isotropic) reduced $R(F)$ to 0.053 and showed clearly that the strongest reflections suffered from extinction. An isotropic extinction correction was applied; the value of the extinction parameter was treated as a variable in the refinement.[10] The final $R(F)$ for 1496 reflections is 0.044.

Comparison of the final structure with the partial false structure found earlier revealed that the carbon atoms (numbered 1, 6, and 7 in Fig. 7.8) of the three-membered ring, all of which have approximately the same y coordinates, are reflected through a point in the false structure to give another grouping having nearly the same set of interatomic vectors. The rest of the false structure is then made up of correct interatomic vectors springing from the incorrect positions.

The final structure given in Fig. 7.8 corroborates the gross structure of Ohta, Sakai, and Hirose and reveals the unknown stereochemistry. The absolute configuration indicated is correct, since it has been shown[3] that treatment of α-cubebene with dry HCl in ether yields (−)-cadinene hydrochloride, the absolute configuration of which is known.

The conjugation in the cyclopropyl ketone moiety inferred from spectral observations is strikingly verified in the geometry of the molecule:

1. The length of the bond connecting the cyclopropane ring to the carbonyl carbon atom, C(7)–C(8), is 1.469 Å, as short as the corresponding bond in α,β-unsaturated ketones and much shorter than the typical sp^3-sp^2 bond, C(8)–C(9), 1.511 Å, on the other side of the carbonyl.
2. The two bonds of the three-membered ring involved in conjugation, C(1)–C(7) and C(6)–C(7), are appreciably longer than C(1)–C(6), which is not involved.
3. The five-membered ring is, of course, not planar but puckered; that is, C(9) is out of the plane of the other atoms, so as to avoid eclipsing of the hydrogen atoms connected to C(9) and C(10). The direction of the puckering is puzzling at first glance – the distance between the hydrogen pointing forward from C(9) and the hydrogen on C(6) is 2.40 Å, fully 0.1 Å shorter than any intermolecular hydrogen-hydrogen contact in the structure, whereas if C(9) had puckered the other way, no apparent disruption of the packing (Fig. 7.9) would have resulted.

Figure 7.9 is a Newman projection looking down the C(7)–C(8) bond. Of the two possible puckering directions depicted, the one actually observed (upper left) tends toward a situation in which the carbonyl bisects the three-membered ring, whereas the alternative (upper right) tends away from this geometry. Electron diffraction studies of cyclopropanecarboxaldehyde,[11] cyclopropyl methyl ketone, and cyclopropanecarboxylic acid chloride[12] show that the favored conformations are

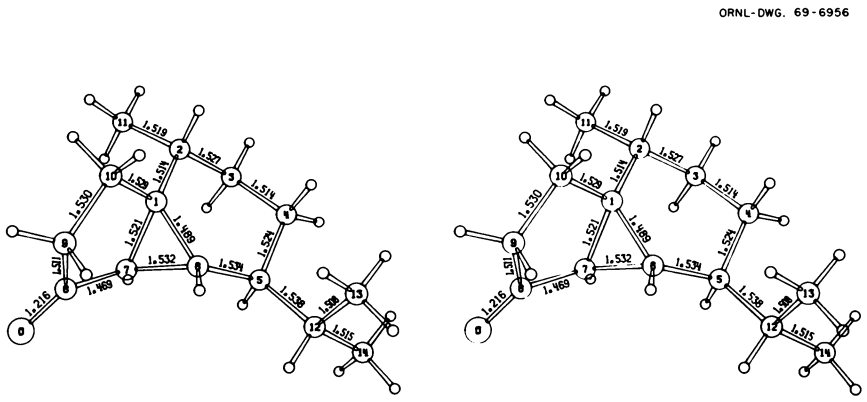

Fig. 7.8. Stereoscopic View of the Nor-β-cubebone. Bond lengths are uncorrected for thermal motion and have standard errors of about 0.004 Å.

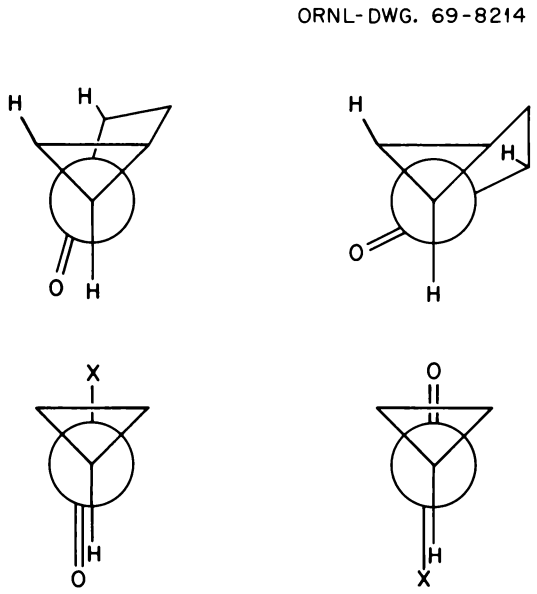

Fig. 7.9. (Top) Newman Projections Showing the Two Possible Conformations of the Five-Membered Ring; (Bottom) The Favored Conformations of Cyclopropanecarboxaldehyde, Methyl Cyclopropyl Ketone, and Cyclopropanecarboxylic Acid Chloride.

those depicted in the bottom of Fig. 7.9. Evidently the H–H contact costs less energy than is gained by increased orbital overlap.

---

[1] A preliminary account of this work was published in the Abstracts of the Eighth International Congress of Crystallography, Stony Brook, New York, August 1969. See *Acta Cryst.* A25, abstract XIII-52, p. S144 (1969).

[2] National Institutes of Health Special Postdoctoral Fellow.

[3] Y. Ohta, T. Sakai, and Y. Hirose, *Tetrahedron Letters* **1966**, 6365.

[4] These experiments were carried out by W. G. Dauben and R. Shavitz, to whom I am obliged for the crystals used in this investigation.

[5] Program FAME, written by R. Dewar and A. Stone, University of Chicago.

[6] J. Karle and H. Hauptman, *Acta Cryst.* 9, 635 (1956).

[7] J. Karle and I. L. Karle, *Acta Cryst.* 21, 849 (1966). Tangent formula refinement was carried out using program PHASEM, written by M. G. B. Drew, Lawrence Radiation Laboratory, University of California, Berkeley.

[8] G. A. Sim, "Aspects of the Heavy-Atom Method," paper 24 in *Computing Methods and the Phase Problem in X-Ray Crystal Analysis,* R. Pepinsky, J. M. Robertson and J. C. Speakman, eds., Pergamon, Oxford, 1961. See also M. M. Woolfson, *Acta Cryst.* 9, 804 (1956).

[9] J. Karle, *Acta Cryst.* B24, 182 (1968).

[10] A correction procedure based on the theory of W. H. Zachariasen, *Acta Cryst.* 23, 558 (1967), has been inserted into the least-squares program ORFLS by A. Vos and C. K. Johnson.

[11] L. S. Bartell and J. P. Guillory, *J. Chem. Phys.* 43, 647 (1965).

[12] L. S. Bartell, J. P. Guillory, and A. T. Parks, *J. Phys. Chem.* 69, 3043 (1965).

A SINGLE-CRYSTAL NEUTRON DIFFRACTION STUDY OF UREA–PHOSPHORIC ACID

E. C. Kostansek[1] W. R. Busing

In a previous neutron diffraction study Worsham and Busing[2] showed that the compound formed from urea and nitric acid is a salt, uronium nitrate, in which the acid hydrogen ion is attached to the urea oxygen atom and forms a moderately strong hydrogen bond to the nitrate ion. An x-ray study of the one-to-one compound of urea and phosphoric acid which was reported by Sundera-Rao, Turley, and Pepinsky[3] showed a very short O...O distance between the two moieties, which implied that the acid proton may be shared equally between them. The neutron diffraction study which we report here confirms that the hydrogen ion is essentially centered in a strong hydrogen bond, so that the substance is intermediate between a salt and an addition compound.

The urea–phosphoric acid compound is orthorhombic, *Pbca,* with lattice parameters[3] $a = 17.68$ Å, $b = 7.48$ Å, $c = 9.06$ Å and eight formula units per cell. Single crystals were grown from aqueous solution, and the intensities of 2079 reflections from a 69.3-mg sample were measured using the Oak Ridge automatic neutron diffractometer.[4] The observations were corrected for absorption[5] and converted to structure factors in the usual way.[6] A three-dimensional Fourier synthesis using signs calculated from the x-ray structure revealed the positions of all seven hydrogen atoms. The atomic coordinates and anisotropic temperature factor coefficients were adjusted by the method of least squares. It was immediately apparent that the data showed the effects of severe extinction, and an isotropic extinction correction[7] was included in the refinement. Even this did not solve the problem completely, and eventually 64 reflections, the strongest of which was observed with an intensity only 4.9% of that calculated, were omitted from the refinement. The agreement factor $R(F^2)$ is now 0.108, but these results are not considered to be final. The atomic coordinates are as follows:

	x	y	z
P	0.3109	0.2783	0.3094
O(1)	0.3389	0.0904	0.3617
O(2)	0.2775	0.3842	0.4352
O(3)	0.2469	0.2509	0.1928
O(4)	0.3795	0.3664	0.2378
O(5)	0.4471	0.6339	0.3109
N(1)	0.5078	0.7834	0.4911
N(2)	0.3965	0.6359	0.5426
C	0.4499	0.6833	0.4466
H(1)	0.4087	0.5047	0.2821
H(2)	0.2977	0.0098	0.3937
H(3)	0.2610	0.1986	0.0952
H(4)	0.5497	0.8067	0.4220
H(5)	0.5121	0.8210	0.5953
H(6)	0.3987	0.6777	0.6481
H(7)	0.3517	0.5664	0.5088

Figure 7.10 is a stereoscopic view of one formula unit and its surroundings. Each of the seven hydrogen atoms is involved in a hydrogen bond with the following distances and angles:

X–H...O	X–H (Å)	H...O (Å)	Angle at H (deg)
O(5)..H(1)..O(4)	1.21	1.22	169
O(1)–H(2)...O(2)	0.99	1.67	174
O(3)–H(3)...O(2)	1.00	1.60	177
N(1)–H(4)...O(4)	0.99	1.96	171
N(1)–H(5)...O(5)	0.99	2.29	145
N(2)–H(6)...O(5)	1.01	2.21	148
N(2)–H(7)...O(2)	1.00	2.00	168

The acid hydrogen, H(1), is shared nearly equally between O(5) of urea and O(4) of phosphoric acid, and the difference between this compound and uronium nitrate can be related to the fact that phosphoric acid is weaker than nitric acid.

Other distances of interest are:

C–O(5)	1.284 Å
C–N(1)	1.330 Å
C–N(2)	1.332 Å
P–O(1)	1.565 Å
P–O(2)	1.508 Å
P–O(3)	1.561 Å
P–O(4)	1.526 Å

Distances in the urea group are intermediate between those found in urea[8] and those in uronium nitrate,[2] a fact which is consistent with the resonance theory discussed by Worsham and Busing.[2]

In the phosphoric acid group, O(2), which makes the shortest bond to phosphorus, has no hydrogen atom of its own but is the acceptor of three hydrogen bonds. Each of the atoms O(1) and O(3), which form the longest bonds to phosphorus, has its own hydrogen atom but accepts no hydrogen bond. Intermediate between these extremes is O(4), which shares its acid hydrogen atom and is the acceptor for one other hydrogen bond.

---

[1]Oak Ridge Associated Universities Summer Student Trainee from Hiram College, Hiram, Ohio, Summer 1969.

[2]J. E. Worsham, Jr., and W. R. Busing, *Acta Cryst.* **B25**, 572 (1969).

[3]R. V. G. Sundera-Rao, J. W. Turley, and R. Pepinsky, *Acta Cryst.* **10**, 435 (1957).

[4]W. R. Busing, H. G. Smith, S. W. Peterson, and H. A. Levy, *J. Phys. (Paris)* **25**, 495 (1964).

[5]W. R. Busing and H. A. Levy, *Acta Cryst.* **10**, 180 (1957).

[6]G. M. Brown and H. A. Levy, *J. Phys. (Paris)* **25**, 469 (1964).

[7]W. H. Zachariasen, *Acta Cryst.* **23**, 558 (1967).

[8]J. E. Worsham, Jr., H. A. Levy, and S. W. Peterson, *Acta Cryst.* **10**, 319 (1957).

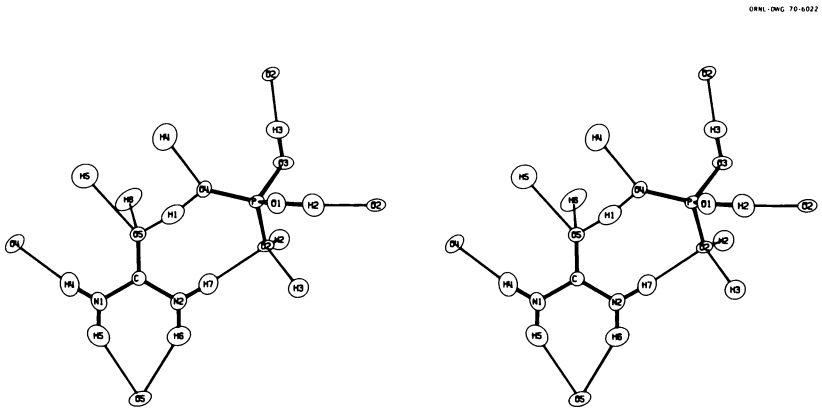

Fig. 7.10. Stereoscopic View of One Formula Unit of Urea–Phosphoric Acid Showing the Hydrogen Bonds to Neighboring Atoms.

CRYSTAL STRUCTURE OF TRI(*p*-BIPHENYLYL)-AMINIUM PERCHLORATE

G. M. Brown G. R. Freeman[1]

The tri(*p*-biphenylyl)aminium cation (**1**) is representative of several known triarylaminium cations,[2] which generally are isolated as the perchlorate salts. These

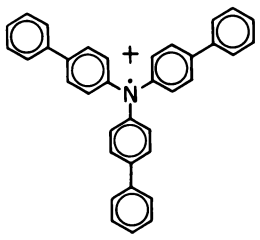

1

free-radical ions are isoelectronic with the corresponding uncharged triarylmethyl radicals and are expected to be similar in structure to the latter more familiar radicals and also to the triarylcarbonium ions and carbanions. There exist in all these species similar possibilities for delocalization of the unshared electron or of charge around the aromatic ring systems. No data are available for the carbanions, but the results of diffraction studies[3-7] suggest that, in general, triarylmethyl radicals and carbonium ions have essentially plane trigonal arrangements of C–C bonds at the central carbon atoms, which correspond in position to the nitrogen atom in the aminium cation. X-ray analyses on tri(*p*-fluorophenyl)amine and tri(*p*-iodophenyl)amine described in last year's annual report[8] suggest that even the triarylamines in general have plane or nearly plane arrangements of the valence bonds at nitrogen. The study described here was undertaken to confirm the expectation that triarylaminium radical cations have a similar geometry for the nitrogen valences.

The particular compound tri(*p*-biphenylyl)aminium perchlorate was chosen for analysis because of its known stability in the solid state.[1] This compound was also thought to be of interest because of the possibility of observing varying effects of crystal environment on the twist from coplanarity of the two rings in the biphenylyl group. It is known (see the convenient tabulation of Suzuki[9]) that the twist angle varies widely among various biphenyl compounds, depending upon what substituents are present on the rings and on the environment of the biphenyl system.

A crystal specimen with minimum and maximum diameters about 0.25 and 0.50 mm was cut from a prism and mounted. From preliminary x-ray precession photographs, the space group was established as $P2_1/c$, and approximate unit-cell parameters were established. Precise values for the cell parameters were obtained by the method of least squares from angle data recorded at about 19°C with the Oak Ridge computer-controlled diffractometer.[10] Data for six reflections in the range 124 to 133° 2θ for Cu $K\alpha_1$ radiation (λ = 1.54051 Å) yielded the following parameters (and standard errors in parentheses): a = 9.842(1) Å, b = 24.442(1) Å, c = 12.501(1) Å, β = 106.77(1)°. The reasonable value 1.322 g/cm^3 is obtained for the calculated density on the assumption of four formula units per cell.

Intensity data for 6025 independent reflections were recorded with the automatic diffractometer and Cu $K\alpha$ radiation to the limit 161.5° in 2θ. The crystal specimen was measured accurately to obtain the necessary data for making absorption corrections[11] and for computing derivatives to be used later in applying corrections for extinction. The value of the absorption coefficient used was 10.88 cm^{-1}; the absorption correction factors on the observed intensity values ranged from 1.25 to 1.41. The raw intensity data and corresponding standard errors were converted in the usual preliminary processing to a set of observed structure-factor squares F_o^2's, with standard errors $\sigma(F_o^2)$'s. The normalized structure factors[12] E were also computed.

The solution for the structure was obtained through use of Long's computer program[13] for direct sign determination by the Sayre[14] equation. All of the 42 atoms of carbon, nitrogen, oxygen, and chlorine in the asymmetric unit were identifiable with peaks in the E map[15] computed with the "best" sign combination for the 730 E's of magnitude $\geq$1.50. After some preliminary cycles of least-squares refinement, starting coordinates for the hydrogen atoms were computed according to chemical-structural considerations, and both the coordinates and the thermal parameters of the hydrogen atoms were adjusted thereafter. In the final refinement cycles, coordinates and anisotropic thermal parameters were adjusted for all atoms, and for each of the five atoms of the perchlorate ion the ten extra parameters of the three-cumulant model[16] were also adjusted. Corrections for mild extinction were applied according to the method of Zachariasen[17] in the least-squares calculations; the extreme correction on the calculated structure factor squares F_c^2's was about 0.85. Final values of the usual measures of goodness of fit[18] are: $R(F)$ = 0.051, $R(F^2)$ = 0.050, $R_w(F^2)$ = 0.087, σ_1 = 1.55.

The shapes of the radical-cation and of the perchlorate ion are shown in the stereoscopic drawings of Figs. 7.11 and 7.12, in which the atoms are represented by their 50% probability ellipsoids.[19] The geometry of the ions is described more precisely by the numerical data in Tables 7.5–7.7 and in Fig. 7.13. Table 7.5 specifies the deviations of various atoms from the exact plane (*T*) of the triangle of carbon atoms about the central nitrogen atom and from the best least-squares planes (*1*, *1'*, *2*, *2'*, *3*, *3'*) through the atoms of the individual six-membered rings. Table 7.6 gives valence angles in the cation and the interplane angles in the cation which are of most interest. Figure 7.13 shows all bond lengths in the cation, and Table 7.7 gives bond lengths and angles in the perchlorate ion.

As may be seen from Table 7.5, no carbon atom is displaced from the best plane of its own ring by more than 0.009 Å, an amount which is hardly to be regarded as significant. On the other hand, generally for all six rings the atoms directly attached to the rings are displaced somewhat more, probably indicating effects of packing in the crystal.

From the data in Table 7.5 for plane *T* it is clear that the configuration described by the nitrogen atom and the three sets of axial atoms of the biphenylyl groups is approximately but not exactly plane. The distance of the nitrogen atom from plane *T* is 0.014 Å, about ten times the standard error of position of the atom along the perpendicular to the plane. This may be a signifi-

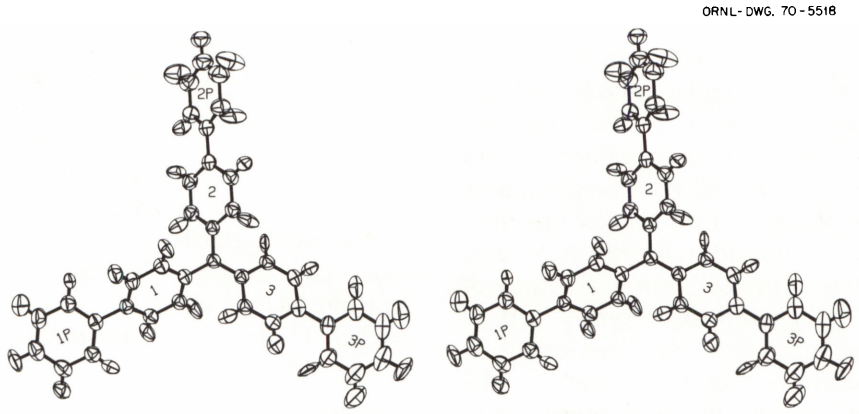

Fig. 7.11. Stereoscopic Drawing of the Tri(*p*-biphenylyl)aminium Cation, Showing 50% Probability Ellipsoids for All Atoms.

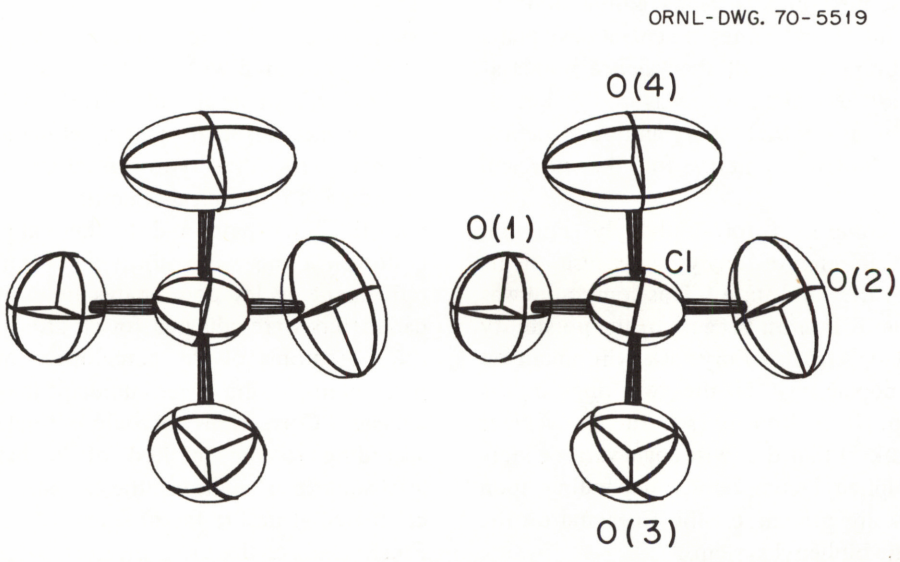

Fig. 7.12. Stereoscopic Drawing of the Perchlorate Ion in Tri(*p*-biphenylyl)aminium Perchlorate, Showing the 50% Probability Ellipsoids.

cant displacement in the formal mathematical sense, but it is clear that the geometry of the nitrogen valences is essentially plane trigonal, as expected. The small displacement of the N atom corresponds to a bending of each C–N bond from the exactly plane configuration by only 0.6°.

The interplane angles *T-1*, *T-2*, and *T-3* are essentially twist angles around the C–N bonds from the hypothetical configuration (physically impossible) in which the carbon triangle *T* and the rings *1*, *2*, and *3* would all be coplanar. These angles have the values 43.5, 45.3, and 26.5°, respectively, all within the range of values found for the corresponding twists in various triphenylamines,[8] triphenylmethyls,[3-4] and triphenylcarbonium ions.[5-7]

The interplane angles *1-1'*, *2-2'*, and *3-3'*, which have the values 36.4, 14.5, and 23.0°, respectively, specify the twist angles about the central bonds of the three

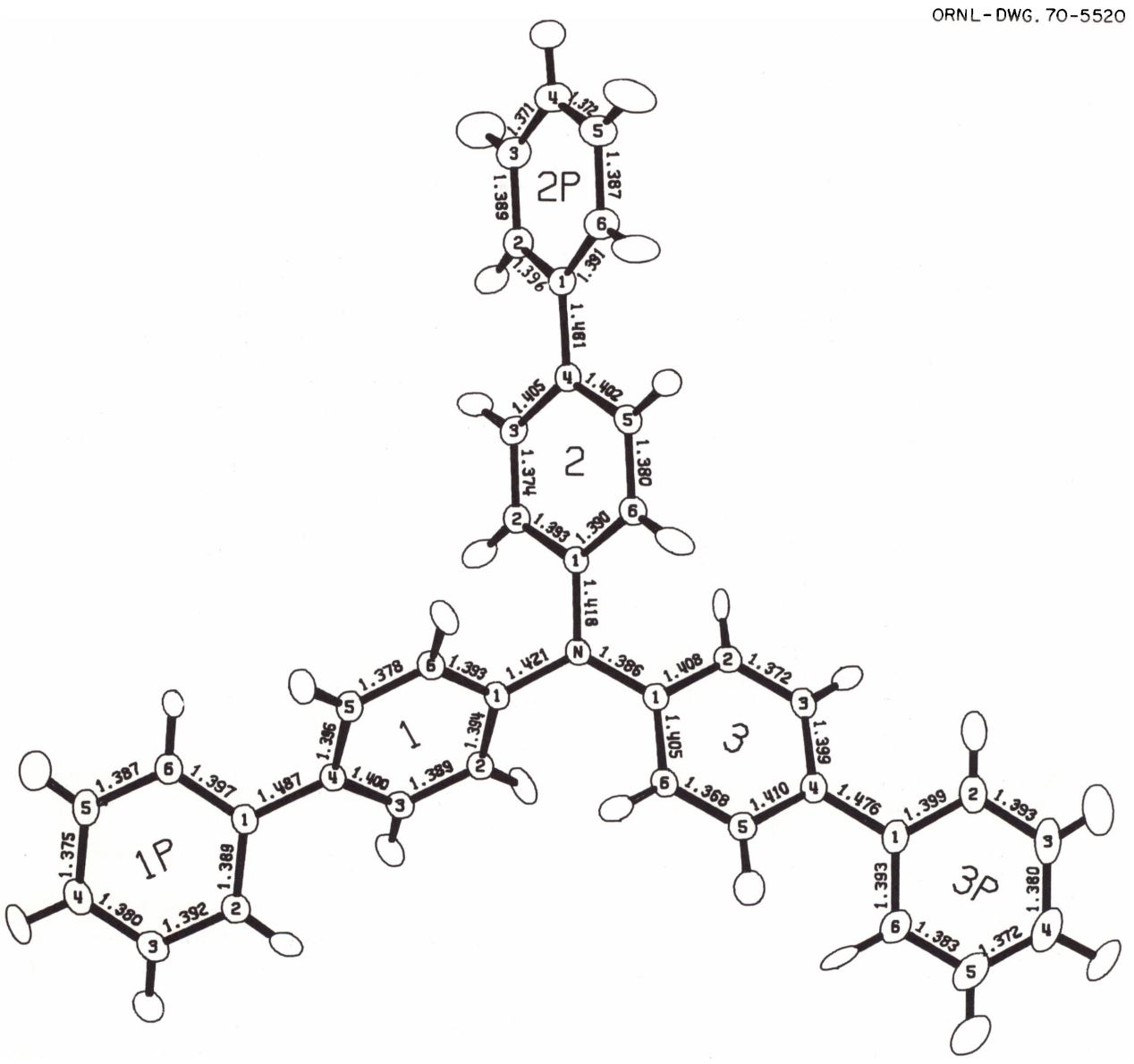

Fig. 7.13. Drawing of the Tri(*p*-biphenylyl)aminium Cation, Showing All C–C and C–N Bond Lengths (Uncorrected for Effects of Thermal Motion). The standard errors of the bond lengths range from about 0.002 Å for bonds at the center of the ion to about 0.003 Å for bonds near the periphery.

Table 7.5. Distances of Various Atoms from Exact Plane *T* Through the Three Carbon Atoms Attached to the Nitrogen Atom and from the Least-Squares Best Planes Through the Six-Membered Rings

The atom numbering scheme is given in Fig. 7.13, where ring *1′* is designated *1P*, and so forth

Atom	Distance from Plane *T* (Å)	Atom	Distance (Å) from Ring Plane –					
			1	*1′*	*2*	*2′*	*3*	*3′*
	× 10^{-3}		× 10^{-3}	× 10^{-3}	× 10^{-3}	× 10^{-3}	× 10^{-3}	× 10^{-3}
N	−14	C(1)	−4	3	−1	3	−6	7
C(4,1)	8	C(2)	5	−8	−8	4	6	−3
C(1,1′)	26	C(3)	−1	6	9	−7	1	−2
C(4,1′)	110	C(4)	−3	1	−2	4	−8	3
C(4,2)	24	C(5)	4	−5	−7	3	8	1
C(1,2′)	56	C(6)	−1	4	8	−6	−1	−6
C(4,2′)	81							
C(4,3)	−1	N[a]	−45		−23		−18	
C(1,3′)	−11	C(1′)[a]	−10		−36		−31	
C(4,3′)	−78	C(4)[a]		28		33		−18

[a]Atoms attached to the six-membered rings for which the best planes were calculated.

Table 7.6. Valence Angles and Interplane Angles in the Tri(*p*-biphenylyl)aminium Radical Cation

See text and caption of Table 7.5 for definitions of interplane angles. The standard errors of the valence angles are in the range 0.1 to 0.2°.

Angles at Nitrogen Atom (deg)

C(1,1)–N–C(1,2)	C(1,1)–N–C(1,3)	C(1,2)–N–C(1,3)
117.1	122.0	120.9

Angles at Carbon Atoms (deg)

Angle	Biphenylyl 1	Biphenylyl 2	Biphenylyl 3
C(6)–C(1)–C(2)	120.3	119.9	118.7
C(1)–C(2)–C(3)	119.6	119.9	120.4
C(2)–C(3)–C(4)	120.9	121.7	121.6
C(3)–C(4)–C(5)	118.2	117.1	117.3
C(4)–C(5)–C(6)	121.7	121.9	122.0
C(5)–C(6)–C(1)	119.4	119.5	120.0
C(6′)–C(1′)–C(2′)	118.7	117.3	118.2
C(1′)–C(2′)–C(3′)	120.4	120.9	120.3
C(2′)–C(3′)–C(4′)	120.2	120.5	120.5
C(3′)–C(4′)–C(5′)	120.0	119.7	119.5
C(4′)–C(5′)–C(6′)	120.3	120.1	120.8
C(5′)–C(6′)–C(1′)	120.5	121.5	120.7
C(3)–C(4)–C(1′)	121.8	121.2	122.0
C(5)–C(4)–C(1′)	120.0	121.7	120.7
C(2′)–C(1′)–C(4)	121.2	121.0	121.3
C(6′)–C(1′)–C(4)	120.1	121.6	120.5
C(2)–C(1)–N	121.0	119.2	120.6
C(6)–C(1)–N	118.8	120.9	120.7

Interplane Angles (deg)

Planes	Angle	Planes	Angle
T–1	43.5	1–1	36.4
T–2	45.3	2–2′	14.5
T–3	26.5	3–3′	23.0

Table 7.7. Bond Lengths and Valence Angles in the Perchlorate Ion

The atom numbers refer to Fig. 7.12. The standard errors of the uncorrected bond lengths and angles are about 0.002 Å and 0.2°.

Bond or Angle	Parameters from Two-Cumulant Refinement		Intermode Distances (Å) and Angles (deg)
	Uncorrected	Corrected	
Bonds			
Cl–O(1)	1.434	1.472	1.453
Cl–O(2)	1.417	1.471	1.431
Cl–O(3)	1.425	1.469	1.447
Cl–O(4)	1.422	1.472	1.446
Angles			
O(1)–Cl–O(2)	109.2	109.6	108.7
O(1)–Cl–O(3)	108.9	108.5	108.6
O(1)–Cl–O(4)	110.0	109.5	110.1
O(2)–Cl–O(3)	109.5	109.3	110.5
O(2)–Cl–O(4)	109.4	109.7	109.5
O(3)–Cl–O(4)	109.8	110.2	109.3

biphenylyl groups. These varied twists, like those about the C–N bonds, are obviously requirements for packing of the cation in the crystal.

There is a most interesting correlation for the C–N bonds among their lengths, interbond angles, and twist angles. The bond N–C(1,3), at 1.386 Å, is shorter than the average of bonds N–C(1,1) and N–C(1,2) by 0.035 Å, about 17 times the standard error of its length. This

significant difference is probably related to the fact that the ring *3* is twisted about 20° less than *1* or *2* from the plane *T*. The lesser twist should make bond N–C(1,3) stronger and shorter than the other two, since the π-orbital overlap integral is proportional to the cosine of the twist angle. It follows from the valence-shell electron-pair repulsion theory of directed valency[20] that the C–N–C angle opposite C(1,3) should be the smallest of the three C–N–C angles, as is observed.

Unfortunately, the significance of this correlation is diminished somewhat by the fact that the expectation of a similar correlation of twists about the three inter-ring bonds of the biphenylyl groups with the lengths of these bonds is not fulfilled. The bond which appears shortest, C(4,3)–C(1,3′), has the intermediate twist.

It is of some significance that we were able to refine successfully the anisotropic thermal parameters of the 27 hydrogen atoms, since this has rarely been done for hydrogen atoms in x-ray analyses until recently. Last year a similar successful refinement for the hydrogen atoms in tri(*p*-fluorophenyl)amine[8] was reported. These successes attest to the quality of our data. Although no detailed analysis of the thermal parameters has been attempted, it is clear from the ellipsoids depicted in Fig. 7.11 that generally they are physically sensible.

The apparent C–H bond lengths show the systematic error of shortening usually observed in x-ray analysis for chemical bonds involving hydrogen atoms. This shortening is attributed to the shifting of the centroids of the hydrogen electron clouds from the proton positions as a result of chemical bonding.[21] In the present case the mean apparent C–H bond length is 0.970 Å, and the rms deviation is 0.028. The minimum and maximum lengths are 0.904 and 1.030 Å respectively. The actual C–H internuclear distance is known to be about 1.08 Å in aromatic compounds.

The determination of the detailed structure of the perchlorate ion in this work is one of the few determinations of even moderate precision ever reported for this ion, and it may be the best one. Perchlorate ions are quite often found to be in a disordered arrangement, which makes it impossible to determine their atomic parameters precisely. In the present case the ions are in an ordered arrangement, though the oxygen atoms are characterized by rather large rms vibrational amplitudes (up to 0.46 Å in magnitude). It was these large amplitudes which suggested the use of the three-cumulant refinement for the atoms of the perchlorate ion. This refinement allowed us to reach the best agreement between F_o^2's and F_c^2's and also allowed calculation of the intermode Cl–O distances,[16] which should be better approximations to the actual mean Cl–O separations than the uncorrected distances obtained from a refinement with the usual two-cumulant model. The corresponding valence-angle estimates defined by the intermode vectors were also computed. However, the way to obtain the most reliable description of the perchlorate ion is to make corrections on the bond lengths and angles through a rigid-body analysis.[22] For this purpose we used the program of C. K. Johnson[23] and the coordinates and anisotropic thermal parameters from the last refinement cycle before the three-cumulant model was introduced. Table 7.7 shows the corresponding uncorrected and corrected bond lengths and angles, along with the intermode distances and angles calculated from the parameters of the three-cumulant model. The agreement among the four Cl–O distances corrected by the rigid-body calculation is extraordinarily good, especially so in view of the large corrections, 0.038 to 0.054 Å. The rms amplitudes associated with the three principal axes of libration of the ion are 12.9, 9.8, and 7.7°.

The average corrected Cl–O bond length of 1.471 Å is in fair agreement with averages of similarly corrected values that have been reported previously: 1.464 Å in nitronium perchlorate,[24] 1.464 Å in monoclinic hydronium perchlorate at −80°C;[25] 1.452 Å in orthorhombic hydronium perchlorate at room temperature.[26,27] In these other cases the individual bond length values differ among themselves by from 0.026 to 0.034 Å.

We thank Professor Robert I. Walter of the University of Illinois at Chicago Circle for suggesting this work and for supplying crystals of the subject compound.

---

[1] Oak Ridge Graduate Fellow from North Texas State University, Denton, under appointment with Oak Ridge Associated Universities.

[2] R. I. Walter, *J. Am. Chem. Soc.* **77**, 5999 (1955).

[3] P. Andersen, *Acta Chem. Scand.* **19**, 622 (1965).

[4] P. Andersen and B. Klewe, *Acta Chem. Scand.* **21**, 2599 (1967).

[5] P. Andersen and B. Klewe, *Acta Chem. Scand.* **19**, 791 (1965).

[6] A. H. Gomes de Mesquita, C. H. MacGillavry, and K. Eriks, *Acta Cryst.* **18**, 437 (1965).

[7] L. L. Koh, *Dissertation Abstr.* **25**, 3860 (1965).

[8] *Chem. Div. Ann. Progr. Rept. May 20, 1969*, ORNL-4437, p. 125.

[9] H. Suzuki, *Electronic Absorption Spectra and Geometry of Organic Molecules*, Academic, New York, 1967.

[10] W. R. Busing *et al.*, *The Oak Ridge Computer-Controlled X-Ray Diffractometer*, ORNL-4143 (1968).

[11]D. J. Wehe, W. R. Busing, and H. A. Levy, *A FORTRAN Program for Calculating Single-Crystal Absorption Corrections,* ORNL-TM-229 (1962).

[12]H. Hauptman and J. Karle, *Solution of the Phase Problem. I. The Centrosymmetric Crystal,* Am. Cryst. Assoc. Monograph No. 3, 1953.

[13]R. E. Long, Ph.D. dissertation, University of California at Los Angeles, 1965.

[14]D. Sayre, *Acta Cryst.* **5,** 60 (1952).

[15]I. L. Karle and J. Karle, *Acta Cryst.* **16,** 969 (1963).

[16]C. K. Johnson, "Generalized Treatments for Thermal Motion," chap. 9 in *Thermal Neutron Diffraction,* B. T. M. Willis, ed., Oxford, 1970.

[17]W. H. Zachariasen, *Acta Cryst.* **A24,** 212 (1968).

[18]Definitions: $R(F)$ and $R(F^2)$ are defined by

$$\Sigma\left||F_o^x| - S^x|F_c^x|\right| \Big/ \Sigma|F_o^x| ,$$

with $x = 1$ and 2 respectively;

$$R_w(F^2) \equiv \left[\Sigma w(F_o^2 - S^2F_c^2)^2 / \Sigma wF_o^4\right]^{1/2} ,$$

$$\sigma_1 \equiv \left[\Sigma w(F_o^2 - S^2F_c^2)^2 / (n - p)\right]^{1/2} ,$$

where p is the number of parameters fitted to the n observations. The factor S is the factor scaling the values $|F_c|$ to the values $|F_o|$.

[19]C. K. Johnson, *OR TEP: A FORTRAN Thermal-Ellipsoid Plot Program for Crystal-Structure Illustrations,* ORNL-3794 revised (1965).

[20]R. J. Gillespie, *J. Chem. Educ.* **40,** 295 (1963).

[21]R. F. Stewart, E. R. Davidson, and W. T. Simpson, *J. Chem. Phys.* **42,** 3175 (1965).

[22]V. Schomaker and K. N. Trueblood, *Acta Cryst.* **B24,** 63 (1968).

[23]C. K. Johnson, "The Effect of Thermal Motion on Interatomic Distances and Angles," in *Crystallographic Computing,* F. R. Ahmed, ed., Munskgaard, Copenhagen, in press.

[24]M. R. Truter, D. W. J. Cruickshank, and G. A. Jeffrey, *Acta Cryst.* **13,** 855 (1960).

[25]C. E. Nordman, *Acta Cryst.* **15,** 18 (1962).

[26]M. R. Truter, *Acta Cryst.* **14,** 318 (1961).

[27]F. S. Lee and G. B. Carpenter, *J. Phys. Chem.* **63,** 279 (1959).

X-RAY DIFFRACTION STUDY OF KRYPTON DIFLUORIDE

P. A. Agron H. A. Levy

The unit cell dimensions $a = 4.60$ Å and $c = 5.83$ Å for krypton difluoride at 8°C were determined by x-ray diffraction using precession photography. The most probable space group is $P4_2/mnm$. The packing of the linear molecules in the crystal differs from that reported for XeF_2.[1] Intermolecular krypton-fluorine distances in the proposed structure indicate that van der Waals forces may be responsible for the increase in the stability of this compound over that observed in the gas phase. A study at low temperature is required for further elucidation of the details of the structure, which are masked by large thermal motion of fluorine atoms at 8°C.

---

[1]H. A. Levy and P. A. Agron, *J. Am. Chem. Soc.* **85,** 214 (1963); S. Siegel and E. Gebert, *J. Am. Chem. Soc.* **85,** 240 (1963).

NEUTRON AND X-RAY DIFFRACTION STUDIES OF XENON HEXAFLUORIDE

H. A. Levy P. A. Agron

Single-crystal diffraction data were collected on the automated ORNL instruments for two phases[1] of xenon hexafluoride. X-ray data for both the monoclinic and cubic phases[2] were taken at 20°C. In addition, neutron data were obtained on the cubic phase of XeF_6 at 3 and −11°C.[2] The observation has been made by several investigators that both phases can apparently be held unchanged for long periods at room temperature but that the monoclinic crystals are disrupted on cooling to 8 to 10°C. The elucidation of the nature of the stability of these phases awaits a complete solution of the two structures.

Recently a structure was proposed[3] for the cubic phase of XeF_6 based on single-crystal x-ray diffraction data obtained at −80°C. According to this proposal both tetramers and hexamers of xenons bridged by fluorine atoms occur. Since neutron diffraction is much more favorable, in this instance, for establishing the positions of the fluorine atoms, the proposed model was tested with the reduced neutron data obtained at −11°C. The discrepancy index,

$$R(F) = \Sigma\left||F_o| - |F_c|\right| \Big/ \Sigma|F_o| = 0.20 ,$$

based on 11 atoms and 79 parameters indicates that the proposed model is not adequate. Since the cubic phase appears to be stable at low temperatures, a neutron diffraction study with reduced thermal motion is called for to establish the fluorine positions.

G. R. Jones has also proposed[4] a possible structure for the monoclinic XeF_6 based on the tetrameric species present in the cubic phase. This model has been applied to a set of neutron data and again is found to give an inadequate fit. The discrepancy index based on 27 atoms and 107 parameters gives $R(F) = 0.25$.

[1]P. A. Agron, C. K. Johnson, and H. A. Levy, *Inorg. Nucl. Chem. Letters* **1**, 145 (1965).

[2]These data were collected in collaboration with S. W. Peterson, Argonne National Laboratory.

[3]R. D. Burbank and G. R. Jones, *Science* **168**, 248 (1970).

[4]Private communication.

DIFFRACTION PATTERN AND STRUCTURE OF LIQUID TRIMETHYLAMINE DECAHYDRATE AT 5°C

C. Folzer[1] R. W. Hendricks[2] A. H. Narten

Trimethylamine is one of a large number of compounds known to form a solid clathrate hydrate; its ideal composition[3] is $4(CH_3)_3N{\cdot}41H_2O$, and its melting point is 5°C. The trimethylamine guest molecules interact strongly with the host water network through the formation of relatively short (2.705 to 2.668 Å) N···H–O hydrogen bonds; for this reason the term "semiclathrate hydrate" has been proposed to distinguish these structures from those of the gas and peralkylammonium salt hydrates[4] in which the guest species is not hydrogen bonded to the host network.

The scattering of x rays from a solution of trimethylamine in water having the same composition as the clathrate crystal has been measured and analyzed at the melting point of the solid hydrate. Two independent sets of large- and small-angle x-ray data have been collected and combined into one; the resulting intensity function (Fig. 7.14) covers a range of scattering angles not previously reported for any liquid. A correlation function $G(r)$ derived from the data is shown in Fig. 7.15 together with the curve for pure water[5] at 4°C.

In the region of radial distances $r < 2.5$ Å, several pronounced maxima are visible which correspond to intramolecular atom-pair interactions. At distances greater than ~2.5 Å, the correlation function of the solution is surprisingly similar to that of pure water; however, some significant small differences are evident. The distinct peak at 2.85 Å (2.84 Å in water) is somewhat smaller, the broad maximum at ~4.5 Å has a slightly different shape, and the very broad peak around 7 Å is somewhat less pronounced in the solution curve. In both the solution and in pure water there are significant deviations from a uniform distance distribution (there is "structure") to about 8 Å. If the positional correlation between water molecules or

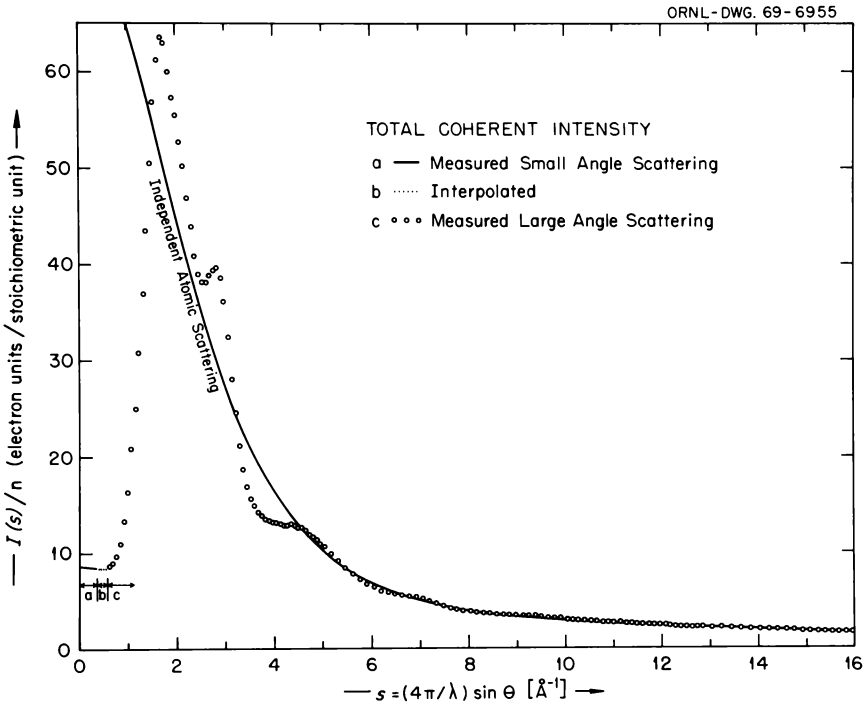

Fig. 7.14. Total Scattered Intensities for Liquid Trimethylamine Decahydrate at 5°C. A stoichiometric unit of solution containing 8.98 mole % trimethylamine and 91.02 mole % water is visualized as representative of the whole solution. The small-angle scattering was measured to values of $s \geq 0.01$ Å^{-1}.

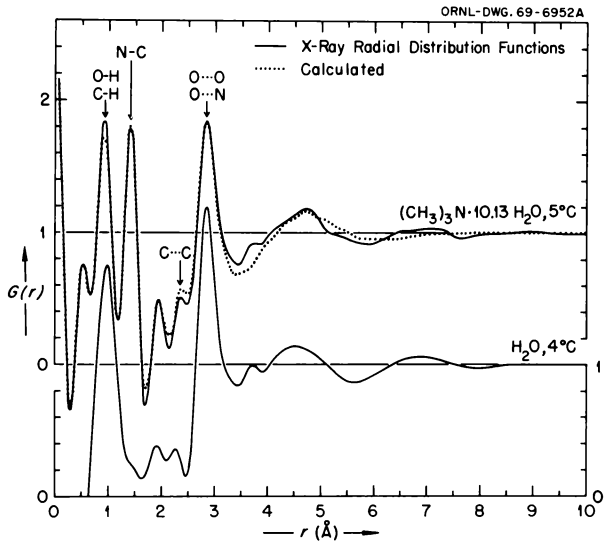

Fig. 7.15. X-Ray Atom-Pair Correlation Functions for Water and Liquid Trimethylamine Decahydrate at the Melting Point. The calculated curve for the solution is based on gas diffraction results below $r \cong 2.5$ Å and on a simple tetrahedral network model for distances $r > 2.5$ Å.

between water and trimethylamine molecules extended to larger distances (as might be the case if the molecules formed large clusters held together by hydrogen bonds, or if regions containing qualitatively different local arrangements or "phases" were present), the intensity function (Fig. 7.14) should exhibit interference maxima in the region of small scattering angles, that is, below the first major diffraction peak at ~1.7 $Å^{-1}$. The observed lack of interference in the small-angle region precludes any significant variation from unity of the correlation function not included in the curves of Fig. 7.15.

The maximum at 2.84 Å in the correlation function of pure water represents[6] ~4.4 O···O interactions per average water molecule, indicating predominantly tetrahedral coordination. The location of the maximum near 4.5 Å, when compared with the nearest-neighbor distance, is a strong indication that the *average* deviation from ideal tetrahedral coordination in both pure water and the solution must be quite small. In the solution, however, the trimethylamine molecules are expected to interact strongly with water through the formation of N···H–O hydrogen bonds, as is known to be the case in the crystalline hydrate;[3] these interactions must therefore contribute significantly to the maximum at 2.85 Å. Let us assume that this peak can be represented by a Gaussian distribution of distances centered at r_0 = 2.85 Å and characteristic of the interactions of y nitrogen atoms and $(1 - y)$ oxygen atoms with $4F$ nearest neighbor atoms, y being the mole fraction of trimethylamine and $F \leqslant 1$ the fractional occupancy of the assumed tetrahedral network. Let the broad maximum around 4.5 Å correspond to a similar distribution of $12F$ average atoms centered at $r_1 = r_0(8/3)^{1/2}$ characteristic of a tetrahedral network. Let higher neighbor interactions and all intermolecular interactions involving hydrogen atoms and methyl groups be described by uniform distributions. Without further specification of the detailed nature of this assumed tetrahedral network of oxygen and nitrogen atoms, we can calculate an intensity function for this very simple model of the trimethylamine solution. Using Eq. 5 of ref. 4 and adjusting by least squares the occupancy factor F and the rms variations in the first- and second-neighbor distances, a value of $F = 0.95$ was found to give the best agreement with the experimental curve for the solution. The correlation function calculated for this model is shown in the dotted curve of Fig. 7.15, and agreement with the experimental curve is surprisingly good. The calculated curve for distances $r < 2.5$ Å is model independent, the parameters describing the intramolecular interactions being taken from gas diffraction results.[7,8] The average coordination number of oxygen (nitrogen) atoms in the solution, 3.8, is thus smaller than the value of 4.4 found for pure water. It should also be noted that a similar model for water gives rather poor agreement with the x-ray data,[6] and this leads to the conclusion that the first coordination sphere of an average molecule is more complex in pure water than in the trimethylamine solution.

Our analysis of the diffraction pattern for the trimethylamine solution supports the idea that the hydrogen bonds between water molecules form an extensive three-dimensional network in which the nitrogen atoms of the amine participate through the formation of N···H–O hydrogen bonds. The detailed features of such a network would of course be short lived, and the local and instantaneous environment of individual molecules is distorted from the average tetrahedral geometry. These small but continuous deviations from the average result in the loss of all positional correlation a few molecular radii away from any starting point, characteristic of a liquid.

Intensity and radial distribution functions calculated for two specific different models for the trimethylamine solution give equally good quantitative agreement with the x-ray data.[9] One model assumes that the tetrahedral network is similar to the ice I structure (ice I model) with none of the cavities occupied by

"interstitial" water molecules and 95% of the network positions being randomly occupied by oxygen and nitrogen atoms. The second model assumes that the short-range order in the solution is, on the average, similar to that found for the solid hydrate, all the large cavities characteristic of this structure[3] being randomly occupied by trimethylamine and water molecules. These two different structural models have the same density, and the calculated distance spectra differ significantly only at relatively large separations, where all positional correlation in the liquid solution has disappeared.

The fact that two models based on qualitatively different crystal structures describe the average short-range order in the liquid trimethylamine solution equally well, illustrates that the three-dimensional configuration of molecules in a liquid cannot be deduced uniquely from one-dimensional diffraction data. However, it has been shown[6] that a clathrate model is incompatible with diffraction measurements on pure water (and hence is unsatisfactory for dilute solutions); it does not afford a continuous transition from dilute to concentrated solutions of trimethylamine in water. The ice I model, on the other hand, is in excellent agreement with the x-ray data on pure water,[10] and it describes quantitatively the radial distribution in other aqueous solutions.[11-13] While this model cannot be proved to be unique, it seems to provide a more satisfactory description of the short-range order found in water and many aqueous systems.

---

[1]Crystallography Laboratory, University of Pittsburgh, Pittsburgh, Pa. 15213.

[2]Metals and Ceramics Division.

[3]D. Panke, *J. Chem. Phys.* **48**, 2990 (1968).

[4]G. A. Jeffrey and R. K. McMullan, *Progr. Inorg. Chem.* **8**, 43 (1967).

[5]A. H. Narten, *X-Ray Diffraction Data on Liquid Water in the Temperature Range 4–200°C*, ORNL-4578 (1970).

[6]A. H. Narten and H. A. Levy, *Science* **165**, 447 (1969).

[7]S. Shibata and L. S. Bartell, *J. Chem. Phys.* **42**, 1147 (1965).

[8]B. Beagley and T. G. Hewitt, *Trans. Faraday Soc.* **64**, 2561 (1968).

[9]C. Folzer, R. W. Hendricks, and A. H. Narten, to be submitted to the *Journal of Physical Chemistry.*

[10]A. H. Narten, M. D. Danford, and H. A. Levy, *Discussions Faraday Soc.* **43**, 97 (1967).

[11]A. H. Narten, *J. Chem. Phys.* **49**, 1962 (1968).

[12]A. H. Narten and S. Lindenbaum, *J. Chem. Phys.* **51**, 1108 (1969).

[13]A. H. Narten, *J. Phys. Chem.* **74**, 765 (1970).

INFRARED AND RAMAN SPECTROSCOPY

SPECTROPHOTOMETRY OF SOLUTIONS OVER WIDE RANGES OF TEMPERATURE AND PRESSURE

W. C. Waggener A. J. Weinberger
R. W. Stoughton

Our efforts to understand the condensed states of simple molecules more nearly completely through studies of their near-infrared spectra as a function of temperature and pressure have continued.

Preliminary results comparing parameters of the four bands observed in the spectrum of orthobaric liquid H_2S in the region 1.1 to 2.2 μ with those of its cogener, H_2O, in the region between 0.8 and 1.6 μ were published.[1] The H_2S spectrum differs from that of H_2O in that the bands of the former are narrower, are in general less intense, and broaden with increasing temperature and decreasing density from the freezing point. This broadening, which must arise from kinetic processes connected with weak intermolecular association, is similar to that which we have observed in pure Lorentzian bands in liquid CO_2,[2] except that the band broadening and shifting for the same range of reduced temperature are in orthobaric liquid CO_2 8 times smaller, indicative of still weaker intermolecular forces.

In view of the unexpected highly Gaussian distribution functions required for a least-squares fit of the 1.6-μ vibrational-band cluster of liquid H_2S, we concluded that H bonding, while much weaker in liquid H_2S than in H_2O, still is a controlling factor in the band profile. Consequently, we have turned to a study of the liquid haloforms,[3] in which H bonding is known to be extremely weak. Harmonic and combination bands involving the C-H stretch (ν_1) with the C-H bending mode (ν_4) are relatively intense compared with the other vibrations present and are more susceptible to band analysis than the summation bands in *n*-hexane and cyclohexane which we have already measured. We are measuring the $3\nu_1$ band of $CHBr_3$ and $CHCl_3$ near 8675 cm^{-1} and both the $2\nu_2 + 2\nu_4$ and the $3\nu_1$ bands centered near 8589 and 8793 cm^{-1}, respectively, in the dilute gas. To date we have measured $CHBr_3$ at 19°, $CHCl_3$ at 19 and −63° (fp), and CHF_3 at 19, −48, and −63°. It is apparent for these haloforms that (1) all the bands exhibit a distinct asymmetry, (2) the CHF_3 band intensities are on the order of one-tenth of those for $CHCl_3$ and $CHBr_3$, and (3) changes in density of CHF_3 have an opposite effect upon the band width and position than observed for $CHCl_3$.

Values of 1.11 and 1.29 for the asymmetry index, defined as the ratio of integrated intensities above and below ν_{max}, were obtained for the $3\nu_1$ bands of $CHBr_3$ and $CHCl_3$, respectively, at 19°C. Overlap of the $2\nu_1 + 2\nu_4$ and $3\nu_1$ bands in the liquid CHF_3 spectra (Fig. 7.16) prevents estimate of their asymmetries, although skewness is apparent in the bands both at 19 and −48°C.

The asymmetry in the two spectra of gaseous CHF_3 (Fig. 7.16) and the asymmetry observed in the spectra of the liquid haloforms suggest that some form of quantized rotation or libration may persist in the liquid state. At −48° (5 atm) the envelopes of the single *P*, *Q*, and *R* rotational branches of each band are clearly resolved. In each case the central *Q* branch is very sharp (~650 liters $mole^{-1}$ cm^{-1}) and incompletely resolved, and the *R* branch is much more intense than the corresponding *P* branch. The asymmetry index for the integrated intensity of each band is about 1.5. At 19° (40 atm), which is near the critical temperature (33°C), the profile of the gas-phase spectrum is clearly approaching that of the orthobaric liquid. The *Q* rotational branch of each band has broadened and become less intense. The *P* and *R* branches are no longer resolved but appear as slight inflections and humps on the low- and high-energy sides of the bands respectively. The asymmetry indices have increased to 1.8 ($2\nu_1 + 2\nu_4$) and 2.0 ($3\nu_1$).

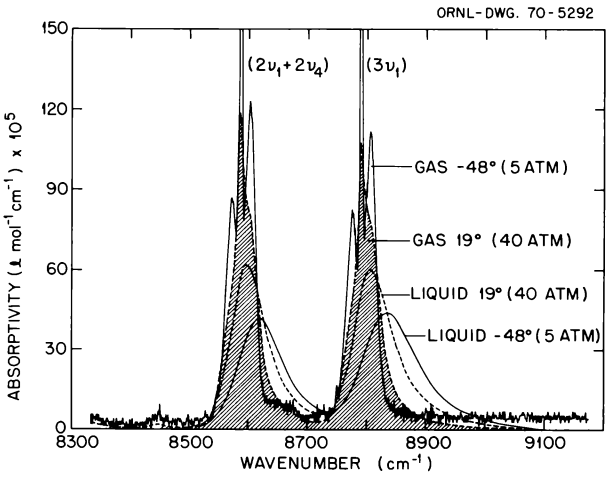

Fig. 7.16. Spectra of Orthobaric Liquid and Gaseous CHF_3 at 19 and 48°C. Taken with a Cary model 14 spectrophotometer provided with a 0 to 0.2 absorbance range. Sample cell, 2.54 cm vs reference cell, 0.25 cm (CCl_4, 25°). Base line for correction of liquid and gas measurements obtained with CCl_4 and vacuum, respectively, in sample cell.

Thus these haloform spectra are more complex than we expected, and the spectra of liquid CHF_3 are qualitatively different from liquid $CHCl_3$ and $CHBr_3$. For $CHCl_3$ the changes in the position and width of the $3\nu_1$ band with temperature are small and negative. However, for liquid CHF_3 $\nu_{max}(3\nu_1)$ increases 32 cm^{-1} between room temperature and −63°, and its estimated half bandwidth increases from 70 to 116 cm^{-1} (also see Fig. 7.16). This very large increase in bandwidth with increasing density and decreasing temperature suggests association in the liquid, and we are particularly interested in measuring the CHF_3 bands to the freezing point (−155°C).

We expect to complete measurements of the liquid haloforms from their respective freezing points to their critical points or to the point of thermal instability. An attempt will then be made to correlate the respective spectra with the size and polarizability of the attached Br, Cl, and F.

For several years we have been concerned with the measurement and interpretation of the spectra of pure liquids. Our equipment, however, was intended primarily for solution spectrophotometry, and we have established some limits of applicability of nitric, sulfuric, and perchloric acids as aqueous solvents up to 250°.[4] This year we plan to make an exploratory study of species present in the aqueous chromate-dichromate system as a function of temperature from 25 to 250°C. The equilibria involved apparently have not been studied as a function of temperature, and almost certainly not above 100°C. Our study should provide fundamental equilibrium and rate data for chromium species which are extremely important oxidizing agents and corrosion inhibitors in the chemical processing industry. We believe that our initial studies of the chromate-dichromate system in dilute acids will lead to other extremely important and profitable studies involving the oxidation states and hydrolytic behavior of chromium, iron, and other members of the first transition series.

Our original Cary model 14 spectrophotometer was replaced with an updated model 14 with a Datex digital system. This instrument, specially built for us, has optimized performance in the wavelength range (0.25 to 3.0 μ) most useful for studies of liquids and solutions in cells with sapphire windows. It can be operated with the infrared source beam reversed to eliminate the several watts of sample heating and permit operation at lower sample temperatures. Furthermore, it is possible to measure photosensitive samples.

We found it impractical to adapt the available machine-language programs for conversion of digital

information on punched tape to processed data stored on magnetic tape. Therefore computer programs written in convenient FORTRAN IV language were developed which were suited to our particular needs for processing the digital data output from the new spectrophotometer and for computing and plotting spectral parameters. The method of W. R. Busing (Chemistry Division) was used to transcribe from paper to magnetic tape. Spectral scan information (identification, wavelength, filter, absorbance, and slit width) is processed and stored on duplicate library magnetic tapes with provisions for editing the tape to remove both machine and human errors from a given data set. From these, calculations, tabulations, and graphs of publishable quality can be generated. Punched tape generated during the day can now be processed, stored, and plotted overnight.

[1]W. C. Waggener, A. J. Weinberger, and R. W. Stoughton, *J. Phys. Chem.* **73**, 3518 (1969).

[2]W. C. Waggener, A. J. Weinberger, and R. W. Stoughton, *J. Phys. Chem.* **71**, 4320 (1967).

[3]W. C. Waggener, A. J. Weinberger, and R. W. Stoughton, *Chem. Div. Ann. Progr. Rept. May 20, 1969*, ORNL-4437, p. 107.

[4]W. C. Waggener, A. J. Weinberger, and R. W. Stoughton, *Appl. Spectry.* **22**, 545 (1968).

INFRARED AND RAMAN SPECTRAL STUDIES ON ^{18}O-ENRICHED POLYCRYSTALLINE KNO_3

M. H. Brooker[1] G. E. Boyd

Isotopic substitution (e.g., ^{18}O, ^{15}N, etc.) in molecular ions in crystalline solids can facilitate the interpretation of vibrational spectroscopic measurements made after radiolytic decomposition by energetic ionizing radiations.[2] Infrared and Raman studies have been performed with polycrystalline samples of 51.7% ^{18}O-enriched KNO_3 by techniques described previously. Band frequencies and assignments from these measurements for the four possible isotopically different species ($N^{16}O_3^-$, $N^{16}O_2{}^{18}O^-$, $N^{16}O^{18}O_2^-$, $N^{18}O_3^-$) are listed in Table 7.8. These frequencies are in excellent agreement with infrared studies of ^{18}O-substituted nitrate in KBr pellets.[3] The four intense Raman bands associated with the totally symmetric stretching vibration appear to have identical molar extinction coefficients and can be used quantitatively to determine ^{18}O isotopic constitution[4] (Fig. 7.17).

Substitution of either one or two ^{18}O atoms on the nitrate ion lowers the symmetry from the D_{3h} point group to C_{2v}. The ν_3 (E' *ca.* 1350 cm^{-1}) and ν_4 (E' *ca.* 710 cm^{-1}) modes split into an A_1 and a B_2 mode (Table 7.8, Fig. 7.18). The separation between these two components is about 15 cm^{-1} in the ν_3 region and

Table 7.8. Vibrational Frequencies and Assignments for Bands Observed in 51.7% ^{18}O-Enriched KNO_3 at Room Temperature[a]

D_{3h} Symmetry					C_{2v} Symmetry				
Frequency (cm^{-1})				Assignment	Frequency (cm^{-1})				Assignment
$N^{16}O_3^-$		$N^{18}O_3^-$			$N^{16}O_2{}^{18}O$		$N^{16}O^{18}O_2$		
Raman	Infrared	Raman	Infrared		Raman	Infrared	Raman	Infrared	
716	715	777	776	(E') ν_4	706	705	694	693	A_1 } ν_4
					699	698	686	685	B_2 }
826	828		816[b]	(A_2'') ν_2		824[b]		819[b]	B_1 ν_2
	846[c]								
1051	1051.0	991	991	(A_1') ν_1	1031	1031	1011	1011	A_1 ν_1
1048[c]	1049.9[c]	988[c]			1028[c]		1008[c]		
	1383[d]		1363[d]	(E') }	1353[b]	1383[d]	1331[b]	1363[d]	B_2 } ν_3
1345		1324[b]		(A_g)[e] } ν_3	1338[b]	1371[d]	1346[b]	1377[d]	A_1 }
1360		1339[b]		(B_g)[e] }					

[a]Assignments are based on a free-ion approximation. A more complete analysis of the spectrum of solid KNO_3 is found from factor group representation; see, for instance, M. H. Brooker and D. E. Irish, *Can. J. Chem.* **48**, 1198 (1970).

[b]Curve resolved from band envelope.

[c]Bands are split due to correlation field coupling; see M. H. Brooker, *J. Chem. Phys.* in press, and "Correlation Field Coupling of Nondegenerate Nitrate Vibrations," contribution in this Section, this report.

[d]Values and assignments from ref. 3.

[e]Factor group assignment.

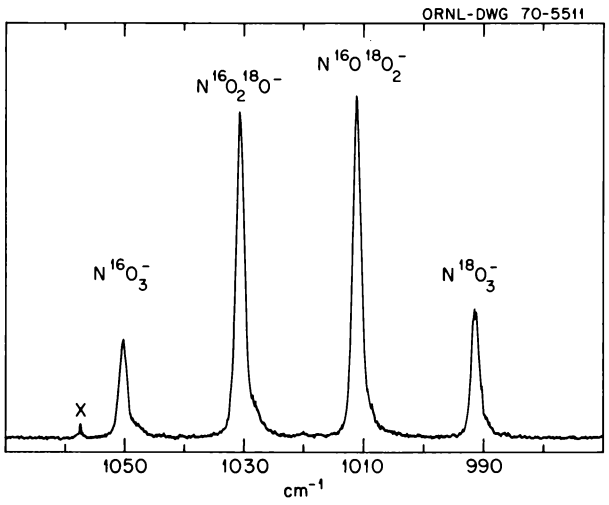

Fig. 7.17. Raman Spectrum of the ν_1 Region of 51.7% ^{18}O-Enriched KNO_3. 1.0 cm^{-1} slit width, 5 X 10^3 counts/sec, 0.5-sec time constant. A weak plasma line is visible at 1057.3 cm^{-1}.

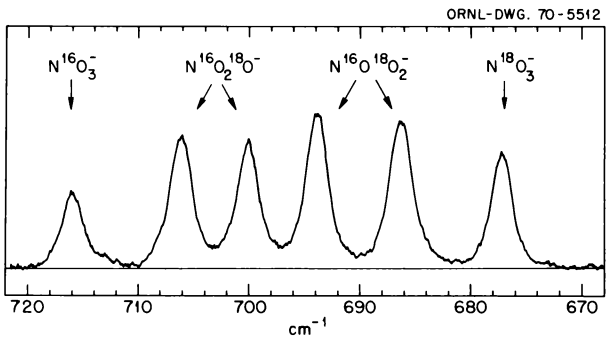

Fig. 7.18. Raman Spectrum of the ν_4 Region of 51.7% ^{18}O-Enriched KNO_3. 1.0 cm^{-1} slit width, 5 X 10^2 counts/sec, 5.0-sec time constant.

6 cm^{-1} in the ν_4 region. A weak shoulder on the low-frequency side of each of the ν_1 Raman components may be assigned to a band due to correlation field splitting. This would indicate that the small mass change on substitution of ^{18}O for ^{16}O is not sufficient to decouple the vibrations of neighboring nitrate ions in the crystal.

In nonenriched KNO_3, lattice frequencies occur at 126 (weak), 85 (intense), and 52 (medium) cm^{-1}. In 51.7% ^{18}O-enriched KNO_3, the frequencies are 120, 80, and 50 cm^{-1} respectively. The relatively large frequency shifts in the bands at *ca.* 120 and 80 cm^{-1} on substitution of the heavier ^{18}O atom would indicate that these bands are essentially librational modes of the nitrate ion, while the 2-cm^{-1} shift in the band at *ca.* 50 cm^{-1} would be consistent with this band being due to a translatory motion of the nitrate ion.

---

[1]Visiting scientist; National Research Council of Canada Postdoctoral Fellow, 1969–70.

[2]M. H. Brooker and G. E. Boyd, "Radiolysis of ^{18}O-Enriched Polycrystalline KNO_3," a contribution in chap. 4, this report.

[3]R. Kato and J. Rolfe, *J. Chem. Phys.* **47**, 1901 (1967).

[4]A. J. Melveger, E. R. Johnson, and E. N. Ladov, *J. Inorg. Nucl. Chem.* **32**, 337 (1970).

IONIC INTERACTIONS IN CRYSTALS: INFRARED AND RAMAN SPECTRA OF POWDERED $Ca(NO_3)_2$, $Sr(NO_3)_2$, $Ba(NO_3)_2$, AND $Pb(NO_3)_2$[1]

M. H. Brooker[2] D. E. Irish[3] G. E. Boyd

Infrared and Raman spectra of the isomorphous cubic crystals $Ca(NO_3)_2$, $Sr(NO_3)_2$, $Ba(NO_3)_2$, and $Pb(NO_3)_2$ have been recorded. The observed vibrational spectra can be interpreted conveniently in terms of a factor group analysis. Splitting of spectral bands previously reported as singlets (Fig. 7.19) was observed under high-resolution conditions achieved with laser Raman spectroscopy. Correlation field splittings of the nitrate ion vibrations were of the order of 50 cm^{-1} in the antisymmetric stretching region; in the regions of the symmetric stretch, antisymmetric bend, and out-of-plane deformation the correlation field splittings were *ca.* 2 cm^{-1}. Multiple attenuated total reflectance (MATR) techniques were useful for obtaining spectra of the strongly absorbing ν_3 region at *ca.* 1380 cm^{-1}.

---

[1]Expanded abstract of paper scheduled to appear in *J. Chem. Phys.* **53** (August 1, 1970).

[2]Visiting scientist; National Research Council of Canada Postdoctoral Fellow, 1969–70.

[3]Department of Chemistry, University of Waterloo, Waterloo, Ontario, Canada.

ORNL-DWG. 69-13280

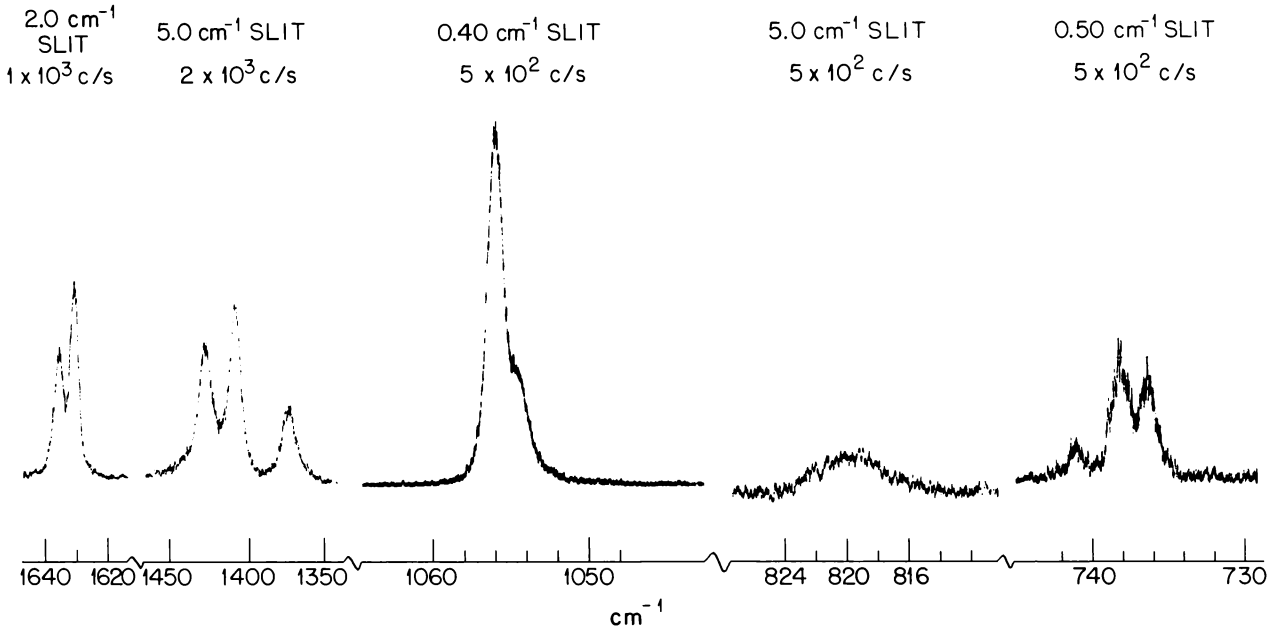

Fig. 7.19. Photograph of Portions of the Raman Spectrum of $Sr(NO_3)_2$. Sample excited with 4880-Å argon ion laser line.

TRANSVERSE OPTICAL FREQUENCIES FROM MULTIPLE ATTENUATED TOTAL REFLECTANCE INFRARED SPECTROSCOPY[1]

M. H. Brooker[2]

The techniques of multiple attenuated total reflectance (MATR) spectroscopy have been found useful for obtaining infrared spectra of strongly absorbing samples. No dispersing medium is required; hence spectra can be obtained free from interfering bands contributed by organic mulling oils and free from possible ion exchange effects common to alkali halide pressed pellets. Theoretically, for infrared reflection spectra each absorption band should give rise to two components: (1) a transverse optical, TO, and (2) a longitudinal optical, LO, mode. We have found that infrared peak frequencies determined with solid samples by MATR methods are the same as those obtained from transmission spectra. Contributions from LO modes do not appear to contribute significantly to the MATR band intensity.

[1]Expanded abstract of a paper to be published in *J. Chem. Phys.*

[2]Visiting scientist; National Research Council of Canada Postdoctoral Fellow, 1969–70.

CORRELATION FIELD COUPLING OF NONDEGENERATE NITRATE VIBRATIONS[1]

M. H. Brooker[2]

Laser Raman spectra have been recorded for several ionic nitrates at relatively high resolution. Band multiplicity in the out-of-plane deformation vibration in its first overtone and in the symmetric stretching regions was observed and has been discussed according to the selection rules for the appropriate factor group representation (Table 7.9). Correlation field splittings are considered to be the result of dipole-dipole interactions and are inversely proportional to the third power of the distance between molecules. The magnitude of the correlation field splitting (Table 7.10) may be related to both the distance between and the relative orientations of the neighboring NO_3^- ions. The magnitude of the correlation field splitting is essentially independent of mass.

Since the vibrational modes in the first overtone region of the out-of-plane vibrations have identical symmetry species and similar frequency, Fermi resonance interaction is possible. Evidence exists for some mixing of the eigenfunctions; however, the observations are not fully consistent with Fermi resonance.

Table 7.9. Vibrational Frequencies for Bands Derived from the Nondegenerate Fundamentals in Ionic Nitrates[a,b]

	ν_1		ν_2		$2\nu_2$
	Raman	Infrared	Raman	Infrared	Raman[c]
$LiNO_3$	1071 (1.0)	i.a.	i.a.	838	1676 (0.016)
$NaNO_3$	1068 (1.0)	i.a.	i.a.	836	1673 (0.012)
KNO_3-I (150°C)	1056 (1.0)	1055[d]	i.a.	836[d]	1672 (0.011)
KNO_3-II (25°C)	1048 (0.04)	1051, {1049.9[d]	826 (0.0005)	828, {828[e] 829[d]	1653 (0.003)
	1051 (0.96)	1051.0}		846 849}	~1664 (0.002)
					~1675 (0.0025)
					1686 (0.003)
$RbNO_3$	1053 (0.08)	1053[f]	836 (<0.0001)	836	1674 (0.019)
	1057 (0.92)	1057[f]			
$CsNO_3$	1047 (0.10)	1047[f]	833 (<0.0001)	834	1668 (0.02)
	1051 (0.90)	1051[f]			
$AgNO_3$	1043 (0.15)			802	1605 (0.005)
	1045 (0.85)	1046	809 (0.003)		1614 (0.006)
$TlNO_3$	1039 (0.10)			819	1639 (0.007)
	1043 (0.90)	1042	821 (0.002)		1643 (0.009)
$Ca(NO_3)_2$	1066 (0.3)			813	1628 (0.006)
	1069 (0.7)		819 (0.001)		1633 (0.004)
$Sr(NO_3)_2$	1054 (0.2)			814	1630 (0.005)
	1056 (0.8)	1055	820 (0.001)		1635 (0.004)
$Ba(NO_3)_2$				817	1634 (0.006)
	1048 (1.0)	1047	820 (0.001)		1638 (0.004)
$Pb(NO_3)_2$	1044 (0.2)			807	1614 (0.005)
	1046 (0.8)	1045	811 (0.002)		1618 (0.004)

[a]Raman intensities relative to the total ν_1 intensity taken as unity are given in parentheses.

[b]Unless otherwise stated, infrared values are the powder values reported by M. H. Brooker and D. E. Irish, *Can. J. Chem.* **48**, 1198 (1970); M. H. Brooker, D. E. Irish, and G. E. Boyd, *J. Chem. Phys.* **53** (1970); also "Ionic Interactions in Crystals: Infrared and Raman Spectra of Powdered $Ca(NO_3)_2$, $Sr(NO_3)_2$, $Ba(NO_3)_2$, and $Pb(NO_3)_2$," a preceding contribution in this Section, this report.

[c]$2\nu_2$ modes are Raman active and infrared forbidden for all centrosymmetric crystals, and Raman and infrared active for noncentrosymmetric crystals.

[d]Oriented single-crystal values obtained from A. A. Shultin and S. V. Karpov, *J. Phys. Chem. Solids* **30**, 1981 (1969); **29**, 475 (1968).

[e]Oriented single-crystal values; M. H. Brooker and D. E. Irish, unpublished work.

[f]Obtained from polycrystalline samples deposited on an AgBr plate. Infrared spectra were recorded under high-resolution conditions on a P.E. 521 grating infrared instrument.

Table 7.10. Properties of Ionic Metal Nitrate Crystals[a]

	Space Group	Molecules per Primitive Cell	NO_3^- Site Symmetry	Relative NO_3^- Orientation	Closest N-N Distance in Unit Cell (Å)	Magnitude of Correlation Field Splitting (cm^{-1})		
						ν_2	$2\nu_2$	ν_1
$LiNO_3$	D_{3d}^6-$R\bar{3}C$	2	D_3	Parallel out-of-plane, coplanar	3.70 4.69	0	0	0
$NaNO_3$	D_{3d}^6-$R\bar{3}C$	2	D_3	Parallel out-of-plane, coplanar	4.07 5.07	0	0	0
KNO_3-I	D_{3d}^6-$R\bar{3}C$	2	D_3	Parallel out-of-plane, coplanar	4.48 5.42	0	0	0
KNO_3-II	D_{2h}^{16}-*Pnma*	4	C_s	Stacked	3.22	20	33	3
$RbNO_3$[b]	C_3^2-$P3_1$	3	C_1	Parallel out-of-plane	4.85	0	0	4
$CsNO_3$[b]	C_3^2-$P3_1$	3	C_1	Parallel out-of-plane	5.20	0	0	4
$AgNO_3$	D_{2h}^{15}-*Pcba*	8	C_1	Off-center, tilted stack	3.85	7	9	2
$TlNO_3$	D_{2h}^{16}-*Pnma*	8	C_s	Mutually perpendicular	4.05	2	4	4
	or C_{2v}^9-$Pbn2_1$	4	C_1	Slightly rotated from perpendicular				
$Ca(NO_3)_2$	T_h^6-*Pa*3	4	C_3	Mutually perpendicular	4.35	6	5	3
$Sr(NO_3)_2$	T_h^6-*Pa*3	4	C_3	Mutually perpendicular	4.50	6	5	2
$Pb(NO_3)_2$	T_h^6-*Pa*3	4	C_3	Mutually perpendicular	4.55	4	4	2
$Ba(NO_3)_2$	T_h^6-*Pa*3	4	C_3	Mutually perpendicular	4.70	4	4	0

[a]Stable room-temperature phases except for KNO_3-I, which is stable above 130°C.

[b]$RbNO_3$ and $CsNO_3$ have been treated on the assumption that the space groups are identical. Distances are based on the pseudocubic unit cells.

[1]Expanded abstract of a paper to be published in *J. Chem. Phys.* (1970).

[2]Visiting scientist; National Research Council of Canada Postdoctoral Fellow, 1969–70.

RAMAN SPECTRUM OF CRYSTALLINE MoF_4

John B. Bates

The Raman spectrum of crystalline MoF_4 has not been reported previously. A sample of this material was supplied in the form of a yellowish-tan solid contained in the bottom of an evacuated quartz reaction flask.[1] The Raman spectrum shown in Fig. 7.20 was measured on a Jarrell-Ash model 25-300 spectrophotometer using both a helium-neon laser (Spectra-Physics 125-A, λ = 6328 Å) and an argon ion laser (Spectra-Physics 141, λ = 4880 Å) source to excite the spectra.

The crystal structure of MoF_4 has not been determined, so an interpretation of the Raman spectrum of this material cannot be given at this time. However, in the likelihood that the unit cell contains MoF_4 tetrahedra, we can propose a tentative assignment of the major features of the spectrum shown in Fig. 7.20. The strong band at 722 cm^{-1} is a totally symmetric crystal component of ν_1 (A_1), and one of the weaker bands at 746, 710, and 690 cm^{-1} may be a second component of ν_1 (the 746 cm^{-1} is a likely candidate for the second ν_1 component). Two of the three weaker bands observed in this region are likely to be crystal components of the ν_3 (F_2) asymmetric stretching mode.

The degenerate bending modes ν_2 (E) and ν_4 (F_2) are giving rise to the low-frequency components observed at 280, 251, and 211 cm^{-1} and to a low-frequency shoulder on the 251-cm^{-1} band observed at about 220 cm^{-1} (Fig. 7.20). The bands observed at 176 and 142

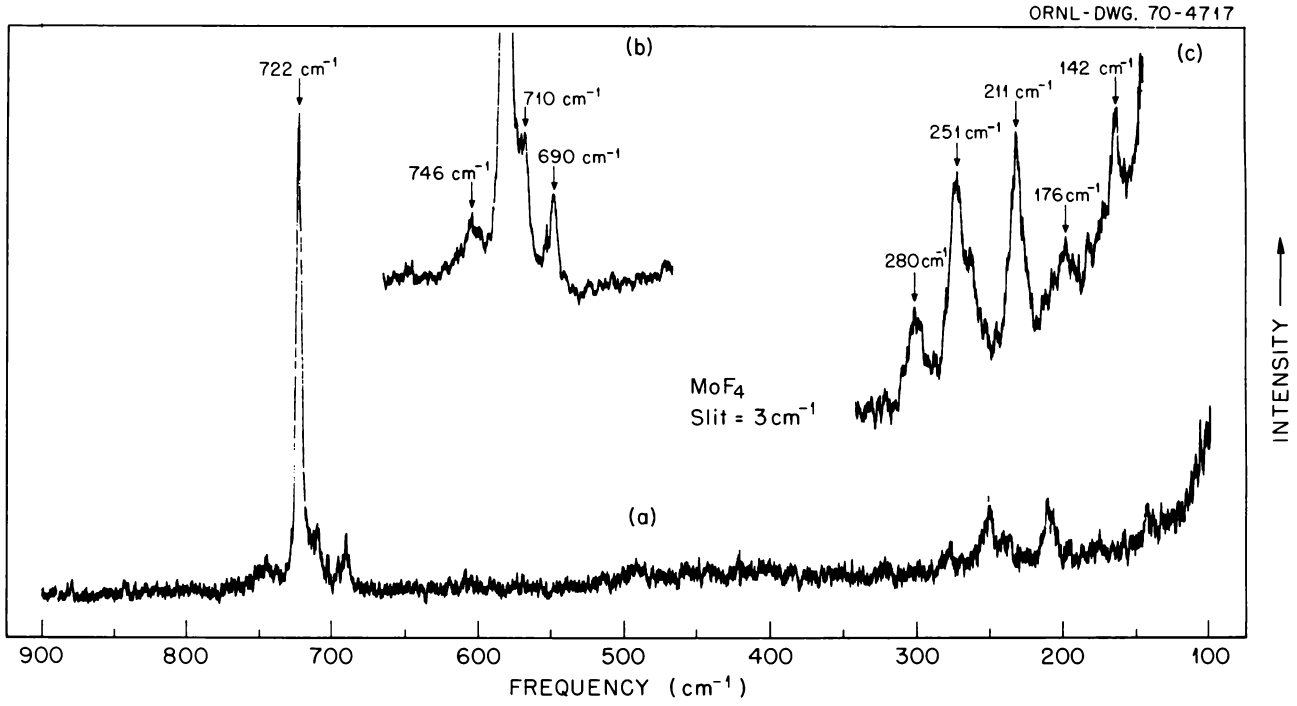

Fig. 7.20. Raman Spectrum of Crystalline MoF_4 at 298°K.

cm^{-1} may be due to external lattice phonons of the MoF_4 lattice, since these frequencies have about the magnitudes expected for librational motions of the MoF_4 tetrahedra.

Although the above assignment of the Raman spectrum of crystalline MoF_4 is only tentative, the reported spectrum can be used to identify MoF_4 in samples of unknown composition. Since our measurements were made on samples of MoF_4 contained in a thick-walled quartz reaction flask, it should be possible to follow the reaction leading to the formation of MoF_4 (and to other fluorides of molybdenum) by continuously measuring the Raman spectrum of the products formed during the course of the reaction.

[1]Samples of MoF_4 were supplied by C. F. Weaver and H. A. Friedman of the Reactor Chemistry Division.

RAMAN SPECTRUM OF POLYCRYSTALLINE MoF_5

John B. Bates

The Raman spectra of polycrystalline samples of MoF_5 were measured at 298°K (Fig. 7.21) and at about 100°K (Fig. 7.22) using the 4880-Å line of an argon laser as the exciting source. The spectrum measured at 298°K was obtained from a sample of crystalline MoF_5 sublimed onto the walls of a quartz reaction flask. This sample was produced in one of the steps in the process leading to the synthesis of MoF_3.[1] By measuring the Raman spectrum of MoF_5 in the reaction vessel, it was not necessary to interrupt the synthesis of MoF_3 at this stage.

A second sample[2,3] of polycrystalline MoF_5 sealed in a quartz tube having an optical flat at one end was

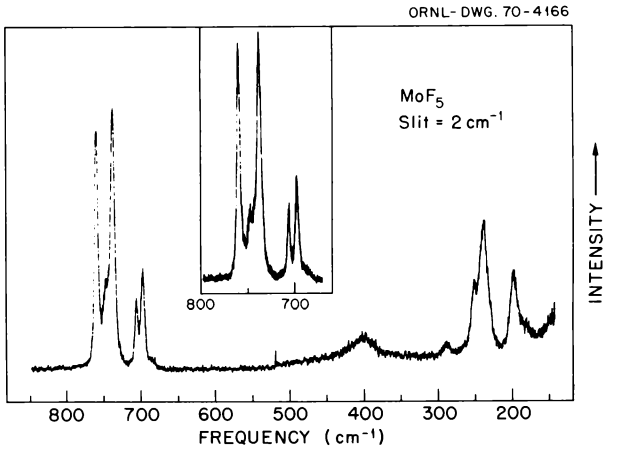

Fig. 7.21. Raman Spectrum of Crystalline MoF_5 at 298°K.

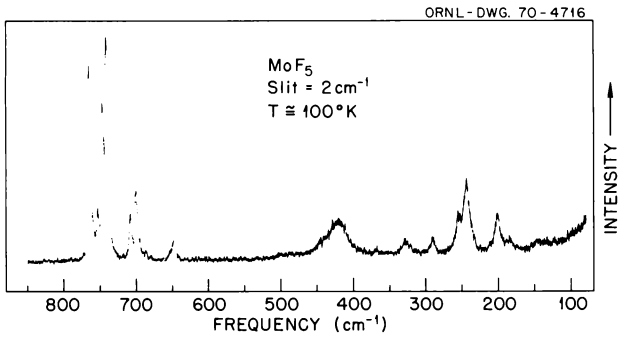

Fig. 7.22. Raman Spectrum of Crystalline MoF_5 at About 100°K.

secured to the brass tail section of a Raman cold cell.[4] Raman spectra of this sample were measured with the tail-section temperature at 77°K. Although a direct measurement was not possible, the temperature at the sample was estimated to be no lower than 100°K.

The Raman spectra of crystalline MoF_5 were interpreted on the basis of the crystal structure data of Edwards *et al.*,[5] in which it was found that the four molybdenum atoms in the primitive unit cell (C_{2h}) occupy two sets of nonequivalent sites. From the irreducible representation for the 69 optical modes of the MoF_5 lattice given by

$$\Gamma^{op}(C_{2h}) = 19A_g + 17B_g + 15A_u + 18B_u ,$$

it would appear that the 36 Raman-active modes would give rise to a complex Raman spectrum of crystalline MoF_5.

Comparison of the observed crystalline spectra with the Raman spectrum of liquid MoF_5[6] suggested an interpretation of the infrared[6] and Raman spectra[7] of crystalline MoF_5 based on two correlation schemes which map the D_{3h} point group of MoF_5 through the C_2 and C_s (nonequivalent) site groups onto the C_{2h} point group isomorphous to the crystallographic C_{2h} factor group. According to this interpretation each nondegenerate D_{3h} molecular mode of MoF_5 will give rise to two Raman-active A_g modes (components) in the crystal, the intensity of each crystal component being comparable with the intensity exhibited by the corresponding molecular mode in the spectrum of the liquid. Each doubly degenerate D_{3h} molecular mode of MoF_5 could exhibit four components in the Raman spectrum of the crystal, but, in the absence of strong correlation field coupling, it is likely that only two components for each of the degenerate modes would be observed.

The spectral activity and qualitative intensity predictions derived from the purely group theoretical analysis of the vibrational spectrum of crystalline MoF_5 are in good agreement with the experimental data (this work and ref. 6). The present analysis provides an alternative to the discussion by Beattie *et al.*[7] in which the vibrational spectra of crystalline NbF_5 and TaF_5, which are isostructural with crystalline MoF_5, were interpreted on the basis of a normal coordinate analysis of the tetrameric Mo_4F_{20} "super" molecule. The predicted intensities for the optical modes of crystalline MoF_5 which would follow from this latter analysis do not appear to agree with the observed intensities (this work and ref. 6).

---

[1] C. F. Weaver and H. A. Friedman, *MSR Program Semiann. Progr. Rept. Aug. 31, 1969,* ORNL-4449, pp. 114–15.

[2] This sample of MoF_5 was kindly supplied by G. M. Begun.

[3] A. C. Rutenberg, *Chem. Div. Ann. Progr. Rept. May 20, 1969,* ORNL-4437, pp. 46–47.

[4] J. B. Bates, "Multiple-Sampling Cold Cell for a Laser-Excited Raman Spectrophotometer," another contribution in this Section, this report.

[5] A. J. Edwards, R. D. Peacock, and R. W. H. Small, *J. Chem. Soc.* **1962**, 4486.

[6] T. J. Quellette, C. T. Ratcliffe, and D. W. A. Sharp, *J. Chem. Soc.* A **1969**, 2351.

[7] I. R. Beattie, K. M. S. Livingston, G. A. Ozin, and D. J. Reynolds, *J. Chem. Soc.* A **1969**, 958.

POLARIZED RAMAN SPECTRA OF SINGLE-CRYSTAL $NaBF_4$

John B. Bates

Measurements of the polarized Raman spectra of oriented single crystals of organic or inorganic compounds allow one to determine the symmetry type of each Raman-active crystal vibration and to study the contribution from each element of the polarizability tensor to the observed scattering. The additional information gained from polarized spectra of single crystals compared with that obtained from spectroscopic measurements made on the corresponding polycrystalline materials is analogous to the gain in information from x-ray diffraction experiments with single crystals rather than with the corresponding crystalline powder, although the difference is not as great in the spectroscopic case.

The polarized Raman spectra of an oriented single crystal of sodium tetrafluoroborate were measured in the internal mode region at 298 and 77°K. The faces of a single crystal[1] of $NaBF_4$ (orthorhombic), which had

been oriented by x-ray diffraction, were polished parallel to the (100), (010), and (001) crystallographic planes; the cell edges had lengths of 5, 2, and 2 mm parallel to the crystallographic *b*, *a*, and *c* axes respectively.

Polarized Raman spectra were measured using a Jarrell-Ash 25-300 spectrophotometer equipped with a Spectra-Physics model 141 argon ion laser. The room-temperature measurements were made on the single crystal mounted at the end of a goniometer and placed at the focus of the incident laser beam. The polarization of the incident radiation (4880 Å) was controlled by a half-wave plate inserted before the condensing lens, and the polarization of the scattered light was determined by a sheet of Polaroid film placed before the entrance slit of the monochromator. A 25-mm-focal-length camera lens was used to collect and collimate the scattered light, which was subsequently brought to a focus at the entrance slit by a 270-mm-focal-length achromatic lens. The aperture of the camera lens was stopped down to *f*/2.8 to minimize the solid angle of light collected. In measuring the polarized Raman spectrum of a single crystal, it is desirable to collect only those scattered light rays which are parallel to the optic axis of the monochromator (and hence parallel to a known crystal axis), since nonparallel (divergent) rays may become depolarized due to birefringence before leaving the crystal.[2,3] The result would be observed as anomalous depolarization ratios and the appearance of residual components. Minimizing the solid angle of light collected will reduce the magnitude of these errors in the observed spectrum.

A second single crystal of $NaBF_4$ was mounted with the (100) face held against the brass block of a Raman cold cell[4] and with the *b* axis parallel to the horizontal plane. Using liquid nitrogen as the coolant, the polarized Raman spectra of $NaBF_4$ were measured as described above. The scattered light in this case was collected by a 100-mm-focal-length camera lens stopped down to *f*/2.8.

At room temperature, $NaBF_4$ belongs to the orthorhombic system.[5,6] The space group was determined to be D_{2h}^{17} (*Cmcm*), and the primitive unit cell contains two BF_4^- ions located on C_{2v} sites.[5,6] Based on the known unit-cell structure, the irreducible representation for the 18 optically active internal modes arising from vibrations of the BF_4^- ions is given by

$$\Gamma^{int}(D_{6h}) = 4A_{1g} + B_{1g} + 2B_{2g} + 2B_{3g} + A_u + 4B_{1u} + 2B_{2u} + 2B_{3u} .$$

The correlation diagram given in Table 7.11 shows the origin of the internal modes of the lattice that are derived from the nine vibrational modes of the isolated tetrahedral BF_4^- ion described by

$$\Gamma(T_d) = A_1 + E + 2F_2 .$$

The results of the polarization measurements are shown in Figs. 7.23 and 7.24 and are summarized in Table 7.12. The notation labeling the different scattering geometries of Figs. 7.23 and 7.24 indicates which element of the crystal polarizability tensor is respon-

Table 7.11. Correlation Diagram for $NaBF_4$

	Molecular Group, T_d	Site Group, $C_{2v}(z)$	Factor Group,[a] D_{2h}	
			A_g	a^2, b^2, c^2
$x^2 + y^2 + z^2$	A_1	A_1	B_{1g}	ac
	A_2	A_2	B_{2g}	bc
$(2z^2 - x^2 - y^2, x^2 - y^2)$	E		B_{3g}	ab
	F_1	B_1	A_u	
x, y, z	F_2	B_2	B_{1u}	b
(xy, xz, yz)			B_{2u}	a
			B_{3u}	c

[a]The *b* axis is unique in the $NaBF_4$ structure, so that $x = c$, $y = a$, and $z = b$ in determining the symmetry of vector or tensor components in the D_{2h} group.

sible for the observed spectrum.[7] Thus, *c(ab)a* indicates that the incident radiation is directed parallel to the *c* axis and polarized parallel to the *a* axis and that the scattered light is collected parallel to the *a* axis and analyzed parallel to the *b* axis.

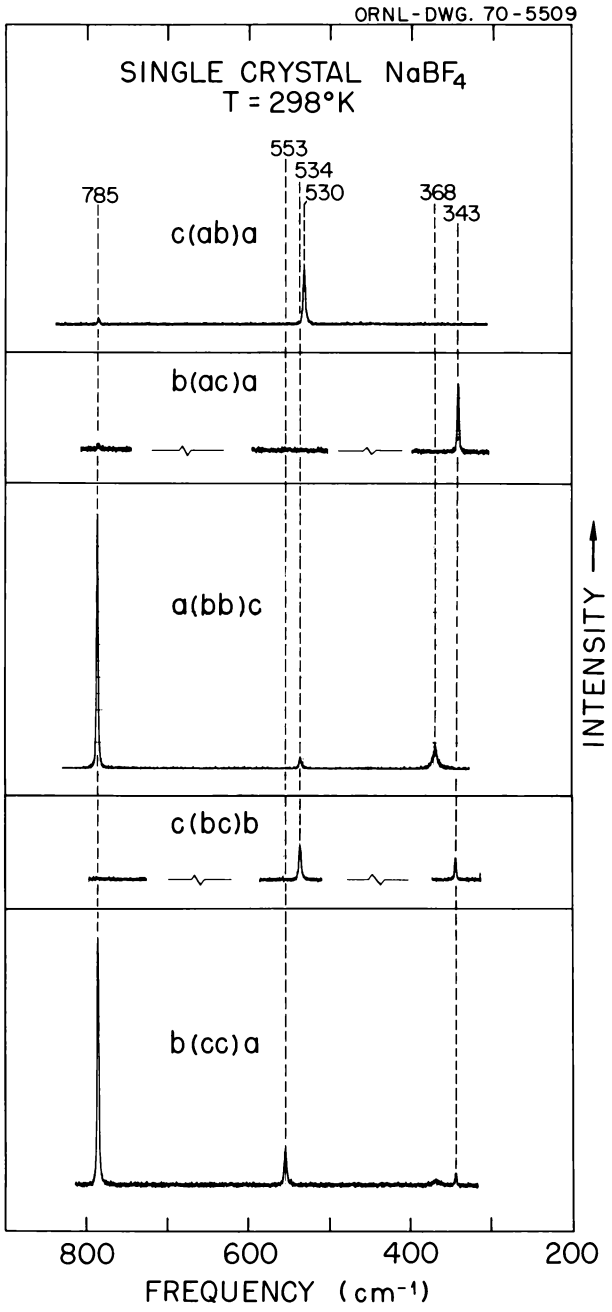

Fig. 7.23. Polarized Raman Spectra of Single-Crystal $NaBF_4$ Measured at 298°K.

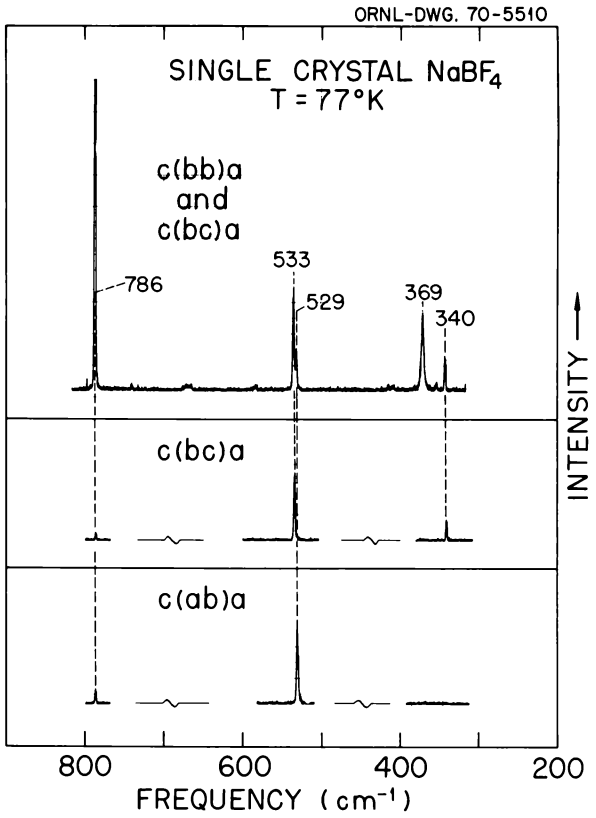

Fig. 7.24. Polarized Raman Spectra of Single-Crystal $NaBF_4$ Measured at 77°K.

Table 7.12. Frequencies and Assignments from the Polarized Raman Spectra of Single-Crystal $NaBF_4$ Measured at 298°K

Mode	Frequency (cm^{-1})			
	A_g	B_{1g}	B_{2g}	B_{3g}
ν_1 (A_1)	785			
ν_2 (E)	368	343		
ν_3 (F_2)	[1111][a]		[1111][a]	1049
ν_4 (F_2)	553		534	530

[a]Polarization measurements of these components are uncertain due to the weakness of these bands.

From the polarization measurements described above, an unambiguous assignment can be made for the Raman-active correlation field components of the vibrational modes of the BF_4^- ion. The crystal structure data for $NaBF_4$ suggest that the *ac* plane is nearly isotropic; this is reflected in the small splitting observed between the B_{2g} and B_{3g} components of the F_2 modes (Table 7.12). Also, because the $NaBF_4$ crystal is nearly optically uniaxial (pseudotetragonal or pseudocubic), depolarization of the incident and scattered radiation

may occur along one of the crystal axes, which would result in the appearance of residual (i.e., theoretically forbidden) components in the Raman spectrum for certain orientations. Indeed, as can be seen in Figs. 7.23 and 7.24, residual components do appear in several of the polarized spectra. However, additional factors such as small errors in crystal alignment or crystal imperfection (mosaic spread) can also be responsible for the appearance of residual components.

The Raman spectra of $NaBF_4$ at 77°K (Fig. 7.24) were nearly identical to the room-temperature spectra, indicating that no phase change occurs at this temperature. Only slight frequency shifts from the room-temperature measurements were observed, and no additional features appeared in the spectra.

[1]Crystals of $NaBF_4$ were kindly supplied by L. O. Gilpatrick, Reactor Chemistry Division.

[2]S. P. S. Porto, J. A. Giordmain, and T. C. Damen, *Phys. Rev.* **147**, 608 (1966).

[3]J. B. Bates, D. M. Thomas, A. Bandy, and E. R. Lippincott, *Spectrochim. Acta*, to be published.

[4]J. B. Bates, "Multiple-Sampling Cold Cell for a Laser-Excited Raman Spectrophotometer," another contribution in this Section, this report.

[5]A. Weiss and K. Zohner, *Phys. Status Solidi* **21**, 257 (1967).

[6]G. Brunton, *Acta Cryst.* **B24**, 1703 (1968).

[7]T. C. Damen, S. P. S. Porto, and B. Tell, *Phys. Rev.* **142**, 570 (1966).

THE RAMAN SPECTRA OF LIQUID AND GASEOUS H_2O AND D_2O AT ELEVATED TEMPERATURES AND PRESSURES

Arvin S. Quist

The Raman spectra of water, both in the liquid and vapor states, have been measured at saturation vapor pressures to the critical temperature, 374°C. Additional measurements have been made to temperatures of 601° on a sample held at a constant density of 0.11 g/cm^3. Similar data on D_2O have been obtained to 436°.

For these measurements the liquids were contained in sealed thick-walled (8 mm o.d., 2 mm i.d.) quartz or Pyrex capillary tubes. Pyrex tubes were satisfactory to temperatures slightly above 300°, at which point they began to be severely attacked by water. The quartz tubes were much more resistant to corrosion; in the experiments where the water density was maintained at 0.11 g/cm^3, no visible attack occurred even at 601°. However, with both types of tubes, sudden failures sometimes occurred.

Special techniques were developed by the ORNL Glass Shop to seal one end of these tubes so that the inner and outer surfaces were essentially flat, parallel, and optically transparent. Each tube, after filling with the required amount of liquid, was sealed (by fusion) under vacuum, and the extra length was removed. Final lengths of the sealed tubes ranged from 1.5 to 2 in.

For the measurements at elevated temperatures, the tubes were inserted vertically into the center of a high-temperature furnace described elsewhere.[1] The 4880-Å laser beam entered the flat end of each tube and passed through its entire length. The scattered light, either from the liquid, vapor, or supercritical fluid, was collected at 90° from the incident beam through a quartz window in the furnace. Collection and focusing of the Raman scattered radiation was accomplished by the same optical arrangement as described in ref. 1.

The Raman bands of water of greatest interest in this study are those from approximately 3200 to 3700 cm^{-1}. The spectra of the liquid in this wavelength region at temperatures from 25 to 373° are presented in Fig. 7.25. The most noticeable features are the rapid decrease in the intensity of the 3250-cm^{-1} shoulder with increasing temperature and the shift in the position of the band maximum from approximately 3420 cm^{-1} at 25° to approximately 3590 cm^{-1} at 373°.

The spectrum of water vapor consists of a single peak, occurring at 3657 cm^{-1} at room temperature[2] and decreasing to approximately 3600 cm^{-1} at the critical temperature and pressure. When this peak was studied at a constant density of 0.11 g/cm^3 from 350° (where the density of the vapor in equilibrium with the liquid is 0.11 g/cm^3) to 601°, the frequency at which the maximum occurred remained essentially invariant, changing only from 3638 to 3634 cm^{-1}. This result is shown in Fig. 7.26, where the wave number of the maximum intensity for the liquid, vapor, and supercritical fluid is plotted vs temperature from 25 to 601°. The peak was somewhat asymmetrical, but the asymmetry decreased with increasing temperature.

Deuterium oxide showed qualitatively the same spectral changes with varying temperature and density as did water. Further experiments on H_2O, D_2O, and their mixtures are continuing. Interpretation of these spectra will be presented when data over a wider range of conditions have been gathered.

[1]A. S. Quist, "A Furnace for Molten-Salt Raman Spectroscopy to 800°C," another contribution in this Section, this report.

[2]W. S. Benedict, N. Gailar, and E. K. Plyer, *J. Chem. Phys.* **24**, 1139 (1956).

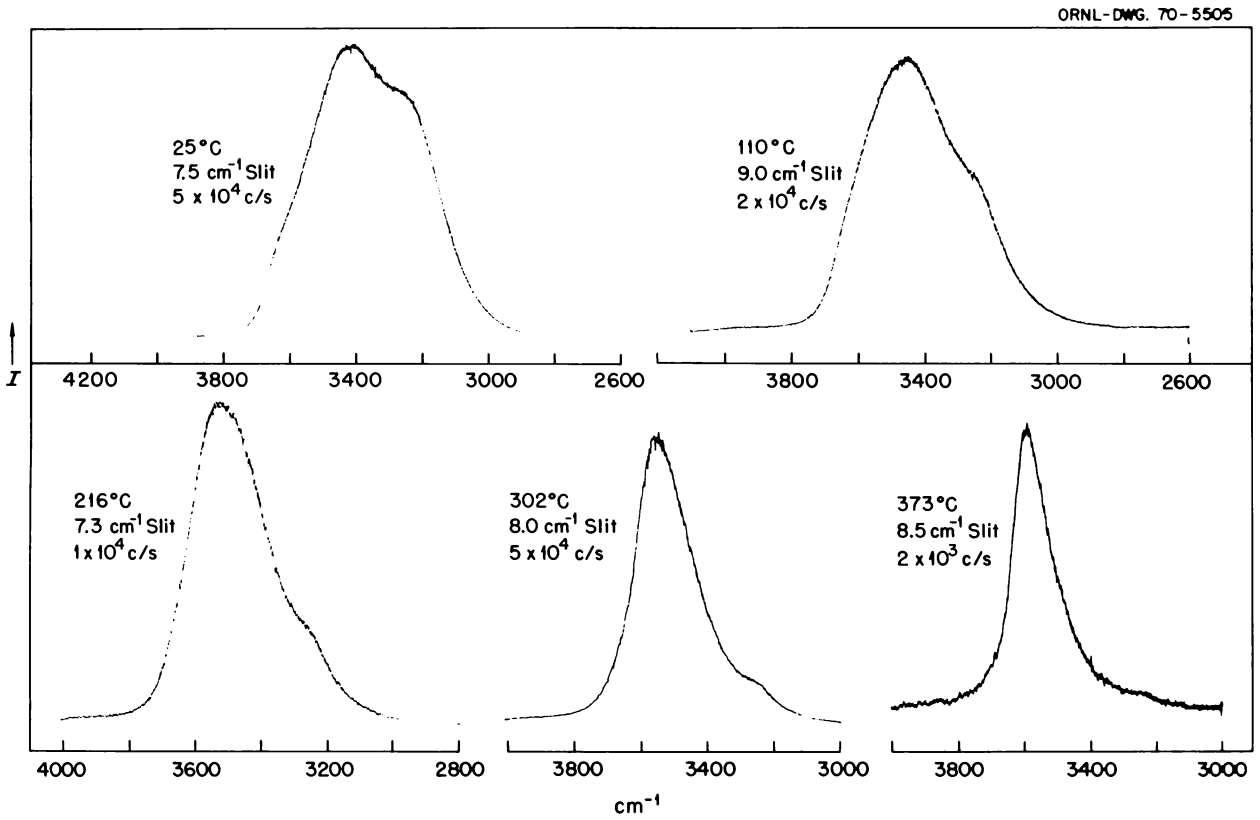

Fig. 7.25. Raman Spectra of Liquid Water at Saturation Vapor Pressure to 373°C.

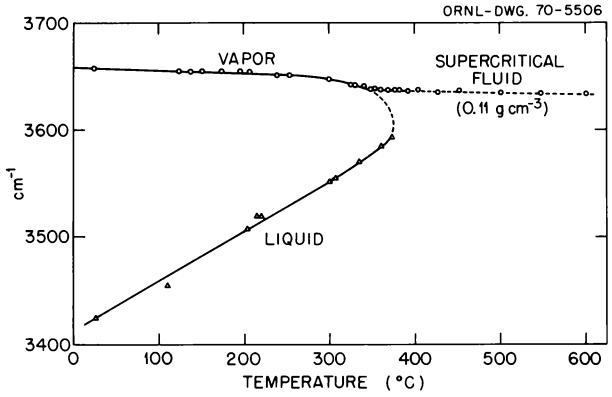

Fig. 7.26. Frequency of the Band Maximum for Liquid and Gaseous Water as a Function of Temperature.

RAMAN SPECTRUM OF MOLTEN $NaNO_3$[1]

M. H. Brooker[2] Arvin S. Quist G. E. Boyd

The Raman spectrum of molten sodium nitrate has been recorded (Table 7.13). Lifting of the degeneracies of the ν_3 (E') and ν_4 (E') modes in molten sodium nitrate was observed and compared with similar effects in aqueous nitrate solutions. A single broad band *ca.* 115 cm^{-1} was attributed to an external lattice-like vibration. The vibrational spectrum of molten sodium nitrate is consistent with a semiordered array of ions in which the NO_3^- ions occupy sites of low symmetry. Local order in the melt may resemble the arrangement of ions found in a particular crystal structure, but the Raman spectrum does not present sufficient information to justify the complete factor group representation proposed by other workers.[3,4]

---

[1] Expanded abstract of paper in *Chem. Phys. Letters* 5, 357 (1970).

[2] Visiting scientist; National Research Council of Canada Postdoctoral Fellow, 1969–70.

[3] K. Williamson, P. Li, and J. P. Devlin, *J. Chem. Phys.* 48, 3891 (1968).

[4] D. W. James and W. H. Leong, *J. Chem. Phys.* 51, 640 (1969).

Table 7.13. Vibrational Frequencies (cm^{-1}) of Molten $NaNO_3$

Raman, This Work,[a] $T = 336°C$	Raman, Ref. 3		Infrared, Ref. 4, $310°C < T < 350°C$
	315°C	360°C	
115 dp (~30 cm^{-1})	~125	140	
	170		
719 dp	718	722 dp	
732 dp			
828 (~20 cm^{-1})			825
			833
			1033
1057 P (17 cm^{-1})	1063	1055 P	1047
1365 P? (60 cm^{-1})			1345
	1398	1398 dp	1390
1420 dp (90 cm^{-1})			1430
1656 P (17 cm^{-1})			

[a]dp, depolarized line; P, polarized line. Bandwidth at half height given in parentheses. Vibrational frequencies showed no significant temperature-dependent variations.

RAMAN SPECTRA OF SOLID AND MOLTEN BeF_2 AND Li_2BeF_4

Arvin S. Quist John B. Bates G. E. Boyd

The solvent for fissile and fertile materials in the molten-salt breeder reactor will probably be a mixture of LiF and BeF_2 with a BeF_2:LiF ratio somewhat less than the composition Li_2BeF_4. However, a melt with the composition Li_2BeF_4 is a possible choice for use as a flush salt and/or as a coolant for future molten-salt reactors. Therefore it is of some importance in establishing a basic understanding of these high-temperature systems to attempt to measure the vibrational spectra of the beryllium-fluorine complexes which may exist in molten LiF-BeF_2 mixtures, not only to gain information on the species that may be present, but also to characterize the bands caused by beryllium-fluorine interactions so that these can be identified in systems containing other complex ions (such as fission product fluorides) dissolved in this solvent.

Raman spectra of molten Li_2BeF_4 have been obtained to 640°C. The melt was contained in windowless nickel cells of the type described elsewhere for these measurements.[1] Sample illumination was performed with the 4880-Å line of a Spectra Physics model 141 argon ion laser. The furnace and optical system also have been described[2] and were used in conjunction with a Jarrell-Ash model 25-300 Raman spectrometer. A typical Raman spectrum for molten Li_2BeF_4 at 533° is shown in Fig. 7.27.

The Raman spectrum of solid BeF_2 was measured from room temperature to its melting point (555°) with the equipment described. For these studies a hand-picked piece of BeF_2 glass approximately 5 mm in height and roughly triangular in cross section was contained in a sealed quartz tube (8 mm o.d., 6 mm i.d.) having a quartz window fused to one end. The spectrum of BeF_2 glass at 25° is presented in Fig. 7.28. The maximum of the most intense band appeared to be near 280 cm^{-1}. Weaker components were observed at approximately 205, 395, and 440 cm^{-1}. The spectrum did not change significantly until devitrification occurred at temperatures near 280°. After devitrification, the observable Raman spectrum contained only a single peak, which was centered near 345 cm^{-1}. Only this single band was observed as the temperature was increased to the melting point of BeF_2. The Raman spectrum of molten BeF_2 has not yet been measured.

It is clear from the observations thus far reported that the present information regarding the vibrational spectra of molten Li_2BeF_4 and solid BeF_2 is far from complete. Definite conclusions regarding the structure of beryllium fluoride melts (based only on spectroscopic evidence) therefore cannot be made at this time. However, comparison of the Raman spectrum of molten Li_2BeF_4 with that of molten $NaBF_4$[3] suggests the following provisional interpretation of the Li_2BeF_4

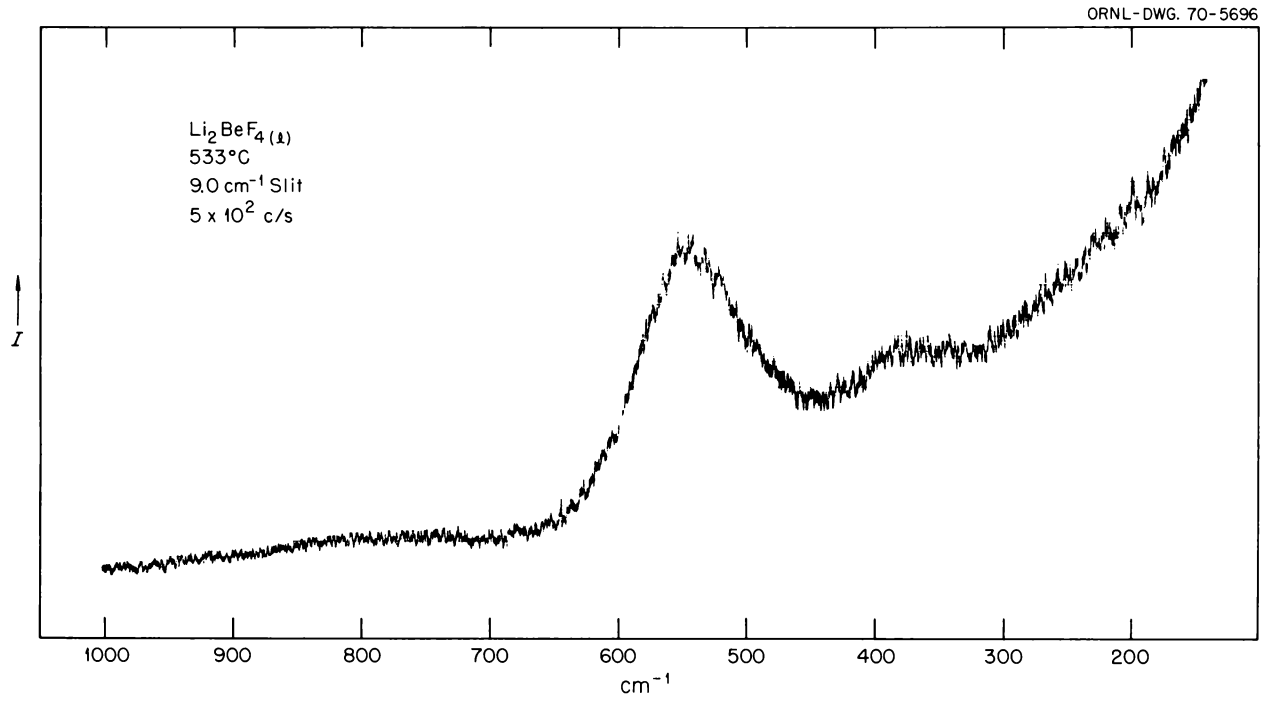

Fig. 7.27. Raman Spectrum of Molten Li_2BeF_4 at 533°C.

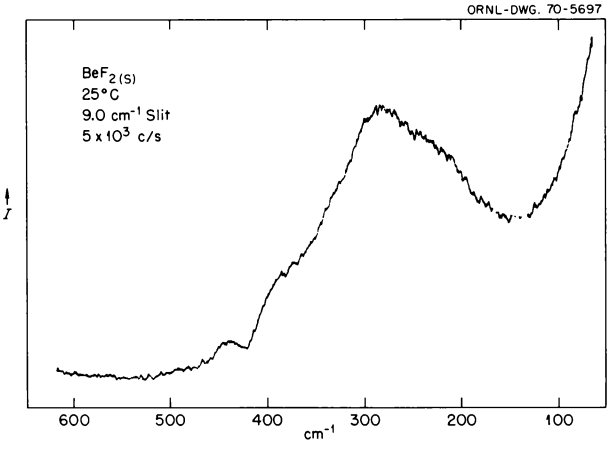

Fig. 7.28. Raman Spectrum of BeF_2 Glass at 25°C.

spectrum, assuming tetrahedral coordination of beryllium in the melt: The strong band observed at ~550 cm^{-1} is the totally symmetric stretching mode. The broad, weak band centered at about 800 cm^{-1} is an asymmetric stretching mode, and the band at 390 cm^{-1} is assigned to a bending mode. A change in the slope of the background scattering between 170 and 300 cm^{-1} (Fig. 7.27) indicates the presence of a weak band with a center estimated to occur at about 240 cm^{-1}. This band also can be assigned to a bending mode.

If the above assignment of the band observed at 550 cm^{-1} to the symmetric beryllium-fluorine stretching mode is correct, then it can be argued that, although beryllium may be tetrahedrally coordinated in molten Li_2BeF_4, each fluorine atom is bicoordinated with two beryllium atoms. By using the ratio of the boron-fluorine and beryllium-fluorine force constants as calculated from the vibrational frequencies observed for diatomic boron-fluorine and beryllium-fluorine[4] and assuming this ratio holds for the tetrahedral species, BF_4^- and BeF_4^{2-}, a value of 670 cm^{-1} was computed for the totally symmetric stretching mode of BeF_4^{2-} based on the value of 779 cm^{-1} observed for ν_1 (A_1) in molten $NaBF_4$.[3] This computed frequency for ν_1 (A_1) of free BeF_4^{2-} ion is probably 10% too low, but the result indicates that the band observed at 550 cm^{-1} in molten Li_2BeF_4 is far below what we expected for the ν_1 mode of free BeF_4^{2-} ions. The lower observed frequency, however, can be explained by allowing bicoordination of the fluorine atoms: sharing fluorine atoms between two beryllium atoms would weaken the beryllium-fluorine bond and hence result in a lowering of the frequencies of the beryllium-fluorine stretching modes. Thus although the spectroscopic studies (and,

consequently, the theoretical interpretation) are not complete and definite conclusions cannot be made at this time, our results indicate that an important feature of a model for molten Li_2BeF_4 will include tetrahedral coordination of the beryllium atoms and bicoordination of the fluorine atoms.

[1] A. S. Quist, "A Windowless Cell for Laser Raman Spectroscopy of Molten Fluorides," another contribution in this Section, this report.

[2] A. S. Quist, "A Furnace for Molten-Salt Raman Spectroscopy to 800°C," another contribution in this Section, this report.

[3] A. S. Quist, J. B. Bates, and G. E. Boyd, "Raman Spectra of Molten $NaBF_4$ to 556°C," following contribution, this report.

[4] G. Herzberg, *Spectra of Diatomic Molecules*, Van Nostrand, New York, 1950.

RAMAN SPECTRA OF MOLTEN $NaBF_4$ TO 556°C

Arvin S. Quist John B. Bates G. E. Boyd

Possible use of molten NaF-$NaBF_4$ mixtures as a low-melting, low-cost coolant for a molten-salt breeder reactor has led to an interest in obtaining an understanding of the properties of this system. The characteristic vibrational spectrum of the BF_4^- ion in these melts has not been obtained until now, primarily because these molten salts rapidly attack the usual optical window materials. However, the recent development of a windowless cell for use in molten-salt Raman spectroscopy has led to successful measurements of the Raman spectrum of molten $NaBF_4$ to 556°C.

Although Raman scattering measurements with polycrystalline $NaBF_4$ have been published,[1] the recent availability of Raman spectrometers designed for use with stable, intense laser light sources has made it possible to obtain a spectrum of the solid material which reveals much more detail than was previously observed. A spectrum of polycrystalline $NaBF_4$,[2] contained in a melting-point glass capillary near 25°, is presented in Fig. 7.29. The sample was illuminated with 4880-Å light from a Spectra Physics model 141 argon ion laser; the scattered light was collected and collimated by a 25-mm-focal-length $f/0.95$ camera lens and focused onto the entrance slit of a Jarrell-Ash model 25-300 Raman spectrometer by a 270-mm-focal-length achromatic lens.

For the measurements on liquid $NaBF_4$, the melt was contained in nickel windowless cells of the type described previously.[3] The resistance-heated furnace and the optics for collecting the Raman-scattered light have also been described.[4] Data were collected from a few degrees above the melting point (408°) to 556°, at which point surface-tension forces were no longer able to contain the melt within the cell. A typical Raman spectrum of molten $NaBF_4$ is presented in Fig. 7.30.

The frequencies of the bands observed in the Raman spectrum of molten $NaBF_4$ at 437°C and in the Raman spectrum of polycrystalline $NaBF_4$ at 25°C are collected in Table 7.14. The tetrahedral BF_4^- ion has four normal modes of vibration, all of which are Raman

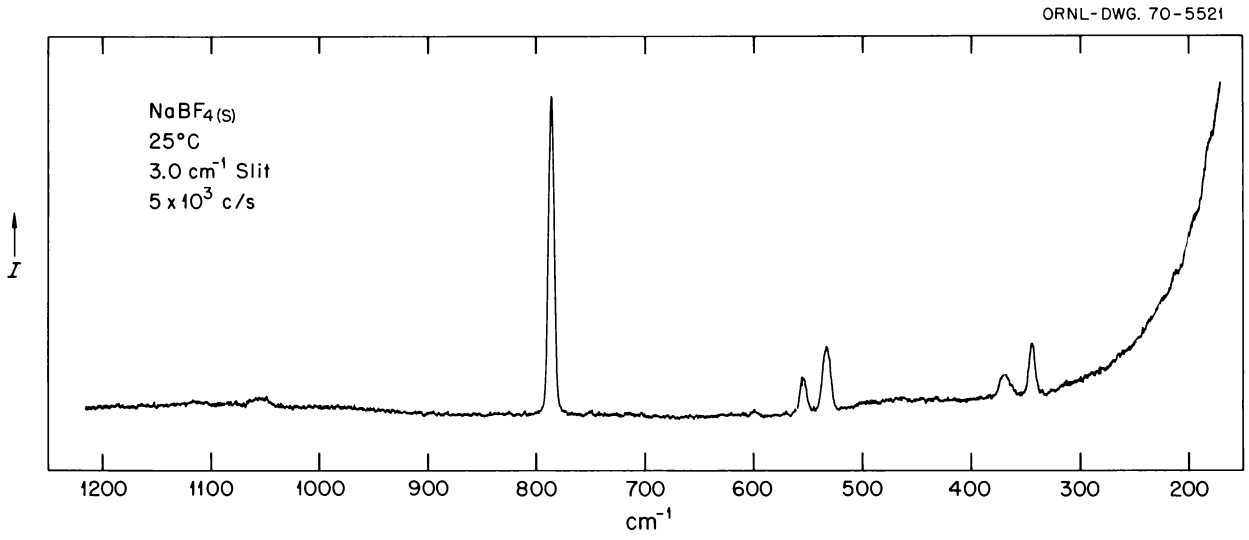

Fig. 7.29. Raman Spectrum of Polycrystalline $NaBF_4$ at 25°C.

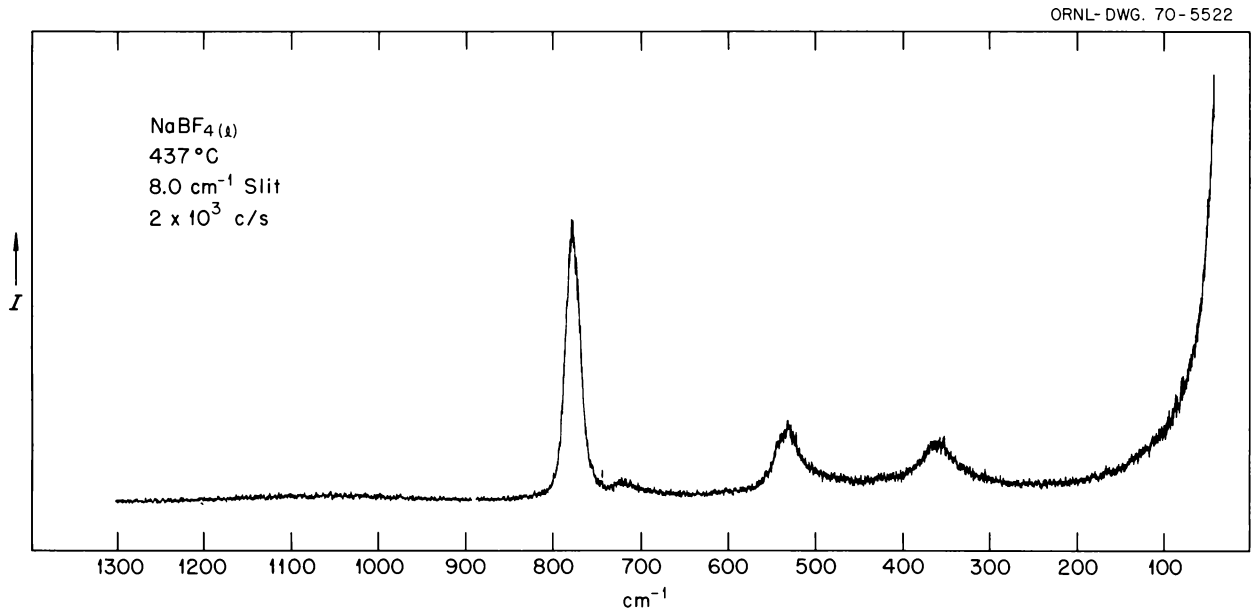

Fig. 7.30. Raman Spectrum of Molten $NaBF_4$ at 437°C.

Table 7.14. Bands Observed in the Raman Spectra of Molten $NaBF_4$ at 437°C and Polycrystalline $NaBF_4$ at 25°C

Frequency (cm^{-1})		Assignment
Melt (437°C)	Polycrystalline (25°C)	(T_d Symmetry)
1075	1090, 1056	ν_3 (F_2)
779	786	ν_1 (A_1)
720		$\nu_3 - \nu_2$ or impurity (?)
535	554, 533	ν_4 (F_2)
362	369, 343	ν_2 (E)

active. The totally symmetric stretching mode, ν_1 (A_1), was observed at 786 cm^{-1} in the polycrystalline solid (25°C) and at 779 cm^{-1} in the spectrum of the melt at 437°C. As the temperature of the melt increases, the ν_1 peak appears to shift slightly to lower frequencies, occurring at 775 cm^{-1} at 556°C. However, a weak band appears on the low-frequency side of ν_1 in the melt spectrum, and its apparent increase in intensity with increase in temperature could be responsible for the apparent shift in the band maximum of ν_1. This weak band, which occurs at about 720 cm^{-1} in the spectrum of the melt at 437°C (Table 7.14), may be due to $\nu_3 - \nu_2$ since an increase in the intensity with increasing temperature is characteristic of a difference tone. It may also be due, however, to an impurity in the melt.

The ν_2 (E) and ν_4 (F_2) bending modes of BF_4^- were observed at 362 and 535 cm^{-1}, respectively, in the spectrum of the melt at 437°C (Table 7.14). These modes were observed to split into two components each in the spectrum of polycrystalline $NaBF_4$ (Table 7.14). The crystal structure of $NaBF_4$ belongs to the D_{2h}^{17} space group[5] with two BF_4^- ions located on C_{2v} sites in the primitive cell. Thus the BF_4^- vibrations give rise to the following Raman-active components in the lattice: $A_1 \rightarrow A_g$, $E \rightarrow A_g + B_{1g}$, and $F_2 \rightarrow A_g + B_{2g} + B_{3g}$. We can expect to observe, then, two components for the ν_2 (E) mode and three components for the ν_4 (F_2) mode. As discussed above, two components were observed for each of these modes in the Raman spectrum of polycrystalline $NaBF_4$; the third component for ν_4 (F_2) was either too weak to be observed under the present experimental conditions or it was accidentally coincident with one of the other two observed components.

The ν_3 (F_2) asymmetric stretching mode of BF_4^- appeared in the Raman spectrum of the melt as a broad, weak band centered at about 1075 cm^{-1} (Fig. 7.30). In the spectrum of the polycrystalline solid, two components were observed for ν_3 at 1090 and 1056 cm^{-1}. As discussed above for the ν_4 (F_2) mode, the third Raman-active component of ν_3 is either too weak to be observed under the present experimental conditions or

the frequency is accidentally coincident with one of the observed frequencies of the other two components.

Both the number of frequencies and intensities of the bands observed in the Raman spectrum of molten $NaBF_4$ (Fig. 7.30 and Table 7.14) are entirely consistent with a tetrahedral structure for the BF_4^- ion in the melt. This result is particularly important in view of the spectroscopic measurements of the beryllium fluoride-containing melts described elsewhere in this report,[6] because it establishes trends for spectral behavior whenever the dominant species in a melt is a free tetrahedral fluoride-containing anion.

---

[1] J. Goubeau and W. Bues, *Z. Anorg. Allgem. Chem.* **268**, 221 (1952).

[2] Supplied by L. O. Gilpatrick of the Reactor Chemistry Division.

[3] A. S. Quist, "A Windowless Cell for Laser Raman Spectroscopy of Molten Fluorides," another contribution in this Section, this report.

[4] A. S. Quist, "A Furnace for Molten-Salt Raman Spectroscopy to 800°C," another contribution in this Section, this report.

[5] G. Brunton, *Acta Cryst.* **B24**, 1703 (1968).

[6] A. S. Quist, J. B. Bates, and G. E. Boyd, "Raman Spectra of Solid and Molten BeF_2 and Li_2BeF_4," preceding contribution, this report.

DYNAMICS OF A POLYMER MODEL FOR MOLTEN Li_2BeF_4: SOME PRELIMINARY RESULTS

John B. Bates

The importance of polymeric structures for interpreting the thermodynamic properties of BeF_2 melts has recently been discussed by C. F. Baes, Jr.[1] The polymeric models considered in this work were based on tetrahedrally coordinated beryllium atoms which are bridged through bicoordinated fluorine atoms to produce a large number of anionic Be_aF_b species. In particular, assuming that beryllium remains fully four-coordinated in the melt, it was concluded in ref. 1 that the Be_nF_{2n+2} chain structures involving shared tetrahedral edges were especially important in melts of high BeF_2 content such as $LiF\text{-}BeF_2$.

In view of the foregoing hypothesis and the current investigations of the Raman spectra of Li_2BeF_4 melts, we have calculated the vibrational spectrum of the Be_nF_{2n+2} polymer assuming the chain length n to be sufficiently large that the effects of end groups can be neglected. The initial calculations were intended to test the assignments proposed for the observed Raman spectrum of molten Li_2BeF_4[2] and, conversely, to test the suitability of the polymeric model in describing the vibrational spectrum of the Li_2BeF_4 melt.

The theory and methods used in calculating the optically active vibrations of the Be_nF_{2n+2} polymer (where n is assumed to be infinitely large) have been described elsewhere.[3] The lattice (polymer) potential function is approximated by a modified valence force field in which the diagonal elements of the matrix are the force constants for the internal coordinates, and the off-diagonal elements are the interaction constants between pairs of internal coordinates. Figure 7.31 shows a segment of the Be_nF_{2n+2} polymer with the primitive unit cell (primitive repeating unit for the polymer) indicated by the dashed outline. The lattice has D_{2h} symmetry; there are two beryllium atoms and four fluorine atoms in the unit cell (Fig. 7.31), and the irreducible representation for the 15 optical modes of the lattice is given by

$$\Gamma^{op}(D_{2h}) = 3A_g + 2B_{1g} + 2B_{2g} + 2B_{3g} + 2B_{1u} + 2B_{2u} + 2B_{3u} .$$

The frequencies for the optically active vibrations of the Be_nF_{2n+2} polymer are obtained from the eigenvalues λ_i of $|G^{op}F^{op} - \lambda E| = 0$, where E is the identity matrix and where G^{op} and F^{op} are given by

$$G^{op}_{tt'} = \sum_{i=1}^{3n} m_i^{-1} B^{op}_{tt'} B^{op}_{t'i}$$

and

$$F^{op}_{uv} = \sum_{l=0} F^{l}_{uv} = \sum_{l=0} \sum_{uvw} Z^{l}_{uvw} \phi^{l}_{w} .$$

In these equations, B^{op} is the optically active B matrix and is defined by

$$B^{op}_{ti} = \sum_{l=0} B^{l}_{ti} ,$$

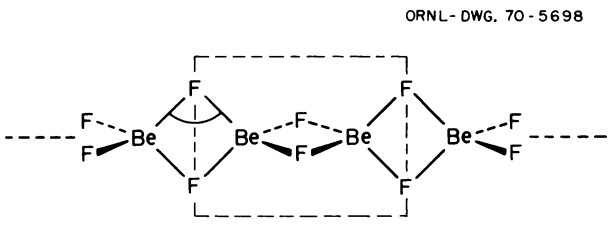

Fig. 7.31. Polymer Model for Molten Li_2BeF_4.

in which the B^l_{ti} are the B matrix elements relating Cartesian displacement coordinates ϵ_i for masses m_i to the internal displacement coordinates, S_t, by the equation

$$S_t = \sum_{l=0} \sum_{i=1}^{3n} B^l_{ti} \epsilon^l_i , \quad t = 1, \ldots 3n ,$$

where n is the number of atoms per primitive cell and the sum over l includes all primitive cells containing atoms involved in defining the internal coordinate S_t. In computing the optically active force-constant matrix, F^{op}, ϕ^l is a one-dimensional array containing valence and interaction constants for the lth cell, and Z^l is the constraint matrix for the lth cell.[3]

The results of the calculation are given in Table 7.15. Only the calculated frequencies corresponding to those bands observed in the Raman spectrum of molten Li_2BeF_4 are given, along with force constants obtained from a least-squares fit of the observed and calculated frequencies. The good agreement between the observed and calculated frequencies for the three modes given in Table 7.15 suggests that the assignment of the Raman spectrum given in another contribution to this report[2] is at least tenable on the basis of a polymeric model for molten Li_2BeF_4. The low value of the beryllium-fluorine stretching force constant and the relatively large stretch-stretch interaction constant (for beryllium-fluorine bonds joined to a common beryllium atom) were expected in view of the bicoordinated fluorine atoms. (For comparison, the value of the hydrogen-fluorine force constant is about 80% lower in the symmetric F-H-F$^-$ ion as compared with the free H-F value.[3]) In addition, as the concentration of BeF_2 increases, the effects due to fluorine bicoordination should become more apparent in the Raman spectrum of molten LiF-BeF_2.

Table 7.15. Calculated Frequencies and Force Constants for Three Optical Modes of the Be_nF_{2n+2} Polymer, and Comparison with Experimental Results

Frequency (cm^{-1})		Assignment
Observed[2]	Calculated	
800	800	Asymmetric Be-F stretch
550	550	Symmetric Be-F stretch
390	390	FBeF bend
	Force Constants	
$F_{Be\text{-}F}$	2.10 mdyn/Å	
$F^1_{Be\text{-}F,\ Be\text{-}F}$	0.17 mdyn/Å (interaction of bonds joined to a common Be atom)	
$H_{F\diagup Be\diagdown F}$	0.54 mdyn-Å/rad^2 (bend between bridging F atoms)	

[1] C. F. Baes, Jr., *J. Solid State Chem.* **1**, 159 (1970).

[2] A. S. Quist, J. B. Bates, and G. E. Boyd, "Raman Spectra of Solid and Molten BeF_2 and Li_2BeF_4," another contribution in this Section, this report.

[3] J. B. Bates, E. R. Lippincott, Y. Mikawa, and R. J. Jakobsen, *J. Chem. Phys.* **52**, 3731 (1970).

A FURNACE FOR MOLTEN-SALT RAMAN SPECTROSCOPY TO 800°C

Arvin S. Quist

A vacuum-tight furnace was designed and constructed for use in measuring the Raman spectra of molten salts to 800°C. This furnace was intended for use in the cell compartment of a Jarrell-Ash model 25-300 laser Raman spectrometer (Jarrell-Ash Company, Waltham, Massachusetts), but it could also be easily adapted for use with other laser Raman systems.

The basic features of this furnace are the same as have been described earlier for use in absorption spectrophotometric studies of molten fluoride salts.[1-3] Major modifications to these previously described furnaces include (1) changing the position of one of the two side windows to the top of the furnace to permit entry of the laser beam, (2) use of cartridge heaters (Watlow, Saint Louis, Missouri) in place of platinum-wire heaters, and (3) use of a bellows assembly to connect the side window to the main body of the furnace. The main features of the present high-temperature furnace assembly are shown in Fig. 7.32.

Twelve ¼-in.-diam cartridge heaters are arranged symmetrically in U-shaped grooves milled in the cylindrical nickel furnace body. Three 2-in.-long heaters are positioned under the viewing port in the side of the nickel body; the other nine cartridge heaters are each 3½ in. long. Maximum output of the 12 120-V heaters is 2100 W. The control Chromel-Alumel thermocouple, connected to a proportional temperature regulator, is positioned in a hole drilled in the nickel furnace body in the side opposite to the viewing port at a point approximately ⅛ in. equidistant from two heaters.

The molten salt whose Raman spectrum is to be measured is held in its container in a cylindrical silver block which fits inside the nickel furnace body. An

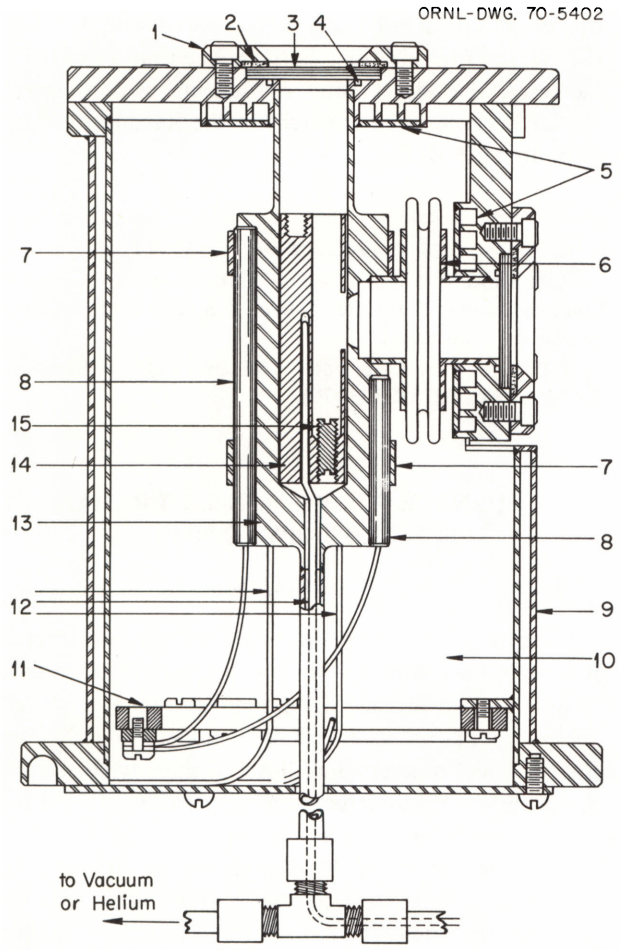

Fig. 7.32. Schematic Cross Section of Furnace. (1) Window flange, (2) Viton window pad, (3) quartz window, (4) O-ring, (5) cooling water channels, (6) nickel bellows, (7) heater clamps, (8) cartridge heaters, (9) water jacket, (10) fibrous insulation, (11) heater-connector assembly, (12) metal-sheathed thermocouples, (13) nickel furnace body, (14) cylindrical silver sample-holder block, (15) sample positioning screw.

adjustment screw at the bottom of the sample holder cavity allows freedom in the initial positioning of the sample holder. A Chromel-Alumel thermocouple located in the interior of the silver block at the same height as the molten salt is used to determine the temperature of the melt.

The laser beam enters the furnace through the top window and is brought to a focus in the molten salt at the center of the viewing port. The Raman-scattered light is collected and collimated by a compound *f*/2 100-mm-focal-length lens positioned adjacent to the side window. A 270-mm-focal-length achromatic lens focuses the collimated light on the entrance slit of an *f*/8.7 double monochromator. The limiting factor in the light-collection system is the aperture stop of the side window of the furnace, which is approximately *f*/2.3.

The entire furnace assembly is supported on a positioning table by three adjustable vertical pins. The positioning table is adjustable in the horizontal plane by two micrometer screws at 90° to each other. This arrangement permits accurate placement of the sample in the laser beam. The complete unit, furnace and positioning table, can be moved easily into and out of the sample compartment of the Jarrell-Ash Raman spectrometer.

The Raman spectra of molten nitrates, fluoroborates, and fluorides have been measured at temperatures to 800° with this furnace. With nitrates a quartz containment cell open to the atmosphere of the furnace interior was used; the interior was either evacuated or contained helium. Molten fluoroborates and fluorides were contained in windowless cells, which are described in the following contribution to this report.

---

[1] J. P. Young and J. C. White, *Anal. Chem.* **31**, 1892 (1959).

[2] J. P. Young, *Anal. Chem. Div. Ann. Progr. Rept. Nov. 15, 1963*, ORNL-3537, p. 26.

[3] J. P. Young, *Inorg. Chem.* **6**, 1486 (1967).

A WINDOWLESS CELL FOR LASER RAMAN SPECTROSCOPY OF MOLTEN FLUORIDES

Arvin S. Quist

A windowless or captive-liquid cell has been designed, fabricated, and utilized to measure the Raman spectra of molten fluorides to temperatures of 800°C. This cell was built for the furnace described earlier[1] and is to be used specifically for laser Raman spectroscopy. Its design is based on the general principles successfully employed for several years in the construction of cells to measure the visible and ultraviolet absorption spectra of fluoride melts.[2] No window materials are necessary; the melt is retained in the cell by surface tension.

A schematic diagram showing dimensions of the windowless cells for Raman studies on molten fluorides is given in Fig. 7.33. These cells are usually constructed from pure nickel or from oxygen-free copper, since these materials are satisfactory container materials for the melts of interest to us. However, they could be constructed from a variety of other materials for use with other molten-salt systems.

Prior to use, the cells are degreased by conventional techniques, and the surface oxides are removed by heating in a hydrogen atmosphere. Filling of the cells

with solid fluorides is carried out in an inert-atmosphere glove box. About 0.3 to 0.4 g of salt is required to fill the cell to a level about $\frac{1}{16}$ to $\frac{1}{8}$ in. above the top of the slot. The filled cells are heated in an evacuated quartz tube to melt the fluoride and to fill the lower portion of the cell completely. This procedure removes most of the trapped air and allows fluoride in excess of that which can be held in the cell by surface tension to escape through the slot. The remaining volume of the melt usually does not escape from the cell during subsequent experimental measurements.

The cell is transferred, after cooling, to a 6-mm-ID, 8-mm-OD quartz tube which has a $\frac{1}{16}$-in.-thick optically flat quartz disk fused to one end. The open end of the metal cell is placed nearest the optical flat. The quartz tube is sealed by fusion under reduced pressure, thereby safely containing the windowless cell holding the fluoride salt in a convenient-sized tube for Raman spectral measurements. This arrangement for containing molten fluorides for laser Raman spectroscopy takes advantage of the desirable optical features of a quartz cell while avoiding the difficulties which arise when molten fluorides come into contact with quartz. The sample is completely enclosed in an inert atmosphere, thus presenting no problems in subsequent experimental manipulations. The containment feature is of particular importance when working with toxic beryllium-containing melts.

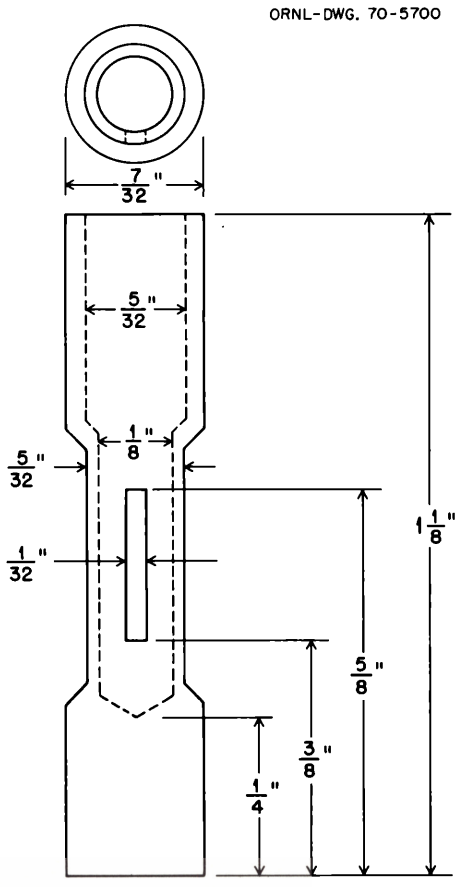

Fig. 7.33. Windowless Cell for Laser Raman Spectroscopy of Molten Fluorides.

Raman spectral measurements on the molten salt are made by placing the sealed quartz tube containing the windowless cell into the central portion, ordinarily a removable silver block, of the resistance-heated furnace described earlier.[1] This quartz tube is held in a vertical position, with the laser beam entering through the optical flat. A 19-in.-focal-length lens is used to bring the beam to a focus at the vertical center of the slot of the windowless cell. Although entry of the laser beam into the molten salt through its concave meniscus causes some divergence, beam defocusing usually is not significant. Most of the incident light passes through the molten salt in such a manner as to give an adequate amount of Raman-scattered light through the slot in the windowless cell. The scattered light is collected at the side port of the furnace by a compound $f/2$ 100-mm-focal-length camera lens. The collimated light is focused on the entrance slit of a double monochromator by a 270-mm-focal-length achromatic lens.

The small width of the slot (0.03125 in.) for the exit of the Raman-scattered light from the windowless cell is not a limiting factor in determining the amount of light which subsequently enters the monochromator. The focused laser beam, with a diameter of less than 0.0004 in., can be considered to be a point source of scattered light. Ordinarily the point of focus of the laser beam will occur in the cross-sectional center of the windowless cell; however, even if the point of focus falls at the rear of the molten-salt-containing cavity, the distance from scattered-light source to slot would be only 0.125 in. Consequently, the maximum f value of the windowless cell would be 0.03125/0.125, or 0.25. This is a much smaller value than the focal ratio of the furnace aperture, approximately $f/2.3$. Therefore, in the present experimental system, the width of the opening in the windowless cell does not limit the amount of scattered light which is transmitted to the double monochromator.

The height of the slot (0.250 in. or 6.3 mm) also is not of major importance in limiting the amount of light reaching the spectrometer. The collecting and collimating lenses give an overall magnification of approximately 3 for optimum light-gathering capacity. Consequently, the magnified image of the slot usually

completely fills the 20-mm-high entrance slit of the monochromator.

Windowless cells of the above design have been used successfully to obtain the Raman spectra of molten fluorides, fluoroborates, and fluorozirconates to temperatures of 800°. Representative spectra so obtained are given in other contributions to this Section of this annual report.

[1] A. S. Quist, "A Furnace for Molten-Salt Raman Spectroscopy to 800°C," preceding contribution, this report.

[2] J. P. Young, *Anal. Chem.* 36, 390 (1964).

MULTIPLE-SAMPLING COLD CELL FOR A LASER-EXCITED RAMAN SPECTROPHOTOMETER

John B. Bates

An inexpensive sample cell for a laser-excited Raman spectrophotometer was designed for measurements to 77°K (liquid nitrogen) for use with a variety of samples including single crystals, powdered solids contained in Pyrex or quartz capillaries, polycrystalline deposits of organic liquids or gases, and liquids which can be contained in quartz or Pyrex tubes.

A schematic side view of the cell is shown in Fig. 7.34. The outer part of the cell is constructed from Pyrex, with flat Pyrex windows sealed directly to the cell body for entrance of the incident laser beam and exit of the scattered light. At the top of the cell near the 45/50 standard-taper ground-glass joint, a vacuum port (three-way stopcock) is joined to the left side of the cell (facing the exit window) and a 12/30 standard-taper ground-glass joint containing thermocouple leads is joined to the right side of the cell (Fig. 7.34*a*).

The inner section of the cryostat is a Pyrex cold finger which terminates in a brass sample block joined to the cold finger through a Kovar seal. A large portion of the sample block (*a*2) is hollowed out to provide for maximum cooling. The sample block is constructed so that opposite faces may provide differing sampling arrangements. The front face of the block, shown in Fig. 7.34*b*, is used for materials (principally powders) contained in quartz or Pyrex capillaries (maximum outside diameter about 2 mm). A capillary is secured to the surface of the horizontal groove with a thin layer of silicone grease. A vertical groove at the center of the face (Fig. 7.34*b*) allows the laser beam entering through the bottom window of the cell to be focused near the center of the capillary.

The flat surface on the opposite face of the sample block (*a*3) has two small brass posts (2 mm square)

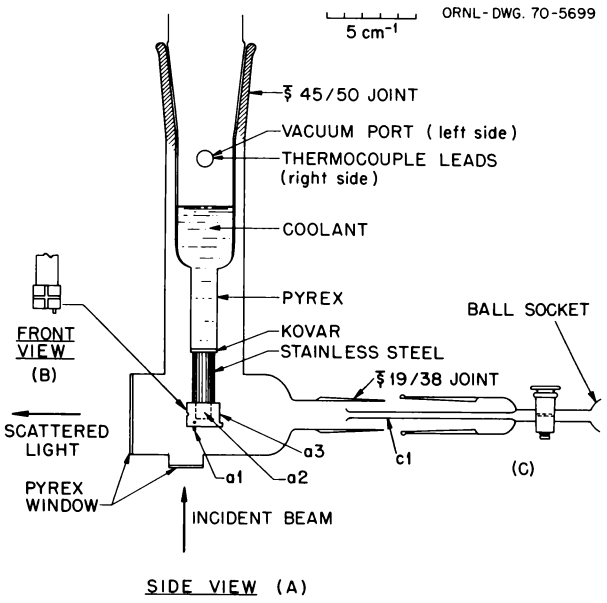

Fig. 7.34. Schematic Side View of the Raman Cold Cell.

which extend outward on either side of the lower edge of the surface to provide support for large single crystals or liquid cells. Single crystals are mounted on the surface of the block by covering one face of the crystal with a thin layer of silicone grease and pressing this face of the crystal against the block. For measuring the Raman spectra of condensed gases, liquids, or matrix-isolated species, the attachment shown in Fig. 7.34*c* is used to form a deposit of the material on the cold surface of the sample block (*a*3). A sample bulb containing the vaporized material is attached to the ball socket, and the vapor is directed onto the block through the flared end of the glass tube (*c*1). The cold finger is then rotated 180° to place the sample in the laser beam.

The temperature near a given sample is measured by a thermocouple attached to the sample block by means of a set screw (*a*1). In some cases, as with single crystals, the thermocouple can be attached directly to the sample. The scattered light from a sample is collected and collimated using a 100-mm-focal-length *f*/2.0 Angenieux s3 camera lens. The cold cell has a clear aperture of about *f*/0.8, so that it is not the limiting stop of the system.

Typical low-temperature Raman spectra which can be obtained with this cold cell are presented in other contributions to this Section of this annual report.[1]

[1] See, for example, J. B. Bates, "Raman Spectrum of Polycrystalline MoF_5," another contribution to this Section, this report.

MICROWAVE AND RADIO-FREQUENCY SPECTROSCOPY

PARAMAGNETIC RESONANCE STUDIES OF LIQUIDS DURING PHOTOLYSIS

Ralph Livingston Henry Zeldes
Jürgen K. Dohrmann[1]

An electron paramagnetic resonance (epr) spectrum has been studied during the photolysis of aqueous solutions of citric acid at room temperature. Three radicals were identified. One is $(HO_2CCH_2)_2\dot{C}OH$, formed from excited citric acid by splitting off the central carboxyl group. In a 3.6 *M* solution at 31°C the *g* value is 2.00314 and there is a 14.52-G hyperfine splitting for four equivalent methylene protons and a 0.63-G splitting for the hydroxyl proton. By addition of strong mineral acid the hydroxyl proton splitting was reduced to zero. This effect is caused by acid-catalyzed exchange of the hydroxyl hydrogen atom. Couplings from carboxyl group protons were not expected and indeed were not seen. A second radical is $HO_2CCH_2C(OH)(CO_2H)\dot{C}H_2$, formed by splitting off an end carboxyl group of excited citric acid. Its *g* value in the above solution is 2.0027, and there is a coupling of 22.3 G to two equivalent $\dot{C}H_2$ protons. Additional unresolved hyperfine structure is present. The third radical is $HO_2CCH_2C(OH)(CO_2H)\dot{C}HCO_2H$, which was most likely produced by abstraction of a hydrogen atom from citric acid by a reactive radical. In the above solution the *g* value is 2.00324, and only a single coupling of 20.90 G to one proton, the $\dot{C}H$ proton, was resolved. This radical was produced from citric acid with very much higher steady-state concentration in a solution which also contained H_2O_2. Photolysis of H_2O_2 gave the reactive OH radical, which quickly abstracted a methylene hydrogen of citric acid. With the higher radical concentration it was possible to resolve further hyperfine structure. Measurements were made both in H_2O and D_2O solutions. A coupling of 0.32 G was found for an exchangeable proton and is assigned to the hydroxyl proton. A coupling of 0.30 G was found for two equally coupled protons and is assigned to the methylene hydrogens in the position γ to the unpaired electron.

Photolysis of aqueous sodium citrate solutions gave a very weak epr spectrum. Only one radical, $^-O_2CCH_2C(OH)(CO_2^-)\dot{C}HCO_2^-$, was identified. This radical, like its triply protonated derivative in citric acid solution, was most likely formed by hydrogen atom abstraction (from citrate ion) by a reactive radical. Here, too, a very much higher radical concentration was produced by the addition of H_2O_2. Measurements were made both in H_2O and D_2O solutions. In a solution having 1.6 *M* sodium citrate and 0.6 *M* H_2O_2 at 38°C, the *g* value is 2.00325. There is a 20.30-G coupling from the $\dot{C}H$ proton, a 0.27-G coupling from an exchangeable proton, which is assigned to the OH proton, a 0.55-G coupling assigned to one of the two CH_2 protons in the γ position, and an 0.11-G coupling assigned to the other CH_2 proton. The nonequivalence of these two γ protons is not surprising, as the coupling for a γ proton (as well as a β proton) is known to depend upon the steric arrangement of the molecule.

Hyperfine splittings from ^{13}C in natural abundance have been studied for several short-lived radicals during photolysis in liquids. A strong spectrum of $\dot{C}H_2COO^-$ was made by photolyzing an aqueous solution containing acetate ion and H_2O_2. With a signal averager, ^{13}C couplings of 32.09 and 13.85 G were found and assigned to the $\dot{C}H_2$ and COO^- carbons respectively. These values indicate that the radical is a planar π radical. A pronounced difference in line intensity (attributed to a difference in line width) was seen for pairs of lines whose separation is given by the larger ^{13}C coupling. The high-field line of such a pair is the broader. From this observation it is concluded that $2g_3 - (g_1 + g_2)$ is negative, where g_3 is the principal *g* value perpendicular to the plane of the radical. A spectrum from $(CH_3)_2\dot{C}OH$ obtained[2] by photolyzing an isopropyl alcohol solution containing acetone was strong enough that ^{13}C lines were seen by conventional chart recording. The coupling for the methyl carbons is 5.35 G, and that for the central carbon is 65.05 G. It is concluded that the unpaired electron is not in a pure *p* orbital; the radical skeleton is not planar. A spectrum for $CH_3COCH_2NO_2\cdot^-$ strong enough to see ^{13}C lines without signal averaging was obtained[3] by photolyzing a basic aqueous solution containing acetone and potassium nitrite. A single ^{13}C coupling of 11.05 G was found and assigned to the carbonyl carbon. The acetoin radical, $CH_3\dot{C}OHCOCH_3$, was studied using the signal averager. The radical was prepared[4] by photolysis of solutions containing 1 or 2% diacetyl in isopropyl alcohol. In strongly acid solution there is rapid exchange[4] between tautomeric forms, which causes the two central carbons as well as the two outer carbons to become equivalent. A single ^{13}C coupling of 5.12 G was found for the rapidly exchanging radical and is attributed to the two central carbons. This radical was also investigated in the absence of acid, where negligible exchange occurs. Without exchange all carbons are inequivalent. Lines due to ^{13}C were seen, and one

coupling of 7.8 G was evaluated. A provisional coupling of 10.8 G for another carbon was found.

Studies of aqueous solutions of tartaric acid during photolysis were continued. A radical, all of whose eight hyperfine lines were in emission rather than absorption, had been found and identified[5] as HOOCCH(OH)ĊH(OH). A second radical had been identified[5] as HOOCĊHCHO, and it was postulated that the first radical was converted to the second by an acid-catalyzed pinacol-like rearrangement similar to that found[6] for a similar radical produced by removal of a hydrogen atom from ethylene glycol. It was believed that emission was seen because the radical had somehow been produced with more molecules in the upper electron spin state than in the lower and because the rearrangement to form the second radical occurred rapidly enough to prevent thermal relaxation processes from producing the higher equilibrium population of the lower electron spin state. Additional observations have now been made in which the pH of the solutions has been varied. This was done to change the (acid catalyzed) rate of conversion of HOOCCH(OH)ĊH(OH) to HOOCĊHCHO. When the pH was increased by reducing the concentration of tartaric acid, the emission spectrum was progressively converted to an absorption spectrum, but at a different rate for the different hyperfine lines. The higher-field hyperfine lines became absorption lines more quickly. This indicates that they have a shorter thermal relaxation time. As was expected, it was found that when the spectrum from HOOCCH(OH)ĊH(OH) was changed to an absorption spectrum by dilution, it could be converted back to an emission spectrum by the addition of strong mineral acid. When the pH was lowered the concentration of HOOCĊHCHO increased greatly. This is consistent with the more rapid transformation of HOOCCH(OH)ĊH(OH) to HOOCCHCHO.

[1] On leave from Institut für Physikalische Chemie der Freien Universität Berlin, Germany.

[2] H. Zeldes and R. Livingston, *J. Chem. Phys.* **45**, 1946 (1966).

[3] H. Zeldes and R. Livingston, *J. Am. Chem. Soc.* **90**, 4540 (1968).

[4] H. Zeldes and R. Livingston, *J. Chem. Phys.* **47**, 1465 (1967).

[5] R. Livingston and H. Zeldes, *Chem. Div. Ann. Progr. Rept. May 20, 1969*, ORNL-4437, p. 115.

[6] R. Livingston and H. Zeldes, *J. Am. Chem. Soc.* **88**, 4333 (1966).

PARAMAGNETIC RESONANCE STUDY OF GAMMA-IRRADIATED SINGLE CRYSTALS OF $KHCO_3$ AND $KDCO_3$

R. W. Holmberg

An electron paramagnetic resonance (epr) study of the radicals formed when single crystals of $KHCO_3$ and $KDCO_3$ are gamma irradiated has been undertaken. Earlier workers[1] have observed the radicals $\dot{C}O_2^-$ and $\dot{C}O_3$ when $KHCO_3$ was irradiated at room temperature. We have not detected $\dot{C}O_2^-$ when the crystals were irradiated at 77°K. The radical $\dot{C}O_3^-$ is formed at the low temperature, but its formation represents only a minor fraction of the radiation damage as seen by epr. Two new radicals were seen predominantly. One is very probably $\dot{C}O_3^{3-}$. Its spectrum in $KHCO_3$ consists of a single broad, slightly anisotropic line which saturates at relatively low microwave power. In $KDCO_3$ additional structure was resolved, presumably arising from weak hyperfine interactions with several nearby potassium nuclei. The other radical has been tentatively identified as $(HCO_3)_2^{\cdot -}$. Such a radical might be formed from the dimeric pairs of bicarbonate ions in the crystal by loss of an electron. It would thus be analogous to the *V* centers seen in alkali halide crystals. Its spectrum in $KHCO_3$ is characterized by a small 1-2-1 hyperfine splitting from two equally coupled protons.

When the crystals were warmed to room temperature, both of these radicals disappeared and $\dot{C}O_2^-$ grew in. When crystals of $KHCO_3$ which had previously been irradiated and warmed to room temperature were reirradiated and observed at 77°K, several triplet-state radicals were seen. These radicals were not detected on first irradiation, even when comparable total irradiation doses were given. An analysis of their *g* and *D* tensors suggests that they are $\dot{C}O_3^-$-$\dot{C}O_3^-$ radical pairs. Presumably the initial radiation forms defect centers which allow $\dot{C}O_3^-$ radicals to be stably trapped in adjacent sites in the crystal lattice.

[1] G. W. Chantry, A. Horsfield, J. R. Morton, and D. H. Whiffen, *Mol. Phys.* **5**, 589 (1962).

ELECTRON SPECTROSCOPY

USE OF SOFT X RAYS IN CHEMICAL ANALYSIS

T. A. Carlson L. D. Hulett[1]

The construction and use of our high-resolution electron spectrometer has been discussed previously.[2]

In our initial work we used an electron gun for promoting Auger lines and a gas discharge tube to obtain the narrow helium resonance line for studying molecular orbitals. This work is continuing, and, in addition, we are now using an x-ray source for measuring the inner-shell binding energies of atoms by means of the photoelectric effect.

The importance of determining the binding energies in the inner shells of atoms as a function of chemical environment has been amply illustrated by Siegbahn and others.[3] The valence shell acts as an outside potential to the inner shells of an atom. Changes in the electron density of the valence shell are reflected by shifts in the binding energies of the inner shells. To measure accurately the binding energy of an inner atomic shell is to offer a threefold analysis: (1) qualitative, each element is characterized by the binding energies of its atomic shell; (2) quantitative, the relative intensity of the photoelectron is proportional to the amount of the different elements present; and (3) interpretive, in the sense that it yields an evaluation of the electron density surrounding the atom, or in crude terms its oxidation state.

We have utilized these capabilities in the following application: (1) studies of chemical shifts of the different elements in tRNA and its components, (2) measurements of chemical shifts of arsenic in various oxidation states, (3) studies of chemical shifts in bromine in KBr, $KBrO_3$, and $KBrO_4$. Item 1 has been previously discussed in part.[4] Here we shall briefly present the data on items 2 and 3.

Figure 7.35 shows a plot of the binding energy (eV) of the 3*d* shell for a series of arsenic-containing compounds as a function of the "calculated charge" on the arsenic. The "calculated charge" is a value obtained by a method suggested by Siegbahn[3] using electronegativity differences between arsenic and its neighboring atoms. A monotonic function is obtained. One

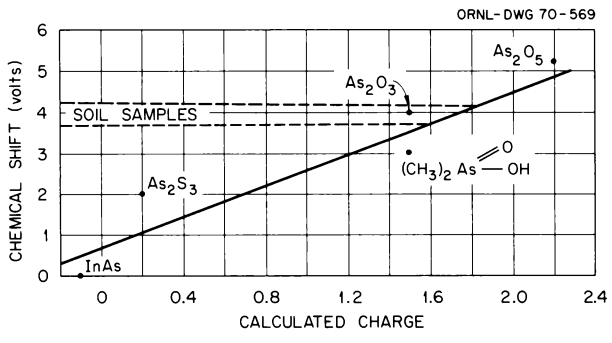

Fig. 7.35. Chemical Shift in Binding Energy (eV) of 3*d* Shell in Arsenic as a Function of Calculated Charge.

of the motivations of the study was to determine whether an electron-spectroscopic method could be used to evaluate the behavior of arsenic in herbicides when exposed to soil. A defoliant containing cacodylic acid, $(CH_3)_2AsOOH$, was added to soil, which was allowed to stand for a week. The arsenic could be observed easily and appeared as a single peak, which indicated a single oxidation state. The principal point here is that electron spectroscopy offers a good opportunity to study what happens to arsenic in various environments in situ.

In Fig. 7.36 is shown a plot of the chemical shift of bromine in different oxidation states. These data are compared with those taken for other halides. The compounds compared are the alkali metal salts of the halides, halites, halates, and perhalates. The solid line represents calculations based on Hartree-Fock wave functions for the free ions analogous to the nominal oxidation states. These calculations, of course, highly exaggerate the chemical effect (electrons are not brought to infinity as suggested by oxidation number). However, by normalizing the calculations at one point, the value for the perchlorate ion, the calculations do explain qualitatively the data for all the halides, namely, a continuous rise in binding energy as one goes

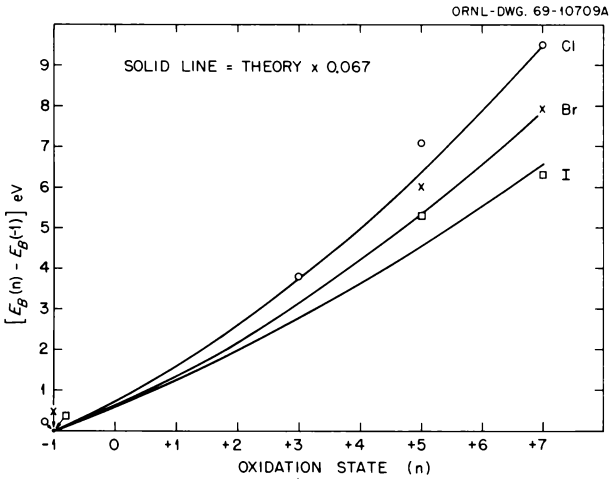

Fig. 7.36. Chemical Shifts in the Inner-Shell Binding Energies of Halogens. $E_B(-1)$ are binding energies taken from data on the halides, oxidation state = -1; $E_B(n)$ are the binding energies taken from the halites ($n = +3$), halates ($n = +5$), and perhalates ($n = +7$). Data on NaCl, NaClO, $NaClO_2$, and $NaClO_3$, shown by ○, are from ref. 3; data on KBr, $KBrO_3$, and $KBrO_4$, shown by x, are from our work; and data on KI, KIO_3, and KIO_4, shown by □, are taken from C. S. Fadley *et al.*, *J. Chem. Phys.* 48, 3779 (1968). The data in each case are normalized to the alkali-metal-ion binding energy. The theory (solid line) comes from Hartree-Fock calculations of the free ion whose charge corresponds to the oxidation number.

to higher oxidation states with the slope increasing for lower Z. Most interesting is the fact that the measurement on perbromate (oxidation number = 7) falls in quite naturally with the rest of the data. Until recently the perbromate had not been prepared, and theoretical speculation that the compound was fundamentally unstable was advanced. The evidence from the present data is that the electron density surrounding bromine in perbromate is close to what one would have expected.

[1] Analytical Chemistry Division.

[2] T. A. Carlson *et al., Phys. Div. Ann. Progr. Rept. Dec. 31, 1968,* ORNL-4395, p. 87; also see B. P. Pullen, T. A. Carlson, W. E. Moddeman, G. K. Schweitzer, W. E. Bull, and F. A. Grim, *J. Chem. Phys.* (in press).

[3] Siegbahn *et al., ESCA: Atomic, Molecular and Solid State Structure Studied by Means of Electron Spectroscopy,* Almqvist and Wiksells Boktryckeri A.B., Uppsala, 1967.

[4] L. D. Hulett and T. A. Carlson, *Clin. Chem.* (in press).

ANGULAR DISTRIBUTION OF PHOTOELECTRONS

T. A. Carlson A. E. Jonas[1]

There are three important pieces of data that ought to be determined for a photoelectron: its energy, its relative intensity, and the angular distribution relative to the incident photon. Measurements of the first two items have been exploited by Turner[2] and others in providing a basis for determining the nature of molecular orbitals for a wide variety of gaseous molecules. Measurements on the angular distribution also offer an important clue as to the nature of the molecular orbital from which the photoelectron is removed, particularly with regard to the nature of the angular momentum. For unpolarized photoelectrons the angular distribution is given as

$$I(\theta) \propto 1 + B \sin^2\theta \quad , \tag{1}$$

where

$$B = \frac{3\beta}{4 - 2\beta},$$

θ is the angle between the incoming photon and outgoing photoelectron, and β is a parameter dependent on the energy of the phtoelectron and the nature of the molecular orbital. As long as we are dealing with dipole absorption, Eq. (1) is true for all cases of atoms and molecules.

It is desirable to combine angular measurements with the high resolution inherent in the helium resonance line, whose energy is 21.22 eV and whose natural width is the order of a few millivolts. Some measurements have been carried out,[3] but the spectrometers used were not high-resolution dispersion instruments, and the scatter of the results obtained is rather large. We have constructed a chamber (Fig. 7.37) containing a gas discharge tube whose angle with respect to the entrance hole can be continuously varied from 140 to 20°. This chamber can be attached to our high-resolution double-focusing electrostatic electron spectrometer. We operate with an energy resolution of 20 to 40 nV, so that vibrational structure can be easily resolved as well as the electron levels. The angular resolution is 3°.

Argon, krypton, and xenon have been studied with the 21.22-eV resonance line of helium and the 16.85- and 16.67-eV resonance lines of neon. Figure 7.38 shows the results for the outermost $p_{3/2}$ shell of each of these rare gases at two different energies. A value of β is chosen to give the best fit to the data. Also plotted are the theoretical predictions of Manson and Cooper.[4] The theoretical predictions lie below the experimental points, but the trends with regard to the dependence on the elements and on the energy are consistent with experiment. The unusual structure noted by McGowan *et al.*[3] for krypton and argon using the near-resonance lines was not seen in our work.

In Fig. 7.39 is plotted the angular dependence for H_2. The agreement with the theoretical prediction[5] of β = 1.75 is excellent. Figure 7.40 shows the results for the first two ionization potentials of nitrogen. The theory[6] is slightly lower in the case of the first orbital. Calculations have not been made for the $A^2\pi_g$ orbital, but experimentally the value of β is lower for the second ionization potential than for the first. Since theory would have predicted actually a higher value of β if we had assumed the second orbital to be a $^2\Sigma_g^+$ state, it would appear that $^2\Sigma_g^+$ better describes the first ionization potential. This conclusion is supported by the nature of the vibrational structure in the photoelectron spectra of the first two ionization potentials.[7] Also plotted in Fig. 7.40 are the relative angular dependences of the different vibrational states. These ratios represent the relative probability that the molecule ion will be left in the various vibrational states as the result of photoionization. The relative transition probabilities to the first three vibrational states of $A\ ^2\Pi_u$ do not seem to have a strong angular dependence, but in striking contrast the relative intensity of lines corresponding to the ν_0 and ν_1 vibrational states of $^2\Sigma_g^+$ are definitely dependent on angle. The ability to

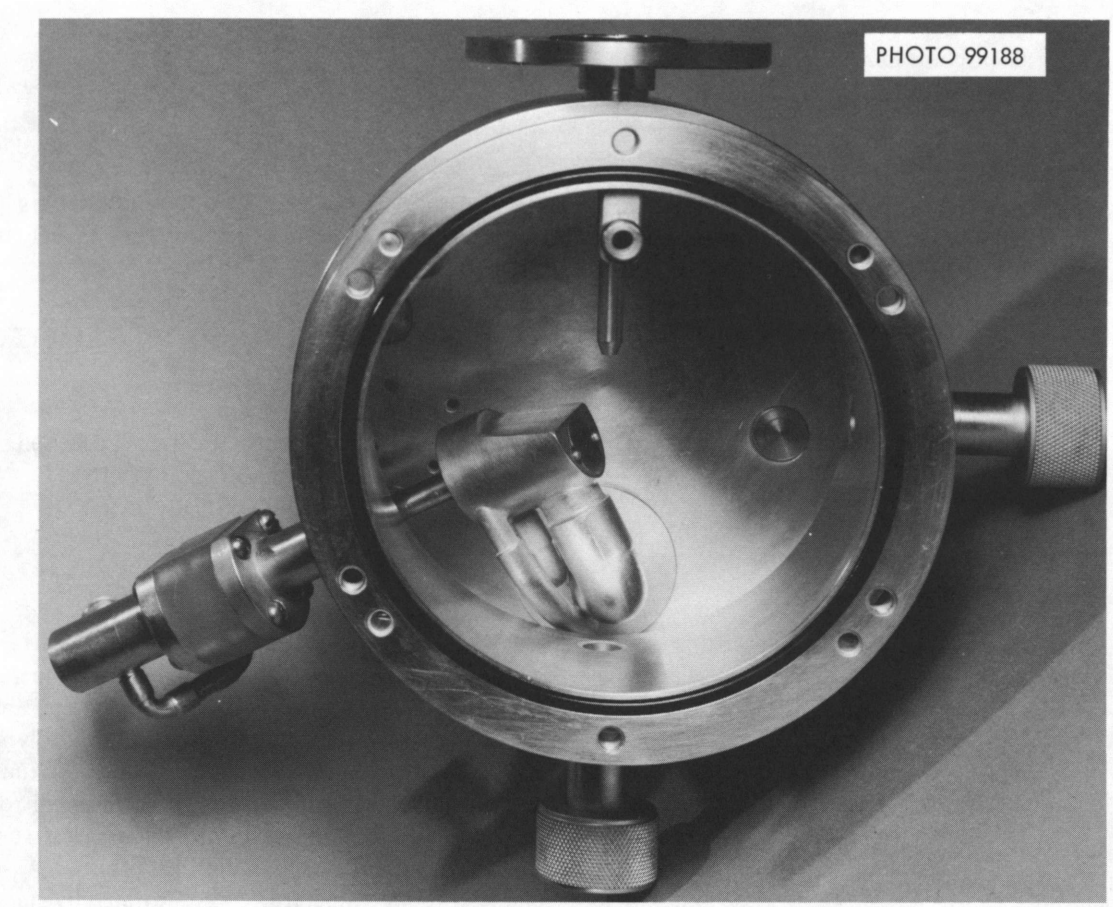

Fig. 7.37. Chamber for Angular Distribution Studies Used with Electron Spectrometer. To the left is the flange which connects to spectrometer. At a 60° angle from the flange is a gas-discharge tube. Diameter of chamber is 15 cm.

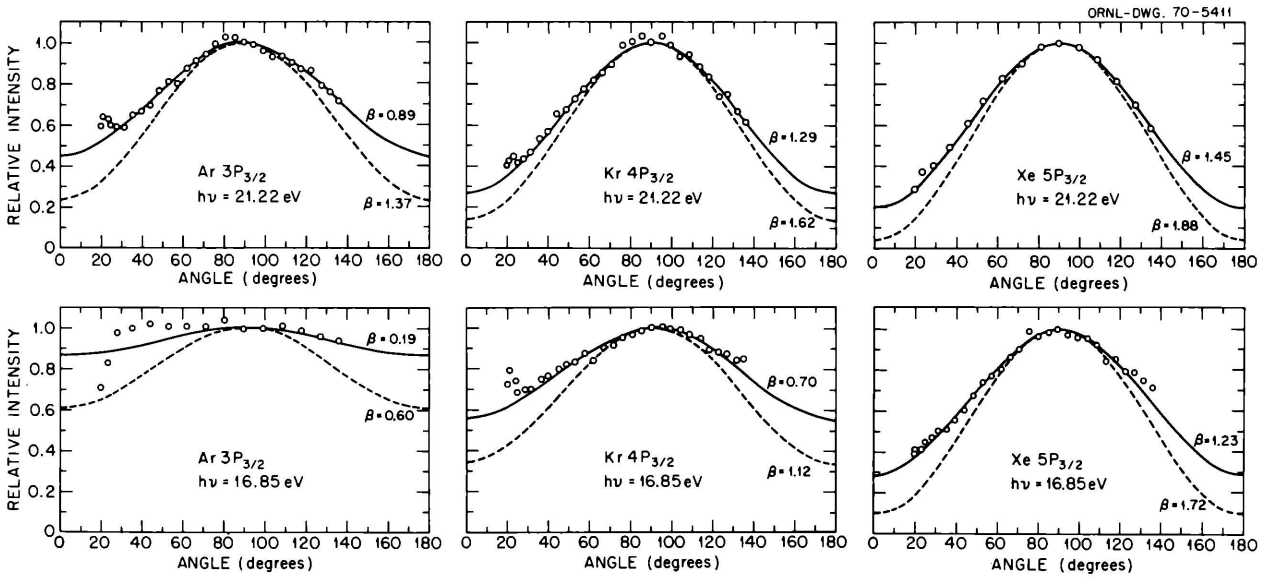

Fig. 7.38. Angular Distribution of Photoelectrons Ejected from the Outermost Orbital of Ar, Kr, and Xe. β is defined in Eq. (1). The solid line is the best fit given by Eq. (1). The dotted line corresponds to calculations from ref. 4.

measure the angular dependence of the vibrational structure arising from photoionization may prove to be another important probe into the nature of molecular orbitals.

---

[1] Guest student from the University of Tennessee, Knoxville.

[2] P. W. Turner, A. D. Baker, C. Baker, and C. R. Brundle, *High Resolution Molecular Photoelectron Spectroscopy*, Wiley, in preparation.

[3] J. Berkowitz and H. Ehrhardt, *Phys. Letters* **21**, 531 (1966); J. A. R. Samson, *Proc. Roy. Soc. (London)* (to be published); J. W. McGowan, D. A. Vroom, and A. R. Comeaux, *J. Chem. Phys.* **51**, 5626 (1969).

[4] S. T. Manson and J. W. Cooper, submitted to the *Physical Review.*

[5] J. C. Tully, R. S. Berry, and B. J. Dalton, *Phys. Rev.* **176**, 95 (1968).

[6] B. Schneider and R. S. Berry, *Phys. Rev.* **182**, 141 (1969).

[7] D. W. Turner and D. P. May, *J. Chem. Phys.* **45**, 471 (1966).

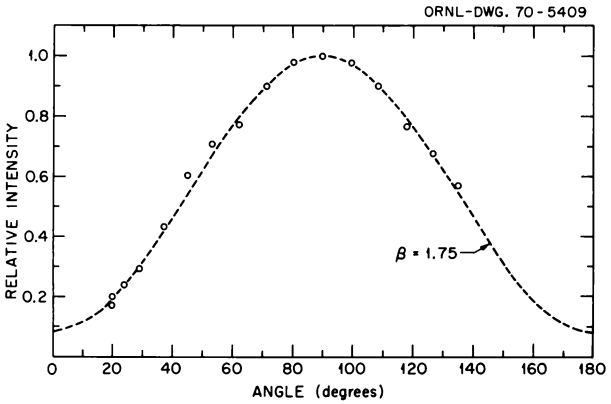

Fig. 7.39. Angular Distribution of Photelectrons Ejected from H_2. Transitions are to the $v = 2$ vibrational level in H_2^+ (which is the most probable transition). The β is that calculated in ref. 5.

MASS SPECTROMETRY AND RELATED TECHNIQUES

CHARACTERIZATION OF VOLATILE AND NONVOLATILE SOLIDS OBTAINED FROM THE GAS-PHASE RADIOLYSIS OF PENTABORANE-9[1,2]

James W. Pinson[3] P. S. Rudolph
Russell Baldock

Cobalt-60 gamma-ray radiolysis at room temperature of pentaborane-9 (mol. wt 63) in the gas phase produced both volatile and nonvolatile polymeric solids. At the completion of each radiolysis run, all solid products were deposited on a liquid-nitrogen-cooled surface. No solid deposits on the glass surface were evident during the radiolysis process. A solid, volatile at room temperature, was separated by standard vacuum techniques and identified by its physical properties and its infrared spectrum as decaborane-16.

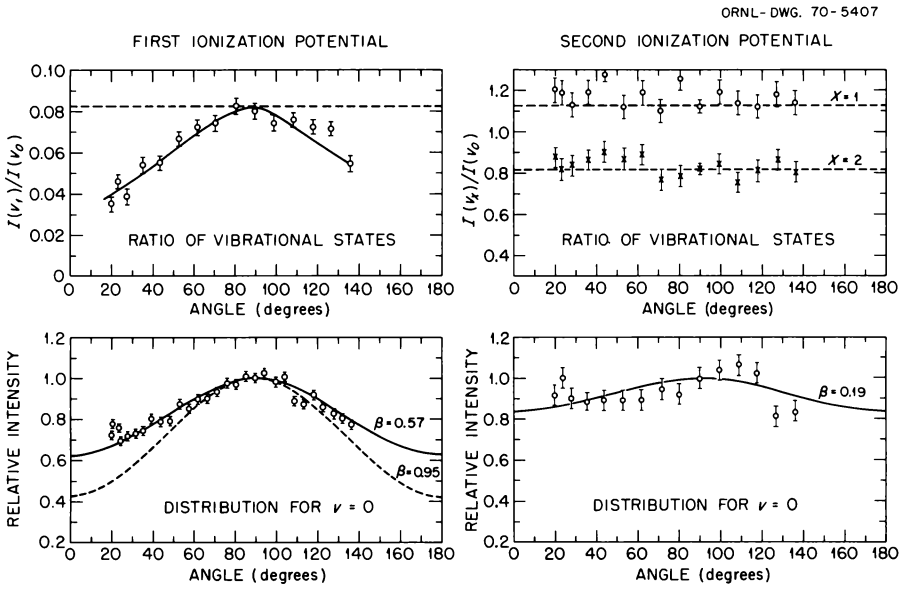

Fig. 7.40. Angular Distributions of Photoelectrons Ejected from N_2. The bottom two graphs show the distribution for the two least-bound orbitals. The solid lines are the best fit using Eq. (1). The dotted line is from theory, ref. 6. The upper two graphs show the relative intensities for transitions to the different vibrational states.

This identification was substantiated by differential thermal analysis (DTA). Nonvolatile solids were separated into a benzene-soluble fraction and an acetone-soluble fraction. Thermal-probe mass-spectral analysis[4] of the acetone-soluble fraction, which constituted approximately 80% of the solids, revealed three main groups whose major peaks were at *m/e* values of 101, 115, and 132. Mass-spectral analysis of the benzene-soluble fraction revealed groups at 125, 180, 231, 285, and 320. Infrared and DTA analyses indicated five distinct types of polymers in this fraction. Infrared analysis showed B-H apex bonds present in the acetone-soluble fraction of the nonvolatile solid indicating nonmolecular-type dimeric "fragments." This bonding was absent in the benzene-soluble fraction of the nonvolatile solid and in the $B_{10}H_{16}$ volatile fraction. DTA data are in agreement with this interpretation. Additional mass-spectral, infrared, DTA, thermogravimetric analysis, and rate studies are being correlated to a previously proposed mechanism.[5]

[1] Research sponsored jointly with the University of Southern Mississippi, Hattiesburg.

[2] Presented at the 159th National Meeting, American Chemical Society, Houston, Tex., Feb. 26, 1970.

[3] Oak Ridge Associated Universities Research Participant from the University of Southern Mississippi, Hattiesburg, summers 1968 and 1969.

[4] Performed by W. T. Rainey, Jr., Analytical Chemistry Division.

[5] J. W. Pinson and T. J. Klingen, *Gamma-Ray Radiolysis of Pentaborane-9 Vapor*, abstract PHYS-173, 156th National Meeting, American Chemical Society, Atlantic City, N.J., Sept. 8–13, 1968.

THE TWO-STAGE MASS SPECTROMETER

Russell Baldock

The two-stage mass spectrometer is being operated in support of the superheavy-element program of the Chemistry Division, currently using extracts from carefully selected samples of mica.[1] Preliminary analyses have been made to establish separation procedures, sample sizes, and the circumvention of interferences by impurities.

[1] R. V. Gentry, J. W. Boyle, and Russell Baldock, "Studies of Pleochroic Haloes," a contribution to Chap. 2, this report.

MOLECULAR BEAM STUDIES

CROSSED-MOLECULAR-BEAM STUDIES OF BIMOLECULAR ASSOCIATION AND UNIMOLECULAR DECOMPOSITION REACTIONS

R. E. Minturn Sheldon Datz

Our studies of the association reactions and "sticky collisions" between amines and BF_3 reported previously[1,2] were terminated because we were once again unable to detect the vibrationally excited intermediate complex we expected to find. Even following apparatus modifications that made our detection system some ten times more sensitive, a signal indicating the existence of a long-lived complex could not be extracted from the noise background. The anomaly noted[2] in the distribution of BF_3 molecules elastically scattered by NH_3 was removed, however, when this experiment was repeated after the modifications indicated above.

The reasons for our repeated failure to observe the predicted excited product molecules from these reactions are still not clear, but since many other types of interesting reactions do exist which may be more amenable to exploitation by crossed-beam techniques, we do not plan to pursue the experiment further.

[1] R. E. Minturn and S. Datz, *Chem. Div. Ann. Progr. Rept. May 20, 1968*, ORNL-4306, p. 170.

[2] R. E. Minturn and S. Datz, *Chem. Div. Ann. Progr. Rept. May 20, 1969*, ORNL-4437, p. 138.

CROSSED-MOLECULAR-BEAM STUDIES OF REACTIONS OF ATOMIC DEUTERIUM WITH HALOGEN MOLECULES

George E. Moore Sheldon Datz
Robert M. Statnick[1]

Product DI molecules from the reaction of D atoms with CH_3I were not detected with the general-purpose crossed-molecular-beam apparatus, in spite of the improvements in signal detection previously described[2] and the elimination of the rf interference from the signal by use of an improved linear amplifier. This result suggests that the yield of product molecules in this reaction is too small for detection in our system; consequently, the reaction of deuterium atoms with a more highly halogenated molecule (such as CBr_4) might be more suitable for study, since then, at least intuitively, the probability of collisions of proper steric orientation for reaction would be increased.[3]

An investigation of the reaction of thermal deuterium atoms with CBr_4 molecules has been undertaken. In initial experiments the deuterium-atom main beam was modulated at 100 Hz, and modulated product DBr was detected using differential pulse counting at $m/e = 83$. However, a very large part of the product DBr was produced not in the gas-phase reaction but in an interaction of modulated gas-phase deuterium atoms with solid CBr_4 (mp 90°), probably at slit edges in the scattering or detector chambers. In current experiments the cross beam of CBr_4 molecules is modulated, but not the deuterium atom beam; although the surface reaction still can take place, modulated DBr can result only from the gas-phase reaction.

---

[1] U.S. Atomic Energy Commission Postdoctoral Fellow under appointment with Oak Ridge Associated Universities.

[2] G. E. Moore, S. Datz, and R. M. Statnick, *Chem. Div. Ann. Progr. Rept. May 20, 1969,* ORNL-4437, p. 141.

[3] Chemical intuition may be unreliable. See, for example, P. R. Brooks, *J. Chem. Phys.* **50,** 5031 (1969).

Publications

NUCLEAR CHEMISTRY

G. Chilosi,[1] G. D. O'Kelley, and E. Eichler, "The Decay of 8.8-min ^{49}Ca to Levels in ^{49}Sc," *Nucl. Phys.* **A136**, 649 (1969).

J. H. Hamilton,[2] F. E. Coffman,[2] A. V. Ramayya,[2] and N. R. Johnson, "Decay of ^{74}As," *Nucl. Phys.* **A132**, 254 (1969).

D. G. Sarantites,[3] N. R. Johnson, and H. W. Boyd,[4] "Levels in ^{110}Cd Populated in the Decay of 69-min ^{110g}In," *Nucl. Phys.* **A138**, 115 (1969).

K. S. Toth,[5] R. L. Hahn, M. F. Roche,[5] and D. S. Brenner,[6] "New Erbium Isotope, ^{155}Er," *Phys. Rev.* **183**, 1004 (1969).

K. S. Toth,[5] R. L. Hahn, C. E. Bemis, Jr., T. H. Handley,[7] and M. F. Roche,[5] "Search for ^{172}Hf Alpha Decay," *J. Inorg. Nucl. Chem.* **32**, 1051 (1970).

R. A. Kuebbing,[8] "Measurements of Transition Probabilities in Some Middle Weight Nuclei," Ph.D. thesis, Case Western Reserve University, Cleveland, Ohio, January 1970.

R. L. Hahn, M. F. Roche,[5] and K. S. Toth,[5] "Alpha Decay of ^{227}U," *Phys. Rev.* **182**, 1329 (1969).

F. Plasil,[9] R. L. Ferguson, and H. W. Schmitt,[9] "Neutron Emission in the Fission of ^{213}At," pp. 505–17 in *Physics and Chemistry of Fission* (Proc. Second IAEA Symposium, Vienna, Austria, July–August 1969), IAEA, Vienna, 1969.

L. H. Niece,[10,11] D. E. Troutner,[10] and R. L. Ferguson, "Independent Yields of ^{95}Zn from Thermal-Neutron Fission of ^{235}U and ^{233}U," *Phys. Rev. C* **1**, 312 (1970).

J. D. Hastings,[10,12] D. E. Troutner,[10] and R. L. Ferguson, "Fractional Cumulative Yields of ^{103}Mo, ^{105}Mo, and ^{106}Mo from Thermal-Neutron Induced Fission of ^{235}U," *Radiochim. Acta* **11**, 51 (1969).

N. G. Runnalls,[10,13] D. E. Troutner,[10] and R. L. Ferguson, "Charge Distribution in Fission: Fractional Cumulative Fission Yields of ^{143}Ba from Thermal-Neutron-Induced Fission of ^{235}U," *Phys. Rev.* **179**, 1188 (1969).

J. F. Emery,[7] J. E. Strain,[7] G. D. O'Kelley, and W. S. Lyon,[7] "Non-Destructive Neutron Activation Analysis of the Allende Meteorite," *Radiochem. Radioanal. Letters* **1**, 137 (1969).

---

[1] Visiting scientist 1964–65; present address: INFN and Istituto di Fisica Superiore, Università di Napoli, Italy.

[2] Physics Department, Vanderbilt University, Nashville, Tenn.

[3] Chemistry Department, Washington University, St. Louis, Mo.

[4] Oak Ridge Associated Universities Research Participant from West Georgia College, Carrollton.

[5] Electronuclear Division.

[6] Chemistry Department, Clark University, Worcester, Mass.

[7] Analytical Chemistry Division.

[8] Oak Ridge Graduate Fellow under appointment with Oak Ridge Associated Universities.

[9] Physics Division.

[10] University of Missouri, Columbia.

[11] Present address: Abbott Laboratories, Chicago, Ill.

[12] Present address: Mound Laboratory, Miamisburg, Ohio.

[13] Present address: Stout State University, Menomonie, Wis.

G. D. O'Kelley, J. S. Eldridge,[7] E. Schonfeld,[14] and P. R. Bell,[14,15] "Elemental Compositions and Ages of Lunar Samples by Non-Destructive Gamma-Ray Spectrometry," *Science* **167**, 580 (1970).

Lunar Sample Preliminary Examination Team (including P. R. Bell,[14,15] J. S. Eldridge,[7] and G. D. O'Kelley), "Preliminary Examination of Lunar Samples from Apollo 11," *Science* **165**, 1211 (1969).

Lunar Sample Preliminary Examination Team (including P. R. Bell,[14,15] J. S. Eldridge,[7] and G. D. O'Kelley), *Lunar Sample Information Catalog – Apollo 11,* Science and Applications Directorate, NASA Manned Spacecraft Center, Aug. 31, 1969.

Lunar Sample Preliminary Examination Team (including P. R. Bell,[14,15] J. S. Eldridge,[7] and G. D. O'Kelley), *Apollo 11 – Preliminary Science Report,* NASA SP-214 (1969).

G. D. O'Kelley, J. S. Eldridge,[7] E. Schonfeld,[14] and P. R. Bell,[14,15] "Primordial Radionuclide Abundances, Solar-Proton and Cosmic-Ray Effects, and Ages of Apollo 11 Lunar Samples by Non-Destructive Gamma-Ray Spectrometry," *Geochim. Cosmochim. Acta, Suppl. 1* **2**, 1407 (1970).

Lunar Sample Preliminary Examination Team (including P. R. Bell,[14,15] J. S. Eldridge,[7] V. A. McKay,[16] G. D. O'Kelley, and R. T. Roseberry[16]), "Preliminary Examination of Lunar Samples from Apollo 12," *Science* **167**, 1325 (1970).

Lunar Sample Preliminary Examination Team (including P. R. Bell,[14,15] J. S. Eldridge,[7] V. A. McKay,[16] G. D. O'Kelley, and R. T. Roseberry[16]), *Lunar Sample Information Catalog – Apollo 12,* Science and Applications Directorate, NASA Manned Spacecraft Center, Report MSC-01512, Jan. 12, 1970.

CHEMISTRY AND PHYSICS OF TRANSURANIUM ELEMENTS

R. J. Silva, R. L. Hahn, M. L. Mallory, C. E. Bemis, P. F. Dittner, O. L. Keller, J. R. Stokely,[7] and K. S. Toth,[5] "Nuclear Chemistry with the Oak Ridge Isochronous Cyclotron," *Proc. Intern. Conf. on the Use of Cyclotrons in Chemistry, Metallurgy and Biology,* Oxford, England, Sept. 22–23, 1969.

J. Halperin, C. E. Bemis, Jr., R. E. Druschel, and J. R. Stokely,[7] "The Thermal Neutron Cross Section and Resonance Integral of ^{252}Cf," *Nucl. Sci. Eng.* **37**, 228 (1969).

E. T. Chulick,[3,17] P. L. Reeder,[3] E. Eichler, and C. E. Bemis, Jr., "Redetermination of Delayed Neutrons from ^{252}Cf," *Radiochim. Acta* **12**, 164 (1969).

O. L. Keller, Jr., J. L. Burnett, T. A. Carlson, and C. W. Nestor, Jr.,[18] "Predicted Properties of the Superheavy Elements. I. Elements 113 and 114, Eka-Thallium and Eka-Lead," *J. Phys. Chem.* **74**, 1127 (1970).

L. J. Nugent, P. G. Laubereau,[19] G. K. Werner,[9] and K. L. Vander Sluis,[9] "Electron-Transfer Absorption in Some Actinide(III) and Lanthanide(III) Tricyclopentadienides and the Standard II-III Cation Oxidation Potentials," *Proc. 8th Rare-Earth Research Conference,* Reno, Nevada, Apr. 19–22, 1970.

M. O. Workman[20] and J. H. Burns, "Studies on the 'Isomeric' Forms of Some β-Diketone Complexes of Europium(III) and Neodymium(III)," *Inorg. Chem.* 8, 1542 (1969).

J. H. Burns and M. D. Danford, "The Crystal Structure of Cesium Tetrakis(hexafluoroacetylacetonato)europate and -americate. Isomorphism with the Yttrate," *Inorg. Chem.* 8, 1780 (1969).

P. G. Laubereau[19] and J. H. Burns, "Tricyclopentadienyl-curium," *Inorg. Nucl. Chem. Letters* **6**, 59 (1970).

---

[14] NASA Manned Spacecraft Center, Houston, Tex.

[15] Now of the Director's Division.

[16] Instrumentation and Controls Division.

[17] Present address: Texas A & M University, College Station.

[18] Mathematics Division.

[19] Visiting scientist from the Federal Republic of Germany, Bonn.

[20] Department of Chemistry, University of Virginia, Charlottesville.

P. G. Laubereau[19] and J. H. Burns, "Microchemical Preparation of Tricyclopentadienyl Compounds of Berkelium, Californium, and Some Lanthanide Elements," *Inorg. Chem.* **9**, 1091 (1970).

ISOTOPE CHEMISTRY

D. A. Lee, "Extraction of Lithium Values," U.S. Pat. 3,479,147 (Nov. 18, 1969).

L. L. Brown and J. S. Drury, "Nitrogen Isotope Effects in the Reduction of Nitrate, Nitrite, and Hydroxylamine to Ammonia. II. The MgO and $CuSO_4$ Systems," *J. Chem. Phys.* **51**, 3771 (1969).

A. C. Rutenberg and J. S. Drury, "Chemical Fractionation of Uranium Isotopes," *J. Inorg. Nucl. Chem.* **31**, 2289 (1969).

G. M. Begun and R. N. Compton,[21] "Threshold Electron-Impact Excitation and Negative-Ion Formation in XeF_6 and XeF_4," *J. Chem. Phys.* **51**, 2367 (1969).

RADIATION CHEMISTRY

C. J. Hochanadel, J. A. Ghormley, and P. J. Ogren,[22] "Pulse Radiolysis of NO: Production of NO_2 and N_2O_3 and the Production and Relaxation of Vibrationally Excited NO," *J. Chem. Phys.* **50**, 3075 (1969).

J. W. Boyle, J. A. Ghormley, C. J. Hochanadel, and J. F. Riley,[23] "Production of Hydrated Electrons by Flash Photolysis of Liquid Water with Light in the First Continuum," *J. Phys. Chem.* **73**, 2886 (1969).

C. J. Hochanadel (book review), *Radiation Chemistry,* vols. I and II, Advan. Chem. Ser. No. 81 (1968), in *Nucl. Sci. Eng.* **36**, 460 (1969).

G. E. Boyd and Q. V. Larson, "Chemistry of Iodine-128 and Iodine-130 Recoils in Neutron-Irradiated Crystalline KIO_3 and KIO_4," *J. Am. Chem. Soc.* **91**, 4639 (1969).

G. E. Boyd and L. C. Brown,[24] "Investigations on the Thermal and Radiolytic Decomposition of Anhydrous Crystalline $KClO_2$," *J. Phys. Chem.* **74**, 1691 (1970).

L. C. Brown[24] and G. E. Boyd, "Microanalytical Method for Determination of Perbromate Ion in the Presence of Macro-Amounts of Other Bromine Anions," *Anal. Chem.* **42**, 291 (1970).

ORGANIC CHEMISTRY

C. J. Collins and C. E. Harding,[25,26] "Ratio of the Rates of Solvent Attack and 3,2–Hydride Shift in the Norbornyl Cation," *J. Am. Chem. Soc.* **91**, 7194 (1969).

H. Kwart,[27] E. N. Givens,[28] and C. J. Collins, "The Acetolysis of 3-Phenyl-2-butylsulfoxonium Ions," *J. Am. Chem. Soc.* **91**, 5532 (1969).

C. J. Collins, "Protonated Cyclopropanes," *Chem. Rev.* **69**, 543 (1969).

C. E. Harding,[25,26] "The Solvolyses of Carbon-14–Labeled 2-(Δ^3-Cyclopentenyl)ethyl Tosylates," Ph.D. thesis, University of Tennessee, Knoxville, August 1969.

---

[21] Health Physics Division.

[22] Department of Chemistry, Maryville College, Maryville, Tenn.

[23] Present address: Lockheed Palo Alto Research Laboratory, Palo Alto, Calif.

[24] Now of the Isotopes Division.

[25] Oak Ridge Graduate Fellow from the University of Tennessee, Knoxville, under appointment with Oak Ridge Associated Universities.

[26] Present address: University of Tübingen, Tübingen, West Germany.

[27] Department of Chemistry, University of Delaware, Newark.

[28] Oak Ridge Graduate Fellow from the University of Delaware, Newark, under appointment with Oak Ridge Associated Universities.

C. J. Collins, M. D. Eckart,[25,29] and V. F. Raaen, "Anion Control of Stereoselectivity During Deaminations," *J. Am. Chem. Soc.* **92**, 1787 (1970).

C. J. Collins and B. M. Benjamin, "Concerted, Backside Displacement and *Exo:Endo* Stereospecificity on Deamination of Substituted Norbornylamines," *J. Am. Chem. Soc.* **92**, 3182 (1970).

B. M. Benjamin and C. J. Collins, "Wagner-Meerwein Rearrangements of Substituted Classical Norbornyl Cations," *J. Am. Chem. Soc.* **92**, 3183 (1970).

PHYSICAL CHEMISTRY

Y. C. Wu,[30] R. M. Rush, and G. Scatchard,[31] "Osmotic and Activity Coefficients for Binary Mixtures of Sodium Chloride, Sodium Sulfate, Magnesium Sulfate, and Magnesium Chloride in Water at 25°. II. Isopiestic and Electromotive Force Measurements on the Two Systems Without Common Ions,"[32] *J. Phys. Chem.* **73**, 2047, 4434 (1969).

M. H. Lietzke and R. W. Stoughton, "Electromotive Force Studies in Aqueous Solutions at Elevated Temperatures. XI. The Thermodynamic Properties of HCl-LiCl Solutions," *J. Tenn. Acad. Sci.* **44**, 66 (1969).

M. H. Lietzke and R. W. Stoughton, "Electromotive Force Studies in Aqueous Solutions at Elevated Temperatures. XII. The Thermodynamic Properties of HCl-CsCl-$BaCl_2$ Mixtures," *J. Inorg. Nucl. Chem.* **31**, 3481 (1969).

R. J. Beshinske[33] and M. H. Lietzke, "Monte Carlo Calculation of Some Thermodynamic Properties of Steam Using a Dipole-Quadrupole Potential," *J. Chem. Phys.* **51**, 2278 (1969).

H. B. Hupf,[34] "The Thermodynamic Properties of Aqueous Hydrochloric Acid–Cesium Chloride–Barium Chloride Mixtures," Ph.D. thesis, University of Tennessee, Knoxville, June 1969.

F. Vaslow, "The Apparent Molal Volumes of the Lithium and Sodium Halides. Critical-Type Transitions in Aqueous Solution," *J. Phys. Chem.* **73**, 3745 (1969).

S. Lindenbaum, L. Leifer,[35] G. E. Boyd, and J. W. Chase,[36] "Variation of Osmotic Coefficients of Aqueous Solutions of Tetra-*n*-alkylammonium Halides at 25 and 65°C," *J. Phys. Chem.* **74**, 761 (1970).

S. Lindenbaum, "Heats of Dilution at 25° of Aqueous Solutions of the Bolaform Electrolyte $[Bu_3N(CH_2)_8NBu_3]X_2$," *J. Phys. Chem.* **73**, 4334 (1969).

G. E. Boyd, "Thermal Effects in Ion Exchange Reactions with Organic Exchangers: Enthalpy and Heat Capacity Changes," *Proc. Intern. Conf. on Ion Exchange in the Process Industries*, Society of Chemical Industry, London (1970).

G. E. Boyd and J. Schubert,[37] "The First Use of Organic and Inorganic Ion Exchangers for Separating Plutonium from Uranium and the Fission Products," *Progress in Nuclear Energy, Series III*, vol. 4, pp. 319–44, Pergamon, London, 1969.

---

[29] Present address: Tennessee Eastman Corp., Kingsport, Tenn.

[30] Present address: National Bureau of Standards, Washington, D.C.

[31] Consultant; Professor of Physical Chemistry, Emeritus, Massachusetts Institute of Technology, Cambridge.

[32] Research jointly sponsored by the Office of Saline Water, U.S. Department of the Interior, and the U.S. Atomic Energy Commission under contract with Union Carbide Corp. and under Contract No. AT-(30-1)-905 with the Massachusetts Institute of Technology.

[33] Department of Chemistry, St. John's University, Jamaica, N.Y.; present address: RCA Research Laboratories, Princeton, N.J.

[34] Isotopes Division; present address: The Medical School, University of Miami, Miami, Fla.

[35] Michigan Technological University, Houghton.

[36] Xerox Corporation Research Laboratories, Rochester, N.Y.

[37] University of Pittsburgh, Pittsburgh, Pa.

S. B. Sachs,[38] W. H. Baldwin, and J. S. Johnson, "Hyperfiltration Studies XVI: Salt Filtration by Dynamically Formed and Cast Poly(Glutamic Acid) and Poly(Acrylic Acid) Membranes,"[39] *Desalination* **6**, 215 (1969).

J. S. Johnson, K. A. Kraus,[40] A. E. Marcinkowsky,[41] H. O. Phillips, and A. J. Shor,[42] "Method of Separating Salts from Aqueous Solutions,"[43] U.S. Pat. 3,449,245 (June 10, 1969).

W. H. Baldwin, R. J. Raridon, and K. A. Kraus,[40] "Properties of Organic-Water Mixtures. X. Activity Coefficients of Sodium Chloride at Saturation in Water Mixtures of Polyglycols and Polyglycol Ethers at 30°,"[43] *J. Phys. Chem.* **73**, 3417 (1969).

C. J. Barton,[42] M. A. Bredig, L. O. Gilpatrick,[42] and Judy A. Fredericksen,[44] "Solubility of Cerium Trifluoride in Molten Mixtures of Lithium, Beryllium, and Thorium Fluorides," *Inorg. Chem.* **9**, 307 (1970).

M. A. Bredig, "The Experimental Evidence for 'Complex Ions' in Some Molten Salt Mixtures," book chapter in *Molten Salts: Characterization and Analysis*, ed. by Gleb Mamantov, Marcel Dekker, New York–London, 1969.

G. H. Cartledge, "Kinetics of Charge and Discharge of the Film on Superpassive Iron," *Chimia (Aarau)* **23**, 450 (1969).

CHEMICAL PHYSICS

J. E. Worsham, Jr.,[45] and W. R. Busing, "The Crystal Structure of Uronium Nitrate (Urea Nitrate) by Neutron Diffraction," *Acta Cryst.* **B25**, 572 (1969).

G. M. Brown, "The Crystal and Molecular Structure of 6-Mercaptopurine Monohydrate. A Second, Independent X-Ray Diffraction Determination," *Acta Cryst.* **B25**, 1338 (1969).

G. R. Freeman,[8] "The Crystal and Molecular Structures of Tri-(*p*-fluorophenyl)-amine and Tri-(*p*-iodophenyl)-amine," Ph.D. dissertation, North Texas State University, Denton, January 1970.

A. H. Narten and H. A. Levy, "Observed Diffraction Pattern and Proposed Models of Liquid Water," *Science* **165**, 447 (1969).

A. H. Narten and H. A. Levy, "Structure of Water," *Science* **167**, 1520 (1970).

A. H. Narten and S. Lindenbaum, "Diffraction Pattern and Structure of the System Tetra-*n*-butylammonium Fluoride–Water at 25°C," *J. Chem. Phys.* **51**, 1108 (1969).

A. H. Narten, "Diffraction Pattern and Structure of Aqueous Ammonium Halide Solutions," *J. Phys. Chem.* **74**, 765 (1970).

W. C. Waggener, A. J. Weinberger, and R. W. Stoughton, "The Near-Infrared Spectrum of Liquid Hydrogen Sulfide," *J. Phys. Chem.* **73**, 3518 (1969).

M. H. Brooker,[46] A. S. Quist, and G. E. Boyd, "Raman Spectrum of Molten $NaNO_3$," *Chem. Phys. Letters* **5**, 357 (1970).

---

[38] Visiting scientist from the Weizmann Institute of Science, Rehovoth, Israel; present address: Gulf General Atomic, San Diego, Calif.

[39] Research sponsored jointly by the Office of Saline Water, U.S. Department of the Interior, and the U.S. Atomic Energy Commission under contract with Union Carbide Corp.

[40] Director's Division.

[41] Present address: Technical Center, Union Carbide Corp., South Charleston, W.Va.

[42] Reactor Chemistry Division.

[43] Based on work sponsored by the Office of Saline Water, U.S. Department of the Interior.

[44] Oak Ridge Associated Universities Research Participant from St. Cloud State College, St. Cloud, Minn.

[45] Chemistry Department, University of Richmond, Richmond, Va.

[46] Postdoctoral Research Fellow from the National Research Council of Canada.

R. W. Holmberg, "ESR Study of $\dot{HCO}$ in Single Crystals of Formic Acid at 77°K," *J. Chem. Phys.* **51**, 3255 (1969).

Z. Luz,[47] A. Reuveni,[47] R. W. Holmberg, and B. L. Silver,[48] "ESR of ^{17}O-Labeled Nitrogen Dioxide Trapped in a Single Crystal of Sodium Nitrite," *J. Chem. Phys.* **51**, 4017 (1969).

M. M. Abraham,[49] C. B. Finch,[50] R. W. Reynolds,[49] and H. Zeldes, "Electron Spin Resonance Spectrum of Divalent Europium in Thorium Dioxide," *Phys. Rev.* **187**, 451 (1969).

T. A. Carlson, C. W. Nestor, Jr.,[18] F. B. Malik,[51] and T. C. Tucker,[18] "Calculations of *K*, *L*, *M*, and *N* Binding Energies and *K* X-Rays for Elements from $Z = 96-120$," *Nucl. Phys.* **A135**, 57 (1969).

M. O. Krause,[52] F. A. Stevie,[53] L. J. Lewis,[54] T. A. Carlson, and W. E. Moddeman,[55] "Multiple Excitation of Neon by Photon and Electron Impact," *Phys. Letters* **31A**, 81 (1970).

T. A. Carlson, W. E. Moddeman,[55] and M. O. Krause,[52] "Electron Shake-Off in Neon and Argon as a Function of Energy of the Impact Electron," *Phys. Rev. A* **1**, 1406 (1970).

T. A. Carlson, W. E. Moddeman,[55] B. P. Pullen,[25,56] and M. O. Krause,[52] "Identification of High Energy Lines in the *K-LL* Auger Spectrum of N_2," *Chem. Phys. Letters* **5**, 390 (1970).

B. P. Pullen,[25,56] "The Construction and Use of a High Resolution Photoelectron Spectrometer," Ph.D. thesis, University of Tennessee, Knoxville, February 1970; ORNL-TM-2794 (February 1970).

F. Schmidt-Bleek,[57] G. Ostrom,[57] and S. Datz, "'Hot' Atomic Halogen Beams from Sputtering of Silver Halides," *Rev. Sci. Instr.* **40**, 1351 (1969).

---

[47]The Weizmann Institute of Science, Rehovoth, Israel.

[48]Technion, Haifa, Israel.

[49]Solid State Division.

[50]Metals and Ceramics Division.

[51]Physics Department, Indiana University, Bloomington.

[52]Thermonuclear Division.

[53]USAEC Fellow in Health Physics from Vanderbilt University, Nashville, Tenn.

[54]Summer student from Morehouse College, Atlanta, Ga.

[55]Graduate student from the University of Tennessee, Knoxville.

[56]Present address: Department of Physical Science, Southeastern Louisiana State College, Hammond.

[57]Department of Chemistry, Purdue University, Lafayette, Ind.; present address: Department of Chemistry, University of Tennessee, Knoxville.

Papers Presented at Scientific and Technical Meetings

NUCLEAR CHEMISTRY

F. E. Coffman,*[1] J. H. Hamilton,[1] A. V. Ramayya,[1] and N. R. Johnson, "Zero Spin for the 1482.6-keV Level in ^{74}Ge from γ-$\gamma(\theta)$," International Conference on Properties of Nuclear States, Montreal, Canada, Aug. 25–30, 1969.

L. L. Riedinger,*[2,3] E. Eichler, V. Fuglsong,[4] G. Hagemann,[4] and B. Herskind,[4] "Coulomb Excitation of ^{154}Gd and ^{166}Er," International Conference on Nuclear Reactions Induced by Heavy Ions, Heidelberg, Germany, July 15–18, 1969.

K. S. Toth,*[5] R. L. Hahn, M. A. Ijaz,[6] and W. M. Sample,[6] "New Isotopes: ^{151}Er, ^{156}Yb, and ^{157}Yb," 1970 Spring Meeting, American Physical Society, Washington, D.C., Apr. 27–30, 1970; *Bull. Am. Phys. Soc.* **15**, 645 (1970).

R. G. Lanier,*[7,8] R. A. Meyer,[9] J. B. Ball,[5] N. R. Johnson, G. D. O'Kelley, and R. K. Sheline,[10] "Levels in ^{161}Tb Excited by the (^{3}He,d) Reaction," 1970 Spring Meeting, American Physical Society, Washington, D.C., Apr. 27–30, 1970; *Bull Am. Phys. Soc.* **15**, 552 (1970).

J. H. Hamilton,*[1] P. E. Little,[1] A. V. Ramayya,[1] and N. R. Johnson, "$M1$ Admixtures in the $2^+(\beta) \rightarrow 2^+$ Transition in ^{178}Hf," 1970 Spring Meeting, American Physical Society, Washington, D.C., Apr. 27–30, 1970; *Bull. Am. Phys. Soc.* **15**, 524 (1970).

P. E. Little,*[1] J. H. Hamilton,[1] A. V. Ramayya,[1] and N. R. Johnson, "Decay of ^{178}Ta," 36th Meeting, Southeastern Section, American Physical Society, University of Florida, Gainesville, Nov. 6–8, 1969; *Bull. Am. Phys. Soc.* **15**, 179 (1970).

N. R. Johnson, "Applications of Quantitative Gamma-Gamma Coincidence Measurements," International Conference on Radioactivity in Nuclear Spectroscopy, Vanderbilt University, Nashville, Tenn., Aug. 11–15, 1969 (invited).

J. H. Hamilton,*[1] N. R. Johnson, L. L. Riedinger,[2,3] D. J. McMillan,[1] A. F. Kluck,[2] and L. C. Whitlock,[1] "Systematics of $K\pi - 0^-$ and 1^- Octupole Bands in Transitional Nuclei," International Conference on Properties of Nuclear States, Montreal, Canada, Aug. 25–30, 1969.

R. L. Ferguson, Franz Plasil,[11] G. D. Alam,[12] and H. W. Schmitt,*[11] "Fragment Energy Correlation Measurements in the Fission of Spontaneously Fissioning Isomers," 1970 Spring Meeting, American Physical Society, Washington, D.C., Apr. 27–30, 1970; *Bull. Am. Phys. Soc.* **15**, 648 (1970).

---

*Speaker.

[1]Physics Department, Vanderbilt University, Nashville, Tenn.

[2]Oak Ridge Graduate Fellow from Vanderbilt University, Nashville, Tenn., under appointment with Oak Ridge Associated Universities.

[3]Present address: Physics Department, University of Notre Dame, Notre Dame, Ind.

[4]Niels Bohr Institute, University of Copenhagen, Copenhagen, Denmark.

[5]Electronuclear Division.

[6]Physics Department, Virginia Polytechnic Institute, Blacksburg.

[7]U.S. Atomic Energy Commission Postdoctoral Fellow under appointment with Oak Ridge Associated Universities.

[8]Present address: Lawrence Radiation Laboratory, Livermore, Calif.

[9]Lawrence Radiation Laboratory, Livermore, Calif.

[10]Florida State University, Tallahassee.

[11]Physics Division.

[12]Guest Scientist from PINSTECH, P.O. Nilore, Rawalpindi, Pakistan.

G. D. Alam,*[12] R. L. Ferguson, Franz Plasil,[11] H. Roesler,[13] and H. W. Schmitt,[11] "Fragment Energy Correlation Measurements for Neutron Induced Fission of ^{234}U as a Function of Neutron Energy," 1970 Spring Meeting, American Physical Society, Washington, D.C., Apr. 27–30, 1970; *Bull. Am. Phys. Soc.* **15**, 648 (1970).

G. D. O'Kelley,* J. S. Eldridge,[14] E. Schonfeld,[15] and P. R. Bell,[15,16] "Elemental Compositions and Ages of Lunar Samples by Non-Destructive Gamma-Ray Spectrometry," Apollo 11 Lunar Science Conference, Houston, Tex., Jan. 5–8, 1970.

G. D. O'Kelley, "Preliminary Gamma-Ray Spectrometry Results on Apollo 12 Samples," Apollo 11 Lunar Science Conference, Houston, Tex., Jan. 5–8, 1970.

G. D. O'Kelley, "Preliminary Examination of Lunar Samples from Apollo 11," Tennessee Academy of Science, Seventy-Ninth Meeting, Sewanee, Tenn., Nov. 21–22, 1969.

G. D. O'Kelley,* J. S. Eldridge,[14] E. Schonfeld,[15] and P. R. Bell,[15,16] "Comparative Radionuclide Concentrations of Apollo 11 and Apollo 12 Samples by Non-Destructive Gamma-Ray Spectrometry," American Geophysical Union, Fifty-First Annual Meeting, Washington, D.C., Apr. 20–24, 1970.

CHEMISTRY AND PHYSICS OF TRANSURANIUM ELEMENTS

C. E. Bemis, Jr., "Nuclear Structure Studies in the Transuranium Region at ORNL," 158th National Meeting, American Chemical Society, New York, Sept. 7–12, 1969; abstract NUCL-78 (invited).

R. J. Silva, R. L. Hahn,* O. L. Keller, K. S. Toth,[5] M. L. Mallory, M. F. Roche,[5] C. E. Bemis, and P. F. Dittner, "Nuclear Chemistry With Heavy Ions at ORNL," 158th National Meeting, American Chemical Society, New York, Sept. 7–12, 1969; abstract NUCL-46 (invited).

R. J. Silva, R. L. Hahn, M. L. Mallory,* C. E. Bemis, P. F. Dittner, O. L. Keller, J. R. Stokely,[14] and K. S. Toth,[5] "Nuclear Chemistry with the Oak Ridge Isochronous Cyclotron," International Conference on the Use of Cyclotrons in Chemistry, Metallurgy, and Biology, Oxford, England, Sept. 22–23, 1969.

O. L. Keller, Jr., "Actinide and Transactinide Elements Production and Research at Oak Ridge," Robert A. Welch Foundation Conferences on Chemical Research. XIII. The Transuranium Elements – The Mendeleev Centennial, Houston, Tex., Nov. 17–19, 1969.

M. R. Schmorak,[17] C. E. Bemis, Jr.,* and M. J. Zender,[18] "Levels in ^{240}Pu Populated in the Decay of ^{240m}Np and in the Alpha Decay of ^{244}Cm," International Conference on Radioactivity in Nuclear Spectroscopy: Nuclear Techniques and Applications, Vanderbilt University, Nashville, Tenn., Aug. 11–15, 1969.

M. R. Schmorak,*[17] C. E. Bemis, Jr., M. Zender,[18] F. Coffman,[1] A. Ramayya,[1] and J. H. Hamilton,[1] "A Two-Phonon Octupole Vibrational Band in ^{240}Pu," 1970 Spring Meeting, American Physical Society, Washington, D.C., Apr. 27–30, 1970; *Bull. Am. Phys. Soc.* **15**, 547 (1970).

R. E. Druschel,* J. Halperin, and C. E. Bemis, Jr., "Half Lives of ^{253}Cf and ^{253}Es," 21st Southeastern Regional Meeting, American Chemical Society, Richmond, Va., Nov. 5–8, 1969; abstract No. 42.

L. J. Nugent, P. G. Laubereau,*[19] G. K. Werner,[11] and K. L. Vander Sluis,[11] "Electron-Transfer Absorption in Some Actinide(III) and Lanthanide(III) Tricyclopentadienides and the Standard II-III Cation Oxidation Potentials," 8th Rare-Earth Research Conference, Reno, Nev., Apr. 19–22, 1970.

---

[13] Guest scientist from Technische Hochschule, Munich, Germany.

[14] Analytical Chemistry Division.

[15] NASA Manned Spacecraft Center, Houston, Tex.

[16] Now of the Director's Division.

[17] Nuclear Data Group.

[18] Oak Ridge Associated Universities Research Participant from Fresno State College, Fresno, Calif.

[19] Visiting scientist from the Federal Republic of Germany, Bonn.

L. J. Nugent, M. W. Swagel,[20] and F. M. Johnson,[20] "Laser-Induced Single- and Double-Photon Excitation and Dissociation in Gaseous Nitrous Oxide" (by abstract only), 36th Meeting, Southeastern Section, American Physical Society, University of Florida, Gainesville, Nov. 6–8, 1969; *Bull. Am. Phys. Soc.* **15**, 164 (1970).

J. H. Burns* and J. R. Peterson,[21] "On the Structures of $AmCl_3$ and $CfCl_3$ and the Ionic Radii of Actinide Elements," American Crystallographic Association, Winter Meeting, New Orleans, La., Mar. 1–5, 1970.

C. E. Bemis, Jr., "Performance and Operating Experience with the Oak Ridge National Laboratory 150-cm Sector Separator," Third American Electromagnetic Isotope Separator Symposium, Brookhaven National Laboratory, Upton, N.Y., Sept. 16–17, 1969 (invited).

ISOTOPE CHEMISTRY

G. M. Begun, "Simple Modification of the Cary Model-81 Raman Spectrophotometer to Permit Use of Laser Light Sources," International Conference on Raman Spectroscopy, Carleton University, Ottawa, Canada, Aug. 4–7, 1969.

RADIATION CHEMISTRY

R. W. Matthews,*[22] H. A. Mahlman, and T. J. Sworski, "Kinetic Evidence for a Primary Yield of NO_3 Radicals in the Radiolysis of Aqueous Nitric Acid Solutions," XXII International Congress of Pure and Applied Chemistry, Sydney, Australia, Aug. 20–27, 1969.

G. E. Boyd, "Recoil and Radiation Chemistry of the Crystalline Alkali-Metal Halates and Perhalates," International Symposium on Chemical Effects of Nuclear Transformations, Cambridge, England, July 1–3, 1969 (invited).

PHYSICAL CHEMISTRY

G. Scatchard,*[23] R. M. Rush, and J. S. Johnson, "The Excess Free Energy and Related Properties of Electrolyte Solutions," symposium on Structures of Water and Aqueous Solutions in honor of T. F. Young, University of Chicago, Chicago, Ill., June 16–18, 1969 (invited).

R. M. Rush and J. S. Johnson,* "Isopiestic Studies on Mixed Perchlorate Solutions," Symposium on Electrolyte Solutions, Middle Atlantic Regional Meeting, American Chemical Society, Newark, Del., Apr. 1–3, 1970 (invited).

G. E. Boyd, "Thermal Effects in Ion Exchange Reactions with Organic Exchangers: Enthalpy and Heat Capacity Changes," International Conference on Ion Exchange in the Process Industries, Society of Chemical Industry, London, England, July 16–18, 1969 (invited).

G. E. Boyd, "Volume Changes in Ion Exchange Reactions," Gordon Research Conference on Ion Exchange, Meriden, N.H., Aug. 18–22, 1969 (invited).

K. Bunzl*[24] and G. E. Boyd, "Donnan Equilibrium in Ion Exchangers," Second Symposium on Ion Exchange, Hungarian Chemical Society, Balatonszeplak, Hungary, Sept. 10–14, 1969 (invited).

F. Nelson, "Some Observations on Mass Transport in Ion Exchange Columns," Gordon Research Conference on Ion Exchange, Meriden, N.H., Aug. 18–22, 1969 (invited).

---

[20] Xerox Corp./EOS Division. Research sponsored by Edgewood Arsenal, U.S. Army.

[21] Department of Chemistry, University of Tennessee, Knoxville.

[22] Visiting scientist from the Australian Atomic Energy Commission Research Establishment, Lucas Heights, New South Wales.

[23] Consultant; Professor of Physical Chemistry, Emeritus, Massachusetts Institute of Technology, Cambridge.

[24] Visiting scientist from Gesellschaft f. Strahlenforschung MBH, Munich, Germany.

R. A. Gilbert, R. H. Busey, C. W. Linsey,[25,26] and R. B. Escue,*[27] "Calorimetric Melting Points and Heats of Fusion for Lead Halides," 158th National Meeting, American Chemical Society, New York, Sept. 7–12, 1969; abstract INOR-30.

R. H. Busey,* C. W. Linsey,[25,26] and R. B. Escue,[27] "High Temperature Enthalpies of Lead Halides," 24th Annual Calorimetry Conference, Portsmouth, N.H., Oct. 14–16, 1969.

F. A. Posey, "Corrosion Processes in Restricted Geometries," Advanced Short Course in Aqueous Corrosion, Ohio State University, Columbus, Oct. 29, 1969 (invited).

CHEMICAL PHYSICS

W. R. Busing, "Least-Squares Refinement of Lattice and Orientation Parameters for Use in Automatic Diffractometry," International Summer School on Crystallographic Computing, International Union of Crystallography Commission on Crystallographic Computing, Carleton University, Ottawa, Canada, Aug. 4–12, 1969 (invited).

P. A. Agron and W. R. Busing,* "A Neutron Diffraction Study of Magnesium Chloride Hexahydrate," Eighth General Assembly and International Congress, International Union of Crystallography, Buffalo, Stony Brook, and Upton, N.Y., and Washington, D.C., Aug. 7–24, 1969.

W. R. Busing, "An Interpretation of the Structures of Alkaline Earth Chlorides in Terms of Interionic Forces," American Crystallographic Association Winter Meeting, Tulane University, New Orleans, La., Mar. 1–5, 1970.

C. K. Johnson, "Introduction to Thermal-Motion Analysis," "The Effect of Thermal Motion on Interatomic Distances and Angles," "Higher Order Statistical Models for Thermal Motion," and "Drawing Crystal Structures by Computer," International Summer School on Crystallographic Computing, International Union of Crystallography Commission on Crystallographic Computing, Carleton University, Ottawa, Canada, Aug. 4–12, 1969 (invited).

C. K. Johnson, "Kinematics of Molecular Motion in Crystals," Eighth General Assembly and International Congress, International Union of Crystallography, Buffalo, Stony Brook, and Upton, N.Y., and Washington, D.C., Aug. 7–24, 1969 (invited).

C. K. Johnson, "Series Expansion Models for Thermal Motion," American Crystallographic Association Winter Meeting, Tulane University, New Orleans, La., Mar. 1–5, 1970.

G. M. Brown, "Neutron Diffraction in the Study of Carbohydrates," Gordon Research Conference on the Chemistry of Carbohydrates, Tilton School, Tilton, N.H., June 9–13, 1969 (invited).

G. M. Brown* and R. Chidambaram,[28] "A Model for Torsional Oscillators in Least-Squares Refinement," Eighth General Assembly and International Congress, International Union of Crystallography, Buffalo, Stony Brook, and Upton, N.Y., and Washington, D.C., Aug. 7–24, 1969 (invited).

G. R. Freeman,*[25,29] H. A. Levy, and G. M. Brown, "Crystal and Molecular Structures of Tri(*p*-fluorophenyl)amine and Tri(*p*-iodophenyl)amine," Eighth General Assembly and International Congress, International Union of Crystallography, Buffalo, Stony Brook, and Upton, N.Y., and Washington, D.C., Aug. 7–24, 1969.

G. M. Brown* and W. E. Thiessen,[30] "The Crystal Structure of Sedoheptulosan Monohydrate," Eighth General Assembly and International Congress, International Union of Crystallography, Buffalo, Stony Brook, and Upton, N.Y., and Washington, D.C., Aug. 7–24, 1969.

---

[25]Oak Ridge Graduate Fellow from North Texas State University, Denton, under appointment with Oak Ridge Associated Universities.

[26]Present address: Emporia College, Emporia, Kan.

[27]Chemistry Department, North Texas State University, Denton.

[28]Visiting scientist 1964–65 from Bhabha Atomic Research Centre, Trombay, Bombay-74, India.

[29]Present address: University of Alabama in Birmingham, University of Alabama Medical Center, Birmingham.

[30]National Institutes of Health Special Postdoctoral Fellow.

H. A. Levy,* W. E. Thiessen,[30] and G. M. Brown, "A Least-Squares Method for Converting Observed Intensities to Normalized Structure Factors," American Crystallographic Association Winter Meeting, Tulane University, New Orleans, La., Mar. 1–5, 1970.

W. E. Thiessen,[30] "Structure and Stereochemistry of α- and β-Cubebene from the Crystal Structure of Nor-β-cubebone," Eighth General Assembly and International Congress, International Union of Crystallography, Buffalo, Stony Brook, and Upton, N.Y., and Washington, D.C., Aug. 7–24, 1969.

W. E. Thiessen,[30] "The Addition Product of an Isocyanide with a Steroidal α,β-Unsaturated Ketone: Structure Determination," American Crystallographic Association Winter Meeting, Tulane University, New Orleans, La., Mar. 1–5, 1970.

A. H. Narten* and H. A. Levy, "Observed Diffraction Pattern and Proposed Models of Liquid Water," Eighth General Assembly and International Congress, International Union of Crystallography, Buffalo, Stony Brook, and Upton, N.Y., and Washington, D.C., Aug. 7–24, 1969 (invited).

C. Folzer*[31] and A. H. Narten, "X-Ray Dirraction Pattern and Structure of Molten $(CH_3)_3N \cdot 10.13\ H_2O$ at 5°C," Eighth General Assembly and International Congress, International Union of Crystallography, Buffalo, Stony Brook, and Upton, N.Y., and Washington, D.C., Aug. 7–24, 1969.

A. H. Narten, "Diffraction Pattern and Correlation Functions of Liquid Gallium," Gordon Research Conference on the Chemistry and Physics of Liquids, Holderness, N.H., Aug. 11–15, 1969.

A. H. Narten, "Diffraction Pattern and Structure of Aqueous Halide Solutions," 158th National Meeting, American Chemical Society, New York, Sept. 7–12, 1969; abstract PHYS-227.

Ralph Livingston, "Paramagnetic Resonance of Liquids During Photolysis," Southeastern Magnetic Resonance Conference, Huntsville, Ala., Sept. 25–26, 1969 (invited).

B. P. Pullen,*[32,33] T. A. Carlson, W. E. Bull,[21] and G. K. Schweitzer,[21] "Photoelectron Spectroscopy of Fluorinated D_{3h}, T_d, $D_{\infty h}$, O_h, and C_{3v} Symmetry Group Compounds," 158th National Meeting, American Chemical Society, New York, Sept. 7–12, 1969; abstract PHYS-176.

W. E. Moddeman,[34] B. P. Pullen,*[32,33] T. A. Carlson, W. E. Bull,[21] and G. K. Schweitzer,[21] "Photoelectron Spectroscopy of Group IV A T_d and C_{3v} Symmetry Group Compounds," 158th National Meeting, American Chemical Society, New York, Sept. 7–12, 1969; abstract PHYS-177.

W. E. Moddeman,*[34] T. A. Carlson, B. P. Pullen,[32,33] and M. O. Krause,[35] "Auger Spectra of Simple Molecules," 158th National Meeting, American Chemical Society, New York, Sept. 7–12, 1969; abstract PHYS-178.

T. A. Carlson, B. P. Pullen,[32,33] W. E. Moddeman,*[34] M. O. Krause,[35] and F. W. Ward,[36] "A High Resolution Electron Spectrometer for Photoelectron and Auger Electron Studies," 158th National Meeting, American Chemical Society, New York, Sept. 7–12, 1969; abstract PHYS-179.

M. O. Krause,*[35] F. A. Stevie,[37] L. J. Lewis,[38] T. A. Carlson, and W. E. Moddeman,[34] "Multiple Ionization of Neon by Electron and Photon Impact," 22nd Conference on Gaseous Electronics, American Physical Society, Gatlinburg, Tenn., Oct. 29–31, 1969.

---

[31] Crystallography Laboratory, University of Pittsburgh, Pittsburgh, Pa.

[32] Oak Ridge Graduate Fellow from the University of Tennessee, Knoxville, under appointment with Oak Ridge Associated Universities.

[33] Present address: Department of Physical Science, Southeastern Louisiana State College, Hammond.

[34] Graduate student from the University of Tennessee, Knoxville.

[35] Thermonuclear Division.

[36] Plant and Equipment Division.

[37] U.S. AEC Fellow in Health Physics from Vanderbilt University, Nashville, Tenn.

[38] Summer student from Morehouse College, Atlanta, Ga.

T. A. Carlson, "Determination of Electron Structure in Molecules by Means of High Resolution Electron Spectroscopy," 27th Annual Pittsburgh Diffraction Conference, Pittsburgh, Pa., Nov. 5–7, 1969 (invited).

B. P. Pullen,[32,33] T. A. Carlson, G. K. Schweitzer,*[21] and W. E. Bull,[21] "High Resolution Electron Spectrometry for Study of Electronic Structure of Molecules," 21st Southeastern Regional Meeting, American Chemical Society, Richmond, Va., Nov. 5–8, 1969; abstract No. 325.

B. P. Pullen,[32,33] T. A. Carlson, W. E. Bull,[21] and G. K. Schweitzer,*[21] "The Photoelectron Spectra of CH_3Cl and CF_3Cl," 21st Southeastern Regional Meeting, American Chemical Society, Richmond, Va., Nov. 5–8, 1969; abstract No. 326.

T. A. Carlson, "Scope of High Resolution Electron Spectroscopy in Chemical Analysis," Eastern Analytical Symposium, New York, Nov. 19–21, 1969 (invited).

L. D. Hulett*[14] and T. A. Carlson, "The Analysis of Compounds of Biological Interest by Electron Spectroscopy," Second Annual Symposium on Automated High Resolution Analysis in the Clinical Laboratory, Oak Ridge National Laboratory, Oak Ridge, Tenn., Mar. 12–13, 1970.

T. A. Carlson, "High Resolution Auger and Photoelectron Spectroscopy," International Symposium on Photoelectron Spectroscopy, University of Tennessee, Knoxville, May 14–15, 1970 (invited).

J. W. Pinson*[39] and P. S. Rudolph, "Characterization of Volatile and Nonvolatile Solids Obtained from the Gas Phase Radiolysis of Pentaborane-9," 159th National Meeting, American Chemical Society, Houston, Tex., Feb. 26, 1970; abstract PHYS-100.

S. Datz, "Molecular Beam Experiments on Inelastic Scattering," Gordon Research Conference on Intermolecular Energy Transfer, Andover, N.H., June 16–20, 1969.

F. Schmidt-Bleek,*[40] G. Ostrom,[40] and S. Datz, "An Atomic Halogen Beam Source for the 0.1 to 10 eV Region," 5th International Hot Atom Chemistry Symposium, Cambridge, England, July 3–5, 1969.

P. F. Dittner* and S. Datz, "Inelastic Scattering of Alkali Atoms and Ions from Hydrogen Molecules," VIth International Conference on the Physics of Electronic and Atomic Collisions, Cambridge, Mass., July 28–Aug. 2, 1969.

S. Datz,* C. D. Moak,[11] B. R. Appleton,[41] M. T. Robinson,[41] and O. S. Oen,[41] "Energy Dependence of Channeled Ion Energy Loss Spectra,"[42] Conference on Atomic Collision Phenomena in Solids, Sussex, England, Sept. 7–12, 1969.

F. Schmidt-Bleek,*[40] G. Ostrom,[40] and S. Datz, "Hot Halogen Atoms from Sputtered Targets," 21st Southeastern Regional Meeting, American Chemical Society, Richmond, Va., Nov. 5–8, 1969; abstract No. 102.

---

[39] Oak Ridge Associated Universities Research Participant from the University of Southern Mississippi, Hattiesburg.

[40] Department of Chemistry, Purdue University, Lafayette, Ind.; present address: Department of Chemistry, University of Tennessee, Knoxville.

[41] Solid State Division.

[42] Collaborative with Solid State Division.

Lectures

NUCLEAR CHEMISTRY

E. Eichler, "Nuclear Chemistry Research at ORNL," Swedish Research Council Laboratory, Studsvik, Sweden, Mar. 10, 1969.

E. Eichler, "Nuclear Spectroscopy in the A = 90 Region," Instituut voor Kernfysisch Onderzoek, Amsterdam, Netherlands, May 21, 1969.

E. Eichler, "The Use of the $(p,n\gamma)$ Process in Nuclear Spectroscopy Studies," Istituto di Fisica Superiore di Firenze, Florence, Italy, July 21, 1969.

E. Eichler, "Nuclear Spectroscopy," Istituto di Fisica Superiore dell Universita di Napoli, Italy, July 28, 1969.

N. R. Johnson, "Some Aspects of Vibrational Behavior in Deformed Nuclei," Seminar, Michigan State University, Lansing, Mar. 18, 1970.

G. D. O'Kelley, "Preliminary Examination of Lunar Samples from Apollo 11," Meeting of Directors of Industrial Research, New York, Sept. 26, 1969; Analytical Group, East Tennessee Section, American Chemical Society, Oak Ridge, Tenn., Oct. 24, 1969; Department of Chemistry, University of Tennessee, Knoxville, Nov. 17, 1969.

G. D. O'Kelley, "The Origin and History of the Moon from Studies of Lunar Samples from Apollo 11 and Apollo 12," National Science Foundation In-Service Science Institute, Knoxville College, Knoxville, Tenn., Mar. 4, 1970; Department of Chemistry, Florida State University, Tallahassee, Mar. 13, 1970; Knoxville Science Club, Knoxville, Tenn., Apr. 3, 1970.

G. D. O'Kelley, "Decay of Neutron-Deficient Nuclides of Mass 89," Department of Chemistry, Florida State University, Tallahassee, Mar. 12, 1970.

G. D. O'Kelley, "A New Look at the Moon: Analysis of Samples from Apollo 11 and Apollo 12," Western Carolinas Section, American Chemical Society, Brevard, N. C., May 5, 1970; Society of Sigma Xi, Vanderbilt University, Nashville, Tenn., May 5, 1970; Savannah River Section, American Chemical Society, Augusta, Ga., May 8, 1970.

CHEMISTRY AND PHYSICS OF TRANSURANIUM ELEMENTS

O. L. Keller, Jr., "Actinide and Transactinide Elements Production and Research at Oak Ridge," North Carolina State University, Raleigh, Dec. 11, 1969.

R. J. Silva, "The Transuranium Elements," Oak Ridge Associated Universities, Oak Ridge, Tenn., July and September 1969.

R. J. Silva, "One Atom at a Time Chemistry," Department of Chemistry Seminar, University of Tennessee, Knoxville, Feb. 25, 1970.

P. F. Dittner, "Production and Detection of Transuranium Elements," Seydel-Woolley Visiting Lectureship, Georgia Institute of Technology, Atlanta, Jan. 19, 1970.

R. L. Hahn, "Beta Emission and Interactions," Symposium on Liquid Scintillation Counting, Oak Ridge Associated Universities, Oak Ridge, Tenn., June 2–20, 1969.

R. L. Hahn, "Experiments at the Oak Ridge Isochronous Cyclotron," Summer Institute for College Science Teachers, Oak Ridge Associated Universities, Oak Ridge, Tenn., Aug. 8, 1969.

R. L. Hahn, "Experiments at the End of the Periodic Table," Physics Department Colloquium, University of Houston, Houston, Tex., Nov. 20, 1969.

L. J. Nugent, "Transuranium Element Production at ORNL and the Luminescence of Cm(III) in Various Liquid Media," Physics Department Colloquium, Vanderbilt University, Nashville, Tenn., May 23, 1969.

L. J. Nugent, "The Man Made Transuranium Elements and Some Recent Spectroscopic Studies of Their Chemical Compounds," American Chemical Society Lecture, University of Louisville, Louisville, Ky., Jan. 29, 1970.

L. J. Nugent, "Intramolecular Energy Transfer and Sensitized Luminescence in Actinide(III) β-Diketone Chelates," Chemistry Department Seminar, University of Louisville, Louisville, Ky., Jan. 29, 1970.

ORGANIC CHEMISTRY

C. J. Collins, "Aufklärung von Reaktionsmechanismen in der organischen Chemie," Gesellschaft Deutscher Chemiker Ortsvergand Wuppertal/Hagen, Wuppertal-Elberfeld, May 21, 1969.

C. J. Collins, "Erinnerungseffekte während Desaminierungen," University of Göttingen, Germany, June 2, 1969; University of Munich, Germany, July 4, 1969.

C. J. Collins, "The Use of Isotopes in Organic Chemistry," Birmingham Southern College, Birmingham, Ala., Nov. 7, 1969; Southern Illinois University, Carbondale, Feb. 6, 1970.

C. J. Collins, "Memory Effects During Deaminations," University of Alabama, Tuscaloosa, Feb. 18, 1970; University of Oklahoma, Norman, Mar. 12, 1970; University of Wisconsin, Milwaukee, Apr. 6, 1970; Northeast Tennessee Section of the American Chemical Society, Emory and Henry College, Emory, Va., May 4, 1970.

PHYSICAL CHEMISTRY

M. H. Lietzke, "Desalination and the Thermodynamics of Sea Water," Dupont Seminar, University of Tennessee, Knoxville, Oct. 9, 1969.

R. J. Herdklotz,[1] "The Thermodynamic Properties of Aqueous Hydrochloric Acid–Metal Chloride Mixtures at Elevated Temperatures," South Carolina Academy of Science, Columbia, Apr. 24, 1970.

E. H. Taylor, "Anomalous Properties, Yes; Anomalous Water, No!" Seminar, Brookhaven National Laboratory, Upton, N.Y., Apr. 8, 1970.

F. A. Posey, "Crevice Corrosion and Pitting of Titanium and Its Alloys," Seminar, Department of Metallurgical Engineering, Ohio State University, Columbus, Ohio, May 29, 1969.

CHEMICAL PHYSICS

C. K. Johnson, "Mathematical Models for Analyzing Bragg Diffraction Data from Crystals with Non-Gaussian Thermal Motion," National Bureau of Standards, Washington, D.C., Jan. 6, 1970.

C. K. Johnson, "On Extracting Information of Chemical Interest from Crystallographic Thermal-Motion Parameters," Iowa State University, Ames, Apr. 30, 1970.

C. K. Johnson, "The Analysis of Skew and Kurtose Thermal-Motion Density Functions," Iowa State University, Ames, May 1, 1970.

W. E. Thiessen,[2] "Applications of Diffraction Methods to Organic Structure Determinations," University of Kansas, Lawrence, Feb. 13, 1970; Clemson University, Clemson, S.C., Sept. 17, 1969.

T. A. Carlson, "Determination of Electronic Structures in Molecules by Means of High Resolution Electron Spectroscopy," Chemistry Seminar, University of Minnesota, Minneapolis, Feb. 19, 1970.

---

[1] Oak Ridge Graduate Fellow from the University of Tennessee, Knoxville, under appointment with Oak Ridge Associated Universities.

[2] National Institutes of Health Special Postdoctoral Fellow.

T. A. Carlson, "Electron Spectroscopy in Chemical Studies," Chemical Physics Seminar, University of Tennessee, Knoxville, Apr. 18, 1970.

P. S. Rudolph, "The Changing Techniques in Radiation Chemistry," Seminar, Thomas More College, Covington, Ky., Apr. 20, 1970.

P. S. Rudolph, "The Mass Spectrometer as a Tool in Radiation Chemistry," Physical Science Seminar, Department of Physics, Thomas More College, Covington, Ky., Apr. 20, 1970.

S. Datz, "Fast Heavy Ion Collision Physics," Institute of Physics, University of Aarhus, Aarhus, Denmark, Aug. 27, 1969.

S. Datz, "Channeling: Motion of Energetic Particles in Solids," Department of Physics, University of Georgia, Athens, Oct. 31, 1969.

Supplementary Activities

STAFF

PROFESSIONAL AND EDUCATIONAL ACTIVITIES

Russell Baldock	Editorial Board, *International Journal of Mass Spectrometry and Ion Physics,* 1968–present.
G. E. Boyd	Nominating Committee, Division of Nuclear Chemistry and Technology, American Chemical Society, 1970.
	Professional Awards Committee, Division of Nuclear Chemistry and Technology, American Chemical Society, 1970–1971.
	Session Chairman, Fifth International Informal Hot-Atom Chemistry Meeting, Cambridge, England, July 3–5, 1969.
	Editorial Advisory Board, *Radiochimica Acta,* 1963–present.
	Honorary Editorial Board, *Radiokhimiia,* Pergamon Press, Inc., 1961–present.
R. H. Busey	Secretary-Treasurer, Calorimetry Conference, 1963–1969.
	Director, Calorimetry Conference, 1969–1971.
W. R. Busing	Vice-President, American Crystallographic Association, 1970.
	Program Chairman, Winter Meeting, American Crystallographic Association, Tulane University, New Orleans, La., Mar. 2–5, 1970.
	Editor, *Transactions of the American Crystallographic Association,* Volume 6, 1970.
T. A. Carlson	Lecturer in Physics, University of Tennessee, Oak Ridge Extension, October 1969–March 1970.
C. J. Collins	Professor of Chemistry, part time, University of Tennessee, Knoxville, January 1964–present.
S. Datz	Steering Committee, International Conference on the Physics of Electronic and Atomic Collisions, International Union of Pure and Applied Physics, 1963–present.
	Program Committee, Division of Electron Physics, American Physical Society, 1969–1970.
	Co-chairman, Conference on Dynamics of Molecular Collisions, Oak Ridge National Laboratory, 1969–1970.
	Editorial Advisory Board, *Atomic Data,* 1969–present.
	Chairman, Gordon Research Conference on Particle-Solid Interactions, 1969–1970.
	ORNL Long Range Planning Group, December 1969–April 1970.
	Guest Professor, Institute of Physics, University of Aarhus, Aarhus, Denmark, April 13–June 12, 1970.
R. L. Hahn	Committee on Major Nuclear Facilities, Division of Nuclear Chemistry and Technology, American Chemical Society, 1970.
	Ad Hoc Committee on the Outside Use of the Super-HILAC, American Physical Society, 1970.
O. L. Keller, Jr.	USAEC Transplutonium Program Committee, 1969–1972.
	Member, Nuclear Physics Survey Panel, National Academy of Sciences, 1969–1970.
K. A. Kraus	Editorial Board, *Journal of Chromatography,* 1958–present.
	Editorial Advisory Board, *Journal of Inorganic and Nuclear Chemistry,* 1958–present.
	Editorial Board, *Desalination,* 1966–present.
M. H. Lietzke	Professor of Chemistry, part time, University of Tennessee, Knoxville, January 1964–present.

Siegfried Lindenbaum	Professor of Biomedical Sciences, part time, University of Tennessee–Oak Ridge Graduate School of Biomedical Sciences, October 1969–present.
Ralph Livingston	Professor of Chemistry, part time, University of Tennessee, Knoxville, January 1964–present.
	ORNL liaison officer for ORNL–University of Tennessee part-time teaching programs, 1968–present.
	Member, Graduate Council, University of Tennessee, Knoxville, January 1970–present.
	Vice-chairman, Southeastern Magnetic Resonance Conference, Columbia, S.C., Oct. 1–2, 1970.
	Co-chairman, ESR Symposium, Division of Physical Chemistry, American Chemical Society, Athens, Ga., Dec. 7–9, 1970.
	Participant, Workshop for Faculties of Traditionally Negro Institutions, Oak Ridge, Tenn., Aug. 4–29, 1969.
	Participant, Southern College University Union Workshop, September and November 1969.
G. E. Moore	Instructor in Chemistry, National Science Foundation In-Service Institute for Secondary School Science Teachers, Knoxville College, Knoxville, Tenn., 1967–present.
G. D. O'Kelley	Professor of Chemistry, part time, University of Tennessee, Knoxville, January 1964–present.
	Subcommittee on Radiochemistry, National Academy of Sciences–National Research Council, 1962–present.
	Lunar Sample Preliminary Examination Team, an advisory committee to the NASA Manned Spacecraft Center, Houston, Tex., 1967–1970.
	Committee on Major Nuclear Facilities, Division of Nuclear Chemistry and Technology, American Chemical Society, 1967–1969.
	Chairman-Elect, Division of Nuclear Chemistry and Technology, American Chemical Society, 1970.
R. J. Raridon	State Sponsor of the Collegiate Division, Tennessee Academy of Science, 1965–present.
	President-Elect, Tennessee Academy of Science, 1970.
R. W. Stoughton	Editorial Advisory Board, *Journal of Inorganic and Nuclear Chemistry*, 1958–present.
E. H. Taylor	Board of Directors, Institute of Catalysis.
	Participant, Workshop for Faculties of Traditionally Negro Institutions, Oak Ridge, Tenn., Aug. 4–29, 1969.
	Participant, Third Summer Conference on "Science for Clergymen," July 7–18, 1969.

FOREIGN MEETINGS AND ACTIVITIES

Meeting and/or Activity	Location	Staff Member(s)
Visiting Professor of Chemistry, Chemisches Institut der Universität Tübingen (September 1968–July 1969)	Tübingen, West Germany	C. J. Collins
Guest scientist, Niels Bohr Institute (August 1968–August 1969)	Copenhagen, Denmark	E. Eichler
International Conference on Nuclear Reactions Induced by Heavy Ions, July 15–18, 1969	Heidelberg, Germany	E. Eichler
International Conference on the Properties of Nuclear States, Aug. 25–30, 1969	Montreal, Canada	E. Eichler
International Symposium on Chemical Effects of Nuclear Transformations, July 1–3, 1969	Cambridge, England	G. E. Boyd
International Conference on Ion Exchange in the Process Industries, Society of Chemical Industry, July 16–18, 1969	London, England	G. E. Boyd
Second Symposium on the Physics and Chemistry of Fission, July 28–Aug. 1, 1969	Vienna, Austria	R. L. Ferguson
International Conference on Raman Spectroscopy, Aug. 4–7, 1969	Carleton University, Ottawa, Canada	G. M. Begun

Meeting and/or Activity	Location	Staff Members(s)
International Summer School on Crystallographic Computing, International Union of Crystallography Commission on Crystallographic Computing, Aug. 4–12, 1969	Carleton University, Ottawa, Canada	W. R. Busing C. K. Johnson
Ninth International Symposium on Free Radicals, Aug. 24–29, 1969	Banff, Canada	R. Livingston
Conference on Atomic Collision Phenomena in Solids, Sept. 7–12, 1969	Sussex, England	S. Datz
International Conference on the Use of Cyclotrons in Chemistry, Metallurgy, and Biology, Sept. 22–23, 1969	Oxford, England	M. L. Mallory

COLLABORATIVE RESEARCH

Institution	Collaborator(s)	Subject	Staff Member(s)
University of Alabama	D. A. Zatko	Study of silver compounds by electron spectroscopy[1]	T. A. Carlson
Andrews University	M. C. Kelley J. R. Van Hise	Search for the 0^+ member of the two-phonon vibrational state in ^{110}Cd	N. R. Johnson
Argonne National Laboratory	A. M. Friedman	Search for fission isomerism in ^{241}Pu	C. E. Bemis, Jr.
Centre D'Etude de L'Energie Nucleaire, Mol, Belgium	P. Fettweis	Decay of ^{101}Tc	G. D. O'Kelley
David Lipscomb College	J. W. Dawson	An investigation of radioactive ^{163}Tm	N. R. Johnson R. J. Silva
University of Delft, Netherlands	B. van Nooijen	Properties of radioactive ^{84}Y and ^{86}Y	N. R. Johnson
University of Delhi, India	S. C. Pancholi	Investigations of the decay properties of ^{84}Y and ^{59}Fe	N. R. Johnson
Florida State University	R. K. Sheline	Levels in ^{161}Tb excited by the (^{3}He,d) reaction and by the decay of 3.7-min ^{161}Gd	N. R. Johnson
Indiana University	F. B. Malik	Use of atomic wave functions[1]	T. A. Carlson
Institute of Nuclear Research, Amsterdam, Netherlands	J. Konijn	Properties of radioactive ^{84}Y	N. R. Johnson
Lawrence Radiation Laboratory, Berkeley	J. Harris M. Nurmia K. Eskola A. Ghiorso	Chemical separation of element 104	R. J. Silva
Lawrence Radiation Laboratory, Livermore	R. G. Lanier	Search for the 0^+ member of the two-phonon vibrational state in ^{110}Cd	N. R. Johnson
	R. G. Lanier R. A. Meyer	Levels in ^{161}Tb excited by the (^{3}He,d) reaction and by the decay of 3.7-min ^{161}Gd	N. R. Johnson G. D. O'Kelley
Maryville College	P. J. Ogren	Pulse radiolysis of nitric oxide	C. J. Hochanadel J. A. Ghormley
Massachusetts Institute of Technology School of Chemical Engineering Practice, Oak Ridge Station	Various teams	Hyperfiltration with dynamically formed membranes	J. S. Johnson K. A. Kraus

[1] In collaboration with the Physics Division.

Institution	Collaborator(s)	Subject	Staff Member(s)
Middle East Technical University, Ankara, Turkey	N. K. Aras	Decay of ^{101}Tc	G. D. O'Kelley
		Level properties of the deformed nucleus ^{184}W	N. R. Johnson
University of Missouri	D. E. Troutner	Independent fission yield studies	R. L. Ferguson
University of Naples, Italy	G. G. Chilosi	Decay of ^{101}Tc	G. D. O'Kelley
NASA Manned Spacecraft Center	E. Schonfeld	Determination of primordial and cosmogenic radionuclide content of lunar material by gamma-ray spectrometry	G. D. O'Kelley
Purdue University	R. C. Hagenauer	Decay of neutron-deficient nuclides of mass 89	G. D. O'Kelley E. Eichler
Savannah State College	M. P. Menon	Decay of 86-sec ^{136}I	E. Eichler N. R. Johnson G. D. O'Kelley
University of Southern Mississippi	J. W. Pinson	Study of solid polymers from the radiolysis of pentaborane-9 vapor	R. Baldock P. S. Rudolph
St. John's University	R. J. Beshinske	Monte Carlo calculations of the thermodynamic properties of water	M. H. Lietzke
University of Tennessee	F. K. Schmidt-Bleek	Chemical accelerator sources	S. Datz
	W. E. Bull G. K. Schweitzer	Use of electron spectroscopy for chemical analysis[1]	T. A. Carlson
Vanderbilt University	J. H. Hamilton A. V. Ramayya F. E. Coffman	Two-phonon octupole states in ^{240}Pu	C. E. Bemis, Jr.
	G. D. Benson R. G. Albridge	Decay of ^{192}Au	G. D. O'Kelley
	G. D. Benson A. V. Ramayya R. G. Albridge	Decay of ^{194}Au to levels in ^{194}Pt	G. D. O'Kelley
	J. H. Hamilton A. V. Ramayya	Systematics of the $K\pi = 0^-$ and 1^- octupole bands in transitional nuclei	N. R. Johnson
		A study of the properties of some vibrational spherical nuclei	N. R. Johnson
		Studies of the vibrational behavior of deformed nuclei	N. R. Johnson
Virginia Polytechnic Institute	M. A. Ijaz and W. M. Sample	Properties of rare-earth alpha emitters	R. L. Hahn
Washington University West Georgia College	D. G. Sarantites H. W. Boyd	Levels in ^{110}Cd populated in the decay of 69-min ^{110g}In	N. R. Johnson
Xerox Corp., Pasadena, Calif.	M. W. Swagel F. M. Johnson	Laser-induced single- and double-photon excitation and dissociation in gaseous nitrous oxide	L. J. Nugent

ANNUAL INFORMATION MEETING AND ADVISORY COMMITTEE

The Annual Information Meeting of the Chemistry Division was held October 8, 1969. Reports presented at the Meeting were:

E. H. Taylor	Introduction
S. Datz	Collision-Induced Vibrational Excitation and Dissociation of Molecular Hydrogen with Energetic Alkali Atoms
T. A. Carlson	The Use of High-Resolution Electron Spectroscopy in Chemical Analysis[1]
G. D. O'Kelley	Determination of Radionuclides in Lunar Samples from Apollo 11
A. R. Jones	Energy Transfer in the Radiolysis of Aliphatic Carboxylic Acids
T. J. Sworski	Kinetic Evidence for a Primary Yield of HSO_4 Radicals in the Radiolysis of Aqueous Sulfuric Acid Solutions
R. Livingston	Paramagnetic Resonance Studies of Liquids
R. A. Gilbert	The High-Temperature Enthalpies of the Lead Halides
W. R. Busing	Interionic and Intermolecular Forces in Crystalline Hydrates
A. H. Narten	Structure in Water and Aqueous Solutions
N. R. Johnson	Vibrational Properties of Nuclei
R. J. Silva	Heavy Actinides and Transactinides
O. L. Keller	Superheavy Elements

Members of the Advisory Committee were:

Prof. Paul D. Bartlett (1966–1969)
Department of Chemistry
Harvard University
Cambridge, Massachusetts 02138

Dr. Gerhart Friedlander, Chairman (1966–1969)
Department of Chemistry
Brookhaven National Laboratory
Upton, Long Island, New York 11973

Dr. Joseph J. Katz (1965–1969)
Argonne National Laboratory
9700 South Cass Avenue
Argonne, Illinois 60439

Prof. Harry H. Sisler (1966–1969)
Dean, College of Arts and Sciences
University of Florida
Gainesville, Florida 32601

VISITING SCIENTISTS

Name	Affiliation	ORNL Research Program	Sponsor
J. L. Atwood	University of Alabama	Transuranium Research Laboratory	ORAU Faculty Research Participation Program
M. C. Banta	East Texas Baptist College	Electrochemical Kinetics	Summer employee (faculty)
L. Blum	University of Puerto Rico	Neutron and X-Ray Diffraction	ORAU Faculty Research Participation Program
M. H. Brooker	University of Waterloo, Waterloo, Ontario	Radiation and Hot-Atom Chemistry of Inorganic Crystalline Solids	National Research Council of Canada
R. Desiderato	North Texas State University	Neutron and X-Ray Diffraction	ORAU Faculty Research Participation Program

Name	Affiliation	ORNL Research Program	Sponsor
J. K. Dohrmann	Freie Universität Berlin, Institut für Physikalische Chemie	Microwave and Radio-Frequency Spectroscopy	Deutsche Forschungsmeinschaft
Leela Ganguly	Louisiana State University	Transuranium Research Laboratory	Louisiana State University
R. V. Gentry	Columbia Union College	Transuranium Research Laboratory	Columbia Union College
E. W. Graham	University of California at Los Angeles	Physical Chemistry	UCLA
R. G. Lanier		Nuclear Chemistry	U.S. AEC Postdoctoral Fellowship Program
P. G. Laubereau	Anorganisch-Chemisches Laboratorium, Technische Hochschule München, Munich, Germany	Transuranium Research Laboratory	Bundesministerium für wissenschaftliche Forschung, Bonn, Federal Republic of Germany
P. J. Ogren	Maryville College	Radiation Chemistry	
C. W. Owens	University of New Hampshire	Radiation and Hot-Atom Chemistry of Inorganic Crystalline Solids	ORAU Faculty Research Participation Program
S. W. Peterson	Argonne National Laboratory	Neutron and X-Ray Diffraction	ANL
M. J. Pikal	University of Tennessee	Physical Chemistry of Polyelectrolyte Systems	
J. W. Pinson	University of Southern Mississippi	Mass Spectrometry	ORAU Faculty Research Participation Program
F. K. Schmidt-Bleek	University of Tennessee	Molecular Beam	Consultant
R. M. Statnick		Molecular Beam	U.S. AEC Postdoctoral Fellowship Program
S. P. Tanner	University of West Florida	Transuranium Research Laboratory	Summer employee (faculty)
W. E. Thiessen		Neutron and X-Ray Diffraction	National Institutes of Health Special Postdoctoral Fellow
W. J. Wallace	Muskingum College	Water Research Program	ORAU Faculty Research Participation Program
M. J. Zender	Fresno State College	Transuranium Research Laboratory	ORAU Faculty Research Participation Program

STUDENTS

GRADUATE

Name	Major Professor and/or Institution	Staff Advisor	Field of Research	Sponsor
J. A. Fahey	J. R. Peterson, University of Tennessee	L. J. Nugent	Transuranium Research Laboratory	Oak Ridge Graduate Fellowship Program
L. Finkel	J. A. Marinsky, State University of New York at Buffalo	G. E. Boyd E. Eichler R. L. Ferguson	Independent fission yields of ^{101}Tc, ^{104}Tc, and ^{105}Tc from thermal-neutron induced fission of ^{235}U	

Name	Major Professor and/or Institution	Staff Advisor	Field of Research	Sponsor
G. R. Freeman	Robert Desiderato, Jr., North Texas State University	H. A. Levy G. M. Brown	The Crystal and Molecular Structures of Tri-(*p*-fluorophenyl)-amine and Tri-(*p*-iodophenyl)-amine (Ph.D. thesis, January 1970)	Oak Ridge Graduate Fellowship Program
D. W. Gosbin	M. H. Lietzke, University of Tennessee	M. H. Lietzke	Monte Carlo calculations of thermodynamic properties of electrolyte solutions	
M. S. Green[2]	W. W. Wyatt, University of Tennessee	B. M. Benjamin	Stereochemistry of 1,2-glycols by nuclear magnetic resonance	ORAU Special Training Division
C. E. Harding	C. J. Collins, University of Tennessee	C. J. Collins	The Solvolyses of ^{14}C-labeled 2-(Δ^3-cyclopentenyl)ethyl Tosylates (Ph.D. thesis, August 1969)	Oak Ridge Graduate Fellowship Program
R. J. Herdklotz	M. H. Lietzke, University of Tennessee	M. H. Lietzke	Thermodynamic properties of aqueous HCl-NaCl-$MgCl_2$ mixtures	Oak Ridge Graduate Fellowship Program
H. B. Hupf[3]	M. H. Lietzke, University of Tennessee	M. H. Lietzke	The Thermodynamic Properties of Aqueous HCl-CsCl-$BaCl_2$ Mixtures (Ph.D. thesis, June 1969)	ORNL
A. E. Jonas	W. E. Bull and G. K. Schweitzer, University of Tennessee	T. A. Carlson	Photoelectron spectroscopy of gaseous molecules[1]	University of Tennessee NASA Research Grant
N. Kashihira	F. K. Schmidt-Bleek, University of Tennessee	S. Datz	Chemical accelerator sources	
A. F. Kluk	J. H. Hamilton, Vanderbilt University	N. R. Johnson	Vibrational behavior of deformed rare-earth nuclei	Oak Ridge Graduate Fellowship Program
R. A. Kuebbing	Case Western Reserve University	E. Eichler J. K. Dickens[4]	Measurements of Transition Probabilities in Some Middle Weight Nuclei (Ph.D. thesis, January 1970)	Oak Ridge Graduate Fellowship Program
C. W. Linsey	R. B. Escue, North Texas State University	R. H. Busey R. A. Gilbert	High-temperature enthalpies of the lead halides – enthalpies and entropies of fusion	Oak Ridge Graduate Fellowship Program
W. E. Moddeman	W. E. Bull and G. K. Schweitzer, University of Tennessee	T. A. Carlson	Auger spectroscopy of gaseous molecules[1]	University of Tennessee NASA Research Grant
G. L. Ostrom	F. K. Schmidt-Bleek, University of Tennessee	S. Datz	Sputtering studies	
B. P. Pullen	W. E. Bull and G. K. Schweitzer, University of Tennessee	T. A. Carlson	The Construction and Use of a High Resolution Photoelectron Spectrometer (Ph.D. thesis, February 1970)[1]	Oak Ridge Graduate Fellowship Program

[2] M.Ed. candidate in the College of Education.

[3] Isotopes Division.

[4] Neutron Physics Division.

Name	Major Professor and/or Institution	Staff Advisor	Field of Research	Sponsor
P. R. Reed	F. K. Schmidt-Bleek, University of Tennessee	C. J. Hochanadel T. J. Sworski	Radiation chemistry of methane	AUA-ANL Pre-doctoral Fellowship
N. Singhal	J. H. Hamilton, Vanderbilt University	N. R. Johnson E. Eichler	Vibrational properties of even-even spherical nuclei	Vanderbilt University
J. N. Stevenson	J. R. Peterson, University of Tennessee	O. L. Keller, Jr.	Transuranium Research Laboratory	

UNDERGRADUATE

Name	Institution	ORNL Research Program	Sponsor
L. L. Ansell	Kansas State College	Organic Chemistry	ORAU Summer Student Trainee Program
R. J. Boulware	Haverford College	Isotope Chemistry	Black Undergraduate Program
K. H. Bowen	University of Mississippi	Molecular Beam	ORAU Summer Student Trainee Program
A. Elaine Cureton	Knoxville College	Water Research Program	Black Undergraduate Program
Linda L. Gainer	Fisk University	Chemistry of Aqueous Systems	Black Undergraduate Program
R. J. Katt	Williams College	Molten Salts	ORAU Summer Student Trainee Program
E. C. Kostansek	Hiram College	Neutron and X-Ray Diffraction	ORAU Summer Student Trainee Program
Ivy W. Nixon	Tennessee State University		ORNL Summer Secretary
Omega N. Norton	Knoxville College	Organic Chemistry	Black Undergraduate Program
J. G. Porterfield	University of Tennessee	Chemistry of Aqueous Systems	Cooperative Education Program
Elizabeth E. Willis	Westhampton College	Chemistry of Aqueous Systems	ORAU Summer Student Trainee Program

ORNL-4581
UC-4 – Chemistry

INTERNAL DISTRIBUTION

1. Biology Library
2–4. Central Research Library
5. Laboratory Shift Supervisor
6. MIT Practice School
7–8. ORNL – Y-12 Technical Library Document Reference Section
9–41. Laboratory Records Department
42. Laboratory Records, ORNL R.C.
43. H. I Adler
44. P. A. Agron
45. C. R. Baldock
46. W. H. Baldwin
47. C. E. Bemis
48. D. S. Billington
49. F. F. Blankenship
50. E. G. Bohlmann
51. C. J. Borkowski
52–56. G. E. Boyd
57. M. A. Bredig
58. R. B. Briggs
59. H. R. Bronstein
60. A. R. Brosi
61. G. M. Brown
62. J. H. Burns
63. R. H. Busey
64. W. R. Busing
65. T. A. Carlson
66. G. H. Cartledge
67. C. J. Collins
68. D. R. Cuneo
69. F. L. Culler
70. M. D. Danford
71. S. Datz
72. J. S. Drury
73. A. S. Dworkin
74. E. Eichler
75. R. L. Ferguson
76. J. L. Gabbard
77. J. A. Ghormley
78. R. A. Gilbert
79. J. H. Gillette
80. W. R. Grimes
81. R. L. Hahn
82. J. Halperin
83. R. F. Hibbs
84. C. J. Hochanadel
85. H. P. Carter
86. C. K. Johnson
87. J. S. Johnson
88. N. R. Johnson
89. W. H. Jordan
90. O. L. Keller
91. M. T. Kelley
92. B. H. Ketelle
93. K. A. Kraus
94. J. A. Lane
95. E. Lamb
96. H. A. Levy
97. M. H. Lietzke
98. T. A. Lincoln
99. S. Lindenbaum
100. J. L. Liverman
101. R. Livingston
102. R. S. Livingston
103. R. N. Lyon
104. H. G. MacPherson
105. Peter Mazur
106. J. R. McNally, Jr.
107–117. G. E. Moore
118. K. Z. Morgan
119. A. H. Narten
120. L. J. Nugent
121. G. D. O'Kelley
122. G. W. Parker
123–124. R. B. Parker
125. F. Plasil
126. J. J. Pinajian
127. F. A. Posey
128. Helen Raaen
129. R. J. Raridon
130. S. A. Reynolds
131. P. S. Rudolph
132. H. W. Schmitt
133. H. E. Seagren
134. E. D. Shipley
135. M. J. Skinner
136. H. G. Smith
137. A. H. Snell
138. R. W. Stoughton
139. D. A. Sundberg
140. T. J. Sworski
141–194. E. H. Taylor
195. R. E. Thoma
196. K. S. Toth
197. D. B. Trauger
198. F. Vaslow
199. G. M. Watson
200. A. M. Weinberg
201. T. E. Willmarth
202. G. Scatchard (consultant)

EXTERNAL DISTRIBUTION

203. H. Miller, Office of Isotope Development, AEC, Washington
204. R. H. Schuler, Radiation Research Laboratories, Mellon Institute, 4400 Fifth Ave., Pittsburgh 13, Pa.
205. Division of Research and Development, AEC, Washington
206. Laboratory and University Division, AEC, ORO
207. Boeing Airplane Company
208. Union Carbide Corporation, Chemicals Division (South Charleston)
209. North American Aviation, Inc.

210. Masaharu Kondo, Professor of Chemistry, Radiation Chemistry Laboratory, Tokyo Metropolitan University, 1-950, Fukasawa-cho, Setagaya-ku, Tokyo, Japan
211. M. Daniels, Department of Chemistry, University College of West Indies, Kingston 7, Jamaica
212. J. P. W. Houtman, Reactor Institute Delft, Technische Hogeschool, Delft, The Netherlands
213. Technion, Israel Institute of Technology, Department of Nuclear Science, Haifa, Israel
214. W. T. Smith, Jr., Department of Chemistry, University of Tennessee, Knoxville
215. J. H. Green, Department of Nuclear and Radiation Chemistry, The University of New South Wales, P.O. Box 1, Kensington, N.S.W., Australia
216. Ingmar Bergstrom, Nobel Institute of Physics, Stockholm 50, Sweden
217. Riki Kobayashi, William Marsh Rice University, Houston, Texas
218. J. A. Swartout, 270 Park Avenue, New York 17, New York
219. W. W. Grigorieff, Assistant to the Executive Director, Oak Ridge Associated Universities
220. Enrico Cerrai, CISE, Milan, Italy
221. H. E. Podall, Office of Saline Water, U.S. Department of the Interior, Washington, D.C.
222. D. E. Troutner, Chemistry Department, University of Missouri, Columbia, Missouri
223. J. H. Hamilton, Physics Department, Vanderbilt University, Nashville, Tennessee
224. W. H. McCoy, Office of Saline Water, U.S. Department of the Interior, Washington, D.C.
225. Sidney Johnson, Office of Saline Water, U.S. Department of the Interior, Washington, D.C.
226. F. H. Coley, Office of Saline Water, U.S. Department of the Interior, Washington, D.C.
227. W. A. Schwartz, Cincinnati Water Research Laboratory, 4676 Columbia Parkway, Cincinnati, Ohio
228. Sidney Langer, Gulf General Atomic, San Diego, California
229. J. R. Peterson, Department of Chemistry, University of Tennessee, Knoxville, Tennessee
230. Library, Wah Chang Albany Corporation, P.O. Box 460, Albany, Oregon
231. S. B. Sachs, Weizmann Institute of Science, Rehovoth, Israel
232. F. Schmidt-Bleek, Department of Chemistry, University of Tennessee, Knoxville, Tennessee
233. F. E. Walker, Chemistry Department, Lawrence Radiation Laboratory, Livermore, California
234. Robert Vandenbosch, Chemistry Department, University of Washington, Seattle, Washington
235. S. R. Mohanty, Department of Chemistry, Utkal University, Bhubaneswar 4, India
236. G. Czapski, Department of Physical Chemistry, The Hebrew University, Jerusalem, Israel
237. Patent Office, AEC, ORO

238–427. Given distribution as shown in TID-4500 under Chemistry Category (25 copies – CFSTI)